ANNALS OF THE RHEUMATIC DISEASES

THE EULAR JOURNAL
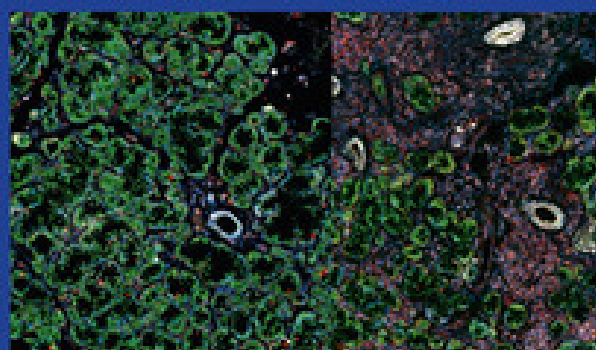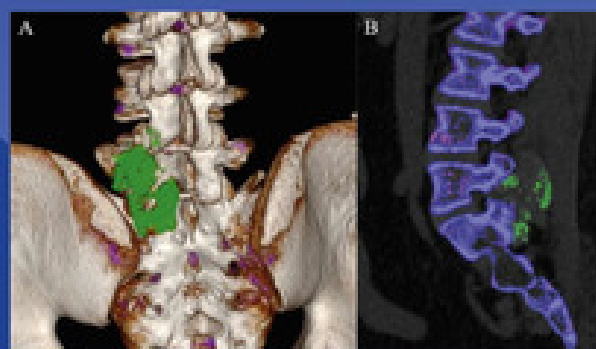
Viewpoint

Medical gaslighting in rheumatology: listening, learning, and leading

Viswaja Kaja [1,*], Kryss Shane[2,3], Adegbenga A. Bankole[4], Anthony D. Slonim[5]

[1] Department of Internal Medicine, Virginia Tech-Carilion School of Medicine, Roanoke, VA, USA

[2] National University, San Diego, CA, USA

[3] Endicott College, Beverly, MA, USA

[4] Department of Rheumatology, Virginia Tech-Carilion School of Medicine, Roanoke, VA, USA

[5] Departments of Internal Medicine and Pediatrics, Health Systems Science and Interprofessional Practice, Virginia Tech-Carilion School of Medicine, Roanoke, VA, USA

OVERVIEW

A strong patient-physician relationship is essential for accurate diagnosis and effective treatment, particularly in patients with chronic, complex diseases. Specialties like rheumatology rely heavily on this relationship. *Medical gaslighting* refers to situations in which healthcare providers unintentionally dismiss or minimize a patient's concerns, leading them to question their own perceptions, judgement, or emotions [1].

The term gaslighting comes from a 1944 film, *Gaslight*, in which a woman is manipulated into doubting her perception of reality. Over time, the term gained mainstream attention, especially on social media, where it developed a negative connotation [2]. Between 2005 and 2025, Google's Relative Interest Score increased for 'medical gaslighting' from 5 to 85 [Shane K, personal communication, May 10th, 2025], and in 2022, Merriam-Webster dictionary named it Word of the Year, reflecting its cultural prominence [3]. Despite growing awareness, medical gaslighting is still underrepresented in peer reviewed literature. In 2020, *JAMA* described a patient whose symptoms were dismissed until a long COVID diagnosis was confirmed [4]. In 2025, ECRI (formerly known as Emergency Care Research Institute), identified medical gaslighting as the top threat to patient safety [5], citing its role in delayed diagnoses, care mismanagement, patient distress, and worsening health disparities. A 2023 HealthCentral survey found that 94% of respondents reported experiencing medical gaslighting by a physician [6].

Rheumatologists are uniquely positioned to recognise and address medical gaslighting, as the specialty often involves patients with chronic, multisystem symptoms lacking clear diagnostic markers. These diseases present with diverse symptoms, variable disease progression and organ system involvement. Diagnosis and treatment depend on synthesising clinical patterns, patient-reported symptoms and laboratory findings over time [7]. The complexity and rarity of these diseases contribute to diagnostic delays and confusion, creating situations that may be perceived as medical gaslighting. As awareness grows, rheumatologists must understand its impact on patient care.

THEORETICAL UNDERPINNINGS

Trust is the foundation of any successful relationship [8]. In his 1949 essay 'The Seven Sins of Medicine', Dr Richard Asher emphasised the importance of good manners in medical practice, noting that subtle or unintentional rudeness could undermine the trust essential to the patient-physician relationship [9]. In rheumatology, this trust is often strained due to the complex nature of disease presentation and progression. Patients may face shifting diagnoses, prolonged uncertainty, and conflicting opinions from multiple providers, making them more vulnerable to medical gaslighting. Even well-meaning but dismissive interactions can erode a patient's confidence if they feel disbelieved or misunderstood. Importantly, trust is bidirectional. Studies suggest that physicians' trust in patients is influenced by perceptions of whether the patient is a 'good' historian, someone who communicates clearly, follows recommendations, and respects clinical authority [10]. When credibility is unconsciously filtered through these expectations, it can lead to biased or inadequate care.

Epistemic injustice, a concept from philosophy, refers to harm done to individuals in their capacity as 'knowers' [11,12]. In medicine, patients are the primary knowers of their symptoms

*Correspondence to Dr Viswaja Kaja.

E-mail address: viswaja.kaja@gmail.com (V. Kaja).

Handling editor Josef S. Smolen.

and lived experiences, even when medical tests fail to explain them. When their accounts are dismissed because of bias, uncertainty, or misalignment with diagnostic norms, testimonial injustice occurs [11,12]. Hermeneutic injustice arises when patients lack the language to describe symptoms and providers lack the interpretive tools to understand them [11,12]. This is especially relevant in rheumatology, where symptoms like fatigue, diffuse pain, or cognitive dysfunction are often difficult to articulate and interpret. These symptoms may appear unrelated or reflect an underlying systemic autoimmune rheumatic disease (SARD). When mutual understanding is compromised, meaningful clinical engagement is lost, and trust is undermined.

RECOGNIZING MEDICAL GASLIGHTING IN RHEUMATOLOGY

The nature of rheumatic disease creates conditions in which medical gaslighting may unintentionally arise. SARDs often present with a constellation of symptoms, increasing the risk of both under- and overdiagnosis. Communicating this uncertainty is challenging, and patients may feel dismissed, especially when their symptoms are attributed to ageing, stress or psychosocial factors, even after thorough clinical evaluation. The Table provides 10 examples of physician statements alongside how patients may interpret them when experiencing perceived medical gaslighting.

Patients are often told their symptoms are 'unexplainable' or 'inconsistent' with rheumatic disease, which may be interpreted as "no one knows what is wrong with me". When fatigue or joint pain is linked to ageing, patients might think "the doctor thinks I'm just getting old". Similarly, if symptoms are attributed to anxiety or depression, instead of diseases like rheumatoid arthritis or systemic lupus erythematosus (SLE), patients may internalise "the doctor thinks I am crazy" [7] (Table). Even if the physician's communication is technically accurate, patients may perceive these explanations as dismissive, eroding trust and damaging the therapeutic relationship. A clear example of medical gaslighting's harm is the development of learned helplessness, where patients lose confidence, self-esteem, and agency, placing them at higher risk for depression and anxiety [13].

Diagnostic challenges

Diagnosing SARDs is inherently difficult due to symptom overlap with functional disorders and possibility of coexisting functional disorders. Preclinical autoimmunity, overlap syndromes and comorbidities such as obesity, chronic pain and osteoarthritis further blur diagnostic clarity and complicate clinical interpretation.

Early in the diagnostic process, patients often report nonspecific symptoms that resemble other diseases, making it hard to distinguish between rheumatic diseases such as rheumatoid arthritis, polymyalgia rheumatica (PMR), SLE, and psoriatic arthritis [7]. Limited knowledge of these diseases among primary care providers can result in medical gaslighting delaying or preventing referrals to rheumatology and prolonging diagnostic delays.

Challenges increase when specific autoantibodies are absent, as in diseases such as polyarteritis nodosa or PMR. Without clear biomarkers, clinicians must rely heavily on clinical judgement and patient-reported symptoms. This reliance may lead to scepticism about the legitimacy of the patient's experience, increasing the risk of perceived or actual gaslighting when symptoms are minimised or attributed to psychological or age-related causes.

One effective strategy to reduce this risk is to shift the emphasis at the initial consultation from diagnosis to understanding and validating how patients experience their disease. Subsequent visits can prioritise reaching a definitive diagnosis. Validated assessment tools support this patient-centred approach, helping patients to describe symptoms and quality of life impacts across multiple domains [14−16]. While these tools are effective, certain aspects of a patient's experience remain underrepresented and would benefit from further refinement. The Figure outlines a framework to guide clinical conversations towards these domains, supporting patients as the primary knowers of their experience.

Certain diseases, such as SLE, fibromyalgia and Ehlers-Danlos Syndrome, are especially prone to misdiagnosis or dismissal [16−18]. These illnesses often present with symptoms such as widespread pain and fatigue, which are difficult to quantify and frequently minimised in clinical settings [Shane K, personal communication, May 10th 2025]. While SARDs often coexist with mental health diseases such as anxiety and depression, referencing psychological factors without proper context or sensitivity may feel dismissive to patients, rather than reflecting comprehensive understanding of their disease.

RECOMMENDATIONS FOR PRACTICE

Providing effective care for patients with complex, multisystem disease requires time, empathy, and consistent engagement. Clinicians must listen, reflect critically, and collaborate with patients, especially when symptoms are nuanced and hard to quantify. To support this model, healthcare systems should adopt policies that allow physicians adequate time with patients, fostering more empathic and patient-centred care.

Shared decision-making should be emphasised, promoting patient autonomy and informed choice, even when patient's preferences diverge from clinical recommendations. However, it is important to maintain clarity: partnering in shared decision-making does not mean relinquishing responsibility for guiding diagnostic evaluation and management.

To address structural contributors to medical gaslighting, particularly those linked to gender, race, sexual orientation, and socioeconomic status, mandatory training in communication, cultural competency and implicit bias should be integrated into rheumatology education [19]. This foundation is essential for

Table
Common statements made by physicians interpreted differently by patients

|	Physician statement	Patient's interpretation
1	Your labs are normal.	They don't want to do anything.
2	This is not typical for this disease.	They think I'm making this up.
3	Let's see if your symptoms subside.	They're hoping I'll go away.
4	Try to stay active, it will help.	They think I'm not doing anything.
5	There is nothing else to do until we see if this medicine works.	They're giving up on me.
6	This doesn't look like anything serious.	They're not taking my suffering seriously.
7	Let's wait for the results.	They don't believe I'm sick.
8	You have already seen several specialists.	They think I'm overreacting.
9	There are no objective signs of inflammation.	They think I'm imagining my symptoms.
10	I expected you to feel better by now.	They said I'm not trying hard enough.
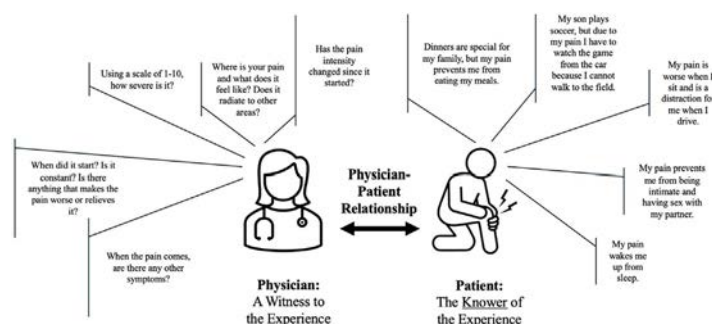
Figure. A cartoon that depicts the differences between standardised assessment questions by a physician using an example of pain and the patient's perspective on what they would like to contribute to the conversation as a 'knower' of the pain experience.

clinicians to be both diagnostically proficient and attuned to patients' lived experiences [17,18,20].

Further research is needed to deepen the understanding of medical gaslighting. A research program that integrates the definitions, perspectives of patients and providers, data, awareness, and action plans for management when it occurs are all areas in which to start investigations. Future studies should explore how systemic biases influence patient-provider interactions and outcomes. Research into medical and patient decision-making is increasingly critical in an era of open access health information and evolving decision support tools. Additionally, new instruments should be developed and validated to help patients express underreported experiences such as sexual health, fatigue, cognitive dysfunction (brain fog), spiritual wellbeing, and treatment burden.

Public advocacy and education should highlight the importance of a collaborative, trusting patient-physician relationship. Tools like patient-reported outcome measures (PROMs) offer shared language for symptom reporting and may empower patients to communicate more confidently. When rheumatologists incorporate PROMs into consultations, they can facilitate more effective dialogue and shared decision-making, helping to mitigate medical gaslighting.

CONCLUSION

The multifaceted nature of SARDs often leads to discordance between quantifiable clinical markers and the patient's subjective experiences, complicating assessment for the provider and communication with the patient. This discordance increases the risk of perceived medical gaslighting. Rheumatologists are uniquely positioned to reduce this risk through sustained, empathic, patient-centred care. Doing so requires addressing unconscious bias, enhancing communication, and advancing research that incorporates both physician and patient voices to improve outcomes and rebuild trust in healthcare.

Competing interests

All authors declare they have no competing interests.

CRediT authorship contribution statement

Viswaja Kaja: Writing − review & editing, Writing − original draft, Visualization, Conceptualization. **Kryss Shane:** Writing − review & editing, Visualization. **Adegbenga A. Bankole:** Writing − review & editing, Supervision. **Anthony D. Slonim:** Writing − review & editing, Visualization, Supervision, Conceptualization.

Funding

Patient consent for publication

Not applicable.

Ethics approval

Not applicable.

Provenance and peer review

Not commissioned; externally peer reviewed.

Orcid

Viswaja Kaja: http://orcid.org/0009-0009-2927-3524

REFERENCES

[1] Shapiro D, Hayburn A. Medical gaslighting as a mechanism for medical trauma: case studies and analysis. Curr Psychol 2024;43:34747–60. doi: 10.1007/s12144-024-06935-0.

[2] Cukor G. Gaslight [video file]. MGM; 1944. Accessed on May 5, 2025. https://archive.org/details/Gaslight_628.

[3] Yadava OP. Medical gaslighting'-an eye-opener. Indian J Thorac Cardiovasc Surg 2023;39(5):441–2. doi: 10.1007/s12055-023-01588-3.

[4] Rubin R. As their numbers grow, COVID-19 "long haulers" stump experts. JAMA 2020;324(14):1381–3. doi: 10.1001/jama.2020.17709.

[5] ECRI. Top 10 patient safety concerns 2025 [Internet] 2025 Mar 10 [cited 2025 May 5]. Available from: https://home.ecri.org/blogs/ecri-thought-leadership-resources/top-10-patient-safety-concerns-2025.

[6] Kennedy LP. What you told us about medical gaslighting [Internet]. HealthCentral 2023 Sep 28 [updatedcited 2025 Jun 28]. Available from: https://www.healthcentral.com/chronic-health/what-you-told-us-about-medical-gaslighting.

[7] Sloan M, Naughton F, Harwood R, Lever E, D'Cruz D, Sutton S, et al. Is it me? The impact of patient-physician interactions on lupus patients' psychological well-being, cognition and health-care-seeking behaviour. Rheumatol Adv Pract 2020 Jul 22;4(2):rkaa037. doi: 10.1093/rap/rkaa037.

[8] Taylor LA, Nong P, Platt J. Fifty years of trust research in health care: a synthetic review. Milbank Q 2023;101(1):126–78. doi: 10.1111/1468-0009.12598.

[9] Asher R. The seven sins of medicine. Lancet 1949;2(6574):358–60. doi: 10.1016/s0140-6736(49)90090-2.

[10] Thom DH, Campbell B. Patient-physician trust: an exploratory study. J Fam Pract 1997;44(2):169–76.

[11] Wilson A, Millard C, Sabroe I. Physician narratives of illness. Lancet 2019; 394(10192):20–1. doi: 10.1016/S0140-6736(19)31501-6.

[12] Sabroe I, Mather S, Wilson A, Hall-Flavin DK, Fricker M, Barron LA, et al. Error, injustice, and physician wellbeing. Lancet 2021;397(10277):872–3. doi: 10.1016/S0140-6736(21)00512-2.

[13] Santoyo-Fexas L, Uriarte Botello RA, Solis CV, Esquivel Valerio JA, Díaz-García RE, Colunga-Pedraza IJ, et al. FRI0076 relationship between depression, learned helplessness, disability and disease activity in patients with rheumatoid arthritis. Ann Rheum Dis 2020;79(suppl 1):615.

[14] Pincus T, Swearingen CJ, Bergman M, Yazici Y. RAPID3 (Routine Assessment of Patient Index Data 3), a rheumatoid arthritis index without formal joint counts for routine care: proposed severity categories compared to disease activity score and clinical disease activity index categories. J Rheumatol 2008;35(11):2136–47. doi: 10.3899/jrheum.080182.

[15] Bruce B, Fries JF. The Stanford Health Assessment Questionnaire: dimensions and practical applications. Health Qual Life Outcomes 2003;1:20. doi: 10.1186/1477-7525-1-20.

[16] Webster KA, Peipert JD, Lent LF, Bredle J, Cella D. The Functional Assessment of Chronic Illness Therapy (FACIT) measurement system: guidance for use in research and clinical practice. In: Kassianos AP, editor. Handbook of quality of life in cancer. Cham: Springer; 2022. p. 79–104. doi: 10.1007/978-3-030-84702-9_6.

[17] Bruce IN, Buie J, Bloch L, Bae SC, Costenbader K, Levy RA, et al. Lupus spectrum ambiguity has long-term negative implications for patients. Lupus Sci Med 2023;10(1):e000856. doi: 10.1136/lupus-2022-000856.

[18] Miklovic T, Sieg VC. Ehlers-Danlos Syndrome. StatPearls [Internet]. Treasure Island (FL): StatPearls Publishing; 2025. Available from: https://www.ncbi.nlm.nih.gov/books/NBK549814/.

[19] Hall WJ, Chapman MV, Lee KM, Merino YM, Thomas TW, Payne BK, et al. Implicit racial/ethnic bias among health care professionals and its influence on health care outcomes: a systematic review. Am J Public Health 2015;105(12):e60–76. doi: 10.2105/AJPH.2015.302903.

[20] Williams YJ, Jantke RL, Jason LA. Chronic fatigue syndrome: case definitions and diagnostic assessment. N Y State Psychol 2014;26:41–5.

Rheumatoid arthritis

Spatial mapping of rheumatoid arthritis synovial niches reveals a LYVE1^{+} macrophage network associated with response to therapy

Julien De Lima[1], Marie-Astrid Boutet[1,2], Olivier Bortolotti[3], Laure-Agnès Chépeaux[4], Yaël Glasson[4], Anne-Sophie Dumé[4], Rachel Lau[2], Paul Humbert[1], Sophie Allain[1], Adrien Le Pluart[1], Alessandra Nerviani[2], Liliane Fossati-Jimack[2], Henri-Alexandre Michaud[4], Jérôme Guicheux[1], Benoit Le Goff[1], Myles J. Lewis[2], Costantino Pitzalis[2,5,6], Gabriel Courties[3], Florence Apparailly[3,7], Frederic Blanchard[1,*]

[1] Nantes Université, ONIRIS, CHU Nantes, INSERM, Regenerative Medicine and Skeleton, RMeS, Nantes, France
[2] Centre for Experimental Medicine and Rheumatology, William Harvey Research Institute, Barts and The London School of Medicine and Dentistry, Queen Mary University of London, London, UK
[3] Institute of Regenerative Medicine and Biotherapy, INSERM, University of Montpellier, Montpellier, France
[4] Plateforme de Cytométrie et d'Imagerie de Masse de Montpellier, Institut de Recherche en Cancérologie de Montpellier, INSERM, University of Montpellier, Institut régional du Cancer de Montpellier, Montpellier, France
[5] IRCCS Humanitas Research Hospital, Milan, Italy
[6] Department of Biomedical Sciences, Humanitas University, Milan, Italy
[7] Clinical Department for Osteoarticular Diseases, University hospital Lapeyronie, Montpellier, France

ARTICLE INFO

ABSTRACT

Objectives: Despite advances in rheumatoid arthritis (RA) treatment, a significant proportion of patients fail to achieve adequate remission. The dynamic cellular and architectural changes within the synovium that underpin therapeutic success remain poorly understood. This study aimed to unravel the synovial landscape during effective RA treatment, identifying key cellular networks and molecular pathways associated with remission.

Methods: We performed high-dimensional imaging mass cytometry on synovial tissues from healthy controls, patients with osteoarthritis, and patients with early RA longitudinally before and after 6 months of conventional synthetic disease-modifying antirheumatic drugs (csDMARD) therapy. Findings were validated using whole-tissue RNA-sequencing and immunofluorescence in larger patient cohorts, and integrated with ligand-receptor analyses from public single-cell RNA-seq datasets and *in vitro* functional coculture assays.

Results: Our deep spatial profiling pinpointed a critical LYVE1^{+}CD206^{+} tissue-resident macrophage network, localised within perivascular niches alongside fibroblasts and vascular cells. This homeostatic network was disrupted in active RA but restored in patients responding well to csDMARDs. This restoration correlated with the re-establishment of specific cell-cell interactions and was governed by distinct molecular pathways, including chemokines, annexins, and TAM

Correspondence to: Dr Frederic Blanchard, RMeS − Regenerative Medicine and Skeleton, 1 place Alexis Ricordeau, 44042 Nantes Cedex 1, France.
E-mail address: frederic.blanchard@univ-nantes.fr (F. Blanchard).

Marie-Astrid Boutet and Olivier Bortolotti contributed equally to this work.

Florence Apparailly and Frederic Blanchard contributed equally to this work.

Handling editor Josef S. Smolen.

(TYRO3, AXL, MERTK) receptors. Functionally, LYVE1$^+$ macrophages demonstrated a regulatory, anti-inflammatory phenotype in vitro, contrasting with proinflammatory myeloid cells.

Conclusions: This study provides an unprecedented spatial and dynamic blueprint of the RA synovium's response to therapy. We identify the LYVE1$^+$ macrophage network as a pivotal component of synovial homeostasis and its restoration as a hallmark of clinical remission. These findings unveil novel cellular and molecular targets, paving the way for more active therapeutic strategies.

WHAT IS ALREADY KNOWN ON THIS TOPIC

- Single-cell transcriptomic analyses have brought unprecedented insights into synovial cell heterogeneity, including macrophages. The proportion of macrophage subtypes varies in response to disease-modifying antirheumatic drugs (DMARD) treatment but their spatial interactions with other synovial cells are understudied.

WHAT THIS STUDY ADDS

- Using single-cell high-dimensional imaging mass cytometry, we identified that tissue-resident LYVE1$^+$ macrophages in perivascular sublining synovial niches were disturbed in active rheumatoid arthritis (RA) but recovered after conventional synthetic DMARD treatment. Several molecular pathways implicated in the restoration of these spatial cell interactions were found to be associated with clinical remission.

HOW THIS STUDY MIGHT AFFECT RESEARCH, PRACTICE OR POLICY

- The combination of transcriptomic and spatial proteomic approaches allows a better elucidation of the interconnections between the stromal microenvironment and the immune cell landscape. This study forms the basis for the development of more targeted, hence more active therapeutic strategies for RA.

INTRODUCTION

Rheumatoid arthritis (RA) affects 0.3% to 1% of the general population worldwide and is characterised by joint inflammation associated with debilitating bone and cartilage erosions. Despite the availability of a large therapeutic arsenal, including conventional synthetic (cs) disease-modifying antirheumatic drugs (DMARDs; eg, methotrexate, MTX), biologic (b) DMARDs (eg, tumour necrosis factor [TNF] inhibitors) and targeted synthetic (ts) DMARDs (eg, JAK inhibitors), around 40% of patients do not adequately respond to these treatments, and RA remains a major public health challenge [1,2]. RA is a prototypic synovitis-driven autoimmune disease and the in-depth characterisation of the synovium has broadened our understanding of RA pathogenesis and led to the development of targeted therapies. There is currently no predictive biomarker of treatment response; consequently, treatment allocation is based on 'trial and error' [3,4]. Recent evidence supports the concept of integrating synovial cellular/molecular signatures into clinical algorithms to help predict response to specific DMARDs and enhance clinical outcome, towards precision medicine [1,5].

Transcriptomic profiling of dissociated tissues using single-cell RNA sequencing (scRNAseq) approaches has brought unprecedented insights into synovial cell heterogeneity, including fibroblasts, macrophages, T and B cells [6−8]. Importantly, key cellular crosstalk and dysregulated signalling pathways involved in RA pathogenesis have been highlighted. A particular role for tissue-resident macrophages (TRM) expressing *MERTK, CD163, TREM2*, and *TIMD4* (and *Cx3cr1* in mice) has been

proposed as a protective tight-junction-forming cell layer that secludes the synovium, and avoids the infiltration of inflammatory cells from the joint cavity [7,9]. Recently, LYVE1$^+$CX3CR1$^+$ TRM were shown to form a sentinel unit around fenestrated capillaries at the lining-sublining interface. In response to systemic immune complex challenge, these macrophages orchestrate neutrophil recruitment and activation of nociceptor neurons [10]. Overall, TRM represent the majority of lining and sublining synovial macrophages in healthy donors and patients with RA in remission, whereas several inflammatory macrophage (IM) subsets, characterised by toll-like receptor activation, interferon signature, alarmin production, or antigen presentation, are enriched in the synovial tissue of patients with active RA [11].

Although these findings have been outstandingly informative, tissue dissociation represents a major limitation inherent to single-cell profiling approaches, as critical cells and spatial information are lost during the sample preparation. Both the stromal microenvironment and immune cell infiltrate spatial function/identity are increasingly recognised as key players of pathogenesis and treatment response in rheumatology, as in oncology [5,12−14]. Recently, spatial transcriptomic revealed that pathogenic and tolerogenic dendritic cells interact with T cells within lining and sublining niches, providing novel opportunities to restore immune homeostasis in RA [15]. However, such single-cell spatial studies remain very sparse in rheumatology.

Here, we performed single-cell high-dimensional imaging mass cytometry (IMC) to spatially analyse and compare the expression of 33 proteins in the synovial tissue from healthy individuals, patients with osteoarthritis (OA) who lack severe inflammatory responses, and matched samples from patients with active early treatment-naïve RA at baseline and at 6 months after starting a csDMARD treatment. IMC analyses were combined with whole-tissue RNA-seq and IF staining validation in large cohorts of RA patients, as well as ligand-receptor investigation of public scRNAseq datasets and functional *in vitro* coculture assays. Overall, this study provides insights into the spatial distribution and the pathogenic connections between synovial niches. It also highlights key pathways relevant for better understanding RA pathogenesis and for the development of novel therapeutic strategies.

METHODS

All methods are described in the supplementary methods file.

Patient and public involvement statement

Although there was no specific patient and public involvement (PPI) when the study here presented was initially conceived, participants have been subsequently involved in surveys to assess the quality and burden of research visits and interventions. Furthermore, patients recruited in Pathobiology of Early Arthritis Cohort (PEAC) are regularly invited to PPI local events

where they are asked to provide feedback on research themes and questions.

RESULTS

Highplexed IMC highlights a high heterogeneity of TRM within the synovial lining and sublining layers

To comprehensively profile the cellular composition and spatial organisation of RA synovium, we took advantage of the various cluster-specific gene markers recently proposed by scRNAseq studies [6,7,16] and developed the workflow presented in Figure 1A. Thirty-three antibodies labelled with unique metal isotopes were validated to identify monocytes and macrophages, including TRM and IM, lymphoid and stromal cells (Fig 1A,B, Supplementary Fig S1A and Supplementary Table S1). Forty high-dimensional images were analysed for a total of 26.85 mm^2 of synovial tissue from 4 healthy donors, 4 patients with OA exhibiting a low inflammatory profile, and 4 patients with active anticitrullinated protein antibody positive (ACPA$^+$) RA (Disease Activity Score—Erythrocyte Sedimentation Rate [DAS28-ESR] ≥ 3.9) at baseline before the initiation of treatment (Supplementary Table S2). For 3 patients with RA, we also included matched posttreatment biopsies at 6 months (Supplementary Fig S1B).

All images were then segmented into 115,411 total cells and an unsupervised clustering approach classified synovial TRM, IM, lymphoid and stromal cells (Fig 1C). By calculating the distance between each cell type from the vascular and lining cells, we obtained a comprehensive spatial cell organisation allowing for the annotation of lining (L-) and sublining (SL-) cell subsets (Fig 1D). IMC subsets were also mapped onto public scRNAseq datasets covering 23,759 synovial cells dissociated from the synovium of patients with RA ($n = 11$), and similar clusters were identified (Fig 1E,F, Supplementary Fig S2A) [7,17].

Importantly, we distinguished 3 distinct TRM subsets based on their differential expression of TIM4, MERTK, and LYVE1. Lining TRM1 (L-TRM1) were CD68$^+$CD163$^+$TIM4$^+$MERTK^{low}, whereas L-TRM2 were CD68$^+$CD163$^+$TIM4$^-$MERTK^{high}, and both expressed the apoptosis marker cleaved-caspase 3 (Fig 1C and Supplementary Fig S3A), which is presumably linked to their efferocytosis capacity [18]. In line with previously published evidence, scRNAseq confirmed that L-TRM1 expressed higher levels of *TIM4* and *TREM2* compared to L-TRM2, and both cell subsets expressed *CD163* and low levels of *MERTK* (Fig 1F) [7]. These L-TRM1 and L-TRM2 populations align with the TREM2^{high} and TREM2^{low} macrophages, respectively, identified by Alivernini et al. [7]. In the sublining, SL-TRM3 were positive for CD206 and LYVE1 (Fig 1B-F), corresponding to LYVE1^{pos} macrophages [7] or the recently characterised perivascular TRM in mice and patients with RA [10,19]. Three distinct tissue-infiltrating CD14$^+$ IM clusters were defined based on varying expression of the alarmin S100A12 (SL-IM1), CD11c and HLA-DR (IM2, antigen-presenting cells) or osteopontin (SPP1, IM3) (Fig 1C-F). These clusters shared features with the S100A12^{pos}, CLEC10A^{pos}, and SPP1^{pos} macrophages previously reported (Supplementary Fig S2B) [7]. A small proportion of IM3 was also positive for KI67 (Fig 1C and Supplementary Fig S3B), suggesting cell proliferation linked to tissue fibrosis [20]. A fourth IM cluster (L-IM4), characterised by the expression of CCR2, IFI6, and granzyme B expression presented an interferon signature, akin to the ISG15^{pos} macrophage cluster [7]. Regarding stromal cells, L-fibroblasts were defined by the expression of podoplanin (PDPN$^+$CD90$^-$), whereas SL-fibroblasts exhibited

CD90/THY1 expression (Fig 1B-D), consistent with previous characterisations [16,21,22]. At the transcriptomic level, L-fibroblasts expressed *PDPN, PRG4, VCAM,* and *CD55,* whereas SL-fibroblasts were characterised by the expression of *THY1, DKK3,* and *CXCL12* (Supplementary Fig S2A). Due to the close proximity between those cells, both smooth muscle cells (aSMA$^+$) and endothelial cells (CD31$^+$) were collectively identified as vascular cells (Fig 1B-E). Overall, our results unveiled distinct spatial organisation within the lining and sublining layers of the synovium.
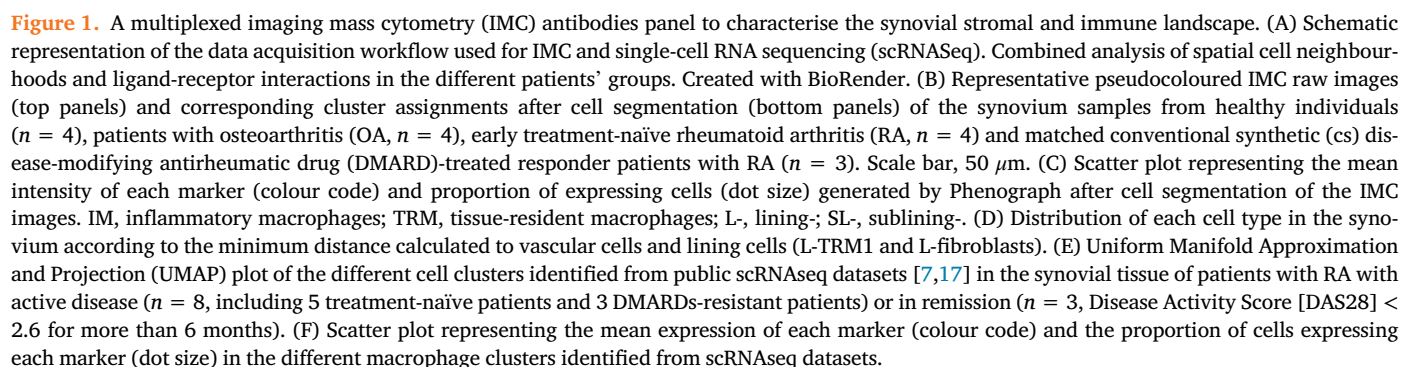
Synovial tissues from patients with active RA are characterised by a significant disruption of SL-TRM3 cellular network

Following the identification of synovial cell subsets, we compared the stromal and immune cell density across patients' groups. As expected, a significant increase in both lymphoid cell subsets (B, plasma, CD4 and/or CD8 T cells) and L-fibroblast cell density was observed in the synovium of patients with RA as compared to healthy donors (Fig 2A-D and Supplementary Fig S4A) [21]. Inversely, the density of TRM, specifically L-TRM2, was decreased in RA compared to OA synovial tissues (Fig 2A-D and Supplementary Fig S4A), and the IM/TRM ratio was significantly increased in active RA compared to healthy donors (Supplementary Fig S4B). Altogether, we highlighted a concomitant infiltration of lymphoid cells and IM, and a reduction of synovial TRM in patients with active early treatment-naïve RA.

To further characterise the communications between individual synovial cells, a permutation test was performed and, within the 5 nearest cell neighbours ($k = 5$) and a distance threshold of 20 μm, we identified interactions and avoidance behaviours between cell cluster pairs (Fig 2E,F) [23]. In healthy individuals, the main synovial cellular network mostly involved sublining cells, including SL-TRM3, SL-fibroblasts and vascular cells. In OA tissues, the interactions involving SL-TRM3 were reduced whereas the interactions involving L-TRM2 and CD4$^+$ T cells were enhanced, especially with L-TRM1 and CD8$^+$ T cells (Fig 2E,F). Importantly, in the synovium of patients with early, active, and treatment-naïve RA, several cell-cell interactions were disrupted compared to healthy tissues, especially the ones involving SL-TRM3 (Fig 2E,F). Furthermore, in RA, disease-specific interactions were revealed, especially involving IM, lymphoid cells, and L-fibroblasts (Fig 2E-F). These analyses therefore highlighted that the synovial infiltration at early stages of RA creates a dense cellular network in which the homeostatic social network involving SL-TRM3 is disrupted.

The definition of spatial multicellular neighbourhoods or niches reveals the dynamic and functional synovial interactions of SL-TRM3

We next explored whether multicellular structural analysis, rather than pairwise cell-cell interactions, would provide further insights into the organisation and dynamic changes of RA synovial tissue. Cells were clustered based on the identity of their neighbours within a radius of 20 μm [24,25], and 9 cellular neighbourhoods (herein called 'niches') were identified, of which 3 were localised in the lining (L1 to L3) and 6 in the sublining (SL1 to 4, ELS1 and 2) (Fig 3A-E). Lining niches were composed of distinct proportions of L-TRM1, L-TRM2, and L-fibroblasts. The 4 sublining niches (SL1-4 niches) were mostly composed of vascular cells, SL-fibroblasts, and SL-TRM3, which was reminiscent of the principal cell network determined in healthy donors (Fig 2E,F). Two additional niches also localised
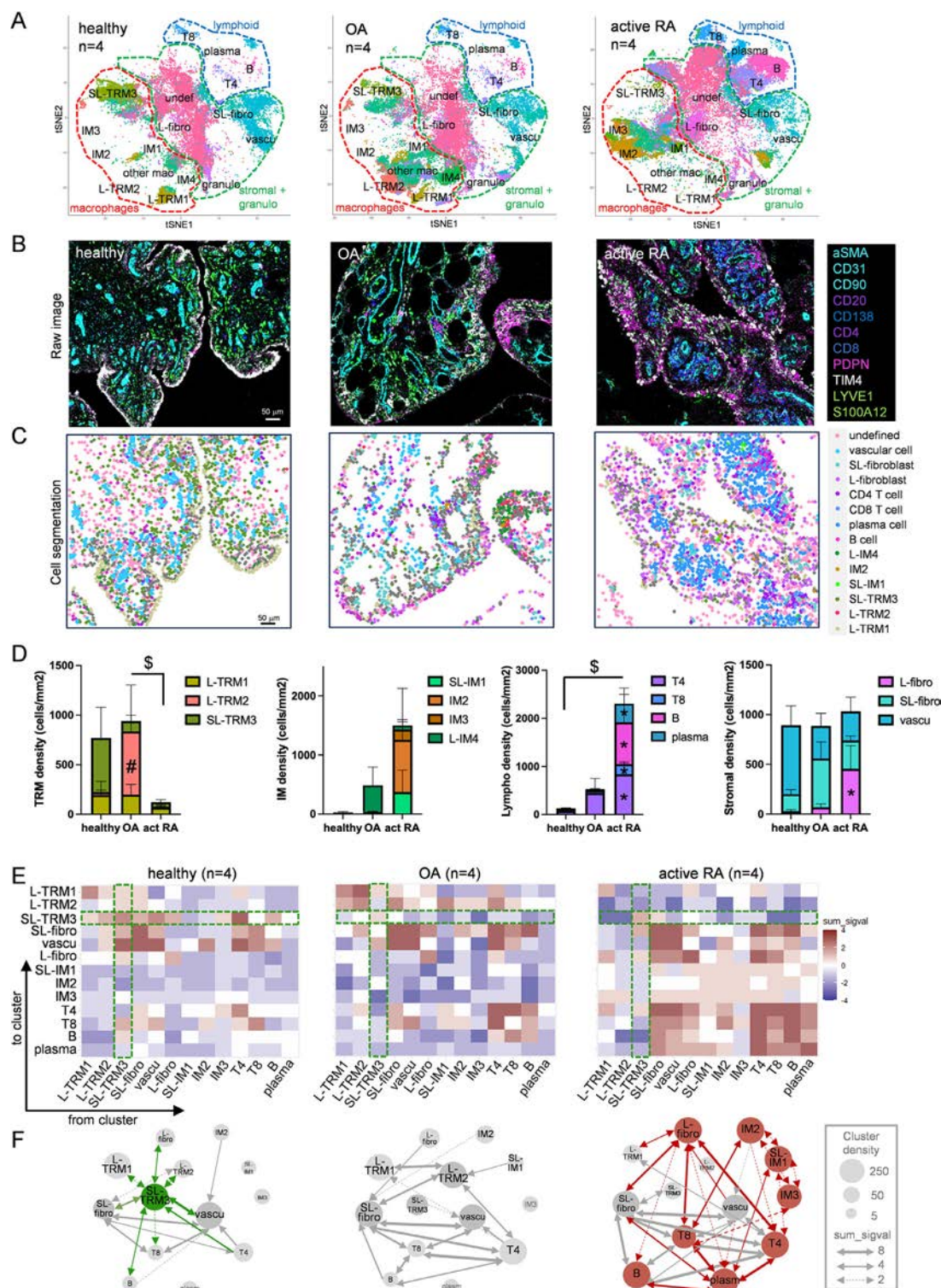
Figure 1. A multiplexed imaging mass cytometry (IMC) antibodies panel to characterise the synovial stromal and immune landscape. (A) Schematic representation of the data acquisition workflow used for IMC and single-cell RNA sequencing (scRNASeq). Combined analysis of spatial cell neighbourhoods and ligand-receptor interactions in the different patients' groups. Created with BioRender. (B) Representative pseudocoloured IMC raw images (top panels) and corresponding cluster assignments after cell segmentation (bottom panels) of the synovium samples from healthy individuals (*n* = 4), patients with osteoarthritis (OA, *n* = 4), early treatment-naïve rheumatoid arthritis (RA, *n* = 4) and matched conventional synthetic (cs) disease-modifying antirheumatic drug (DMARD)-treated responder patients with RA (*n* = 3). Scale bar, 50 μm. (C) Scatter plot representing the mean intensity of each marker (colour code) and proportion of expressing cells (dot size) generated by Phenograph after cell segmentation of the IMC images. IM, inflammatory macrophages; TRM, tissue-resident macrophages; L-, lining-; SL-, sublining-. (D) Distribution of each cell type in the synovium according to the minimum distance calculated to vascular cells and lining cells (L-TRM1 and L-fibroblasts). (E) Uniform Manifold Approximation and Projection (UMAP) plot of the different cell clusters identified from public scRNAseq datasets [7,17] in the synovial tissue of patients with RA with active disease (*n* = 8, including 5 treatment-naïve patients and 3 DMARDs-resistant patients) or in remission (*n* = 3, Disease Activity Score [DAS28] < 2.6 for more than 6 months). (F) Scatter plot representing the mean expression of each marker (colour code) and the proportion of cells expressing each marker (dot size) in the different macrophage clusters identified from scRNAseq datasets.

Figure 2. Synovial cell densities and interactions are altered in patients with active treatment-naïve rheumatoid arthritis (RA). (A) t-distributed stochastic neighbor embedding (t-SNE) plot of the different cell subsets represented in the synovial tissue of healthy individuals ($n = 4$), patients with osteoarthritis (OA, $n = 4$) and active treatment-naïve rheumatoid arthritis (active RA, $n = 4$) patients. Macrophages (red), lymphoid (blue), and stromal (green) cell types are encircled. (B,C) Representative pseudocoloured imaging mass cytometry (IMC) images of stromal (aSMA, CD31, PDPN, and CD90) and immune cell markers (CD20, CD138, CD4, CD8, TIM4, LYVE1, and S100A12) of the synovium samples from healthy individuals, patients with osteoarthritis (OA) and active RA (B), and corresponding subset assignments after cell segmentation (C). Scale bar, 50 μm. (D) Cell densities of tissue-resident macrophages (TRM), inflammatory macrophages (IM), lymphoid cells, and stromal cells are presented for patients belonging to the healthy, OA and active RA (act RA) group. One-way analysis of variance (Kruskal-Wallis) with Dunn's correction was performed: $, adjusted P value < .05 for total TRM and total lymphoid cells; #, adjusted P value < .05 compared with active RA; *, adjusted P value < .05 compared with healthy. (E) Heatmaps showing the cell-cell interactions as the sum of the significant values calculated for each patient (sum_sigval) belonging to the healthy ($n = 4$), OA ($n = 4$) and active RA ($n = 4$) group. Brown squares indicate interactions; blue squares indicate avoidance between each cell pair. Interactions implicating SL-TRM3 are highlighted in green. (F) Schematic representation of the pairwise cell interactions, considering cluster densities (circle size) and sum_sigval values (arrow thickness) as calculated in (E). RA-specific interactions compared to both healthy and OA synovium are shown in red, interactions implicating SL-TRM3 cells that were lost in active RA synovium compared to healthy are shown in green.
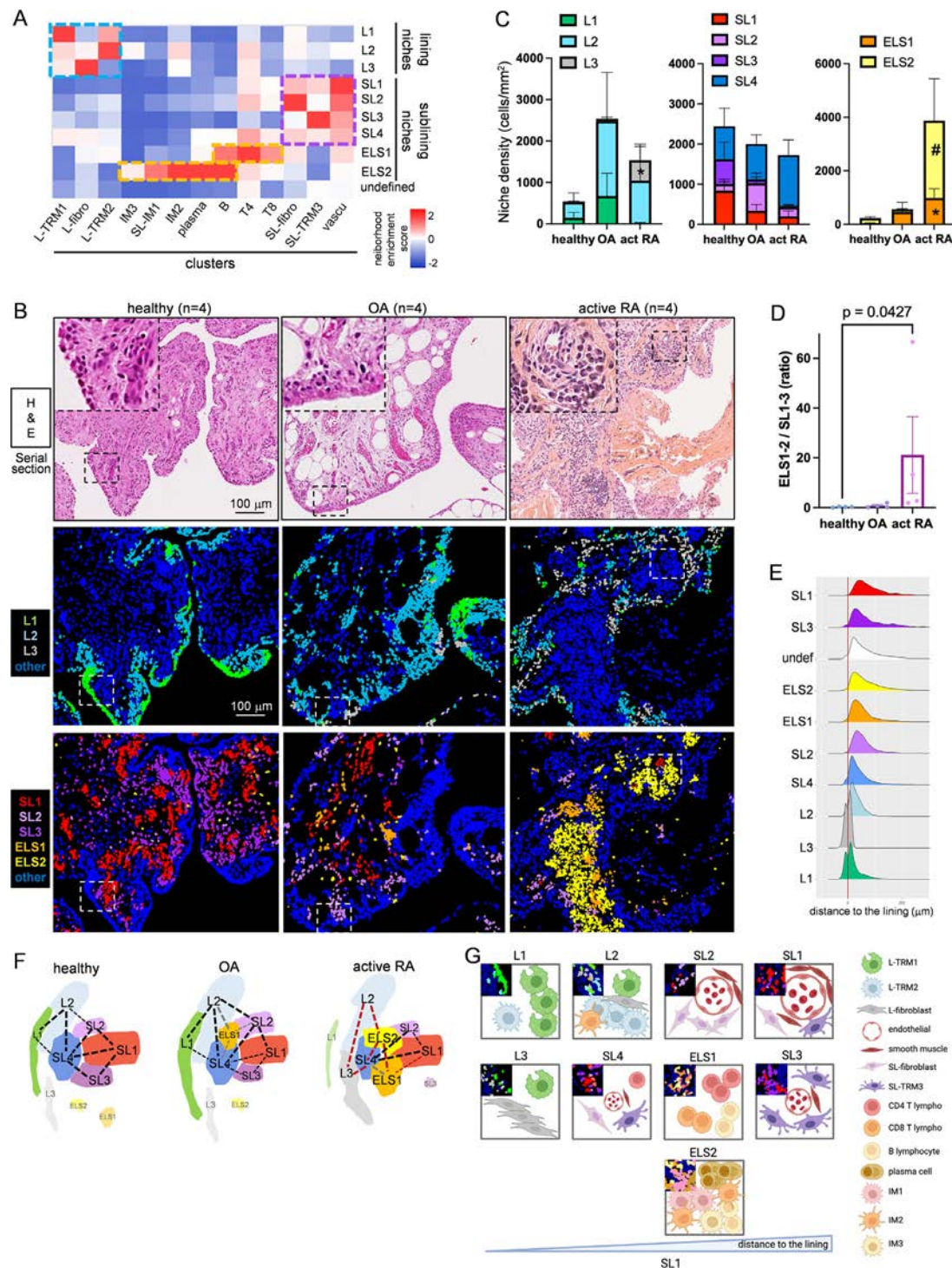
Figure 3. The spatial organisation of the synovial niches is altered in patients with active treatment-naïve rheumatoid arthritis (RA). (A) Heatmap representing the neighbourhood enrichment score of each cell subset across 10 niches defined in the 15 synovial tissues analysed. Lining niches are highlighted in light blue, sublining niches in purple, and ectopic lymphoid structures (ELS) niches in orange. (B) Representative hematoxylin and eosin (H&E) staining (top panels) and corresponding images of the lining (middle panels) or sublining and ELS (bottom panels) niches in the 3 patients' groups. (C) Niche densities are presented in the patients belonging to the healthy ($n = 4$), osteoarthritis (OA, $n = 4$) and active RA (active RA, $n = 4$) group. One-way analysis of variance (Kruskal-Wallis) with Dunn's correction was performed: *, adjusted P value < .05 compared to healthy; #, adjusted P value < .05 compared to OA. (D) Ratio of ELS1-2 densities to SL1-3 densities in the 3 patients' groups. (E) Distribution of each niche in the synovium according to the minimum distance calculated to the lining cells (L-TRM1 and L-fibroblasts). (F) Schematic representation of the niches' spatial organisation, considering the niche densities, distances to the lining and their interactions. Basal niche interactions in healthy and OA samples are provided in black and grey, additional interactions between niches observed specifically in active RA are shown in red. (G) Schematic representation of the cell type composition and proportions in each niche. Created with BioRender. Representative images of the cell subsets in each niche are shown as insets.

in the sublining compartment were composed of lymphoid cells and IM tightly packed together, forming ectopic lymphoid structures (ELS) [5,26,27]. While the ELS1 niche was mostly composed of lymphoid cells, namely B cells, CD4 and CD8 T cells, the ELS2 niche included B cells, plasma cells, but also the 3 IM subtypes (Fig 3A). Representative images of the niches localisation are shown in Figure 3B. Importantly, ELS1, ELS2, and L3 niches were significantly more abundant in active RA samples,

compared to healthy donors or patients with OA (Fig 3C and Supplementary Fig S5A). According to the changes in density of SL1, SL2, and SL3 niches, the ELS1-2/SL1-3 ratio was significantly increased in active RA compared to healthy donors (Fig 3D).

While each niche can represent the site of unique and local cellular interactions, distinct niches may also interact to support additional biological events [25]. Spatial niche interaction graphs were generated for each patient group (Supplementary Fig S6A) and provided a comprehensive locoregional niches map based on the strength of the interactions between niches, their density, and their precise tissue location (Fig 3E-G). In healthy donors, the main interactions were observed between L1, L2, SL1, SL2, SL3, and SL4 niches. Of interest, the cells in these niches (TRM, fibroblasts and vascular cells) are considered tissue resident or structural cells, thus highlighting the features of a homeostatic synovial interaction map. In OA synovium, a similar cartography was observed but a central position of the ELS1 niche, interacting with L2, SL2, and SL4 niches, was underlined (Fig 3F). In patients with active RA, the L3, ELS1, and ELS2 synovial niches composed of all infiltrating proinflammatory immune cells and L-fibroblasts, established novel interactions between them and with the homeostatic niches, therefore highlighting profound alterations compared to the homeostatic picture (Fig 3F). Furthermore, in the RA cellular interactive map, the loss of L1 and SL3 niches involvement, as well as the disruption of specific interactions, such as L2 with SL2 or with SL4, were observed (Fig 3F,G). Altogether, these results indicated that the cellular infiltration characterising the RA synovial tissue has a profound impact on the whole synovial architecture and the underlying cellular communications. As observed at the individual cell level (Fig 2), these results notably confirmed that the perivascular SL3 niche, mainly composed of SL-TRM3, was profoundly altered in patients with early active and treatment-naïve RA.

SL-TRM3 are reestablished following efficient csDMARD treatment

To study the impact of csDMARD treatment on the altered synovial cellular network observed in patients with active RA, we next performed paired analyses of patients with matched RA ($n = 3$) before therapeutic intervention and 6 months following efficient csDMARD treatment with MTX and sulfasalazine (SZP). The density of SL-TRM3 was significantly increased following treatment as assessed by IMC (Fig 4A and Supplementary Fig S4C). Whole-tissue RNA-seq performed on the tissues analysed by IMC confirmed that the expression of *LYVE1* was significantly increased in synovial biopsies posttreatment ($n = 3$, Fig 4B). Importantly, the upregulation of *LYVE1* was further validated in a larger cohort of csDMARD (MTX, SZP or hydroxychloroquine) responder lympho-myeloid and ACPA$^+$ patients from the PEAC ($n = 11$ paired baseline and 6-month samples, Fig 4C) [26,28]. Noteworthy, this increase of synovial *LYVE1* expression was not observed in poor-responder patients (Fig 4C). Similar results were observed when including patients with other pathotypes and ACPA$^-$ status ($n = 54$ paired samples, Supplementary Fig S7A). Baseline *LYVE1* expression was consistently lower in synovial biopsies with a lympho-myeloid pathotype compared to diffuse-myeloid or pauci-immune pathotypes, and it correlated negatively with disease activity and other clinic-radiographic parameters (Supplementary Fig S7B, C).

Six months following efficient MTX/SZP treatment, the cellular interactions involving SL-TRM3 cells were partially reestablished, for example, with L-fibroblasts, L-TRM2 and vascular cells (Fig 4D,E). In addition, MTX/SZP treatment induced novel interactions, such as between SL-TRM3 and plasma cells, whereas preexisting interactions persisted posttreatment, such as with SL-fibroblasts and CD4 T cells (Fig 4D,E). These cellular interactions were visualised on raw images of LYVE$^+$ SL-TRM3 in their tissue microenvironment and their corresponding spatial graphs, highlighting clear proximities between SL-TRM3, SL-fibroblasts, vascular cells and T cells, especially in patients with RA 6 months following MTX/SZP treatment (Fig 4F,G). Interestingly, upon MTX/SZP treatment and along with the increase of SL1 and SL3 niches proportion (Fig 4H,I and Supplementary Fig S5B), SL3 reestablished significant connections with SL1 and SL4 (Fig 4I,J and Supplementary Fig S6B), as observed in healthy conditions (Fig 3F). Overall, good response to MTX/SZP therapy was associated with a partial recovery of the basal healthy synovial cartography, with a particular involvement of SL-TRM3.

scRNAseq ligand-receptor analysis underlines SL-TRM3 cellular pathways linked to disease activity

To further elucidate the pathways governing SL-TRM3 communications within the synovial niches in relation to disease activity, we next performed IF staining of SL-TRM3 (sublining CD68$^+$, MERTK$^+$, TIM4$^-$ cells). Synovia were collected from an independent cohort of patients with established ACPA$^+$ RA with active disease (DAS28 > 2.6, $n = 13$) or in remission (DAS28 < 2.6, $n = 7$) following cs- and/or b-DMARD treatments (Supplementary Table S2). A significantly higher SL-TRM3 density was evident in patients with RA in remission compared to those with active RA (Fig 5A). This pattern held true when including patients with ACPA$^-$ RA or when restricting the analysis to patients with RA treated solely with csDMARDs (Supplementary Fig S7D, E).

We further analysed public scRNAseq datasets from synovial cells dissociated from the synovium of patients with ACPA$^+$ active ($n = 8$) and remission ($n = 3$) RA introduced previously (Fig 1E,F, Supplementary Table S2) [7,17]. Several ligand-receptor interactions involving SL-TRM3 were induced in the synovial tissue of patients with RA in remission when compared to active RA (Fig 5B,C and Supplementary Fig S8). Of note, SL-TRM3 from patients with RA in remission were found to display enhanced response to chemokines (*CXCL12*, macrophage migration inhibitory factor [*MIF*]), annexins (*ANXA1*), amyloid-beta precursor protein (*APP*), and colony stimulating factor 1 (*CSF1*); these ligands being expressed by the main SL-TRM3 neighbours highlighted above (Fig 4), such as L- and SL-fibroblasts, vascular cells, plasma cells and CD4 T cells (Fig 5B). Inversely, SL-TRM3 from patients with active RA were highly stimulated by collagens and fibronectin (*FN1*) (Supplementary Fig S9A).

Conversely, SL-TRM3 from patients with RA in remission were major producers of chemokines (*CCL2, CCL3, CXCL12, CXCL16*), TNF family members (*TNFSF12, TNFSF13B*), Growth Arrest Specific 6 (*GAS6*), and C-type lectin domain family 2 member B (*CLEC2B*), with potent effects on their main neighbours such as L-TRM2, CD4 T cells, plasma cells, vascular cells and fibroblasts (Fig 5C). Of note, SL-TRM3 from patients with active RA were characterised by the production of fibronectin and alarmin (*S100A8*) (Supplementary Fig S9B).

Differential expression of selected ligands and receptors by SL-TRM3 from active versus remission RA was confirmed in a larger cohort of patients (Fig 5D and Supplementary S9C). A majority of genes upregulated in remission RA SL-TRM3 were
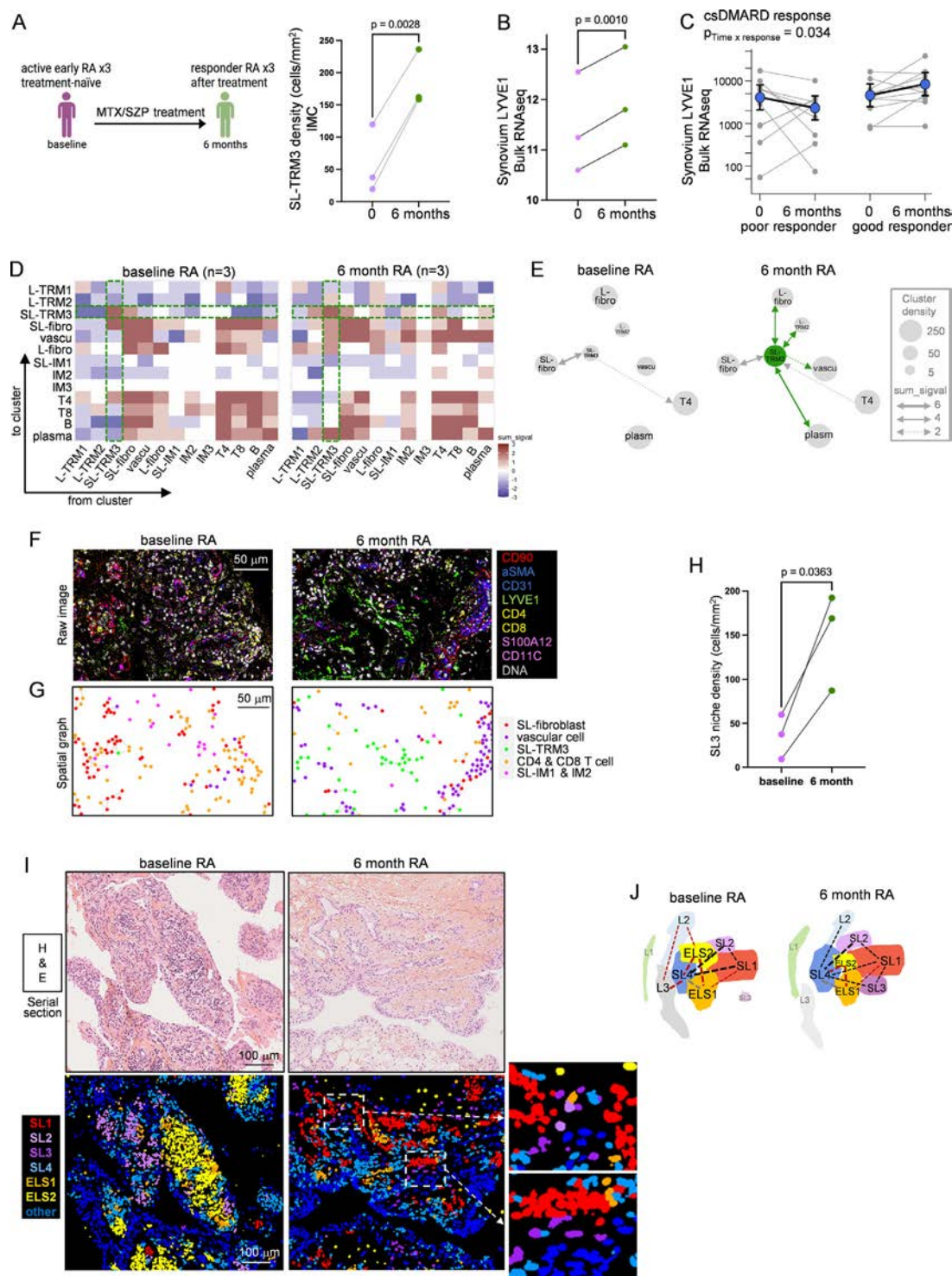
Figure 4. Partial recovery of the synovial architecture following efficient conventional synthetic disease-modifying antirheumatic drug (csDMARD) treatment. (A) Synovium samples were obtained from patients with active treatment-naïve rheumatoid arthritis (RA) at baseline ($n = 3$) and 6 months following efficient treatment with csDMARD (methotrexate [MTX]/sulfasalazine [SZP]) from the same patients ($n = 3$). Paired analysis of SL-TRM3 densities in patients with RA at baseline and 6 months post-csDMARD treatment was performed on the imaging mass cytometry (IMC) images. Paired Student's t-tests were performed. (B, C) Paired plots for baseline and 6-month *LYVE1* bulk RNA-seq counts in the 3 patients analysed previously (B) and in all lympho-myeloid and anticitrullinated protein antibody positive (ACPA$^+$) patients who achieved poor or good clinical responses to csDMARD treatment (C) ($n = 21$, delta Disease Activity Score—Erythrocyte Sedimentation Rate [DAS28-ESR] ≥ 2.8) in the Pathobiology of Early Arthritis Cohort (PEAC). Paired Student's t-tests were performed in (B). In (C), differences between *LYVE1* bulk RNA-seq counts in pretreatment and posttreatment samples were assessed using a negative binomial generalised linear mixed effects model with time and response as fixed effects and patient as random effects ($p_{\text{Time} \times \text{response}}$). Coloured points show regression line of fitted mixed-effect model (estimated marginal means), with error bars showing 95% CIs (fixed effects). Grey points and lines show raw paired count data. (D) Heatmaps generated using the IMC images and showing the cell-cell interactions as the sum of the significant values calculated for each patient (sum_sigval) belonging to the active RA at baseline ($n = 3$) and 6 months post-csDMARD treatment ($n = 3$) group. Brown squares indicate interactions; blue squares indicate avoidance between each cell pair. Interactions implicating SL-TRM3 are highlighted in green. (E) Schematic representation of the pairwise cell interactions, considering cluster densities (circle size) and sum_sigval values (arrow thickness) as calculated in (D). Interactions implicating SL-TRM3 that were induced 6 months post-csDMARD treatment compared to baseline are shown in green. (F) Representative IMC raw images in the synovium samples from healthy individuals ($n = 4$)

highly expressed in their healthy/OA counterparts, indicating these genes were diminished in active RA and recovered upon remission (Supplementary Fig S9D). Pathway analyses of the top 200 upregulated genes in SL-TRM3 from remission RA versus active RA revealed distinct biological processes related to antigen processing and presentation (*MHC-II* genes, *CD74*), regulation of TNF production (*GAS6, TNFAIP3*) and negative regulation of immune/inflammatory response (*TREM2, CD46*), suggesting an important role in the response to treatment (Fig 5E). Inversely, in active RA, SL-TRM3 were characterised by high expression of genes implicated in the recognition of pathogens (viral process, *CD209* and *MRC1* genes) and purine metabolic process (*PGK1, NDUFB3*), suggesting an active role in immune response (Supplementary Fig S9E). Genes upregulated in remission RA versus healthy/OA SL-TRM3 were involved in antigen processing, regulation of memory T cell and germinal centre formation, suggesting an adaptive immune regulatory role (Supplementary Fig S9F). Furthermore, genes upregulated in both healthy/OA and remission RA versus active RA SL-TRM3 implicated regulation of the immune system and response to corticosteroid (*TGFB1, FOS, FOXO3*), suggesting recovery of a protective phenotype in remission.

To experimentally probe the functional attributes of these synovial macrophage subsets, we generated LYVE1^{+-} MERTK^{+}HLA-DR^{low} (SL-TRM3 surrogate) and LYVE1^{--} MERTK^{-}HLADR^{high} (IM surrogate) macrophages for coculture with RA patient-derived fibroblast-like synoviocytes (RA-FLS) (Fig 5F,G). Upon Lipopolysaccharide (LPS) stimulation, LYVE1^{+} macrophages failed to induce IL-6 secretion by RA-FLS, in stark contrast to LYVE1^{-} macrophages, which promoted IL-6 via IL1A/B release (inhibited by IL-1R antagonist) (Fig 5H,I). This functional distinction, demonstrating a dampened proinflammatory capacity for LYVE1^{+} macrophages, complements our spatial mapping data and their remission-associated transcriptomic profile.

Altogether, our findings underscore a distinct negative regulatory role for LYVE1^{+}/SL-TRM3 in modulating inflammatory responses, sharply contrasting with proinflammatory HLADR-^{high}/IM macrophages. The differential cellular interactions and pathways involving SL-TRM3 in active versus remission RA are schematically summarised in Figure 6.

DISCUSSION

Here, we provided a comprehensive synovial cell and niche social network mapping by performing multiplex, single-cell spatial analysis of the human synovial tissue using IMC. This approach allowed us to decipher the spatial organisation of the main tissue resident/homeostatic or infiltrating/inflammatory myeloid, lymphoid, and stromal cells. We highlighted the presence of 7 macrophage subsets, for which the spatial features and expression profile expanded the diversity described so far in the literature [6−8,11,29]. We then identified the presence of 9 relevant synovial niches, of which 3 were localised in the lining

(L1 to L3) and 6 in the sublining (SL1 to 4, ELS1 and 2), providing a niche map similar to the one recently obtained using spatial transcriptomic analyses [15].

We first underlined that 2 distinct TRM subsets can be found in the lining layer, depending on their expression of TIM4 and MERTK. Whether L-TRM2 represents the proinflammatory state of L-TRM1 that lost barrier and homeostatic functions or originates from a different precursor now deserves further studies [7,11]. We also observed that lining fibroblasts expressing podoplanin (PDPN) were expanded in RA and mainly localised in the L3 niche, where, as previously described in the literature [16,21,29], they assume a central position by connecting with lining L-TRM1 cells but also with sublining cells and niches. This expansion matched with a reduction of the density and frequency of the L1 niche mainly composed of L-TRM1 cells in RA, confirming previous studies that demonstrated a significant disruption of the lining myeloid barrier that physically secludes the joint in homeostatic conditions [4,7,9,11].

Within the sublining compartment, different subsets of IM and lymphoid cells were shown to communicate together and form 2 distinct ELS niches. Such ELS organisation recapitulates the architecture of secondary lymphoid organs [30−32]. The ELS1 niche corresponded to a T cell-rich zone, whereas the ELS2 niche resembled the B cell-rich area. In the context of active RA and before any treatment intervention, both ELS niches were also strongly connected with resident sublining fibroblasts (PDPN^{-}CD90^{+}) near vascular vessels belonging to the SL1 and SL4 niches, consistent with the described presence of activated stromal cells and high endothelial venules, respectively [30 −32]. Importantly, we also highlighted the presence of different subtypes of IM within the ELS2 niche. Although analysing the expression of additional markers would be necessary to further characterise ELS cells, our data clearly indicate that several inflammatory myeloid cells with potent roles on monocyte and fibroblast activation (IM1, S100A12^{+}), antigen presentation (IM2, HLA-DR^{+}), neutrophil activation and matrix remodelling (IM3, SPP1^{+}) [6,7,11,15,33−35] are localised in closed proximity to the cells involved in ELS functions and enriched in active RA.

Despite the availability of a large variety of cs-, b-, and ts-DMARDs approved for the treatment of RA, 40% of patients still do not respond to treatment, understanding molecular signatures underlying the variety of clinical and treatment-response phenotypes remains one of the major areas of research in rheumatology. Here, we focused our analyses on patients with RA who, 6 months following MTX/SZP treatment, presented a good or moderate response, in order to decipher the complex biological mechanisms driving the suppression of inflammation. We demonstrated that a key cellular social network involved in the homeostasis of healthy synovium comprised SL-TRM3, SL-fibroblasts, and vascular cells in SL1 to 4 niches, while, in active RA, the paucity of SL-TRM3 cells induced profound changes in the SL1 and SL3 organisation. Similarly, recent work highlighted that LYVE1^{+} macrophages are significantly associated with

and patients with RA at baseline ($n = 3$) and 6 months post-csDMARD treatment ($n = 3$) showing SL-fibroblasts (CD90+), vascular cells (aSMA+ or CD31+), SL-TRM3 (LYVE1+), T cells (CD4+ or CD8+), SL-IM1 (S100A12+), and IM2 (CD11C+). (G) Corresponding spatial graphs presenting the interactions (grey nodes) between SL-fibroblasts (red), vascular cells (purple), SL-TRM3 (green), T (orange), SL-IM1 and IM2 (pink) in the 3 patients' groups. (H) Paired analysis of SL3 niche densities in patients with RA at baseline and 6 months post-csDMARD treatment. Paired Student's t-tests were performed. (I) Representative hematoxylin and eosin (H&E) staining (top panels) and corresponding images of the sublining and ectopic lymphoid structures (ELS) (bottom panels) niches in the synovium of patients with RA at baseline and 6 months post-csDMARD treatment. (J) Schematic representation of the niches' spatial organisation, considering the niche densities, distances to the lining and their interactions. Basal niche interactions previously observed in healthy and osteoarthritis (OA) samples are provided in black and grey; additional interactions between niches observed specifically in RA samples are shown in red (refers to Fig 3F).
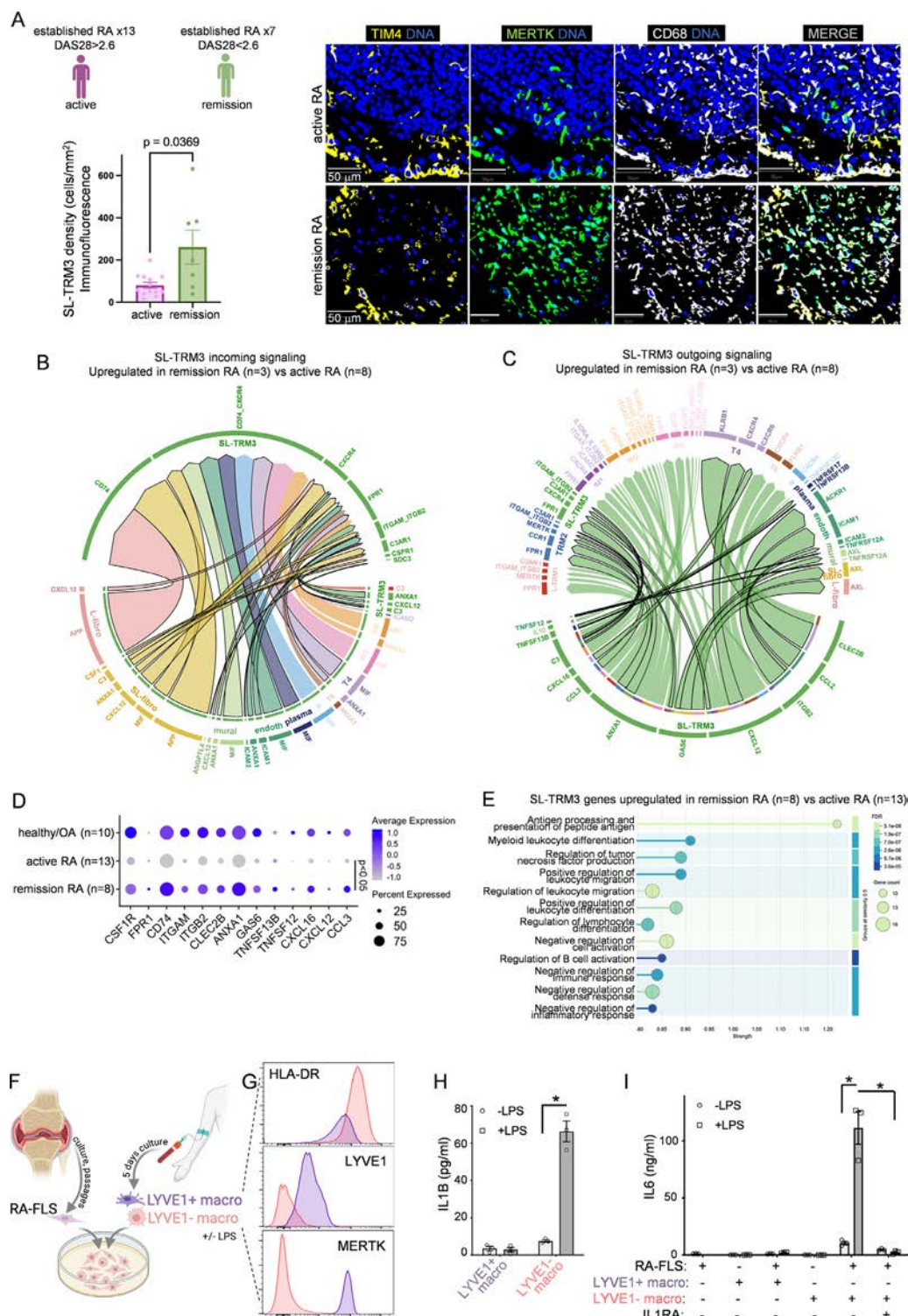
Figure 5. scRNAseq ligand-receptor analysis underlines the existence of cellular pathways involving SL-TRM3 and linked to disease activity. (A) Synovium samples were obtained from patients with active established anticitrullinated protein antibody positive (ACPA⁺) rheumatoid arthritis (RA) (*n* = 13, Disease Activity Score [DAS28] > 2.6) and from patients under remission (*n* = 7, DAS28 < 2.6). IF staining was performed to determine SL-TRM3 (sublining CD68⁺ MERTK⁺ TIM4⁻) cell density. Mann-Whitney U tests were performed. Representative images are shown. (B, C) Public scRNAseq datasets [7,17] were used to analyse the potent ligand-receptor interactions between SL-TRM3 and other synovial cells in the synovium of patients with ACPA⁺ RA with active disease (*n* = 8, comprising 5 treatment-naïve patients and 3 disease-modifying antirheumatic drugs (DMARDs)-resistant patients) or in remission (*n* = 3, DAS28 < 2.6 for more than 6 months). Chord diagrams of all upregulated incoming and outgoing interactions (except MHC interactions) involving SL-TRM3 in remission RA versus active RA samples. Sender cells are presented at the start of the arrows and receiver cells at the end. Main interacting neighbours described in Fig 4E are highlighted in bold, and their interactions with SL-TRM3 are presented with bordered arrows. (D, E) Public scRNAseq datasets [7,17,47] were used to analyse differentially expressed genes in SL-TRM3 from patients with anticitrullinated protein antibody positive (ACPA⁺) RA with active disease (*n* = 13, comprising 6 treatment-naïve patients and 7 DMARDs-resistant patients) versus in remission (*n* = 8, DAS28 < 2.6 for more than 6 months). Gene expression in SL-TRM3 from healthy controls (*n* = 6) and patients with OA (*n* = 4) is also shown. Scatter plot representing the mean expression of selected upregulated genes in remission RA (colour code) and proportion of expressing SL-TRM3 (dot size) (D). Plot showing Gene Ontology (GO) biological pathways identified with STRING-db using upregulated genes in SL-TRM3 in remission RA versus active RA (E). (F) Fibroblast-like synoviocytes (RA-FLS) from active patients with RA (*n* = 4) were cocultured
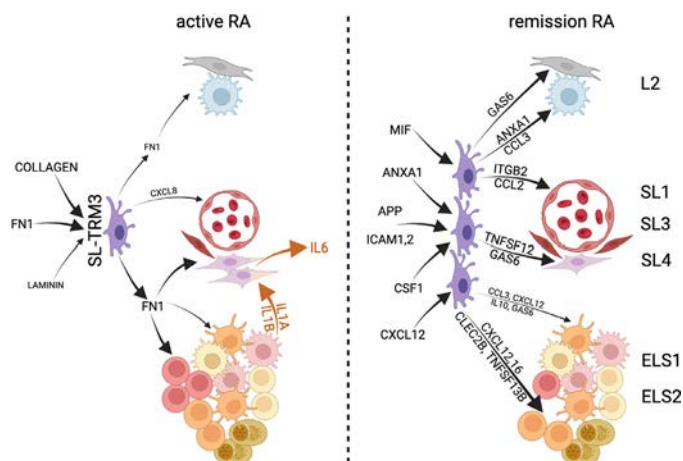
Figure 6. Proposed model of SL-TRM3 cell interactions in rheumatoid arthritis (RA). Schematic representation of the differential cell-cell communications and implicated molecular pathways established by SL-TRM3 in the synovium of active versus patients with RA in remission. Pathways implicating the main SL-TRM3 neighbours are highlighted in higher font and arrow size. Communications between IM and fibroblasts are presented in orange. Location of the cells in their respective niches is also provided. Created with BioRender.

specific cell-type abundance phenotypes enriched for fibroblasts, endothelial, and myeloid cells in a large cohort of patients with RA [8]. Importantly, MTX/SZP treatment was able to induce a partial recovery of the basal homeostatic synovial cartography allowing, for example, a partial restoration of SL-TRM3, and the re-establishment of interactions with TRM, lymphoid and stromal cells similar to the healthy or OA situation. Similarly, we observed that *LYVE1* expression was enhanced after csDMARD treatment, especially in responder patients with RA, and that SL-TRM3 cells were also more abundant in patients with RA in remission. Perivascular SL-TRM3 cells are positive for the hyaluronan receptor LYVE1 and the mannose receptor CD206, and are thought to control homeostatic collagen production, leukocyte infiltration, and fibrosis [10,11,36,37]. More recently, LYVE1$^+$ macrophages have been shown to restrain the inflammatory and fibrotic phenotype of shoulder capsular fibroblasts through upregulation of genes and pathways involved in extracellular matrix organisation and remodelling [38], confirming their beneficial functions.

We further dissected the molecular pathways involved in SL-TRM3 communications by combining IMC with public scRNA-seq datasets analyses, and explored a large number of cell-cell communications based on ligand-receptor interactions. In the synovial tissue of patients with RA in remission, SL-TRM3 could be recruited and regulated by chemokines, anti-inflammatory mediators, and macrophage growth factors such as *MIF, CXCL12, ANXA1,* and *CSF1* [39,40]. They are themselves characterised by a negative regulation of immune and inflammatory responses and could influence other immune and stromal cells through chemokines (eg, *CCL2, CXCL16*), TNF family members (*TNFSF12* and *13B*), and *CLEC2B* [41,42]. Importantly, upon efficient treatment, SL-TRM3 expressed high levels of *GAS6*

ligand to stimulate stromal cells and macrophages upon binding to its receptors, *AXL* and *MERTK*. TAM (TYRO3, AXL, and MERTK) receptors have been shown to negatively regulate the inflammatory cascade involved in RA pathophysiology and mediate phagocytosis of apoptotic cells [7,28,43]. Our *in vitro* coculture assays provide direct functional support for this regulatory role, demonstrating that LYVE1$^+$/SL-TRM3 surrogate macrophages, unlike their LYVE1$^-$ counterparts, exhibit a dampened proinflammatory capacity by failing to induce significant IL-1B/IL-6 production. These collective findings strongly support the development of TAM-targeted therapeutic strategies to foster inflammation resolution in arthritis [7,11,28,44−46]. Although further *in vitro* validation is warranted, our combined analyses provide novel insights into the complex interplay governing synovial homeostasis and therapeutic response.

Our findings must be considered in the context of some limitations. While our high-dimensional IMC approach provides unprecedented cellular resolution, we recognise the inherent heterogeneity of synovitis in RA. To address this challenge, our initial discovery phase focused on a limited number of well-defined, homogeneous early patients with RA, treatment-naïve, ACPA-positive, and exhibiting a lympho-myeloid pathotype, initiating MTX/SZP therapy. Key findings were subsequently validated in larger, albeit more heterogeneous, cohorts (eg, the PEAC for bulk RNA-seq and an independent cohort of established RA for IF), following a standard translational research strategy. Future studies should aim to confirm whether similar molecular perturbations are present in tissues with diverse histopathological profiles (eg pauci-immune and diffuse-myeloid) [5] or in patients with differing ACPA status. Nevertheless, in accordance with our IMC results from MTX/SZP-treated patients, our IF staining demonstrated that SL-TRM3 density was also associated with disease activity in a broader cohort of patients with established RA treated with various cs- and b-DMARDs. While this supports the robustness of our findings across disease stages and treatment regimens, future studies involving larger, homogeneously treated cohorts will be valuable to dissect drug-specific effects from the more general synovial remodelling associated with remission.

In summary, our study provides a comprehensive, spatially resolved characterisation of the synovial microenvironment across healthy individuals, patients with active RA, and those receiving csDMARD therapy. While primarily descriptive, this approach was deliberately chosen to address key gaps in our understanding of in situ cellular dynamics within the RA synovium, particularly how these are modulated by treatment. Given the urgent need for predictive biomarkers and more precisely targeted therapies in RA, a foundational understanding of the cellular and structural changes associated with therapeutic response is essential. In this context, our detailed mapping of the LYVE1$^+$ macrophage network and its niche remodelling during MTX/SZP-induced remission represents an important step. By capturing these spatial alterations, our findings offer new insights into the cellular mechanisms underlying synovial homeostasis and generate testable hypotheses for future mechanistic and interventional studies.

with LYVE$^+$ and LYVE$^-$ macrophages generated from blood monocytes of a healthy donor. (G, H) Macrophages were characterised by flow cytometry and Enzyme-Linked Immunosorbent Assay (ELISA) for their expression of HLA-DR, LYVE1, MERTK, and IL1B. (I) Following Lipopolysaccharide (LPS) stimulation (100 ng/ml), LYVE$^-$ macrophages induced the secretion of IL6 by RA-FLS through IL1B (inhibited by the IL1 receptor antagonist IL1RA), whereas LYVE1$^+$ macrophages did not. One representative experiment of 4 independent experiments with FLS from 4 different patients with RA is shown. Mann-Whitney *U* tests were performed: *, $P < .05$.

Competing interests

CRediT authorship contribution statement

Julien De Lima: Writing − review & editing, Visualization, Methodology, Data curation, Writing − original draft, Validation, Formal analysis. **Marie-Astrid Boutet:** Writing − original draft, Formal analysis, Writing − review & editing, Methodology, Conceptualization. **Olivier Bortolotti:** Methodology, Data curation, Formal analysis. **Laure-Agnès Chépeaux:** Investigation, Methodology, Formal analysis. **Yaël Glasson:** Methodology, Formal analysis, Validation, Investigation. **Anne-Sophie Dumé:** Methodology, Formal analysis, Investigation. **Rachel Lau:** Formal analysis, Data curation. **Paul Humbert:** Investigation, Methodology, Formal analysis. **Sophie Allain:** Methodology, Formal analysis, Investigation. **Adrien Le Pluart:** Formal analysis, Investigation, Data curation. **Alessandra Nerviani:** Resources, Conceptualization, Methodology. **Liliane Fossati-Jimack:** Methodology, Resources, Conceptualization. **Henri-Alexandre Michaud:** Writing − review & editing, Resources, Conceptualization, Software, Methodology. **Jérôme Guicheux:** Writing − original draft, Writing − review & editing, Supervision. **Benoit Le Goff:** Validation, Resources, Writing − review & editing, Supervision. **Myles J. Lewis:** Methodology, Data curation, Writing − review & editing, Formal analysis. **Costantino Pitzalis:** Validation, Project administration, Conceptualization, Writing − review & editing, Resources, Funding acquisition. **Gabriel Courties:** Writing − review & editing, Methodology, Conceptualization, Validation, Data curation. **Florence Apparailly:** Writing − original draft, Supervision, Funding acquisition, Writing − review & editing, Validation, Project administration, Conceptualization. **Frederic Blanchard:** Writing − original draft, Validation, Resources, Methodology, Formal analysis, Conceptualization, Writing − review & editing, Visualization, Supervision, Project administration, Funding acquisition, Data curation.

Acknowledgements

Funding

Patient consent for publication

Not applicable.

Ethics approval

All procedures related to RA biopsies for IMC analysis were performed following written informed consent and were approved by the hospital's ethics committee (REC 05/Q0703/198). Other RA, OA and control biopsies were obtained following written patient's informed consent and ethics approval was granted by the Nantes University Hospital ethics committee (DC-2011- 1399).

Provenance and peer review

Not commissioned; externally peer reviewed.

Supplementary materials

Supplementary material associated with this article can be found in the online version at doi:10.1016/j.ard.2025.07.019.

Orcid

Julien De Lima: http://orcid.org/0000-0002-0191-9479
Olivier Bortolotti: http://orcid.org/0000-0002-3669-8215
Yaël Glasson: http://orcid.org/0000-0002-5072-7078
Rachel Lau: http://orcid.org/0000-0002-8330-8048
Paul Humbert: http://orcid.org/0000-0003-1208-5550
Adrien Le Pluart: http://orcid.org/0000-0002-4513-6054
Liliane Fossati-Jimack: http://orcid.org/0000-0003-3757-3999
Gabriel Courties: http://orcid.org/0000-0002-0003-7407
Frederic Blanchard: http://orcid.org/0000-0003-1055-2573

REFERENCES

[1] Lewis MJ, Pitzalis C. Progress continues in prediction of the response to treatment of RA. Nat Rev Rheumatol 2023;19:68–9.

[2] GBD 2019 Diseases and Injuries Collaborators. Global burden of 369 diseases and injuries in 204 countries and territories, 1990-2019: a systematic analysis for the Global Burden of Disease Study 2019. Lancet Lond Engl 2020;396:1204–22.

[3] Aletaha D, Neogi T, Silman AJ, Funovits J, Felson DT. Bingham CO 3rd, et al. 2010 rheumatoid arthritis classification criteria: an American College of Rheumatology/European League Against Rheumatism collaborative initiative. Ann Rheum Dis 2010;69:1580–8.

[4] Boutet M-A, Courties G, Nerviani A, Le Goff B, Apparailly F, Pitzalis C, et al. Novel insights into macrophage diversity in rheumatoid arthritis synovium. Autoimmun Rev 2021;20:102758.

[5] Rivellese F, Surace AEA, Goldmann K, Sciacca E, Çubuk C, Giorli G, et al. Rituximab versus tocilizumab in rheumatoid arthritis: synovial biopsy-based biomarker analysis of the phase 4 R4RA randomized trial. Nat Med 2022;28:1256–68.

[6] Zhang F, Wei K, Slowikowski K, Fonseka CY, Rao DA, Kelly S, et al. Defining inflammatory cell states in rheumatoid arthritis joint synovial tissues by integrating single-cell transcriptomics and mass cytometry. Nat Immunol 2019;20:928–42.

[7] Alivernini S, MacDonald L, Elmesmari A, Finlay S, Tolusso B, Gigante MR, et al. Distinct synovial tissue macrophage subsets regulate inflammation and remission in rheumatoid arthritis. Nat Med 2020;26:1295–306.

[8] Zhang F, Jonsson AH, Nathan A, Millard N, Curtis M, Xiao Q, et al. Deconstruction of rheumatoid arthritis synovium defines inflammatory subtypes. Nature 2023;623:616–24.

[9] Culemann S, Grüneboom A, Nicolás-Ávila JÁ, Weidner D, Lämmle KF, Rothe T, et al. Locally renewing resident synovial macrophages provide a protective barrier for the joint. Nature 2019;572:670–5.

[10] Hasegawa T, Lee CYC, Hotchen AJ, Fleming A, Singh R, Suzuki K, et al. Macrophages and nociceptor neurons form a sentinel unit around fenestrated capillaries to defend the synovium from circulating immune challenge. Nat Immunol 2024;25:2270–83.

[11] Kurowska-Stolarska M, Alivernini S. Synovial tissue macrophages in joint homeostasis, rheumatoid arthritis and disease remission. Nat Rev Rheumatol 2022;18:384–97.

[12] Moldoveanu D, Ramsay L, Lajoie M, Anderson-Trocme L, Lingrand M, Berry D, et al. Spatially mapping the immune landscape of melanoma using imaging mass cytometry. Sci Immunol 2022;7:eabi5072.

[13] Karimi E, Yu MW, Maritan SM, Perus LJM, Rezanejad M, Sorin M, et al. Single-cell spatial immune landscapes of primary and metastatic brain tumours. Nature 2023;614:555–63.

[14] Buckley CD, Ospelt C, Gay S, Midwood KS. Location, location, location: how the tissue microenvironment affects inflammation in RA. Nat Rev Rheumatol 2021;17:195–212.

[15] MacDonald L, Elmesmari A, Somma D, Frew J, Di Mario C, Madhu R, et al. Synovial tissue myeloid dendritic cell subsets exhibit distinct tissue-niche localization and function in health and rheumatoid arthritis. Immunity 2024;57:2843–62 e12.

[16] Wei K, Korsunsky I, Marshall JL, Gao A, Watts GFM, Major T, et al. Notch signalling drives synovial fibroblast identity and arthritis pathology. Nature 2020;582:259–64.

[17] Floudas A, Smith CM, Tynan O, Neto N, Krishna V, Wade SM, et al. Distinct stromal and immune cell interactions shape the pathogenesis of rheumatoid and psoriatic arthritis. Ann Rheum Dis 2022;81:1224–42.

[18] Boada-Romero E, Martinez J, Heckmann BL, Green DR. The clearance of dead cells by efferocytosis. Nat Rev Mol Cell Biol 2020;21:398–414.

[19] Montgomery AB, Chen SY, Wang Y, Gadhvi G, Mayr MG, Cuda CM, et al. Tissue-resident, extravascular Ly6c-monocytes are critical for inflammation in the synovium. Cell Rep 2023;42:112513.

[20] Papazoglou A, Huang M, Bulik M, Lafyatis A, Tabib T, Morse C, et al. Epigenetic regulation of profibrotic macrophages in systemic sclerosis-associated interstitial lung disease. Arthritis Rheumatol 2022;74:2003–14.

[21] Croft AP, Campos J, Jansen K, Turner JD, Marshall J, Attar M, et al. Distinct fibroblast subsets drive inflammation and damage in arthritis. Nature 2019;570:246–51.

[22] Friščić J, Böttcher M, Reinwald C, Bruns H, Wirth B, Popp SJ, et al. The complement system drives local inflammatory tissue priming by metabolic reprogramming of synovial fibroblasts. Immunity 2021;54:1002–21 e10.

[23] Jackson HW, Fischer JR, Zanotelli VRT, Ali HR, Mechera R, Soysal SD, et al. The single-cell pathology landscape of breast cancer. Nature 2020;578:615–20.

[24] Schürch CM, Bhate SS, Barlow GL, Phillips DJ, Noti L, Zlobec I, et al. Coordinated cellular neighborhoods orchestrate antitumoral immunity at the colorectal cancer invasive front. Cell 2020;182:1341–59 e19.

[25] Bhate SS, Barlow GL, Schürch CM, Nolan GP. Tissue schematics map the specialization of immune tissue motifs and their appropriation by tumors. Cell Syst 2022;13:109–30 .e6.

[26] Lewis MJ, Barnes MR, Blighe K, Goldmann K, Rana S, Hackney JA, et al. Molecular portraits of early rheumatoid arthritis identify clinical and treatment response phenotypes. Cell Rep 2019;28:2455–70 .e5.

[27] Humby F, Lewis M, Ramamoorthi N, Hackney JA, Barnes MR, Bombardieri M, et al. Synovial cellular and molecular signatures stratify clinical response to csDMARD therapy and predict radiographic progression in early rheumatoid arthritis patients. Ann Rheum Dis 2019;78:761–72.

[28] Nerviani A, Boutet M-A, Ghirardi GM, Goldmann K, Sciacca E, Rivellese F, et al. Axl and MerTK regulate synovial inflammation and are modulated by IL-6 inhibition in rheumatoid arthritis. Nat Commun 2024;15:2398.

[29] Kuo D, Ding J, Cohn IS, Zhang F, Wei K, Rao DA, et al. HBEGF+ macrophages in rheumatoid arthritis induce fibroblast invasiveness. Sci Transl Med 2019;11:eaau8587.

[30] Meednu N, Rangel-Moreno J, Zhang F, Escalera-Rivera K, Corsiero E, Prediletto E, et al. Dynamic spectrum of ectopic lymphoid B cell activation and hypermutation in the RA synovium characterized by NR4A nuclear receptor expression. Cell Rep 2022;39:110766.

[31] Nerviani A, Pitzalis C. Role of chemokines in ectopic lymphoid structures formation in autoimmunity and cancer. J Leukoc Biol 2018;104:333–41.

[32] Antonioli L, Fornai M, Pellegrini C, Masi S, Puxeddu I, Blandizzi C. Ectopic lymphoid organs and immune-mediated diseases: molecular basis for pharmacological approaches. Trends Mol Med 2020;26:1021–33.

[33] MacDonald L, Alivernini S, Tolusso B, Elmesmari A, Somma D, Perniola S, et al. COVID-19 and RA share an SPP1 myeloid pathway that drives PD-L1 + neutrophils and CD14+ monocytes. JCI Insight 2021;6:e147413.

[34] Simmons DP, Nguyen HN, Gomez-Rivas E, Jeong Y, Jonsson AH, Chen AF, et al. SLAMF7 engagement superactivates macrophages in acute and chronic inflammation. Sci Immunol 2022;7:eabf2846.

[35] Cooles FAH, Anderson AE, Lendrem DW, Norris J, Pratt AG, Hilkens CMU, et al. The interferon gene signature is increased in patients with early treatment-naive rheumatoid arthritis and predicts a poorer response to initial therapy. J Allergy Clin Immunol 2018;141:445–8 e4.

[36] Lim HY, Lim SY, Tan CK, Thiam CH, Goh CC, Carbajo D, et al. Hyaluronan receptor LYVE-1-expressing macrophages maintain arterial tone through hyaluronan-mediated regulation of smooth muscle cell collagen. Immunity 2018;49:326–41 e7.

[37] Chakarov S, Lim HY, Tan L, Lim SY, See P, Lum J, et al. Two distinct interstitial macrophage populations coexist across tissues in specific subtissular niches. Science 2019;363 eaau0964.

[38] Ng MTH, Borst R, Gacaferi H, Davidson S, Ackerman JE, Johnson PA, et al. A single cell atlas of frozen shoulder capsule identifies features associated with inflammatory fibrosis resolution. Nat Commun 2024;15:1394.

[39] Sugimoto MA, Vago JP, Teixeira MM, Sousa LP. Annexin A1 and the resolution of inflammation: modulation of neutrophil recruitment, apoptosis, and clearance. J Immunol Res 2016;2016:8239258.

[40] Farr L, Ghosh S, Moonah S. Role of MIF cytokine/CD74 receptor pathway in protecting against injury and promoting repair. Front Immunol 2020; 11:1273.

[41] Yamana J, Morand EF, Manabu T, Sunahori K, Takasugi K, Makino H, et al. Inhibition of TNF-induced IL-6 by the TWEAK-Fn14 interaction in rheumatoid arthritis fibroblast like synoviocytes. Cell Immunol 2012;272:293–8.

[42] Fergusson JR, Smith KE, Fleming VM, Rajoriya N, Newell EW, Simmons R, et al. CD161 defines a transcriptional and functional phenotype across distinct human T cell lineages. Cell Rep 2014;9:1075–88.

[43] Pagani S, Bellan M, Mauro D, Castello LM, Avanzi GC, Lewis MJ, et al. New insights into the role of Tyro3, Axl, and mer receptors in rheumatoid arthritis. Dis Markers 2020;2020:1614627.

[44] Giroud P, Renaudineau S, Gudefin L, Calcei A, Menguy T, Rozan C, et al. Expression of TAM-R in human immune cells and unique regulatory function of MerTK in IL-10 production by tolerogenic DC. Front Immunol 2020;11:564133.

[45] Zizzo G, Hilliard BA, Monestier M, Cohen PL. Efficient clearance of early apoptotic cells by human macrophages requires M2c polarization and MerTK induction. J Immunol. 1950 2012;189:3508–20.

[46] Waterborg CEJ, Beermann S, Broeren MGA, Bennink MB, Koenders MI, van Lent PLEM, et al. Protective role of the MER tyrosine kinase via efferocytosis in rheumatoid arthritis models. Front Immunol 2018;9:742.

[47] Chou C-H, Jain V, Gibson J, Attarian DE, Haraden CA, Yohn CB, et al. Synovial cell cross-talk with cartilage plays a major role in the pathogenesis of osteoarthritis. Sci Rep 2020;10:10868.

Rheumatoid arthritis

Influence of canstatin on fibroblast-driven hypervascularisation in rheumatoid arthritis

Corinna Heck[1], Birgit Zimmermann-Geller[1], Sophie Haun[1], Frederik Lötfering[1], Paula Welbrink[1], Daria Kürsammer[1], Klaus W. Frommer [1], Mona Arnold-Gräf[1], Adelheid Korb-Pap [2], Anna Knothe[1], Nils Schulz [1], Stefan Simianer[1], Ingo Tarner[1], Walter Hermann[1], Christoph Biehl[3], Stefan Günther [4], Jürgen Steinmeyer [5], Katrin S. Lips [6], Markus Rickert[5], Stefan Rehart[7], Ulf Müller-Ladner[1], Elena Neumann [1,*]

[1] Department of Rheumatology and Clinical Immunology, Justus Liebig University Giessen, Campus Kerckhoff, Bad Nauheim, Germany
[2] Institute of Musculoskeletal Medicine, University Hospital Muenster, Muenster, Germany
[3] Department of Trauma, Hand and Reconstructive Surgery, University Hospital Giessen, Germany
[4] Max-Planck-Institute for Heart- and Lung Research, CPI - DNA & RNA Technologies, DZHK - Advanced Molecular Analytics Platform RheinMain, Bad Nauheim, Germany
[5] Department of Orthopaedics and Orthopaedic Surgery, University Hospital Giessen and Marburg, Giessen, Germany
[6] Experimental Trauma Surgery, Justus Liebig University Giessen, Giessen, Germany
[7] Department of Trauma, Hand and Reconstructive Surgery, University Hospital Giessen, Giessen, Germany

ARTICLE INFO

ABSTRACT

Objectives: Hypervascularisation is a dominant feature of the inflamed synovium in rheumatoid arthritis (RA). As RA synovial fibroblasts (RASFs) are key cells of synovial pathophysiology and are located adjacent to the aberrant endothelial cells (ECs), we hypothesised that this interaction might be responsible for the pathological hypervascularisation.

Methods: In the severe combined immunodeficiency (SCID) mouse model for RA, RASF-mediated helix-like vessel (HLV) formation was described and modulated by canstatin, an antiangiogenic collagen IV fragment that blocks the angiopoietin (ANGPT)/Tie2 pathway in EC. ANGPT2/CD31 and CXCL2 immunofluorescence on implants and human synovium was performed. RASF were stimulated with interleukin (IL)-1β once or repetitively and immunoassays, real-time polymerase chain reaction and RNA sequencing were performed. Two-dimensional (2D) tube formation and 3-dimensional spheroid-based assays using human umbilical vein ECs and fluorescent-stained RASF with/without canstatin, IL-11 and CXCL2 were evaluated.

Results: In SCID mice, RASF-specific HLV formation started early and increased until day 30. The number of HLV was significantly reduced by canstatin. Compared to osteoarthritis synovium, ANGPT2 was significantly upregulated in RA vessels. Repetitive RASF stimulation significantly decreased IL-6, IL-11 and CXCL-2 compared to RASF stimulated once with IL-1β. When RASF was stimulated once, CXCL2 and IL-11 were significantly reduced along with 2D tube formation, while repetitive stimulation significantly attenuated hypervascularisation. RNAseq revealed underlying pathways leading to altered tube formation.

*Correspondence to Dr Elena Neumann, Department of Rheumatology and Clinical Immunology, Justus Liebig University Giessen, Campus Kerckhoff, Bad Nauheim, Germany.
E-mail address: e.neumann@kerckhoff-klinik.de (E. Neumann).
Handling editor Josef S. Smolen.

Conclusions: We showed that RASF affect vascularisation *in vitro* and *in vivo*. The results support the idea that canstatin is able to alter the RASF pathological HLV formation. In the SCID mouse model, this was regulated on a molecular level mediated by ANGPT2 in a vascular endothelial growth factor A-independent manner, contributing significantly to one of the central aspects of RA pathophysiology.

WHAT IS ALREADY KNOWN ON THIS TOPIC

- Increased and altered angiogenesis in the inflamed synovium of patients with RA is an early pathological feature.
- Fibroblasts are able to remodel the ECM and to interact with the vascular system as angiogenesis is mediated by complex interactions of EC, fibroblasts, macrophages and ECM.
- Vessel maturity, stability and survival are regulated by the balance of pro- and anti-angiogenic factors, including VEGF and the angiopoietin (ANGPT)1/Tie-2 system. Under pathological conditions, such as cellular activation and local hypoxia in RA, this balance is disturbed leading to abnormal ANGPT2 expression and competitive ANGPT2-Tie2 binding.
- In the severe combined immunodeficiency (SCID) mouse model of RA it was shown that RASF migrate beyond tissue borders.
- RASF-mediated matrix degradation results in a local release of matrix-associated proteins such as the angiogenic inhibitor canstatin, a fragment of type IV collagen, which inhibits angiogenesis by blocking ANGPT1-induced proliferation of EC.

WHAT THIS STUDY ADDS

- RASF specifically induce helix-like vessel (HLV) formation in the SCID mouse model of RA early after RASF implantation. ANGPT2 was detectable in SCID mouse implants and RA synovial tissue.
- In 3D and 2D tube formation assays, RASF and RASF-conditioned media significantly altered tube formation which was further enhanced by stimulation of RASF with IL-1β.
- Repetitive IL-1β stimulation of RASF partially restored tube formation compared to RASF stimulated once. RNAseq showed that the top 50 differentially expressed genes were mainly associated with autoimmune diseases, vascular diseases and diseases affecting the immune system, including IL 11 and CXCL2, factors able to alter angiogenesis VEGF-independently.
- Tube formation assays showed that CXCL2 and IL-11 altered network formation. Canstatin was significantly higher in RA serum compared to healthy controls.
- Canstatin altered tube formation in both 2D and 3D tube formation assays. In the SCID-mouse model, canstatin did not alter RASF invasion but reduced the number of HLV in ipsilateral implants.

HOW THIS STUDY MIGHT AFFECT RESEARCH, PRACTICE OR POLICY

- In RA synovium, activated RASF exert a considerable influence on pathological vascularization by interacting with EC. Here, we observed an RASF-induced pathological HLV formation.
- Integrated RNA sequencing, functional angiogenesis and molecular analysis showed that ANGPT2 may play a role in HLV formation and that RASF influence pathological angiogenesis involving factors such as IL-11 and CXCL2.
- Addition of ANGPT2, despite inhibiting VEGF, was able to partially restore tube formation. ANGPT2 positive vessels were observed at all time points in all implants, suggesting a role of ANGPT2 during HLV development and new vessel formation.
- The matrix fragment canstatin reduced 2D and 3D tube formation, thus confirming the anti-angiogenic canstatin-effect on EC by altering tube shapes without triggering apoptosis at the concentrations used.
- In the SCID mouse model, canstatin primarily acted on EC-RASF interactions significantly reducing the RASF-mediated formation of HLV, providing a promising lead compound to inhibit altered vessel formation in RA.

INTRODUCTION

Increased angiogenesis in the inflamed synovium of patients with rheumatoid arthritis (RA) is an early pathological feature [1,2]. Angiogenesis defines the process of new capillary formation by sprouting of preexisting vessels [1,3], which is mediated by complex interactions of endothelial cells (ECs), fibroblasts, macrophages and the extracellular matrix (ECM) [3]. Angiogenesis starts with EC activation, disruption of the vascular basement membrane and surrounding ECM and the migration of ECs. Fully differentiated ECs are able to sprout after exposure to increased concentrations of proangiogenic factors such as vascular endothelial growth factor A (VEGF-A), leading to formation and maturation of newly formed vessels, which consist of EC forming the inner lining and pericytes surrounding the vascular tubes [1,3,4]. Normally, vessel maturity, stability and survival are regulated by the balance of pro- and antiangiogenic factors, including vascular endothelial growth factor (VEGF), the angiopoietin (ANGPT)-1/Tie-2 system, platelet-derived growth factor B and/or transforming growth factor-β [3]. Under pathological conditions, this balance is disturbed leading to altered angiogenesis and ANGPT2 signalling [5].

Vascular regulators such as ANGPT2, which is mainly expressed by ECs, is found to be dysregulated in RA-associated altered angiogenesis [5−7]. EC-specific ANGPT1/2 signalling is mediated by Tie2. ANGPT1−Tie2 activation promotes stabilisation of mature vessels and vascular integrity but inhibits inflammatory gene expression and leukocyte recruitment [8]. Pathological conditions result in abnormal ANGPT2 expression and competitive ANGPT2−Tie2 binding, disturbing the stabilising effect of ANGPT1.

ANGPT2 promotes EC inflammation and vascular leakage by reducing the integrity of EC junctions. ANGPT2-mediated inhibition of Tie2 also influences immune signalling resulting in leukocyte adhesion to the vessel walls with transmigration into surrounding tissues and the release of proinflammatory and proangiogenic cytokines [5,8,9]. ANGPT2 acts synergistically with VEGF-A and enhances angiogenesis associated with RA [7].

Cellular activation and local hypoxia in RA promote the expression of VEGF-A, leading to ANGPT2-mediated blocking of the ANGPT1 effect on proliferation, migration and budding of ECs, thereby destabilising blood vessels and inducing synovial angiogenesis [2,5].

The associated process of ECM degradation and alterations of the synovial ECM is mediated by RA synovial fibroblasts (RASFs) [10−12]. RASF express high amounts of adhesion molecules, matrix metalloproteinases (MMPs), proinflammatory cytokines (eg, interleukin [IL]-6, IL-11) and toll-like receptors (TLR) [13]. TLR stimulation results in the release of VEGF-A by RASF, which facilitates interactions with the vascular system [13]. In the severe combined immunodeficiency (SCID) mouse model of RA, it was demonstrated that RASFs migrate beyond tissue borders from an ipsilateral implantation site to a contralaterally implanted cartilage matrix through the vascular system by degrading the consecutive matrix subsequently invading the cartilage at both sites [14].

RASF-mediated matrix degradation results in a local release of matrix-associated proteins such as the angiogenic inhibitor canstatin, which is a fragment of the NC1 domain of the type IV collagen α2 chain. It is ubiquitously expressed in the basement membrane and is part of the interstitial matrix including the lining layer of the synovial membrane in RA patients [15,16]. Canstatin treatment or overexpression suppresses tumour growth by inhibiting angiogenesis and lymphangiogenesis and inhibits tube formation and migration of human lymphatic ECs by blocking ANGPT1-induced proliferation [17]. RASF-mediated degradation of ECM releases matrix fragments, which contribute to the invasive and prodestructive phenotype of RASFs [18]. Fibroblasts are able to remodel the ECM by modifying collagens and interacting with the vascular system in the process of wound healing [19].

Due to the RASF-mediated increased angiogenesis in RA synovium, RASF−EC interactions were analysed in this study with focus on vessel formation modulated by canstatin and respective molecular pathways *in vitro* and *in vivo*.

MATERIALS AND METHODS

See supplementary file.

RESULTS

RASF invasion into cartilage over time in the SCID mouse model of RA

RASF invasion in the SCID mouse model was evaluated at days (d) 12/18/24/30/40/45 after implantation (Supplementary Material S1). On day 12, RASF-mediated cartilage invasion was observed in ipsilateral and contralateral implants. Ipsilaterally, the strongest increase of RASF invasion was found between days 18 and 40, while the invasion increased similarly in contralateral implants. RASF invasion further increased until day 45 in ipsilateral implants. RASF invasion was similar in ipsilateral and contralateral implants.

RASFs specifically induce helix-like vessel formation in the SCID mouse model of RA

Vessel formation into implants was analysed in the SCID mouse model between days 3 and 45. Helix-like vessels (HLVs) were only detectable after RASF implantation because implantation without RASF did not result in HLV formation on days 3 and 6, suggesting a RASF-specific HLV induction (Supplementary Material S2).

HLV formation was observed when implanting RASFs in ipsilateral and contralateral implants from day 3 until day 45 (Fig 1A). Ipsilaterally, more HLVs were observed compared to contralateral implants over the entire time period. On day 3, HLVs were thin with weak blood circulation, whereas on day 40 and day 45, HLV thickness and circulation increased at both sites. Based on the number of HLVs, the kinetics of HLV formation (Fig 1B) could be divided into 3 phases (Fig 1C).

During phase 1 (days 3-18), the formation of HLVs already started and was comparable with only a slight increase in HLVs in ipsilateral implants. In contrast, contralateral implants showed a strong increase of HLVs during phase 1. Phase 2 (days 18-30) was characterised by a strong increase in HLV formation in ipsilateral implants. Contralaterally, this increase was observed with a delay between days 24 and 40. Phase 3 (days 30-45) marked the last phase showing a decrease in HLVs in ipsilateral and contralateral implants. Ipsilaterally, the decrease started at day 30 and contralaterally at day 40. Of note, the decrease of the number of HLVs was comparable at both sites.

Angiopoietin-2 in SCID mouse implants and human synovial tissue

ANGPT2 was analysed in ipsilateral and contralateral implants (Fig 2A). Serial sections were stained for ANGPT2, and CD31 was used as a EC marker control. Immunofluorescence revealed that ANGPT2 was expressed in contralateral and ipsilateral implants (days 3-12). Ipsilateral implants expressed more ANGPT2 compared to contralateral implants at day 9. On day 12, ANGPT2 expression was again similar in ipsilateral and contralateral implants (Fig 2A). As comparison, human synovial tissue of osteoarthritis (OA) and RA patients was stained for ANGPT2 and CD31 (Fig 2B). The ANGPT2 signal was significantly stronger in RA than OA patients, suggesting an ANGPT2-specific role in altered RA blood vessels. To confirm the effect of RASF on ANGPT2 expression by ECs, human umbilical vein endothelial cells (HUVECs) were cultured alone or in coculture with RASFs (number of HUVECs as ANGPT2-expressing cells was the same in both settings) showing an upregulation of ANGPT2 in cocultures compared to EC alone at the RNA level (Fig 2C). However, the RASF-induced ANGPT2 protein increase was low after 6 hours but increased at later timepoints (5% after 4 hours vs 14% after 48 hours).

RASF-mediated influence on angiogenesis in vitro

A 2-dimensional (2D) tube formation assay was performed with/without the addition of 15% RASFs (Calcein-AM, green fluorescent) to HUVECs. RASFs influenced tube formation by significantly reducing tube thickness after 4 hours (Fig 3A) and 8 hours (Fig 3B) compared to tube formation by HUVECs alone. Additionally, RASF altered EC sprouting in the 3-dimensional (3D) spheroid-based sprout assay by significantly increasing the area of spheroids after 24 hours but reducing tube formation leading to a diffuse sprouting of ECs instead of aligning into tubes (Fig 3C). To investigate whether cell−cell contact between ECs and RASFs was required, tube formation with HUVECs alone was compared to HUVECs cultured with RASF-conditioned medium with/without IL-1β stimulation of RASF. The same interfering effect on cell network formation could be observed with RASF-conditioned medium (Fig 3D) which was further enhanced by conditioned medium from RASFs stimulated with IL-1b.

Influence of repetitive activation of RASFs and ECs in vitro

The area of the cell network formed was measured in the tube formation assay with RASFs being added to HUVECs after having been stimulated once and up to 3 times (repetitively) with IL-1β (Supplementary Material S3). Unstimulated RASFs significantly reduced the area of the cell network after 4 hours ($P < .0001$, n = 4, Fig 4A) compared to HUVEC monoculture. RASFs stimulated once with IL-1β further reduced the network area compared to unstimulated RASFs ($P < .038$), while RASFs stimulated 3 times significantly restored tube formation compared to RASFs stimulated once ($P = .029$), leading to the formation of a significant larger area of cell network comparable to the effect of unstimulated RASFs after the third stimulation.
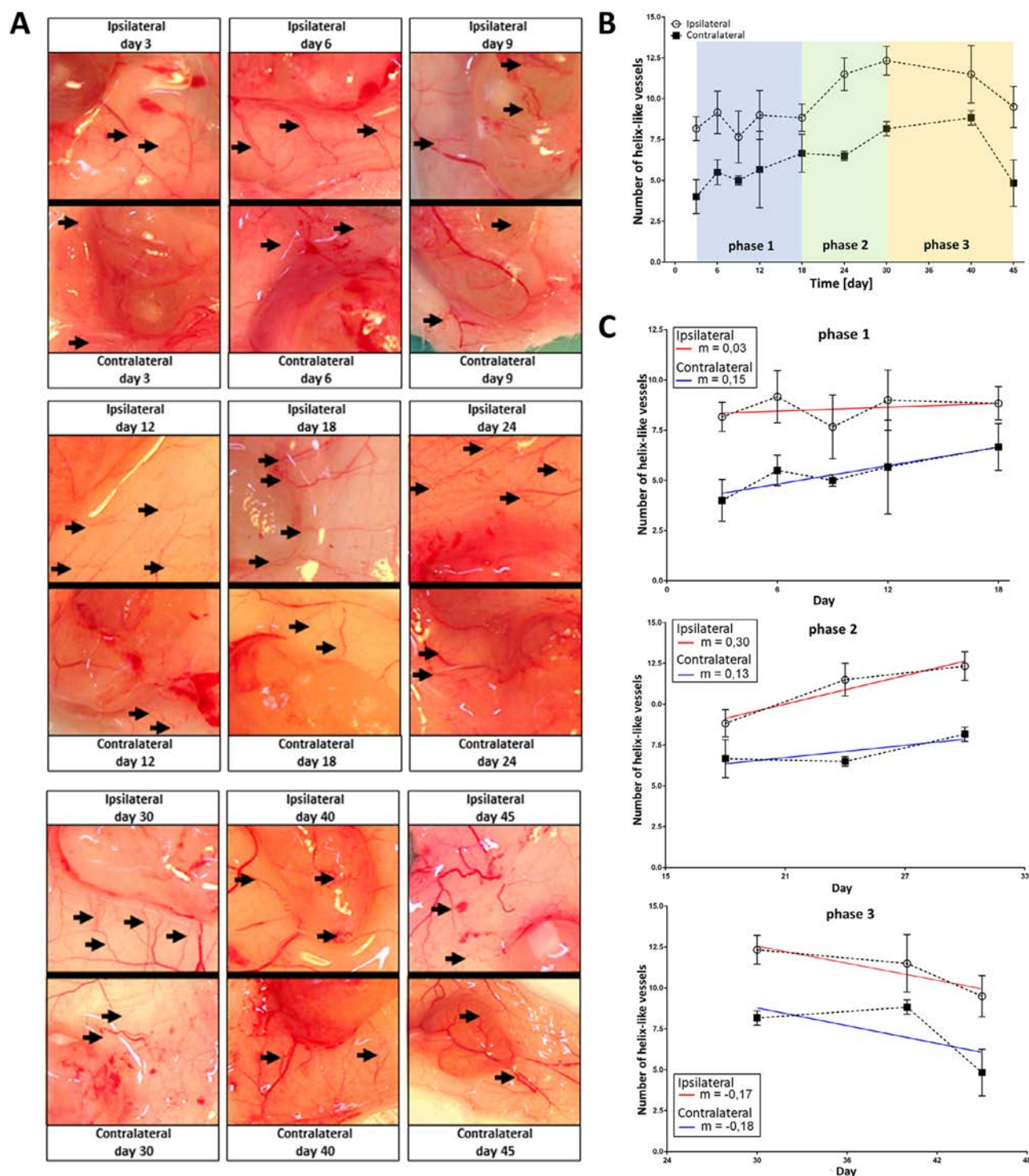
Figure 1. Formation of RASF-induced HLVs between day 3 and 45. A, Representative pictures of ipsi- and contralateral implants on d3 to 45 containing HLVs (black arrows) are shown. B, HLV formation was quantified in representative implant areas on days 3, 6, 9, 12, 18, 24, 30, 40 and 45 ipsi- and contralaterally (means of biological replicates calculated and used for statistics (n = 3), standard error). C, The development of HLVs between days 3 and 45 could be divided in 3 phases. In phase 1 (days 3-18), the number of HLVs increased contralaterally but not ipsilaterally. In phase 2 (days 18-30), the number of HLVs increased ipsilaterally but not contralaterally. In phase 3 (days 30-45), the number of HLV decreased at both sides. Slopes are shown for ipsi- (red) and contralateral (blue) implants. HLV, helix-like vessel; RASF, rheumatoid arthritis synovial fibroblasts.

`Furthermore, the secretion of IL-6 in RASFs and HUVECs in mono- and coculture after repetitive stimulation with IL-1β was measured (Fig 4B). RASFs stimulated once showed a significant increase in IL-6 levels compared to unstimulated controls. After subsequent repetitive RASF stimulation, a significantly lower increase in IL-6 levels compared to the first stimulation ($P < .0001$) was observed. In contrast, repetitive stimulation of HUVECs did not show a reduced response after repetitive stimulation ($P = .08$) and IL-6 production was lower compared to RASFs. Interestingly, repetitive stimulation of HUVECs + 15% RASFs resulted in a high and significant increase in IL-6 levels for each subsequent stimulation ($P = .01$). Thus, RASF−EC interactions significantly altered the reduced response of RASF to repetitive stimulation in monoculture.

Furthermore, VEGF-A, the chemokine IL-8 and MMP-3 were measured in supernatants of repetitively stimulated RASFs.
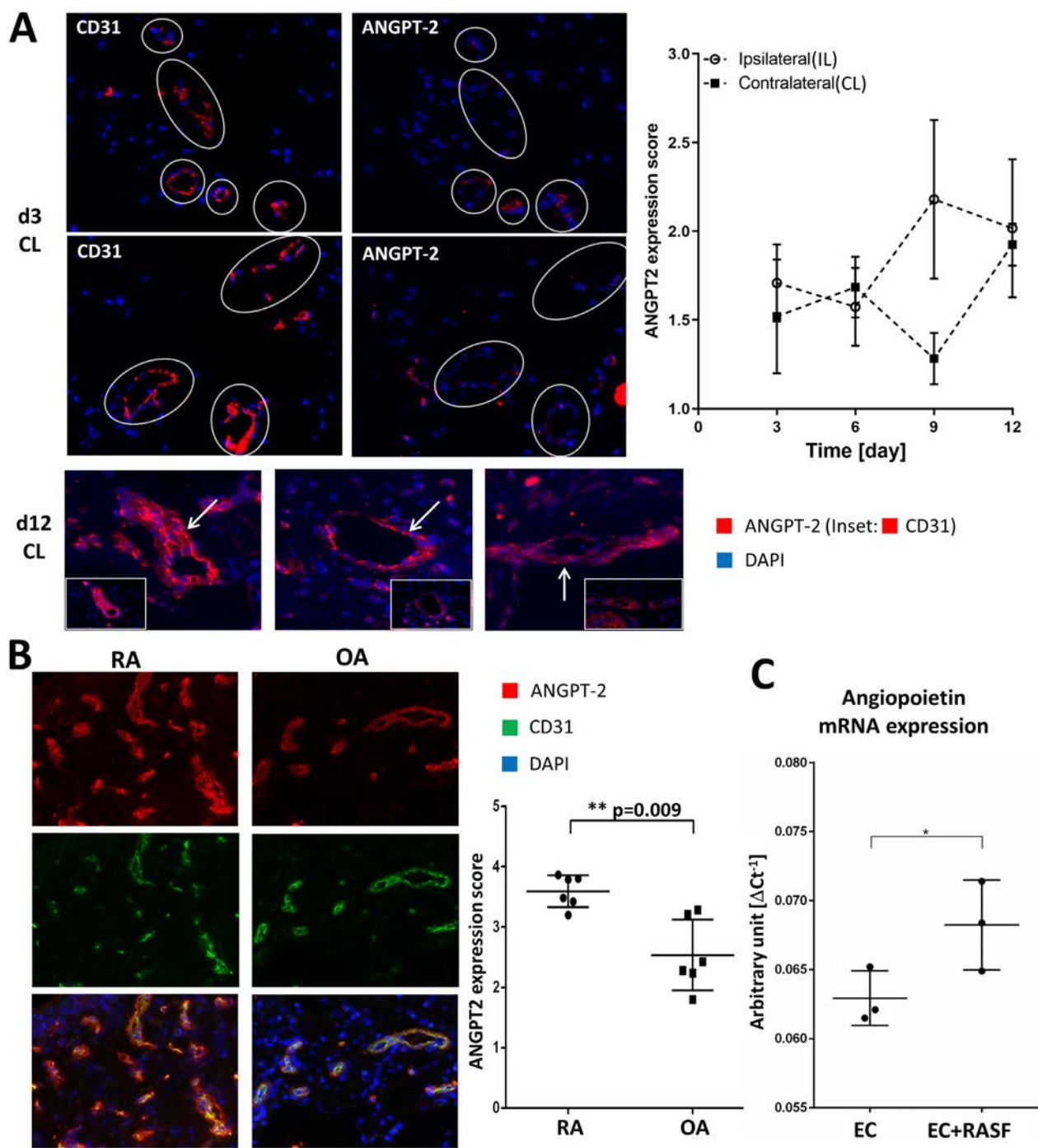
Figure 2. Expression of ANGPT2 in SCID mouse implants and human synovial tissue. A, Serial sections of ipsi- and contralateral implants were stained for ANGPT2 and CD31 as control on days 3, 6, 9 and 12. Examples for days 3 and 12 for contralateral implants are shown. Vessels were identified using the CD31 signal and ANGPT2 signal evaluated in each vessel using a score of 1 (ANGPT2 negative or weak ANGPT2 signal) to 4 (strong ANGPT2 signals, stronger than CD31 signals). On days 3 and 6, the ANGPT2 signal was detectable in ipsi- and contralateral implants; however, on day 9, the ANGPT2 signal was higher in ipsilateral implants. Means from all implants with the same RASF were calculated. The mean ± standard error from n = 3 biological replicates (RASFs from 3 different patients) was calculated. B, Immunofluorescence of ANGPT2/CD31 costaining on human RA and OA tissue was performed and the overlay quantitatively evaluated using CD31 as basis to identify vessels. The score in costainings ranged from 1 (ANGPT2 negative) to 4 (strong ANGPT2, stronger than CD31). ANGPT2 was significantly upregulated in RA vs OA patients (n = 6, P = .009, means ± SD). C, ANGPT2 mRNA expression by HUVECs was significantly increased by addition of RASFs after 6 hours (n = 3). For statistics, the Mann −Whitney U test was performed. Pictures are shown in 400-fold magnification. ANGPT2, angiopoietin 2; HLV, helix-like vessel; HUVEC, human umbilical vein endothelial cell; OA, osteoarthritis; RASF, rheumatoid arthritis synovial fibroblasts; SCID, severe combined immunodeficiency.

Interestingly, IL-8, MMP-3 and VEGF-A did not show differences between the first and third RASF stimulation in contrast to IL-6 (Fig 4C), with the latter showing that the repetitive stimulation effect of RASF observed in the tube formation experiment was not VEGF mediated.

Influence of repetitive IL-1β stimulation of RASFs on gene expression

`The influence of repetitive stimulated RASFs was further evaluated using RNAseq. RNA expression from RASF stimulated once
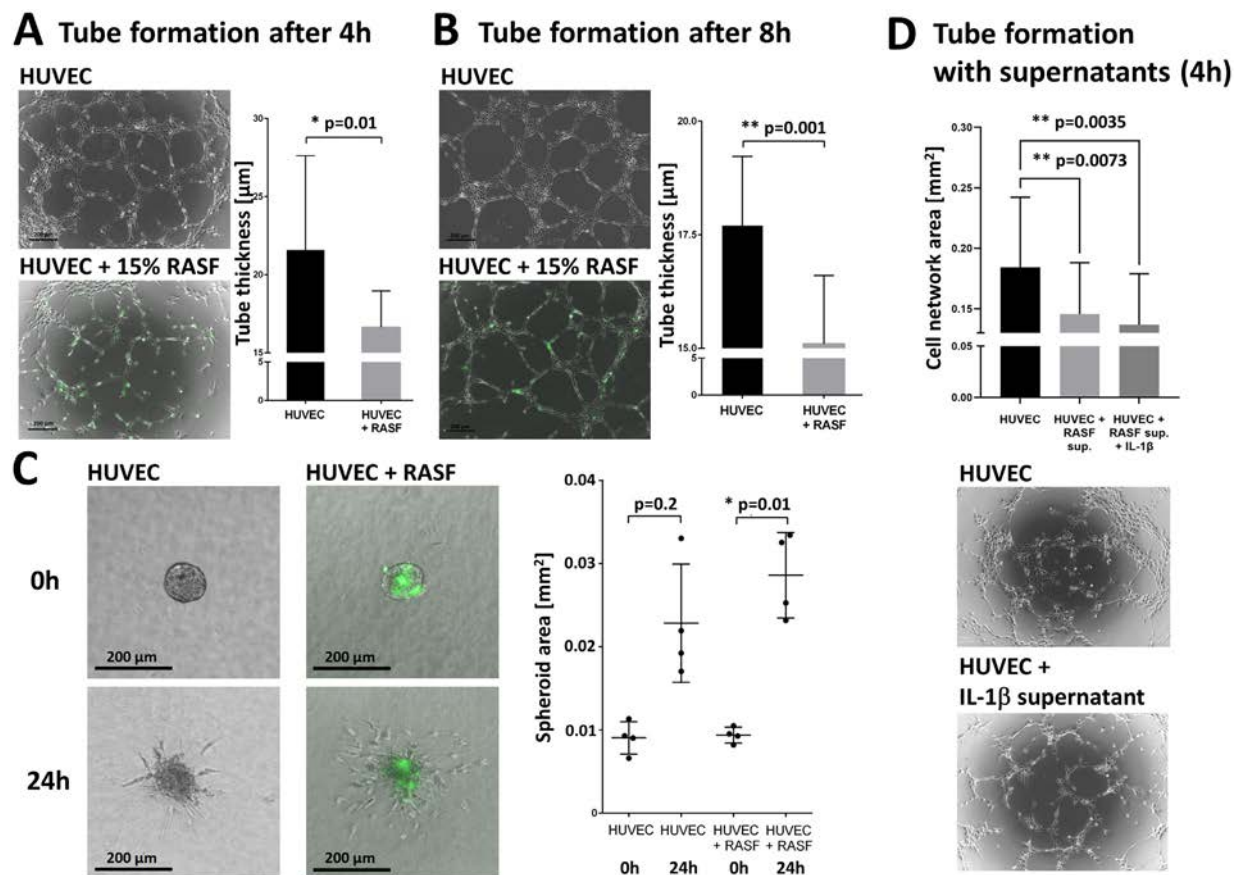
Figure 3. RASF significantly altered angiogenesis in vitro in 2D tube formation and 3D-spheroid-based sprout assays. 15% Calcein-AM stained RASFs (green) were added to HUVECs in the tube formation assay on Matrigel coating (A, B) as well as to the collagen matrix of the 3D spheroid-based sprout assay (C). RASFs significantly reduced tube thickness already after 4 (A) and 8 hours (B) of tube formation (n = 10). For statistics, the Mann−Whitney U test was used. C, Representative pictures of the 3D spheroid-based sprout assay after 0 and 24 hours (100-fold magnification) are shown. RASFs significantly increased the spheroid area by promoting EC sprouting after 24 compared to 0 hours (n = 4). For statistics, the Friedman's test including Dunn's multicomparison correction was used. D, Tube formation using RASF-conditioned supernatants showed a statistically significant reduced cell network area compared to control, which was further disturbed by adding conditioned media from IL-1 β stimulated RASFs (n = 10). For statistics, the Friedman's test including Dunn's multicomparison correction was used. Means $\pm$ SDs are shown. HLV, helix-like vessel; HUVEC, human umbilical vein endothelial cell; RASF, rheumatoid arthritis synovial fibroblasts; 3D, 3-dimensional; 2D, 2-dimensional.

and 3 times (repetitively) was assessed, and gene and pathway analysis between once and thrice stimulated RASF was performed.

Results of RNAseq showed that the top 50 differentially expressed genes (DEGs) were mainly associated with autoimmune diseases, vascular diseases and diseases affecting the immune system (Fig 5A). Interestingly, pathway analysis also revealed that genes involved in tumour necrosis factor α (TNF α) signalling pathways and pathways associated with RA were expressed significantly different between single and repetitive RASF stimulation (Fig 5A,B, marked in green). In contrast, genes involved in VEGF-mediated signalling pathways were not differentially expressed (Fig 5B, marked in blue), confirming the measurements at the protein level (Fig 4C). Evaluation of the top 10 signalling pathways showed that the TNF-associated signalling pathways induced in the first stimulation were significantly lower after the third stimulation (bars in red, Fig 5C). The top 50 DEG were further evaluated (Fig 5D). For this, expression profiles for each of the top 50 DEG were generated. Three different expression profiles were identified. Genes with a significant upregulation after first stimulation compared to control but a significant downregulation after third compared to the first stimulation were assigned to expression profile 1. Five (*STC1, BMP6, CXCL2, IL-11* and *ELOVL7)* of the top 50 DEG showed this expression profile. Literature research revealed that IL-11 and CXCL2 might play an RASF-mediated role in the altered

angiogenesis observed in RA and were further evaluated because these factors are able to alter angiogenesis VEGF independently [20,21]. The significant reduction in IL-11 (*P* < .001) and CXCL2 (*P* = .004) after the third compared to first stimulation were verified at the protein level (Fig 5E). On a functional level, the tube formation assay using 25, 50, or 100 ng/mL CXCL2 showed that CXCL2 was able to reduce the area of network formation at all concentrations (Fig 6A). The area of network formation reduced by CXCL2 was restored to the control level by the addition of the CXCL2 inhibitor SB225002 (Fig 6B). IL-11 also altered the area of network formation and the effect could be reversed using a neutralising IL-11 antibody (Fig 6C,D). IL-11 und CXCL2 signals were detectable in ipsilateral implants at early time points with CXCL2 showing stronger expression. A weaker signal for CXCL2 was detectable in canstatin-treated implants (Fig 6E). To evaluate the role of VEGF, bevacizumab was used inhibiting tube formation, which could in part be restored by ANGPT2. When using ECM medium without VEGF, a similar effect of ANGPT2 was observed (Fig 6F).

Influence of canstatin on RASF−EC interactions in vitro

Due to the activating role of matrix fragments on RASFs, the effect of canstatin on RASF−EC interactions was evaluated. To
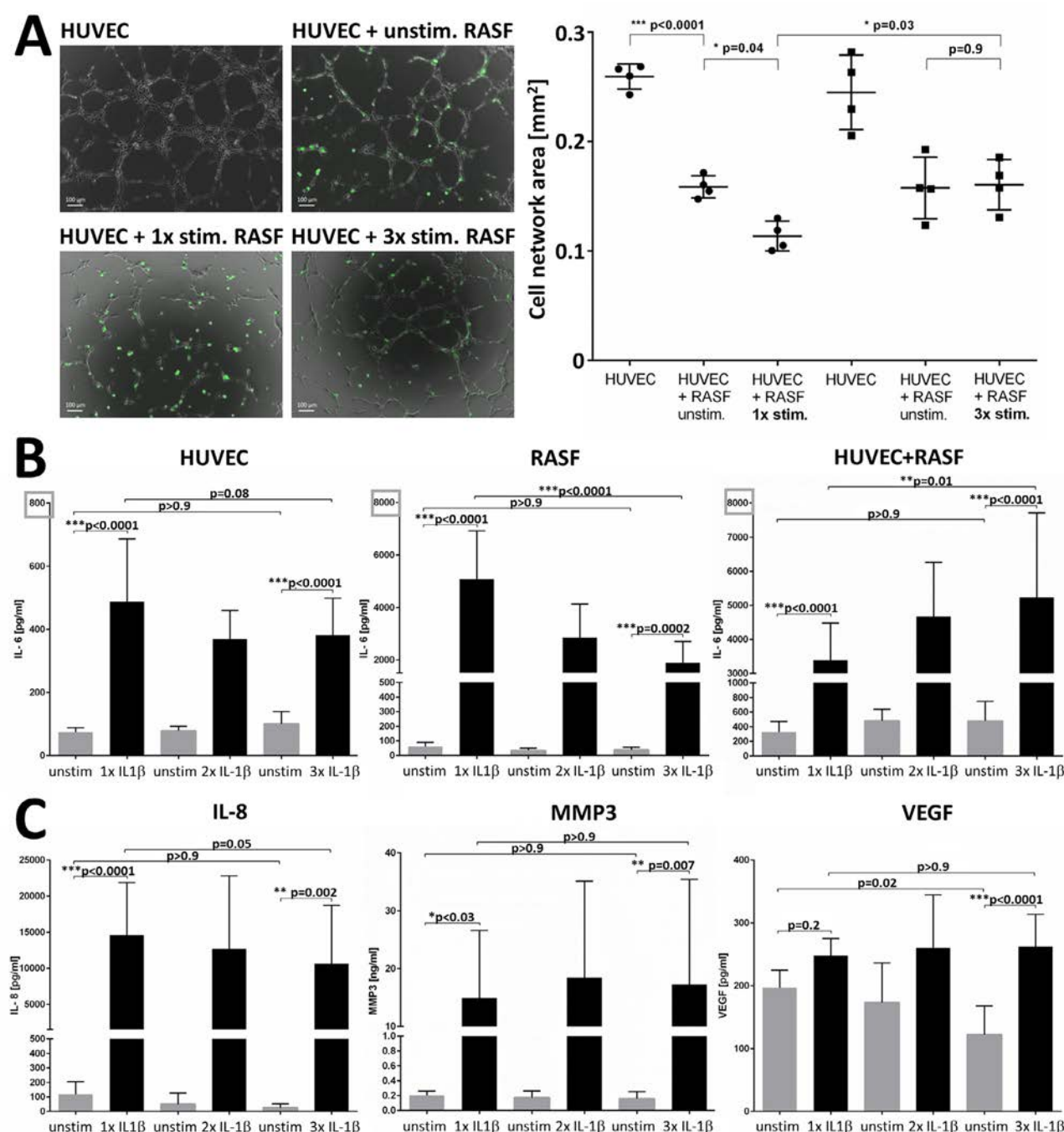
Figure 4. Repetitive stimulation of RASF significantly attenuated the proinflammatory effect of IL-1β on angiogenesis by altering IL-6 secretion in mono- and coculture with HUVEC in vitro. (A) RASF were stimulated 3 times (repetitively) with IL-1β. Each step consisted of IL-1β stimulation for 16 hours followed by a recovery for 8 hours. After first and third stimulation, IL-1β-stimulated or unstimulated RASFs (green, 15% of HUVEC numbers) were added to HUVECs in the tube formation assay. Unstimulated RASFs significantly reduced the area covered with cell network compared to HUVEC monoculture. RASF stimulated once significantly further reduced the area of cell network. Repetitively stimulated RASFs significantly attenuated the proinflammatory effect of once stimulated RASFs because repetitively stimulated RASFs did not show differences compared to unstimulated RASFs (n = 4). B, RASFs and HUVECs were repetitively stimulated with IL-1β in mono- and coculture. Repetitive stimulation of RASF in monoculture led to a significantly lower induction of IL-6 after the third stimulation compared to stimulation once (RASF 1st: 5076 ± 1730 pg/mL vs 3rd: 1890 ± 758 pg/mL, P < .0001) but not in HUVEC monoculture (1st: 488 ± 186 pg/mL vs 3rd: 382 ± 109 pg/mL, P = .08). Of note, HUVECs alone produced lower amounts of IL-1 compared to RASFs and coculture (y-scale bar, grey frame). Repetitive stimulation of HUVECs and RASFs in coculture resulted in a significant IL-6 upregulation after third stimulation compared to once (1st vs 3rd: P = .02, n = 8). C, Repetitive stimulation of RASFs did not affect IL-8, MMP-3 and VEGF secretion (n = 7). A-C, For statistical analysis, one-way ANOVA was used including Sidak's test for multicomparison correction, means ± SDs are shown. ANOVA, analysis of variance; HLV, helix-like vessel; HUVEC, human umbilical vein endothelial cell; IL, interleukin; MMP, matrix metalloproteinase; RASF, rheumatoid arthritis synovial fibroblasts; VEGF, vascular endothelial growth factor.

identify the physiological concentrations, canstatin was measured in serum of RA patients. Canstatin was significantly upregulated in RA compared to healthy controls (P < .001), but not compared to OA (Fig 7A). Canstatin stimulation of HUVECs in

the tube formation assay for 4 or 8 hours did not affect tube thickness (data not shown). However, prestimulation of HUVECs with canstatin for 20 hours before use in the tube formation assay resulted in a significant reduction of tube thickness
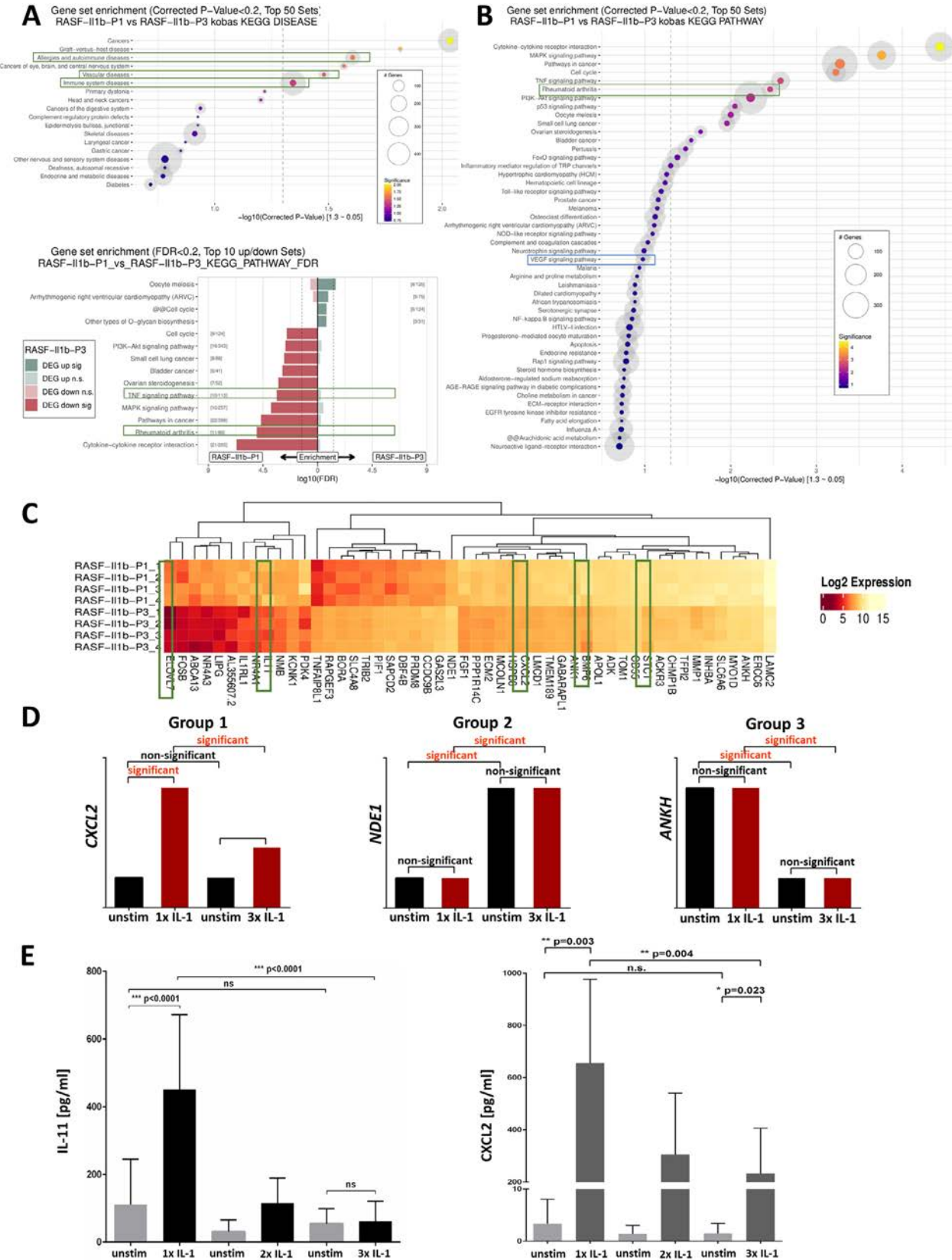
Figure 5. Influence of repetitive IL-1β stimulation on RASF gene and protein expression. RASFs were stimulated thrice with IL-1β for 16 hours. A recovery step without IL-1β for 8 hours followed after each stimulation. RNAseq was performed after the first and third stimulation followed by pathway analyses and top 50 DEG identification. A, Diseases associated with the top 50 DEG between first and third RASF stimulation are shown. B, Signalling pathways associated with the top 50 DEG between first and third RASF stimulation are shown. Shaded in grey is the number of DEG significantly associated with a specific disease (A) or signalling pathway (B). Significantly enriched DEGs within pathways were determined from the KEGG Pathway database using the KOBAS web server. Dashed line marks significantly different gene groups between first and third stimulation. Gene groups right of the dashed line have a significance level of P < .05. Significance values using the lower scale were obtained from the negative decadic logarithm of the corrected P value. In (A), 2 corresponds to the highest and 0.75 to the lowest significance level. Among the top 6 diseases, the main gene groups were autoimmune diseases, vascular diseases and diseases affecting the immune system (marked green). In (B), 4 corresponds to the highest and 1 to the lowest significance level. Genes associated with RA and TNFα signalling pathways were significantly different (marked green) in contrast

after 8 hours, but not after 4 hours (Fig 7B). Therefore, the longer-term effect of canstatin on HUVEC−RASF interactions and canstatin prestimulated HUVECs was used in further experiments. Additional stimulation of prestimulated HUVECs with additional canstatin in the tube formation assay significantly further reduced tube thickness after 4 and 8 hours (Fig 7C, HUVECs vs. HUVECs + 0.5 µg/mL canstatin). The addition of RASFs to canstatin prestimulated HUVECs did not significantly influence tube thickness after 4 and 8 hours (Fig 7C). The addition of RASFs to canstatin prestimulated HUVECs and additional stimulation with 0.5 µg/mL canstatin in the tube formation assay did not further significantly alter tube thickness after 4 and 8 hours (Fig 7C). Canstatin did not induce ANGPT2 in HUVECs alone after 6 or 48 hours (0% and 2% ANGPT2 induction by canstatin, n = 3) or in HUVEC/RASF cocultures (5% and 6% ANGPT2 induction).

Canstatin significantly influenced angiogenesis in the 3D spheroid-based sprout assay (Fig 7D). The area of spheroids was lower directly after generation of spheroids (defined as 0 h) with canstatin (Fig 7E, left graph). This effect was stronger after 24 hours because canstatin significantly reduced the area of sprouting spheroids also after the addition of RASFs (added at time point 0 h) (Fig 7E, right graph). Canstatin did not induce apoptosis in RASFs or ECs at the concentrations used for the 2D and 3D assays (Supplementary Methods).

Influence of canstatin on RASF-mediated cartilage invasion and HLV formation in vivo

To evaluate the influence of canstatin regarding cartilage invasion and HLV formation, canstatin was added to ipsi- and contralateral implants during implantation. Canstatin did not affect RASF-mediated invasion at the ipsi- or contralateral side (Fig 8A). Although the invasion score was higher for implants without canstatin at most time points (Fig 8A), the difference was not statistically significant (example day 40 at both sides: Fig 8B). Interestingly, canstatin significantly reduced the number of HLVs in ipsilateral implants on day 3, whereas contralateral implants did not show differences under canstatin treatment (Fig 8C,D). On day 45, the number of HLVs was identical in ipsilateral and contralateral implants with/without canstatin (Fig 8C,E). The course of HLV formation differed under the influence of canstatin in ipsilateral implants (RASF directly coimplanted with cartilage ± canstatin, Fig 8F). In phases 1, 2 and 3, there were fewer HLVs observed in ipsilateral implants containing canstatin compared to ipsilateral implants without canstatin. The only exceptions were day 9 and day 45, which showed similar numbers of HLVs in ipsilateral implants ± canstatin. The total number of vessels (HLV together with normal-shaped vessels) did not differ between implants with/without addition of canstatin (not shown).

Furthermore, ANGPT2 expression was also altered in vessels of ipsilateral implants containing canstatin. At day 6, ipsilateral

implants without canstatin showed lower ANGPT2 signals compared to ipsilateral implants with canstatin but higher signals at day 9 and day 12. In contrast, the contralateral implants with canstatin showed higher ANGPT2 signals at all time points (days 3-12) compared to contralateral implants without canstatin (Fig 8G).

DISCUSSION

In RA synovium, activated RASFs exert a considerable influence on pathological vascularisation by interacting with ECs. HLVs and a similar kinetic observed in our study also occur in the context of other diseases. Diseases of the coronary vessels and peripheral arteries lead to the maturation of pathological collateral vessels with helix-like structure [22−25]. Following arterial occlusion, weakly perfused collateral vessels are supplied with more blood, and ECs are activated by increased blood flow because of altered pressure, which causes maturation of collateral vessels [26]. Pathological collateral vessels exhibit a tortuous vessel shape, which shows similarities to RA synovium, but also HLVs observed after RASF implantation into SCID mice. Here, we observed an RASF-induced pathologic HLV formation. Integrated RNA sequencing, functional angiogenesis and molecular analysis showed that ANGPT2 may play a role in HLV formation and that RASF influence pathological angiogenesis involving factors such as IL-11 and CXCL2. Interestingly, addition of ANGPT2 while inhibiting VEGF, resulting in disturbed tube formation, was able to in part restore tube formation.

HLV formation could be divided into early phase 1 of RASF-mediated HLV formation, phase 2 with HLV accumulation and phase 3 with reduction of accumulated HLV. Compared to normal arterial vessels, collateral vessels show an increased expression of ANGPT2 [27]. In our study, ANGPT2 was already detectable ipsilaterally and contralaterally in SCID mouse implants between day 3 and 12. ANGPT2 expression was observed at all time points and all ipsilateral and contralateral implants, suggesting a role of ANGPT2 during HLV development. ANGPT2 plays a crucial role in the destabilisation of blood vessels [28], representing a very early event in new vessel formation. Regarding the presence of ANGPT2 already at day 3 and the higher levels of ANGPT2 in ipsilateral implants at day 9, ANGPT2 might be a marker for early molecular alterations in HLV formation. We also found a significantly higher ANGPT2 expression in RA compared to OA synovium, suggesting an involvement of ANGPT2 in RA. The synovium analysed originated from knee joints removed during joint replacement surgery. Therefore, pathological processes involved in altered vascularisation had existed for years. Consequently, ANGPT2 might be a marker of long-term vascular changes, which can be evaluated using long-term models such as the SCID mouse model but not short-term culture systems such as 2D tube formation. Local cell activation due to chronic inflammation, tissue damage and long-term treatment may influence synovial cells,

---

to genes associated with VEGF signalling pathways (marked blue). C, Top10 signalling pathways with upregulated DEG (green) and downregulated (red) pathways are shown. D, Heatmap of the top 50 DEGs comparing first and repetitive third stimulation of RASF (log2 of the top 50 DEG expression values). Based on the expression profiles of the top 50 DEG, subgroup profiles were identified. All top 50 DEG could be assigned to one of the 3 groups: group 1 included genes showing a significant weaker induction of gene expression after third IL-1β stimulation compared to the third (marked green, example for CXCL2). Groups 2 and 3 did not show this effect (group 2, example NDE1; group 3, example ANKH). E, Repetitive RASF stimulation significantly reduced IL-11 (P < .001) and CXCL2 (P = .004) protein secretion after third compared to first stimulation. Means ± SDs are shown (n = 8). For statistical analysis, one-way ANOVA was used including Sidak's test for multicomparison correction. ANOVA, analysis of variance; DEG, differentially expressed gene; IL, interleukin; KEGG, Kyoto Encyclopedia of Genes and Genomes; RASF, rheumatoid arthritis synovial fibroblasts; TNF, tumour necrosis factor.
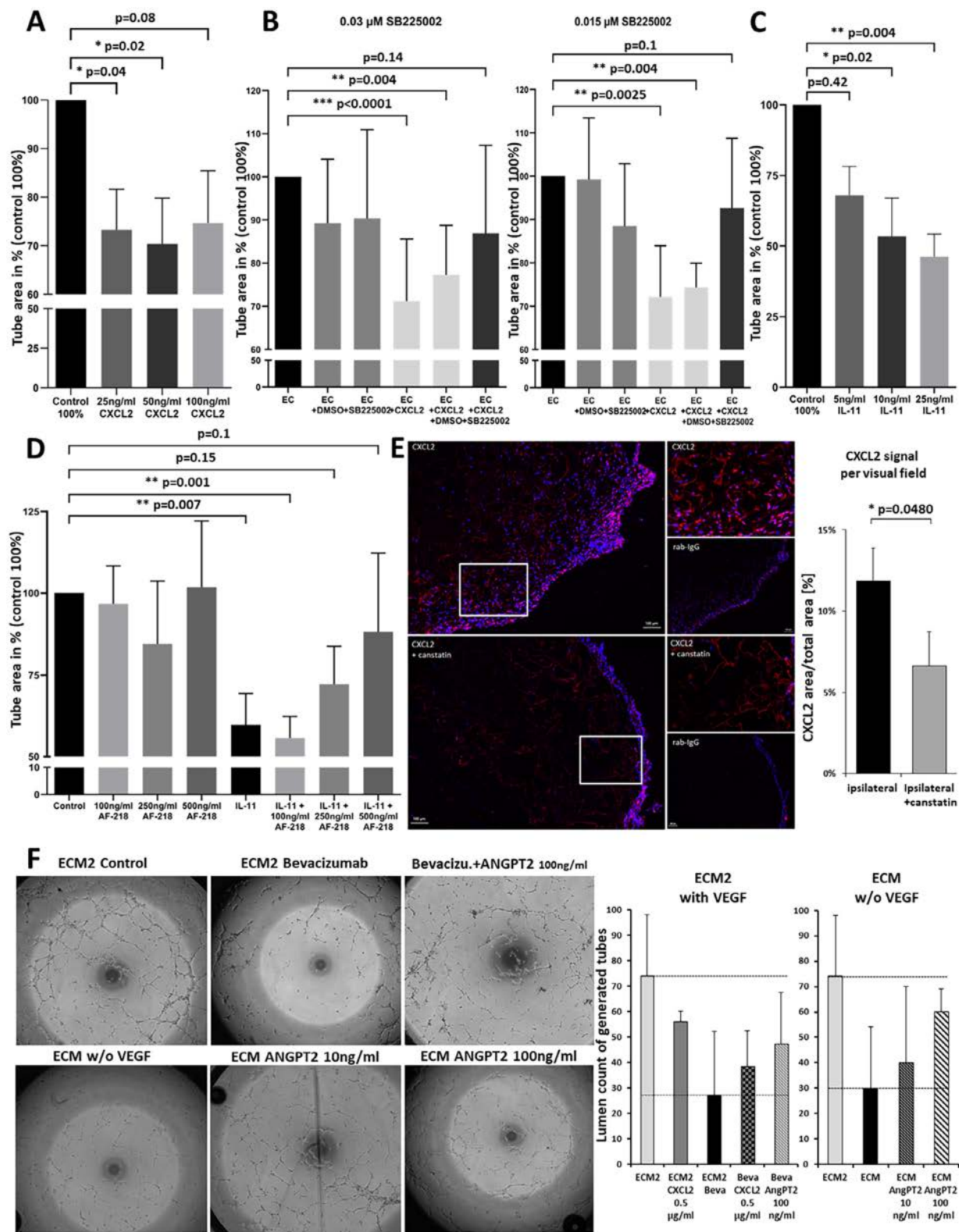
Figure 6. Effects of CXCL2 and IL-11 on 2D tube formation. A, The tube formation assay was performed for 4 hours with/without the addition of CXCL2. CXCL2 decreased the area of tube formation at all concentrations used (n = 5 each). B, The area of tube formation reduced by 50 ng/mL CXCL2 was restored to control level by the addition of 0.015 (n = 6) or 0.03 μM (n = 8) of the CXCL2 inhibitor SB225002 (SB) in DMSO as solvent. C, IL-11 reduced the area of network formation at all concentrations used with the strongest and statistically significant effects with 10 and 25 ng/mL IL-11 (n = 5 each). D, IL-11 (10 ng/mL) induced reduction could be restored with the IL-11 neutralising antibody AF-218 at the higher concentrations used (250 and 500 ng/mL). E, Immunofluorescence for CXCL2 in ipsilateral implants with/without canstatin treatment (+ canstatin). Quantification of days 3 to 9 showed a significant lower CXCL2 area per visual field in implants without canstatin. F, 2D tube formation with bevacizumab led to disturbed tube formation compared to ECM2 control containing VEGF. Addition of ANGPT2 improved tube formation. Similarly, tube formation in ECM without VEGF led to reduced tube formation compared to ECM2 which could in part be restored by addition of ANGPT2. Means ± SDs are shown. For statistics, a Friedman's test including Dunn's multicomparison correction was used. ANGPT2, angiopoietin 2; ANOVA, analysis of variance; DMSO, dimethyl sulfoxide; IL, interleukin; RASF, rheumatoid arthritis synovial fibroblasts; TNF, tumour necrosis factor; 2D, 2-dimensional.
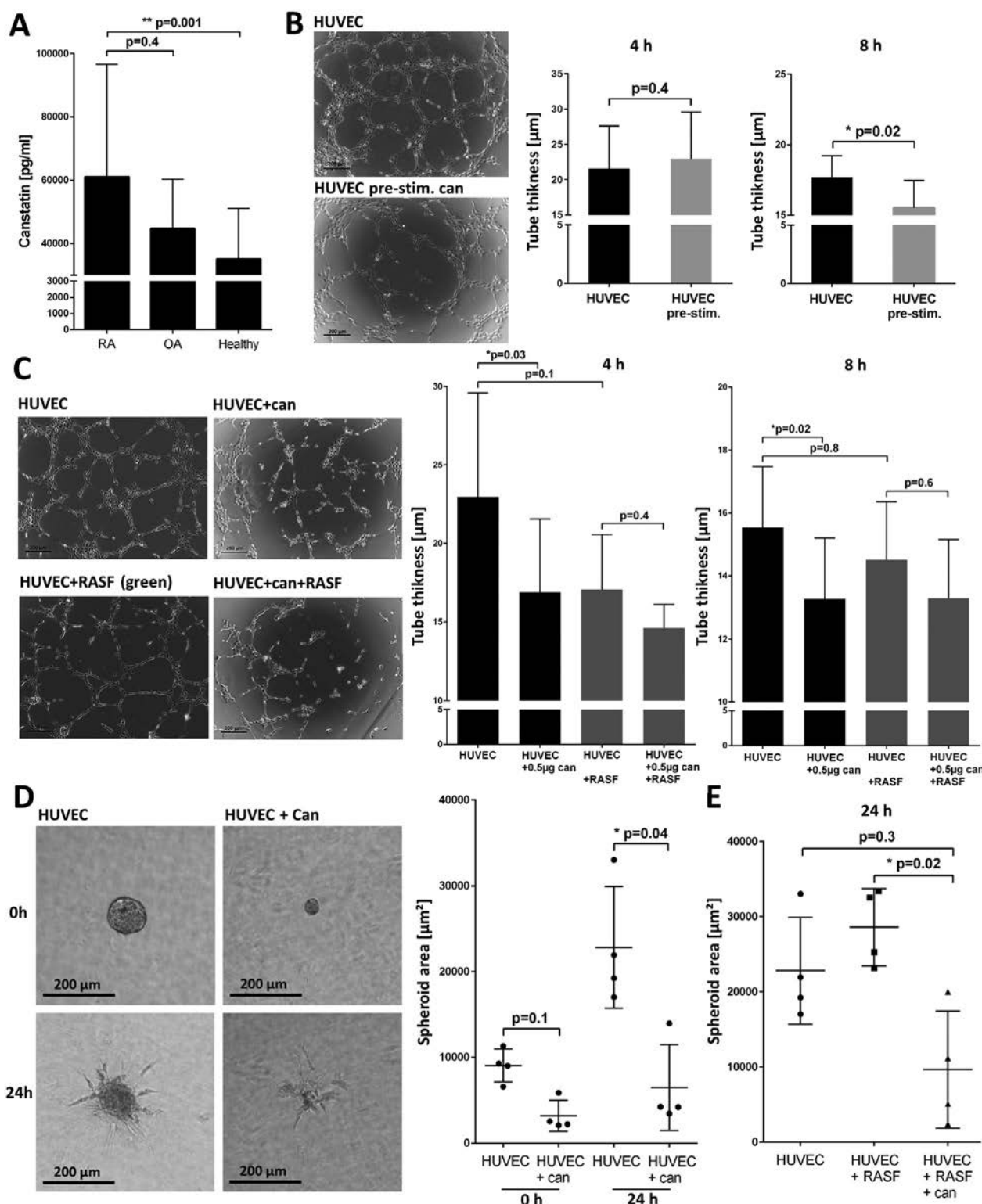
Figure 7. Influence of canstatin on angiogenesis with focus on RASF−EC interactions *in vitro*. A, Canstatin was measured in RA (n = 27), OA (n = 8) and healthy control (n = 20) serum. Canstatin was significantly upregulated in RA patients compared to healthy controls (61.1 ng/mL vs 35.1 ng/mL) but not compared to OA (44.7 ng/mL). For statistics Kruskal−Wallis test including Dunn's multicomparison correction was used. B, Representative pictures of the 2D tube formation assay (100-fold magnification) are shown. Assays were performed for 4 or 8 hours with unstimulated HUVECs or HUVEC prestimulated with canstatin for 20 hours before use. Tube thickness was significantly reduced after 8 hours when HUVECs were prestimulated, but not after 4 hours (n = 10 each). For statistics, the Wilcoxon signed-rank test was used. C, Representative pictures of the tube formation assay (100-fold magnification): Canstatin prestimulated HUVECs (HUVEC); canstatin prestimulated HUVECs treated with additional canstatin in the tube formation assay (HUVEC + can); canstatin prestimulated HUVECs with 15% unstimulated RASFs (green) (HUVEC + RASF); and canstatin prestimulated HUVECs with 15% unstimulated RASF (green) with additional canstatin in the assay (HUVEC + can + RASF). Additional canstatin stimulation of prestimulated HUVECs resulted in a significant reduction of tube thickness after 4 and 8 hours compared to prestimulated HUVECs without additional canstatin. RASF did not alter tube thickness of prestimulated HUVECs after 4 or after 8 hours (P = .8) significantly. Additional canstatin stimulation of prestimulated HUVECs did not further reduce tube thickness after 4 or 8 hours when RASFs were added. For statistics, Kruskal−Wallis test including Dunn's multicomparison correction was performed. D, Representative pictures of 3D spheroid-based sprout assay are shown (100-fold magnification). The area of spheroids was measured directly after spheroid generation (0 h) and 24 hours after starting spheroid sprouting. Stimulation of

including RASFs, leading to epigenetic imprinting. Therefore, findings discussed here may differ in RASFs from the initial phase of RA. ANGPT2 and VEGF act synergistically via Notch signalling and may thus contribute to altered vascularisation in the inflamed RA synovium [7]. Endothelial Notch signalling is involved in EC migration and polarisation [29]. Therefore, it is possible that long-term synergism between ANGPT2 and VEGF in RA contributes to altered vessel formation.

Comparing collateral vessels with HLV formation, collateral vessels were analysed 6 to 16 weeks after induction [27,30], while HLVs already occurred on day 3 after RASF implantation. RASF-induced HLVs might occur early because of the altered RASF expression profile. Activated RASFs usually express factors such as VEGF [31]. VEGF-A-overexpressing mice formed more collateral vessels between day 13.5 and day 14.5 of embryogenesis compared to mice expressing reduced VEGF-A [32]. Accordingly, the increased VEGF expression by RASF could accelerate HLV formation.

Our study showed an RASF-mediated influence on ECs by reducing tube thickness and the formed tube network area *in vitro* already after 4 hours. Cultured RASF express increased basic fibroblast growth factor (bFGF) and IL-6 levels, which can be strongly increased by proinflammatory stimulation [13]. Previous studies showed that bFGF and IL-6 significantly reduce VE-cadherin expression in HUVEC [33,34], a mechanism potentially contributing to HLV formation. However, RASF-conditioned supernatants were able to alter tube formation without contact between RASFs and ECs.

To clarify the influence of inflammatory episodes on RASF and factors released by RASF in the context of vascularisation, RASF were repetitively stimulated with IL-1β. RASF secreted significantly less IL-6 as a result of repeated IL-1β activation compared to RASF activated once. This effect observed for several parameters appears like an 'inflammatory adjustment' to repeated activation. Some studies describe a similar effect, for example in macrophages that develop tolerance to lipopolysaccharide-induced TLR immune responses and express fewer proinflammatory genes after repeated activation based on changes in signal transduction and epigenetic modifications [35−38].

Two studies described that synovial fibroblast (SF) produce significantly more IL-6 after repeated TNFα stimulation compared to fibroblasts stimulated once [39,40]. This is contrary to our results using IL-1β given that IL-6-induction was already reduced after double stimulation of RASFs with IL-1β. An explanation could be the different stimulation schemes and cytokines used. In the 2 studies, SFs were stimulated with TNFα for 24 hours, after which the fibroblasts had a recovery period of 24 hours before being stimulated twice with TNFα [39,40]. In our study, RASFs were stimulated 3 times with IL-1β for 16 hours each time, with a recovery period of 8 hours. Indeed, repetitive stimulation of RASF with TNFα showed a slight increase in IL-6 secretion compared to first stimulation (Supplementary Material S4) suggesting an IL-1β-specific inflammatory adjustment. Interestingly, parameters including angiogenesis-related factors such as VEGF did not show a reduced response after repetitive stimulation with IL-1β or TNFα in our stimulation schemes. This was

also confirmed at protein level. Crowley et al [39] identified NF-κB as possible regulator in RASF priming as a result of repeated TNFα activation, which was not significantly altered after repetitive IL-1β activation.

The repetitive stimulation effect on RASFs was also observed functionally. After the addition of RASFs stimulated once with IL-1β to HUVECs, the area of formed tube network was reduced significantly compared to unstimulated RASFs. This effect was less pronounced after addition of repetitively stimulated RASFs. Therefore, repetitive IL-1β-activation of RASFs had a significant influence on the functional interactions with ECs.

VEGF-independent factors may additionally influence angiogenesis such as IL-11 and CXCL2. Both were expressed at significantly lower levels after repetitive stimulation of RASFs. IL-11 is secreted by fibroblasts, osteoblasts and ECs. IL-11 activates the JAK/STAT and Pi3K/AKT/mTORC1 signalling pathways [41]. In relation to vascularisation and RA, a publication suggested a dual role for IL-11 in RA. Specifically, IL-11 increased infiltration of both SFs and vessels into the hyperplastic RA synovium by binding directly to its endothelial receptor IL-11Rα [20]. This is in line with our findings that IL-11 contributed to altered network formation in the 2D tube formation assay.

CXCL2 is expressed by various cell types such as ECs, mast cells and T cells. CXCL2 can interact with EC by its receptor CXCR2 and influence new vessel formation in a VEGF-independent manner [21]. It was shown that CXCL2 stimulated proliferation, migration and sprouting of HUVECs, while sprouting of HUVECs was reduced after CXCR2 blockade [21]. In our study, CXCL2 also influenced HUVECs by significantly reducing tube thickness and area of network formation. RASFs stimulated once secreted significantly more CXCL2 than unstimulated RASFs. Therefore, the high CXCL2 levels released by RASFs stimulated once may lead to the significantly reduced tube thickness, while the lower CXCL2 levels release by repetitively stimulated RASFs attenuates this effect.

During RASF-induced matrix degradation, matrix fragments including antiangiogenic collagen type IV fragments are released which further activate RASF [18]. In our study, prestimulation of HUVECs with canstatin for 20 hours and subsequent tube formation showed a canstatin-mediated significant reduction of tube thickness and area of spheroids. Collagen IV is ubiquitously present in the basement membrane of the vascular EC layer [15]. Following collagen IV-mediated degradation mediated by interactions with the α1 and α2 chains of the NC1 domain, the antiangiogenic collagen IV fragment canstatin is released [42].

Although canstatin is a relatively unknown molecule, several studies showed an antiangiogenic canstatin effect on ECs [15,17,43−45]. Canstatin binds to the HUVEC surface via integrins and thus inhibits VEGF-mediated signal transduction via the PI3K/AKT signalling pathway, resulting in inhibition of migration, proliferation and tube formation [45]. Canstatin triggers apoptosis in EC and tumour cells [15,46−49]. The antiangiogenic canstatin effect observed in our study could be due to the blocked VEGF signal transduction via integrins described by Zhu et al [45] because tube formation was stimulated via VEGF in the culture medium and the HUVECs require VEGF for the

HUVECs with 0.5 µg/mL canstatin (can) resulted in a significant reduction of the spheroid area after 24 hours compared to unstimulated HUVEC (n = 4). For statistics, Friedmann's test including Dunn's multicomparison correction was used. E, Area of spheroids containing HUVECs, RASFs and canstatin was significantly reduced after 24 hours compared to spheroids containing HUVECs and RASFs only (n = 4). For statistics, Kruskal−Wallis test including Dunn's multicomparison correction was used. Means ± SDs are shown. ANOVA, analysis of variance; can, canstatin; EC, endothelial cell; HUVEC, human umbilical vein endothelial cell; IL, interleukin; OA, osteoarthritis; RA, rheumatoid arthritis; RASF, rheumatoid arthritis synovial fibroblasts; 3D, 3-dimensional; TNF, tumour necrosis factor; 2D, 2-dimensional.
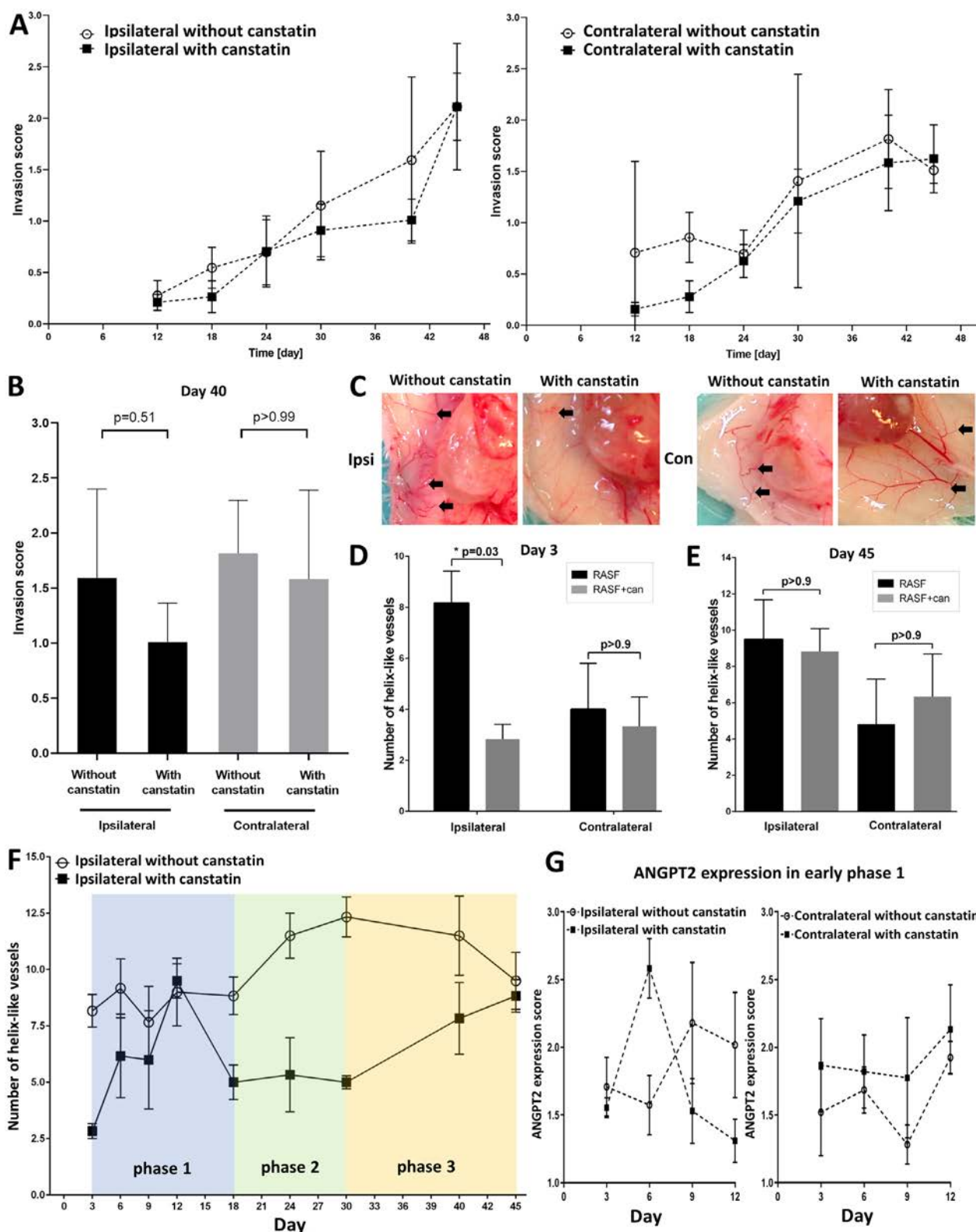
Figure 8. Influence of canstatin on RASF-mediated invasion and HLV formation in SCID mice. A, RASF together with human cartilage in a gelatine matrix were subcutaneously coimplanted ± 0.5 μg/mL canstatin at the ipsilateral side. Contralaterally, human cartilage in a gelatine matrix ± 0.5 μg/mL canstatin was implanted. Invasion scores for days 12 to 45 after implantation ±canstatin showed similar scores at the ipsi- and contralateral side with mostly higher scores in implants without canstatin (n = 3 biological replicates based on means for experimental replicates per group). B, RASF invasion did not significantly differ between ipsi- and contralateral implants ±canstatin (example: day 45) although values for implants without canstatin were higher (n = 3 biological replicates). Mean ± SD; statistics: Kruskal−Wallis test including Dunn's multicomparison correction. C, Representative pictures of ipsi- (I) and contralateral (C) implants ±canstatin (can) on day 3 containing HLVs (black arrows). Canstatin significantly reduced HLV numbers in ipsilateral implants on day 3 (D) but not on day 45 (E). Means ± SDs of HLV in ipsi- and contralateral implants ±canstatin are shown. Statistics D, E: Kruskal−Wallis test including Dunn's multicomparison correction (n = 3). F, HLV formation between days 3 and 45 in ipsilateral implants under the influence of canstatin. Number of HLV were quantified in representative areas (same size) of ipsilateral implants ±canstatin on days 3 to 45 (n = 3, standard error is shown). (G) Expression of ANGPT2 in SCID mouse implants for 3 animal series and human synovial tissue are shown. Serial sections of SCID mouse implants ±canstatin were stained for ANGPT2 and CD31 as control (400-fold magnification). The ANGPT2 signal

correct formation of the cell network. Earlier studies demonstrated that canstatin may cause focal adhesion kinase phosphorylation mediated by interaction with $\alpha v\beta 3$ and/or $\alpha v\beta 5$ integrins resulting in AKT phosphorylation. As a result, the caspase-3 cascade is activated, and apoptosis is induced [46,48]. We excluded apoptosis induction in RASFs and HUVECs with the canstatin concentrations used. Therefore, this apoptosis cascade was not responsible for the observed reduced spheroid area.

Canstatin did not change RASF-mediated altered angiogenesis *in vitro*. In the SCID mouse model, RASF-mediated invasion was not significantly reduced. Therefore, canstatin may not primarily act on RASFs but on EC−RASF interactions. Canstatin significantly reduced RASF-mediated HLV without reducing angiogenesis in general. This could be related to ANGPT2 signalling since canstatin can reduce Tie2 receptor expression in HUVECs [17], which is bound by ANGPT1 and ANGPT2, leading to its autophosphorylation [50]. Accordingly, canstatin could reverse the effects of RASF-mediated enhanced ANGPT2 expression, leading to an imbalance between ANGPT1 and ANGPT2 binding to Tie2 in ECs as well as direct ANGPT2 binding. Thus, canstatin could contribute to the reduction of HLVs induced by ANGPT1. Consequently, canstatin-mediated inhibition of Tie2 might prevent Tie2-mediated ANGPT2 signalling and alter the ANGPT2/ANGPT1 balance, while VEGF signalling would be not affected. This could explain why specific formation of altered HLVs was reduced by canstatin but not general vessel formation. CXCL2 signal was reduced in canstatin-treated implants potentially contributing to the reduced HLV formation as discussed above. Of note, evaluation of canstatin stability in human serum for 45 days did not show a decrease in canstatin (Supplementary Methods) suggesting canstatin may remain in the implant until blood vessel infiltration takes place (days 24-45).

CONCLUSION

Taken together, we showed that RASFs affect neovascularisation *in vitro*. The results show that canstatin is able to alter the interaction of RASFs with ECs and the subsequent pathological HLV formation. On molecular level, RASF-mediated altered angiogenesis involves IL-11, CXCL-2 and ANGPT2, contributing significantly to altered angiogenesis in RA.

Competing interests

The authors declare no competing interests.

Acknowledgements

Contributors

CH, BZG, SH, FL, PW, DK, and EN designed the experiments. CH, BZG, SH, FL, PW, DK, MAG, AKP, AK, NS, SS, IT, WH, CB, SG, JS, KSL, MR, and SR performed the experiments. CH, BZG, SH, FL, PW, DK, KWF, MAG, AKP, AK, NS, SS, IT, WH, CB, SG, and SR evaluated the experiments. CH, KWF, and SG conducted statistical analyses. JS, KSL, MR, and SR organised and performed in vivo experiments. UML and EN supervised the project. CH, BZG, and EN wrote the manuscript. SH, FL, PW, DK, KWF, MAG, AKP, AK, NS, SS, IT, WH, CB, SG, JS, KSL, MR, SR, and UML contributed to manuscript preparation.

Funding

Patient consent for publication

Not applicable.

Ethics approval

The studies involving human participants were reviewed and approved by Ethics Committee of the Justus-Liebig-University of Giessen. The patients/participants provided their written informed consent to participate in this study. The animal study was reviewed and approved by local ethics authorities of the Justus-Liebig-University of Giessen.

Provenance and peer review

Not commissioned, externally peer reviewed.

Patient and public involvement

Patients and/or the public were not involved in the design, or conduct, or reporting, or dissemination plans of this research.

Supplementary materials

Supplementary material associated with this article can be found in the online version at doi:10.1016/j.ard.2025.05.019.

Orcid

Klaus W. Frommer: http://orcid.org/0000-0003-2374-964X
Adelheid Korb-Pap: http://orcid.org/0000-0002-0106-903X
Nils Schulz: http://orcid.org/0009-0000-0378-3766
Stefan Günther: http://orcid.org/0000-0002-5594-4549
Jürgen Steinmeyer: http://orcid.org/0000-0002-4053-503X
Katrin S. Lips: http://orcid.org/0000-0003-3320-7545
Elena Neumann: http://orcid.org/0000-0001-7609-5964

was evaluated compared to the CD31 signal. The score ranged from 0: ANGPT2 negative to 3: strong ANGPT2 signal, stronger than CD31. On day 6, ANGPT2 signal was higher in ipsilateral implants with canstatin compared to ipsilateral implants without canstatin. However, on days 9 and 12, ANGPT2 signal was higher in ipsilateral implants without canstatin. In contralateral implants, ANGPT2 signal was higher in contralateral implants with canstatin. Means for all implants with RASF from the same patient were calculated; n = 3 biological RASF replicates are shown (mean ± standard error). ANGPT2, angiopoietin 2; ANOVA, analysis of variance; can, canstatin; HLV, helix-like vessel; HUVEC, human umbilical vein endothelial cell; RASF, rheumatoid arthritis synovial fibroblasts; SCID, severe combined immunodeficiency.

REFERENCES

[1] Elshabrawy HA, Chen Z, Volin MV, Ravella S, Virupannavar S, Shahrara S. The pathogenic role of angiogenesis in rheumatoid arthritis. Angiogenesis 2015;18:433–48.

[2] Wang Y, Wu H, Deng R. Angiogenesis as a potential treatment strategy for rheumatoid arthritis. Eur J Pharmacol 2021;910:174500.

[3] Azizi G, Boghozian R, Mirshafiey A. The potential role of angiogenic factors in rheumatoid arthritis. Int J Rheum Dis 2014;17:369–83.

[4] Adams RH, Alitalo K. Molecular regulation of angiogenesis and lymphangiogenesis. Nat Rev Mol Cell Biol 2007;8:464–78.

[5] Akwii RG, Sajib MS, Zahra FT, Mikelis CM. Role of angiopoietin-2 in vascular physiology and pathophysiology. Cells 2019;8:471.

[6] Dai C, Kuo SJ, Zhao J, Jin L, Kang L, Wang L, et al. Correlation between genetic polymorphism of angiopoietin-2 gene and clinical aspects of rheumatoid arthritis. Int J Med Sci 2019;16:331–6.

[7] Gao W, Sweeney C, Walsh C, Rooney P, McCormick J, Veale DJ, et al. Notch signalling pathways mediate synovial angiogenesis in response to vascular endothelial growth factor and angiopoietin 2. Ann Rheum Dis 2013; 72:1080–8.

[8] Wu Q, Xu WD, Huang AF. Role of angiopoietin-2 in inflammatory autoimmune diseases: a comprehensive review. Int Immunopharmacol 2020; 80:106223.

[9] Akwii RG, Sajib MS, Zahra FT, Tullar P, Zabet-Moghaddam M, Zheng Y, et al. Angiopoietin-2-induced lymphatic endothelial cell migration drives lymphangiogenesis via the beta1 integrin-RhoA-formin axis. Angiogenesis 2022;25:373–96.

[10] Neumann E, Lefèvre S, Zimmermann B, Geyer M, Lehr A, Umscheid T, et al. Migratory potential of rheumatoid arthritis synovial fibroblasts: additional perspectives. Cell Cycle 2010;9:2286–91.

[11] Smith MH, Gao VR, Periyakoil PK, Kochen A, DiCarlo EF, Goodman SM, et al. Drivers of heterogeneity in synovial fibroblasts in rheumatoid arthritis. Nat Immunol 2023;24:1200–10.

[12] Wei K, Korsunsky I, Marshall JL, Gao A, Watts GFM, Major T, et al. Notch signalling drives synovial fibroblast identity and arthritis pathology. Nature 2020;582:259–64.

[13] Bartok B, Firestein GS. Fibroblast-like synoviocytes: key effector cells in rheumatoid arthritis. Immunol Rev 2010;233:233–55.

[14] Lefèvre S, Knedla A, Tennie C, Kampmann A, Wunrau C, Dinser R, et al. Synovial fibroblasts spread rheumatoid arthritis to unaffected joints. Nat Med 2009;15:1414–20.

[15] Kamphaus GD, Colorado PC, Panka DJ, Hopfer H, Ramchandran R, Torre A, et al. Canstatin, a novel matrix-derived inhibitor of angiogenesis and tumor growth. J Biol Chem 2000;275:1209–15.

[16] Poduval P, Sillat T, Beklen A, Kouri VP, Virtanen I, Konttinen YT. Type IV collagen alpha-chain composition in synovial lining from trauma patients and patients with rheumatoid arthritis. Arthritis Rheum 2007;56:3959–67.

[17] Hwang-Bo J, Yoo KH, Park JH, Jeong HS, Chung IS. Recombinant canstatin inhibits angiopoietin-1-induced angiogenesis and lymphangiogenesis. Int J Cancer 2012;131:298–309.

[18] Lefèvre S, Schwarz M, Meier FMP, Zimmermann-Geller B, Tarner IH, Rickert M, et al. Disease-specific effects of matrix and growth factors on adhesion and migration of rheumatoid synovial fibroblasts. J Immunol 2017;198:4588–95.

[19] Bainbridge P. Wound healing and the role of fibroblasts. J Wound Care 2013;22:407–8 410-12.

[20] Elshabrawy HA, Volin MV, Essani AB, Chen Z, McInnes IB, Van Raemdonck K, et al. IL-11 facilitates a novel connection between RA joint fibroblasts and endothelial cells. Angiogenesis 2018;21:215–28.

[21] Urbantat RM, Blank A, Kremenetskaia I, Vajkoczy P, Acker G, Brandenburg S. The CXCL2/IL8/CXCR2 pathway is relevant for brain tumor malignancy and endothelial cell function. Int J Mol Sci 2021;22:2634.

[22] Faber JE, Chilian WM, Deindl E, van Royen N, Simons M. A brief etymology of the collateral circulation. Arterioscler Thromb Vasc Biol 2014;34:1854–9.

[23] Ginsberg MD. The cerebral collateral circulation: Relevance to pathophysiology and treatment of stroke. Neuropharmacology 2018;134:280–92.

[24] Nishijima Y, Akamatsu Y, Weinstein PR, Liu J. Collaterals: implications in cerebral ischemic diseases and therapeutic interventions. Brain Res 2015;1623:18–29.

[25] Schaper W. Collateral circulation: past and present. Basic Res Cardiol 2009;104:5–21.

[26] Schirmer SH, van Nooijen FC, Piek JJ, van Royen N. Stimulation of collateral artery growth: travelling further down the road to clinical application. Heart 2009;95:191–7.

[27] Zhang H, Chalothorn D, Faber JE. Collateral vessels have unique endothelial and smooth muscle cell phenotypes. Int J Mol Sci 2019;20:3608.

[28] Lekas M, Lekas P, Mei SH, Deng Y, Dumont DJ, Stewart DJ. Tie2-dependent neovascularization of the ischemic hindlimb is mediated by angiopoietin-2. PLoS One 2012;7:e43568.

[29] Swaminathan B, Youn SW, Naiche LA, Du J, Villa SR, Metz JB, et al. Endothelial Notch signaling directly regulates the small GTPase RND1 to facilitate Notch suppression of endothelial migration. Sci Rep 2022;12:1655.

[30] Cai WJ, Kocsis E, Luo X, Schaper W, Schaper J. Expression of endothelial nitric oxide synthase in the vascular wall during arteriogenesis. Mol Cell Biochem 2004;264:193–200.

[31] Ospelt C, Gay S, Klein K. Epigenetics in the pathogenesis of RA. Semin Immunopathol 2017;39:409–19.

[32] Lucitti JL, Mackey JK, Morrison JC, Haigh JJ, Adams RH, Faber JE. Formation of the collateral circulation is regulated by vascular endothelial growth factor-A and a disintegrin and metalloprotease family members 10 and 17. Circ Res 2012;111:1539–50.

[33] Kayakabe K, Kuroiwa T, Sakurai N, Ikeuchi H, Kadiombo AT, Sakairi T, et al. Interleukin-6 promotes destabilized angiogenesis by modulating angiopoietin expression in rheumatoid arthritis. Rheumatology (Oxford) 2012; 51:1571–9.

[34] Wu JC, Yan HC, Chen WT, Chen WH, Wang CJ, Chi YC, et al. JNK signaling pathway is required for bFGF-mediated surface cadherin downregulation on HUVEC. Exp Cell Res 2008;314:421–9.

[35] Biswas SK, Lopez-Collazo E. Endotoxin tolerance: new mechanisms, molecules and clinical significance. Trends Immunol 2009;30:475–87.

[36] Foster SL, Hargreaves DC, Medzhitov R. Gene-specific control of inflammation by TLR-induced chromatin modifications. Nature 2007;447:972–8.

[37] Foster SL, Medzhitov R. Gene-specific control of the TLR-induced inflammatory response. Clin Immunol 2009;130:7–15.

[38] Seeley JJ, Ghosh S. Tolerization of inflammatory gene expression. Cold Spring Harb Symp Quant Biol 2013;78:69–79.

[39] Crowley T, O'Neil JD, Adams H, Thomas AM, Filer A, Buckley CD, et al. Priming in response to pro-inflammatory cytokines is a feature of adult synovial but not dermal fibroblasts. Arthritis Res Ther 2017;19:35.

[40] Friščić J, Böttcher M, Reinwald C, Bruns H, Wirth B, Popp SJ, et al. The complement system drives local inflammatory tissue priming by metabolic reprogramming of synovial fibroblasts. Immunity 2021;54:1002–1021.e10.

[41] Du X, Williams DA. Interleukin-11: review of molecular, cell biology, and clinical use. Blood 1997;89:3897–908.

[42] Rebustini IT, Myers C, Lassiter KS, Surmak A, Szabova L, Holmbeck K, et al. MT2-MMP-dependent release of collagen IV NC1 domains regulates submandibular gland branching morphogenesis. Dev Cell 2009;17:482–93.

[43] Hou WH, Wang TY, Yuan BM, Chai YR, Jia YL, Tian F, et al. Recombinant mouse canstatin inhibits chicken embryo chorioallantoic membrane angiogenesis and endothelial cell proliferation. Acta Biochim Biophys Sin (Shanghai) 2004;36:845–50.

[44] Magnon C, Opolon P, Ricard M, Connault E, Ardouin P, Galaup A, et al. Radiation and inhibition of angiogenesis by canstatin synergize to induce HIF-1alpha-mediated tumor apoptotic switch. J Clin Invest 2007;117:1844–55.

[45] Zhu L, Guo Z, Zhang J, Yang Y, Liu C, Zhang L, et al. Recombinant human arresten and canstatin inhibit angiogenic behaviors of HUVECs via inhibiting the PI3K/Akt signaling pathway. Int J Mol Sci 2022;23:8995.

[46] Kanazawa H, Imoto K, Okada M, Yamawaki H. Canstatin inhibits hypoxia-induced apoptosis through activation of integrin/focal adhesion kinase/Akt signaling pathway in H9c2 cardiomyoblasts. PLoS One 2017;12:e0173051.

[47] Okada M, Morioka S, Kanazawa H, Yamawaki H. Canstatin inhibits isoproterenol-induced apoptosis through preserving mitochondrial morphology in differentiated H9c2 cardiomyoblasts. Apoptosis 2016;21:887–95.

[48] Panka DJ, Mier JW. Canstatin inhibits Akt activation and induces Fas-dependent apoptosis in endothelial cells. J Biol Chem 2003;278:37632–6.

[49] Xing YN, Deng P, Xu HM. Canstatin induces apoptosis in gastric cancer xenograft growth in mice through the mitochondrial apoptotic pathway. Biosci Rep 2014;34:e00106.

[50] Davis S, Aldrich TH, Jones PF, Acheson A, Compton DL, Jain V, et al. Isolation of angiopoietin-1, a ligand for the TIE2 receptor, by secretion-trap expression cloning. Cell 1996;87:1161–9.

Psoriatic arthritis

Inhibition of structural damage progression with the selective interleukin-23 inhibitor guselkumab in participants with active PsA: results through week 24 of the phase 3b, randomised, double-blind, placebo-controlled APEX study

Philip J. Mease [1,2,*], Christopher T. Ritchlin [3], Laura C. Coates [4],
Alexa P. Kollmeier [5], Bei Zhou [6], Yusang Jiang [6], Karen Bensley [6], Koeun Im [7],
Rattandeep Batra [8], Soumya D. Chakravarty [9,10], Proton Rahman [11],
Désirée van der Heijde [12]

[1] Rheumatology Research, Providence Swedish Medical Center, Seattle, WA, USA
[2] University of Washington School of Medicine, Seattle, WA, USA
[3] Department of Medicine, Allergy/Immunology and Rheumatology, University of Rochester Medical Center, Rochester, NY, USA
[4] Nuffield Department of Orthopaedics, Rheumatology and Musculoskeletal Sciences, University of Oxford, Botnar Research Centre, Oxford, UK
[5] Johnson & Johnson, San Diego, CA, USA
[6] Johnson & Johnson, Spring House, PA, USA
[7] Johnson & Johnson, Cambridge, MA, USA
[8] Johnson & Johnson, Toronto, ON, Canada
[9] Johnson & Johnson, Horsham, PA, USA
[10] Drexel University College of Medicine, Philadelphia, PA, USA
[11] Craig L Dobbin Genetics Research Centre, Faculty of Medicine, Division of Rheumatology, Memorial University of Newfoundland, St. Johns, NL, Canada
[12] Leiden University Medical Center, Leiden, The Netherlands

ARTICLE INFO

ABSTRACT

Objectives: The APEX study evaluated the effects of guselkumab, a fully human, dual-acting monoclonal antibody able to bind CD64 and selectively inhibit the interleukin (IL)-23p19 subunit, on clinical and radiographic outcomes in active psoriatic arthritis (PsA).
Methods: APEX (ongoing, phase 3b, double-blind, placebo-controlled) randomised (5:7:7) biologic-naïve adults with active PsA (≥3 tender, ≥3 swollen joints; C-reactive protein ≥0.3 mg/dL; ≥2 erosive joints) to subcutaneous guselkumab 100 mg every 4 weeks (Q4W); guselkumab 100 mg at week 0, week 4, then every 8 weeks (Q8W); or placebo every 4 weeks. Primary (proportion of participants achieving ≥20% improvement in American College of Rheumatology response criteria [ACR20]) and major secondary (total PsA-modified van der Heijde-Sharp [vdH-S] score least squares mean [LSM] change from baseline) endpoints at week 24 were multiplicity-controlled for comparing each guselkumab group versus placebo.

*Correspondence to Dr. Philip J. Mease, Rheumatology Research, Providence Swedish Medical Center, Seattle, WA, USA.
E-mail address: pmease@philipmease.com (P.J. Mease).
Handling editor Josef S. Smolen.

Results: Among 1020 participants (Q4W: 273; Q8W: 371; placebo: 376), significantly greater proportions of participants receiving guselkumab Q4W (66.6%) and Q8W (68.3%) versus placebo (47.0%) achieved ACR20 at week 24 (both $P < 0.001$). Baseline mean total vdH-S scores were 26.7 to 27.7 across groups; guselkumab Q4W- and Q8W-treated participants exhibited significantly lower rates of radiographic progression versus placebo at week 24 (total vdH-S score LSM change: 0.55 and 0.54 vs 1.35; $P = 0.002$ and $P < 0.001$, respectively). Through week 24, 38.2%, 42.5%, and 37.3% of participants receiving guselkumab Q4W, Q8W, and placebo, respectively, had ≥1 adverse event, with no new safety signals.

Conclusions: Guselkumab, a fully human monoclonal antibody able to bind CD64 and simultaneously inhibit the IL-23p19 subunit, provided significantly higher rates of clinical improvement and significant inhibition of structural damage progression versus placebo, with no new safety signals, at week 24 in biologic-naïve participants with active and erosive PsA.

WHAT IS ALREADY KNOWN ON THIS TOPIC

- Substantial proportions of patients with psoriatic arthritis (PsA) exhibit structural joint damage, which can be monitored via standard radiography and quantified using the PsA-modified van der Heijde-Sharp score. Radiographic progression in PsA is associated with impaired physical function, diminished health-related quality of life, and long-term disability. Guselkumab is a monoclonal antibody that selectively and potently binds and inhibits the p19 subunit of interleukin (IL)-23, a key regulator in the inflammatory pathways involved in PsA. Guselkumab 100 mg administered subcutaneously at week 0, week 4, then every 8 weeks has been approved worldwide to treat the signs and symptoms of active PsA. To date, no IL-23p19-subunit inhibitor has been approved by the United States Food and Drug Administration for inhibition of structural joint damage progression.

WHAT THIS STUDY ADDS

- The global, phase 3b, randomised, placebo-controlled APEX study was designed to further evaluate the effects of 2 guselkumab dosing regimens on clinical and radiographic outcomes and safety in participants with active PsA. Among the 1020 participants evaluated for efficacy, those receiving either guselkumab every 4 or 8 weeks demonstrated statistically significantly lower rates of radiographic progression at week 24 than did those receiving placebo (major secondary endpoint); guselkumab slowed rates of both erosion and joint space narrowing progression. Additionally, while the efficacy of guselkumab on nail disease has been evaluated in participants with psoriasis, this was now assessed for the first time in a phase 3 study dedicated to participants with PsA. Guselkumab-treated participants demonstrated mean percent improvements in psoriatic nail disease at week 24 versus worsening with placebo. Outcomes assessing improvements in the American College of Rheumatology response criteria and almost clear/completely clear skin and safety findings through 6 months of guselkumab were consistent with its known therapeutic profile in active PsA and moderate-to-severe psoriasis.

HOW THIS STUDY MIGHT AFFECT RESEARCH, PRACTICE OR POLICY

- Inhibiting progression of structural joint damage is an important treatment goal for patients with active PsA and their treating clinicians. Together with previous studies demonstrating the significant multidomain efficacy (including novel APEX results exhibiting improvements in psoriatic nail disease) and favourable safety profile of guselkumab, radiographic findings from APEX now establish guselkumab as the only therapy targeting the IL-23p19 subunit to comprehensively address treatment goals, including preservation of joint health, that are of high importance to patients and health care providers.

INTRODUCTION

Psoriatic arthritis (PsA), a chronic, heterogeneous, inflammatory disease affecting the joints and skin, can substantially diminish health-related quality of life (HRQoL) [1,2]. The persistent inflammation seen in PsA can lead to joint destruction, visualised as erosions and joint space narrowing (JSN) by standard radiography [3]. Progressive joint damage in PsA is associated with substantial impairment of physical function and higher levels of disability [4,5]. Diagnostic delays as short as 6 months have been associated with development of erosive disease and poorer physical function [6]. In observational studies, 25% to 39% of patients with early PsA had erosions visible on standard radiography [7,8] and up to 47% exhibited damage within the first 2 years [6]. Therefore, inhibiting progression of structural joint damage is a key treatment goal for patients with PsA.

International PsA treatment recommendations support using biologics for patients with active disease despite use of conventional synthetic disease-modifying antirheumatic drugs (csDMARDs) or with poor prognostic indicators, including radiographic damage [9−11]. The biologic DMARD guselkumab, a fully human, dual-acting monoclonal antibody that selectively inhibits the interleukin (IL)-23p19 subunit, is approved to treat moderate-to-severe plaque psoriasis, active PsA, and moderately-to-severely active ulcerative colitis and Crohn's disease [12,13]. In phase 3 studies of adults with active PsA, guselkumab (100 mg every 4 weeks [Q4W] or at weeks 0 and 4 then every 8 weeks [Q8W]) demonstrated significant improvements across disease domains, and in physical function and HRQoL, compared with placebo [14−16]. Guselkumab benefits were sustained through up to 2 years of treatment while maintaining a favourable safety profile [14,17−19]. In DISCOVER-2 (biologic-naïve population), participants receiving guselkumab Q4W exhibited significantly less radiographic progression at week 24 (assessed by PsA-modified van der Heijde-Sharpe [vdH-S] score) versus placebo; the numerically lower rates of radiographic progression seen with guselkumab Q8W compared with placebo were not statistically significant [16]. Guselkumab Q8W is globally approved to treat the signs and symptoms of active PsA [12]. In the European Union, the Q4W regimen is approved for use in patients at high risk of joint damage [20].

The phase 3b APEX study (NCT04882098) is further evaluating the effects of both guselkumab dosing regimens (Q4W and Q8W) on PsA signs and symptoms and radiographic progression in a population with active and erosive disease. Here, we report primary efficacy and safety results for the double-blind placebo-controlled phase (weeks 0-24) of this 3-year study.

METHODS

Participants and study design

APEX is an ongoing phase 3b, multicentre, randomised, double-blind, placebo-controlled study [21]. Eligible adults had PsA for ≥6 months; met the ClASsification criteria for Psoriatic ARthritis [22]; had active disease (≥3 swollen joints, ≥3 tender joints, C-reactive protein [CRP] ≥0.3 mg/dL) despite treatment with standard nonbiologic therapies (ie, csDMARDs, apremilast, and/or nonsteroidal anti-inflammatory drugs [NSAIDs]), ≥2 erosive joints on baseline radiographs of the hands and feet (centrally read by 2 readers with an adjudicator); and ≥1 psoriatic plaque ≥2 cm or psoriatic nail changes.

Individuals with arthritis mutilans or other inflammatory disease that could confound efficacy evaluations and those with unstable suicidal ideation or suicidal behaviour within 6 months of screening were excluded. Participants were naïve to biologics and Janus kinase inhibitors; the following were not permitted within the specified timeframe prior to the first study agent administration: topical (2 weeks), systemic (4 weeks), or phototherapy (4 weeks) treatment that could confound psoriasis evaluations; systemic immunosuppressants (4 weeks); csDMARDs (other than methotrexate [MTX], sulfasalazine, hydroxychloroquine, or leflunomide; 4 weeks); experimental antibody or biological therapy (6 months); intramuscular or intravenous corticosteroids (4 weeks); or lithium (4 weeks).

Participants were randomised (5:7:7) to subcutaneous administration of guselkumab 100 mg Q4W; guselkumab 100 mg at weeks 0, 4, then Q8W; or placebo with crossover to guselkumab Q4W at week 24. Concomitant stable NSAIDs, oral corticosteroids (≤10 mg/d prednisone equivalent), and select csDMARDs (MTX [≤25 mg/wk], sulfasalazine [≤3 g/d], hydroxychloroquine [≤400 mg/d], and leflunomide [≤20 mg/d]) were permitted. Through week 24, participants could not receive >2 concomitant csDMARDs or MTX with leflunomide. At week 16, participants with <20% improvement from baseline in both swollen and tender joint counts (SJC/TJC) qualified for early escape and could initiate or increase the dose of 1 permitted concomitant medication (up to allowed maximum dose) at the investigator's discretion.

APEX is being conducted in accordance with the Declaration of Helsinki and Good Clinical Practice guidelines. An Institutional Review Board (IRB) or Ethics Committee at each site (central IRB in the United States: Advarra; Pro00049187) approved the protocol. All participants provided written informed consent. Neither patients nor members of the public were involved in the design, conduct, reporting, or dissemination plans of this research.

Randomisation and masking

Treatment group assignments employed randomly permuted blocks and 4 composite stratification levels: 1 level comprised participants with baseline radiographs exhibiting a high degree of variability between the readers and 3 stratification levels characterised participants based on predicted risk of progression. Informed by prior studies of participants with PsA [21], a combination of concomitant corticosteroid use (yes/no), baseline number of erosive joints, difference between readers in the baseline number of erosive joints, and/or most recently determined serum CRP level classified participants as having high radiographic variability, no progression risk (NP), low-to-moderate progression risk (LMP), or risk of rapid progression (RP)

(Supplementary Methods). Guselkumab and placebo were provided in identical prefilled syringes; all participants received the same number of injections at all timepoints. Participants, investigators, and study site staff remained blinded to treatment assignments through week 48.

Assessments

Clinician assessments of joint disease included SJC (0-66), TJC (0-68), and physician's global assessment of disease activity (visual analogue scale [VAS] 0-10). Dactylitis and enthesitis were evaluated using the Dactylitis Severity Score (DSS; 0 = none; 4 = severe; total = 0-60) [23,24] and Leeds enthesitis index (LEI; presence or absence of pain at each of 6 anatomical locations; total = 0-6 [25]), respectively. A blinded independent assessor determined joint counts, DSS, and LEI.

Psoriatic skin disease activity was assessed using the Psoriasis Area and Severity Index (PASI; 0-72) [26] and Investigator's Global Assessment (IGA) of psoriasis (0 = clear; 4 = severe) [27]. The modified Nail Psoriasis Severity Index (mNAPSI) [28] assessed each fingernail for pitting, onycholysis, oil-drop dyschromia, crumbling, leukonychia, splinter haemorrhages, hyperkeratosis, and red spot in the lunula (range: each nail 0-13; total 0-130). Participants reported their pain (Patient's Assessment of Pain; VAS 0-10 cm), physical function (Health Assessment Questionnaire-Disability Index [HAQ-DI]; 0-3) [29], and overall disease activity (Patient's Global Assessment of Disease Activity [arthritis]; VAS 0-10 cm), which are components of the American College of Rheumatology (ACR) response criteria [30].

Radiographs of the hands (posteroanterior) and feet (anteroposterior) were obtained at baseline and week 24. Radiographic progression was evaluated using the PsA-modified vdH-S score that assesses erosions and JSN in 40 joints of the hands and 12 joints of the feet with separate annotation of pencil-in-cup (PIC) and gross osteolysis (GO) deformities (maximal erosion score [320] + maximal JSN score [208] = maximal total score [528]) [31,32]. Images were scored independently by 2 blinded central readers and a blinded adjudicator (if the absolute difference between the 2 readers' change scores was ≥3). Scores from the 2 readers (or the adjudicator and 1 reader with the closest score) were averaged to determine the change score per patient. The smallest detectable change and interreader agreement were determined (Supplementary Methods).

Participants were monitored for adverse events (AEs). Serum samples were collected at regular intervals to measure haematology and chemistry laboratory parameters and determine the presence of antibodies to guselkumab (validated immunoassay method).

Outcomes

The primary and major secondary endpoints at week 24 were the proportion of participants achieving ≥20% improvement in the ACR response criteria (ACR20) [30] and least squares mean (LSM) change from baseline in total PsA-modified vdH-S score. Other secondary endpoints included the proportions of participants achieving ACR20, ACR50 (≥50% improvement), and ACR70 (≥70% improvement) over time; no radiographic progression at week 24 (2 definitions: change in PsA-modified vdH-S score ≤0 and ≤0.5); and minimal disease activity (MDA) [33] at week 24. LSM changes in DSS and LEI and LSM percent change in mNAPSI at week 24 were assessed among those affected at baseline (score >0). LSM change from baseline in HAQ-DI was also determined at week 24.

Among participants with ≥3% psoriatic body surface area (BSA) and IGA ≥2 at baseline, response rates for achieving ≥90% or 100% improvement in PASI (PASI 90/PASI 100), clear or almost clear skin (IGA 0/1 response: IGA of 0 or 1 and ≥2-grade improvement from baseline), and completely clear skin (IGA 0) at week 24 were determined.

Statistical analyses

Assuming a 60% ACR20 response rate at week 24 with guselkumab versus 35% with placebo, sample sizes of 250, 350, and 350 for the Q4W, Q8W, and placebo groups, respectively, were estimated to provide >99% statistical power to detect a significant treatment difference for each guselkumab regimen using a 2-sided Chi-square test at a significance level of $\alpha = 0.05$. Assuming respective overall mean (SD) changes from baseline in total PsA-modified vdH-S score of 0.25 (3.1), 0.45 (3.1), and 1.13 (3.2), sample sizes of 250, 350, and 350 were estimated to provide ≥90% (Q4W vs placebo) and 80% (Q8W vs placebo) power to detect a significant treatment difference (2-sided $\alpha = 0.05$).

Treatment group differences for the primary and major secondary endpoints were tested in the following sequence, only if all preceding endpoints demonstrated significance versus placebo: ACR20 at week 24 for (1) Q4W versus placebo and (2) Q8W versus placebo and change in PsA-modified vdH-S score from baseline to week 24 for (3) Q4W versus placebo and (4) Q8W versus placebo. Other P values were not multiplicity-controlled and considered nominal.

Efficacy data were analysed by randomised treatment group. Participants from Ukrainian sites rendered unable to support key study operations (ie, all participants were projected to miss primary and major secondary endpoint assessments or to miss ≥2 doses of study intervention prior to week 24) were excluded from efficacy analyses. The resulting population constitutes the modified full analysis set (mFAS). For analyses of ACR20/50/70 through week 24, participants who met treatment failure criteria (discontinued study agent for any reason other than natural disaster [ND; COVID-19 pandemic] or major disruption [MD; Ukraine/Russia crisis]; initiated or increased the dose of csDMARDs or oral corticosteroids; or initiated protocol-prohibited therapy for PsA) were considered nonresponders. Data from participants who discontinued study agent or with severe treatment noncompliance due to ND/MD were imputed using multiple imputation (MI) at all subsequent timepoints or at the next timepoint, respectively. Other missing data were imputed using nonresponder imputation (NRI). Severe noncompliance was defined as missing ≥30% of doses prior to a given timepoint, ie, ≥2 doses for week 24 analyses. The mean response rate, over the 200 MI datasets, was reported. Treatment group comparisons were based on the combined standardised Wilson-Hilferty transformation of the Cochran-Mantel-Haenszel test statistic, stratified by composite randomisation levels, from each MI dataset.

For changes from baseline in total PsA-modified vdH-S score and erosion/JSN subscores at week 24, data from participants with discontinuation of study agent/severe noncompliance due to ND/MD were not used, and MI was employed for all missing data; treatment failure rules were not applied. LSM changes and corresponding P values between each guselkumab and placebo groups were determined using an analysis of covariance model including baseline PsA-modified vdH-S score, treatment group, and composite stratification levels. The proportion of participants with no progression was determined similarly; P values were determined by standardised Wilson-Hilferty transformation of the Cochran-Mantel-Haenszel test statistic, stratified by composite randomisation levels, from each MI dataset. LSM changes in PsA-modified vdH-S score and response rates for achieving change ≤0 were determined (post hoc) among participants in the NP, LMP, and RP stratification levels.

Sensitivity analyses including all randomised participants and employing different approaches for handling missing data and model covariates were performed to evaluate the robustness of the primary and major secondary endpoints (Supplementary Methods).

For all other secondary outcomes at week 24, after application of treatment failure rules, data from participants with study agent discontinuation/severe noncompliance due to ND/MD were not used. For binary endpoints, any other missing data were imputed by NRI; response rates and P values were determined using a generalised linear mixed model. For continuous endpoints, other missing data were not imputed; LSM changes and P values were determined using mixed-effect model for repeated measures. Both models included treatment group, visit, an interaction term of visit with treatment group, and composite stratification level.

Safety analyses included all participants who received ≥1 study agent administration. The frequency and types of AEs were summarised by actual treatment received. Major adverse cardiovascular events (MACEs) were prespecified as nonfatal myocardial infarction, nonfatal stroke, and cardiovascular death. Common Terminology Criteria for Adverse Events (CTCAE 5.0) maximum toxicity grades were used to determine abnormalities in aspartate aminotransferase (AST) and alanine aminotransferase (ALT) levels; results were summarised by randomised treatment group and concomitant MTX use.

RESULTS

Participants

The 247 study sites across 29 countries in 4 regions (Supplementary Results) screened 2811 patients and enrolled and randomised 1054 participants. Data were collected from June 17, 2021, through December 30, 2024. Thirty-four participants from 5 Ukrainian sites (unable to carry out key study operations due to MD) were excluded from efficacy analyses. In the resulting mFAS of 1020 participants (Q4W 273; Q8W 371; placebo 376), a majority met the criteria for the composite stratification NP level (n = 588; 57.6%) followed by LMP (n = 267; 26.2%), RP (n = 94; 9.2%), and high radiographic variability (n = 71; 7.0%; Supplementary Fig S1). Through week 24, 38 participants (Q4W 3.3%; Q8W 4.0%; placebo 3.7%) discontinued the study agent; ≥96% in each group completed study treatment (Supplementary Fig S1).

Baseline characteristics of the mFAS were well balanced across treatment groups (Table 1). The mean age was 53 years, 55% were male, and 83% were White. Baseline disease characteristics were consistent with established moderately-to-severely active PsA (mean duration ~7 years; SJC 11.9; TJC 20.7), with moderately impaired physical function (mean HAQ-DI 1.2). Mean erosion (13.4-13.7), JSN (13.3-14.0), and total (26.7-27.7) PsA-modified vdH-S scores were similar across treatment groups.

Efficacy

The primary and major secondary endpoints were met. Significantly greater proportions of participants receiving

Table 1

Baseline demographics, disease characteristics, and prior and concomitant medications for APEX participants[a]

	Guselkumab 100 mg		Placebo (N = 376)	Total (N = 1020)
	Q4W (N = 273)	Q8W (N = 371)		
Demographics				
Age, y	52.2 ± 13.2	53.2 ± 12.9	53.5 ± 13.0	53.0 ± 13.0
Sex[b]				
Female	124 (45.4)	172 (46.4)	163 (43.4)	459 (45.0)
Male	149 (54.6)	199 (53.6)	213 (56.6)	561 (55.0)
Race				
White	233 (85.3)	305 (82.2)	311 (82.7)	849 (83.2)
Asian	38 (13.9)	61 (16.4)	61 (16.2)	160 (15.7)
Native Hawaiian or Other Pacific Islander	2 (0.7)	2 (0.5)	0	4 (0.4)
American Indian or Alaska Native	0	0	2 (0.5)	2 (0.2)
Black or African American	0	2 (0.5)	0	2 (0.2)
Not reported	0	1 (0.3)	1 (0.3)	2 (0.2)
Weight, kg	85.6 ± 20.1	83.2 ± 17.4	83.1 ± 18.2	83.8 ± 18.5
BMI, kg/m^2	29.4 ± 6.0	29.0 ± 5.6	28.9 ± 5.7	29.1 ± 5.7
Disease characteristics				
PsA duration, y	7.5 ± 7.1	7.2 ± 7.6	7.2 ± 6.9	7.3 ± 7.2
ACR response components				
Number of swollen joints, 0-66	11.6 ± 9.4	12.1 ± 8.5	11.8 ± 8.9	11.9 ± 8.9
Number of tender joints, 0-68	21.2 ± 14.6	20.6 ± 13.4	20.5 ± 13.9	20.7 ± 13.9
Physician's global assessment, 0-10 cm VAS	6.4 ± 1.6	6.4 ± 1.6	6.2 ± 1.7	6.3 ± 1.7
Patient's assessment of pain, 0-10 cm VAS	5.9 ± 2.2	5.9 ± 2.1	5.9 ± 2.1	5.9 ± 2.1
Patient's global assessment, 0-10 cm VAS	5.9 ± 2.2	5.9 ± 2.1	5.9 ± 2.0	5.9 ± 2.1
HAQ-DI, 0-3	1.2 ± 0.7	1.2 ± 0.6	1.2 ± 0.7	1.2 ± 0.7
CRP, mg/dL	1.7 ± 2.9	1.5 ± 2.0	1.7 ± 2.5	1.6 ± 2.5
Radiographic damage				
PsA-modified vdH-S score, 0-528	27.7 ± 47.6	26.7 ± 43.4	26.8 ± 42.2	27.0 ± 44.1
Erosion score, 0-320	13.7 ± 24.3	13.4 ± 21.9	13.4 ± 20.7	13.5 ± 22.1
JSN score, 0-208	14.0 ± 24.2	13.3 ± 22.8	13.4 ± 22.4	13.5 ± 23.0
Psoriasis assessments				
Psoriatic BSA, 0-100%	15.0 (19.2)	16.5 (21.9)	16.3 (21.5)	16.0 (21.0)
IGA, N	269	364	370	1003
2	81 (30.1)	134 (36.8)	137 (37.0)	352 (35.1)
3	92 (34.2)	115 (31.6)	117 (31.6)	324 (32.3)
4	15 (5.6)	25 (6.9)	31 (8.4)	71 (7.1)
Participants with BSA ≥3% and IGA ≥2	159 (58.2)	231 (62.3)	223 (59.3)	613 (60.1)
PASI score, 0-72	7.6 ± 8.3	8.3 ± 10.1	8.2 ± 9.5	8.1 ± 9.4
mNAPSI, N	269	364	369	1002
Participants with mNAPSI >0	163 (60.6)	228 (62.6)	257 (69.6)	648 (64.7)
Score, 0-130	23.4 ± 22.8	19.8 ± 20.3	19.4 ± 18.7	20.6 ± 20.4
Dactylitis and enthesitis				
Participants with dactylitis	119/271 (43.9)	143/364 (39.3)	167/372 (44.9)	429/1007 (42.6)
DSS, 1-60	10.8 ± 11.5	11.0 ± 12.8	10.2 ± 10.5	10.6 ± 11.6
Participants with enthesitis	157/271 (57.9)	214/365 (58.6)	218/372 (58.6)	589/1008 (58.4)
LEI score, 1-6	3.2 ± 1.8	3.0 ± 1.7	3.0 ± 1.6	3.1 ± 1.7
Prior and concomitant medications				
Prior medications				
csDMARDs	248 (90.8)	345 (93.0)	340 (90.4)	933 (91.5)
2	57 (20.9)	82 (22.1)	79 (21.0)	218 (21.4)
≥3	9 (3.3)	21 (5.7)	16 (4.3)	46 (4.5)
Apremilast	4 (1.5)	11 (3.0)	7 (1.9)	22 (2.2)
Concomitant medications at baseline				
csDMARDs	181 (66.3)	256 (69.0)	256 (68.1)	693 (67.9)
MTX	161 (59.0)	222 (59.8)	226 (60.1)	609 (59.7)
Dose, mg/wk	15.0 ± 4.3	15.0 ± 4.3	15.0 ± 4.5	15.0 ± 4.4
2 csDMARDs	6 (2.2)	13 (3.5)	6 (1.6)	25 (2.5)
Oral corticosteroids	43 (15.8)	54 (14.6)	71 (18.9)	168 (16.5)
Dose equivalent to prednisone, mg/d	6.2 ± 2.4	6.0 ± 2.7	5.5 ± 1.9	5.8 ± 2.3
NSAIDs	161 (59.0)	199 (53.6)	222 (59.0)	582 (57.1)

ACR, American College of Rheumatology; BMI, body mass index; BSA, body surface area; CRP, C-reactive protein; csDMARD, conventional synthetic disease-modifying antirheumatic drug; DSS, Dactylitis Severity Score; HAQ-DI, Health Assessment Questionnaire-Disability Index; IGA, Investigator's Global Assessment of psoriasis; JSN, joint space narrowing; LEI, Leeds enthesitis index; mNAPSI, modified Nail Psoriasis Severity Index; MTX, methotrexate; NSAID, nonsteroidal anti-inflammatory drug; PASI, Psoriasis Area and Severity Index; PsA, psoriatic arthritis; Q4/8W, every 4/8 weeks; VAS, visual analogue scale; vdH-S, van der Heijde-Sharp.

Data are mean ± SD, n (%), or n/N (%) unless otherwise noted.

[a] Baseline characteristics are reported for the modified full analysis set, excluding 34 participants who were enrolled at 5 sites in Ukraine that could not carry out key study operations.

[b] Participant sex was reported by the investigators by selecting one of the following options: female, male, unknown, or undifferentiated.
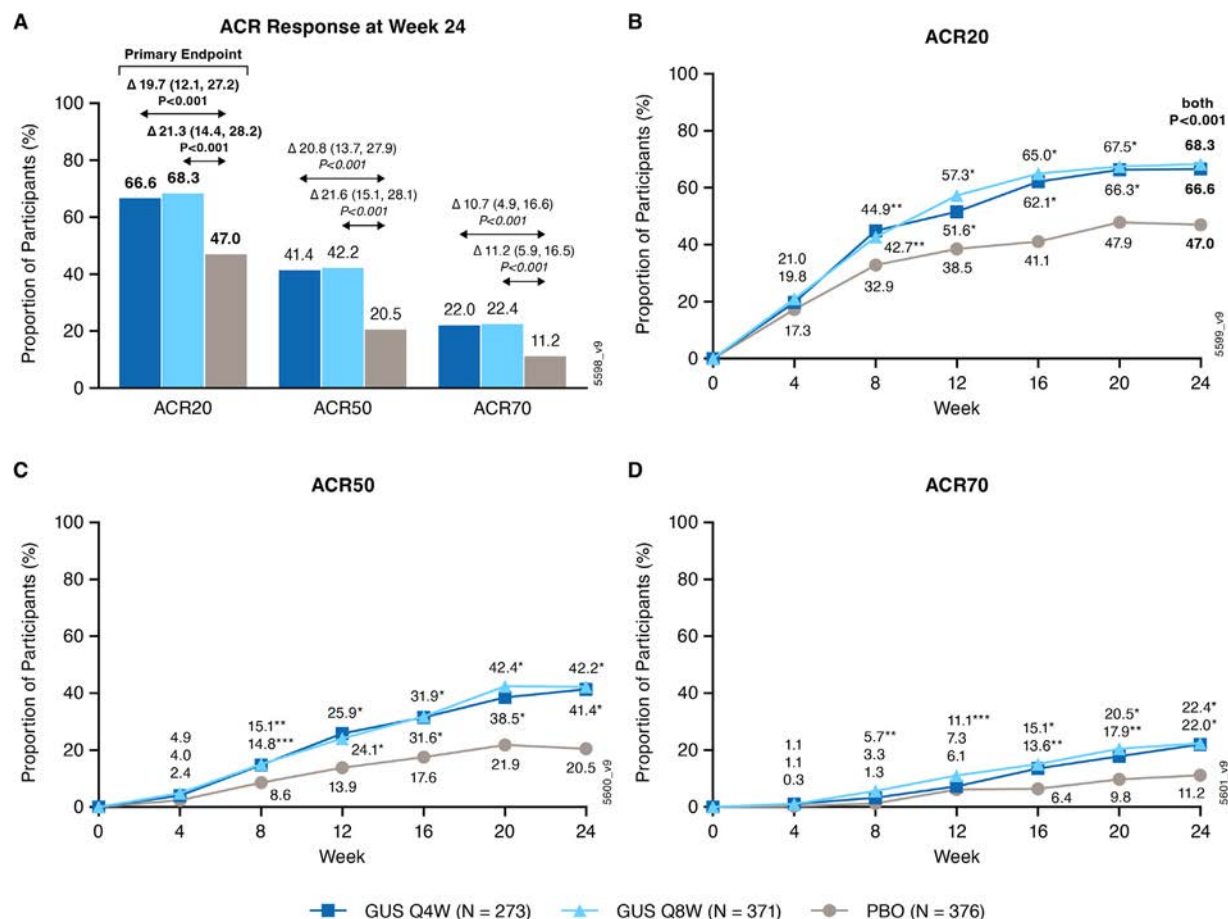
Figure 1. ACR20, ACR50, and ACR70 responses at week 24 (A) and over time (B, C, D). Nominal *$P \leq 0.001$, **$P < 0.01$, ***$P < 0.05$ versus placebo. Italicised P values in panel A are nominal. Data presented as proportion of patients achieving ACR20/50/70 response with adjusted rate differences (95% CI) between each guselkumab group and the placebo group based on the combined Wald statistic (with the Cochran-Mantel-Haenszel weight) for each multiple imputation dataset. ACR20/50/70, $\geq 20\%/\geq 50\%/\geq 70\%$ improvement in the American College of Rheumatology response criteria; GUS, guselkumab; PBO, placebo; Q4W/Q8W, every 4/8 weeks.

guselkumab Q4W (66.6%) and Q8W (68.3%) versus placebo (47.0%) achieved ACR20 response at week 24 (both multiplicity-controlled $P < 0.001$; Fig 1A, B). Results were consistent across primary endpoint sensitivity analyses (Supplementary Fig S2; Supplementary Table S1). Higher proportions of participants in the Q4W and Q8W versus placebo groups achieved the more stringent ACR50 (41.4% and 42.2% vs 20.5%, respectively; both nominal $P < 0.001$) and ACR70 (22.0% and 22.4% vs 11.2%, respectively; both nominal $P < 0.001$) responses at week 24 (Fig 1C, D). Separation from placebo was observed as early as week 8 across these outcomes (Fig 1).

At week 24, guselkumab-treated participants demonstrated significantly lower rates of radiographic progression versus placebo (LSM change: Q4W 0.55 [$P = 0.002$]; Q8W 0.54 [$P < 0.001$]; placebo 1.35) (Fig 2A). Results were verified across sensitivity analyses (Supplementary Table S2). Participant-level data also supported a clear separation in rates of radiographic progression through week 24 between those receiving either guselkumab regimen versus placebo (Fig 2B). Guselkumab-treated participants exhibited less progression of erosions (LSM change: Q4W 0.35 and Q8W 0.32 versus placebo 0.87; nominal $P = 0.002$ and $P < 0.001$, respectively) and JSN (Q4W 0.22 and Q8W 0.24 versus placebo 0.50; nominal $P = 0.025$ and $P = 0.027$, respectively) (Fig 2A). Greater proportions of guselkumab-treated participants showed no progression of structural joint damage at week 24, defined as change in total vdH-S score ≤ 0 (Q4W 67.3% and Q8W 62.8% vs placebo 53.0%; nominal

$P < 0.001$ and $P = 0.007$, respectively) or ≤ 0.5 (Q4W 77.7% and Q8W 74.7% vs placebo 67.7%; nominal $P = 0.007$ and $P = 0.038$, respectively). Participants in the NP stratum generally had smaller LSM changes in vdH-S score and higher rates of achieving change ≤ 0 at week 24, followed by those in the LMP and RP strata (Supplementary Table S3). No participant without PIC/GO at baseline and available data at week 24 (Q4W 240; Q8W 321; placebo 323) developed these features through week 24.

Among the 42.6% of participants with dactylitis at baseline (Table 1), those receiving guselkumab had greater improvements in DSS at week 24 (LSM change: Q4W −8.4 and Q8W −9.1 vs placebo −6.6; nominal $P = 0.004$ and $P < 0.001$, respectively). At baseline, 58.4% of participants had enthesitis (Table 1); LSM changes in LEI at week 24 were −1.8 for both Q4W and Q8W versus −1.7 for placebo (both nominal $P > 0.05$).

Improvements in physical function were also observed at week 24; participants in the Q4W and Q8W groups reported greater LSM improvements in HAQ-DI score versus placebo (−0.41 and −0.42 vs −0.27, respectively; both nominal $P < 0.001$).

Among the 60.1% of participants with $\geq 3\%$ psoriatic BSA and IGA ≥ 2 at baseline, higher proportions of guselkumab Q4W- and Q8W-treated than placebo-treated participants achieved clear or almost clear skin (PASI 90: 69.4% and 60.0% vs 22.0%, respectively; IGA 0/1 response: 72.8% and 67.9% vs 31.3%, respectively) or completely clear skin (PASI 100: 37.6% and 39.5% vs 11.6%, respectively; IGA 0: 50.9% and 52.4% vs 14.6%,
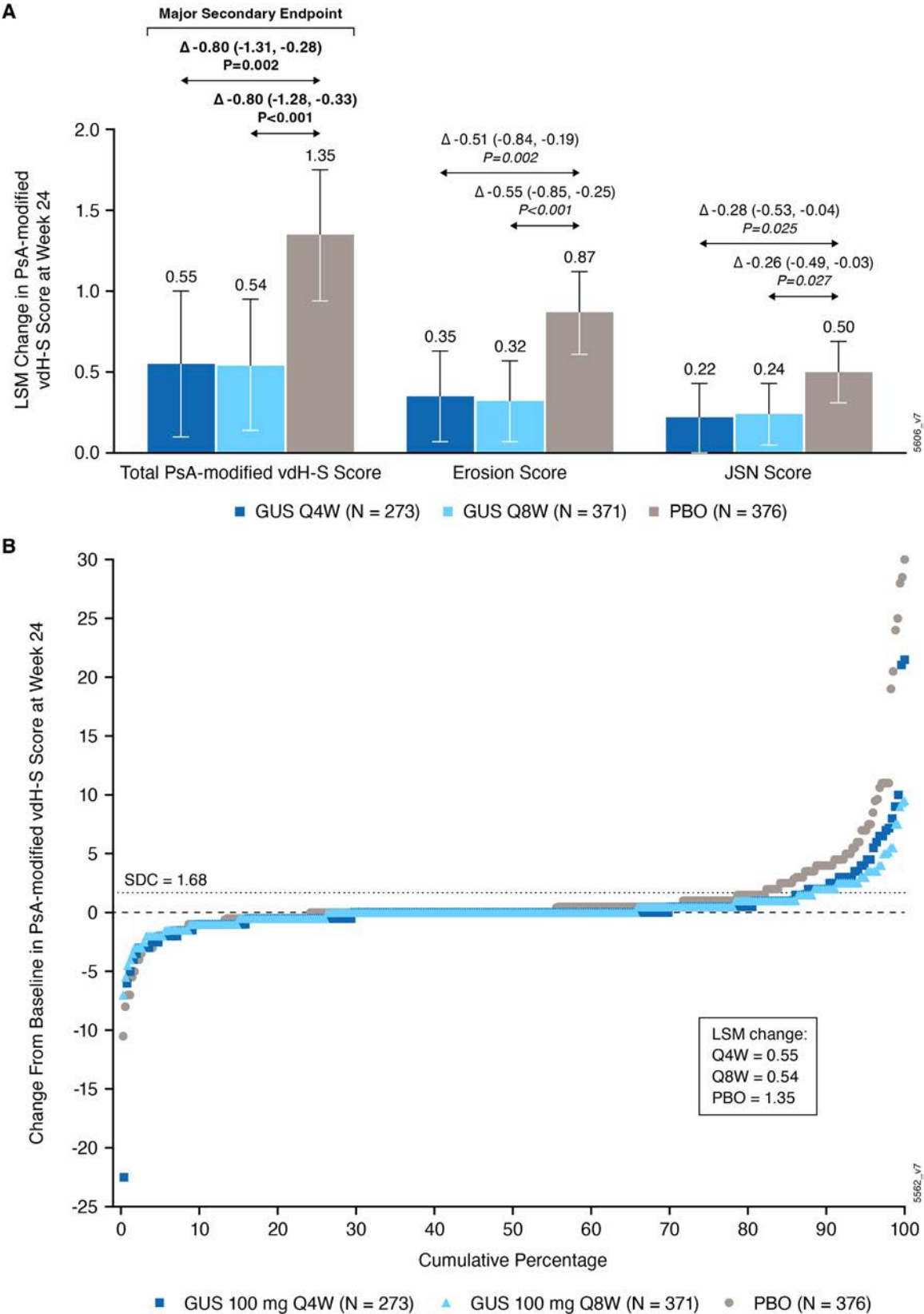
Figure 2. Change from baseline in total PsA-modified vdH-S score and erosion and JSN subscores at week 24 (A) and probability plot for change from baseline in total PsA-modified vdH-S score at week 24 for individual participants (B). Italicised *P* values are nominal. Data presented as LSM change in PsA-modified vdH-S score from baseline to week 24, with LSM differences (95% CI) between each guselkumab group and the placebo group determined by analysis of covariance from each multiple imputation dataset. The intraclass correlation estimates for total vdH-S scores were 0.85 at week 0, 0.84 at week 24, and 0.43 for change from week 0-24. GUS, guselkumab; JSN, joint space narrowing; LSM, least squares mean; PBO, placebo; PsA-modified vdH-S score, psoriatic arthritis-modified van der Heijde-Sharp score; Q4W/Q8W, every 4/8 weeks; SDC, smallest detectable change.
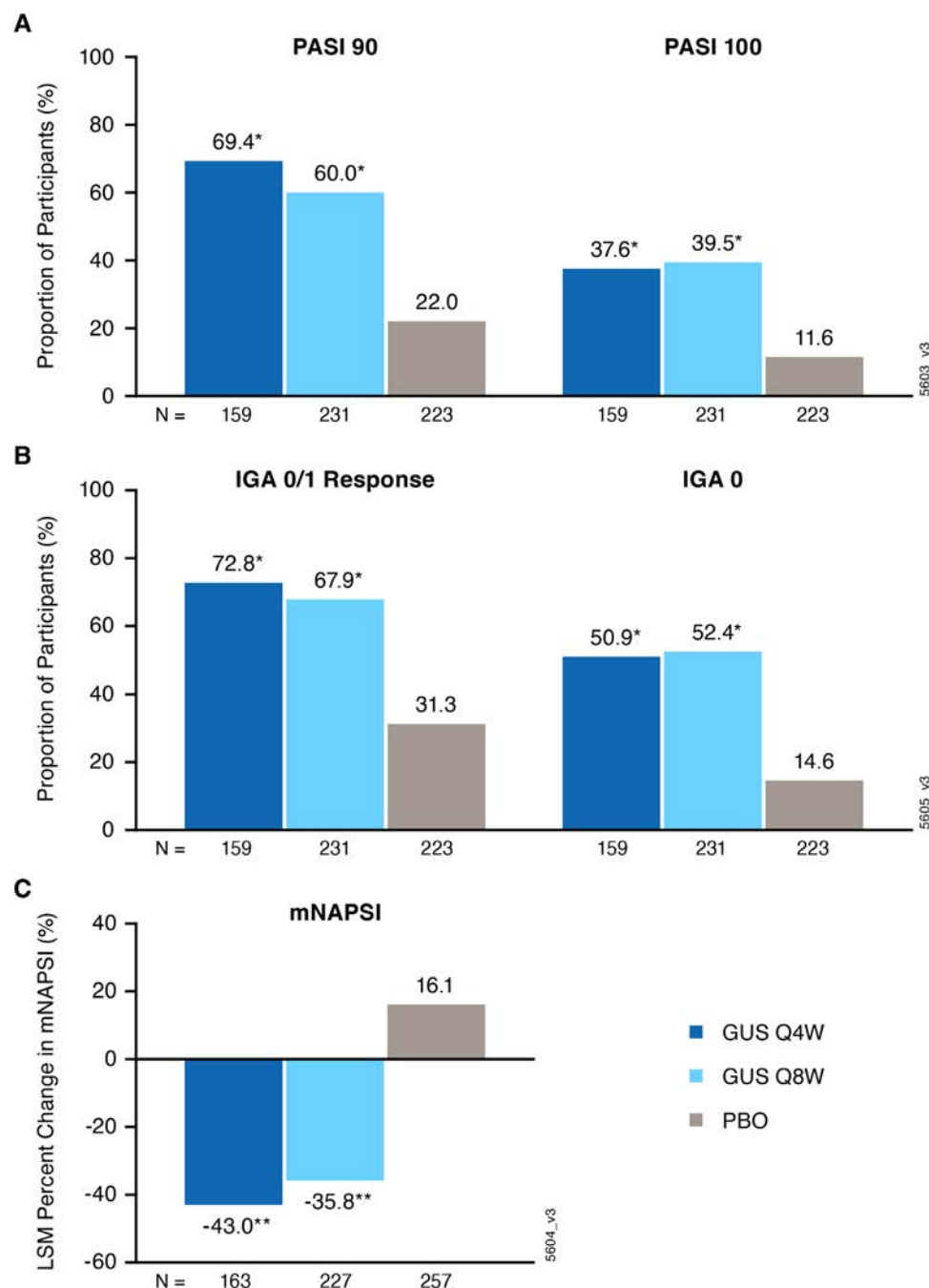
Figure 3. Among participants with BSA ≥3% and IGA ≥2 at baseline, proportions achieving ≥90% (PASI 90) and 100% (PASI 100) improvement in PASI (A) and proportions achieving IGA 0/1 response and IGA 0 (B) at week 24. IGA 0/1 response is defined as an IGA score of 0 (cleared) or 1 (minimal) and ≥2 grade improvement from baseline. LSM percent change in mNAPSI at week 24 among participants with baseline mNAPSI >0 (C). Nominal *P < 0.001, **P < 0.01 versus placebo. BSA, body surface area; GUS, guselkumab; IGA, Investigator's Global Assessment of psoriasis; LSM, least squares mean; mNAPSI, modified Nail Psoriasis Severity Index; PASI, Psoriasis Area and Severity Index; PBO, placebo; Q4W/Q8W, every 4/8 weeks.

respectively) (all nominal P < 0.001; Fig 3A, B). Among participants with mNAPSI >0, those in the Q4W and Q8W groups exhibited improvements at week 24, while those receiving placebo showed worsening nail disease (LSM percent change: Q4W −43.0 and Q8W −35.8 vs 16.1; both nominal P = 0.002; Fig 3C).

The MDA composite endpoint is an established treatment target for patients with PsA. Greater proportions of guselkumab-treated participants achieved MDA at week 24 versus placebo (Q4W 29.6%; Q8W 27.7%; placebo 13.7%; both nominal P < 0.001).

Safety

Through week 24, 38.2%, 42.5%, and 37.3% of participants in the Q4W, Q8W, and placebo groups, respectively, had ≥1 AE

(Table 2). Infections were the most common type of AE (Q4W 18.6%; Q8W 23.5%; placebo 21.0%), the most frequent (>5%) of which were upper respiratory tract infection (Q4W 15 [5.4%]; Q8W 20 [5.2%]; placebo 22 [5.7%]) and COVID-19 (9 [3.2%]; 22 [5.7%]; 21 [5.4%], respectively). No participant had an opportunistic infection or active tuberculosis. Five (1.8%) participants in the Q4W, 12 (3.1%) in the Q8W, and 10 (2.6%) in the placebo groups had a serious AE (SAE). Serious infections were uncommon (Q4W 2 [0.7%]; Q8W 5 [1.3%]; placebo 1 [0.3%]): 4 participants had COVID-19 (1 each in the Q4W [fatal] and placebo groups; 2 in the Q8W group), 2 had pneumonia (both Q8W group), 1 had appendicitis (Q8W), and 1 had diverticulitis (Q4W). No events of new-onset inflammatory bowel disease (IBD) occurred. One participant each had a MACE

Table 2
Summary of adverse events through week 24 in APEX participants

	Guselkumab 100 mg			
	Q4W (N = 280)	Q8W (N = 388)	Combined (N = 668)	Placebo (N = 386)
Mean follow-up, wk	24.0	23.9	24.0	23.8
Participants with ≥1				
AE	107 (38.2)	165 (42.5)	272 (40.7)	144 (37.3)
AE occurring in >5% of participants in any treatment group				
Upper respiratory tract infection	15 (5.4)	20 (5.2)	35 (5.2)	22 (5.7)
COVID-19	9 (3.2)	22 (5.7)	31 (4.6)	21 (5.4)
SAE	5 (1.8)	12 (3.1)	17 (2.5)	10 (2.6)
AE leading to discontinuation	2 (0.7)	6 (1.5)	8 (1.2)	1 (0.3)
Infection	52 (18.6)	91 (23.5)	143 (21.4)	81 (21.0)
Serious infection	2 (0.7)	5 (1.3)	7 (1.0)	1 (0.3)
Opportunistic infection	0	0	0	0
Active tuberculosis	0	0	0	0
Malignancy	0	2 (0.5)	2 (0.3)	0
MACE	0	1 (0.3)	1 (0.1)	0
VTE	1 (0.4)	1 (0.3)	2 (0.3)	1 (0.3)
Clinically important hepatic disorder[a]	0	0	0	0
Anaphylactic or serum sickness reaction	0	0	0	0
Injection-site reaction[b]	8 (2.9)	2 (0.5)	10 (1.5)	0
Death	1 (0.4)	0	1 (0.1)	0

AE, adverse event; MACE, major adverse cardiovascular event; Q4/8W, every 4/8 weeks; SAE, serious adverse event; VTE, venous thromboembolism.
Data are n (%) unless otherwise noted.
[a] Clinically important hepatic disorders were prespecified as AE terms within the Medical Dictionary for Regulatory Activities category of Drug-Related Hepatic Disorders that met the criteria for an SAE or led to study agent discontinuation.
[b] Injection-site reactions were defined as any adverse reaction at a study intervention injection site.

(myocardial infarction in a participant with multiple cardiovascular risk factors; Q8W group, no change in dose), prostate cancer (elderly male; Q8W group, discontinued guselkumab), and renal cancer (elderly male; Q8W group, discontinued guselkumab). As noted above, 1 participant (elderly unvaccinated male in the Q4W group) died due to COVID-19 after receiving the study agent at week 4.

Eight (2.9%) and 2 (0.5%) participants receiving guselkumab Q4W and Q8W, respectively, had an injection-site reaction; all were considered mild by study investigators and resolved. No anaphylactic or serum sickness reaction occurred.

The incidence of ALT and AST increases, most commonly grade 1 (9.4%-10.4% and 6.3%-8.9%, respectively), was similar across the treatment groups through week 24 (Supplementary Table S4). No participant had an ALT or AST increase meeting SAE criteria or leading to study agent discontinuation. One participant each in the Q4W and Q8W groups had a grade 2 ALT increase; another participant receiving guselkumab Q4W had a grade 2 increase in AST. In the placebo group, 3 participants had a grade 2 AST increase; all 3 also had ALT increases (2 grade 2 and 1 grade 3). One other participant receiving placebo had a grade 2 ALT increase. No participant had a grade 4 ALT increase or grade 3/4 AST increase. The occurrence of grade 1 ALT and AST increases was generally higher among participants receiving (10.2%-11.9% and 6.9%-9.6%, respectively) versus not receiving (5.3%-10.5% and 4.6%-7.9%, respectively) concomitant MTX, with no apparent differences between the placebo and guselkumab groups. The single participant with a grade 3 ALT increase was receiving placebo without concomitant MTX.

Immunogenicity

Through week 24, 280 and 386 participants in the guselkumab Q4W and Q8W groups, respectively, received ≥1 guselkumab administration and had ≥1 post-baseline serum sample. Of these, 19 (6.0%) and 23 (6.0%) participants, respectively, in the Q4W and Q8W groups tested positive for antibodies to guselkumab, with the majority having low titres. Five participants (Q4W 4 [1.4%]; Q8W 1 [0.3%]) tested positive for neutralising antibodies.

DISCUSSION

The APEX study, conducted to further evaluate guselkumab 100 mg Q4W and Q8W in participants with active PsA, met its primary clinical and major secondary radiographic endpoints. These findings establish guselkumab, a dual-acting monoclonal antibody, as the only selective IL-23p19-subunit inhibitor demonstrating both significant improvement in PsA signs and symptoms and significant inhibition of structural damage progression with both dosing schedules. The significantly lower rates of radiographic progression with guselkumab Q4W or Q8W versus placebo were confirmed across multiple sensitivity analyses and supported by participant-level changes in the total PsA-modified vdH-S score. Importantly, guselkumab inhibited progression of both joint erosions and JSN and afforded higher rates of no structural damage progression at week 24 (change ≤0 or ≤0.5) versus placebo. In addition to meeting the ACR20 primary endpoint required by regulatory agencies, substantial proportions of guselkumab-treated participants achieved the more stringent ACR50 (>40%) and ACR70 (nearly one-quarter) criteria, reflecting important and meaningful improvements in signs and symptoms of joint disease activity. Across these clinical measures, separation from placebo was seen as early as week 8. Additionally, participants receiving guselkumab reported greater improvements in physical function than those receiving placebo. Guselkumab treatment also provided high rates of clear or almost clear skin (approximately two-thirds achieved IGA 0/1) and complete skin clearance (>50% achieved IGA 0), as well as substantial improvement in psoriatic nail disease at week 24, an

early timepoint to effect change in this difficult-to-treat domain. Notably, APEX is the first phase 3 study assessing guselkumab effects on psoriatic nail disease in participants with active PsA, and the findings were consistent with those from previous studies of participants with moderate-to-severe psoriasis [34].

Within the class of IL-23p19-subunit inhibitors approved to treat adults with active PsA, only guselkumab has demonstrated significant inhibition of structural damage in this population [35]. Guselkumab is a fully human monoclonal antibody with a native Fc region, while the modified Fc region of risankizumab contains L234A and L235A (ie, LALA) substitutions [36] known to attenuate binding to Fcγ receptors such as CD64 [37]. A series of *in vitro* analyses explored potential implications of CD64 binding on the function of IL-23−targeting monoclonal antibodies by employing CD64$^+$ myeloid cells, the primary source of the aberrant IL-23 expression in patients with PsA [38]. These experiments showed that guselkumab, but not risankizumab, is able to both bind CD64 on the cell surface and simultaneously capture IL-23 secreted from these cells, and that guselkumab demonstrates Fc-dependent enhanced potency compared with risankizumab for inhibiting IL-23 signalling [13]. The long-term clinical significance of these *in vitro* findings has not been established; additional studies are needed to explore the potential impact of the observed molecular differences on patient outcomes.

The pattern and frequency of AEs in APEX were consistent with the known safety profile of guselkumab in patients with PsA, psoriasis, ulcerative colitis, and Crohn's disease [12,39]. Few participants had an SAE or serious infection, and no participant developed an opportunistic infection, active tuberculosis, or new-onset IBD. One unvaccinated participant died due to COVID-19 (Q4W group; after receiving the week 4 administration). No new safety signals were identified.

APEX results are strengthened by the relatively large study population and high retention through week 24 (≥96%). Significant differences between guselkumab and placebo in the primary and major secondary endpoints were supported by multiple sensitivity analyses. Additionally, APEX employed an objective and validated instrument for assessing radiographic progression (PsA-modified vdH-S score), and all radiographs were centrally scored by blinded independent readers. APEX enrolled participants with active PsA and evidence of erosive disease, an appropriate cohort for evaluating effects of treatment on inhibition of structural damage progression. The study's innovative randomisation strategy, employing 4 composite stratification levels incorporating reader variability in scoring baseline radiographs, concomitant corticosteroid use, number of erosive joints, and CRP level, ensured balance across treatment groups for interreader variability (1 level) and predicted risk of progression (3 levels). While the strata based on predicted risk of radiographic progression and underlying criteria were not intended for use in clinical practice, post hoc analyses indicated that participants in the NP stratum generally exhibited the smallest changes in total vdH-S score and the highest rates of nonprogression (change ≤0) and thus consistency with the stratification assignments. Across the 3 strata, guselkumab-treated participants generally had numerically lower mean changes and higher response rates than in the placebo group; however, comparisons among treatment arms and across strata are limited by the small sample sizes and post hoc nature of these analyses.

In the absence of a consensus definition for identifying and enrolling participants with an increased risk of radiographic progression, eligibility criteria for previous studies evaluating the efficacy of advanced PsA therapies on inhibition of radiographic progression have utilised various combinations of baseline SJC/TJC, CRP, and number of erosive joints [16,40−44]. The overall baseline disease activity of the APEX population, indicative of high levels of joint disease, is generally consistent with that reported in these studies.

The 6-month placebo-controlled period may be relatively short for ascertaining changes in outcomes such as structural damage and nail disease. However, radiographic and nail assessments in APEX are planned to continue through 3 years [21], allowing longer-term evaluation of structural damage and nail outcomes. Relatively high placebo responses were observed for some endpoints, including ACR response and changes in dactylitis and enthesitis. Placebo responses have been steadily increasing over time in randomised controlled trials, and this pattern may be associated with more frequent enrolment of participants from countries with varied socioeconomic status and limited access to advanced therapies, as observed in a recent analysis [45]. Further, both DSS and LEI rely on manual detection, which can be complicated by common comorbidities, such as obesity and fibromyalgia [46,47]. In contrast, outcomes based on more objective measures, such as radiographic, skin, and nail instruments, demonstrated clear separation between both guselkumab dosing regimens and placebo.

The findings from APEX not only confirm the highly favourable benefit-risk profile of guselkumab Q4W and Q8W in treating the signs and symptoms of active PsA across a broad range of patient types [14−16] but also support guselkumab as the only IL-23p19-subunit inhibitor to demonstrate statistically significant inhibition of radiographic progression in this population. As such, guselkumab is unique in its ability to comprehensively address important treatment goals, including preservation of joint health, shared by patients with PsA and their health care providers.

Competing interests

Contributors

PJM, CTR, LCC, APK, BZ, YJ, KB, KI, RB, SDC, PR, and DvdH conceptualised the study. BZ and YJ performed formal analysis. PJM, CTR, LCC, APK, BZ, YJ, KB, KI, RB, SDC, PR, and DvdH provided supervision. PJM, CTR, LCC, APK, BZ, YJ, KB, KI, RB, SDC, PR, and DvdH participated in writing, reviewing, and editing the manuscript. All authors reviewed and approved the manuscript for submission.

Patient consent for publication

Not applicable.

Ethics approval

APEX is being conducted in accordance with the Declaration of Helsinki and Good Clinical Practice guidelines. An Institutional Review Board (IRB) or Ethics Committee at each site (central IRB in the United States: Advarra; Pro00049187) approved the protocol.

Provenance and peer review

Not commissioned; externally peer reviewed.

Data availability statement

The data sharing policy of Johnson & Johnson is available at https://innovativemedicine.jnj.com/our-innovation/clinical-trials/transparency. As noted on this site, requests for access to the study data can be submitted through the Yale Open Data Access (YODA) Project site at http://yoda.yale.edu.

Supplementary materials

Supplementary material associated with this article can be found in the online version at doi:10.1016/j.ard.2025.08.006.

ORCID

Philip J. Mease: http://orcid.org/0000-0002-6620-0457
Christopher T. Ritchlin: http://orcid.org/0000-0002-2602-1219
Laura C. Coates: http://orcid.org/0000-0002-4756-663X
Alexa P. Kollmeier: http://orcid.org/0000-0002-2059-7866
Rattandeep Batra: http://orcid.org/0009-0003-7039-2441
Soumya D. Chakravarty: http://orcid.org/0000-0001-7957-838X
Proton Rahman: http://orcid.org/0000-0002-4521-2029
Désirée van der Heijde: http://orcid.org/0000-0002-5781-158X

REFERENCES

[1] Gladman DD, Antoni C, Mease P, Clegg DO, Nash P. Psoriatic arthritis: epidemiology, clinical features, course, and outcome. Ann Rheum Dis 2005;64 (suppl 2) ii14-7. doi: 10.1136/ard.2004.032482.

[2] Ritchlin CT, Colbert RA, Gladman DD. Psoriatic arthritis. N Engl J Med 2017;376(21):957−70. doi: 10.1056/NEJMra1505557.

[3] Brown AK. How to interpret plain radiographs in clinical practice. Best Pract Res Clin Rheumatol 2013;27(2):249−69. doi: 10.1016/j.berh.2013.03.004.

[4] Kerschbaumer A, Baker D, Smolen JS, Aletaha D. The effects of structural damage on functional disability in psoriatic arthritis. Ann Rheum Dis 2017;76(12):2038−45. doi: 10.1136/annrheumdis-2017-211433.

[5] Zangger P, Gladman DD, Bogoch ER. Musculoskeletal surgery in psoriatic arthritis. J Rheumatol 1998;25(4):725−9.

[6] Haroon M, Gallagher P, FitzGerald O. Diagnostic delay of more than 6 months contributes to poor radiographic and functional outcome in psoriatic arthritis. Ann Rheum Dis 2015;74(6):1045−50. doi: 10.1136/annrheumdis-2013-204858.

[7] Hen O, Di Matteo A, Dubash SR, De Marco G, Tan AL, Emery P, et al. High prevalence of radiographic erosions in early, untreated PsA: results from the SpARRO cohort. RMD Open 2024;10(2):e003841. doi: 10.1136/rmdopen-2023-003841.

[8] Ruta S, Jaldin Cespedes R, Cuellar L, Mareco J, Aguerre D, García Salinas R. Psoriatic arthritis: differential features at the time of clinical presentation in a large cohort of patients with polyarthralgia. Eur J Rheumatol 2023;10 (1):12−7. doi: 10.5152/eurjrheum.2022.22035.

[9] Coates LC, Soriano ER, Corp N, Bertheussen H, Callis Duffin K, Campanholo CB, et al. Group for Research and Assessment of Psoriasis and Psoriatic Arthritis (GRAPPA): updated treatment recommendations for psoriatic arthritis 2021. Nat Rev Rheumatol 2022;18(8):465−79. doi: 10.1038/s41584-022-00798-0.

[10] Gossec L, Kerschbaumer A, Ferreira RJO, Aletaha D, Baraliakos X, Bertheussen H, et al. EULAR recommendations for the management of psoriatic arthritis with pharmacological therapies: 2023 update. Ann Rheum Dis 2024;83 (6):706−19. doi: 10.1136/ard-2024-225531.

[11] Singh JA, Guyatt G, Ogdie A, Gladman DD, Deal C, Deodhar A, et al. Special Article: 2018 American College of Rheumatology/National Psoriasis Foundation guideline for the treatment of psoriatic arthritis. Arthritis Rheumatol 2019;71(1):5−32. doi: 10.1002/art.40726.

[12] Tremfya: Package insert. Horsham, PA: Janssen Biotech, Inc.; 2025.

[13] Sachen KL, Hammaker D, Sarabia I, Stoveken B, Hartman J, Leppard KL, et al. Guselkumab binding to CD64$^+$ IL-23−producing myeloid cells enhances potency for neutralizing IL-23 signaling. Front Immunol 2025;16:1532852. doi: 10.3389/fimmu.2025.1532852.

[14] Coates LC, Gossec L, Theander E, Bergmans P, Neuhold M, Karyekar CS, et al. Efficacy and safety of guselkumab in patients with active psoriatic arthritis who are inadequate responders to tumour necrosis factor inhibitors: results through one year of a phase IIIb, randomised, controlled study (COSMOS). Ann Rheum Dis 2022;81(3):359−69. doi: 10.1136/annrheumdis-2021-220991.

[15] Deodhar A, Helliwell PS, Boehncke WH, Kollmeier AP, Hsia EC, Subramanian RA, et al. Guselkumab in patients with active psoriatic arthritis who were biologic-naive or had previously received TNFα inhibitor treatment (DISCOVER-1): a double-blind, randomised, placebo-controlled phase 3 trial. Lancet 2020;395(10230):1115−25. doi: 10.1016/S0140-6736(20)30265-8.

[16] Mease PJ, Rahman P, Gottlieb AB, Kollmeier AP, Hsia EC, Xu XL, et al. Guselkumab in biologic-naive patients with active psoriatic arthritis (DISCOVER-2): a double-blind, randomised, placebo-controlled phase 3 trial. Lancet 2020;395(10230):1126−36. doi: 10.1016/S0140-6736(20)30263-4.

[17] McInnes IB, Rahman P, Gottlieb AB, Hsia EC, Kollmeier AP, Chakravarty SD, et al. Efficacy and safety of guselkumab, an interleukin-23p19-specific monoclonal antibody, through one year in biologic-naïve patients with psoriatic arthritis. Arthritis Rheumatol 2021;73(4):604−16. doi: 10.1002/art.41553.

[18] McInnes IB, Rahman P, Gottlieb AB, Hsia EC, Kollmeier AP, Xu XL, et al. Long-term efficacy and safety of guselkumab, a monoclonal antibody specific to the p19 subunit of interleukin-23, through two years: results from a phase III, randomized, double-blind, placebo-controlled study conducted in

biologic-naive patients with active psoriatic arthritis. Arthritis Rheumatol 2022;74(3):475–85. doi: 10.1002/art.42010.

[19] Ritchlin CT, Helliwell PS, Boehncke WH, Soriano ER, Hsia EC, Kollmeier AP, et al. Guselkumab, an inhibitor of the IL-23p19 subunit, provides sustained improvement in signs and symptoms of active psoriatic arthritis: 1 year results of a phase III randomised study of patients who were biologic-naive or TNFα inhibitor-experienced. RMD Open 2021;7(1):e001457. doi: 10.1136/rmdopen-2020-001457.

[20] Tremfya (EMA): Package insert. Leiden, The Netherlands: Janssen B.V.; 2022.

[21] Ritchlin CT, Coates LC, Mease PJ, van der Heijde D, Song J, Jiang Y, et al. The effect of guselkumab on inhibiting radiographic progression in patients with active psoriatic arthritis: study protocol for APEX, a Phase 3b, multicenter, randomized, double-blind, placebo-controlled trial. Trials 2023;24(1):22. doi: 10.1186/s13063-022-06945-y.

[22] Taylor W, Gladman D, Helliwell P, Marchesoni A, Mease P, Mielants H, et al. Classification criteria for psoriatic arthritis: development of new criteria from a large international study. Arthritis Rheum 2006;54(8):2665–73. doi: 10.1002/art.21972.

[23] Gladman DD, Inman RD, Cook RJ, Maksymowych WP, Braun J, Davis JC, et al. International spondyloarthritis interobserver reliability exercise−the INSPIRE study: II. Assessment of peripheral joints, enthesitis, and dactylitis. J Rheumatol 2007;34(8):1740–5.

[24] Gladman DD, Ziouzina O, Thavaneswaran A, Chandran V. Dactylitis in psoriatic arthritis: prevalence and response to therapy in the biologic era. J Rheumatol 2013;40(8):1357–9. doi: 10.3899/jrheum.130163.

[25] Healy PJ, Helliwell PS. Measuring clinical enthesitis in psoriatic arthritis: assessment of existing measures and development of an instrument specific to psoriatic arthritis. Arthritis Rheum 2008;59(5):686–91. doi: 10.1002/art.23568.

[26] Fredriksson T, Pettersson U. Severe psoriasis−oral therapy with a new retinoid. Dermatologica 1978;157(4):238–44. doi: 10.1159/000250839.

[27] Langley RGB, Feldman SR, Nyirady J, van de Kerkhof P, Papavassilis C. The 5-point Investigator's Global Assessment (IGA) Scale: a modified tool for evaluating plaque psoriasis severity in clinical trials. J Dermatolog Treat 2015;26(1):23–31. doi: 10.3109/09546634.2013.865009.

[28] Cassell SE, Bieber JD, Rich P, Tutuncu ZN, Lee SJ, Kalunian KC, et al. The modified Nail Psoriasis Severity Index: validation of an instrument to assess psoriatic nail involvement in patients with psoriatic arthritis. J Rheumatol 2007;34(1):123–9.

[29] Fries JF, Spitz P, Kraines RG, Holman HR. Measurement of patient outcome in arthritis. Arthritis Rheum 1980;23(2):137–45. doi: 10.1002/art.1780230202.

[30] Felson DT, Anderson JJ, Boers M, Bombardier C, Furst D, Goldsmith C, et al. American College of Rheumatology. Preliminary definition of improvement in rheumatoid arthritis. Arthritis Rheum 1995;38(6):727–35. doi: 10.1002/art.1780380602.

[31] van der Heijde D, Sharp J, Wassenberg S, Gladman DD. Psoriatic arthritis imaging: a review of scoring methods. Ann Rheum Dis 2005;64(suppl 2) ii61-4. doi: 10.1136/ard.2004.030809.

[32] van der Heijde DMFM, van Leeuwen MA, van Riel PL, Koster AM, van 't Hof MA, van Rijswijk MH, et al. Biannual radiographic assessments of hands and feet in a three-year prospective followup of patients with early rheumatoid arthritis. Arthritis Rheum 1992;35(1):26–34. doi: 10.1002/art.1780350105.

[33] Coates LC, Fransen J, Helliwell PS. Defining minimal disease activity in psoriatic arthritis: a proposed objective target for treatment. Ann Rheum Dis 2010;69(1):48–53. doi: 10.1136/ard.2008.102053.

[34] Foley P, Gordon K, Griffiths CEM, Wasfi Y, Randazzo B, Song M, et al. Efficacy of guselkumab compared with adalimumab and placebo for psoriasis in specific body regions: a secondary analysis of 2 randomized clinical trials. JAMA Dermatol 2018;154(6):676–83. doi: 10.1001/jamadermatol.2018.0793.

[35] Kristensen LE, Keiserman M, Papp K, McCasland L, White D, Carter K, et al. Efficacy and safety of risankizumab for active psoriatic arthritis: 100-week results from the phase 3 KEEPsAKE 1 randomized clinical trial. Rheumatol Ther 2024;11(3):617–32. doi: 10.1007/s40744-024-00654-5.

[36] Singh S, Kroe-Barrett RR, Canada KA, Zhu X, Sepulveda E, Wu H, et al. Selective targeting of the IL23 pathway: generation and characterization of a novel high-affinity humanized anti-IL23A antibody. mAbs 2015;7(4):778–91. doi: 10.1080/19420862.2015.1032491.

[37] Hale G. Living in LALA land? Forty years of attenuating Fc effector functions. Immunol Rev 2024;328(1):422–37. doi: 10.1111/imr.13379.

[38] Mehta H, Mashiko S, Angsana J, Rubio M, Hsieh YM, Maari C, et al. Differential changes in inflammatory mononuclear phagocyte and T-cell profiles within psoriatic skin during treatment with guselkumab vs. secukinumab. J Invest Dermatol 2021;141(7):1707–1718.e9. doi: 10.1016/j.jid.2021.01.005.

[39] Strober B, Coates LC, Lebwohl MG, Deodhar A, Leibowitz E, Rowland K, et al. Long-term safety of guselkumab in patients with psoriatic disease: an integrated analysis of eleven phase II/III clinical studies in psoriasis and psoriatic arthritis. Drug Saf 2024;47(1):39–57. doi: 10.1007/s40264-023-01361-w.

[40] Mease PJ, McInnes IB, Kirkham B, Kavanaugh A, Rahman P, van der Heijde D, et al. Secukinumab inhibition of interleukin-17A in patients with psoriatic arthritis. N Engl J Med 2015;373(14):1329–39. doi: 10.1056/NEJMoa1412679.

[41] Mease PJ, van der Heijde D, Ritchlin CT, Okada M, Cuchacovich RS, Shuler CL, et al. Ixekizumab, an interleukin-17A specific monoclonal antibody, for the treatment of biologic-naive patients with active psoriatic arthritis: results from the 24-week randomised, double-blind, placebo-controlled and active (adalimumab)-controlled period of the phase III trial SPIRIT-P1. Ann Rheum Dis 2017;76(1):79–87. doi: 10.1136/annrheumdis-2016-209709.

[42] McInnes IB, Anderson JK, Magrey M, Merola JF, Liu Y, Kishimoto M, et al. Trial of upadacitinib and adalimumab for psoriatic arthritis. N Engl J Med 2021;384(13):1227–39. doi: 10.1056/NEJMoa2022516.

[43] Kristensen LE, Keiserman M, Papp K, McCasland L, White D, Lu W, et al. Efficacy and safety of risankizumab for active psoriatic arthritis: 24-week results from the randomised, double-blind, phase 3 KEEPsAKE 1 trial. Ann Rheum Dis 2022;81(2):225–31. doi: 10.1136/annrheumdis-2021-221019.

[44] McInnes IB, Asahina A, Coates LC, Landewé R, Merola JF, Ritchlin CT, et al. Bimekizumab in patients with psoriatic arthritis, naive to biologic treatment: a randomised, double-blind, placebo-controlled, phase 3 trial (BE OPTIMAL). Lancet 2023;401(10370):25–37. doi: 10.1016/S0140-6736(22)02302-9.

[45] Kerschbaumer A, Steiner M, Khalili S, Shehab A, Jordanov A, Wildner B, et al. Global recruiting patterns affect placebo response rates in clinical trials of psoriatic arthritis and plaque psoriasis. Arthritis Rheumatol. Published online June 30, 2025. doi: 10.1002/art.43302.

[46] Rebollo-Giménez A, Martínez-Estupiñán L, Olivas-Vergara O, Fuensalida-Novo G, Garrido J, Mejía A, et al. How variable is the volar subcutaneous tissue of the digits on B-mode and color Doppler ultrasound in non-psoriatic individuals and could it be included in a dactylitis score? Ultraschall Med 2021;42(6):643–51. doi: 10.1055/a-1168-6636.

[47] Kaeley GS, Eder L, Aydin SZ, Gutierrez M, Bakewell C. Enthesitis: a hallmark of psoriatic arthritis. Semin Arthritis Rheum 2018;48(1):35–43. doi: 10.1016/j.semarthrit.2017.12.008.
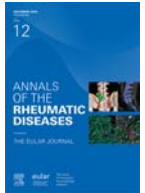
Axial spondyloarthritis

Healthy human enthesis stromal cells mediate immunoregulation via the CD39/CD73 adenosine ectonucleotidase pathway

Ala Altaie [1,#], Davide Simone [2,#], Nicole McDermott [1], Heather Owston [1], Moustafa Attar [2], Liying Jin [2], Chi Wong [1], Peter R. Loughenbury [3], Borse Vishal [3], Tristan McMillan [3], Christopher D. Buckley [2], Stephen N. Sansom [2,§,*], Dennis McGonagle [1,§,*]

[1] Leeds Institute of Rheumatic & Musculoskeletal Medicine, St James Hospital, University of Leeds, Leeds, United Kingdom
[2] Kennedy Institute of Rheumatology, Nuffield Department of Orthopaedics, Rheumatology and Musculoskeletal Sciences, University of Oxford, Oxford, United Kingdom
[3] Leeds Teaching Hospitals NHS Trust, Leeds, United Kingdom

ARTICLE INFO

ABSTRACT

Objectives: Entheseal inflammation (ligament and tendon insertions) and subclinical intestinal inflammation are both hallmarks of the seronegative spondyloarthropathy (SpA) diseases. While regulatory T cells (Tregs) are key to intestinal homeostasis, entheseal homeostatic mechanisms are poorly understood in humans.

Methods: Single-cell RNA sequencing of entheseal tissue, comparative transcriptomic analysis with intestinal tissue datasets, and functional analysis of entheseal stromal populations were undertaken. Functional immunomodulation by entheseal mesenchymal stromal cells (MSCs) was evaluated via coculture with activated T cells. CD39/CD73 pathway involvement was confirmed using pharmacological inhibition and transcriptional profiling.

Results: Single-cell RNA sequencing of 27,348 entheseal cells revealed a lower frequency of Tregs in the T cells of the enthesis ($2.60\% \pm 0.36\%$) compared to those of the ileum ($7.37\% \pm 4.47\%$) and colon ($18\% \pm 8.59\%$). We found that entheseal fibroblasts expressed key immunomodulatory markers, including CD39 (*ENTPD1*) and CD73 (*NT5E*), which were further upregulated upon coculture with activated T cells. Entheseal MSCs significantly suppressed T cell proliferation (up to 89%, $P < .0001$) in an adenosine-dependent manner. Transcriptional profiling revealed that entheseal MSC cocultured with activated T cells upregulated genes of known functional importance in Treg, including *IL10*, *IDO1*, *PTGS2*, *HLA-G*, and *CD274*. In this assay, dual CD39/CD73 inhibition restored T cell proliferation by ~48% ($P = .0004$), confirming that entheseal MSC-mediated immunomodulation acts in part through an adenosine-mediated mechanism.

Conclusions: The normal spinal enthesis harbours an immunoregulatory cellular environment related to entheseal MSCs that utilises the CD39/CD73 adenosine ectonucleotidase axis that may help maintain local immune homeostasis, while the same adenosine ectonucleotidase immunoregulatory pathway is likely dependent on Treg function in the intestine. This has broad implications for understanding the cellular bases of immune dysregulation in the gut-joint axis and could help guide tissue-specific therapy in SpA.

*Correspondence to Drs. Stephen Sansom and Dennis McGonagle.
E-mail addresses:* stephen.sansom@kennedy.ox.ac.uk (S.N. Sansom), d.g.mcgonagle@leeds.ac.uk (D. McGonagle).
# Ala Altaie and Davide Simone contributed equally to this study and are considered as joint first authors.
§ Stephen N. Sansom and Dennis McGonagle contributed equally to this study and are considered joint last authors.

WHAT IS ALREADY KNOWN ON THIS TOPIC

- Entheseal inflammation and subclinical intestinal inflammation are both hallmarks of the seronegative spondyloarthropathy diseases.
- The intestine is a site rich in immune cells, whereas entheseal soft tissue anchorage sites are mostly composed of fibroblasts and are subject to high biophysical stress.
- How immune regulation occurs at the enthesis is poorly understood.

WHAT THIS STUDY ADDS

- We built a single-cell RNA sequencing atlas of human entheseal tissue. We found that the healthy human enthesis has fewer regulatory T cells than are present in healthy human intestinal tissue.
- We showed that entheseal fibroblasts are capable of robustly inhibiting T cell proliferative responses. Native entheseal fibroblasts robustly expressed CD39 (*ENTPD1*) and CD73 (*NT5E*), which mediate the adenosine ectonucleotidase immunoregulatory pathways—a key element of Treg immunomodulation.
- Entheseal fibroblast cocultured with activated T cells further upregulated CD39 (*ENTPD1*) and CD73 (*NT5E*), and pharmacological inhibition of these factors significantly reduced immunomodulation.

HOW THIS STUDY MIGHT AFFECT RESEARCH, PRACTICE OR POLICY

- The normal spinal enthesis harbours a unique immunoregulatory cellular environment that is distinct from the intestine.
- Entheseal fibroblasts utilise molecular immunoregulatory mechanisms that are shared with regulatory T cells, and some of these could be tractable for future development of therapy for enthesitis.

INTRODUCTION

The seronegative spondyloarthritis (SpA) family constitutes a cluster of inflammatory diseases predominantly afflicting musculoskeletal structures, skin, eye, and the intestine. While substantial progress has been made in unravelling the cellular make-up and the pathogenic mechanisms within the skin and intestine [1,2], the immune dynamics of the enthesis—a central site of musculoskeletal inflammation in SpA—remain largely uncharted [3]. Of particular note, subclinical intestinal inflammation is common in SpA, but there is a therapeutic disconnect between drug efficacy in the intestinal and axial skeleton. In the axial skeleton, interleukin (IL)-17 antagonism is effective but may simultaneously be associated with nonefficacy or even the precipitation of intestinal inflammation [4–8]. This suggests that fundamental differences may exist between normal spinal and intestinal immunity in SpA.

The healthy human spinal enthesis contains fibroblasts also known as mesenchymal stromal cells (MSCs) due to the ability of such cells to differentiate into osteoblast, adipocyte and chondrocyte lineage cells (ref our MSC enthesis paper). Furthermore, myeloid cells, conventional T cells, and various innate immune cell populations, including $\gamma\delta$ T cells and innate lymphoid cells (ILCs), have been reported [9]. Given that entheses are sites of high biophysical stress, microdamage and microinflammation, identification of the cellular mechanism(s) that govern normal entheseal immunoregulation and immune homeostasis is of central importance for understanding the etiopathology and informing the targeted treatment of human SpA [10].

Regulatory T cells (Tregs) are important for peripheral tolerance in many tissues with their absence in the gut resulting in potentially fatal neonatal colitis [11]. Moreover, it is noteworthy that subclinical colitis and dysbiosis frequently occur in SpA spectrum diseases [7,12]. The basis for the presence of both entheseal and intestinal inflammation in SpA spectrum disorders remains incompletely understood. The reason why intestinal inflammation typically remains subclinical in SpA, in contrast to that of axial and peripheral joints, is unknown. If a common disease process is assumed, it is possible that, commensurate with it being a barrier site, the gut harbours different immunomodulatory mechanisms than are found in healthy entheses, which are sterile tissues.

In a previous report, using bulk RNA-seq and cytometric analysis, we noted a paucity of Tregs in the normal soft tissue and bony anchorage of the spinal enthesis [9], suggesting that other cell types may provide immune tolerance and tissue homeostasis. One of the key shared pathways between Tregs and stromal cells for mediating immunosuppression is the CD73/CD39 adenosine pathway [13–15]. This mechanism relies on the enzymatic actions of CD39 (ectonucleoside triphosphate diphosphohydrolase 1 [E-NTPDase1]) and CD73 (ecto-5′- nucleotidase [Ecto5′Ntase]). CD39 catalyses the hydrolysis of adenosine triphosphate (ATP) and adenosine diphosphate (ADP) into 5′-adenosine monophosphate, which is subsequently converted into adenosine by CD73 [15]. This process plays a critical role in immune regulation by producing adenosine, a potent immunosuppressive molecule [16,17]. Notably, both entheseal soft tissue MSCs (EST-MSCs) and perientheseal bone MSCs (PEB-MSCs) are known to exhibit surface expression of CD73 [18].

Here, we generated the first single-cell atlas of the human spinal enthesis to assess the presence of immunomodulatory cell populations in the soft tissue and bony anchorage of the enthesis. We propose that the reduced frequency of Tregs in the healthy spinal enthesis compared to intestinal tissues is compensated for by shared specialised regulatory functions of entheseal MSCs. In keeping with this concept, we demonstrate that entheseal MSCs are capable of suppressing activated T cells via the adenosine pathway.

METHODS

Approval was obtained from the Northwest-Greater Manchester West Research Ethics Committee (16/NW/0797). Tissue was obtained from patients undergoing elective spinal surgery for either scoliosis correction or lumbar decompression. Samples included interspinous ligament enthesis and adjacent bone anchorage tissue from regions macroscopically free of inflammation or gross pathology. The interspinous ligament is anatomically distant from primary degenerative or deformity-related changes and is not typically involved in these disease processes. Full details of sample processing and generation of single-cell data using the 10× Genomics Chromium platform are described in the Supplementary Methods. Single-cell data analysis was processed using cellhub pipelines (https://github.com/sansomlab/cellhub) and the downstream computational analyses performed as described in the Supplementary Methods. T cell assays, immunoassay, cytokine measurements, bulk RNA identities sequencing, CD73/CD39 antagonism assays, and statistical analyses were performed as described in the Supplementary Methods.

RESULTS

Generation of a single-cell atlas of human spinal enthesis

We used single-cell RNA sequencing to investigate the cellular basis of immunomodulation in the enthesis (Fig 1A). After quality control (see Methods), we clustered 27,348 single-cell transcriptomes from 4 paired peri-entheseal bone (PEB) and entheseal soft tissue (EST samples, identifying 17 transcriptionally distinct immune cell subsets (Fig 1B,C). These comprised myeloid cells (including progenitors, mature neutrophils, and monocytes), B cells at different stages of differentiation, T cells, erythroid cells including precursors and MSCs (Supplementary Fig S1B,C). The presence of differentiating B and myeloid cells, along with nucleated erythroid cells, is likely attributable to the inclusion of bone marrow in the digested samples.

Comparative composition analysis of the EST and PEB samples showed that most cell subsets were present at both anatomical sites, with the exception of endothelial cells and fibroblasts, which were found almost exclusively in the soft tissue entheseal region (Fig 1D, Supplementary Fig S1A). This shift in MSC composition aligns with known ligamentous soft tissue structure, where mechanical fibroblast lineage cells are more abundant compared to mineralised zones and the underlying trabecular regions that are rich in marrow lineage cells but have a paucity of fibroblasts. Conversely, plasma cells, early B cells (pre-B and pro-B cells) and erythroid cells were more abundant in the bone-associated region (reflecting the presence of bone marrow tissue in the sampled enthesis bony anchorage region).

Extraction and reanalysis of myeloid cells revealed the presence of distinct monocyte and neutrophils clusters (Fig 1D), arranged along a continuum suggestive of a potential differentiation trajectory (Supplementary Fig S1D). These led to (i) 2 *VCAN* and *S100A4* expressing monocyte populations (monocyte 1,2) and (ii) 3 subsets of neutrophils, which were characterised by expression of S100A8/9 cells (neutrophils 1) and *CD24* and *LCN2* (neutrophils 2 and 3). The higher-resolution clustering of the myeloid space also allowed the separation of common myeloid progenitors (characterised by *ELANE, MPO*), pro-myelocytes (*DEFA3, CD24*) and mast cells (*CPA3, HDC*) (Fig 1D and Supplementary Fig S1E). To investigate which myeloid cell populations might contribute to cytokine production in the enthesis under inflammatory conditions such as SpA, we examined the expression of known inflammatory mediators (Fig. 1C). Tumour necrosis factor (*TNF*), *IL1B,* and *IL6* expression were found predominantly in mature monocytes. Neutrophils, in contrast, were the principal myeloid source of *CXCL8* (encoding IL-8) in the healthy spinal enthesis, as previously observed [19], while *MIF*, an emerging inflammatory mediator in SpA [20], was broadly expressed by monocytic subsets (Fig 1E). Lastly, *PTGS2*, encoding COX-2, was found in both mature neutrophils and monocytes.

T cell diversity and reduced Tregs in the spinal enthesis

To characterise the entheseal T and natural killer (NK) cell populations, we extracted and reanalysed these cells separately, adopting a bespoke strategy to integrate T cells from the bone and soft tissue (see Methods, Supplementary Fig S2A). We identified 11 T cell and NK subpopulations, including rare, specialised lymphocyte subsets previously described in entheseal studies, such as $\gamma\delta$ T cells, ILCs, and tissue-resident memory cells (Fig 2A,B; Supplementary Fig S2B).

A small population of Tregs was also detected (Fig 2A-C). Given our previous finding of a paucity of conventional (CD4 + CD25 + FOXP3 +) Tregs in the spinal enthesis [9], we compared the immunomodulatory phenotype and frequency of cells from the enthesis with those identified in a aingle-cell RNA sequencing (scRNA-seq) study of the intestine [2], another site of inflammatory involvement in SpA [21] (Fig 2D,E).

At the transcriptional level, entheseal and intestinal Tregs showed similar expression of *FOXP3, TIGIT, IL2RA,* and *CTLA4*. *IKZF2*, which encodes Helios, was detected in a much larger fraction of entheseal Tregs, indicating that a greater proportion of entheseal Tregs were thymic-derived, while the lower levels of *IKZF2* in the intestinal Treg population were consistent with the large numbers of peripherally induced Treg known to be present in the gut [22] (Fig 2D). Entheseal Tregs also showed more frequent expression of *TGFB1* [23]. Within the total T cell population, Tregs were present at a lower frequency in the T cell population of the healthy enthesis (2.60% ± 0.36%) compared to that of the healthy ileum (7.37% ± 4.47%) and healthy colon (18% ± 8.59%) (Fig 2E). For an annotation-free assessment of the regulatory potential of T cell in the enthesis, we scored the expression of Treg 'signature genes' in all T cells from the enthesis and intestine [24]. While most T cells in both tissues showed low regulatory scores, a subset of healthy intestinal T cells had high Treg signature scores (>0.5). In contrast, no T cells from the healthy enthesis showed high Treg signature scores (Supplementary Fig S2C). The entheseal T cell populations showed a lower cytotoxicity scores than T cells from the gut [25], potentially explaining the reduced frequency of Tregs present in the enthesis (Supplementary Fig S2C). To help confirm our findings, we also examined T cells from a murine enthesis dataset [26]. This analysis was limited by low T cell numbers, but consistent with our observations of low Treg frequency in the human enthesis, we did not detect Foxp3 messenger RNA (mRNA) or identify any cell predicted to be a Treg by automated annotation.

We hypothesised that the paucity of Tregs (and absence of T cells with high Treg signature scores) in the stromal compartment of the enthesis, compared to the intestine, might reflect the differing immunomodulatory requirements at these sites. Unlike the enthesis, the gut is a barrier site in which cytotoxic lymphocytes are important for host defence. Intestinal Tregs are essential for maintaining homeostasis and orchestrating tolerogenic responses to the microbiota [27,28]. In contrast, we reasoned that, at the enthesis, immunomodulation of inflammatory signals resulting from sterile physical stress and microdamage may rely on MSCs to maintain immune homeostasis rather than Tregs.

Enthesis-derived MSCs suppress T cell proliferation and modulate cytokine levels in a dose-dependent manner

To evaluate the immunomodulatory potential of EST-MSCs and PEB-MSCs, a direct contact coculture assay was conducted. Stimulated T cells were cocultured with EST-MSCs or PEB-MSCs at ratios of 1:1, 1:2, 1:4, and 1:8 (MSCs to stimulated T cells) for 5 days. Unstimulated T cells were negative controls, and stimulated T cells without MSCs were positive controls. On day 5 of coculture, T cells in suspension were collected from the supernatants and the suppression of their proliferation was assessed using flow cytometry, with gating on the CD45 + CD90−CD4 + CD25- population (Fig 3A,B). The proliferation index was then calculated and normalised to that of stimulated T cells. Coculturing with EST-MSCs and PEB-MSCs significantly
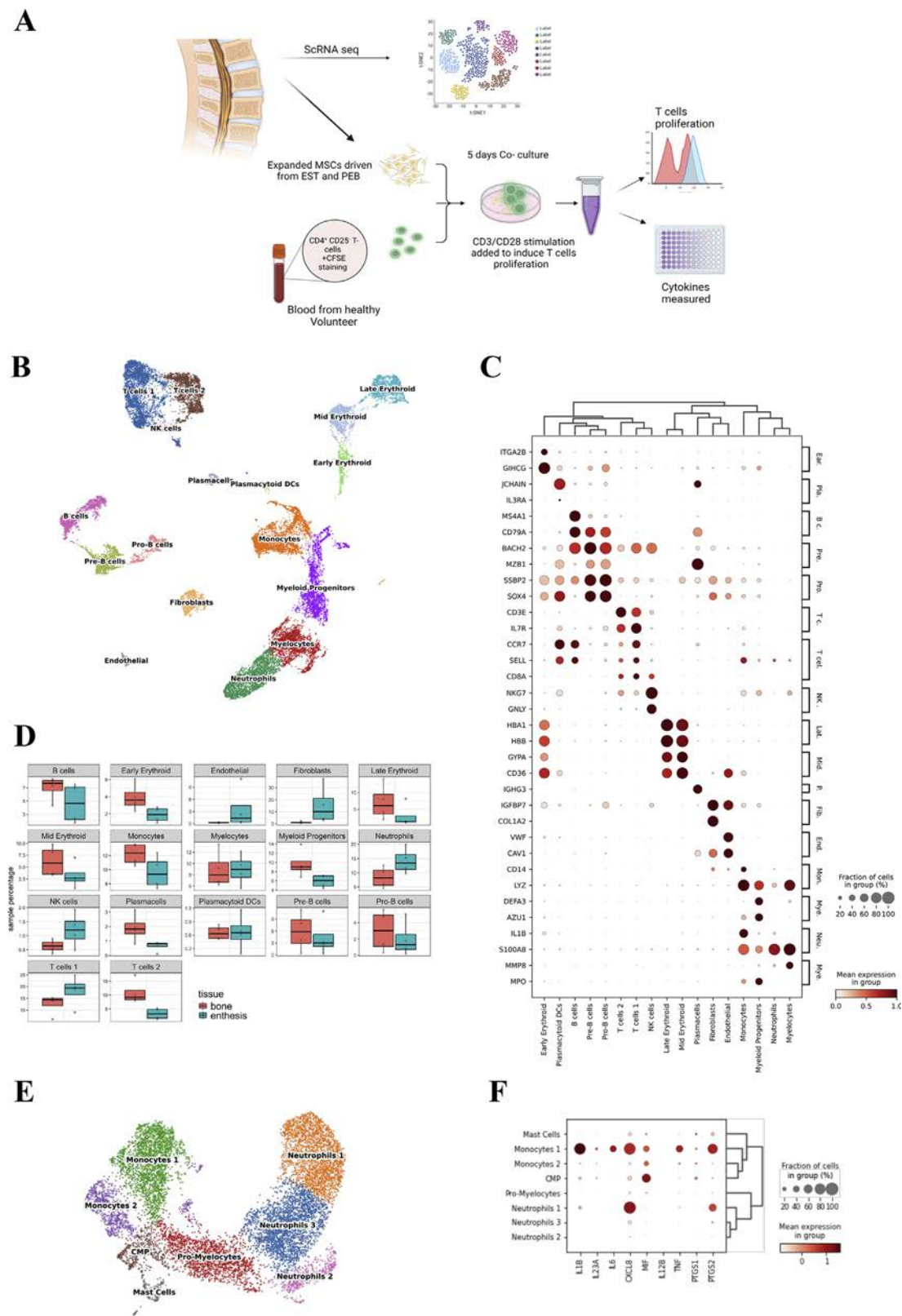
Figure 1. Single-cell atlas of the spinal enthesis: (A) schematic diagram outlining the study methodology. (B) The Uniform Manifold Approximation and Projection (UMAP) shows the annotated map of 27,348 single cells from peripheral enthesis bone (PEB) and entheseal soft tissue (EST). (C) Dot plot showing marker gene expression across identified cell clusters, with colour intensity indicating normalised expression and dot size representing the fraction of expressing cells. (D) The boxplots show the cellular composition by anatomical site within the enthesis complex. (E) The UMAP shows visualisation of myeloid cell subpopulations. (F) The dot plot shows the expression levels of key inflammatory mediators in the entheseal myeloid cell populations. CMP, common myeloid progenitor; MSC, mesenchymal stromal cell.
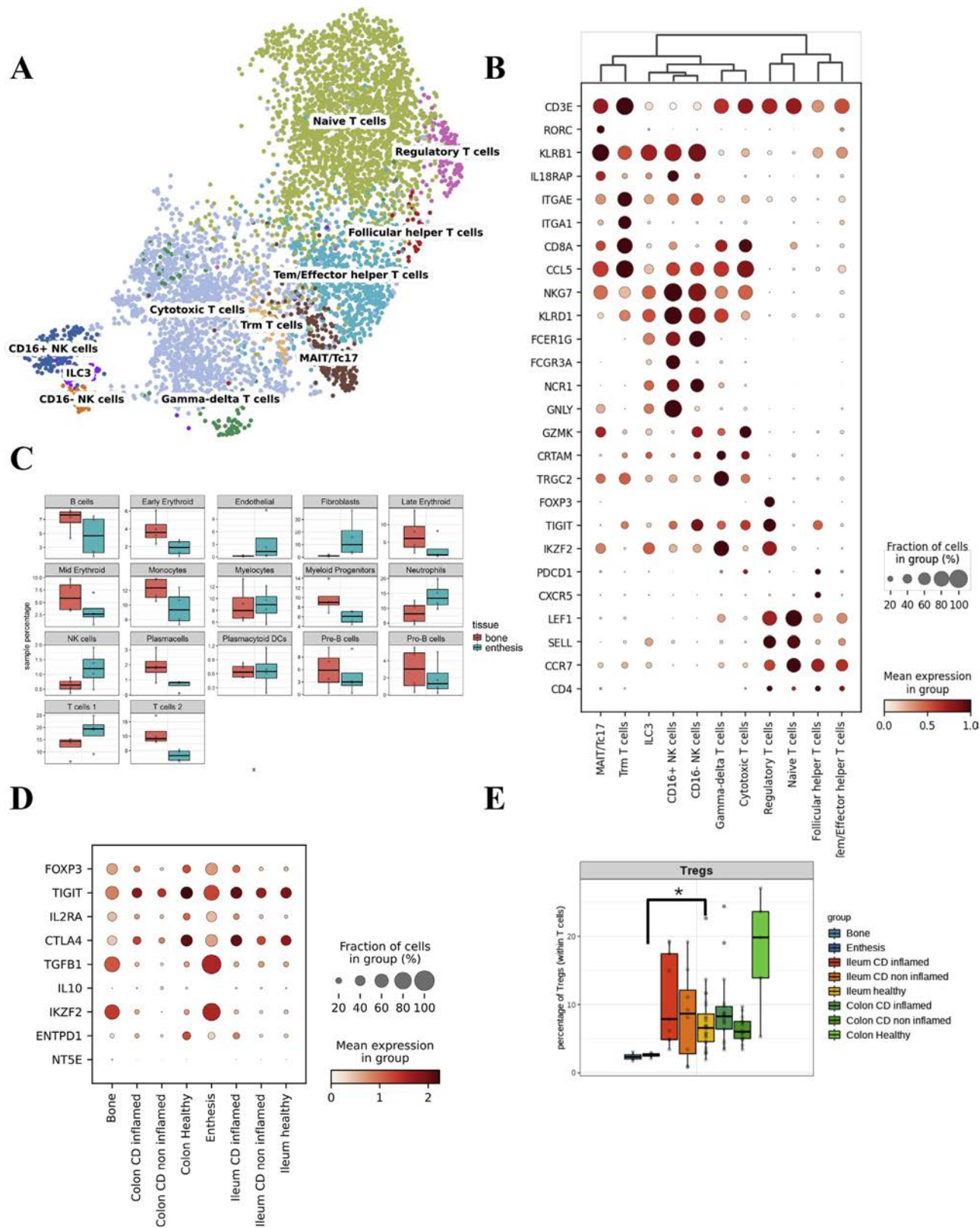
Figure 2. T cell subpopulations in the spinal enthesis: (A) UMAP visualisation of T cell transcriptomes from the spinal enthesis, showing distinct sub-populations. (B) Dot plot displaying marker gene expression across identified T cell clusters. (C) Cluster percentages across entheseal soft tissue and bone regions. (D) Regulatory marker expression in FOXP3+ regulatory T cells (Tregs) from enthesis tissue and intestinal sites (Crohn's disease and healthy controls). (E) Proportion of Tregs in total T cell populations across different anatomical sites (bone/enthesis n = 4, ileum n = 8-24, colon n = 5-17). Tregs were significantly lower in the enthesis compared to the intestine (Wilcoxon rank sum test, $P = .002$).
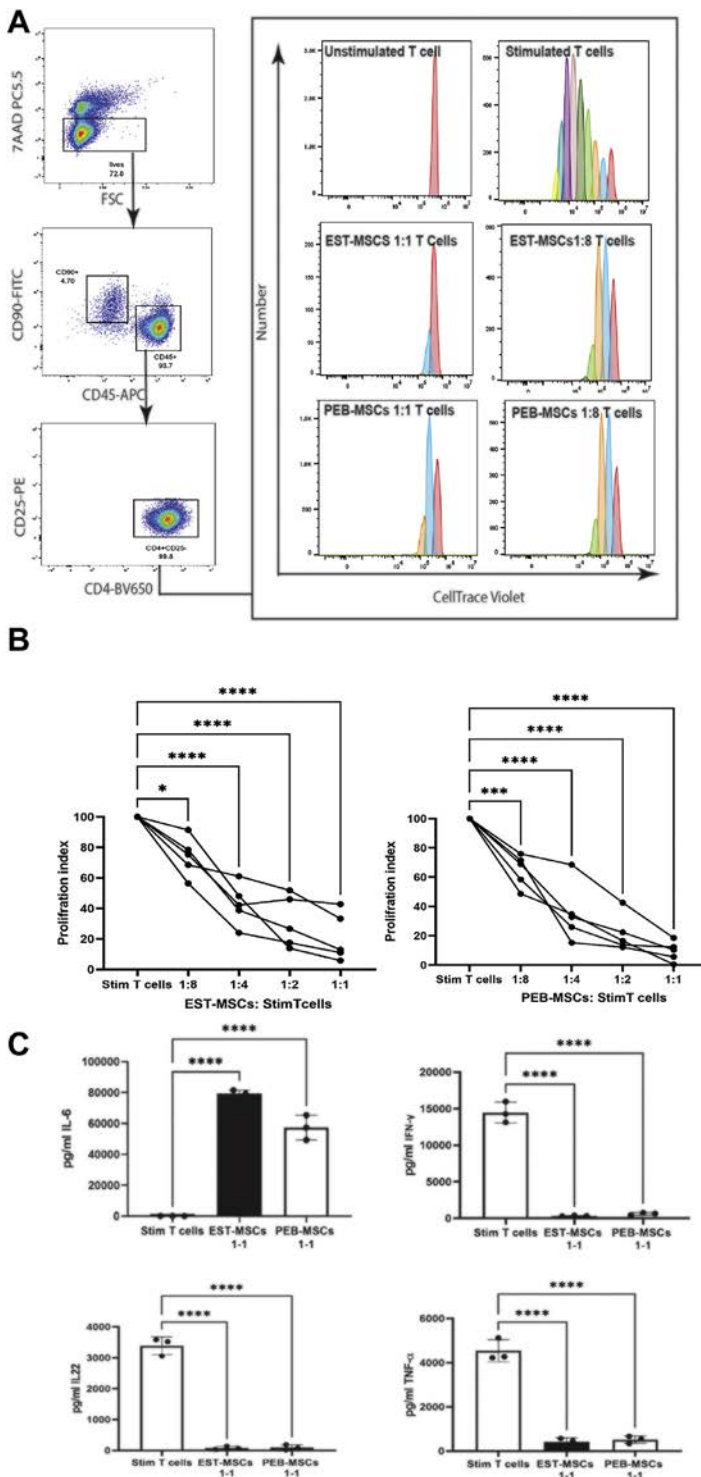
Figure 3. Immunomodulatory effects of EST-MSCs and PEB-MSCs on stimulated T cells: (A) T cells were cocultured with EST-MSCs or PEB-MSCs for 5 days, stained with CD90, CD45, CD4, CD25, and 7AAD for viability assessment. CD45+CD90−CD4+CD25−T cells were gated and analysed for proliferation. Histograms show proliferation suppression across increasing T cell ratios (n = 5). (B) Comparative analysis of T cell proliferation suppression by EST-MSCs (left) and PEB-MSCs (right) at varying ratios. Stimulated T cells alone serve as a positive control. (C) Cytokine levels (TNF-α, IFN-γ, IL-22, IL-6) in coculture supernatants were quantified (n = 3). Statistical significance was assessed using 1-way ANOVA ($P < .05$, $P < .001$, $P < .0001$). Error bars represent mean ± SD. FSC, forward scatter; ANOVA, analysis of variance; EST, entheseal soft tissue; IL, interleukin; IFN, interferon; MSC, mesenchymal stromal cell; TNF, tumour necrosis factor; PEB, peri-entheseal bone.

suppressed the proliferation of stimulated T cells. The most substantial suppression was observed at a 1:1 ratio of MSCs:T cells, with a proliferation index of 21.2% for EST-MSCs ($P < .0001$) and 9.5% for PEB-MSCs ($P < .0001$). As the MSCs:T cells ratio decreased, the proliferation index increased (Fig 3B): 31.2% ($P < .0001$), 42.9%($P < .0001$), and 74.1% ($P = .0205$) for EST-MSCs and 21.5% ($P < .0001$), 35.5% ($P < .0001$), and 64.7% ($P = .0006$) for PEB-MSCs at ratios of 1:2, 1:4, and 1:8, respectively. No significant difference was found between the abilities of EST-MSCs and PEB-MSCs to suppress T cell proliferation ($P = .746$), suggesting that EST-MSCs and PEB-MSCs suppressed T cell proliferation in a dose-dependent manner.

Additionally, cytokine levels were measured in the supernatants of cocultured cells at the 1:1 ratio, where the most

significant suppression of T cell proliferation was observed. The T cell proliferation-related cytokines TNF-a, interferon-y, and IL-22 were significantly reduced with both EST-MSCs and PEB-MSCs ($P < .0001$). On the other hand, IL-6 was significantly increased at 1:1 ratio with both EST-MSCs and PEB-MSCs ($P < .0001$), consistent with its known abundant production by fibroblasts and also potentially its known immunoregulatory role in T cells [30] (Fig 3C).

Spinal enthesis-derived MSCs suppress T cell activation through CD39/CD73 axis

To explore the immunosuppressive mechanism mediated by spinal enthesis MSCs, we assessed the surface expression of the
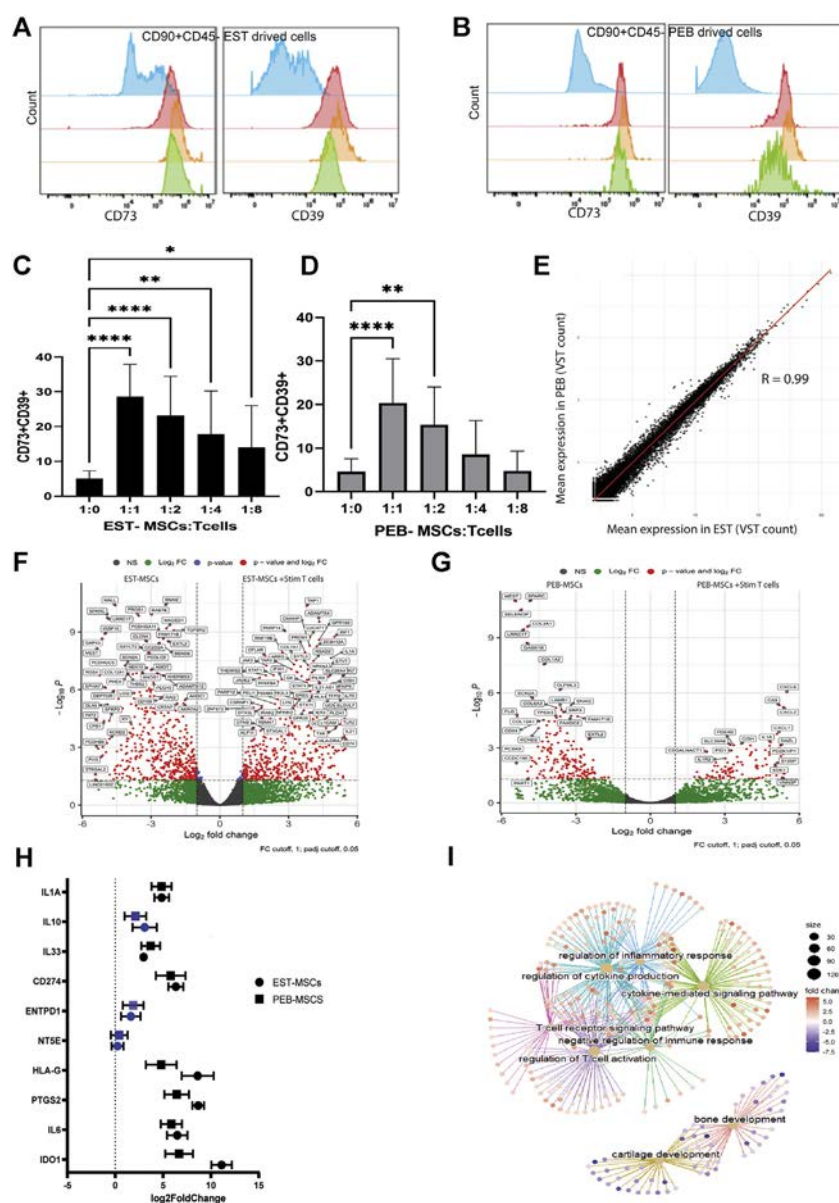
Figure 4. Mechanism of T cell Suppression by EST-MSCs and PEB-MSCs: (A, B) Flow cytometry histograms illustrating CD73 and CD39 expression on native CD90 + CD45− EST and PEB-MSCs. Blue histograms represent unstained controls, while red, orange, and green indicate stained cells (n = 3). (C, D) CD73 and CD39 expression on EST-MSCs and PEB-MSCs after coculture with stimulated T cells for 5 days at varying ratios (n = 5). Statistical significance assessed via 1-way ANOVA, with $P < .05$ considered significant. Error bars represent mean ± SD. (E) Pairwise correlation of average gene expression between EST and PEB-MSCs. Each point represents 1 gene. Pearson correlation coefficient (r > 0.99) (F, G) Volcano plots displaying differentially expressed genes in EST-MSCs and PEB-MSCs (n = 3) after coculture with stimulated T cells (1:1 ratio), compared to controls. (H) Log fold change of differentially expressed genes in cocultured EST-MSCs and PEB-MSCs with stimulated T cells, compared to MSCs without inhibitors (n = 3). (I) Cnet plot illustrating upregulated and downregulated pathways via gene set enrichment analysis (GSEA). Expression intensity is colour-coded (blue = upregulated, red = downregulated) relative to controls (MSCs only). VST, variance stabilizing transformation; ANOVA, analysis of variance; EST, entheseal soft; MSC, mesenchymal stromal cell; TNF, tumour necrosis factor; PEB, peri-entheseal bone.

CD39/CD73 axis markers on resting entheseal MSCs and on MSCs expanded in culture after their coculture with stimulated T cells.

Cells derived from uncultured CD90 + CD45− EST and PEB showed expression of CD73 and CD39 (Fig 4A,B). A significant difference was observed in the coexpression of CD73 + CD39 between EST CD90 + CD45− cells and PEB CD90 + CD45− cells, with proportions of 2.08 and 51.93, respectively (P = .0143) (Supplementary Fig S3). We next investigated whether the expression of CD39 and CD73 by entheseal MSCs could be induced by stimulated T cells. Coculture of EST-MSCs and PEB-MSCs with stimulated T cells led to an elevation in the expression levels of CD39 and CD73, with the highest expression observed at a 1:1 ratio compared to the negative control (MSCs without T cells) ($P < .0001$) (Fig 4C,D). In keeping with their comparable immunosuppressive function, the transcriptomes of EST and PEB-MSCs were highly similar, showing a Pearson correlation of r > 0.99 (Fig 4E), and a differential expression analysis (DESeq2, Benjamini−Hochberg adjusted $P < .05$, log$_2$ fold change > 1) identified no genes with significant differential expression between the 2 populations (Supplementary Fig S3B).

To further delineate the mechanism of T cell proliferation suppression, we performed bulk RNA-seq profiling of cocultures of spinal enthesis MSCs and T cells. MSCs cocultured with stimulated T cells had a significantly different transcriptomic profile to the MSCs with no coculture. In EST-MSCs, coculture with stimulated T cells upregulated 390 and downregulated 306 genes (DESeq2, Padj < .05, |log2FoldChange| > 2) (Fig 4F; Supplementary File S1). Key significantly upregulated transcripts included those encoding *IDO1* (11-fold, Padj < .0001), *PTGS2* (8.7-fold, Padj < .0001), *IL1A* (4.9-fold, Padj < .0001), *IL6* (6.5-fold, Padj < .0001), and *IL33* (3.0-fold Padj < .0001). While these latter cytokines are well known for their proinflammatory functions, their expression in both fibroblasts and MSCs has also been associated with context-specific immunoregulatory effects, including modulation of T cell responses and support of immune homeostasis [29,30]. Immune checkpoint regulators such as *HLA-G* (8.6-fold, Padj < .0001) and CD274 (6.3-fold, Padj < .0001) were also significantly upregulated. Transcripts from the genes encoding CD39 and CD73 (*ENTPD1* and *NT5E*) showed small, nonsignificant increases compared to MSCs with no coculture (Fig 4H).

Table

Functional enrichment analysis results using gene set enrichment analysis

| | | EST-MSCs | | PEB-MSCs | |
| | | EST | | PEB | |
ID	Description	NES	*P*adj	NES	*P*adj
GO:0050727	Regulation of inflammatory response	1.869168673	1.36834E−06	1.790646268	1.19929E−05
GO:0019221	Cytokine-mediated signalling pathway	2.495508595	1E−10	2.568040444	1E−10
GO:0050863	Regulation of T cell activation	2.374466468	1E−10	2.457049726	1E−10
GO:0060348	Bone development	−1.957946691	1.63464E−06	−1.815266647	4.20194E−05
GO:0051216	Cartilage development	−1.920879981	5.70038E−06	−1.924765499	9.65674E−06

EST, entheseal soft; MSC, mesenchymal stromal cell; PEB, peri-entheseal bone.

This table presents the identified upregulated and downregulated pathways obtained from gene enrichment set analysis, including the normalised enrichment score (NES) and corresponding *P*adj.

In PEB-MSCs, 90 transcripts were upregulated and 119 were downregulated (Fig 4G; Supplementary File S2). Similar trends were observed, with significant upregulation of IDO1 (6.7-fold, *P*adj < .0001), PTGS2 (6.4-fold, *P*adj < .00001), IL1A (4.8-fold, *P*adj < .0001), IL6 (5.9-fold, *P*adj < .0001), and CD274 (5.7-fold, *P*adj < .05). As for the PEB-MSCs, *ENTPD1* and *NT5E* showed small, nonsignificant increases (Fig 4H).

Gene set enrichment analysis revealed shared enrichment in key immunosuppressive pathways in both MSC types. These included 'regulation of inflammatory response' (normalised enrichment score [NES] = 1.87, *P*adj < .0001 for EST-MSCs, NES = 1.79, *P*adj < .0001 for PEB-MSCs), 'Cytokine-mediated signalling' (NES = 2.49 *P*adj < .0001 for EST-MSCs, 2.56 *P*adj < .0001 for PEB-MSCs), and 'Regulation of T cell activation' (NES = 2.37 *P*adj < .0001 for EST-MSCs, 2. *P*adj < .0001 for PEB-MSCs) (Table). Downregulated pathways included 'Cartilage development' (NES = −1.92 for both MSC types) and 'Bone development' (NES = −1.95 *P*adj < .0001 for EST-MSCs, −1.81 *P*adj < .0001 for PEB-MSCs), indicating a shift from differentiation to immunoregulation (Fig 4I, Table).

Several genes known to be upregulated in *in vitro* Treg suppression assays were also significantly increased in EST-MSCs and (2.1-fold, *P*adj = .008) in PEB-MSCs) including *IDO1, PTGS2,* CD274, *IL10,* and *HLA-G* in addition to *IL33* (3.0-fold, *P*adj < .00001), further highlighting the role of these MSCs in immunomodulation associated with Treg function (Fig 4G).

Taken together, these findings confirm that MSCs from both EST and PEB upregulate multiple transcripts associated with Treg-mediated suppression when cocultured with activated T-cells, with EST-MSCs showing consistently higher expression levels.

Entheseal ENTPD1 derived immunoregulatory MSCs express CXCL12

To identify whether native entheseal MSCs exhibited regulatory functions, we performed a separate analysis of these from our single-cell atlas, which predominantly originated from the soft tissue entheseal portion of each sample, consistent with the higher cellularity of this location. High-resolution clustering revealed 7 groups, including tendon cells (TMND + fibroblasts) and myofibroblasts (*MYL9, ACTA2*) (Fig 5A,B). Among the remaining clusters, we hypothesised that the CXCL12+ cells, expressing *ENTPD1* and *LEPR* [31] (Fig 5C), and at least in part *NGFR* (encoding CD271 that is a marker for native MSCs), likely contained cells with immunoregulatory transcript expression. CXCL12+ cells were enriched in the bone marrow enthesis anchorage locations compared to soft tissue, in keeping with the

known role of CXCL12 (which encodes for SDF-1) in regulating haematopoiesis (Fig 5D). Conversely, *NT5E* expression was more diffuse across various MSC cell subsets. Given that contact with activated T cells upregulates these markers (Fig 4C,D), it is plausible that more than 1 subtype of MSCs may be involved in maintaining enthesis integrity and promoting immune homeostasis. To help confirm our findings, we examined 2 publicly available single-cell RNA-seq datasets from murine enthesis tissue [26,32]. While we did not find an identical counterpart to the human CXCL12+ regulatory MSCs, both *Nt5e* (CD73) and *Entpd1* (CD39) were expressed in the adult murine enthesis samples from both datasets (Supplementary Fig S4). Together, these data support the conclusion that fibroblast populations capable of immunomodulatory functions are conserved in human and mice entheses. While TNMD + SCX + MKX + cells are canonically associated with tendon/ligament, their enrichment in PEB-derived clusters may reflect either true anatomical extension into adjacent bone as small entheses have a relatively paucity of fibrocartilage compared to large ones, thus making microanatomical dissection technically challenging and resulting in partial tissue overlap during dissection. Other hitherto undefined factors may be involved, but this limitation does not affect our broader immunoregulatory findings, which were validated in anatomically separated cultures. Future studies incorporating spatial validation techniques such as immunohistochemistry (IHC) or Visium-based transcriptomics are warranted to map the tissue distribution of tenogenic and stromal subsets with greater anatomical resolution. Further, in one of the samples, we noted the presence of a cluster of cells that co-expressed *Entpd1*, *Nt5e*, *Cxcl12*, and *Tgfb1* (GSE182997 cluster 2; Supplementary Fig S4). Together, these data support the conclusion that fibroblast populations capable of immunomodulatory functions are conserved in human and mice entheses.

MSC-mediated adenosine pathway involvement modulates T cell proliferation

Given that CD73 and CD39 were both expressed by EST-MSCs and PEB, we tested the capacity of entheseal MSCs to mediate immunomodulation via the adenosine pathway. EST-MSCs and PEB-MSCs were treated with specific inhibitors targeting CD73 and CD39 (APCP and POM-1, respectively). These cells were subsequently cocultured with stimulated T cells at both 1:1 and 1:4 ratios, and single and double blockage experiments were conducted, and the impact on the suppression of T cell proliferation was determined at day 5.

To verify adenosine production and inhibition, we quantified the total adenosine production in the supernatant and observed
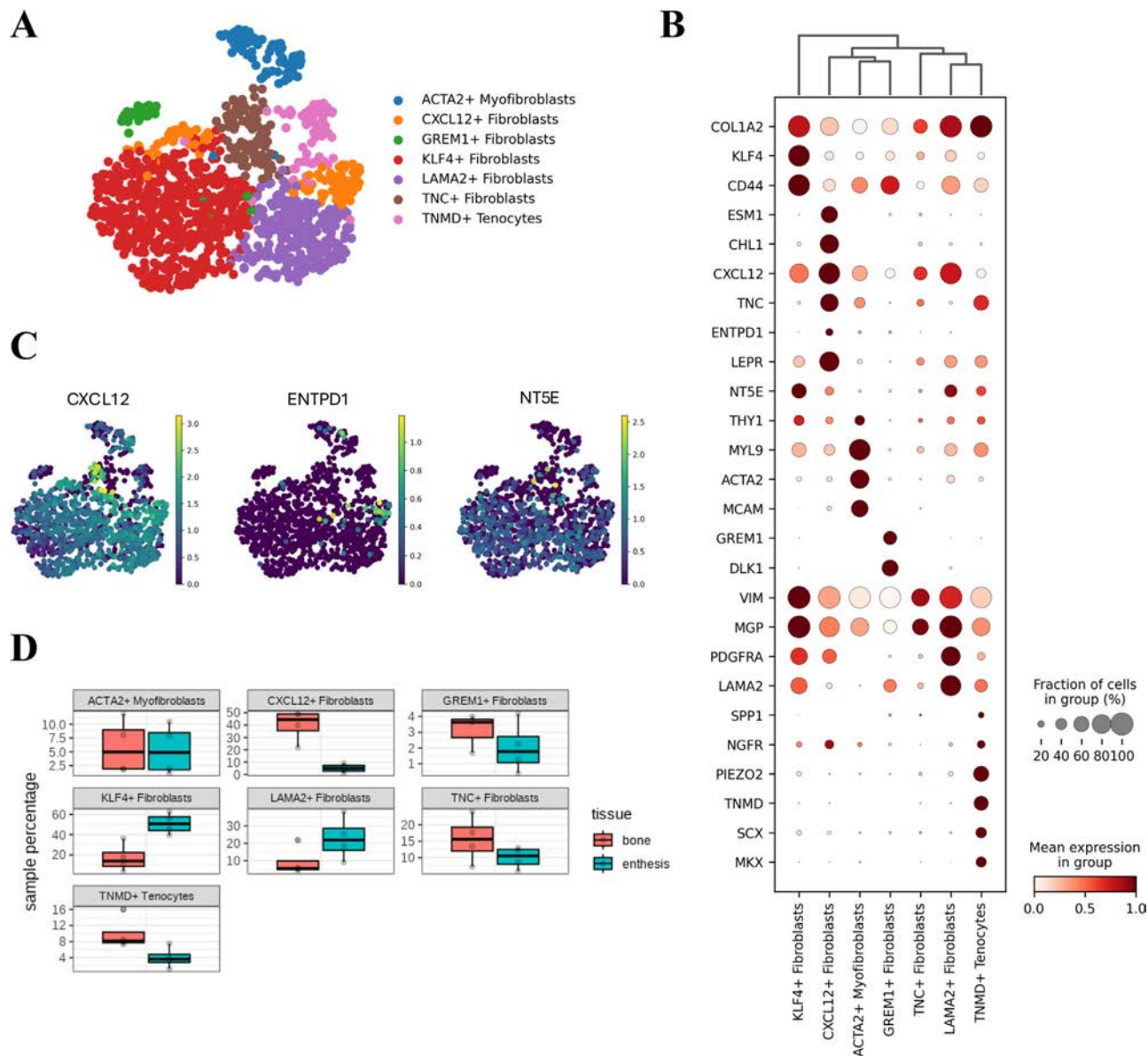
Figure 5. Stromal cells in the enthesis express CXCL12 and ENTPD1: (A) UMAP visualisation of stromal cells from the spinal enthesis, displaying distinct cellular clusters. (B) Dot plot showing marker gene expression across identified stromal cell subsets. (C) Expression of markers of CXCL12+ fibroblasts. (D) Cluster percentages across tissue sites.

a significantly increased adenosine production at a 1:1 coculture compared to MSCs alone ($P < .0001$) (Fig 6A). However, the blockade of CD39 and/or CD73 on MSCs cocultured with stimulated T cells substantially reduced adenosine production ($P < .0001$) compared to untreated cocultured MSCs.

Next, we assessed the impact of adenosine inhibition on the ability of MSCs to control the proliferation of stimulated T cells. We observed an increase in the proliferation index of T cells by 18% ($P = .2934$) and 35% ($P = .2934$) with EST-MSCs and PEB-MSCs pretreated with the CD73 blocker APCP. Similarly, at a 1:1 ratio, the proliferation increased by 12% ($P = .8397$) and 26% ($P = .8397$) with EST-MSCs and PEB-MSCs pretreated with the CD39 blocker POM-1, compared to cocultured T cells with untreated MSCs. Dual blockade of CD39 and CD73 led to a 47% and 48% increase in T cell proliferation with EST-MSCs ($P = .0004$) and PEB-MSCs ($P = .0004$) (Fig 6B,C). Similar comparisons were made at a 1:4 ratio, for which the pretreatment of EST-MSCs and PEB-MSCs with APCP increased T cell proliferation by 29% ($P = .3542$) and 20% ($P = .3542$), respectively.

Likewise, T cell proliferation increased by 39% and 20% following POM-1 treatment with EST-MSCs and PEB-MSCs, respectively ($P = .1639$). However, pretreatment of EST-MSCs and PEB-MSCs with both APCP and POM-1 resulted in the loss of the ability to suppress T cell proliferation, as evidenced by a 90% and 87% increase in the proliferation index of T cells cocultured with EST-MSC and PEB-MSCs, respectively ($P < .0001$) compared to cocultured T cells with untreated MSCs (Fig 6B,C).

To explore the effects of adenosine pathway inhibition on MSC-mediated immunoregulation, we performed bulk RNA-seq on EST- and PEB-derived enthesis MSC cocultured with activated T cells in the presence or absence of CD73 and CD39 inhibitors (APCP and POM-1, respectively).

To visualise transcriptomic changes following dual CD39/CD73 blockade, we generated a volcano plot comparing EST-MSCs/PEB-MSCs cocultured with activated T cells ± APCP and POM-1 combined (Fig 6D). Several immunomodulatory transcripts of interest—including *IDO1, HLA-G, IL1A, IL6, PTGS2, IL10, NT5E, ENTPD1,* and *CD274*—were consistently
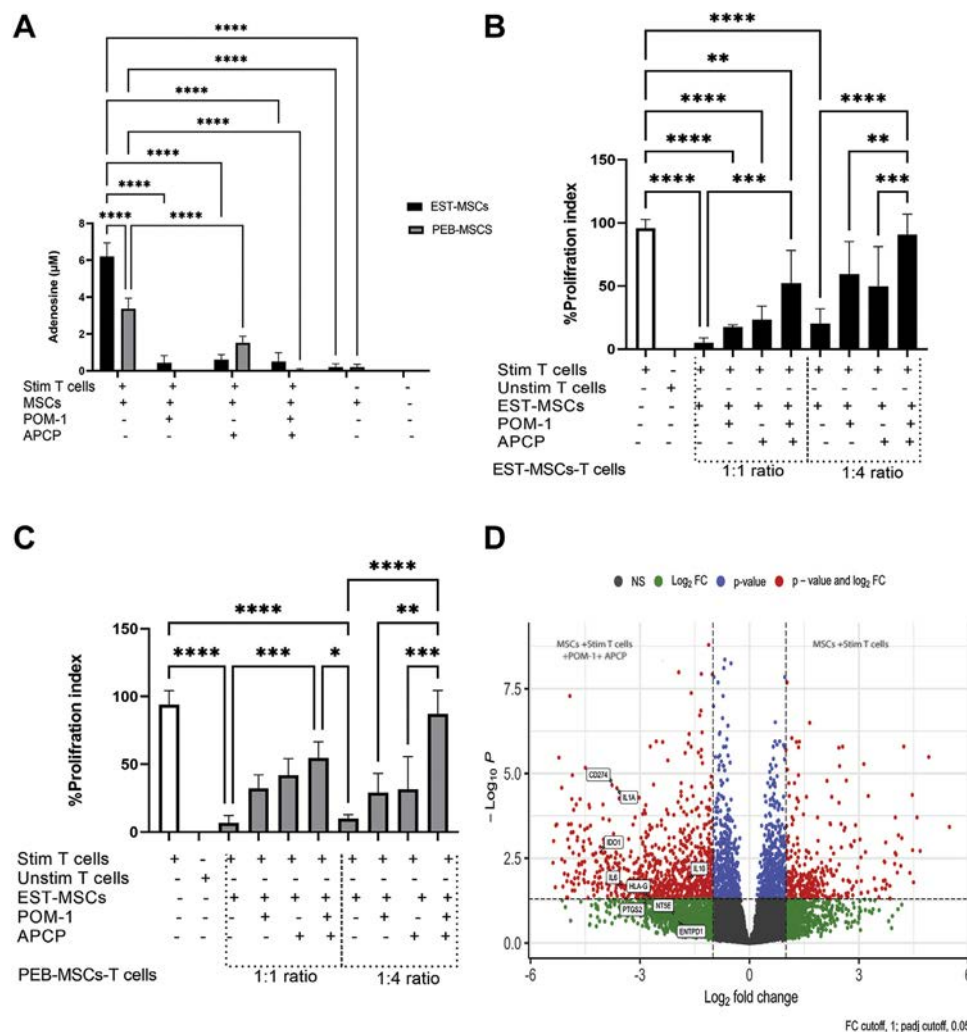
Figure 6. Impact of adenosine pathway inhibition on MSC-mediated immunosuppression of activated T cells: (A) total adenosine levels in supernatants from EST-MSCs and PEB-MSCs pretreated with CD73 inhibitor (APCP) and CD39 inhibitor (POM-1), followed by coculture with stimulated T cells at varying ratios (n = 3). (B, C) T cell proliferation index after coculture with EST-MSCs and PEB-MSCs pretreated with 50 μM APCP and 100 μM POM-1 at 1:1 and 1:4 ratios (n = 5). (D) Volcano plot showing differentially expressed genes in MSCs following coculture with activated T cells versus MSCs treated with APCP and POM-1. Red dots represent significantly upregulated genes (adjusted $P < .05$; $|\log_2 FC| > 1$) (n = 3). EST, entheseal soft; MSC, mesenchymal stromal cell; PEB, peri-entheseal bone; POM-1, sodium polyoxotungstate; APCP, α, ß-methylene ADP.

downregulated with fold changes exceeding the $\log_2(FC)$ threshold of -1. MSCs, transcripts were downregulated following inhibition including *IDO1* (-4.07 fold, Padj $= .002$), *PTGS2* (-2.8 fold, Padj $= .05$), *IL1A* (-3.6-fold, Padj $< .0001$), *IL6* (-3.4fold, Padj $< .05$), *HLA-G* (-2.6 fold, Padj $< .05$), and *CD274* (-3.7-fold, Padj $< .0001$) (Supplementary File S3 and Supplementary Fig S3C).

DISCUSSION

The enthesis is a biomechanically dynamic interface between tendons or ligaments and bone. It constantly undergoes microdamage and repair and is a key site of pathology in SpA [33,34]. The existence of a gut-joint and a gut-enthesis axis in SpA is also well-recognised but the immunological mechanisms underlying shared entheseal and intestinal immune homeostasis remain poorly understood [35]. This study provides the first detailed single-cell atlas of healthy human spinal enthesis, offering new insights into its cellular architecture and immunoregulatory dynamics. A key finding from our study was the paucity of FOXP3+ Tregs that we observed in the enthesis relative to the gut [2,9]. This low entheseal Treg presence contrasts with the

robust immunosuppressive environment maintained at the enthesis, implicating MSCs as the key contributors to local immune regulation, a function that complements, rather than replaces, canonical Treg-mediated tolerance seen in other tissues. Given that MSCs are especially abundant in the EST adjacent to fibrocartilage in the soft tissue side of the enthesis further supports a key role of this pathway at that location. By leveraging multiple pathways, including the CD73/CD39 adenosine axis, which is also operative in stromal cells from other tissues, MSCs appear to be to contribute to the regulation of immune responses in the enthesis, potentially compensating for the paucity of entheseal Tregs in health, ensuring immune homeostasis in this mechanically stressed tissue [17,18]. Nevertheless, it is plausible that the relative absence of Tregs at entheseal sites may help to explain their susceptibility to inflammation and damage in SpA. It is tempting to speculate that the immunosuppressive capacity of MSCs can be overcome by the infiltration of 'arthritogenic' self-reactive T cells into these normally sterile tissues [36].

The CD73/CD39 adenosine axis plays a vital role in MSC-mediated immunoregulation [14]. This pathway catalyses the conversion of extracellular ATP and ADP, released during tissue

stress or injury, into immunosuppressive adenosine [17,37]. Our findings demonstrate that both EST-MSCs and PEB-MSCs express CD73 and CD39, with further upregulation observed in the presence of activated T cells. While *ENTPD1* (CD39) and *NT5E* (CD73) transcripts showed only modest, statistically insignificant, changes compared to MSCs without coculture, the increased surface protein levels (Fig 4C) suggested that the surface levels of these factors are regulated post-transcriptionally. The translation efficiency and stability of CD39/CD73 proteins may be modulated independently of mRNA levels, leading to increased surface expression [38]. Another possibility is intracellular trafficking, where CD39/CD73 might have an intracellular reservoir that is trafficked to the membrane under coculture conditions, contributing to elevated surface levels [39]. Additionally, protein recycling and shedding could be involved, with CD39/CD73 undergoing rapid cycling between intracellular compartments and the plasma membrane. Additionally, a reduction in protein turnover could lead to accumulation on the surface [40]. This dynamic response underscores the adaptive capacity of MSCs to modulate inflammation in response to local signals. However, in SpA, this pathway may become dysregulated or overwhelmed by chronic inflammation and elevated levels of proinflammatory cytokines [12,14].

Consistent with a role of this pathway in immunosuppression, inhibition of CD73/CD39 led to a significant reduction in adenosine levels, a 50% increase in T cell proliferation, and downregulation of key immunosuppressive transcripts, including *IDO1*, *PTGS2*, *IL10*, and *HLA-G*. Although we observed partial reversal of MSC-mediated suppression with pharmacologic CD39 and CD73 blockade, we acknowledge that these inhibitors —particularly POM-1—can have off-target effects on other nucleotidases. Our approach mitigated this by applying inhibitors exclusively to MSCs and confirming that T cell only viability and proliferation were unaffected. While siRNA or blocking antibodies could provide complementary validation, transfection efficiency in primary MSCs is low and donor-to-donor variability further limits standardisation. This limitation of our study could be addressed in future by the use of genetic or antibody-based strategies to inhibit the adenosine pathway. We acknowledge that pharmacologic inhibition, even transient, may reprogramme MSC transcriptional or metabolic states, and thus the observed effects on T cells may not solely reflect acute adenosine pathway blockade. Gene knockdown or clustered regularly interspaced short palindromic repeats (CRISPR)-based deletion of *ENTPD1* and *NT5E* in MSCs would provide complementary mechanistic validation and is a priority for future work.

Our observation that CD73/CD39 inhibition led to approximately a 50% increase in T cell proliferation indicates that EST/ PEB-MSCs employ additional immunosuppressive mechanisms that complement the CD73/CD39 axis, and we found evidence that MSCs can utilise multiple immunomodulatory pathways to suppress inflammation and promote immune tolerance. Transcriptomic profiling revealed upregulation of several key molecules during MSC-T cell interactions [41,42]. These molecules collectively contribute to the suppression of T cell proliferation, modulation of cytokine production, and promotion of tolerogenic immune phenotypes. Notably, EST-MSCs demonstrated consistently higher expression of these molecules compared to PEB-MSCs, reflecting site-specific functional adaptations at the entheseal soft tissue and bone anchorage. The upregulation of *IDO1*, a key enzyme in tryptophan metabolism, highlights its role in creating an immunosuppressive microenvironment, while the elevation of PGE2 (mediated by *PTGS2*) underscores the importance of lipid mediators in MSC-driven immune modulation [30,43].

The observed overexpression of checkpoint molecules such as CD274 and HLA-G further indicates the convergence of MSCs and Tregs on shared immunoregulatory mechanisms, supporting the hypothesis that MSCs act as surrogate immune regulators in the enthesis. Although transcriptomic profiling revealed consistent upregulation of key immunomodulatory genes (eg, *IDO1*, *PTGS2*, *IL6*, *HLA-G*, *CD274*), we recognise that post-transcriptional regulation may alter protein output. Similar to our validation of CD39 and CD73 levels by flow cytometry, assessment of these additional immunomodulatory factors using protein-based techniques (eg, ELISA or immunoblotting) will be important for future studies of their roles in entheseal immunomodulation. We noted enthesis MSC upregulation of several cytokine transcripts widely known for their proinflammatory roles, including *IL6*, *IL1A*, and *IL33,* following T cell coculture. The functions of these factors is however known to be context-specific, and when produced by stromal cells they have been shown to promote Treg induction, control local inflammation, and support tissue tolerance [44,45] In particular, MSC-derived IL-6 has been shown to support Treg stability, promote the development of myeloid-derived suppressor cells, to contribute to immune resolution in barrier tissues and to suppress T cell proliferation [30,46,47], in support of the concept that enthesis MSC-derived IL-6 may contribute to local immune homeostasis.

MSCs have emerged as pivotal orchestrators of immunomodulation in addition to their well-recognised multilineage differentiation capacity in skeletal tissues [48] Within the spinal enthesis, 2 distinct subpopulations of multipotential MSCs have been previously identified: a PEB-derived stroma (PEB-MSCs) and interspinous ligament EST-derived stroma (EST-MSCs), as defined according to ISCT guidelines ref. Both populations share the ability to undergo multilineage differentiation into skeletal tissue elements, including bone [49]. It is known that MSCs exert multifaceted immunosuppressive effects on various immune cells, including B and T cells, NK cells [50]. These effects are mediated by the secretion of soluble factors such as IDO1, PGE2, TGF-β, IL-10, and IL-6, as well as by direct T cell −cell interactions, including via PD-L1.

While MSCs with immunomodulatory potential were first described in culture-expanded bone marrow fractions and thereafter in other tissues, our data provide the first description of these cells in the context of enthesis immunobiology [48,51]. While this property is not exclusive to the enthesis, its presence in a tissue with a low Treg frequency and known susceptibility to inflammation is notable. The immunosuppressive capacity of MSCs/stromal cells is well-documented in other tissues, including the skin and bone marrow, and has been therapeutically exploited in conditions such as graft-vs-host disease using MSC-based therapies (eg, Ryoncil). Indeed, dermal fibroblasts and other tissue-resident stromal cells can suppress immune responses via similar mechanisms [51]. Therefore, our findings extend these principles to the spinal enthesis and support the concept that resident MSCs help maintain local immune homeostasis in mechanically stressed, immune-sparse environments. Future comparative studies using fibroblasts from other uninflamed tissues (eg. skin or lung) may further delineate tissue-specific versus shared features of stromal immunoregulation. Finally, we unexpectedly noted that TNMD+ SCX+ MKX + cells, which are canonically associated with tendon/ligament, were more enriched at the bony anchorage side of the enthesis but both EST and PEB-derived cells had broadly similar immunoregulatory capabilities. Future studies incorporating spatial validation techniques such as IHC or Visium-based transcriptomics are warranted to map the tissue distribution of these stromal subsets with greater anatomical resolution

Our findings have significant implications for the pathophysiology and treatment of SpA [52]. Dysregulation of MSC pathways, particularly the CD73/CD39 axis, may underpin the immune imbalance observed in SpA, providing a rationale for targeting the enhancement adenosine levels via CD73/CD39 pathway manipulation. The identification of regulatory MSC subsets also opens new avenues for precision targeting of specific niches within the enthesis. However, as in murine arthritis models, it is recognised that during the induction of enthesitis that Treg and other cells may migrate from the intestine to the enthesis and thus may assume increased importance during inflammation [53]. Some TNF transgenic models specifically exhibit intestinal and an enthesitis immunopathology [54]. When this TNF-dependent SpA model is crossed with the depletion of Tregs (DEREG) mice, Tregs accumulate in arthritic joint [55]. Nevertheless, the translocation of Tregs to inflamed joints in human SpA, and their possible functional contribution, if present, remains to be investigated.

In conclusion, our findings reveal an immunoregulatory function for MSCs in the human enthesis, extending observations made in other tissue-resident stromal cells, and support their potential role for these cells in normal enthesis immune homeostasis. The dynamic interplay between MSCs and immune cells, mediated by pathways such as CD73/CD39, underscores the adaptive nature of enthesis immune regulation. Future research should focus on comparing healthy and SpA-affected entheses at single-cell resolution, elucidating the mechanisms by which inflammation disrupts MSC function, and explore innovative MSC-based therapies. In summary, compared to the intestine, we found a paucity of entheseal Tregs but evidence that entheseal MSCs subsumed functional attributes of Tregs. These findings have implications for a better understanding of the translational immunology of human SpA, particularly in relation to tissue-specific stromal−immune interactions.

Funding

Competing interests

All authors declare they have no competing interests.

CRediT authorship contribution statement

Ala Altaie: Writing − original draft, Visualization, Validation, Methodology, Investigation, Formal analysis, Data curation, Conceptualization. **Davide Simone:** Writing − original draft, Visualization, Formal analysis. **Nicole McDermott:** Data curation. **Heather Owston:** Data curation. **Moustafa Attar:** Data curation. **Liying Jin:** Data curation. **Chi Wong:** Data curation. **Peter R. Loughenbury:** Resources. **Borse Vishal:** Resources. **Tristan McMillan:** Resources. **Christopher D. Buckley:** Writing − review & editing. **Stephen N. Sansom:** Writing − review & editing, Supervision, Conceptualization. **Dennis McGonagle:** Writing − review & editing, Supervision, Funding acquisition, Conceptualization.

Patient consent for publication

Written informed consent was obtained from all participants.

Ethics approval

Ethical approval for the study was approved by the Northwest-Greater Manchester West Research Ethics Committee (REC:16/NW/0797). And were in accordance with the Decleration of Helsinki-Ethical Principles for Medical Research Involving Human Subjects.

Provenance and peer review

Not commissioned; externally peer reviewed.

Data availability statement

The single-cell RNAseq data generated in this study have been deposited in the GEO database under accession code GSE292866 (raw data) and Zenodo database under accession 15090823 (processed data).

Supplementary materials

Supplementary material associated with this article can be found in the online version at doi:10.1016/j.ard.2025.09.001.

Orcid

Ala Altaie: http://orcid.org/0000-0002-9203-1490

REFERENCES

[1] Hughes TK, Wadsworth 2nd MH, Gierahn TM, Do T, Weiss D, Andrade PR, et al. Second-strand synthesis-based massively parallel scRNA-Seq reveals cellular states and molecular features of human inflammatory skin pathologies. Immunity 2020;53(4):878–94 .e7.

[2] Kong L, Pokatayev V, Lefkovith A, Carter GT, Creasey EA, Krishna C, et al. The landscape of immune dysregulation in Crohn's disease revealed through single-cell transcriptomic profiling in the ileum and colon. Immunity 2023;56(2):444–58 .e5.

[3] Benjamin M, McGonagle D. Entheses: tendon and ligament attachment sites. Scand J Med Sci Sports 2009;19(4):520–7.

[4] Manasson J, Wallach DS, Guggino G, Stapylton M, Badri MH, Solomon G, et al. Interleukin-17 Inhibition in spondyloarthritis is associated with subclinical gut microbiome perturbations and a distinctive interleukin-25-driven intestinal inflammation. Arthritis Rheumatol 2020;72(4):645–57.

[5] Qaiyum Z, Lim M, Inman RD. The gut-joint axis in spondyloarthritis: immunological, microbial, and clinical insights. Semin Immunopathol 2021;43(2):173–92.

[6] Gracey E, Vereecke L, McGovern D, Fröhling M, Schett G, Danese S, et al. Revisiting the gut-joint axis: links between gut inflammation and spondyloarthritis. Nat Rev Rheumatol 2020;16(8):415–33.

[7] Mauro D, Nakamura A, Haroon N, Ciccia F. The gut-enthesis axis and the pathogenesis of Spondyloarthritis. Semin Immunol 2021;58:101607.

[8] Ritchlin C, Adamopoulos IE. Axial spondyloarthritis: new advances in diagnosis and management. BMJ 2021;372:m4447.

[9] Watad A, Rowe H, Russell T, Zhou Q, Anderson LK, Khan A, et al. Normal human enthesis harbours conventional CD4 + and CD8 + T cells with regulatory features and inducible IL-17A and TNF expression. Ann Rheum Dis 2020;79(8):1044–54.

[10] Schett G, Lories RJ, D'Agostino M-A, Elewaut D, Kirkham B, Soriano ER, et al. Enthesitis: from pathophysiology to treatment. Nat Rev Rheumatol 2017;13(12):731–41.

[11] Uhlig HH. Monogenic diseases associated with intestinal inflammation: implications for the understanding of inflammatory bowel disease. Gut 2013;62(12):1795–805.

[12] Rosenbaum JT, Davey MP. Time for a gut check: evidence for the hypothesis that HLA−B27 predisposes to ankylosing spondylitis by altering the microbiome. Arthritis Rheum 2011;63(11):3195–8.

[13] de Oliveira Bravo M, Carvalho JL, Saldanha-Araujo F. Adenosine production: a common path for mesenchymal stem-cell and regulatory T-cell-mediated immunosuppression. Purinergic Signal 2016;12(4):595–609.

[14] Saldanha-Araujo F, Ferreira FIS, Palma PV, Araujo AG, Queiroz RHC, Covas DT, et al. Mesenchymal stromal cells up-regulate CD39 and increase adenosine production to suppress activated T-lymphocytes. Stem Cell Res 2011;7(1):66–74.

[15] Deaglio S, Dwyer KM, Gao W, Friedman D, Usheva A, Erat A, et al. Adenosine generation catalyzed by CD39 and CD73 expressed on regulatory T cells mediates immune suppression. J Exp Med 2007;204(6):1257–65.

[16] Eltzschig HK, Ibla JC, Furuta GT, Leonard MO, Jacobson KA, Enjyoji K, et al. Coordinated adenine nucleotide phosphohydrolysis and nucleoside signaling in posthypoxic endothelium: role of ectonucleotidases and adenosine A2B receptors. J Exp Med 2003;198(5):783–96.

[17] Antonioli L, Pacher P, Vizi ES, Haskó G. CD39 and CD73 in immunity and inflammation. Trends Mol Med 2013;19(6):355–67.

[18] Russell T, Watad A, Bridgewood C, Rowe H, Khan A, Rao A, et al. IL-17A and TNF modulate normal human spinal entheseal bone and soft tissue mesenchymal stem cell osteogenesis, adipogenesis, and stromal function. Cells 2021;10(2):341.

[19] Stavre Z, Bridgewood C, Zhou Q, Maeda Y, Huang T-T, Karman J, et al. A role for neutrophils in early enthesitis in spondyloarthritis. Arthritis Res Ther 2022;24(1):24.

[20] Nakamura A, Zeng F, Nakamura S, Reid KT, Gracey E, Lim M, et al. Macrophage migration inhibitory factor drives pathology in a mouse model of spondyloarthritis and is associated with human disease. Sci Transl Med 2021;13(616):eabg1210.

[21] Leirisalo-Repo M, Turunen U, Stenman S, Helenius P, Seppälä K. High frequency of silent inflammatory bowel disease in spondylarthropathy. Arthritis Rheum 1994;37(1):23–31.

[22] Tanoue T, Atarashi K, Honda K. Development and maintenance of intestinal regulatory T cells. Nat Rev Immunol 2016;16(5):295–309.

[23] Read S, Greenwald R, Izcue A, Robinson N, Mandelbrot D, Francisco L, et al. Blockade of CTLA-4 on CD4+CD25+ regulatory T cells abrogates their function in vivo. J Immunol 2006;177(7):4376–83.

[24] Ferraro A, D'Alise AM, Raj T, Asinovski N, Phillips R, Ergun A, et al. Interindividual variation in human T regulatory cells. Proc Natl Acad Sci USA 2014;111(12):E1111–20.

[25] Watson RA, Tong O, Cooper R, Taylor C, Sharma PK, de Los, Aires AV, et al. Immune checkpoint blockade sensitivity and progression-free survival associates with baseline CD8(+) T cell clone size and cytotoxicity. Sci Immunol 2021;6(64):eabj8825.

[26] Fang F, Xiao Y, Zelzer E, Leong KW, Thomopoulos S. A mineralizing pool of Gli1-expressing progenitors builds the tendon enthesis and demonstrates therapeutic potential. Cell Stem Cell 2022;29(12):1669–84 .e6.

[27] Whibley N, Tucci A, Powrie F. Regulatory T cell adaptation in the intestine and skin. Nat Immunol 2019;20(4):386–96.

[28] Clemente JC, Manasson J, Scher JU. The role of the gut microbiome in systemic inflammatory disease. BMJ 2018;360:j5145.

[29] Wen YH, Lin H-Q, Li H, Zhao Y, Lui VWY, Chen L, et al. Stromal interleukin-33 promotes regulatory T cell-mediated immunosuppression in head and neck squamous cell carcinoma and correlates with poor prognosis. Cancer Immunol Immunother 2019;68(2):221–32.

[30] Dorronsoro A, Lang V, Ferrin I, Fernández-Rueda J, Zabaleta L, Pérez-Ruiz E, et al. Intracellular role of IL-6 in mesenchymal stromal cell immunosuppression and proliferation. Sci Rep 2020;10(1):21853.

[31] Bo-O Zhou, R Yue, Murphy MM, Peyer JG, Morrison SJ. Leptin-receptor-expressing mesenchymal stromal cells represent the main source of bone formed by adult bone marrow. Cell Stem Cell 2014;15(2):154–68.

[32] Zhang T, Wan L, Xiao H, Wang L, Hu J, Lu H. Single-cell RNA sequencing reveals cellular and molecular heterogeneity in fibrocartilaginous enthesis formation. Elife 2023;12:e85873.

[33] Benjamin M, McGonagle D. The enthesis organ concept and its relevance to the spondyloarthropathies. Adv Exp Med Biol 2009;649:57–70.

[34] McGonagle D, Benjamin M, Tan AL. The pathogenesis of psoriatic arthritis and associated nail disease: not autoimmune after all? Curr Opin Rheumatol 2009;21(4):340–7.

[35] Zaiss MM, Zaiss MM, Jones RM, Schett G, Pacifici R. The gut-bone axis: how bacterial metabolites bridge the distance. J Clin Invest 2019;129(8):3018–28.

[36] Penkava F, Sansom S, Bowness P. Pathogenic T-cell clones in axial spondyloarthritis: what is the evidence? Rheumatology (Oxford) 2024;63(suppl 2):ii4–6.

[37] Eltzschig HK, Carmeliet P. Hypoxia and inflammation. N Engl J Med 2011;364(7):656–65.

[38] Boo SH, Kim YK. The emerging role of RNA modifications in the regulation of mRNA stability. Review Exp Mol Med 2020;52(3):400–8.

[39] Allard B, Longhi MS, Robson SC, Stagg J. The ectonucleotidases CD39 and CD73: novel checkpoint inhibitor targets. Immunol Rev 2017;276(1):121–44.

[40] Yegutkin GG. Nucleotide- and nucleoside-converting ectoenzymes: Important modulators of purinergic signalling cascade. Biochim Biophys Acta 2008;1783(5):673–94.

[41] Shi Y, Hu G, Su J, Li W, Chen Q, Shou P, et al. Mesenchymal stem cells: a new strategy for immunosuppression and tissue repair. Cell Res 2010;20(5):510–8.

[42] Haghighitalab A, Matin MM, Amin A, Minaee S, Bidkhori HR, Doeppner TR, et al. Investigating the effects of IDO1, PTGS2, and TGF-β1 overexpression on immunomodulatory properties of hTERT-MSCs and their extracellular vesicles. Sci Rep 2021;11(1):7825.

[43] Mandapathil M, Hilldorfer B, Szczepanski MJ, Czystowska M, Szajnik M, Ren J, et al. Generation and accumulation of immunosuppressive adenosine by human CD4+CD25highFOXP3+ regulatory T cells. J Biol Chem 2010;285(10):7176–86.

[44] Kobie JJ, Shah PR, Yang L, Rebhahn JA, Fowell DJ, Mosmann TR. T regulatory and primed uncommitted CD4 T cells express CD73, which suppresses effector CD4 T cells by converting 5′-adenosine monophosphate to adenosine. J Immunol 2006;177(10):6780–6.

[45] Weber R, Groth C, Lasser S, Arkhypov I, Petrova V, Altevogt P, et al. IL-6 as a major regulator of MDSC activity and possible target for cancer immunotherapy. Cell Immunol 2021;359:104254.

[46] West NR. Coordination of immune-stroma crosstalk by IL-6 family cytokines. Front Immunol 2019;10:1093.

[47] Na H, K-Il Im, Kim N, Lee J, Gil S, Min G-J, et al. The IL-6 signaling pathway contributes critically to the immunomodulatory mechanism of human decidua-derived mesenchymal stromal cells. iScience 2024;27(5):109783.

[48] Gao F, Chiu SM, Motan DAL, Zhang Z, Chen L, Ji H-L, et al. Mesenchymal stem cells and immunomodulation: current status and future prospects. Cell Death Dis 2016;7(1):e2062.

[49] Dominici M, K-Le Blanc, Mueller I, Slaper-Cortenbach I, Marini Fc, Krause Ds, et al. Minimal criteria for defining multipotent mesenchymal stromal cells. The International Society for Cellular Therapy position statement. Cytotherapy 2006;8(4):315–7.

[50] Zhao Q, Ren H, Han Z. Mesenchymal stem cells: immunomodulatory capability and clinical potential in immune diseases. J Cell Immunother 2016;2(1):3–20.

[51] Haniffa MA, Wang X-N, Holtick U, Rae M, Isaacs JD, Dickinson AM, et al. Adult human fibroblasts are potent immunoregulatory cells and functionally equivalent to mesenchymal stem cells. J Immunol 2007;179(3):1595–604.

[52] Mauro D, Simone D, Bucci L, Ciccia F. Novel immune cell phenotypes in spondyloarthritis pathogenesis. Semin Immunopathol 2021;43(2):265–77.

[53] Lefferts AR, Norman E, Claypool DJ, Kantheti U, Kuhn KA. Cytokine competent gut-joint migratory T cells contribute to inflammation in the joint. Front Immunol 2022;13:932393.

[54] Jacques P, Lambrecht S, Verheugen E, Pauwels E, Kollias G, Armaka M, et al. Proof of concept: enthesitis and new bone formation in spondyloarthritis are driven by mechanical strain and stromal cells. Ann Rheum Dis 2014;73(2):437–45.

[55] Venken K, Jarlborg M, Decruy T, Mortier C, Vlieghe C, Gilis E, et al. Distinct immune modulatory roles of regulatory T cells in gut versus joint inflammation in TNF-driven spondyloarthritis. Ann Rheum Dis 2023;82(8):1076–90.

Systemic lupus erythematosus

Development of an MHC imputation panel highlights independent contributions of HLA amino acid residues and *C4* copy number variations to SLE risk

Chae-Yeon Yu [1,2], Dong Mun Shin [3], Sung Min Kim [3], Yui Taek Lee [1], Sungwon Jeon [4,5,6,7], Sehwan Chun [1], So-Young Bang [8,9], Hye-Soon Lee [8,9], Xianyong Yin [10], Yong Cui [11,12], Xuejun Zhang [13], Jong Bhak [4,5,14,15], Soon Ji Yoo [1], Young Jin Kim [3,*], Bong-Jo Kim [3,*], Sang-Cheol Bae [8,9,*], Kwangwoo Kim [1,2,*]

[1] Department of Biology, Kyung Hee University, Seoul, Republic of Korea

[2] Department of Biomedical and Pharmaceutical Sciences, Kyung Hee University, Seoul, Republic of Korea

[3] Division of Genome Science, Department of Precision Medicine, National Institute of Health, Cheongju, Republic of Korea

[4] Korean Genomics Center, Ulsan National Institute of Science and Technology, Ulsan, Republic of Korea

[5] AgingLab, Ulsan, Republic of Korea

[6] Geromics Inc., Suwon, Republic of Korea

[7] Clinomics Inc., Ulsan, Republic of Korea

[8] Department of Rheumatology, Hanyang University Hospital for Rheumatic Diseases, Seoul, Republic of Korea

[9] Hanyang University Institute for Rheumatology Research and Hanyang Institute of Bioscience and Biotechnology, Seoul, Republic of Korea

[10] Department of Epidemiology, School of Public Health, Nanjing Medical University, Jiangsu, China

[11] Department of Dermatology, China-Japan Friendship Hospital, Capital Medical University, Beijing, China

[12] Department of Dermatology, China-Japan Friendship Hospital, Beijing, China

[13] Institute of Dermatology, Anhui Medical University, Hefei, Anhui, China

[14] Department of Biomedical Engineering, College of Information-Bio Convergence Engineering, Ulsan National Institute of Science and Technology, Ulsan, Republic of Korea

[15] Personal Genomics Institute, Genome Research Foundation, Osong, Republic of Korea

ARTICLE INFO

ABSTRACT

Objectives: Systemic lupus erythematosus (SLE) is a complex autoimmune disease strongly associated with the major histocompatibility complex (MHC) region, but precisely pinpointing the risk variants remains challenging. This study aimed to comprehensively profile SLE-driving variants using a newly developed East Asian MHC imputation reference panel, capable of simultaneously imputing diverse MHC variants, including multilevel human leukocyte antigen (HLA) variants and copy number variations (CNVs) of *C4* elements, such as *C4A, C4B,* and human endogenous retrovirus (HERV).

Methods: Using the whole-genome-sequencing (WGS) data from ∼2000 Korean samples, we genotyped and phased MHC variants, including HLA variants and *C4*-related CNVs, to construct an MHC reference panel. Imputation performance of the panel was assessed through leave-one-out cross-validation and validated using WGS and droplet digital polymerase chain reaction

Correspondence to Dr. Young Jin Kim, Dr. Bong-Jo Kim, Dr. Sang-Cheol Bae, Dr. Kwangwoo Kim.

E-mail addresses: inthistime@korea.kr (Y.J. Kim), kbj6181@korea.kr (B.-J. Kim), scbae@hanyang.ac.kr (S.-C. Bae), kkim@khu.ac.kr (K. Kim).

CYY and DMS contributed equally.

Handling editor Josef S. Smolen.

methodology. The panel was applied to 2 independent SLE genome-wide association study data-sets, followed by stepwise conditional analyses, fine-mapping, and model comparisons.

Results: The MHC panel achieved high imputation accuracies of 95% for HLA and 94% for *C4* at the haploid-level. Independent contributions to SLE risk were identified from 6 amino acid positions altering the epitope-binding surfaces of HLA-DRB1 and HLA-C. Reduced *C4A* copy numbers and increased HERV copy numbers, collectively lowering C4 protein levels, were associated with increased SLE risk, independent of HLA variants. Our refined MHC-SLE association model provided superior explanations for SLE risk over previous association models in an independent Korean population.

Conclusions: This study enhanced the understanding of HLA and *C4* in SLE pathogenesis and holds promise for advancing MHC association studies for immune-mediated inflammatory disorders in East Asians using our MHC panel, accessible via https://coda.nih.go.kr/usab/kis/intro.do.

WHAT IS ALREADY KNOWN ON THIS TOPIC

- Systemic lupus erythematosus (SLE) is strongly associated with genetic variations in the major histocompatibility complex (MHC) region, which encompasses numerous immune-related genes including human leukocyte antigen (HLA) genes and complement component *C4*, within a region of extensive linkage disequilibrium.
- The genetic complexity of *C4* has resulted in the lack of comprehensive MHC imputation reference panels that include both HLA and *C4* variants. Most studies have focused on either *C4* or HLA separately, making it challenging to disentangle their relationship and assess their independent effects on SLE.

WHAT THIS STUDY ADDS

- This study developed a high-accuracy MHC imputation reference panel capable of simultaneously imputing HLA variants, *C4*-related copy number variations (CNVs), and other MHC variants.
- Independent contributions to SLE risk were identified from 6 amino acid positions altering HLA-DRB1 and HLA-C epitope-binding surfaces, as well as from reduced *C4A* and increased human endegenous retrovirus (HERV) copy numbers, which collectively lower C4 protein levels.
- A refined MHC-SLE association model is proposed, which integrates HLA missense variants and *C4*-related CNVs, providing superior explanations for SLE risk compared to previous models.

HOW THIS STUDY MIGHT AFFECT RESEARCH, PRACTICE OR POLICY

- We have made our MHC imputation panel publicly available, enabling large-scale studies of MHC-related diseases in East Asian populations and improving the identification of causal genetic variants in complex disorders.
- By elucidating the independent roles of HLA and *C4* in SLE, this study offers a framework for refining genetic risk models, paving the way for improved personalised risk assessments.
- The study presents a generalizable methodology for developing CNV imputation panels, combining haplotype clustering with deep learning-based models and iterative optimisation. This approach can be applied to other complex genetic regions where CNV characterisation poses challenges.

INTRODUCTION

Systemic lupus erythematosus (SLE) is a common polygenic autoimmune disorder characterised by self-tolerance breakdown and impaired nuclear antigen clearance [1]. As of 2025, over 200 SLE-associated loci have been identified, with the major histocompatibility complex (MHC) region exerting particularly strong effects [2,3]. The MHC region, enriched with immune-related genes, exhibits extensive linkage disequilibrium (LD),

exceptionally dense distribution of genetic variants, and the presence of copy number variations (CNVs), making it challenging to accurately characterise individuals' genetic variants and dissect genetic association signals [4].

Our previous studies on human leukocyte antigen (HLA) associations in SLE have demonstrated the crucial role of structural changes in the epitope-binding groove of HLA-DR molecules, driven by HLA-DRB1 missense variants encoding amino acid positions 11, 13, 26, and 37 in multiple Asian populations [5−7]. Haplotypes defined by these residues explained the majority of MHC-associated SLE risk, effectively capturing the known SLE-risk classical alleles of *HLA-DRB1*, such as *HLA-DRB1*15:01* and *HLA-DRB1*03:01* [5].

In parallel, some studies have reported genetic associations of the complement component gene *C4*, located near *HLA-DRB1*, with SLE. *C4* is crucial in the human immune system, facilitating the clearance of dead or damaged cell debris. Its genetic architecture is highly complex, involving coding variants, insertions of human endogenous retrovirus (HERV) sequences, and CNVs. *C4* encodes 2 functionally distinct isoforms, *C4A* and *C4B*, which differ by 4 amino acid residues within positions 1101 to 1106 and exhibit differential affinities for their molecular targets associated with different biological pathways [8,9]. Additionally, HERV insertion in intron 9 of *C4A* or *C4B* creates long forms of *C4A* or *C4B*, which are associated with decreased *C4* expression in blood [10]. Most importantly, total copy number of *C4* varies widely among individuals, mostly ranging from 2 to 8 copies, consisting of various copy numbers of both *C4A* and *C4B*, with and without HERV segments. Therefore, the variance in expression levels of the functionally distinct C4A and C4B isoforms in a general population is attributed mainly to the CNV of *C4*, with additional modulation by the HERV insertion [9]. However, the complex genomic architecture of *C4* requires relatively low-throughput, expensive technologies to characterise individuals' genetic variants, limiting most *C4*-SLE association studies to relatively small sample sizes [11−17]. Furthermore, due to the lack of an imputation reference panel that simultaneously infers both HLA and *C4* variants along with other MHC variants, previous *C4* genetic association studies have focused solely on the effects of the *C4* CNV on SLE, without considering the compounding effects of HLA variants [11−17].

A recent study by Kamitaki et al [18] reported a primary MHC-SLE association signal at *C4*, rather than *HLA-DRB1*03:01* using data from large European and African ancestral populations. Although the primary genetic effect could not be distinctly attributed to either *C4* CNVs or *HLA-DRB1*03:01* in European ancestry due to relatively high LD, a joint logistic regression analysis for *C4* CNVs and *HLA-DRB1*03:01* in African Americans revealed a sole association of *C4* CNVs with SLE, whereas *HLA-DRB1*03:01* showed no significant association. This

finding challenges the long-held belief regarding *HLA-DRB1* associations with SLE, suggesting that the SLE-MHC association, traditionally attributed to *HLA-DRB1*, may instead be driven by CNVs of *C4* alleles.

However, we urge cautious interpretation of these results for several reasons. First, the study reported very poor imputation accuracy in *C4* copy number calls among African populations, potentially impacting the reliability of the findings. Second, the most significant variant was not mapped to *C4* in either ancestry. In an unconditional analysis, the study observed a stronger significant association of *HLA-DRB1*03:01* compared to the *C4* CNV in Europeans. Similarly, another recent European study identified *HLA-DQB*02:01* as the most significant variant for SLE rather than *C4* CNVs [19]. In Africans, *HLA-DRB1*15:03*, known as the most significant classical allele in this population, also showed a stronger association with SLE compared to the *C4* CNVs, in their study and others [20,21]. Third, adjusting solely for *HLA-DRB1*03:01* may not fully capture the multi-allelic nature of *HLA-DRB1* associations. Residual effects after conditioning on *HLA-DRB1*03:01* are expected to remain substantial around and within *HLA-DRB1*. Furthermore, in African ancestry, *HLA-DRB1*03:01* contributes much less to the risk of SLE.

In our present study, we developed an innovative MHC imputation reference panel from whole-genome sequencing (WGS) data to comprehensively analyse MHC associations in SLE using large-scale genome-wide association study (GWAS) data. Unlike existing MHC reference panels, our panel allows for the simultaneous imputation of copy numbers for *C4A, C4B*, and HERV, as well as amino acid residues and classical alleles of 8 major HLA genes, along with neighbouring single-nucleotide polymorphisms (SNPs) and indels across the MHC region. The imputation performance of our reference panel has been assessed through various approaches, achieving a high level of accuracy. Applying our imputation reference panel to large SLE GWAS datasets, we uncovered multiple independent genetic contributions from *HLA-DRB1, C4*, and *HLA-C*, proposing a novel SLE-MHC association model. The analysis schematic of this study is illustrated in Figure 1.

METHODS

Detailed methods are provided in Supplementary Methods.

RESULTS

Development of the MHC reference panel for HLA and C4 imputation

The MHC reference panel for imputing diverse MHC variants, including HLA and *C4* variants, was constructed to include >3000 haplotypes of the general Korean population, based on WGS data from 2 independent experimental batches. To achieve this, we genotyped 289 classical alleles of 8 major HLA genes at the G-group resolution (Supplementary Fig S1), which were further defined as 102 1-field and 267 2-field resolutions, covering 1,440 amino acid positions [22].

The diploid copy numbers of *C4, C4A, C4B*, and HERV were estimated using Genome STRiP [23], based on read depth and the allele-specific read ratio between *C4A* and *C4B* (Supplementary Fig S2). Diploid copy numbers of *C4* ranged from 2 to 8, *C4A* from 0 to 5, *C4B* from 0 to 6 and HERV from 1 to 7 in the reference samples (Supplementary Fig S3). The most common combination included 4 copies of *C4*, consisting of 2 *C4A* copies, 2 *C4B* copies, and at least 2 copies of HERV (Fig 2A). The

accuracy of WGS-based *C4*-typing was validated by droplet digital polymerase chain reaction (ddPCR) technology [24,25] across 127 additional Korean samples (Supplementary Figs S4 and S5), showing highly reliable concordance rates (99.2% for *C4*, 98.4% for *C4A*, 99.2% for *C4B*, and 99.2% for HERV) (Fig 2B). The observed distributions of diploid copy numbers align with those reported in other populations [16,17,19].

To separate each diploid copy number of *C4A, C4B*, and HERV into haploid copy numbers, haplotype clustering was performed using unsupervised machine learning with Gaussian mixture variational autoencoder (GMVAE) models, followed by the cyclic coordinate descent method (Fig 3A-B, Supplementary Table S1, Supplementary Fig S6), as detailed in Supplementary Methods. The frequency distributions of determined haploid copy numbers for *C4A, C4B*, and HERV showed single-modal patterns, each centred around one copy, which accounted for the copy-number genotype distributions (Fid 3C−D). Stochastically inferred diploid copy numbers from the haplotype frequencies matched the observed diploid copy numbers, indicating that *C4* CNVs followed Hardy-Weinberg equilibrium (Supplementary Table S2).

Finally, we assembled the MHC imputation reference panel by incorporating and phasing a comprehensive set of 55,632 MHC variants, including HLA variants, *C4*-related CNVs, and other SNPs and indels in 1,537 quality control (QC)-passed samples.

To assess the imputation performance of the developed panel, leave-one-out cross-validation was conducted by sequentially excluding each reference sample, masking its *C4* and HLA variants, and imputing them using the MHC reference panel with the remaining reference samples. For HLA genes, concordance rates averaged 99.2% at one-field, 97.6% at 2-field, and 97.3% at G-group resolution. For *C4*-related CNVs, our imputation demonstrated high reliability, achieving an overall concordance rate of 94.4% for *C4A, C4B*, and HERV haploid copy numbers, and 90.2% ($r^2 = 0.83$) at diploid level (Table 1). This was slightly better than a previous *C4* imputation approach (e.g. $r^2 = 0.78$ and 0.65 for *C4A* in Europeans and Africans, respectively) [18]. Additionally, the vast majority (95.2%) of discordant results showed only one-copy differences between imputed and observed copy numbers (Supplementary Tables S3 and S4).

Application of the MHC reference panel to large-scale SLE GWAS datasets

We applied the new MHC reference panel to impute MHC variants, including HLA and *C4* variants, in 2 Korean SLE GWAS datasets (discovery dataset, n = 73,148; replication datasets, n = 4,551; Supplementary Table S5), achieving high imputation quality scores (Supplementary Fig S7).

To further validate the imputation accuracy, we compared imputed results with directly genotyped results from 127 QC-passed samples, using WGS for HLA classical alleles and ddPCR for *C4*-related CNVs. Concordance rates were high, with 95.3% at 2-field HLA alleles and 89.8% for *C4*-related CNVs at diploid level, consistent with results from leave-one-out cross-validation of the MHC reference panel (Table 1).

Additionally, correlation analysis of imputed *C4*-related CNVs and plasma C4 protein levels in 1,284 patents replicated known effects: higher *C4* copy numbers increased plasma C4 protein levels, whereas higher HERV inserts decreased them ($P_{C4} = 8.8 \times 10^{-69}$ and $P_{HERV} = 2.9 \times 10^{-23}$; Fig 4; Supplementary Table S6). This reinforces the reliability of our *C4* CNV imputation. No differential regulatory

A MHC variants genotyping
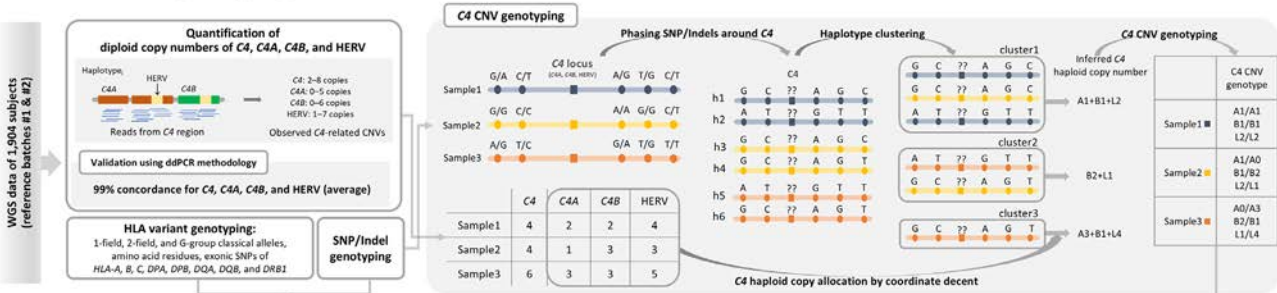
B Reference construction and evaluation
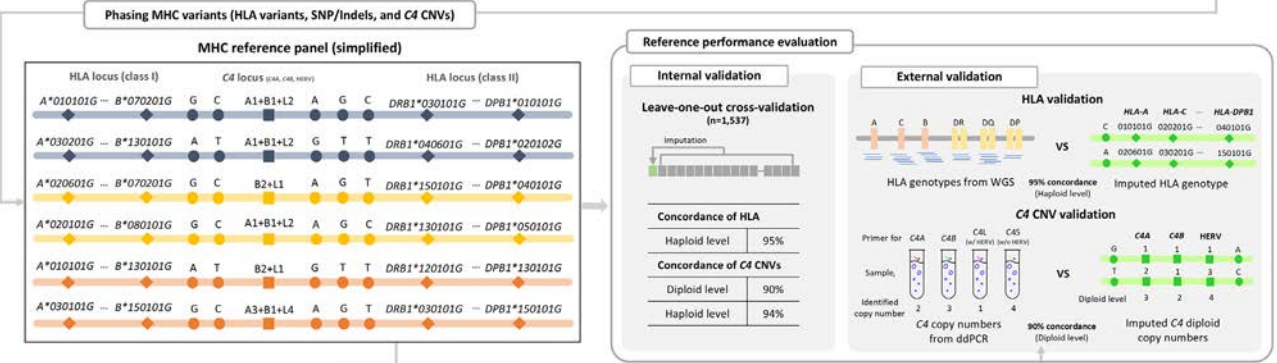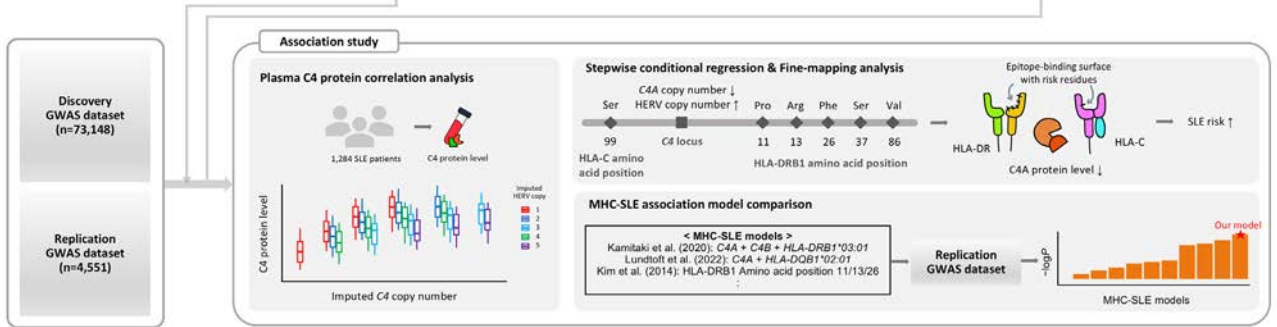

C Disease association analysis

Figure 1. Overview of the study design. The schematic diagram illustrates the key analysis steps of the study. A, To construct an MHC imputation reference panel, WGS data from 1,904 samples in 2 independent batches were used to genotype classical alleles and amino acid residues in 8 major HLA genes, CNVs of *C4*-related elements, and other MHC SNPs/indels. For *C4*, the WGS-based quantification of copy numbers was performed at the diploid level, and the reliability of this quantification method was further validated using ddPCR. The diploid copy numbers of *C4A, C4B,* and HERV were then segregated into haploid copy numbers through unsupervised haplotype clustering and determining the most likely haploid copy number of each *C4*-related element using a cyclic coordinate descent method, based on the WGS-based diploid copy numbers across the reference individuals. For instance, the example cluster 'cluster1' comprises 3 haplotypes that are likely to possess a single-copy of *C4A,* a single-copy of *C4B,* and 2 copies of HERV (designated as A1 + B1 + L2). B, The MHC imputation reference panel was constructed by phasing all binary-coded MHC variants into haplotypes. Its imputation performance was evaluated based on the concordance rates between actual and imputed data from both reference and external samples. C, The newly developed imputation reference panel was applied to 2 independent SLE GWAS datasets: discovery and replication datasets. Plasma C4 protein levels measured in 1,284 SLE patients were analysed for correlations with imputed *C4*-related copy numbers, revealing a positive correlation with *C4* copy number and a negative correlation with HERV copy number. Finally, through stepwise conditional and fine-mapping analyses, 3 independent signals were identified at *HLA-DRB1, C4,* and *HLA-C*, which included key variants contributing to the risk of SLE: amino acid positions 11, 13, 26, 37, and 86 in the epitope-binding pocket of HLA-DRB1, position 99 in the epitope-binding pocket of HLA-C, and the copy numbers of *C4A* and HERV in *C4*. Our refined MHC association model was compared with previous models using the replication dataset, evaluating model significance to confirm that the variants identified through our fine-mapping analysis provided the most robust explanation for SLE risk. CNV, copy number variation; ddPCR, digital droplet polymerase chain reaction; GWAS, genome-wide association study; HLA, human leukocyte antigen; MHC, major histocompatibility; SLE, systemic lupus erythematosus; WGS, whole-genome sequencing.

effects of *C4A* and *C4B* CNVs were observed on C4 production (Supplementary Table S6).

Primary SLE association at HLA-DRB1 tagged by 5 amino acids in the epitope-binding groove

We performed a stepwise conditional regression analysis to unravel multiple independent SLE association signals across the MHC region (28−34 Mb on chromosome 6; hg38) using the

discovery GWAS dataset. The genetic associations of HLA classical alleles, HLA amino acid residues, SNPs, indels, and the diploid and haploid copy numbers of *C4*-related elements with SLE risk were assessed using logistic regression or likelihood ratio test (LRT) adjusting for the top 5 principal components and sex.

We identified the primary association signal at *HLA-DRB1*, with the most significant association occurring at amino acid position 13 ($P_{LRT} = 3.16 \times 10^{-59}$), followed by position 11 ($P_{LRT} = 1.58 \times 10^{-49}$), which is in strong LD with position 13
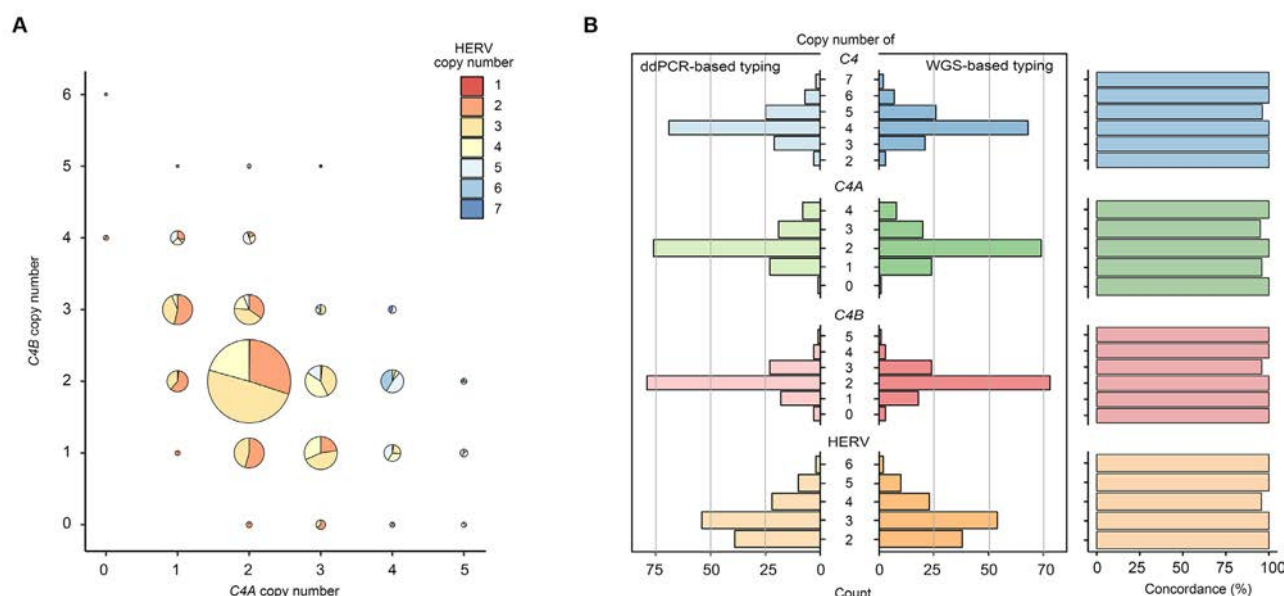
Figure 2. Distribution of diploid copy numbers of *C4*. A, The joint distribution of diploid copy numbers of *C4A, C4B*, and HERV was examined using WGS data for reference samples (n = 1,537). The size of each data point is proportional to the frequency of samples with the corresponding combination of *C4A* and *C4B* copy numbers. Each data point is a pie chart illustrating the distribution of HERV copy numbers for the given combination of *C4A* and *C4B* copy numbers. B, The reliability of the *C4* copy number quantification method using WGS data was evaluated by comparing WGS-based results with ddPCR-based results from 127 non-reference samples. The bi-directional histogram shows the distribution of diploid copy numbers of *C4, C4A, C4B*, and HERV, as determined by ddPCR (left) and the WGS-based approach (right). Concordance rates between the 2 methods are displayed in the bar plot on the right end, according to each copy number of *C4* genes and related elements (≥98.4%). ddPCR, digital droplet polymerase chain reaction; WGS, whole-genome sequencing.

(r^2 = 0.81) (Fig 5A, 6A−G). Among the HLA classical alleles, *HLA-DRB1*15:01:01G* (P = 4.90 × 10^{-50}) and *HLA-DQB1*06:02:01G* (P = 7.11 × 10^{-48}) exhibited the most significant association with SLE risk, both of which are well-established as SLE-risk alleles in East Asian populations (Fig 5A).

Given the complex nature of long-range haplotypes, which may include key amino acid combinations involving residues at positions 13 and 11 that tag specific *HLA-DRB1* classical alleles, we further investigated additional independent associations within *HLA-DRB1* at the amino acid level. After accounting for positions 13 and 11, we identified independent associations at amino acid positions 37 (P_{LRT} = 1.54 × 10^{-15}) and 26 (P_{LRT} = 8.36 × 10^{-14}), which showed moderate residue correlation (r^2 = 0.42) (Fig 6B,H). These positions provided similar model fits for SLE association (P_{LRT} = 1.59 × 10^{-71} for positions 11-13-37 and P_{LRT} = 8.65 × 10^{-70} for positions 11-13-26), which have already been reported in previous studies [5,6]. Considering the uncertainty of the secondary SLE-risk amino acid position, we accounted for both positions 26 and 37 in the next round of stepwise conditional regression. After conditioning on positions 11, 13, 26, and 37, we newly identified amino acid position 86 (P_{LRT} = 4.93 × 10^{-10}; Fig 6C,I). Adding or excluding position 26 in the conditional regression model did not change the statistical significance of position 86. No additional significant positions were detected after conditioning on the amino acid position 11, 13, 26, 37, and 86 (Fig 6D).

The amino acid associations were confirmed in the replication GWAS dataset, revealing highly consistent residue-specific effect sizes (Fig 6G-I) and increased significance in the combined analysis of both datasets (Supplementary File S1). Moreover, the 3 signals derived from the 5 identified amino acid positions exhibited the best SLE association model fit among all possible combinations of HLA-DRB1 amino acid positions in LRTs, accounting for the differences in the number of residues as indicated by the degree of freedom (Supplementary Fig S8). These

positions are located in close spatial proximity within the epitope-binding pocket of HLA-DR molecules (Fig 6J).

Based on these findings, amino acid haplotypes of 5 key positions were tested for SLE associations, identifying 16 haplotypes (frequency > 0.5%), including 5 SLE-risk and 7 SLE-protective haplotypes ($P_{combined}$ < .05; Supplementary Table S7). The amino acid haplotype model effectively explained SLE associations of various classical alleles, including well-known SLE-risk alleles such as *HLA-DRB1*15:01* (PRSFV) in East Asians, as well as alleles specific to Europeans (*HLA-DRB1*03:01*, SSYNV) and Africans (*HLA-DRB1*15:03*, PRSFV), despite their low or absent frequencies in the Korean population. Similarly, *HLA-DRB1*13:02* and *HLA-DRB1*14:03*, previously reported as significant SLE-protective alleles [26], were found to have the SLE-protective haplotype SSPNG. Taken together, this suggests that amino acid haplotypes not only provide a parsimonious disease association model compared to the conventional model using classical alleles but also demonstrate a highly transferable model across different ancestries.

Dissecting the secondary SLE association revealed that decreased C4A *and increased HERV copy numbers confer the risk of SLE, independent of* HLA-DRB1

To determine if there were additional independent MHC associations beyond *HLA-DRB1*, we conducted a conditional analysis that adjusted for all *HLA-DRB1* G-group alleles with frequencies greater than 0.5%, thereby eliminating the influence of *HLA-DRB1* on the SLE associations. Using the discovery GWAS dataset, we identified a secondary signal within the *C4* and observed moderate correlation with *HLA-DRB1*, which was adequately controlled for in the logistic regression model (Fig 5B; Supplementary Table S8). We found that the diploid copy numbers of *C4A* showed the most significant association in the conditional analysis (P = 1.97 × 10^{-14}), which was much stronger
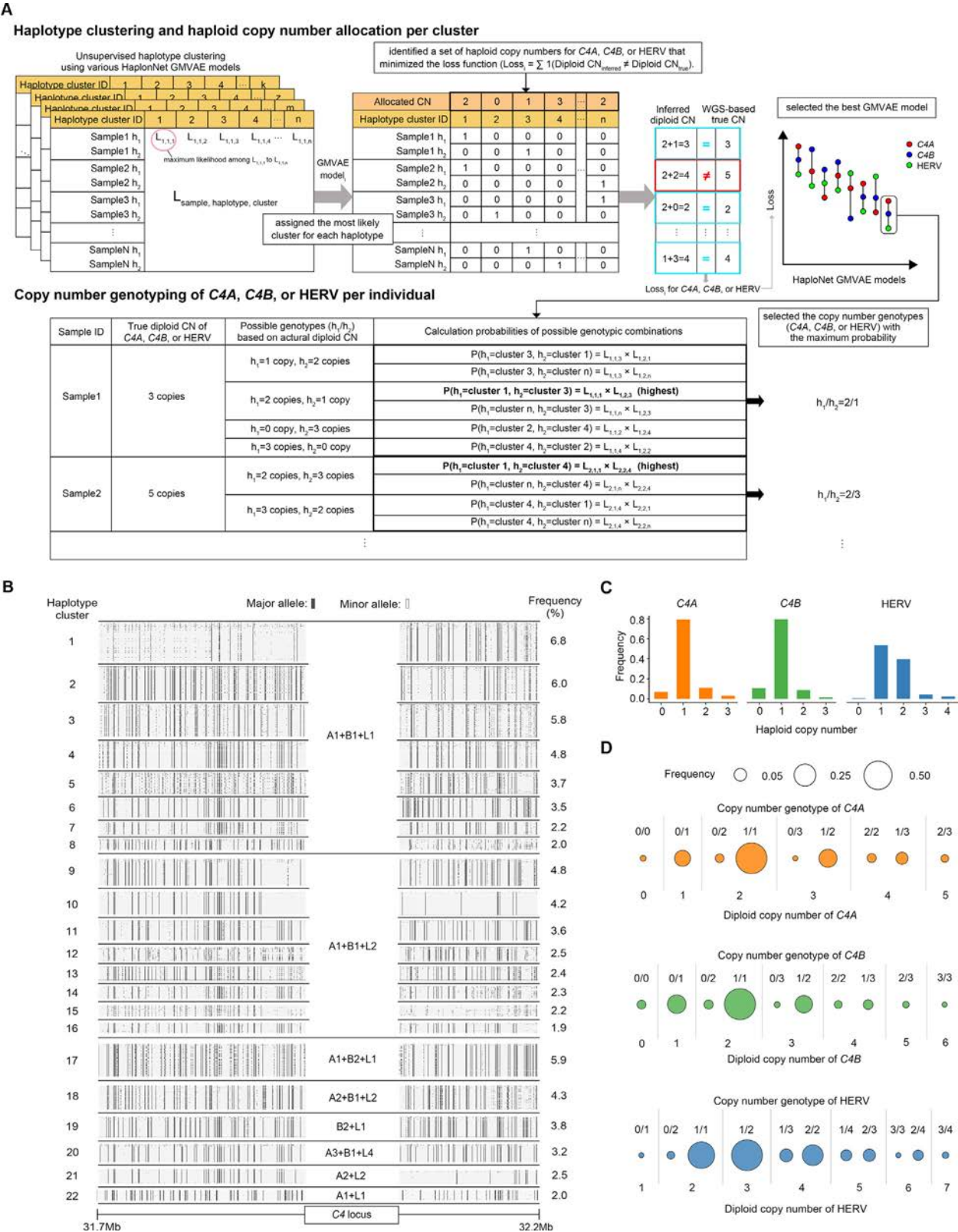
Figure 3. Segregating the diploid copy numbers of *C4A, C4B,* and HERV into haploid copy numbers. A, Unsupervised haplotype clustering was performed using various GMVAE models based on phased SNPs and indels near *C4* in reference samples, estimating the likelihood of each haplotype belonging to each cluster. For each GMVAE model, each haplotype was assigned to the cluster with the highest likelihood. The most likely haploid copy number for each cluster was then determined using a cyclic coordinate descent method, which iteratively minimised the loss function about the difference between inferred and true diploid copy numbers across reference samples. The GMVAE model with the lowest average loss for *C4A, C4B,* and HERV was selected for subsequent procedures. Individuals' CNV genotypes, consisting of 2 haploid copy numbers for *C4A, C4B,* and HERV, were determined as the most likely haploid copy number combinations, evaluated by multiplying the normalised likelihoods for the 2 haplotypes belonging to specific clusters, and aligned with the actual diploid copy numbers. B, Haplotype clustering analysis near the *C4* region (31.7–32.2 Mb on chromosome 6, hg38) identified 47 haplotype clusters. The most common clusters representing 80% of all haplotypes are visualised, along with allocated copy number compositions and frequencies. Each row represents a haplotype, where black and white dots indicate major and minor alleles of biallelic variants upstream and downstream of *C4*, respectively. The *C4* composition is labelled using the initials and copy numbers of *C4A* (A), *C4B* (B), and

Table 1

Concordance rates between imputed and actual data for HLA classical alleles and *C4* CNVs from leave-one-out cross-validation and external sample validation

	HLA								
	HLA-A	*HLA-B*	*HLA-C*	*HLA-DPA1*	*HLA-DPB1*	*HLA-DQA1*	*HLA-DQB1*	*HLA-DRB1*	Total
Leave-one-out cross validation (N = 1537)									
One-field level, %	99.6	99.0	99.9	97.5	98.3	99.9	100.0	99.1	99.2
Two-field level, %	97.7	97.8	99.3	92.7	98.2	99.9	99.5	95.5	97.6
G-group level, %	97.5	97.7	99.3	91.2	98.1	99.9	99.5	95.5	97.4
External sample validation (N = 127)[a]									
One-field level, %	99.3	94.5	98.3	94.1	96.9	99.3	99.3	96.9	97.1
Two-field level, %	97.2	93.1	98.3	89.3	96.9	98.3	97.9	91.7	95.3
G-group level, %	96.9	92.8	97.6	87.9	96.9	98.3	97.9	91.7	95.0

	C4			
	C4A	*C4B*	HERV	Total
Leave-one-out cross validation (N = 1,537)				
Haploid-level, %	94.4	94.7	94.1	94.4
Diploid-level, % (r^2)[b]	90.1 (0.80)	90.1 (0.80)	91.5 (0.90)	90.5 (0.83)
External sample validation (N = 127)[c]				
Diploid-level, %	90.3	89.7	90.3	90.1

CNV, copy number variation; ddPCR, digital droplet polymerase chain reaction; HLA, human leukocyte antigen; MHC, major histocompatibility; SLE, systemic lupus erythematosus; WGS, whole-genome sequencing.

[a] HLA alleles imputed from MHC SNPs were compared with those genotyped from WGS data to calculate concordance rates in 127 external nonreference samples.

[b] Pearson correlation coefficients were calculated between typed (based on WGS data) and imputed *C4*-related copy numbers using reference samples.

[c] Concordance rates were calculated between ddPCR-typed and imputed copy numbers for *C4A*, *C4B*, and HERV.

than the copy numbers of *C4B* ($P = 1.09 \times 10^{-7}$) and HERV ($P = 1.85 \times 10^{-2}$), as well as the total gene copy number of *C4* ($P = 5.37 \times 10^{-2}$) (Fig 5B). The lower copy number of *C4A* was associated with a higher risk of SLE, with a per-copy odds ratio (OR) of 0.70 and a 95% confidence interval (CI) from 0.63 to 0.76 (Fig 6K). This association pattern was consistently observed at the haploid-level, with *C4A* showing the strongest significance among the *C4*-related CNVs ($P = 3.34 \times 10^{-12}$; Fig 5B). Compared with 1 haploid copy of *C4A* as the reference, the deficiency of *C4A* increased SLE risk (OR = 1.36, 95% CI = 1.18 −1.57, $P = 2.38 \times 10^{-5}$), whereas the gain of *C4A* copy showed a protective effect (OR = 0.75, 95% CI = 0.67−0.83, $P = 8.87 \times 10^{-8}$).

As previously known, the haploid-level copy numbers of *C4A*, *C4B* and HERV are in LD with each other (Supplementary Table S1). To understand the overall effect of *C4*-related CNVs and estimate the mutually independent SLE-risk effects of each *C4*-related CNV, we conducted a joint conditional regression analysis using the diploid copy number of *C4A, C4B*, and HERV, adjusting for *HLA-DRB1* and genetic background (Table 2). This joint model revealed a significant contribution of *C4*-related CNVs to SLE susceptibility ($P_{LRT} = 1.80 \times 10^{-15}$), exhibiting significant, independent associations of *C4A* ($P = 4.12 \times 10^{-11}$, per-copy OR = 0.69, 95% CI = 0.62−0.77) and HERV ($P = 1.13 \times 10^{-2}$, per-copy OR = 1.10, 95% CI = 1.02−1.19), but not *C4B* ($P = .24$). In contrast to the effects of the *C4A* CNV, the copy number of HERV was positively associated with the risk of SLE (Fig 6K). However, the known biological effects of both decreased *C4A* copy number and increased HERV copy number are the same, collectively resulting in decreased *C4A*

expression, as supported by our correlation analysis between plasma C4 protein levels and the copy number of *C4* and HERV in our study cohort (Fig 4C).

All *C4*-related association signals involving *C4A* and HERV were robustly validated in the replication GWAS dataset, and demonstrated increased significance in combined analyses incorporating both discovery and replication GWAS datasets (Figs 5B and 6K; Table 2; Supplementary File S1).

We also investigated previously reported sex bias in *C4*-SLE associations using a logistic regression model with an interaction term between sex and *C4*-related CNVs, but found no evidence of sex-biased effect sizes on SLE (Supplementary Table S9). Indeed, plasma C4 protein levels normalised by the *C4* copy number were consistent between males and females in 1,284 SLE patients (Supplementary Fig S9, Supplementary Table S6).

Tertiary association signals at HLA-C *amino acid position 99*

After conditioning on *HLA-DRB1* and *C4*, the tertiary signal was identified at HLA-C amino acid position 99 in the combined analysis but not in the discovery dataset alone ($P_{LRT} = 5.39 \times 10^{-7}$; $P_{combined} = 1.87 \times 10^{-9}$; Figs 5C and 6E,L; Supplementary File S1). This highly polymorphic position, with 4 possible residues, showed consistent effect sizes across the discovery and replication datasets (Fig 6L). Located in the centre of the peptide-binding groove of HLA-C (Fig 6M), position 99 has been associated with other immune-mediated disorders [27,28]. Among its residues, serine was associated with an increased risk of SLE, whereas cysteine was protective (Table 2). Serine at position 99 primarily tags *HLA-C*07:02* in Koreans, which belongs

HERV (L; long form). For instance, 'A3 + B1 + L4' denotes the combination of 3 haploid copies of *C4A*, a single-copy of *C4B*, and 4 copies of HERV (meaning all *C4* copies are in long form). C, Distribution of haploid copy numbers for *C4A, C4B*, and HERV in reference samples are displayed on the bar plots. D, the frequencies of CNV genotypes are plotted according to diploid copy numbers of each *C4*-related elements. CNV, copy number variation; GMVAE, Gaussian mixture variational autoencoder; SNP, single-nucleotide polymorphism.

Table 2
Joint effects of *C4*-related CNVs on SLE risk, adjusted for *HLA-DRB1* effects

Multivariate model	CNV term	Discovery GWAS dataset			Replication GWAS dataset			Combined		
		Per-copy OR (95% CI)	P	P_{LRT}	Per-copy OR (95% CI)	P	P_{LRT}	Per-copy OR (95% CI)	P	P_{LRT}
SLE ~ *C4A* + *C4B* + Cov	*C4A*	0.73 (0.66−0.81)	9.77×10^{-10}	6.52×10^{-15}	0.69 (0.53−0.89)	3.71×10^{-3}	5.43×10^{-3}	0.73 (0.66−0.80)	2.14×10^{-11}	8.86×10^{-17}
	C4B	1.12 (1.02−1.23)	1.68×10^{-2}		1.01 (0.79−1.29)	9.64×10^{-1}		1.10 (1.01−1.20)	2.66×10^{-2}	
SLE ~ *C4* + HERV + Cov	*C4*	0.88 (0.80−0.96)	5.38×10^{-3}	8.32×10^{-3}	0.74 (0.59−0.94)	1.22×10^{-2}	1.75×10^{-2}	0.86 (0.79−0.94)	4.92×10^{-4}	5.17×10^{-4}
	HERV	1.10 (1.02−1.18)	1.57×10^{-2}		1.26 (1.03−1.53)	2.36×10^{-2}		1.12 (1.04−1.20)	2.29×10^{-3}	
SLE ~ *C4A* + HERV + Cov	**_C4A_**	**0.67 (0.61−0.74)**	**2.40×10^{-16}**	**5.48×10^{-16}**	**0.64 (0.5−0.81)**	**2.63×10^{-4}**	**4.75×10^{-4}**	**0.67 (0.61−0.73)**	**5.70×10^{-19}**	**7.18×10^{-19}**
	HERV	**1.12 (1.05−1.20)**	**1.13×10^{-3}**		**1.23 (1.02−1.47)**	**2.71×10^{-2}**		**1.13 (1.06−1.21)**	**1.39×10^{-4}**	
SLE ~ *C4B* + HERV + Cov	*C4B*	1.25 (1.15−1.36)	2.92×10^{-7}	1.16×10^{-6}	1.14 (0.91−1.43)	2.66×10^{-1}	2.34×10^{-1}	1.23 (1.14−1.34)	2.92×10^{-7}	6.47×10^{-7}
	HERV	1.00 (0.93−1.07)	9.58×10^{-1}		1.10 (0.92−1.32)	3.00×10^{-1}		1.01 (0.95−1.08)	6.62×10^{-1}	
SLE ~ *C4A* + *C4B* + HERV + Cov	*C4A*	0.69 (0.62−0.77)	4.12×10^{-11}	1.80×10^{-15}	0.61 (0.46−0.80)	3.71×10^{-4}	1.15×10^{-3}	0.68 (0.62−0.76)	1.50×10^{-13}	3.83×10^{-18}
	C4B	1.06 (0.96−1.18)	2.24×10^{-1}		0.90 (0.69−1.17)	4.19×10^{-1}		1.04 (0.95−1.14)	4.16×10^{-1}	
	HERV	1.10 (1.02−1.19)	1.13×10^{-2}		1.26 (1.04−1.54)	1.87×10^{-2}		1.12 (1.05−1.20)	1.34×10^{-3}	

Multivariate logistic regression was performed to assess SLE-risk across various models, adjusting for dataset, sex, the top 5 genotypic principal components, and G-group *HLA-DRB* classical alleles. P_{LRT} values were calculated using likelihood ratio tests, comparing model fits of each multivariate model with the nested logistic model excluding CNV terms. The model with the lowest P_{LRT} value is highlighted in bold.
CNV, copy number variation; OR, odds ratio; CI, confidence interval; CN, copy number; GWAS, genome-wide association study.

to a previously reported long-range SLE-risk haplotype in Europeans, though its independent effect has not been investigated [20,29,30]. Cysteine at position 99 is mostly found in *HLA-C*01:02*, which has been associated with other diseases but not with SLE [31−33].

SLE-MHC association model comparison in the Korean population

We then focused on evaluating the fit of our SLE-MHC association model to assess its performance relative to previously proposed SLE-MHC association models [5,6,18,19]. To avoid overfitting, our association model included only the variants identified from the discovery dataset, comprising amino acid positions 11, 13, 26, 37, and 86 in HLA-DRB1, along with the diploid copy numbers of *C4A* and HERV, whereas excluding HLA-C amino acid position 99 identified in a combined analysis. The model fit was subsequently evaluated in the replication GWAS dataset.

Our model demonstrated a strong association with a P_{LRT} value of 5.50×10^{-11} in the replication dataset (Fig 6N), outperforming all previous SLE-MHC association models, as indicated by P_{LRT} values that accounted for differences in the number of variables (or degrees of freedom). Notably, some previous models included European-specific alleles, such as *HLA-DRB1*03:01* or *HLA-DQB1*02:01*. To account for this, we re-evaluated these models by substituting the European-specific alleles with the East Asian-specific SLE-risk allele *HLA-DRB1*15:01* or its strong proxy allele *HLA-DQB1*06:02* ($r^2 = 0.94$ in Koreans). Although this substitution improved model performance, the association significance level remained weaker than that of our comprehensive MHC model. These findings emphasise the importance of considering the collective effects of multiple *HLA-DRB1* classical alleles (tagged by missense variants) as well as the diploid copy numbers of *C4A* and HERV. Additionally, when we incorporated the tertiary association at amino acid position 99 of HLA-C, identified only through the combined datasets, the fit of our association model improved, as expected ($P = 1.91 \times 10^{-12}$; Fig 6N).

DISCUSSION

This study delved into the genetic associations within the MHC region using 2 independent Korean SLE case-control datasets, leveraging a newly developed MHC imputation reference panel. Our findings underscore the significant, independent associations of *HLA-DRB1, C4*, and *HLA-C* with the risk of SLE. The MHC-SLE association model we proposed outperformed other models comprising variants reported in previous MHC fine-mapping studies, as evaluated in the Korean replication cohort. Model comparisons using this independent replication dataset were conducted on an independent replication dataset based on LRTs that accounted for differences in degrees of freedom, ensuring fair and robust comparisons.

Importantly, this is the first study to investigate the disease effects of *C4* CNVs while adjusting for the multiallelic effects of *HLA-DRB1*. There has been debate regarding whether *HLA-DRB1* or *C4* is the primary driver of SLE in the MHC region, and whether the associations of SLE with *HLA-DRB1* and *C4*, which are in LD, are independent of each other [34]. Our conditional association model, which controlled for the influence of *HLA-DRB1* on SLE risk, identified the most significant association at *C4*, revealing that a lower copy number of *C4A* and, for the first time, a higher copy number of HERV were independently associated with an increased risk of SLE. Plasma C4 analysis indicated that C4 proteins levels are predominantly influenced by the total
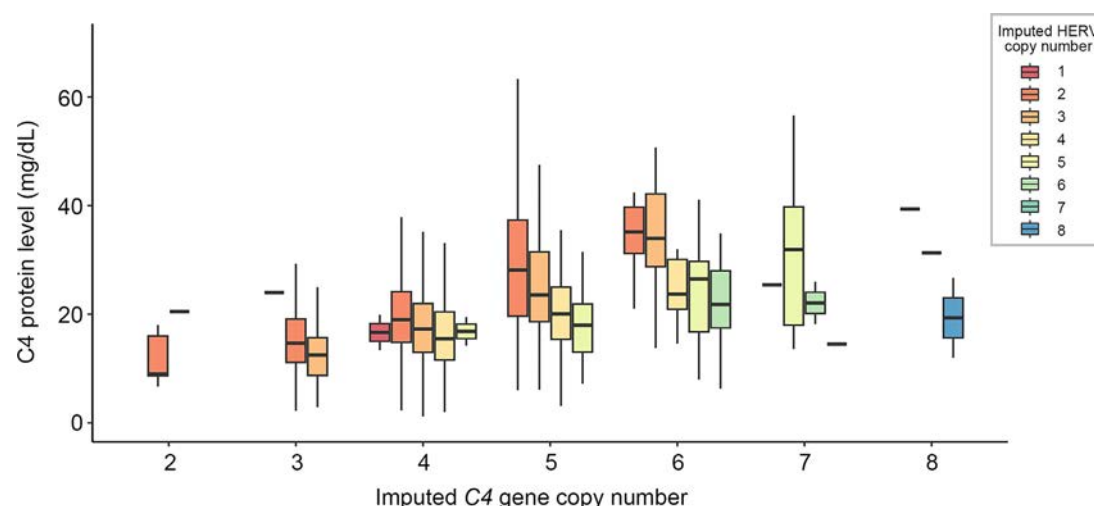
Figure 4. Association of plasma C4 protein levels with imputed *C4* and HERV copy numbers in SLE patients. The boxplot displays the relationship between plasma C4 protein levels and imputed *C4* copy numbers, further stratified by imputed HERV copy numbers in 1,284 SLE patients. A significant positive correlation is observed between *C4* copy numbers and protein levels ($P = 8.8 \times 10^{-69}$), while HERV copy numbers show a negative correlation ($P = 2.9 \times 10^{-23}$). One outlier with C4 protein levels over 100mg/dL from a sample with 6 HERV-inserted *C4* copies was omitted from the plot. SLE, systemic lupus erythematosus.

copy number of *C4*, with no evidence of allele-specific regulatory effects between *C4A* and *C4B*. Additionally, a HERV element, inserted within *C4*, leads to down-regulation of plasma C4 proteins. Considering both the genetic associations with SLE and protein levels, these findings suggest that the reduced production of the C4A protein isoform, functionally distinct from the C4B isoform, is driven by both low *C4A* copy numbers and HERV-mediated attenuation. This reduction plays a crucial role in SLE pathogenesis, particularly through *C4A*-specific pathways such as the regulation of autoreactive B cells [35].

Our fine-mapping study benefitted from the relatively less extensive LD in Koreans compared to Europeans, along with the use of a high-accuracy MHC imputation reference panel. Previous studies have demonstrated that European populations exhibit larger and more extended LD within the MHC region compared to African and Asian populations, likely due to population-specific factors such as lower recombination rates, resulting in slower decay of LD in Europeans [18,19,36−39]. Consistently, European SLE-MHC association analyses have reported long-range SLE-risk haplotypes involving multiple HLA genes in extensive LD, spanning MHC class I and II regions, such as the *C*07:01−B*08:01−DRB1*03:01−DQB1*02:01* haplotype [19,29].

Indeed, recent analyses including Kamitaki et al [18], whose study is detailed in the Introduction section, found that the significance of *C4* CNV effects was comparable to that of well-known risk classical alleles in Europeans [19]. However, the strong correlations between *C4* and HLA in Europeans posed challenges in distinguishing the independent effect of *C4*, especially considering the strong correlation between the SLE-risk *C4* haplotype (single-copy, short-form *C4B*) and SLE-risk HLA alleles, including *HLA-DRB1*03:01, HLA-DRB1*08:01*, and *HLA-DQB1*02:01* ($r^2 >$ 0.7) [18,19,36]. Conversely, findings from African populations revealed weaker correlations between *C4* and HLA variants (maximum r^2 between *C4* haplotypes and HLA alleles = 0.31), making it easier to pinpoint the independent association signal of *C4*. However, in their study, the imputation accuracy for *C4* in Africans was quite poor, and their conditional model controlling only for *HLA-DRB1*03:01* does

not fully support their conclusion that the primary signal driving the risk of SLE is derived from *C4* [18].

In Asian populations, the particularly strong association between *HLA-DRB1* and SLE risk has been well-established [5,6]. In our current study, the association of *C4* was initially overshadowed by the predominant effect of *HLA-DRB1* in the unconditional analysis ($P_{combined}$ of *C4A* = 1.48×10^{-6}). However, as correlations between *HLA-DRB1* classical alleles and *C4*-related haploid copy numbers were generally low (e.g. $r^2 \leq 0.06$ with *HLA-DRB1*03:01*; $r^2 \leq 0.002$ with *HLA-DRB1*15:01*) to at most moderate (maximum r^2 between *C4*-related haploid copy numbers and other *HLA-DRB1* alleles = 0.45; Supplementary Table S8), this allowed our conditional analysis to pinpoint the secondary association signal at *C4*. Especially, *HLA-DRB1*03:01*, the well-established SLE-risk allele among Europeans, was not common in our East Asian cohort (imputed allele frequency = 2.0%; 96.0% of individuals had no copies, 3.8% had 1 copy, and only 0.05% had 2 copies). Notably, the effect size and direction of the *C4A* copy number remained consistent after excluding all *HLA-DRB1*03:01* carriers, with an OR of 0.87 (95% CI = 0.82−0.92) in the full sample, and 0.87 (95% CI = 0.82−0.93) in non-carriers. These results indicate that the observed *C4A* signal is not explained by linkage with *HLA-DRB1*03:01*. Similarly, the exclusion of individuals carrying *HLA-DRB1*15:01*, a predominant risk allele in East Asians, did not result in a substantial change in the association statistics for *C4A* CNVs (OR = 0.88, 95% CI = 0.82−0.94), indicating that the *C4* signal is not driven by linkage to *HLA-DRB1*15:01* either. These results together support that the association of *C4* CNVs with SLE risk in East Asians reflects an independent effect, rather than tagging of *HLA-DRB1* classical alleles.

We developed the first MHC imputation reference panel capable of simultaneously imputing various HLA variants, *C4*-related CNVs, and other MHC variants. The *C4* gene, despite its biological relevance to autoimmune diseases like SLE, has been relatively underexplored compared to HLA genes, largely due to complexity of its genetic structure. In this study, we leveraged WGS data from large-scale general Korean cohorts to characterise *C4* alleles and CNVs using an existing reliable computational approach [18,23].
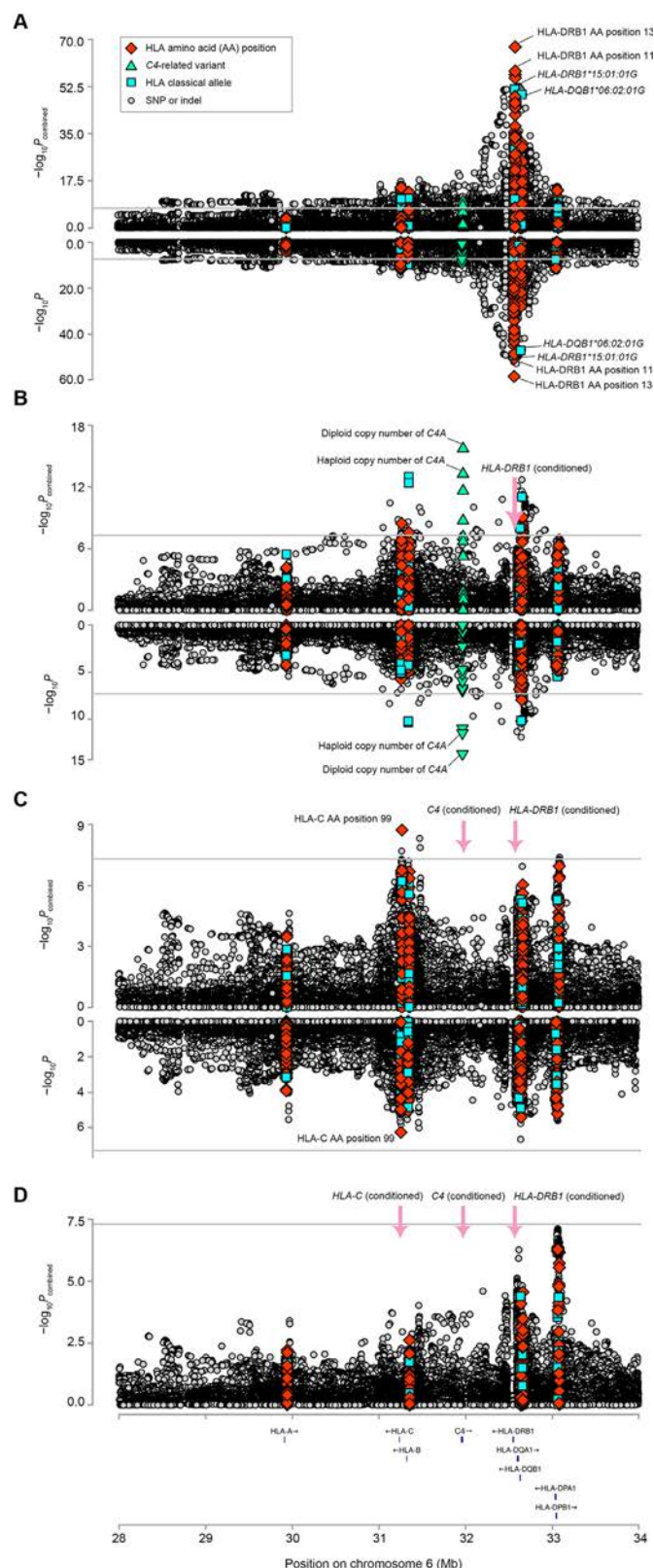
One of the major challenges was accurately defining haploid-level copy numbers from WGS-derived diploid copy numbers. To address this, we employed haplotype clustering with deep learning-based models and an iterative optimisation method to determine the most likely copy numbers of *C4A, C4B,* and HERV. This method not only allowed us to construct an MHC imputation reference panel with high-accuracy for *C4*-related CNVs, but it also holds significant potential for broader applications in other studies dealing with complex CNV genotyping. Nonetheless, our imputation panel has a limitation that it only includes copy number information for *C4A, C4B,* and HERV in each homologous chromosome pair, leading to ambiguity in determining how many copies of *C4A* and *C4B* are in the long form with the HERV insert. This ambiguity is particularly pronounced in haplotypes where both *C4A* and *C4B* alleles are present but the number of HERV copies is fewer than the combined total of *C4A* and *C4B*.

To validate the imputation performance of our reference panel, we rigorously evaluated the imputation accuracy through various methods, including cross-validation with internal and external samples, that compares imputed data with actual data from WGS and ddPCR technologies. These evaluations consistently demonstrated superior imputation accuracy for both HLA variants and *C4*-related CNVs. We have made this imputation panel publicly available via an imputation server (https://coda.nih.go.kr/usab/kis/intro.do), providing other researchers with a valuable tool to better understand causal variants in the MHC region, especially for inflammatory diseases in East Asian populations.

In summary, we have demonstrated an enhanced SLE-MHC association model from the Korean population through the development of a novel MHC imputation reference panel. This advancement not only enriches our understanding of the biological mechanisms underlying the role of HLA and *C4* in SLE pathogenesis but also holds promise for refining genetic risk assessments for SLE. To evaluate its generalisability and transferability across diverse genetic backgrounds, further assessment in other ancestral populations will be important. Furthermore, the application of our MHC panel is poised to significantly advance the investigation of MHC associations in other immune-mediated disorders within East Asian populations, paving the way for further insights and progress in personalised medicine.

Figure 5. Independent SLE association signals at *HLA-DRB1, C4,* and *HLA-C*. MHC-SLE association results from stepwise conditional regression analyses are shown in mirror regional association plots. The lower section of each mirror plot represents analysis results from the discovery GWAS dataset, while the upper section shows results from combined analyses incorporating both discovery and replication GWAS datasets. Significance levels were calculated using logistic regression for binary-coded variables (e.g., presence of an HLA classical allele or a *C4*-related haploid copy number allele) and for diploid copy numbers of *C4*-related elements, and using LRTs for multi-allelic variants (e.g., HLA amino acid positions with multiple residues, *C4*-related CNVs with multiple haploid copy number alleles). The grey horizontal line indicates the genome-wide significance threshold ($P = 5.0 \times 10^{-8}$). A, Unconditional analysis identified the strongest association within *HLA-DRB1*. Amino acid positions 13 exhibited the highest significance ($P = 3.16 \times 10^{-59}$; $P_{combined} = 5.35 \times 10^{-68}$) followed by position 11 ($P = 1.58 \times 10^{-49}$; $P_{combined} = 1.82 \times 10^{-56}$), while *HLA-DRB1*15:01:01G* was the most significantly associated allele ($P = 4.90 \times 10^{-50}$; $P_{combined} = 2.51 \times 10^{-52}$). B, After conditioning on all G-group classical alleles of *HLA-DRB1*, a secondary signal was uncovered at *C4*, with the diploid copy number ($P = 1.97 \times 10^{-14}$; $P_{combined} = 1.86 \times 10^{-16}$) and haploid copy number ($P = 3.34 \times 10^{-12}$; $P_{combined} = 5.34 \times 10^{-14}$) of the *C4A* allele showing the strongest associations. C, Conditioning on all G-group *HLA-DRB1* classical alleles and diploid copy numbers of all *C4* elements (*C4A, C4B,* and HERV) revealed a tertiary signal within *HLA-C* in the combined analysis, with amino acid position 99 exhibiting the most significant association ($P = 1.87 \times 10^{-9}$). No tertiary signal was detected in the discovery GWAS dataset alone. D, After conditioning on *HLA-DRB1, C4,* and *HLA-C* in the combined analysis, no significant variants were identified. CNV, copy number variation; GWAS, genome-wide association study; HLA, human leukocyte antigen; LTR, long terminal repeat; MHC, major histocompatibility; SLE, systemic lupus erythematosus; WGS, whole-genome sequencing.
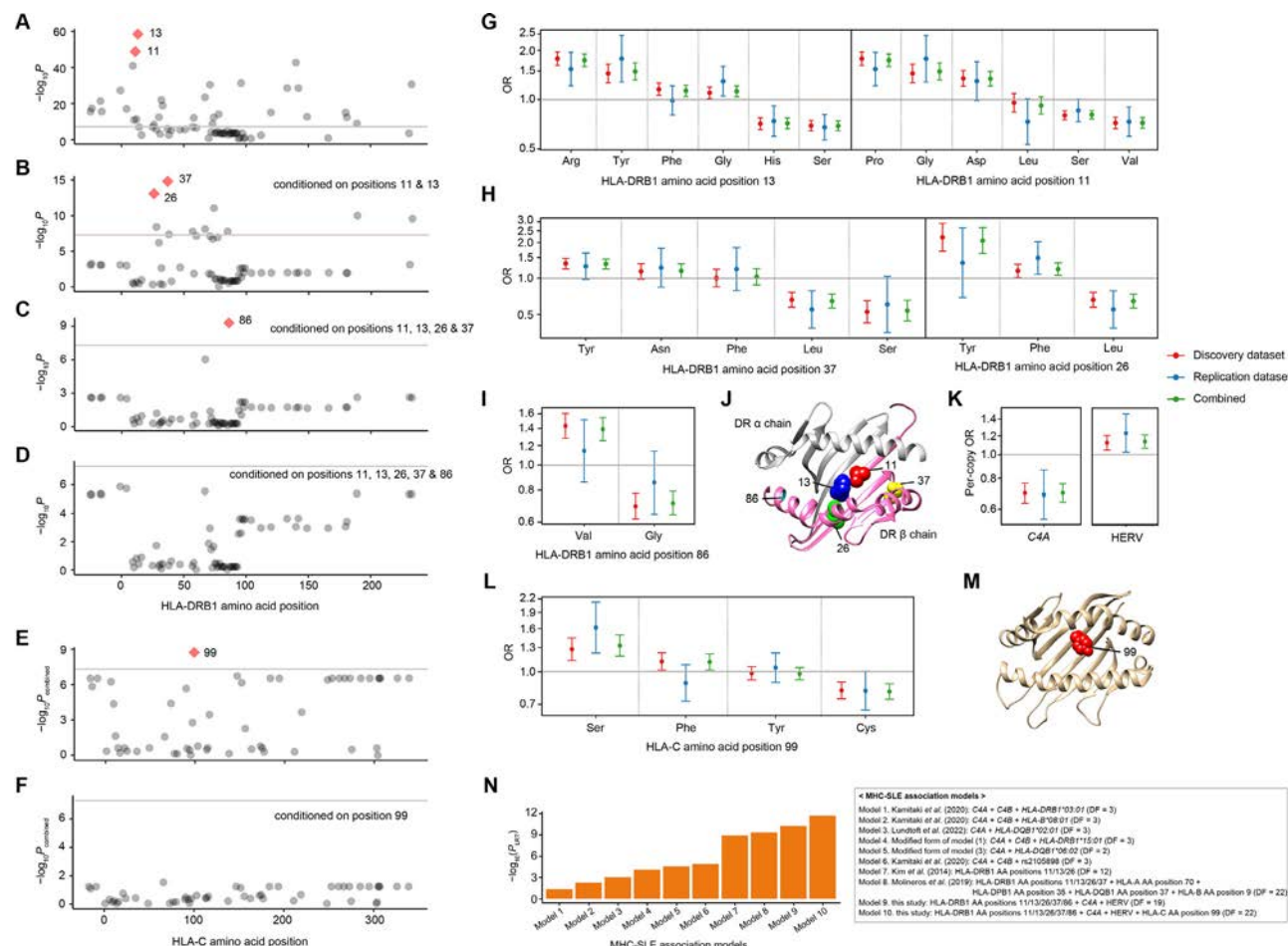
Figure 6. Key SLE-associated variants within *HLA-DRB1*, *C4*, and *HLA-C*. A−F, Stepwise conditional analyses at the amino acid level pinpointed independently SLE-associated positions, with HLA-DRB1 positions identified in the discovery dataset and HLA-C positions identified in the combined discovery and replication datasets. A, Position 13 and its correlated position 11 were identified in HLA-DRB1. B, Conditioning on positions 13 and 11 identified independent signals at position 37 (or 26). C, Position 86 was identified when conditioned on positions 13, 11, 37, and 26. D, No significant positions remained in HLA-DRB1 after conditioning on all five identified positions ($P < 5.0 \times 10^{-8}$). E, Conditioning on *HLA-DRB1* and *C4* identified HLA-C amino acid position 99. F, No additional HLA-C positions were significant after conditioning on position 99 along with *HLA-DRB1* and *C4*. G-I, ORs (dots) with 95% CIs (error bars) for amino acid residues, observed in stepwise conditional analysis, are plotted for HLA-DRB1 positions 13 and 11 (G), positions 37 and 26 (H), and position 86 (I), across datasets: discovery (N = 73,148, red), replication (N = 4,551, blue), and combined (N = 77,699, green). J, The 5 identified amino acid positions are located on the epitope-binding groove of the HLA-DR beta chain. K, Per-copy ORs with 95% CIs for *C4A* and HERV are plotted across datasets. Effect estimates for *C4A* were adjusted for *HLA-DRB1* and other covariates, whereas those for HERV were adjusted for *HLA-DRB1*, *C4A*, and the same set of covariates. L, ORs with 95% CIs for residues at HLA-C position 99, conditioned on *HLA-DRB1* and *C4*, are plotted across datasets. M, Amino acid position 99 is located on the epitope-binding groove of HLA-C. N, P_{LRT} values from the replication dataset for previously proposed and our MHC-SLE association models are plotted. To address potential overfitting, Model 9 was derived from the discovery dataset, excluding the *HLA-C* signal. Model 10 represents the full association model of this study, including the *HLA-C* signal. Our MHC-SLE association models, containing the identified signals, achieved the highest significance whether or not the *HLA-C* signal was included ($P_{Model\_9} = 5.50 \times 10^{-11}$; $P_{Model\_10} = 1.91 \times 10^{-12}$). AA, amino acid; CI, confidence interval; DF, degree of freedom; GWAS, genome-wide association study; HLA, human leukocyte antigen; OR, odds ratio; MHC, major histocompatibility; SLE, systemic lupus erythematosus.

Patient consent for publication

Not applicable.

Provenance and peer review

Not commissioned; externally peer reviewed.

Ethics approval

Analyses involving whole-genome sequencing data were approved by the Institutional Review Boards (IRBs) of UNIST (UNISTIRB-15-19-A, UNISTIRB-16-13-C) and the Korean Disease Control and Prevention Agency (KDCA) (2022-02-04-P-A, KDCA-2024-02-09-R-01). Recruitment of systemic lupus erythematosus patients and healthy controls was approved by the IRBs of Hanyang University (HY-12-005-16, HY-16-07-20, HY-16-129-15) and the Korea National Institute of Health. All participants provided written informed consent prior to inclusion in the study.

Data availability statement

Raw WGS data from reference batch #1 will be available as possible upon request and after approval from the Korean Genomics Center's review board in UNIST. Raw WGS data from reference batch #2 will be available as possible upon request and after approval from KNIH. The SLE GWAS datasets were collected by Hanyang University. This individual-level genotype and phenotype data are protected and are not available due to data privacy laws. The code of all tools used for analyses in this paper is publicly available and has been presented in the Methods section. Custom codes used to analysis are available at https://github.com/KimLabKHU/MHC-_reference_panel.

Supplementary materials

Supplementary material associated with this article can be found in the online version at doi:10.1016/j.ard.2025.06.2121.

Orcid

Chae-Yeon Yu: http://orcid.org/0000-0002-3938-7025
Yui Taek Lee: http://orcid.org/0000-0002-1516-5276
Sehwan Chun: http://orcid.org/0000-0001-8846-4341
Xianyong Yin: http://orcid.org/0000-0001-6454-2384
Young Jin Kim: http://orcid.org/0000-0002-4132-4437
Sang-Cheol Bae: http://orcid.org/0000-0003-4658-1093
Kwangwoo Kim: http://orcid.org/0000-0001-8926-6216

REFERENCES

[1] Hoi A, Igel T, Mok CC, Arnaud L. Systemic lupus erythematosus. Lancet 2024;403(10441):2326–38.
[2] Guga S, Wang Y, Graham DC, Vyse TJ. A review of genetic risk in systemic lupus erythematosus. Expert Rev Clin Immunol 2023;19(10):1247–58.
[3] Ha E, Bae SC, Kim K. Recent advances in understanding the genetic basis of systemic lupus erythematosus. Semin Immunopathol 2022;44(1):29–46.
[4] Trowsdale J, Knight JC. Major histocompatibility complex genomics and human disease. Annu Rev Genomics Hum Genet 2013;14:301–23.
[5] Kim K, Bang SY, Lee HS, Okada Y, Han B, Saw WY, et al. The HLA-DRβ1 amino acid positions 11-13-26 explain the majority of SLE-MHC associations. Nat Commun 2014;5:5902.
[6] Molineros JE, Looger LL, Kim K, Okada Y, Terao C, Sun C, et al. Amino acid signatures of HLA Class-I and II molecules are strongly associated with SLE susceptibility and autoantibody production in Eastern Asians. PLoS Genet 2019;15(4):e1008092.
[7] Sun C, Molineros JE, Looger LL, Zhou XJ, Kim K, Okada Y, et al. High-density genotyping of immune-related loci identifies new SLE risk variants in individuals with Asian ancestry. Nat Genet 2016;48(3):323–30.
[8] Goicoechea de Jorge E, López Lera A, Bayarri-Olmos R, Yebenes H, Lopez-Trascasa M. Rodríguez de Córdoba S. Common and rare genetic variants of complement components in human disease. Mol Immunol 2018;102:42–57.
[9] Yang Y, Chung EK, Zhou B, Blanchong CA, Yu CY, Füst G, et al. Diversity in intrinsic strengths of the human complement system: serum C4 protein concentrations correlate with C4 gene size and polygenic variations, hemolytic activities, and body mass index. J Immunol 2003;171(5):2734–45.
[10] Kerick M, Acosta-Herrera M, Simeón-Aznar CP, Callejas JL, Assassi S, Group International SSc, et al. Complement component C4 structural variation and quantitative traits contribute to sex-biased vulnerability in systemic sclerosis. NPJ Genom Med 2022;7(1):57.
[11] Zhou D, King EH, Rothwell S, Krystufkova O, Notarnicola A, Coss S, et al. Low copy numbers of complement C4 and C4A deficiency are risk factors for myositis, its subgroups and autoantibodies. Ann Rheum Dis 2023;82(2):235–45.
[12] Pereira KMC, Perazzio S, Faria AGA, Moreira ES, Santos VC, Grecco M, et al. Impact of C4, C4A and C4B gene copy number variation in the susceptibility, phenotype and progression of systemic lupus erythematosus. Adv Rheumatol 2019;59(1):36.
[13] Mulvihill E, Ardoin S, Thompson SD, Zhou B, Yu GR, King E, et al. Elevated serum complement levels and higher gene copy number of complement C4B are associated with hypertension and effective response to statin therapy in childhood-onset systemic lupus erythematosus (SLE). Lupus Sci Med 2019;6(1):e000333.
[14] Jüptner M, Flachsbart F, Caliebe A, Lieb W, Schreiber S, Zeuner R, et al. Low copy numbers of complement C4 and homozygous deficiency of C4A may predispose to severe disease and earlier disease onset in patients with systemic lupus erythematosus. Lupus 2018;27(4):600–9.
[15] Lintner KE, Patwardhan A, Rider LG, Abdul-Aziz R, Wu YL, Lundström E, et al. Gene copy-number variations (CNVs) of complement C4 and C4A deficiency in genetic risk and pathogenesis of juvenile dermatomyositis. Ann Rheum Dis 2016;75(9):1599–606.
[16] Chen JY, Wu YL, Mok MY, Wu YJ, Lintner KE, Wang CM, et al. Effects of complement C4 gene copy number variations, size dichotomy, and C4A deficiency on genetic risk and clinical presentation of systemic lupus erythematosus in East Asian populations. Arthritis Rheumatol 2016;68(6):1442–53.
[17] Lv Y, He S, Zhang Z, Li Y, Hu D, Zhu K, et al. Confirmation of C4 gene copy number variation and the association with systemic lupus erythematosus in Chinese Han population. Rheumatol Int 2012;32(10):3047–53.
[18] Kamitaki N, Sekar A, Handsaker RE, de Rivera H, Tooley K, Morris DL, et al. Complement genes contribute sex-biased vulnerability in diverse disorders. Nature 2020;582(7813):577–81.
[19] Lundtoft C, Pucholt P, Martin M, Bianchi M, Lundström E, Eloranta ML, et al. Complement C4 copy number variation is linked to SSA/Ro and SSB/La autoantibodies in systemic inflammatory autoimmune diseases. Arthritis Rheumatol 2022;74(8):1440–50.
[20] Hanscombe KB, Morris DL, Noble JA, Dilthey AT, Tombleson P, Kaufman KM, et al. Genetic fine mapping of systemic lupus erythematosus MHC

associations in Europeans and African Americans. Hum Mol Genet 2018;27 (21):3813–24.

[21] Langefeld CD, Ainsworth HC, Cunninghame Graham DS, Kelly JA, Comeau ME, Marion MC, et al. Transancestral mapping and genetic load in systemic lupus erythematosus. Nat Commun 2017;8:16021.

[22] Dilthey AT, Mentzer AJ, Carapito R, Cutland C, Cereb N, Madhi SA, et al. HLA*LA-HLA typing from linearly projected graph alignments. Bioinformatics 2019;35(21):4394–6.

[23] Handsaker RE, Van Doren V, Berman JR, Genovese G, Kashin S, Boettger LM, et al. Large multiallelic copy number variations in humans. Nat Genet 2015;47(3):296–303.

[24] Sekar A, Bialas AR, de Rivera H, Davis A, Hammond TR, Kamitaki N, et al. Schizophrenia risk from complex variation of complement component 4. Nature 2016;530(7589):177–83.

[25] Bell AD, Usher CL, McCarroll SA. Analyzing copy number variation with droplet digital PCR. Methods Mol Biol 2018;1768:143–60.

[26] Furukawa H, Kawasaki A, Oka S, Ito I, Shimada K, Sugii S, et al. Human leukocyte antigens and systemic lupus erythematosus: a protective role for the HLA-DR6 alleles DRB1*13:02 and *14:03. PLoS One 2014;9(2): e87792.

[27] Shimizu C, Kim J, Eleftherohorinou H, Wright VJ, Hoang LT, Tremoulet AH, et al. HLA-C variants associated with amino acid substitutions in the peptide binding groove influence susceptibility to Kawasaki disease. Hum Immunol 2019;80(9):731–8.

[28] Pidala J, Wang T, Haagenson M, Spellman SR, Askar M, Battiwalla M, et al. Amino acid substitution at peptide-binding pockets of HLA class I molecules increases risk of severe acute GVHD and mortality. Blood 2013 Nov 21;122 (22):3651–8.

[29] Morris DL, Taylor KE, Fernando MM, Nititham J, Alarcón-Riquelme ME, Barcellos LF, et al. Unraveling multiple MHC gene associations with systemic lupus erythematosus: model choice indicates a role for HLA alleles and non-HLA genes in Europeans. Am J Hum Genet 2012;91(5):778–93.

[30] Morris DL, Fernando MM, Taylor KE, Chung SA, Nititham J, Alarcón-Riquelme ME, et al. MHC associations with clinical and autoantibody manifestations in European SLE. Genes Immun 2014;15(4):210–7.

[31] Wang CC, Shen CH, Lin GC, Chen YM, Chen IC. Association of HLA alleles with cephalosporin allergy in the Taiwanese population. Sci Rep 2024;14 (1):17167.

[32] Irish Schizophrenia Genomics Consortium and the Wellcome Trust Case Control Consortium 2. Genome-wide association study implicates HLA-C*01:02 as a risk factor at the major histocompatibility complex locus in schizophrenia. Biol Psychiatry 2012 Oct 15;72(8):620–8.

[33] Fujita KI, Matsumoto N, Murase R, Takeshima K, Ishida H, Kubota Y. Associations of HLA-C*01:02 and HLA-B*46:01 with regorafenib-induced erythema multiforme in Japanese patients with metastatic colorectal cancer. Clin Transl Sci 2023;16(10):1741–7.

[34] Fernando MM, Vyse TJ. Major histocompatibility complex and SLE editor. In: Lahita RG, editor. Lahita's systemic lupus erythematosus. Elsevier; 2021.

[35] Simoni L, Presumey J, van der Poel CE, Castrillon C, Chang SE, Utz PJ, et al. Complement C4A regulates autoreactive B cells in murine lupus. Cell Rep 2020;33(5):108330.

[36] Boteva L, Morris DL, Cortés-Hernández J, Martin J, Vyse TJ, Fernando MM. Genetically determined partial complement C4 deficiency states are not independent risk factors for SLE in UK and Spanish populations. Am J Hum Genet 2012;90(3):445–56.

[37] de Bakker PI, McVean G, Sabeti PC, Miretti MM, Green T, Marchini J, et al. A high-resolution HLA and SNP haplotype map for disease association studies in the extended human MHC. Nat Genet 2006;38(10):1166–72.

[38] McElroy JP, Cree BA, Caillier SJ, Gregersen PK, Herbert J, Khan OA, et al. Refining the association of MHC with multiple sclerosis in African Americans. Hum Mol Genet 2010;19(15):3080–8.

[39] Frisse L, Hudson RR, Bartoszewicz A, Wall JD, Donfack J, Di Rienzo A. Gene conversion and different population histories may explain the contrast between polymorphism and linkage disequilibrium levels. Am J Hum Genet 2001;69(4):831–43.

Systemic lupus erythematosus

Integrative spatial multiomics analysis reveals regulatory mechanisms of VCAM1 $^+$ proximal tubule cells in lupus nephritis

Junyu Wang [1,2], Ao Zheng [1,2], Nianping Liu [1,3], Zhen Tan [1], Yu Shi [2], Tianyi Ma [2], Songwen Luo [2], Lin Zhu [2], Zhou Zhou [1], Feifei Yuan [4], Tiekun Li [5], Yuyan Gong [6], Jingwen Fang [2,7], Lu Liu [8], Xuejun Zhang [8], Sang-Cheol Bae [9], Chikashi Terao [10], Zhu Chen [1], Xiaomei Li [1], Guosheng Wang [1,*], Kun Qu [1,3,11,*], Chuang Guo [1,2,12,*]

[1] Department of Rheumatology and Immunology, The First Affiliated Hospital of USTC, State Key Laboratory of Eye Health, Division of Life Sciences and Medicine, School of Basic Medical Sciences, University of Science and Technology of China, Hefei, China
[2] Division of Life Sciences and Medicine, University of Science and Technology of China, Hefei, China
[3] School of Biomedical Engineering, Suzhou Institute for Advanced Research, University of Science and Technology of China, Suzhou, China
[4] Division of Nephrology, Nanfang Hospital, Southern Medical University, Guangzhou, China
[5] Nanjing Kingmed Center for Clinical Laboratory Co, Ltd, Nanjing, Jiangsu, China
[6] SeekGene BioSciences Co, Ltd, Beijing, China
[7] HanGene Biotech, Hefei, Anhui, China
[8] Institute of Dermatology, Anhui Medical University, Anhui, China
[9] Department of Rheumatology, Hanyang University Hospital for Rheumatic Diseases, Hanyang University Institute for Rheumatology Research, Hanyang Institute of Bioscience and Biotechnology, Seoul, Republic of Korea
[10] Laboratory for Statistical and Translational Genetics Analysis, RIKEN Center for Integrative Medical Sciences, Wako, Saitama, Japan
[11] Institute of Artificial Intelligence, Hefei Comprehensive National Science Center, Hefei, China
[12] School of Pharmacy, Bengbu Medical University, Bengbu, China

ARTICLE INFO

ABSTRACT

Objectives: Lupus nephritis (LN) is a severe complication of systemic lupus erythematosus (SLE), characterised by kidney inflammation, tubular injury, and interstitial fibrosis. However, the spatial organisation of these heterogeneous cell populations and their regulatory mechanisms in LN remain poorly understood. The objective of this study was to investigate the regulatory mechanisms underlying region-specific kidney lesions and tubular damage in LN.
Methods: We performed single-cell multiome and spatial transcriptomic analyses on kidney biopsy samples from patients with LN and controls, integrating data from the largest East Asian SLE genome-wide association studies (GWAS) (208,370 samples) to date. Validation experiments were performed using multiplex immunohistochemistry (mIHC), *in vitro* lentiviral-mediated transcription factor overexpression, and functional stimulation assays.
Results: We identified *VCAM1*-expressing proximal tubule (PT_VCAM1) cells as components of an LN-specific inflammatory niche (niche 5) localised in the kidney cortex. Both in silico and *in vitro* experiments demonstrated that interactions between PT_VCAM1 cells and myofibroblasts,

*Correspondence to Dr Chuang Guo, Kun Qu, Guosheng Wang.
E-mail addresses: gswang0551@163.com (G. Wang), qukun@ustc.edu.cn (K. Qu), gchuang@ustc.edu.cn (C. Guo).
Junyu Wang, Ao Zheng, and Nianping Liu contributed equally to this work.

as well as immune cells in niche 5, promote their epithelial-mesenchymal transition. Trajectory analysis suggested that PT_VCAM1 cells originate from a failed-repair pathway in proximal tubule cells, regulated by transcriptional networks involving BACH2. Integrative GWAS analysis further linked SLE-associated risk single-nucleotide polymorphisms to *cis*-regulatory elements specific to PT_VCAM1 cells, including single-nucleotide polymorphisms within the distal enhancer of the *BMP2K* locus, which establishes a BACH2 motif.

Conclusions: Collectively, our findings characterise PT_VCAM1 cells as injury-responsive cell states that contribute to the inflammatory and fibrotic niche in LN, linking genetic predisposition to cellular injury and disease progression.

KEY MESSAGES

WHAT IS ALREADY KNOWN ON THIS TOPIC

- Lupus nephritis (LN) is a severe complication of systemic lupus erythematosus (SLE), characterised by tubular epithelial dysfunction, immune cell infiltration, and progressive fibrosis.
- Recent studies have identified key LN-associated immune cell subpopulations, such as granzyme K$^+$ CD8 T cells and CD163$^+$ dendritic cells.
- Genome-wide association studies (GWAS) have identified susceptibility candidates that contribute to the dysfunction of immune subpopulations in SLE.

WHAT THIS STUDY ADDS

- Using single-cell multiome and spatial transcriptomic sequencing, we identified a distinct inflammatory microenvironment in the renal cortex of patients with LN (niche 5), characterised by the colocalisation of *VCAM1*-expressing proximal tubule (PT_VCAM1) cells, myofibroblasts, and immune cells.
- PT_VCAM1 cells exhibited a "failed-repair" phenotype, regulated by a core transcriptional network involving 4 transcription factors, with BACH2 emerging as a potential novel therapeutic target.
- The increased presence of myofibroblasts and immune cells within niche 5 facilitated interactions with PT_VCAM1 cells through several ligands, including COL4A1, SPP1, and transforming growth factor (TGF)-β1, thereby promoting epithelial-mesenchymal transition (EMT) in PT_VCAM1 cells.
- Integrative GWAS analysis revealed associations between SLE risk single-nucleotide polymorphisms (SNPs) and PT_VCAM1-specific *cis*-regulatory elements, including variants in the distal enhancer of the *BMP2K* locus. These variants were shown to create a BACH2 motif, reinforcing the failed-repair phenotype in PT_VCAM1 cells.

HOW THIS STUDY MIGHT AFFECT RESEARCH, PRACTICE OR POLICY

- Our study presents a comprehensive mapping of the spatial architecture and regulatory mechanisms in the human LN kidney, revealing spatial and genetic influences on PT_VCAM1 cells in promoting inflammatory and fibrotic remodelling.
- Our multiomics strategy, which identified causal variants specific to distinct cell subpopulations, offers a framework for developing precision therapeutics targeting cell types implicated in LN pathogenesis.

INTRODUCTION

Lupus nephritis (LN) is a severe complication of systemic lupus erythematosus (SLE), affecting up to two-thirds of patients with SLE and contributing to morbidity and mortality [1]. LN is characterised by immune cell infiltration, tubular epithelial injury, and progressive fibrosis. Immune cells, including macrophages, T cells, and B cells, infiltrate kidney tissues and initiate inflammatory responses that exacerbate fibrosis and kidney damage [2,3]. Tubular epithelial cells, particularly proximal tubule (PT) cells, also contribute to local inflammation through the secretion of inflammatory mediators and interactions with immune and stromal cells [4,5]. Elucidating these interactions within their spatial context is fundamental to advancing our understanding of LN pathogenesis.

Recent single-cell sequencing studies have identified transcriptional programs in LN-associated immune cell subpopulations, such as APOE$^+$ monocytes, granzyme K$^+$ CD8 T cells, and CD163$^+$ dendritic cells [2,4,6,7]. However, the role of tubular epithelial subpopulations, such as PT cells in LN, remains insufficiently explored. PT cells are essential for kidney function and exhibit subpopulation-specific heterogeneity in healthy and diseased conditions [5]. For instance, healthy kidneys feature PT-S1, PT-S2, and PT-S3 as primary subpopulations, whereas diseased kidneys exhibit PT cell subpopulations such as *VCAM1*-expressing PT (PT_VCAM1) cells [8,9]. PT_VCAM1 cells are enriched in fibrotic microenvironments and are implicated in immune cell recruitment and inflammation [10]. Despite these insights, the mechanisms driving the transition of conventional PT cells into PT_VCAM1 cells and the regulatory pathways associated with this process remain unresolved. Addressing these gaps could provide a mechanistic framework for understanding the progression of LN and other kidney pathologies.

Genetic predispositions significantly contribute to the development of LN, with genome-wide association studies (GWAS) identifying numerous genetic risk variants associated with lupus, primarily in noncoding regions of the genome [11]. These studies implicate *cis*-regulatory elements (CREs) in the regulation of genes associated with LN pathogenesis [12,13]. However, challenges remain in prioritising these variants to specific cellular populations as well as clarifying how these variants affect cellular function or contribute to disease pathogenesis. Integrating GWAS data with single-cell and spatial transcriptomics (STs) offers a systematic framework to link CREs with specific cell types and evaluate their influence on transcriptional regulation in LN.

This study integrates single-cell multiome sequencing and ST to delineate cellular niches, intercellular interactions, and genetic regulatory mechanisms in LN kidneys. We identified 6 kidney niches, including an inflammatory niche (niche 5) in the kidney cortex of patients with LN, which is enriched with immune cells, myofibroblasts (MyoFIB), and PT_VCAM1 cells. PT_VCAM1 cells exhibited a profibrotic and proinflammatory phenotype, arising from a failed-repair pathway regulated by BACH2. Integrative GWAS fine-mapping linked SLE-associated single-nucleotide polymorphisms (SNPs) to PT_VCAM1-specific CREs. These findings highlight spatial and genetic influences on PT_VCAM1 cells in promoting inflammatory and fibrotic remodelling in LN kidneys.

METHODS

Details of the methods are available in the online Supplementary Methods.

RESULTS

Multimodal single-cell profiling of kidney cells in human LN

We obtained kidney tissue samples from 8 patients with LN and used adjacent nontumour tissues from 2 patients with kidney tumour as control samples (Supplementary Table S1). We then performed paired single-nucleus RNA sequencing (snRNA-seq) and single-nucleus assay for transposase-accessible chromatin sequencing (snATAC-seq) using the 10× multiome platform, which enables the concurrent measurement of RNA expression and chromatin accessibility within the same nuclei (Fig 1A and Supplementary Fig S1A). After rigorous filtering of RNA and chromatin accessibility data, we retained 41,543 high-quality nuclei. To expand our dataset, we integrated additional snRNA-seq and snATAC-seq datasets from 5 control samples [8]. Unlike our paired dataset, these public datasets contain separate populations of nuclei for snRNA-seq and snATAC-seq from the same samples. In total, this integration resulted in 64,479 nuclei for snRNA data and 72,472 nuclei for snATAC data, with each nucleus containing an average of 2078 genes and 17,523 fragments (Supplementary Fig S1B).

Following batch effect correction across samples and unsupervised clustering, we identified 35 distinct cell subpopulations in the transcriptomic data, subsequently categorised into 13 cell types (Fig 1B-D and Supplementary Fig S1C-E). These cell subpopulations represented a wide range of kidney cell types, including those located in the cortex, medullary ray, and outer medulla. Moreover, the identified cell subpopulations exhibited extensive similarities to those derived from publicly available human kidney cell datasets [3,8] (Supplementary Fig S1F,G), validating the accuracy of the cell clustering. Additionally, leveraging the high-resolution cell subpopulation annotations obtained from snRNA-seq, we used the Seurat label transfer approach [14] to map these annotations to the snATAC-seq cells. This process resulted in cell cluster annotations within the snATAC-seq data that showed high consistency with those identified in publicly available snATAC-seq data from human kidney cells [3] (Fig 1C and Supplementary Fig S2A,B).

To evaluate cellular and molecular alterations between LN samples and control samples, we quantified the proportions of each identified cell type relative to the total cell population, as well as the number of differentially expressed genes (DEGs) and differentially accessible regions (DARs) by comparing LN samples with control samples within each cell type (Fig 1E,F and Supplementary Table S2). In patients with LN, we observed a significant increase in the proportion of infiltrating immune cells (Padjusted $= .014$), consistent with previous reports, indicating that enhanced immune activation contributes to LN pathogenesis [4]. Furthermore, we found a significant reduction in podocyte populations (Padjusted $= .0041$), in line with histopathological evidence that podocyte loss compromises glomerular filtration integrity [15]. Although the proportion of PT cells did not show a statistically significant change, this cell type exhibited the highest number of DEGs and DARs, indicating extensive alterations in their biological function in LN. Collectively, our multiome atlas provided a detailed molecular characterisation of LN, revealing substantial changes in both cell-type proportions and gene expression profiles compared with controls.

Niche 5 is characterised by increased MyoFIB, immune infiltrates, and PT_VCAM1 cells

To investigate the cellular neighbourhoods surrounding significantly altered cell subpopulations, we prepared 10-μm cryosections from 11 kidney tissue samples for ST profiling, comprising 8 from patients with LN and 3 from control samples (Fig 2A and Supplementary Fig S1). We also expanded our cohort by incorporating 1 publicly available control sample from the study by Melo Ferreira et al [16]. After stringent quality control, our ST dataset comprised 6410 spots, with an average of 17 cells and 3292 detected genes per spot (Supplementary Fig S3A,B). We then applied Cell2location [17] to assign cell-type probabilities to each spot and subsequently used SPACEL [18] for joint analysis across all slices, identifying 6 distinct cellular niches (niche 1-6) in patients with LN and control samples (Fig 2B and Supplementary Fig S3C,D). Pathologist annotations of haematoxylin and eosin (H&E)-stained images delineated the cortical, medullary ray, and outer medulla regions (Fig 2C and Supplementary Fig S3E).

Notably, niche 5 was significantly enriched in the cortical region of LN samples, whereas niche 2 predominated in the cortex of control samples (Fig 2D and Supplementary Fig S3F,G). These 2 niches recapitulated known tissue features, representing kidney tubules (niche 2) and atrophied kidney tubules (niche 5), respectively (Supplementary Fig S4A). Other niches, including niche 1 (cortex), niche 3 (medullary rays), and niche 4 (outer medulla), showed no significant differences between LN and control samples (Supplementary Fig S3F,G). Further analysis of the cell type composition of LN/control-enriched niches revealed that niche 5 was notably enriched with MyoFIB, PT_VCAM1 cells, and various immune cell populations, including *CD163*-expressing M2 macrophages (Mac_M2), *ITGAX*-expressing macrophages (Mac_ITGAX), CD8 T cells, and plasma cells (Fig 2E-H and Supplementary Fig S4B). Cell types within niche 5 exhibited higher colocalisation scores compared with those in other niches, suggesting a distinct microenvironment structure (Supplementary Fig S4C). Moreover, Moran's I analysis revealed that PT_VCAM1 cells exhibited significantly increased spatial aggregation in LN kidneys (Supplementary Fig S4D).

To validate the presence of a cellular neighbourhood coenriched with MyoFIB, PT_VCAM1 cells, and immune cells in the cortex of patients with LN, we first utilised SeekSpace to analyse the spatial coordinates of bona fide single-cell transcriptomes from an additional patients with LN across 2 replicates. This approach identified high-quality single cells and successfully mapped 27 out of 35 cell subpopulations in 10× multiome datasets (Supplementary Fig S5A-E). We observed spatial colocalisation of PT_VCAM1 cells, MyoFIB, and immune cells in the cortical regions (Supplementary Fig S5F,G). Furthermore, we performed multiplex immunohistochemistry (mIHC) staining using 4′,6′-dia midino-2-phenylindole (DAPI) and antibodies targeting AQP1, VCAM1, α-SMA (*ACTA2*), and CD45 (*PTPRC*) in 3 LN samples and 3 control samples. The results revealed significantly higher numbers of PT_VCAM1 cells, MyoFIB, and immune cells in the cortical region of patients with LN (Fig 2I, J), with these cell types showing close spatial proximity to each other (Supplementary Fig S6A).

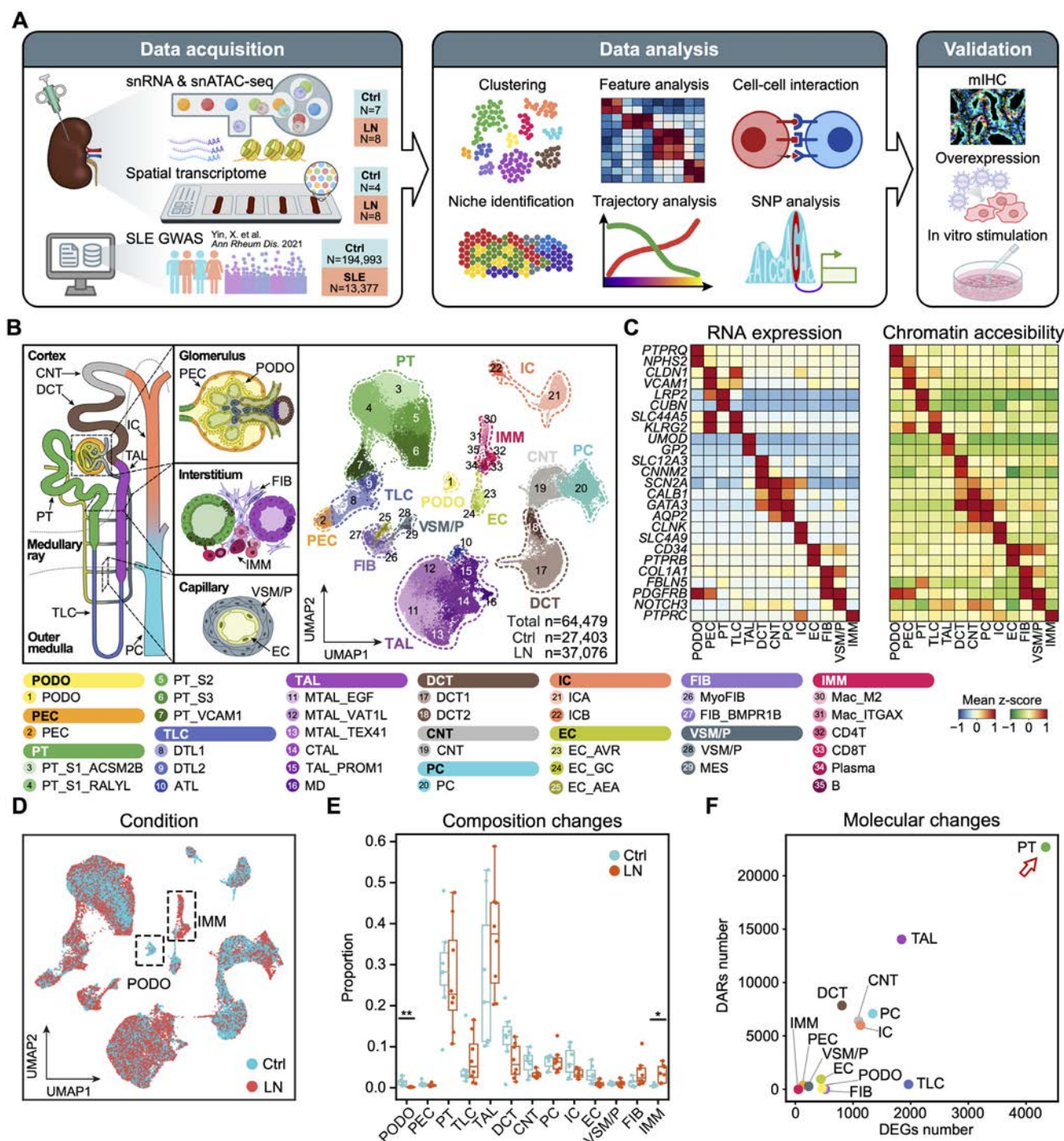DEG analysis across distinct cellular niches revealed that niche 5 exhibited elevated expression of complement genes

Figure 1. Single-cell multiomics profiling of human lupus nephritis (LN). A, Schematic overview of the study design. B, Scheme of the kidney, with cell-type distribution indicated by colour (left), and uniform manifold approximation and projection (UMAP) visualisation of single-nucleus RNA sequencing (snRNA-seq) data from all samples, coloured by cell subpopulations (right). Dashed circles highlight cell types. C, Heatmaps showing z-score−transformed gene expression (left) and chromatin accessibility (right) of canonical marker genes across the 13 cell types. D, UMAP visualisation of snRNA-seq data from all samples, coloured by condition. Cell types with significant proportional differences between control (Ctrl) and LN are highlighted with dashed rectangles. E, Box plots comparing the cell proportion of each cell type between Ctrl and LN samples. Statistical significance was assessed using a 2-sided Wilcoxon rank-sum test, and P values were adjusted using the Benjamini-Hochberg correction (*Padjusted < .05; **Padjusted < .01). F, Scatter plot showing the number of differentially expressed genes (DEGs) and differentially accessible regions (DARs) across the 13 cell types, comparing LN and Ctrl conditions. snATAC-seq, single-nucleus assay for transposase-accessible chromatin sequencing; SLE, systemic lupus erythematosus; SNP, single-nucleotide polymorphism; mIHC, multiplex immunohistochemistry; PODO, podocyte; PEC, parietal epithelial cell; PT, proximal tubule cell; TLC, thin limb cell; TAL, thick ascending limb cell; DCT, distal convoluted tubule cell; CNT, connecting tubule cell; PC, principal cell; IC, intercalated cell; EC, endothelial cell; FIB, fibroblast; VSM/P, vascular smooth muscle cell or pericyte; IMM, immune cell; PT_VCAM1, *VCAM1*-expressing proximal tubule cell; DTL1, descending thin limb cell type 1; DTL2, descending thin limb cell type 2; ATL, ascending thin limb cell; MTAL_EGF, *EGF-expressing* medullary thick ascending limb cell; MTAL_VAT1L, *VAT1L-expressing* medullary thick ascending limb cell; MTAL_TEX41, *TEX41-expressing* medullary thick ascending limb cell; CTAL, cortical thick ascending limb cell; TAL_PROM1, *PROM1-expressing* thick ascending limb cell; MD, macula densa cell; DCT1, distal convoluted tubule cell type 1; DCT2, distal convoluted tubule cell type 2; ICA, alpha-intercalated cell; ICB, beta-intercalated cell; EC_AVR, ascending vasa recta endothelial cell; EC_GC, glomerular capillary endothelial cell; EC_AEA, afferent/efferent arteriole endothelial cell; MyoFIB, myofibroblast; FIB_BMPR1B, *BMPR1B-expressing* fibroblast; MES, mesangial cell; Mac_M2, *CD163-expressing* M2 macrophage; Mac_ITGAX, *ITGAX-expressing* macrophage.
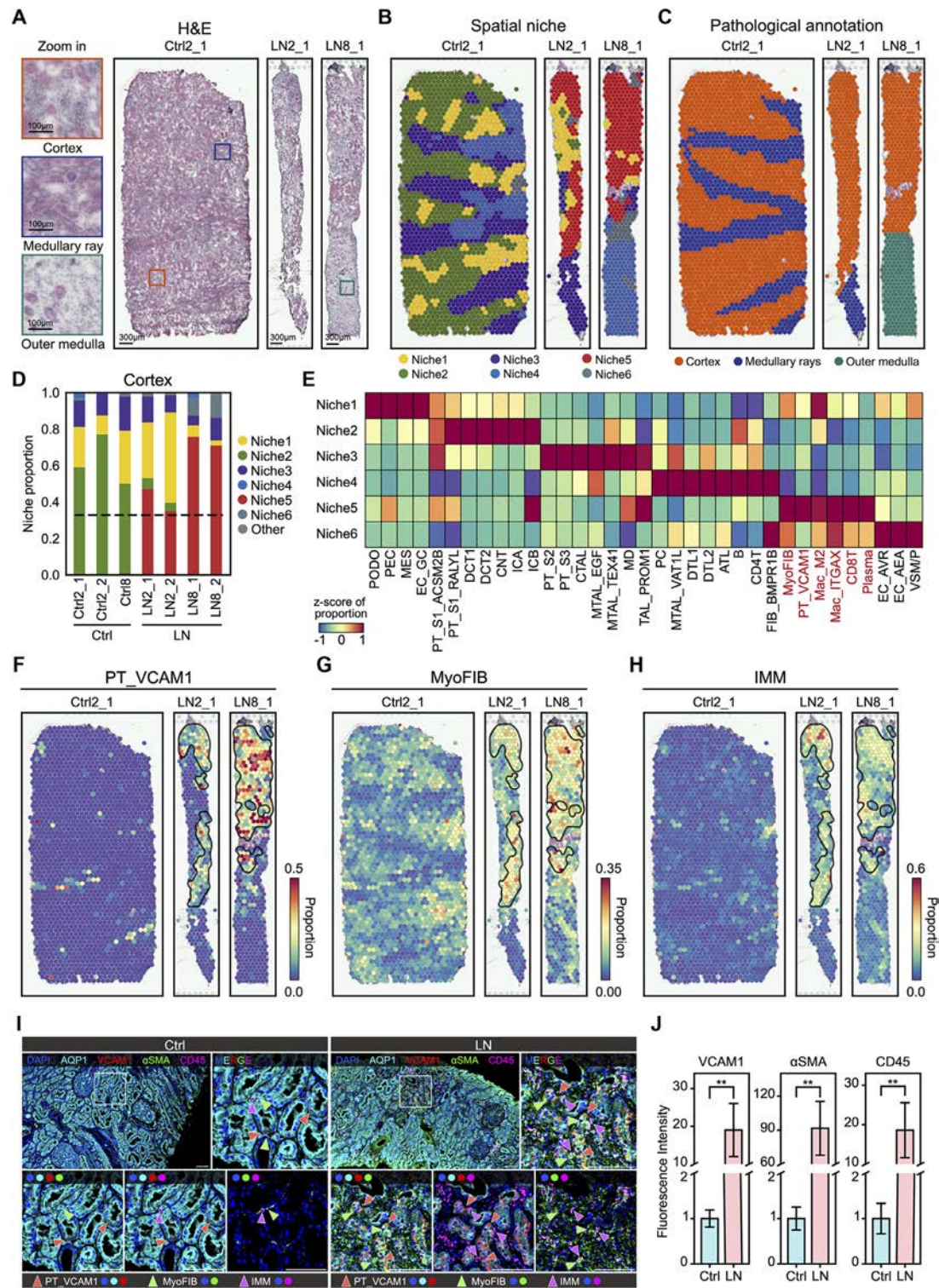
Figure 2. Identification and cellular composition of distinct niches in lupus nephritis (LN). A, Haematoxylin and eosin (H&E)-stained images of representative control (Ctrl) and LN samples, with zoomed-in views of the cortex, medullary rays, and outer medulla regions shown on the left. B and C, Spatial niches (B) and pathological annotations (C) of representative samples. D, Stacked bar plot showing the niche composition in the cortex region. The dashed line indicates the mean proportion of the dominant niche in the cortex region. E, Heatmap showing the cellular composition of cell subpopulations across 6 distinct niches. F-H, Spatial distribution of cellular composition calculated by Cell2location for VCAM1-expressing proximal tubule (PT_VCAM1) cells (F), myofibroblasts (MyoFIB) (G), and immune cells (H) in representative Ctrl and LN samples. Niche 5 is outlined in black lines. I, Multiplex immunohistochemistry (mIHC) staining of representative Ctrl and LN samples, with each panel consisting of 5 subpanels: 1 full image and 4 magnified views of regions outlined by white squares. The zoomed-in views include a merged image and 3 images showing the colocalisation of 2 cell types in pairs. Scale bar = 100 μm. J, Bar plot showing the fluorescence intensity of VCAM1, α-SMA, and CD45 between Ctrl and LN samples. Statistical significance was assessed using a one-sided Student's t-test (**$P < .01$; n = 3 per group). PODO, podocyte; PEC, parietal epithelial cell; PT, proximal tubule cell; DTL1, descending thin limb cell type 1; DTL2, descending thin limb cell type 2; ATL, ascending thin limb cell; MTAL_EGF, *EGF*-expressing medullary thick ascending dimb cell; MTAL_VAT1L, *VAT1L*-expressing medullary thick ascending limb cell; MTAL_TEX41, *TEX41*-expressing medullary thick ascending limb cell; CTAL, cortical thick ascending limb cell; TAL_PROM1, *PROM1*-expressing thick ascending limb cell; MD, macula densa cell; DCT1, distal convoluted tubule cell type 1; DCT2, distal convoluted tubule cell type 2; CNT, connecting tubule cell; PC, principal cell; ICA, alpha-intercalated cell; ICB, beta-intercalated cell; EC_AVR, ascending vasa recta endothelial cell; EC_GC, glomerular capillary endothelial cell; EC_AEA, afferent/efferent arteriole endothelial cell; FIB_BMPR1B, *BMPR1B*-expressing fibroblast; VSM/P, vascular smooth muscle cell or pericyte; MES, mesangial cell; IMM, immune cell; Mac_M2, *CD163*-expressing M2 macrophage; Mac_ITGAX, *ITGAX*-expressing macrophage.

(eg, *C3* and *C1S*), chemokines (eg, *CCL5* and *CCL19*), and collagen-related genes (eg, *COL3A1* and *COL4A1*), suggesting inflammatory signalling and active extracellular matrix (ECM) remodelling in this niche (Supplementary Fig S7A-C and Supplementary Table S3). To further evaluate the clinical relevance of niche 5, we analysed microarray-derived gene expression profiles of 45 pretreatment patients with LN [19] and assessed correlations with established clinical indicators of disease severity, including serum creatinine and proteinuria levels. The niche 5 signature (ie, DEGs identified in niche 5) showed a positive correlation with both serum creatinine (R = 0.318, *P* = .033) and proteinuria levels (R = 0.290, *P* = .053) (Supplementary Fig S7D,E). Collectively, these observations underscore that in the cortical regions of patients with LN, the disruption of normal tissue architecture sustains an inflammatory milieu involving PT_VCAM1 cells, MyoFIB, and immune cells, which is positively correlated with increased disease severity.

PT_VCAM1 cells display a failed-repair state derived from PT_S1_RALYL cells, with their transition regulated by BACH2

PT cells are primary sites of kidney injury and contribute to disease progression across both acute and chronic etiologies [5,20,21]. Given that PT_VCAM1 cells constitute a cellular component of the LN-enriched inflammatory niche (ie, niche 5), we sought to investigate the functional characteristics of PT cells. We identified 5 distinct PT cell subsets (Fig 3A and Supplementary Fig S8A-D), which correspond to the anatomical segments of PT, ranging from PT-S1 (subdivided into PT_S1_ACSM2B and PT_S1_RALYL) to PT-S3. Notably, PT_VCAM1 cells were distinguished by a high expression of injury-associated markers, such as *CDH6, VCAM1*, and *HAVCR1* [3,21,22] (Fig 3B), resembling the *VCAM1*-expressing injured PT cell population previously described as failed-repair PT cells in an ischaemia-reperfusion injury (IRI) mouse model [20]. A hypergeometric test confirmed significant overlap in DEG comparison between PT_VCAM1 cells and failed-repair PT cells (Fig 3C, Supplementary Fig S8E, and Supplementary Table S4).

Notably, similar PT_VCAM1 populations have also been reported in chronic settings such as autosomal dominant polycystic kidney disease (ADPKD), where they contribute to inflammatory and fibrotic responses [9]. Cross-disease comparison (see Supplementary Methods)—including COVID-19-associated acute kidney injury (COV-AKI), acute kidney injury (AKI), diabetic kidney disease (DKD), and hypertensive chronic kidney disease (H-CKD)—revealed that PT_VCAM1 cells in LN exhibited a distinct transcriptomic profile characterised by enhanced activation of interferon-stimulated genes (eg, *IFI44, MX1*, and *IFIT3*) (Supplementary Fig S9A-E), suggesting that the interferon-driven signature of PT_VCAM1 cells is a unique feature of the autoimmune context of LN. Furthermore, deconvolution analysis of bulk transcriptomic data from kidney tissues of 16 patients with proliferative LN—before and after cyclophosphamide treatment [23]—demonstrated that patients with a higher proportion of PT_VCAM1 cells exhibited poorer therapeutic response (*P* = .0128) (Supplementary Fig S9F). This observation was further supported by analysis of a 45-patient microarray dataset [19], where *VCAM1* expression levels showed a positive correlation with serum creatinine (R = 0.358, *P* = .016) and proteinuria (R = 0.357, *P* = .016), highlighting its potential as a biomarker for disease severity and treatment outcome prediction in LN (Supplementary Fig S9G,H).

To investigate whether PT_VCAM1 cells originate from specific PT cell subsets, we applied a diffusion map [24] and PAGA graph [25] to explore potential differentiation trajectories. Both analyses revealed a close relationship between PT_VCAM1 cells and PT_S1_RALYL cells, suggesting a possible lineage connection between the 2 cell clusters (Fig 3D and Supplementary Fig S10A). This hypothesis was further supported by the spatial colocalisation of PT_VCAM1 and PT_S1_RALYL cell clusters within kidney tissue sections (Fig 3E and Supplementary Figs S5G, 10B). A comparative analysis between PT_S1_RALYL and PT_S1_ACSM2B cells, the latter expressing mature PT markers (eg, *ACSM2A* and *SLC22A6*) indicative of a healthy state, revealed that PT_S1_RALYL cells had elevated expression of injury-associated genes (eg, *CDH6, NFIA*, and *NFIB*) (Supplementary Fig S10C,D). This suggested that PT_S1_RALYL cells represent an intermediate injury-responsive state, potentially linking normal PT cells to the injury-prone PT_VCAM1 cells.

Building on this, we utilised both Multivelo [26] and Palantir [27] to infer the differentiation trajectory between PT-S1 cells and PT_VCAM1 cells. Both methods yielded consistent results, delineating 2 distinct differentiation trajectories (Fig 3F). The first trajectory (path 1) connected PT_S1_RALYL cells to PT_S1_ACSM2B cells, suggesting a successful injury-repair pathway. In contrast, the second trajectory (path 2) led from PT_S1_RALYL cells to PT_VCAM1 cells, representing a failed-repair path that results in the injury-associated phenotype. Pseudotime ordering analysis further confirmed these trajectories, showing that path 1 is characterised by a high expression of mature PT markers, such as *ACSM2A* and *ACSM2B,* at its terminal stage (Supplementary Fig S10E-G and Supplementary Table S5). In contrast, path 2 exhibited upregulation in the expression of genes related to proinflammatory responses (eg, *TNFSF10* and *CX3CL1*), profibrotic signalling (eg, *ITGA3* and *COL4A1*), and injury markers (eg, *VIM* and *HAVCR1*) (Fig 3G and Supplementary Fig S10F, G). Consistently, the enhancer landscape along this trajectory revealed progressively increased chromatin accessibility at regulatory regions of the proinflammatory (eg, *CSF1* and *IL32*) and profibrotic genes (eg, *ITGA3* and *COL4A1*) (Supplementary Fig S10H,I). To further explore the regulatory networks underlying these differentiation trajectories, we used SCENIC+ [28] to identify potential transcription factors (TFs). We found that the PT_S1_RALYL cells enriched putative TFs similar to both PT_S1_ACSM2B and PT_VCAM1 cells, indicating that PT_S1_RALYL cells occupy an intermediate state with the potential to differentiate towards either a successful or failed-repair pathway (Fig 3H).

In addition, we examined how TFs specifically regulate the differentiation processes along each trajectory and constructed regulatory networks for both paths (Supplementary Table S6). Peroxisome proliferator-activated receptor alpha (PPARA), a known TF that could protect the kidney against injury [29], was putatively involved in regulating the path 1 process (Supplementary Fig S11A). We also identified 4 core TFs—BACH2, NFAT5, KLF6, and FOSL2—that regulate path2, each targeting more than 50 downstream genes (Fig 3I and Supplementary Fig S11B). NFAT5, a well-established regulator of cellular responses to hypertonic stress, exhibited a positive correlation with the severity of proteinuria in patients with LN [30,31]. Similarly, KLF6, whose loss in PT cells has been shown to protect against kidney fibrosis in mouse models [32], also plays a known regulatory role.

Additionally, we observed that BACH2, a TF associated with oxidative stress and immune response regulation [33], regulates the largest number of downstream genes during the PT_VCAM1
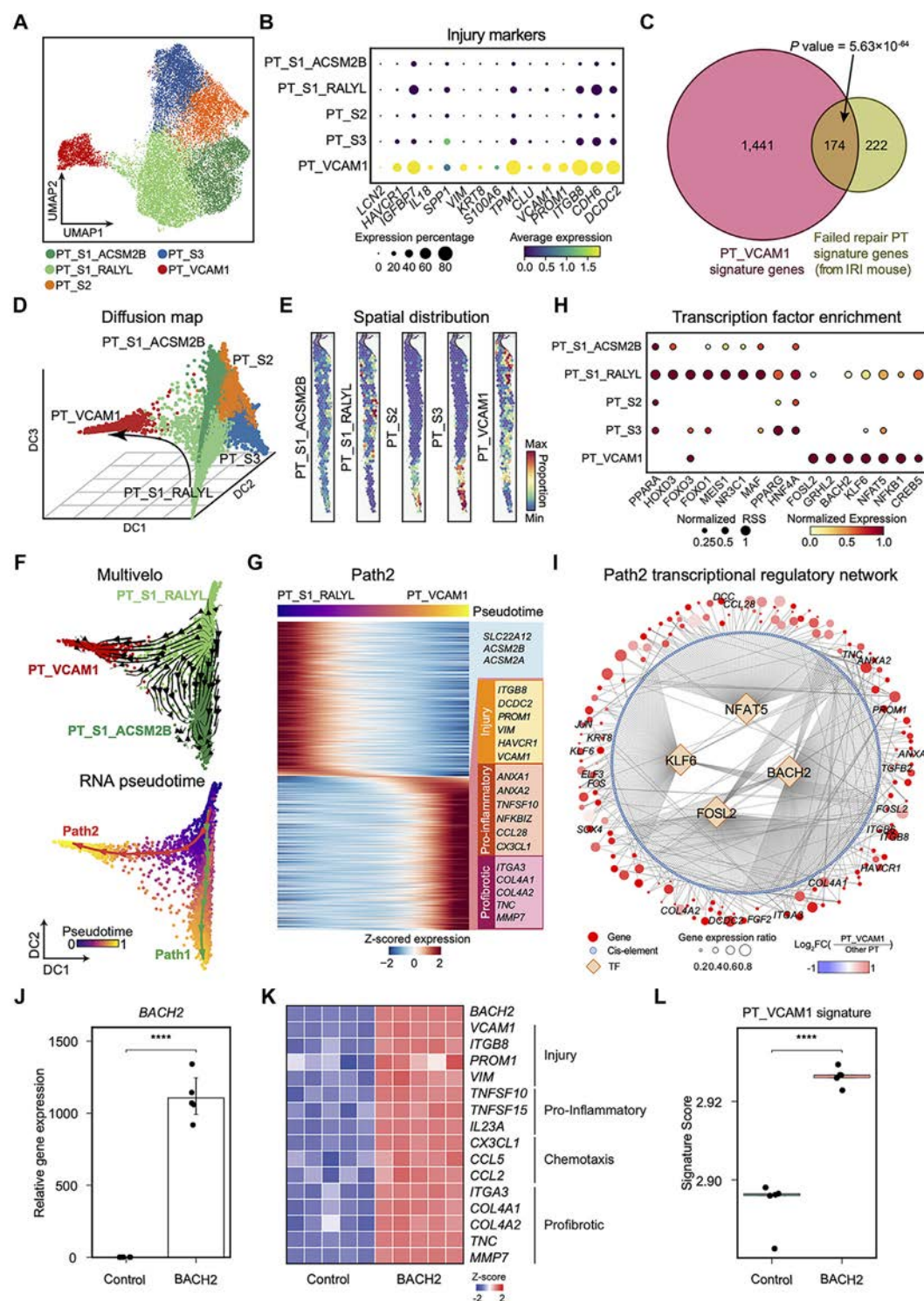
Figure 3. Regulatory networks of *VCAM1*-expressing proximal tubule (PT_VCAM1) cells. A, Uniform manifold approximation and projection (UMAP) visualisation of proximal tubule (PT) cells in single-nucleus RNA sequencing (snRNA-seq data), coloured by PT subpopulations. B, Dot plot showing the average gene expression of injury markers across PT subpopulations. C, Venn diagram showing the overlap between the differentially expressed genes (DEGs) of PT_VCAM1 cells and failed-repair PT cells. Statistical significance was determined by a hypergeometric test. D, Diffusion map showing the PT cells in snRNA-seq data, coloured by PT subpopulations. This visualisation is based on the first 3 eigenvectors of the diffusion map, highlighting the closest proximity between the PT_VCAM1 and PT_S1_RALYL cells. E, Spatial distribution of cellular composition calculated by Cell2location for PT subpopulations in a representative lupus nephritis (LN) sample. F, Diffusion maps for PT_S1 and PT_VCAM1 cells overlaid with velocity vectors from MultiVelo (top, shown as streamlines) and pseudotime trajectories (bottom). Cells are coloured by PT clusters (top) and inferred pseudotime (bottom), respectively. G, Heatmap of genes differentially expressed along the path 2 trajectory, with cells ordered by pseudotime and genes ordered by their maximum expression values. Representative genes are shown on the right. H, Dot plot displaying normalised regulon specificity scores (RSS) and expression of the top enriched transcription factors (TFs) across PT cell types. I, Three-layer regulatory networks depicting the *cis*-regulatory architecture of TFs, regulatory peaks, and target genes in path 2. Circle sizes represent gene expression ratios, while colour intensities indicate log fold changes (FCs). Only edges with a correlation coefficient greater than 0.05 were retained; edge colour and thickness are for visualisation purposes only and do not convey biological meaning. J, Relative gene expression of *BACH2* in BACH2-overexpressing and control HK-2 cells. Statistical significance was assessed using a 2-sided Student's t-test (****$P < .0001$; n = 5). K, Heatmap displaying z-scaled expression levels of selected DEGs in control and BACH2-overexpressing HK-2 cells. L, Box plot showing PT_VCAM1 signature scores in control and BACH2-overexpressing HK-2 cells. Statistical significance was evaluated using a 2-sided Student's t-test (****$P < .0001$; n = 5). IRI, ischaemia-reperfusion injury.

cell-state transition (Supplementary Fig S11B,C). Both the deviation score of the BACH2 motif and its gene expression were elevated at early stages along the trajectory, suggesting that BACH2 functions as a key transcriptional regulator contributing to the PT_VCAM1-associated injury process (Supplementary Fig S11D,E). To validate the role of BACH2 in promoting injury-related phenotypes, we overexpressed BACH2 in HK-2 cells (Fig 3J and Supplementary Fig S11F) and observed upregulation of injury markers (eg, *VCAM1* and *VIM*), proinflammatory responses (eg, *TNFSF10* and *CX3CL1*), and profibrotic signalling (eg, *ITGA3* and *COL4A1*) (Fig 3K). Consistently, the expression of PT_VCAM1 cell signature genes was significantly increased in BACH2-overexpressing cells (Fig 3L), supporting the functional contribution of BACH2 to the PT_VCAM1 cell phenotype.

PT_VCAM1 cells are involved in the fibrotic niche through ECM remodelling and immune cell recruitment

Intercellular communication is a fundamental process in the repair of injured tissues. To elucidate the impact of ligand-receptor (LR) interactions on the PT_VCAM1 cells and, in turn, the influence of this cell cluster on neighbouring cell types, we integrated single-cell and ST data, incorporating spatial proximity into our analyses (Fig 4A). Specifically, we applied the global Moran's statistic [34], a measure of spatial autocorrelation, to identify spatially coexpressed LR pairs in the CellChat database [35]. We then used COMMOT [36], which incorporates LR competition and interaction distances, to infer niche-specific cell−cell communication networks (Fig 4A). Our analysis found that PT_VCAM1 cells primarily received interactions from
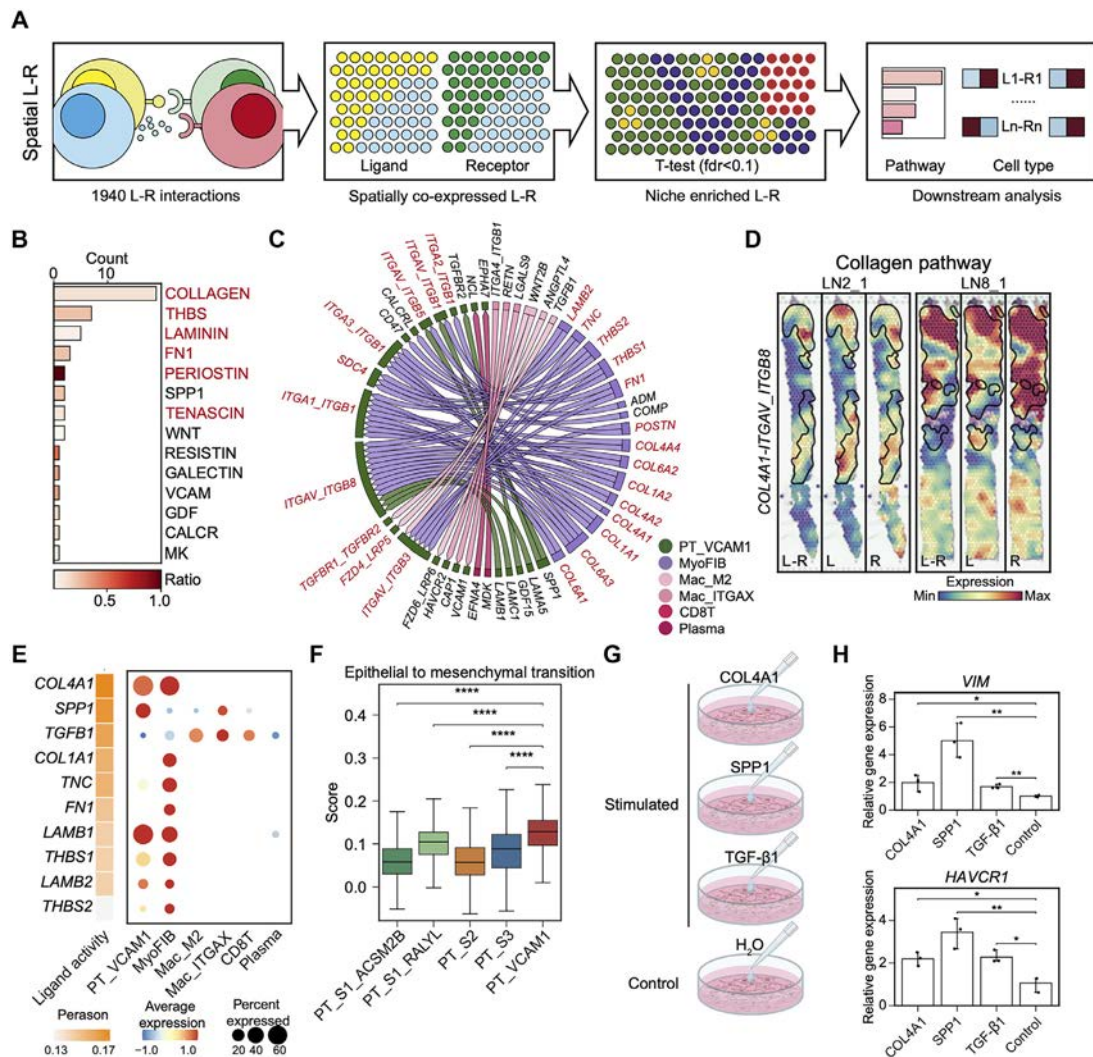

Figure 4. *VCAM1*-expressing proximal tubule (PT_VCAM1)-centric cell−cell interaction network. A, Schematic of the strategy for analysing cell−cell interactions based on spatial transcriptomics (ST) data. B, Bar plots illustrating the enrichment of signalling pathways in interactions between PT_VCAM1, acting as a receiver, and niche 5-specific cell types. C, Chord diagrams depicting interactions between PT_VCAM1, acting as a receiver, and niche 5-specific cell types. D, Smoothed spatial expression of *COL4A1-ITGAV_ITGB8* pairs, *COL4A1,* and *ITGAV_ITGB8* in representative lupus nephritis (LN) samples. Niche 5 is outlined in black. E, Heatmap showing NicheNet's ligand activity predictions with PT_VCAM1-related genes (left) and dot plot depicting the expression patterns of these ligands across niche 5-enriched cell populations (right). F, Box plot depicting the epithelial-mesenchymal transition (EMT) scores across proximal tubule (PT) cell subpopulations. Statistical significance was assessed using a 2-sided Wilcoxon rank-sum test (****$P < .0001$). G, Schematic representation of the strategy for *in vitro* stimulation of human kidney-2 (HK-2) cells, an immortalized human proximal tubular epithelial cell line derived from normal adult kidney. H, Bar plots showing the relative gene expression of *VIM* (top) and *HAVCR1* (bottom) in HK-2 cells across different stimulation conditions. Statistical significance was assessed using a 2-sided Student's t-test (**$P < .01$, *$P < .05$; n = 3 per group). L, ligand; L-R, ligand-receptor; Mac_ITGAX, *ITGAX*-expressing macrophages; Mac_M2, CD163-expressing M2 macrophages; MyoFIB, myofibroblast; R, receptor; TGF, transforming growth factor.

surrounding cells involving ECM components, including collagen, thrombospondin (*THBS*), laminin, fibronectin (*FN1*), periostin (*POSTN*), and tenascin (*TNC*) (Fig 4B,C and Supplementary Table S7). These ECM-encoding genes were predominantly expressed by MyoFIB and PT_VCAM1 cells, which engaged integrin receptors on the PT_VCAM1 cells (Fig 4D and Supplementary Fig S12A-C). Among these ECM components, *TNC*, known to impair tubular integrity and drive kidney fibrosis via integrin signalling, may contribute to the profibrotic niche observed in PT_VCAM1 cells [37].

To examine the impact of these interactions on the gene expression of PT_VCAM1 cells, we applied NicheNet [38] to prioritise ligands modulating upregulated genes in the late stages of path 2 (Fig 4E). Eight out of the top 10 prioritised ligands were epithelial-mesenchymal transition (EMT)-related genes, including *COL4A1, COL1A1, TNC,* and *FN1*, aligning with previous studies that link EMT to kidney fibrosis [39,40] (Supplementary Table S8). *TGFB1* was also identified as a key ligand interacting with *TGFBR1* and *TGFBR2* receptors on the PT_VCAM1 cells (Fig 4E and Supplementary Fig S12D). This ligand is secreted by immune cells, including macrophages and CD8 T cells, and has been demonstrated to induce EMT in kidney disease [41]. The impact of transforming growth factor (TGF)-β1 signalling was supported by our findings, which showed that PT_VCAM1 cells exhibited the highest EMT scores among all PT cell clusters (Fig 4F and Supplementary Fig S12E). To validate whether the predicted ligands promote kidney fibrosis and EMT in PT cells, we stimulated human PT epithelial cells (PTECs) with the top 3 ligands—COL4A1, SPP1, and TGF-β1—and evaluated their effects on *VIM* and *HAVCR1* expression (Fig 4G). Our results demonstrated that all 3 ligands significantly induced higher expression of *VIM* and *HAVCR1* in PTECs (Fig 4H). Furthermore, we also observed a marked upregulation of *BACH2* in PTECs upon *in vitro* stimulation (Supplementary Fig S12F).

We then investigated how PT_VCAM1 cells influence their neighbouring microenvironment and found that PT_VCAM1 cells secreted chemokines such as *CX3CL1* and *CXCL12*, which engaged *CX3CR1* and *CXCR4* on immune cells, facilitating targeted recruitment to injury sites (Supplementary Fig S13A-C and Supplementary Table S7). Concomitantly, local immune cell populations, particularly CD8 T cells, exhibited elevated cytokine secretion and activation signatures in LN samples (Supplementary Fig S13D-G). In parallel, PT_VCAM1 cells produced ECM-related ligands that could bind *CD44* on MyoFIB and CD8 T cells, potentially enhancing cell adhesion and sustaining the fibrotic niche (Supplementary Fig S13B,C). Collectively, these findings reveal the pivotal role of PT_VCAM1 cells in modulating ECM deposition, EMT induction, and immune cell recruitment through spatially coordinated LR interactions, highlighting their central role in pathological tissue remodelling.

GWAS mapping prioritises causal variants facilitating kidney fibrosis in PT_VCAM1 cells

To gain cell-type−specific insights into the role of genetic variants in LN, we performed a fine-mapping genetic analysis using fgwas with an SLE GWAS dataset comprising 208,370 East Asian samples [21] (Fig 5A and Supplementary Fig S14A). As expected, SLE-associated SNPs were significantly enriched in candidate CREs specific to immune cells, such as B cells, Mac_M2, Mac_ITGAX, and CD4 T cells, corroborating their established roles in LN pathogenesis [6,7]. Notably, we also observed

significant enrichment of SLE SNPs in CREs specific to endothelial and epithelial cells, particularly PT_VCAM1 cells, suggesting previously unrecognised genetic influences on kidney epithelial cells (Fig 5B). To understand the functional effects of these SNPs, we obtained 26,304 disease-associated SNPs (referred to as "prioritised SNPs") by integrating genome-wide significant SNPs ($P < 5 \times 10^{-8}$) with those that exhibit high posterior probability (posterior probability of association [PPA] > 0.01) across various cell types. Linking these SNPs to gene expression through cell-type−specific accessible peaks revealed 4520 SNP-gene pairs, 34% of which were validated in expression quantitative trait loci (eQTL) studies [42,43] (Supplementary Fig S14B and Supplementary Table S9), demonstrating the high resolution and accuracy of our approach.

To further investigate the expression patterns of genes linked to the prioritised SNPs, we performed gene expression clustering across cell subpopulations, identifying 8 distinct gene clusters (C1-C8; Fig 5C and Supplementary Table S10). Clusters C1 to C4 and C6 were significantly enriched in niche 5 (Supplementary Fig S14C,D), suggesting that the GWAS SNPs have a genetic predisposition for LN progression. For example, SNPs in the *CD44* locus, such as rs2785201, were linked to increased expression of *CD44* in CD4 and CD8 T cells, potentially influencing immune cell recruitment and inflammation via interactions with hyaluronan [44] (Supplementary Fig S15A-C). Moreover, *COL4A1*, which encodes a subunit of type IV collagen, has been identified as a pivotal marker influenced by genetic variants associated with LN susceptibility [45]. We identified a distinct SNP (rs4284503) in a distal CRE specific to the PT_VCAM1 cells, coaccessible with the *COL4A1* promoter (Fig 5D,E). The distal CRE was located within the *COL4A2* gene body and linked to the expression of both *COL4A1* and *COL4A2* (Fig 5F), potentially reflecting the promoter proximity of these 2 genes. Moreover, our results suggest predominant expression of *COL4A1* in PT_VCAM1 cells and MyoFIB, which may drive PT cell injury and promote EMT (Fig 4E,H). The high expression of *COL4A1* in PT_VCAM1 cells was also validated by our SeekSpace data (Supplementary Fig S15D).

Using a gapped k-mer support vector machine (gkm-SVM) approach [46], we identified 63 SNPs that significantly affect the TF binding motif (Supplementary Table S11), including rs4472162, which enhances chromatin accessibility at a *BMP2K* upstream CRE in PT_VCAM1 cells by creating a BACH2 motif (Fig 5G,H). The upregulation of BMP2K promotes the degradation of HNF1B and HNF4A, key TFs essential for PTEC identity [47], aligning with the loss of HNF4A enrichment observed in PT_VCAM1 cells (Fig 3H). Electrophoretic mobility shift assays (EMSAs) further demonstrated that the SLE risk allele (A>T) at rs4472162 significantly enhances BACH2 binding affinity to the *BMP2K* enhancer region (Supplementary Fig S15E,F). Additionally, we also identified a SNP (rs113607426) located within an intron of *SLC17A3*, and the accessibility of this peak was positively associated with the gene expression of 3 solute carrier family 17 member genes (*SLC17A1, SLC17A3,* and *SLC17A4*) (Supplementary Fig S15G-J). SLC17 transporters are type I phosphate transporters expressed in the kidney and liver [48]. However, the pathogenic roles of these transporters in LN remain unclear. Collectively, these findings reveal how genetic variants converge on specific cell types within LN-enriched niche 5, uncovering the regulatory mechanisms that drive fibrosis and inflammation. These insights provide a framework for understanding genetic predispositions in LN and identifying potential therapeutic targets.
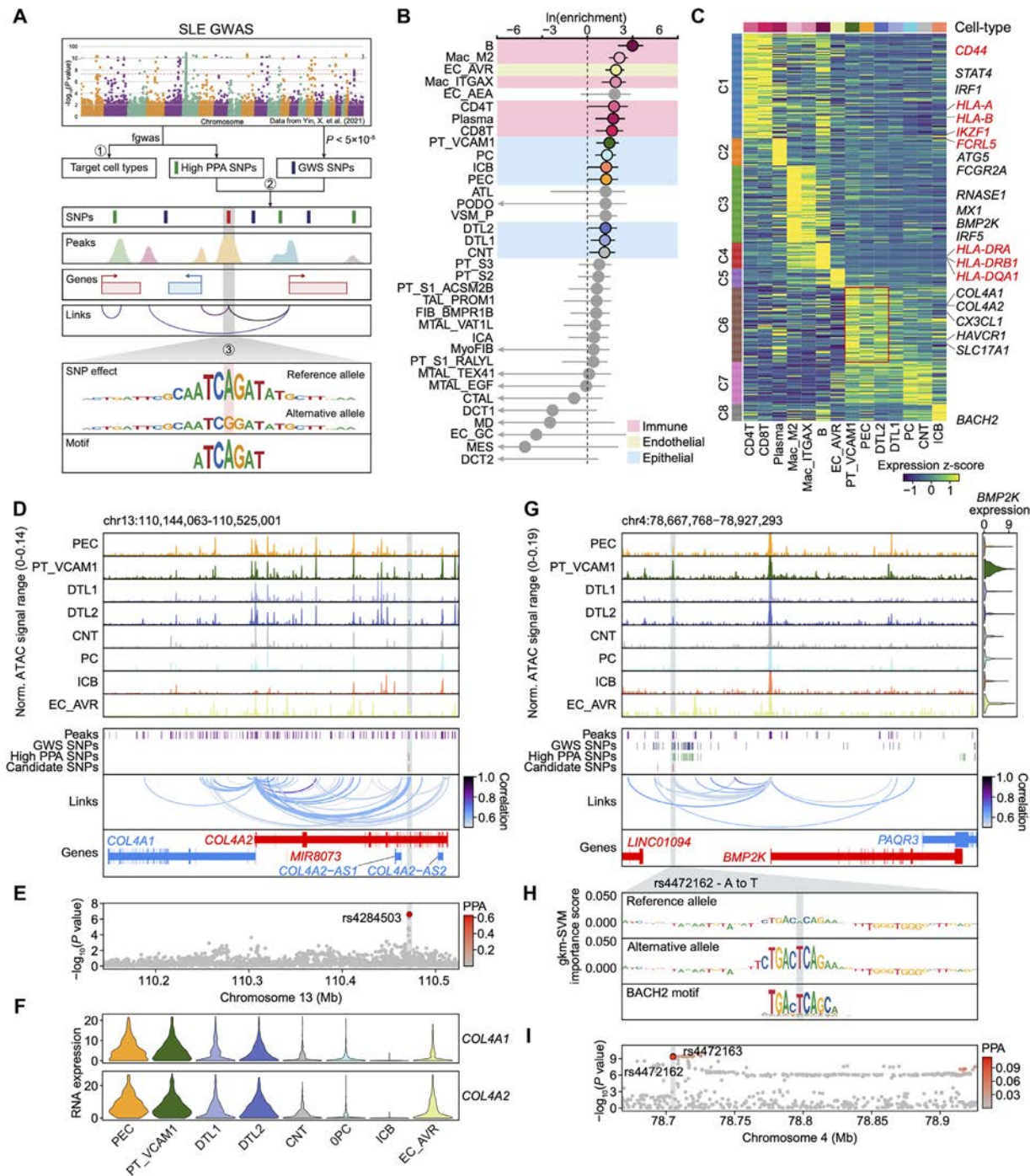
Figure 5. Cell-type-specific genetic risk locus analysis in lupus nephritis (LN). A, Schematic representation of the strategy employed to identify potential causative single-nucleotide polymorphisms (SNPs), their associated gene targets, and the prediction of their impact on transcription factor binding site accessibility. B, Lollipop plot displaying systemic lupus erythematosus (SLE) ln(enrichment) within cell-type−specific *cis*-regulatory elements (CREs). Cell types with positive enrichment and a 95% CI lower bound below zero are shaded in grey. Data represent ln(enrichment) ± 95% CI derived from fgwas. C, Clustered heatmap illustrating the expression profiles of genes associated with candidate SNPs for each cell type. Representative genes are labelled, with gene names in red indicating fine-mapped SNP-to-gene associations supported by public expression quantitative trait loci (eQTL) data from the GTEx portal and the Susztak Lab. D, Normalised chromatin accessibility for cell-type−specific pseudo-bulk tracks surrounding the *COL4A1/COL4A2* locus in SLE heritability-enriched nonimmune cell types. The positions of assay for transposase-accessible chromatin sequencing (ATAC-seq) peaks, genome-wide significant (GWS) SNPs, high posterior probability of association (PPA) SNPs, and candidate functional SNPs are shown below the ATAC-seq tracks. Significant peak-to-gene linkages are indicated by loops connecting the promoter to corresponding peaks. E, Magnified Manhattan plot of the region shown in (D) coloured by PPA level. The candidate SNP is outlined in black. F, Violin plots depicting the expression levels of *COL4A1* and *COL4A2* across the cell types shown in (D). G, As in (D), but for the *BMP2K* locus. *BMP2K* expression levels are shown in the violin plot for each cell type to the right. H, GkmExplain importance scores for the 50 bp region surrounding rs4472162, which creates a BACH2 motif in a CRE linked to *BMP2K* expression. The effect and noneffect alleles for the gapped k-mer support vector machine (gkm-SVM) model are based on the model trained on the VCAM1-expressing proximal tubule (PT_VCAM1) cluster. I, As in (E), but for the region shown in (G). GWAS, genome-wide association studies; PODO, podocyte; PEC, parietal epithelial cell; PT, proximal tubule cell; DTL1, descending thin limb cell type 1; DTL2, descending thin limb cell type 2; ATL, ascending thin limb cell; MTAL_EGF, *EGF*-expressing medullary thick ascending limb cell; MTAL_VAT1L, *VAT1L*-expressing medullary thick ascending limb cell; MTAL_TEX41, *TEX41*-expressing medullary thick ascending limb cell; CTAL, cortical thick ascending limb cell; TAL_-PROM1, *PROM1*-expressing thick ascending limb cell; MD, macula densa cell; DCT1, distal convoluted tubule cell type 1; DCT2, distal convoluted

DISCUSSION

Previous studies using single-cell RNA sequencing have provided valuable insights into the roles of immune and epithelial cells in LN [2,4,6,7,49]. However, the detailed cellular organisation and cell−cell interactions within the local microenvironment remain poorly understood. In this study, we employed single-cell multiome sequencing and ST to analyse kidney samples from patients with LN and controls. Our findings revealed a unique LN-associated cellular niche (niche 5), which was positively correlated with serum creatinine and proteinuria levels. This niche, characterised by increased immune cell infiltration and MyoFIB accumulation, also harboured a subpopulation of PT_VCAM1 cells exhibiting a "failed-repair" phenotype. These cells contribute to disease progression by amplifying the inflammatory and profibrotic microenvironment, linking their dysfunction to kidney fibrosis and tubular atrophy—key features predictive of poor kidney outcomes in LN [9,20].

Our study identified niche 5 as a distinct cortical microenvironment of LN, characterised by immune cell infiltration and MyoFIB accumulation—both recognised as contributors to kidney damage [4]. Within this niche, PT_VCAM1 cells emerged as a key epithelial population associated with fibrosis progression, with their abundance significantly higher in cyclophosphamide nonresponders compared with responders. Furthermore, *VCAM1* expression in the tubulointerstitium positively correlated with serum creatinine and proteinuria, highlighting PT_VCAM1 cells and *VCAM1* as potential tissue-level biomarkers of disease severity and treatment response in LN.

Trajectory analysis further demonstrated that PT_VCAM1 cells originate from intermediate-injury PT precursors (PT_S1_RALYL), tracing a continuum from early to late injury states. This finding refines the current understanding of epithelial cell-state transitions in LN and aligns with prior studies on kidney fibrosis [5,20]. Mechanistically, our research underscores the dynamic interplay between PT_VCAM1 cells and local immune cells, which is partially induced by the TGF-β1−mediated EMT process. These insights suggest that TGF-β receptor kinase inhibitors, such as galunisertib, may hold therapeutic potential in mitigating PT fibrotic reprogramming in LN.

Immune cells have long been recognised as contributors to LN pathogenesis [4,7]; our study provides insights into the role of genetic variants within PT_VCAM1 cells associated with kidney fibrosis. Among the identified variants, rs4284503 in the distal region of the *COL4A1* locus was found to enhance collagen deposition via PT_VCAM1 cells. While *COL4A1* overexpression in fibroblasts and endothelial cells has been linked to kidney fibrosis [50], our study highlights a previously unrecognised role of *COL4A1* regulation in PT cells.

Beyond *COL4A1*, we identified additional SLE-associated variants that influence the binding motifs of TFs. Notably, *BMP2K*, encoding bone morphogenetic protein 2-inducible kinase, emerged as a key gene in the pathogenic process. Knockout studies of *BMP2K* have shown that its absence restores normal PTEC function [47], indicating the role of *BMP2K* in disturbing tubular integrity. We identified a distal *BMP2K* variant, rs4472162,

that creates a de novo BACH2 binding motif, consistent with our gene regulatory network analysis, positioning BACH2 as a central regulator of the failed-repair PT_VCAM1 program. These findings nominate both BMP2K inhibitors (eg, Cerdulatinib [MedChemExpress] and SGC-AAK1-1) and BACH2 modulators (eg, compound 8) as candidate therapeutic agents for targeting this pathogenic epithelial niche in LN.

Despite the strengths of our integrative approach, several limitations should be acknowledged. The relatively small patient cohort limited our ability to fully capture the heterogeneity of LN. Needle biopsy, required for LN tissue sampling, brings challenges to the comprehensive exploration of kidney injury. Furthermore, the naturally low abundance of immune cells in kidney tissues limited our ability to explore their functional role; sorting immune cells for subsequent investigation could provide deeper insights into the impact of genetic variants on immune cell function. Additionally, 10× multiome workflows require nuclei isolation, which may limit the detection of cytoplasmic transcripts and certain cell states, particularly those of granulocytes. Nevertheless, our work provides a comprehensive understanding of the spatial architecture of LN tissues, the interplay between cell types in pathogenic hotspots, and the regulatory programs associated with kidney injury, laying the groundwork for potential therapeutic strategies targeting both immune and kidney tubular cells.

Competing interests

KQ is the chief scientific advisor of HanGene Biotech and Bassfish Technology. The other authors declare that they have no competing interests.

CRediT authorship contribution statement

Junyu Wang: Writing − original draft, Visualization, Validation, Methodology, Data curation. **Ao Zheng:** Visualization, Methodology, Formal analysis, Data curation. **Nianping Liu:** Writing − original draft, Methodology, Formal analysis, Data curation. **Zhen Tan:** Visualization, Resources. **Yu Shi:** Methodology, Data curation. **Tianyi Ma:** Software, Data curation. **Songwen Luo:** Visualization, Data curation. **Lin Zhu:** Methodology. **Zhou Zhou:** Validation. **Feifei Yuan:** Visualization, Validation. **Tiekun Li:** Visualization. **Yuyan Gong:** Validation, Data curation. **Jingwen Fang:** Visualization. **Lu Liu:** Resources. **Xuejun Zhang:** Resources. **Sang-Cheol Bae:** Resources. **Chikashi Terao:** Resources. **Zhu Chen:** Resources. **Xiaomei Li:** Resources. **Guosheng Wang:** Supervision, Resources. **Kun Qu:** Writing − review & editing, Supervision, Project administration, Funding acquisition, Conceptualization. **Chuang Guo:** Writing − review & editing, Supervision, Resources, Project administration, Funding acquisition, Data curation, Conceptualization.

Acknowledegments

---

tubule cell type 2; CNT, connecting tubule cell; PC, principal cell; ICA, alpha-intercalated cell; ICB, beta-intercalated cell; EC_AVR, ascending vasa recta endothelial cell; EC_GC, glomerular capillary endothelial cell; EC_AEA, afferent/efferent arteriole endothelial cell; MyoFIB, myofibroblast; FIB_BMPR1B, *BMPR1B*-expressing fibroblast; VSM/P, vascular smooth muscle cell or pericyte; MES, mesangial cell; Mac_M2, *CD163*-expressing M2 macrophage; Mac_ITGAX, *ITGAX*-expressing macrophage.

at the Institute of Health and Medicine, Hefei Comprehensive National Science Center, for providing experimental platforms.

Contributors

CG and KQ conceived the project. GW collected clinical samples and interpreted clinical data with the help of ZC and XL. JW, CG, and KQ designed experiments. JW performed the experiments and conducted the sample preparation with the help of ZT, LZ, ZZ, and TL. JW and AZ performed data analysis with the help of YS, TM, SL, FY, YG, and JF. XZ, S-CB, CT, and LL provided the GWAS data. CG, KQ, JW, NL, and AZ wrote the manuscript with the help of all the other authors. KQ and CG supervised the entire project. All the authors read and approved the final manuscript.

Funding

Patient consent for publication

Written informed consent was obtained from all participants.

Ethics approval

Ethical approval was granted by the ethics committee of the First Affiliated Hospital of the University of Science and Technology of China (No. 2024-KY-265).

Provenance and peer review

Not commissioned; externally peer reviewed.

Data availability statement

Processed spatial transcriptomics, snRNA-seq, and snATAC-seq generated in this study are available at the Zenodo data archive (https://doi.org/10.5281/zenodo.15868389). The raw sequencing data generated in this study—including single-cell multiome, spatial transcriptomics, and bulk RNA sequencing (RNA-seq)—have been deposited in the Genome Sequence Archive (GSA) at the BIG Data Center, National Genomics Data Center, China National Center for Bioinformation/Beijing Institute of Genomics, and Chinese Academy of Sciences (accession number: PRJCA035165). The data are publicly accessible at https://ngdc.cncb.ac.cn/gsa-human. The publicly available data sources used in this study are as follows: (1) snRNA-seq and snATAC-seq data from human kidney control samples (Muto et al) were obtained from the Gene Expression Omnibus (GEO) (GSE151302); (2) snRNA-seq data from the human kidney atlas (Lake et al [3]) were obtained from GEO (GSE183277); (3) single-cell RNA sequencing (scRNA-seq) data of human lupus nephritis kidney immune cells (Arazi et al [2]) were accessed from the ImmPort repository (SDY997); (4) Microarray data from human lupus nephritis kidney biopsy samples (Parikh et al [19]) were obtained from GEO (GSE200306); (5) Bulk RNA-seq data (n = 25) from kidney tissues of 16 patients with proliferative LN (Bulusu et al [23]) were obtained from GEO (PRJNA1080019); (6) the GWAS summary statistics of the SLE GWAS dataset, comprising 208,370 East Asian samples, were obtained from the coauthor upon request [11].

Declaration of generative AI and AI-assisted technologies in the writing process

During the preparation of this work the authors used ChatGPT 4.0 in order to improve the language and readability. After using this tool, the authors reviewed and edited the content as needed and take full responsibility for the content of the publication.

Supplementary materials

Supplementary material associated with this article can be found, in the online version, at doi:10.1016/j.ard.2025.08.015.

Orcid

Junyu Wang: http://orcid.org/0009-0000-0621-3435
Ao Zheng: http://orcid.org/0009-0004-6494-4382
Nianping Liu: http://orcid.org/0000-0002-9044-6457
Zhen Tan: http://orcid.org/0000-0002-9988-5587
Tianyi Ma: http://orcid.org/0009-0000-8386-3431
Sang-Cheol Bae: http://orcid.org/0000-0003-4658-1093
Zhu Chen: http://orcid.org/0000-0003-0828-1583
Chuang Guo: http://orcid.org/0000-0002-3912-0793

REFERENCES

[1] Mok CC, Teng YKO, Saxena R, Tanaka Y. Treatment of lupus nephritis: consensus, evidence and perspectives. Nat Rev Rheumatol 2023;19(4):227–38. doi: 10.1038/s41584-023-00925-5.

[2] Arazi A, Rao DA, Berthier CC, Davidson A, Liu Y, Hoover PJ, et al. The immune cell landscape in kidneys of patients with lupus nephritis. Nat Immunol 2019;20(7):902–14. doi: 10.1038/s41590-019-0398-x.

[3] Lake BB, Menon R, Winfree S, Hu Q, Melo Ferreira R, Kalhor K, et al. An atlas of healthy and injured cell states and niches in the human kidney. Nature 2023;619(7970):585–94. doi: 10.1038/s41586-023-05769-3.

[4] Chen W, Jin B, Cheng C, Peng H, Zhang X, Tan W, et al. Single-cell profiling reveals kidney CD163(+) dendritic cell participation in human lupus nephritis. Ann Rheum Dis 2024;83(5):608–23. doi: 10.1136/ard-2023-224788.

[5] Li H, Dixon EE, Wu H, Humphreys BD. Comprehensive single-cell transcriptional profiling defines shared and unique epithelial injury responses during kidney fibrosis. Cell Metab 2022;34(12) 1977-98.e9. doi: 10.1016/j.cmet.2022.09.026.

[6] Tang Y, Zhang Y, Li X, Xu R, Ji Y, Liu J, et al. Immune landscape and the key role of APOE+ monocytes of lupus nephritis under the single-cell and spatial transcriptional vista. Clin Transl Med 2023;13(4):e1237. doi: 10.1002/ctm2.1237.

[7] Wu C, Jiang S, Chen Z, Li T, Gu X, Dai M, et al. Single-cell transcriptomics reveal potent extrafollicular B cell response linked with granzyme K(+) CD8 T cell activation in lupus kidney. Ann Rheum Dis 2024;84(3):451–66. doi: 10.1136/ard-2024-225876.

[8] Muto Y, Wilson PC, Ledru N, Wu H, Dimke H, Waikar SS, et al. Single cell transcriptional and chromatin accessibility profiling redefine cellular heterogeneity in the adult human kidney. Nat Commun 2021;12(1):2190. doi: 10.1038/s41467-021-22368-w.

[9] Muto Y, Dixon EE, Yoshimura Y, Wu H, Omachi K, Ledru N, et al. Defining cellular complexity in human autosomal dominant polycystic kidney disease by multimodal single cell analysis. Nat Commun 2022;13(1):6497. doi: 10.1038/s41467-022-34255-z.

[10] Abedini A, Levinsohn J, Klötzer KA, Dumoulin B, Ma Z, Frederick J, et al. Single-cell multi-omic and spatial profiling of human kidneys implicates the

fibrotic microenvironment in kidney disease progression. Nat Genet 2024;56 (8):1712–24. doi: 10.1038/s41588-024-01802-x.

[11] Yin X, Kim K, Suetsugu H, Bang SY, Wen L, Koido M, et al. Meta-analysis of 208370 East Asians identifies 113 susceptibility loci for systemic lupus erythematosus. Ann Rheum Dis 2021;80(5):632–40. doi: 10.1136/annrheumdis-2020-219209.

[12] Gallagher MD, AS Chen-Plotkin. The post-GWAS era: from association to function. Am J Hum Genet 2018;102(5):717–30. doi: 10.1016/j.ajhg.2018.04.002.

[13] Hon CC, Ramilowski JA, Harshbarger J, Bertin N, Rackham OJ, Gough J, et al. An atlas of human long non-coding RNAs with accurate 5′ ends. Nature 2017;543(7644):199–204. doi: 10.1038/nature21374.

[14] Hao Y, Stuart T, Kowalski MH, Choudhary S, Hoffman P, Hartman A, et al. Dictionary learning for integrative, multimodal and scalable single-cell analysis. Nat Biotechnol 2024;42(2):293–304. doi: 10.1038/s41587-023-01767-y.

[15] Davidson A. What is damaging the kidney in lupus nephritis? Nat Rev Rheumatol 2016;12(3):143–53. doi: 10.1038/nrrheum.2015.159.

[16] Melo Ferreira R, Sabo AR, Winfree S, Collins KS, Janosevic D, Gulbronson CJ, et al. Integration of spatial and single-cell transcriptomics localizes epithelial cell-immune cross-talk in kidney injury. JCI Insight 2021;6(12):e147703. doi: 10.1172/jci.insight.147703.

[17] Kleshchevnikov V, Shmatko A, Dann E, Aivazidis A, King HW, Li T, et al. Cell2location maps fine-grained cell types in spatial transcriptomics. Nat Biotechnol 2022;40(5):661–71. doi: 10.1038/s41587-021-01139-4.

[18] Xu H, Wang S, Fang M, Luo S, Chen C, Wan S, et al. SPACEL: deep learning-based characterization of spatial transcriptome architectures. Nat Commun 2023;14(1):7603. doi: 10.1038/s41467-023-43220-3.

[19] Parikh SV, Malvar A, Song H, Shapiro J, Mejia-Vilet JM, Ayoub I, et al. Molecular profiling of kidney compartments from serial biopsies differentiate treatment responders from non-responders in lupus nephritis. Kidney Int 2022;102(4):845–65. doi: 10.1016/j.kint.2022.05.033.

[20] Kirita Y, Wu H, Uchimura K, Wilson PC, Humphreys BD. Cell profiling of mouse acute kidney injury reveals conserved cellular responses to injury. Proc Natl Acad Sci U S A 2020;117(27):15874–83. doi: 10.1073/pnas.2005477117.

[21] Hinze C, Kocks C, Leiz J, Karaiskos N, Boltengagen A, Cao S, et al. Single-cell transcriptomics reveals common epithelial response patterns in human acute kidney injury. Genome Med. Genome Med. 2022;14(1):103. doi: 10.1186/s13073-022-01108-9.

[22] Klocke J, Kim SJ, Skopnik CM, Hinze C, Boltengagen A, Metzke D, et al. Urinary single-cell sequencing captures kidney injury and repair processes in human acute kidney injury. Kidney Int 2022;102(6):1359–70. doi: 10.1016/j.kint.2022.07.032.

[23] Bulusu SN, Bavikatte AN, Shah S, Murthy SSN, Kommoju V, Mariaselvam CM, et al. Renal and peripheral blood transcriptome signatures that predict treatment response in proliferative lupus nephritis-a prospective study. Immunology 2025;174(4):470–80. doi: 10.1111/imm.13891.

[24] Haghverdi L, Buettner F, Theis FJ. Diffusion maps for high-dimensional single-cell analysis of differentiation data. Bioinformatics 2015;31(18):2989–98. doi: 10.1093/bioinformatics/btv325.

[25] Wolf FA, Hamey FK, Plass M, Solana J, Dahlin JS, Göttgens B, et al. PAGA: graph abstraction reconciles clustering with trajectory inference through a topology preserving map of single cells. Genome Biol 2019;20(1):59. doi: 10.1186/s13059-019-1663-x.

[26] Li C, Virgilio MC, Collins KL, Welch JD. Multi-omic single-cell velocity models epigenome-transcriptome interactions and improves cell fate prediction. Nat Biotechnol 2023;41(3):387–98. doi: 10.1038/s41587-022-01476-y.

[27] Setty M, Kiseliovas V, Levine J, Gayoso A, Mazutis L, Pe'er D. Characterization of cell fate probabilities in single-cell data with Palantir. Nat Biotechnol 2019;37(4):451–60. doi: 10.1038/s41587-019-0068-4.

[28] Bravo González-Blas C, De Winter S, Hulselmans G, Hecker N, Matetovici I, Christiaens V, et al. SCENIC+: single-cell multiomic inference of enhancers and gene regulatory networks. Nat Methods 2023;20(9):1355–67. doi: 10.1038/s41592-023-01938-4.

[29] Ledru N, Wilson PC, Muto Y, Yoshimura Y, Wu H, Li D, et al. Predicting proximal tubule failed repair drivers through regularized regression analysis of single cell multiomic sequencing. Nat Commun 2024;15(1):1291. doi: 10.1038/s41467-024-45706-0.

[30] Hao S, Bellner L, Zhao H, Ratliff BB, Darzynkiewicz Z, Vio CP, et al. NFAT5 is protective against ischemic acute kidney injury. Hypertension 2014;63(3):e46–52. doi: 10.1161/HYPERTENSIONAHA.113.02476.

[31] Yoo EJ, Oh KH, Piao H, Kang HJ, Jeong GW, Park H, et al. Macrophage transcription factor TonEBP promotes systemic lupus erythematosus and kidney injury via damage-induced signaling pathways. Kidney Int 2023;104(1):163–80. doi: 10.1016/j.kint.2023.03.030.

[32] Piret SE, Guo Y, Attallah AA, Horne SJ, Zollman A, Owusu D, et al. Kruppel-like factor 6-mediated loss of BCAA catabolism contributes to kidney injury in mice and humans. Proc Natl Acad Sci U S A 2021;118(23):e2024414118. doi: 10.1073/pnas.2024414118.

[33] Zhou Y, Wu H, Zhao M, Chang C, Lu Q. The Bach family of transcription factors: a comprehensive review. Clin Rev Allergy Immunol 2016;50(3):345–56. doi: 10.1007/s12016-016-8538-7.

[34] Li Z, Wang T, Liu P, Huang Y. SpatialDM for rapid identification of spatially co-expressed ligand-receptor and revealing cell-cell communication patterns. Nat Commun 2023;14(1):3995. doi: 10.1038/s41467-023-39608-w.

[35] Jin S, Guerrero-Juarez CF, Zhang L, Chang I, Ramos R, Kuan CH, et al. Inference and analysis of cell-cell communication using CellChat. Nat Commun 2021;12(1):1088. doi: 10.1038/s41467-021-21246-9.

[36] Cang Z, Zhao Y, Almet AA, Stabell A, Ramos R, Plikus MV, et al. Screening cell-cell communication in spatial transcriptomics via collective optimal transport. Nat Methods 2023;20(2):218–28. doi: 10.1038/s41592-022-01728-4.

[37] Zhu H, Liao J, Zhou X, Hong X, Song D, Hou FF, et al. Tenascin-C promotes acute kidney injury to chronic kidney disease progression by impairing tubular integrity via alphavbeta6 integrin signaling. Kidney Int 2020;97(5):1017–31. doi: 10.1016/j.kint.2020.01.026.

[38] Browaeys R, Saelens W, Saeys Y. NicheNet: modeling intercellular communication by linking ligands to target genes. Nat Methods 2020;17(2):159–62. doi: 10.1038/s41592-019-0667-5.

[39] Grande MT, Sánchez-Laorden B, López-Blau C, De Frutos CA, Boutet A, Arévalo M, et al. Snail1-induced partial epithelial-to-mesenchymal transition drives renal fibrosis in mice and can be targeted to reverse established disease. Nat Med 2015;21(9):989–97. doi: 10.1038/nm.3901.

[40] Lovisa S, LeBleu VS, Tampe B, Sugimoto H, Vadnagara K, Carstens JL, et al. Epithelial-to-mesenchymal transition induces cell cycle arrest and parenchymal damage in renal fibrosis. Nat Med 2015;21(9):998–1009. doi: 10.1038/nm.3902.

[41] Shen B, Liu X, Fan Y, Qiu J. Macrophages regulate renal fibrosis through modulating TGFbeta superfamily signaling. Inflammation 2014;37(6):2076–84. doi: 10.1007/s10753-014-9941-y.

[42] Liu H, Doke T, Guo D, Sheng X, Ma Z, Park J, et al. Epigenomic and transcriptomic analyses define core cell types, genes and targetable mechanisms for kidney disease. Nat Genet 2022;54(7):950–62. doi: 10.1038/s41588-022-01097-w.

[43] Consortium GTEx. The GTEx Consortium atlas of genetic regulatory effects across human tissues. Science 2020;369(6509):1318–30. doi: 10.1126/science.aaz1776.

[44] Kadoya H, Yu N, Schiessl IM, Riquier-Brison A, Gyarmati G, Desposito D, et al. Essential role and therapeutic targeting of the glomerular endothelial glycocalyx in lupus nephritis. JCI Insight 2020;5(19):e131252. doi: 10.1172/jci.insight.131252.

[45] Chung SA, Brown EE, Williams AH, Ramos PS, Berthier CC, Bhangale T, et al. Lupus nephritis susceptibility loci in women with systemic lupus erythematosus. J Am Soc Nephrol 2014;25(12):2859–70. doi: 10.1681/ASN.2013050446.

[46] Turner AW, Hu SS, Mosquera JV, Ma WF, Hodonsky CJ, Wong D, et al. Single-nucleus chromatin accessibility profiling highlights regulatory mechanisms of coronary artery disease risk. Nat Genet 2022;54(6):804–16. doi: 10.1038/s41588-022-01069-0.

[47] Mao L, Zhang T, Li Z, Yao W, Cai Y, Li C, et al. Kidney repair through chemically-induced revitalization of renal tubular epithelial cell. Cell Press; 2024 in press. doi: 10.17632/bz47sbmtw2.1.

[48] Reimer RJ. SLC17: a functionally diverse family of organic anion transporters. Mol Aspects Med 2013;34(2-3):350–9. doi: 10.1016/j.mam.2012.05.004.

[49] Der E, Suryawanshi H, Morozov P, Kustagi M, Goilav B, Ranabothu S, et al. Tubular cell and keratinocyte single-cell transcriptomics applied to lupus nephritis reveal type I IFN and fibrosis relevant pathways. Nat Immunol 2019;20(7):915–27. doi: 10.1038/s41590-019-0386-1.

[50] Li H, Li D, Ledru N, Xuanyuan Q, Wu H, Asthana A, et al. Transcriptomic, epigenomic, and spatial metabolomic cell profiling redefines regional human kidney anatomy. Cell Metab 2024;36(5):1105–25. e10. doi: 10.1016/j.cmet.2024.02.015.

Antiphospholipid syndrome

Genetic and epigenetic dysregulation of CR1 is associated with catastrophic antiphospholipid syndrome

Nikhil Ranjan[1], Michael A. Cole[1], Gloria F. Gerber[1], Mark A. Crowther[2], Evan M. Braunstein[1], Daniel Flores-Guerrero[1], Kathy Haddaway[3], Alexis Reed[1], Michael B. Streiff[1], Keith R. McCrae[4], Michelle Petri[5], Shruti Chaturvedi[1], Robert A. Brodsky[1,*]

[1] Division of Hematology, Department of Medicine, Johns Hopkins University School of Medicine, Baltimore, MD, USA

[2] Department of Medicine, McMaster University, Hamilton, ON, Canada

[3] Transfusion Medicine Division, The Johns Hopkins Hospital, Baltimore, MD, USA

[4] Departments of Hematology-Oncology, and Cardiovascular and Metabolic Sciences, Lerner Research Institute, Cleveland Clinic, Cleveland, OH, USA

[5] Division of Rheumatology, Department of Medicine, Johns Hopkins University School of Medicine, Baltimore, MD, USA

ARTICLE INFO

ABSTRACT

Objectives: Catastrophic antiphospholipid syndrome (CAPS) is a complement-driven thrombotic disorder, characterised by widespread thrombosis and multiorgan failure. We identified rare germline variants including complement receptor 1 (*CR1*) in 50% of patients with CAPS. Here, we define *CR1* dysregulation mechanisms (genetic/epigenetic) underlying complement-mediated thrombosis in CAPS and support C5 inhibition as a potential therapy.

Methods: We quantified CR1 expression by flow cytometry across haematopoietic cell types. CRISPR/Cas9 genome editing of TF-1 (erythroleukaemia) cells was performed to generate *CR1* 'knock-out' and 'knock-in' lines with patient-specific *CR1* variants. Multiomics analysis was performed to investigate the role of methylation in patients with reduced CR1 expression. Functional impact of low CR1 was assessed by complement-mediated cell killing using modified Ham assay, cell-bound complement degradation products through flow cytometry, and circulatory immune complexes in serum samples through ELISA.

Results: CR1 expression in erythrocytes was markedly reduced on CAPS erythrocytes (n = 9, 21.80%) compared to healthy controls (HCs; n = 35, 84.04%), with promoter hypermethylation emerging as a plausible epigenetic mechanism for *CR1* downregulation. Novel germline variant (*CR1*-V2125L; *rs202148801*) mitigated CR1 expression and increased complement-mediated cell death of knock-in cell lines. Erythrocytes from the patient with the *CR1*-V2125L variant had low CR1 expression. Levels of circulating immune complexes, which are bound and cleared by CR1 on erythrocytes, were higher in acute CAPS (n = 3, 25.55 µg Eq/mL) than HCs (n = 3, 7.445 µg Eq/mL). Five patients were treated with C5 inhibition which mitigated thrombosis.

Conclusions: Genetic or epigenetic-mediated CR1 deficiency is a potential hallmark of CAPS and predicts response to C5 inhibition.

*Correspondence to Dr. Robert A. Brodsky, Division of Hematology, Department of Medicine, Johns Hopkins University School of Medicine, Baltimore, MD, USA.
E-mail address: brodsro@jhmi.edu (R.A. Brodsky).

What is already known on this topic

- CAPS is a rare, life-threatening manifestation of antiphospholipid antibodies (aPL) with a high mortality rates despite current standard of care therapy.
- Complement activation is implicated in the disease pathogenesis, however the primary molecular drivers of CAPS remain unclear.

What this study adds

- Establishes low CR1 as a central pathogenic driver in CAPS, moving beyond antiphospholipid antibody profile as the sole predictor of disease severity. CR1 expression influenced by genetic polymorphisms and epigenetic modifications can serve as a novel biomarker to help identify patients at the higher risk of anticoagulation refractory APS or CAPS.
- Targeting the terminal complement cascade with C5 inhibitors (e.g., eculizumab) prevents thrombosis in CAPS patients with low CR1. This redirects research toward complement regulators and their intersection with thrombosis.

How this study might affect research, practice or policy

- Screening for CR1 expression by flow cytometry could improve early identification of high-risk APS/CAPS patients.
- C5 inhibitors offer a promising therapeutic strategy for CAPS patients by reducing complement-mediated thrombosis. CR1 expression may serve as a biomarker in CAPS patients to identify candidates who may benefit from complement-targeted therapy.

INTRODUCTION

Antiphospholipid syndrome (APS) is a thromboinflammatory disorder characterised by arterial or venous thrombosis and/or recurrent fetal loss in the presence of persistent antiphospholipid antibodies (aPL), namely lupus anticoagulant (LA), anticardiolipin, and/or anti-β2 glycoprotein-I antibodies [1,2]. The rate of recurrent thrombosis in APS may exceed 20% within the first 2 years despite anticoagulation [3−5]. 'Catastrophic' APS (CAPS) is a rare subset (~1%-2%) of APS, characterised by rapidly developing widespread thrombosis and multiorgan failure and is associated with high morbidity and mortality [1,6]. Currently, no biomarkers predict the risk of developing CAPS, and it is unclear what differentiates APS and CAPS from a biological perspective. Indefinite anticoagulation with a vitamin K antagonist is the standard of care for thrombotic APS; however, this treatment is suboptimal for some patients with anticoagulant-refractory thrombosis and those with CAPS.

Complement is implicated in the pathophysiology of thrombosis in CAPS, and complement inhibition has been successfully used to treat anticoagulant-refractory thrombosis in APS and CAPS [7−10]. We demonstrated abnormal complement activation in >85% of CAPS sera [11,12] and found that 48% (9/19) of patients with CAPS had rare germline variants in complement regulatory genes, a rate that is comparable to atypical haemolytic uraemic syndrome, a prototypical complement-mediated thrombotic disorder [13,14]. Of these, 44% (4/9) harboured novel rare single-nucleotide variants (SNVs) in complement receptor 1 (*CR1*).

CR1 encodes a ~160 to 300 kDa transmembrane glycoprotein expressed on neutrophils, B lymphocytes, erythrocytes, and monocytes but not on platelets [15−18]. CR1 regulates complement through C4b and C3b binding and plays a dominant role in the clearance of soluble immune complexes [19−22]. Similar to

complement factor H, CR1 possesses decay-accelerating activity, leading to the dissociation of the C3 or C5 convertase, and acts as a cofactor for complement factor I in the cleavage of C4b and C3b [19,20,22−25]. Erythrocytes express 100 to 1000 CR1 molecules per cell [26]. CR1 also carries the Knops blood group system, which currently includes 13 antigens with 5 antithetical antigen pairs (Kn^a/Kn^b, McC^a/McC^b, Sl^a/Vil, KCAM/KDAS, DACY/YCAD) [27]. The Helgeson phenotype, previously considered to be the Knops 'null' phenotype, is serologically defined as Kn(a-) McC(a-) Sl(a-) Yk(a-) and is characterised by extremely low CR1 expression on erythrocytes (<100 CR1 molecules per cell) [27,28]. SNVs in the *CR1* gene are linked to reduced CR1 expression. Previously described variants associated with the Helgeson phenotype include rs11118133: A > T, rs2274567: A > G (represents the DACY- YCAD + phenotype) and rs3811381: C > G [26,29−31]. A recent study identified an SNV on *CR1* (rs11117991: T > C) that disrupts a GATA1-binding site and reduces CR1 expression on erythrocytes [32]. GATA1 is a transcription factor crucial for regulating gene expression in erythroid cells; however, *CR1* expression in granulocytes (neutrophils, basophils, and eosinophils) and monocytes is governed PU.1 [16,33,34].

Here, we demonstrate that patients presenting clinically with CAPS have reduced CR1 expression, consistent with Helgeson-like phenotype. This reduced expression may be attributed to germline mutations or hypermethylation in *CR1*. CR1 deficiency leads to impaired clearance of immune complexes, complement dysregulation, and a severe thrombotic phenotype mitigated by C5 inhibition *in vitro* and *in vivo*. We propose that CR1 deficiency will help identify patients at the highest risk of refractory APS or CAPS and those likely to benefit from complement inhibition.

METHODS

Patient classification and samples

We included patients with APS or CAPS enrolled in the Johns Hopkins Complement Associated Disorders Registry as well as healthy controls (HCs) without known APS or thrombosis. Patients were enrolled in the registry based on the International Society on Thrombosis and Hemostasis criteria for APS [2]. All patients with CAPS and the majority of patients in the APS cohort without a history of CAPS also met American College of Rheumatology/European Alliance of Associations for Rheumatology 2023 criteria for APS [35]. Recurrent thrombosis was confirmed by imaging at any time before enrolment or during follow-up in the registry. For patients with multiple tests for aPLs, we report the results drawn closest to the study sample. Definite or probable CAPS was diagnosed according to international consensus criteria, including involvement of 3 or more organs, development of manifestations within a week, histologic confirmation of small vessel thrombosis, and laboratory confirmation of the presence of aPLs [36]. Definite CAPS requires all 4 criteria, while probable CAPS is diagnosed if 3 criteria are met [36]. We included patients with both definite and probable CAPS because the outcomes of patients with probable CAPS are comparable to those of patients with definite CAPS [37] (Table 1). Clinically, it is often challenging to obtain a tissue biopsy to confirm microvascular thrombosis, resulting in many patients having 'probable' CAPS. In order to establish a suitable baseline reference for erythrocyte CR1 expression, the HC cohort for this observational study included adults (≥18 years old) and was not strictly matched by age or comorbidity status.

Table 1

Clinical features for patients with CAPS/probable CAPS

Patient identification	Age, sex	APS laboratory criteria[a]	Thrombotic and obstetric history	Thrombotic trigger	CAPS manifestations	CAPS treatment	Current treatment	CR1 % expression
P1	39, F	Triple positive; primary	HELLP x3, fetal death x2, PVT, renal failure VTE on anticoagulation	Pregnancy	Renal failure, thrombocytopenia, and elevated transaminases	Plasma exchange, high-dose corticosteroids, anticoagulation	Anticoagulation, no further TE outside pregnancy	15.2
P2	42, M	Triple positive; primary	Stroke, biopsy-proven thrombotic vasculopathy of toes	None	Transient ischaemic attack, myocardial infarction, and diffuse alveolar haemorrhage	Anticoagulation, antiplatelet agents, corticosteroids, rituximab, C5i	Continues on C5i, anticoagulation stopped, no further TE	8.4
P3	53, M	Triple positive; secondary	DVT, PE, myocardial infarction	Infection	Thrombocytopenia, liver injury, proteinuria, encephalopathy, bilateral adrenal haemorrhage	Anticoagulation, hydroxychloroquine, plasma exchange, corticosteroids, rituximab, C5i	Continues on C5i and anticoagulation, no further TE	1.9
P4	57, F	LAC; secondary	Recurrent PE on anticoagulation, multiple episodes of ischaemic colitis, adrenal infarction, ischaemic retinopathy and TIA	None	Pulmonary embolism, TIA, ischaemic colitis, ischaemic retinopathy	Anticoagulation, antiplatelet agents, hydroxychloroquine, rituximab, C5i	Continues on C5i; anticoagulation stopped, 1 DVT post-op in the setting of delayed C5i	23
P5	25, F	LAC; secondary	Recurrent DVT (both on and off anticoagulation), placental abruption, chronic thrombocytopenia, HELLP syndrome	Pregnancy			Anticoagulation, hydroxychloroquine	20.9
P6	56, M	Triple positive; primary	Recurrent DVT on anticoagulation, IVC filter thrombosis, renal vein thrombosis, stroke	None			Anticoagulation, aspirin, hydroxychloroquine	27.2
P7	58, M	LAC, aCL IgM; primary	SMA thrombosis, SMV thrombosis, PVT	Surgery, infection	Progressive SMV thrombosis, bilateral adrenal haemorrhage, stroke, splenic infarcts	IVIg, plasma exchange, anticoagulation, C5i	Anticoagulation, C5i	15.9
P8	51, M	Triple positive, primary	LLE arterial thrombosis	None	Thrombocytopenia. DAH, acute renal failure with renal TMA	Plasma exchange, steroids, anticoagulation and IVIg, C5i	Continues on C5i, hydroxychloroquine, warfarin and clopidogrel	56.3
P9	23, M	Triple positive, primary	Recurrent venous thrombosis including cerebral vein thrombosis, bilateral leg arterial thrombosis	Noncompliance with anticoagulant	Bilateral limb-threatening leg ischaemia	Thrombotic storm treated with prednisone, plasmapheresis and unfractionated heparin transitioned to fondaparinux	Anticoagulation, aspirin, hydroxychloroquine	27.4

aβ2GPI, anti β2 glycoprotein-I antibodies; aCL, anticardiolipin antibodies; APS, antiphospholipid syndrome; C5i, C5 inhibitor; DAH, diffuse alveolar haemorrhage; DVT, deep vein thrombosis; HELLP, haemolysis, elevated liver enzymes and low platelets; IVC, inferior vena cava; IVIg, intravenous immunoglobulin; LAC, lupus anticoagulant; LLE, left lower extremity; PE, pulmonary embolism; PVT, portal vein thrombosis; SMA, superior mesenteric artery; SMV, superior mesenteric vein; TE, thromboembolism; TIA, transient ischaemic attack; TMA, thrombotic microangiopathy; VTE, venous thromboembolism.

[a] Primary APS is defined in the absence of a second underlying autoimmune disorder, commonly lupus, whereas secondary APS occurs in the setting of a concomitant diagnosis of a defined autoimmune disorder.

We excluded control participants with aPL positivity, autoimmune disorders, or other diseases known to decrease CR1 expression, including active malaria and a history of Alzheimer's disease [19,38,39]. In this manuscript, we use "sex" to refer to the biological classification of the subjects as male (M) or female (F), determined by chromosomal and/or anatomical characteristics.

Blood was collected by venipuncture in EDTA and serum separation tubes. Serum was allowed to clot before centrifugation at 4 °C, then separated and stored at −80 °C. Whole blood was used to isolate genomic DNA for sequencing. This study was approved by the Institutional Review Board at Johns Hopkins University and was conducted in accordance with the Declaration of Helsinki. All patients provided written informed consent and were not involved in the design, conduct, reporting, or dissemination plans of this research.

CR1 expression by flow cytometry

Whole blood or ammonium-chloride-potassium lysed cells were washed, suspended in Hanks Balanced Salt Solution + 1% BSA (HBSSA), and stained with fluorescent dye-conjugated CR1 antibody for 30 minutes at room temperature (Supplementary Fig S1A and S5). Flow cytometry was performed using Cytoflex S (Beckman Coulter) and analysed using FlowJo.

Targeted sequencing, multiomics, and CRISPR Cas9-mediated gene editing

Genomic DNA was isolated using a DNeasy Blood & Tissue Kit (Qiagen) and quantified with Qubit fluorometric assay. A total of 50 ng of DNA was used for library preparation using a custom-seq panel of 24 complement regulatory genes described in Supplementary Table S1 (Illumina). To understand the methylation fraction on *CR1*, we performed whole genome sequencing and multiomics using duet multiomics evoC kit (Biomodal).

The CRISPR/Cas9 system was used to generate CR1 knockout (KO) and knock-in (KI) cell lines through homology-directed repair (Supplementary Fig S2). The experiments described were performed on 5 cell lines—TF-1^{WT}, TF-1$^{CR1−/−}$, TF-1^{V2125L}, TF-1^{G2109S}, and TF-1^{S1982G} unless mentioned otherwise.

Modified Ham

Modified Ham (mHam) assay was performed with TF-1^{WT}, TF-1$^{CR1−/−}$, TF-1^{V2125L}, and TF-1^{G2109S} cells as previously described [12]. Normal human serum (NHS) was treated as indicated with heat inactivation (HI) for 30 minutes at 56 °C to inactivate complement proteins or addition of targeted complement inhibitors. Following incubation of the cells, serum viability was measured using a WST-1 dye.

Bioluminescent mHam

Bioluminescent mHam (bio-mHam) was performed as previously described [40]. Bioluminescent HEK293$^{PIGA−/−}$ cells were incubated with patient serum after respective treatment (HI and complement inhibitors). Luminescence was monitored serially and per cent relative luminescence at 1 hour was calculated as the luminescence of cells treated with the patient serum compared to cells treated with the sample's heat-inactivated control. A relative 1-hour luminescence of ~12% defines the positive threshold for abnormal complement activity, corresponding to the lower 85th percentile.

Complement fragment deposition through flow cytometry

Each cell line was incubated with NHS at 37 °C for various durations between 5 and 90 minutes. Cells were washed with HBSSA and stained with C3c and C3dneo murine monoclonal antibodies (mAbs) (Quidel) at 5 μg/mL for 30 minutes at 4 °C followed by anti-mouse AF488 (Invitrogen) antibody for 30 minutes at 4 °C. Cells were washed and resuspended in HBSSA for flow cytometry analysis using a Cytoflex S flow cytometer (Beckman Coulter). Data were collected from at least 10,000 cells and analysed using FlowJo.

Quantification and statistical analysis

Descriptive statistics and analysis were performed using Prism10 (GraphPad). Data are represented as mean ± SD.

A complete description of experimental details can be found in the supplemental data.

RESULTS

Patient cohort and samples

A total of 11 patients with CAPS, 8 with thrombotic APS, and 35 HCs were evaluated. Clinical presentation and characteristics of the CAPS and APS groups are detailed in Table 1 and Table 2 respectively. Among the 11 patients with CAPS, CR1 sequencing was completed in 8 patients (3 had not consented to genetic

Table 2

Clinical feature of APS patient cohort.

Patient identification	Age (y), sex	Abs profile	TE history	CR1 % expression
APS1	23, M	LAC, secondary	Myocardial infarction	76.3
APS2	70, F	LAC, primary	PE, DVT	74.1
APS3	53, M	LAC, primary	Arterial thrombosis (necrotic toes), thrombocytopenia	85.4
APS4	33, F	aCL IgM aβ2GPI IgM,[a] primary	Stroke	85.2
APS5	40, F	aCL IgM,[a] primary	Late fetal loss	88.9
APS6	43, F	Triple positive, primary	Recurrent DVT and PE	92.4
APS7	37, M	aβ2GPI IgG, primary	Bilateral retinal vein occlusion, myocardial infarction	82.2
APS8	70, F	LAC, aCL IgM, secondary	PE	97.9

aβ2GPI, anti-β2 Glycoprotein-I antibodies; aCL, anticardiolipin antibodies; ACR, American College of Rheumatology; APS, antiphospholipid syndrome; DVT, deep vein thrombosis; EULAR, European Alliance of Associations for Rheumatology; LAC, lupus anticoagulant; PE, pulmonary embolism.

[a] Meets International Society on Thrombosis and Hemostasis criteria for APS, not ACR/EULAR.
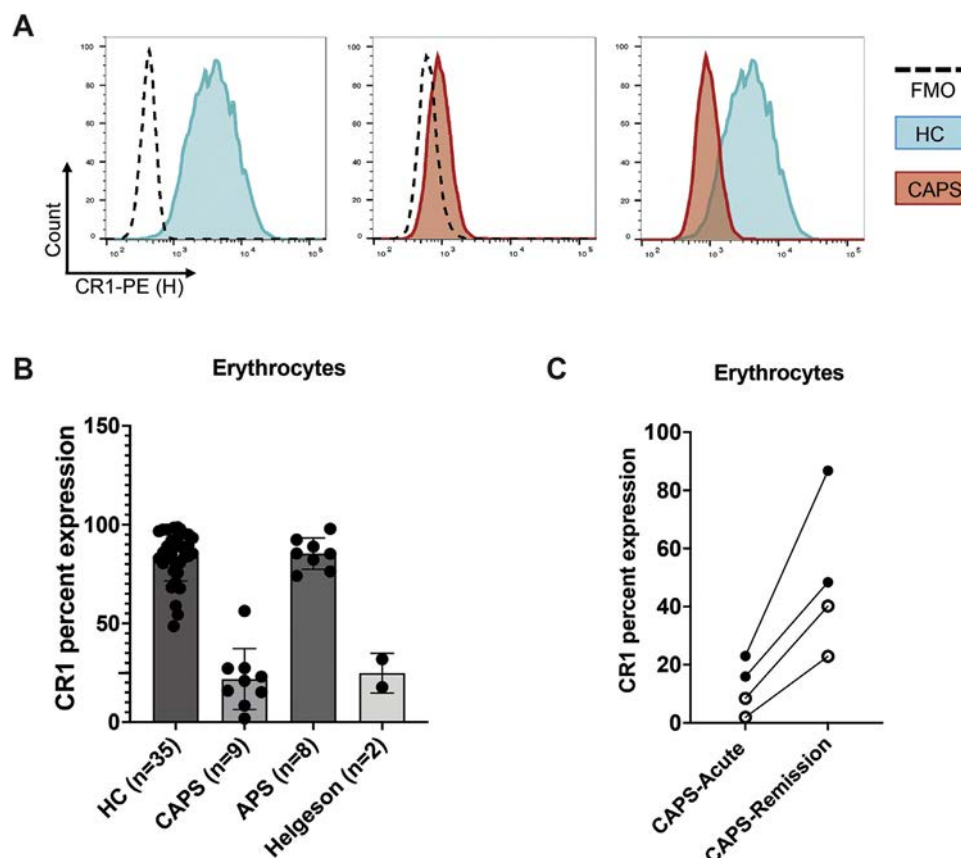
Figure 1. Loss of complement receptor 1 (CR1) impairs immune clearance and makes antiphospholipid syndrome (APS) catastrophic. (A) Representative histograms of CR1 expression [antibody conjugated with phycoerythrin (PE) fluorochrome] in whole blood samples from healthy control (HC; blue) or patient with catastrophic antiphospholipid syndrome (CAPS) (red). Dashed line represents fluorescence minus one (FMO) control. (B) CR1 expression in erythrocytes from HC (82.40% ± 12.96, n = 34), CAPS (21.80% ± 15.44, n = 9), APS (85.30% ± 7.912, n = 8), and Helgeson phenotype (24.80% ± 7.1, n = 2). (C) CR1 expression in serial samples from patients with CAPS representing increased CR1 expression during the remission phase (49.58% ± 10.04) of the disease as compared to the acute phase (12.30% ± 4.572). Patients identified with Helgeson phenotype (rs11117991) are represented as hollow circles. Data are represented as mean ± SD.

studies), and erythrocytes to evaluate CR1 expression were available for 9 (the other 2 were deceased).

Loss of CR1 makes APS catastrophic

Building on previous findings that revealed novel germline variants in 48% of patients with CAPS, we evaluated CR1 expression in our CAPS cohort. CR1 expression was significantly reduced in patients with CAPS (n = 9, 21.80% ± 15.44) compared to the patients with APS (n = 8, 85.30% ± 7.912) and HCs (n = 35, 82.40% ± 12.58). The mean erythrocyte CR1 expression for the Helgeson phenotype controls (obtained from the Johns Hopkins transfusion medicine division, n = 2) was 24.80% ± 10.04 (Fig 1A,B, refer to Supplementary Fig S1B for median fluorescence intensity [MFI]).

Serial samples from patients with CAPS P2, P3, P4, and P7 were collected during the acute and remission phase of CAPS. Samples collected during the remission phase showed significantly higher CR1 expression (49.58% ± 27) compared to the acute phase (12.30% ± 9.144), suggesting a loss of CR1 during the acute phase of the disease (Fig 1C).

CR1 polymorphisms and patient-specific cell line models

CR1 variants were found in 4 of 8 patients with CAPS who underwent sequencing. None of the sequenced control samples (HC, n = 7 and APS, n = 8) had *CR1* variants. The index

patient, first identified with a CR1 variant in our cohort, was a 36-year-old female (P1) with APS (LA and high titre anticardiolipin IgG) with multiple venous and arterial thrombotic events despite anticoagulation and 3 pregnancy losses and was evaluated during her fourth pregnancy. The mHam assay was negative at 17 weeks of gestation; however, the mHam assay became positive at 23 weeks (44.5% cell killing) (Fig 2B). Two days later, she developed thrombocytopenia, liver function tests elevation, and hypoxaemic respiratory failure consistent with either CAPS or haemolysis elevated liver enzymes and low platelets. Targeted sequencing for 24 complement regulatory genes (Supplementary Table S1), identified a heterozygous missense mutation in *CR1* (*CR1*^{V2125L}; rs202148801, Fig 2A), which was verified by Sanger sequencing. Pedigree analysis of samples collected from her family members revealed that both her mother and brother carried the same heterozygous variant (Fig 2C-G) but never presented with any disease manifestations most likely due to lack of aPL.

Missense variants in *CR1* were identified in 3 additional patients (Table 3 and Supplementary Table S2). We generated 2 KI cell line models with the CAPS patient-specific variants (V2125L from P1 and S1982G from PD1; Supplementary Fig S1). We also identified the *CR1*-G2109S variant (*CR1*^{G2109S}; negative control) in a woman without APS who presented with pre-eclampsia (separate cohort). These variants were studied because they were located either within the same exon (G2109S) or in adjacent exons (S1982G, Fig 3A).
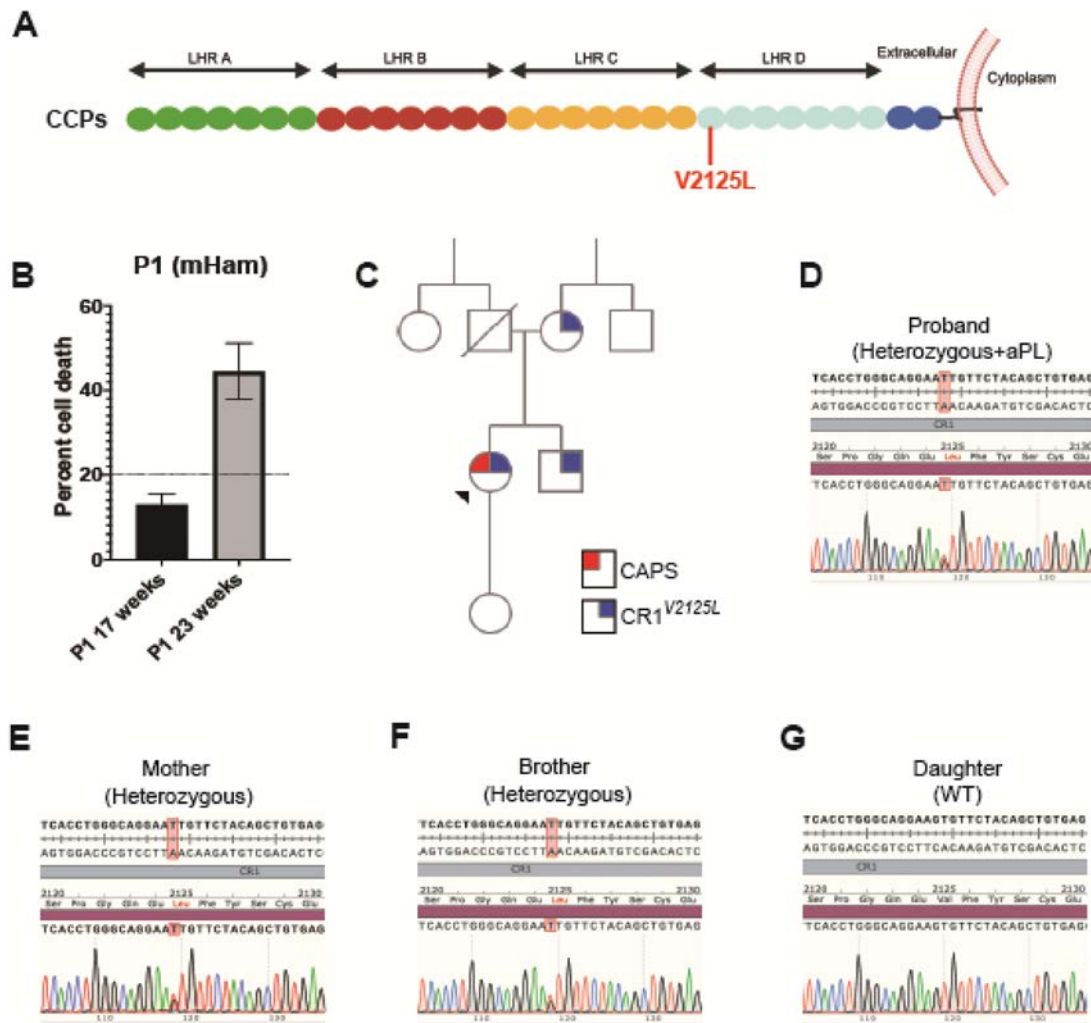
Figure 2. Novel complement receptor 1 (CR1) variants and pedigree tree. (A) Overview of CR1 protein, which contains 4 long homologous regions (LHRs A, B, C, and D). Each LHR consists of 7 complement control proteins (CCPs). *CR1* variant V2125L was identified in CCP22. (B) Modified Ham (mHam) assay demonstrated complement-mediated cell death in patient 1 (P1) at 23 weeks compared to the 17-wk sample. The dashed line represents the threshold for a positive mHam assay. (C) Pedigree tree of the proband's family indicates a heterozygous point mutation (V2125L) in the proband. (D-G) Highlighted regions in the chromatograms of Sanger sequencing reveal that her mother and brother are carrying the same mutation, but the daughter did not have any mutations representing wild type (WT) sequence. aPL, antiphospholipid.

CR1-V2125L (rs202148801) abolishes CR1 mRNA and protein expression

We evaluated *CR1* expression in the respective cell lines (TF-1^{WT}, TF-1$^{CR1−/−}$, TF-1^{V2125L}, TF-1^{G2109S}, and TF-1^{S1982G}) cells. To evaluate the role of the variant, the coding sequence was PCR amplified from 3 regions using specific primers (Fig 3A, Supplementary Table S3). We found that the V2125L mutation abolishes *CR1* full-length mRNA expression to levels consistent with the CR1 KO, whereas the G2109S and S1982G variants did not affect *CR1* transcription (Fig 3B). Flow cytometry, immunofluorescence and western blot analysis also confirmed that surface expression of CR1 was reduced in TF-1^{V2125L} cells when compared to the TF-1^{WT}, TF-1^{G2109S}, and TF-1^{S1982G} (Fig 3C-F). Western blot analysis revealed a low molecular weight (black arrow in Fig 3E) CR1 protein in TF-1^{V2125L} which suggests the V2125L polymorphism yields an allotypic size variant, either by aberrant mRNA splicing or unequal crossing over and loss in the long homologous regions, as described previously [41].

To determine whether the V2125L variant in *CR1* induces protein misfolding and subsequent proteasomal degradation, potentially leading to CR1 loss, we treated TF-1^{WT} and TF-1^{V2125L} cells with the proteasome inhibitor bortezomib. However, CR1 expression levels remain unchanged in TF-1^{V2125L} (Supplementary Fig S3).

Polymorphisms and hypermethylation resulting in CR1 downregulation

Polymorphisms on *CR1*, rs2274567: G, *Hind*III on intron 27 rs11118133: T and rs11117991:C, have been previously reported to reduce CR1 expression and are associated with the Helgeson phenotype. We performed targeted sequencing and investigated these previously reported polymorphisms in our cohort of patient with CAPS and found that P2 and P3 had all 3 Helgeson variants whereas P1, who possessed the novel germline variant, *CR1* SNV rs202148801 (V2125L) linked to low CR1 expression, lacked the previously identified Helgeson variants (Table 3). Two patients, despite low erythrocyte CR1, lacked all known *CR1* polymorphisms (Table 3). We next investigated the methylation profile of *CR1* gene in HCs and the CAPS cohort. All patients with CAPS except (P1) displayed a hypermethylated profile in the CR1 promoter region as compared to controls (Fig 4A,B), suggesting transcriptional silencing as an alternative

Table 3

CR1 genotyping of patients with CAPS

Sample	Previously reported polymorphisms			Novel polymorphisms		
	SNV: A3650G (rs2274567)	SNV: HindIII (rs11118133)	SNV: GATA1 (rs11117991)	SNV: V2125L (rs202148801)	SNV: H1503G (rs758055423)	CR1 % expression
P1[a]	Absent	Absent	Absent	Present	Absent	15.2
P2	Present	Present	Present	Absent	Absent	8.4
P3	Present	Present	Present	Absent	Absent	1.9
P4	Present	Present	Absent	Absent	Absent	23
P5	Absent	Absent	Absent	Absent	Absent	20.9
P6	NS	NS	NS	NS	NS	27.2
P7	Present	Present	Absent	Absent	Absent	15.9
P8	Absent	Absent	Absent	Absent	Present	56.3
P9	Absent	Absent	Absent	Absent	Absent	27.4
PD1[b]	NS	NS	NS	NS	NS	-
PD2[b]	NS	NS	NS	NS	NS	-

CR1, complement receptor 1; NS, not sequenced; SNV, single-nucleotide variant.

[a] TF-1 knock-in (KI) cell lines were generated, because these were the first identified CR1 variants.

[b] Deceased.

mechanism for CR1 regulation. To investigate further, CR1 expression across haematopoietic cells, lymphocytes, and neutrophils was also analysed since they too express CR1. In erythroid cells, CR1 expression is primarily regulated by GATA1, whereas PU.1 plays a dominant role in the development and function of neutrophils and lymphocytes [16].

We observed significant loss of CR1 in neutrophils (n = 4, 53.99 ± 24.09) and lymphocytes (n = 4, 5.96 ± 1.582) in the CAPS cohort as compared to HC neutrophils (n = 6, 92.06 ± 2.964) and lymphocytes (n = 6, 11.84 ± 6.894; Fig 4C-F). Taken together, these results suggest that transcriptional silencing of CR1 due to hypermethylation in the CR1 promotor region can lead to a Helgeson-like phenotype.

Low CR1 modulates cell surface complement fragment deposition and increases complement-mediated cell death

We next examined the functional consequences of the low CR1 on cell surface. First, we analysed complement activation and deposition on different cell lines using C3c and C3dg monoclonal antibodies. Following C3b deposition, factor H in the serum and CR1 can serve as the cofactor for the conversion of C3b to iC3b. Final degradation of iC3b into C3c and C3dg is CR1-dependent [21]. C3b deposition and its cleavage fragments were monitored using flow cytometry with C3c and C3dneo mAbs. Monoclonal anti-C3c detects uncleaved C3b and iC3b while monoclonal anti-C3d ab detects C3b, iC3b, and C3dg. No C3b cleavage was observed on TF-1$^{CR1-/-}$ and TF-1^{V2125L} when compared to TF-1^{WT} (31.77%), TF-1^{G2109S} (49.78%), and TF-1^{S1982G} (44.25%) after 90 minutes (Fig 5A,B, Supplementary Fig S4A and Supplementary Table S4). C3c deposition was significantly higher in cells lacking CR1 (TF-1$^{CR1-/-}$ and TF-1^{V2125L}) (Fig S3B).

Further, we performed the mHam assay using the 4-cell line to assess the impact of the $CR1^{V2125L}$ on complement regulation [12]. TF-1^{V2125L} cells were as susceptible to complement-mediated cell death induced by NHS as TF-1$^{CR1-/-}$ cells (∼21% and 23%, respectively), and were more susceptible to complement-mediated killing than TF-1^{WT} (7%) and TF-1^{G2109S} (5%) cells (Fig 5C).

Low CR1 increases circulating immune complexes

To test the hypothesis that an increase in circulating immune complexes (CICs) due to low CR1 contributes to increased complement activation, we quantified CIC-C1q ELISA in serum from patients with acute CAPS, CAPS in remission, thrombotic APS, and HCs. CICs were significantly increased in sera from acute CAPS (CIC-C1q = 14.32 μg Eq/mL; CIC-C3 = 25.55 μg Eq/mL) compared to CAPS sera collected in remission (CIC-C1q = 3.798 μg Eq/mL and CIC-C3 = 11.40 μg Eq/mL), HCs (CIC-C1q = 3.267 μg Eq/mL and CIC-C3 = 7.445 μg Eq/mL), and patients with APS (CIC-C1q = 3.913 μg Eq/mL and CIC-C3 = 6.316 μg Eq/mL) (Fig 5D,E).

CAPS is triggered through classical complement activation

We next assessed complement-mediated cell killing induced by sera from patient with CAPS (remission or acute) using the bio-mHam. Serum samples collected from patients with acute CAPS led to higher complement-mediated cell killing of the HEK293$^{PIGA-/-}$ bioluminescent cells compared to sera from patients with CAPS in remission (Fig 6A,B). As compared to their respective serum collected during the acute CAPS episode, subsequent serum samples from 5 patients treated with therapeutic terminal complement inhibition (C5i) demonstrated significant inhibition of complement-mediated cell death (Fig 6C, D). In vitro addition of the classical pathway inhibitor (sutimlimab) and C5i (eculizumab) but not factor D inhibitor (ACH-5548/ACH-4471) to serum from patients with acute CAPS rescued the cells from complement-mediated cell death, confirming that complement activation in CAPS is predominantly through the classical pathway

C5 inhibition mitigates thrombosis in CAPS

Five patients from the CAPS cohort (P2, P3, P4, P7, and P8) were treated with either eculizumab or ravulizumab at the discretion of the treating clinician (duration of therapy 2 months to 9 years). Eculizumab and ravulizumab were administered at the doses recommended for treatment of atypical haemolytic uraemic syndrome, at maintenance dosing of 900 mg every 2 weeks for eculizumab and 3300 or 3600 mg of ravulizumab every 8 weeks depending on weight. Collectively, these patients had over 40 thrombotic events despite therapeutic anticoagulation before therapeutic C5 inhibition. Since starting therapy, there has been only 1 thrombotic event when P4 received her eculizumab 1 week after it was due. Since restarting eculizumab, she has had no further thromboses despite discontinuing her anticoagulation over 1 year ago. The swimmer plot summarises the thrombotic events and duration of C5i (Fig 6E).
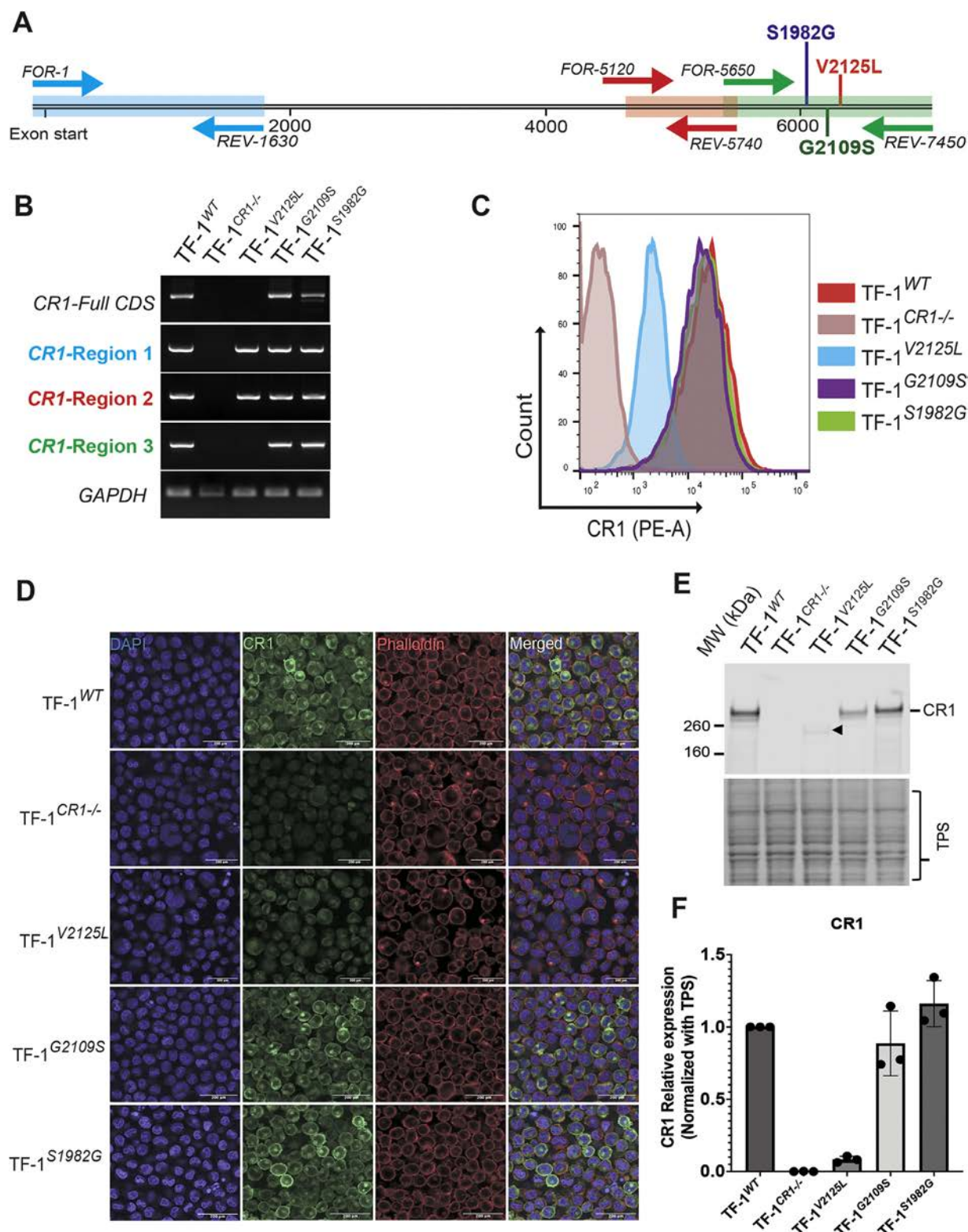
Figure 3. V2125L abolishes complement receptor 1 (CR1) expression. (A) Representation of *CR1* coding sequence (CDS). CDS was PCR (polymerase chain reaction) amplified from 3 regions: region 1 (blue), region 2 (red), and region 3 (green) to analyse the role of variants of unknown significance. Specific primer sets are described in Supplementary Table S2. (B) Isolated RNA from respective cells was subjected to RT-PCR (reverse transcriptase-PCR) for cDNA synthesis. cDNA templates were used for semi-quantitative PCR demonstrating that the V2125L variant results in failure to fully transcribe *CR1,* whereas variants G2109S and S1982G did not affect *CR1* transcription. (C) Flow cytometry analysis represents CR1 expression [antibody conjugated with phycoerythrin (PE) fluorochrome] on respective cell surfaces TF-1^{WT}, TF-1$^{CR1−/−}$, TF-1^{V2125L}, TF-1^{G2109S} and TF-1^{S1982G}. (D) Immunofluorescence staining shows that CR1 expression (green) is significantly reduced in TF-1^{V2125L}. Nuclei are stained with DAPI (4′,6-diamidino-2-phenyl-indole, blue) and phalloidin (red) was used to stain the actin cytoskeleton. The images were captured using a Leica SP8 confocal microscope. The scale bar in the figure insets represents 200 μm. (E) Western blotting represents CR1 protein expression in TF-1^{WT}, TF-1$^{CR1−/−}$, TF-1^{V2125L}, TF-1^{G2109S}, and TF-1^{S1982G}. Black arrowhead represents a possible allotypic variant caused by the V2125L mutation. A total protein stain was used to verify equal loading of proteins. (F) Densitometric quantification of relative CR1 expression through western blot. Images representative of n = 3 experiments. Data are presented as mean ± SD.
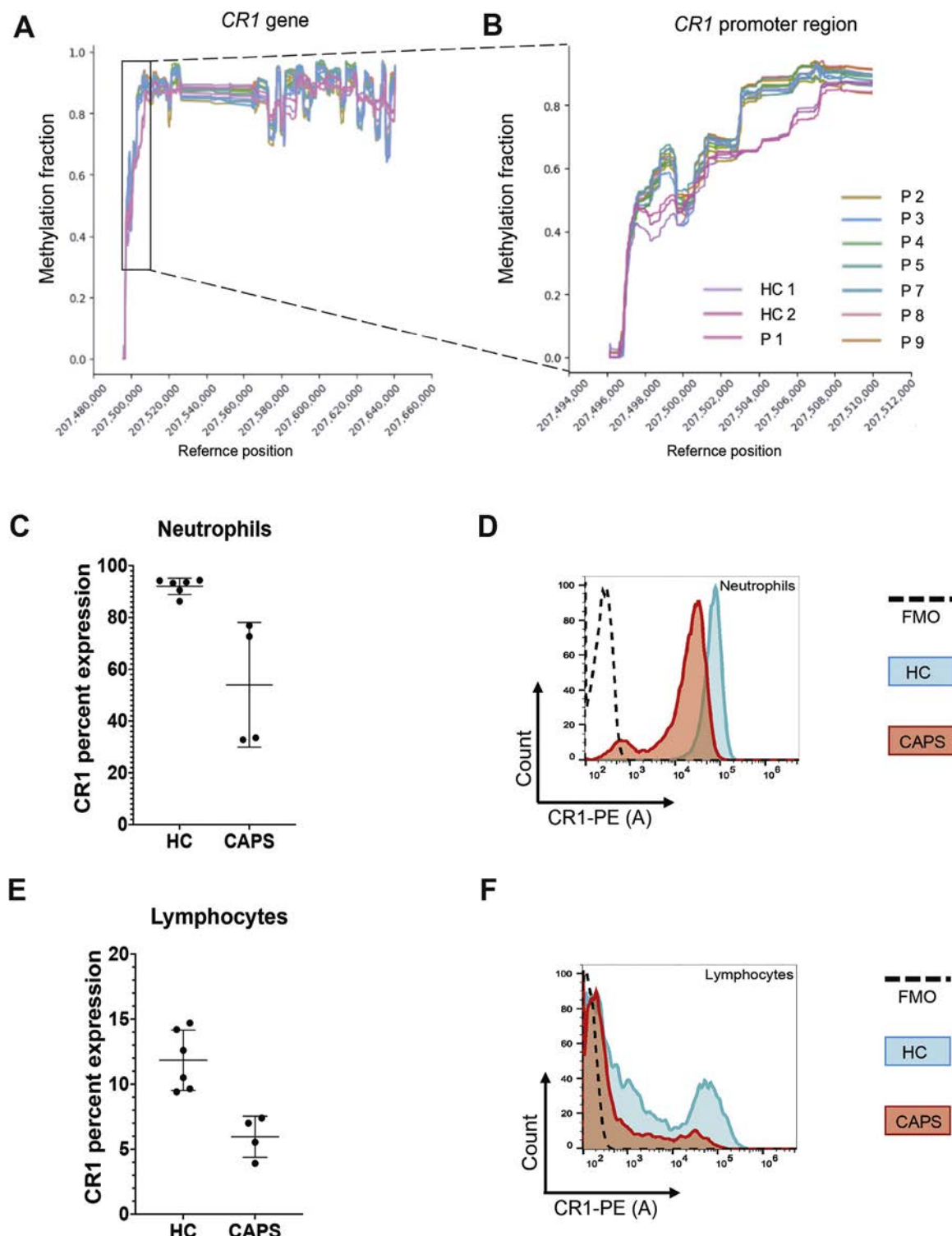
Figure 4. Hypermethylation results in complement receptor 1 (*CR1*) downregulation. (A) Representation of methylation fraction profile of *CR1* gene on the *X*-axis and with the reference position on the *Y*-axis. (B) Inset of the methylation fraction around *CR1* promoter region in healthy controls (HCs) and patients with catastrophic antiphospholipid syndrome (CAPS). Showing hypermethylation in patients with CAPS except index patient (P1) with V2125L SNV as compared to the HCs. (C-F) CR1 per cent expression was assessed by flow cytometry in (C) neutrophils and (E) lymphocytes of HCs (n = 6) and patients with CAPS (n = 4). Live cells were gated using Live/Dead dye, CD45 staining was used to gate the lymphocytes and CD15 staining was used to gate neutrophils. The neutrophils with CR1 on the cell surface were determined by CD15+ CR1+ cell population. Fluorescence minus one (FMO) controls were used to determine the positive threshold and define the background signal. (D) Example histogram of CR1 expression in neutrophils, and (F) lymphocytes. Data are represented as mean ± SD.

DISCUSSION

Complement dysregulation in a subset of patients with APS predisposes to inflammation and thrombotic events and is a feature of CAPS [11,42−44]. Here, we demonstrate that a severe reduction in CR1 expression on erythrocytes, in APS, is a biomarker for severe APS/CAPS. We demonstrate that low CR1 results from novel germline variants in *CR1* (*CR1*[V2125L], rs202148801) or hypermethylation of the *CR1* promoter region which may occur in the context of previously described CR1
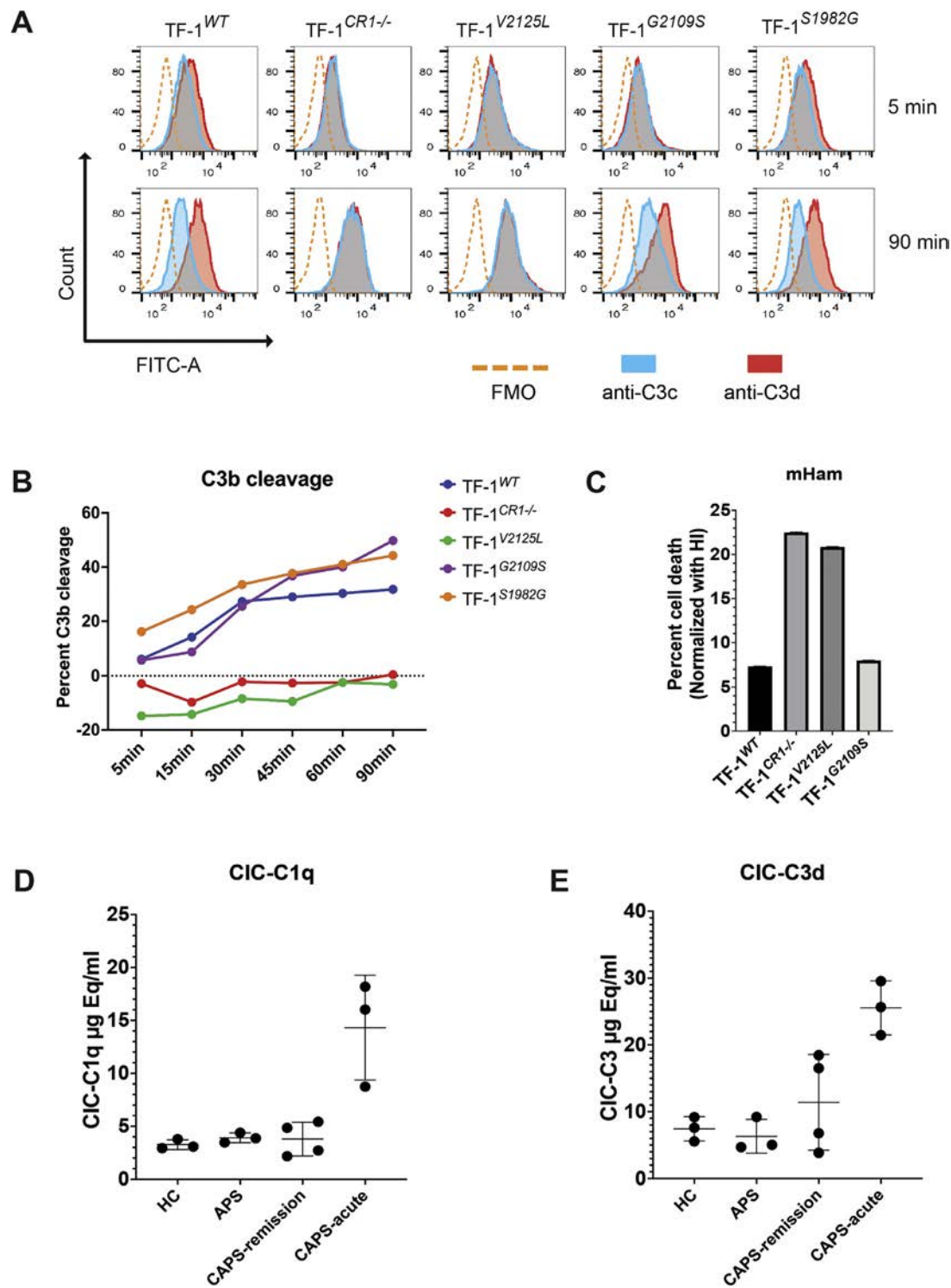
Figure 5. Absence of complement receptor 1 (CR1) leads to complement dysregulation and enhances complement-mediated cell death. (A) Cell lines were exposed to normal human serum (NHS) for 5 to 90 minutes and surface C3b and its fragments were detected by flow cytometry. Representative images at 5 and 90 minutes for each cell line are shown. Monoclonal anti-C3c detects uncleaved C3b and iC3b while monoclonal anti-C3d ab detects C3b, iC3b, and C3d, g. FITC (fluorescein isothiocyanate) labelled goat anti-mouse was used as the secondary ab. Blue solid lines represent C3c deposition and red solid line represents C3d deposition, dashed line represents fluorescence minus one (FMO) control, exposed only to secondary ab. C5 inhibitor was used in the serum to ensure the viability of the cells. (B) Representative example of C3b cleavage in the cell lines. Time course of C3b cleavage demonstrates the inability of cells to cleave C3b to C3d,g without CR1. Data represent median fluorescence intensity (MFI), representative analysis of n = 3 experiments. (C) Modified Ham (mHam) test was performed to analyse complement-mediated cell death in the following cell lines: TF-1^{WT} (7%), TF-1$^{CR1−/−}$ (~23%), TF-1^{V2125L} (~21%) and in TF-1^{G2109S} (~5%). (D) Serum specimens (diluted 1:50) from represented cohorts were subjected to ELISA (enzyme-linked immunosorbent assay) immunoassay to evaluate immune complexes bound to immobilised human C1q purified protein and (E) ability of immune complexes to covalently bind C3 fragments. The µg Eq/mL concentration for each sample is represented in healthy control (HC), n = 3; APS, n = 3; catastrophic antiphospholipid syndrome (CAPS)-remission, n = 4; CAPS-acute, n = 3. Data are represented as mean ± SD.
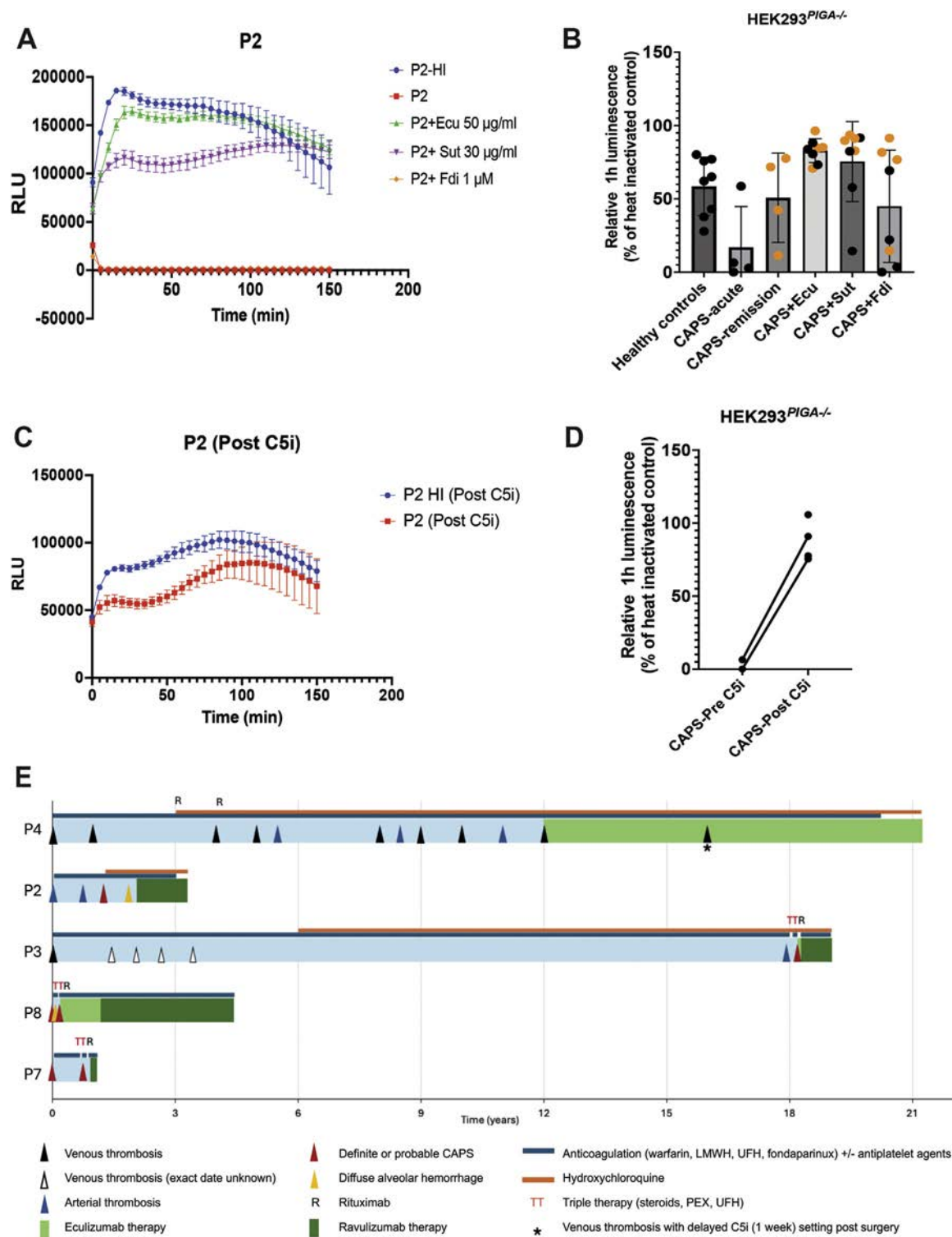
Figure 6. Bioluminescent mHam (bio-mHam) represents enhanced complement activation and efficacy of C5i in catastrophic antiphospholipid syndrome (CAPS). HEK293$^{PIGA−/−}$ cells were used for monitoring complement activation in CAPS sera through bio-mHam assay. Relative luminescence units (RLU) were measured every 5 minutes for 2.5 hours. (A) Representative example of CAPS sera on *PIGA*KO cells with or without heat inactivation (HI), eculizumab (Ecu, 50 μg/mL), sutimlimab (Sut, 30 μg/mL), or ACH-5548 (Fdi, 1 μM). (B) Summary of relative luminescence at 1 hour for healthy controls (HCs, n = 8), CAPS (acute, n = 3 or remission, n = 4), with the addition of eculizumab, sutimlimab, and Fdi. CAPS remission samples are represented as orange dots. (C) Representative example to monitor the efficacy of therapeutic C5i in CAPS sera after C5i therapeutic treatment. (D) Summary of significant reduction of complement-mediated cell killing after C5i therapy in patients with acute CAPS. Data are represented as mean ± SD. (E) Swimmer plot illustrating the timeline of venous thrombosis, arterial and microvascular thrombotic events and CAPS episodes in patients receiving C5 inhibition (C5i) therapy. Therapy durations for eculizumab and ravulizumab are depicted with green and dark green regions, respectively. P2 and P4 are off anticoagulation. LMWH, low molecular weight heparin; PEX, plasmapheresis exchange; UFH, unfractionated heparin.

variants associated with the Helgeson phenotype such as rs11117991. Acquired loss of CR1 in the acute phase of CAPS may also result from proteolytic cleavage of immune complexes bound to erythrocyte CR1 by macrophages of the reticuloendothelial system [33], as is reported in systemic lupus erythematosus [17]. However, our finding of reduced CR1 on leukocytes in CAPS suggests that genetic and epigenetic mechanisms play an important role. We show that functionally CR1 deficiency leads to impaired clearance of immune complexes promoting ongoing classical complement activation, as evidenced by an increase in CICs and classical pathway activation in sera from patients with acute CAPS. Finally, we demonstrate that complement inhibition at C5 inhibits classical pathway activation *ex vivo* and therapeutic C5 inhibition *in vivo* blocks complement activation and prevents thrombosis in patients with CAPS, overcoming the pathological consequences of CR1 deficiency. Together with our previous findings in APS [36], this study supports the potential benefit of complement-targeted therapies to improve patient outcomes and prevent recurrent thrombosis.

We demonstrate a potential association between severe APS/CAPS and the Helgeson-like phenotype (low CR1). Of 9 patients, 8 in the CAPS cohort met the criteria for the Helgeson-like phenotype on their erythrocytes (Fig 1B), whereas none of the HCs or patients with APS displayed this phenotype. CR1 expression in CAPS erythrocytes was markedly reduced to an average of 26% of HC levels, closely resembling the Helgeson phenotype (30%), whereas erythrocytes from the APS cohort showed normal expression levels at 103% of the HC mean. The Helgeson phenotype was originally identified serologically; however, serologic evaluation of Knops antigens is often not feasible due

to a lack of available ABO-compatible antisera. Additionally, variations in antibody potency and antigen expression between erythrocytes of similar phenotypes may lead to discrepancies when positive reactivity is observed for erythrocytes with low CR1 copy number [28]. Erythrocyte flow cytometry appears to be a simple screening approach to identify patients with APS who may be at risk of developing CAPS. We correlated CR1 expression in our CAPS cohort with the already known Helgeson variants and uncovered a novel SNV, $CR1^{V2125L}$ (rs202148801) that results in low CR1 expression leading to a Helgeson-like phenotype. Of 8 sequenced patients with CAPS (Table 3), 6 (75%) harboured SNV associated with low CR1 expression and 2 had rs11117991 (25%), which was demonstrated by Wu et al [32], to block GATA1 binding.

GATA1 is primarily recognised for its role in erythroid cells, whereas the transcription factor PU.1 is essential for the development and function of myeloid cells (eg, neutrophils, monocytes) and lymphoid cells [16]. Our findings reveal that hypermethylation in the CR1 promoter region may play a significant role in regulating its expression in patients with CAPS. All patients with CAPS, except P1, exhibited a similar hypermethylation profile in the CR1 promoter region compared to HC, suggesting epigenetic silencing as a potential mechanism underlying CR1 deficiency. Furthermore, CR1 expression in neutrophils and lymphocytes from patients with CAPS was reduced to 58.6% and 50.3% of HC levels, respectively, indicating systemic downregulation across haematopoietic cell types. These observations suggest that CR1 expression is governed not only by genetic predisposition but also by epigenetic modifications, such as promoter hypermethylation, reflecting a dynamic inter-
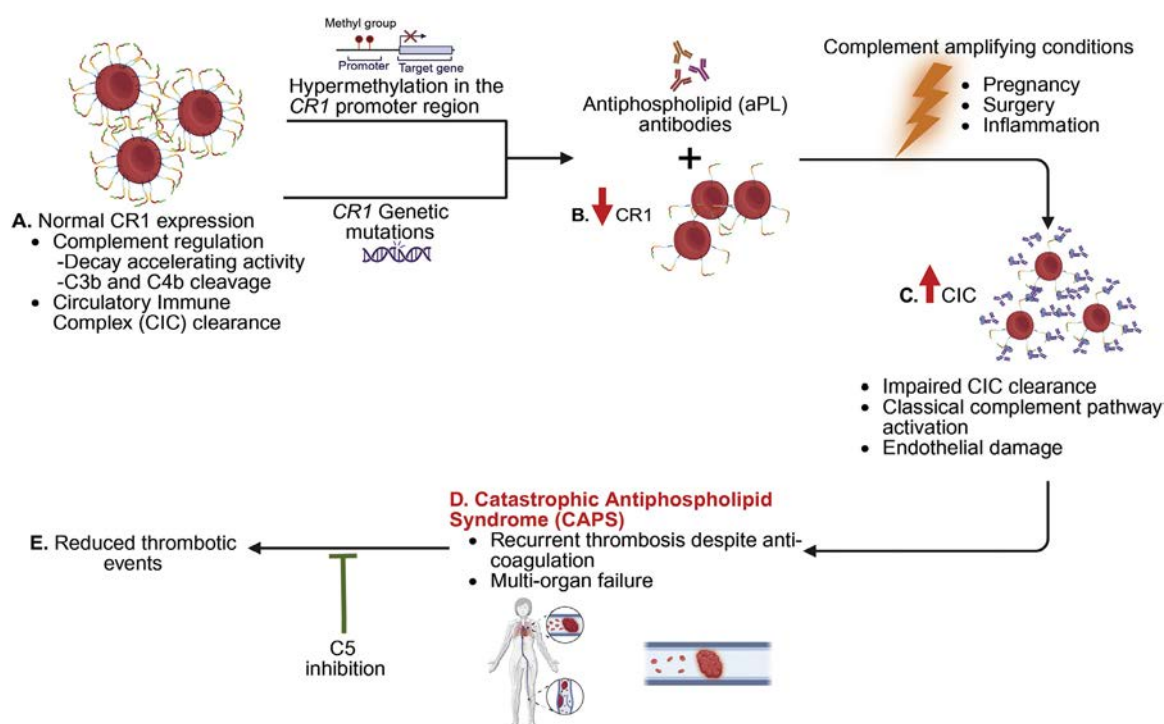

Figure 7. Complement receptor 1 (CR1) deficiency drives complement-mediated pathogenesis in catastrophic antiphospholipid syndrome (CAPS). (A) CR1 is essential for complement regulation through clearing circulating immune complexes (CICs), decay-accelerating activity and acts as a cofactor for factor I mediated cleavage of C3b and C4b, resulting in their inactivation and regulation of the immune response. (B) *CR1* genetic variations (eg, V2125L) and promoter hypermethylation downregulate CR1 on erythrocytes, neutrophils, and B-cells. Low CR1 levels combined with antiphospholipid (aPL) antibodies and complement amplifying conditions (such as pregnancy, surgery, or infections) results in (C) impaired CIC clearance. This triggers complement overactivation, endothelial damage, and recurrent thrombosis despite anticoagulation. (D) These pathological processes promote multiorgan failure and establish CAPS. (E) C5 inhibition, targeting the terminal complement cascade represents a therapeutic strategy for CAPS. Created with BioRender.com.

play between inherited and environmentally influenced regulatory factors. This hypothesis is further reinforced by the observed increased CR1 expression during clinical remission in patients with CAPS with the Helgeson phenotype (P2 and P3, Fig 1C).

Dysregulation in the function of CR1 may amplify classical complement activation by failing to control immune complexes, a known activator of the classical pathway. Indeed, almost 90% of patients with CAPS have evidence of classical complement activation by serologic assays compared to roughly 35% of patients with thrombotic APS [36]. Using a patient-specific variant cell line, we characterised the consequences of reduced CR1 expression that lead to increased C3b deposition and enhanced complement-mediated cell death. A major function of CR1 is to bind and process C3b/C4b-coated immune complexes [19]. Low CR1 influences immune adherence by reducing the binding of opsonised immune complexes containing C3b and C4b to erythrocytes, leading to an inflammatory response [45−47]. We observed a significantly increased level of immune complexes in the serum of patients with acute CAPS as compared to HCs and remission patients with CAPS.

The aetiology of CAPS is multifactorial with genetic and environmental factors contributing to the pathogenesis. Our index case (P1) exemplifies this hypothesis. She inherited the CR1 mutation (*V2125L*) from her mother who did not exhibit thrombosis or pregnancy-related complications, most likely because she did not have aPL. Moreover, P1 developed CAPS manifestations only in the setting of pregnancy, a well-established complement amplifying condition, although she had had macrovascular thrombosis before pregnancy. Our study extends the previous case reports and a small series of eculizumab therapy suggesting that C5 inhibition is efficacious in patients with CAPS [48,49]. We extend these observations by identifying 2 potential biomarkers (erythrocyte CR1 expression and the bio-mHam) to identify patients who are most likely to respond to complement inhibition. Importantly, we show for the first time that it may be feasible to stop anticoagulation in patients with CAPS, but this will need validation in larger trials. Two patients (P2 and P4) are off anticoagulation for over 6 and 13 months, respectively; thus, similar to paroxysmal nocturnal haemoglobinuria, the prototypic complement-driven thrombophilia, long-term anticoagulation may not be required for patients well-controlled on complement inhibitors [50,51].

There are limitations in our study. First, the cohort size is small and the follow-up for patients treated with C5i is relatively short. Second, larger cohorts of patients with CAPS and APS are needed to confirm the association between CR1 deficiency and CAPS and the predictive value of the bio-mHam for response to C5 inhibition. Lastly, more patients are needed to confirm the cellular and molecular mechanisms of the Helgeson-like phenotype in CAPS.

In summary, CAPS is a multihit disorder of classical complement activation mediated by aPL, impaired immune complex handling, and environmental triggers in the presence of marked CR1 deficiency on erythrocytes. CR1 deficiency exhibits a genetic and epigenetic association with Helgeson-like phenotype, serves as a novel biomarker for CAPS, and is a potential screening tool for risk stratification and response to therapy. The severe suppression of CR1 across multiple cell types (erythrocytes, neutrophils, and lymphocytes) in patients with CAPS highlights the need for further investigation into therapeutic strategies targeting epigenetic regulation to restore CR1 function (Fig 7). C5i inhibition appears highly efficacious in preventing thrombosis in CAPS, although large multicentre, prospective trials are needed to confirm this finding.

Competing interests

Acknowledgements

Contributors

NR designed research, performed research, analysed data, and wrote the first draft. MAC designed research, performed research, analysed data, and edited/wrote the paper. GFG designed research and edited/wrote the paper. MAC reviewed research data and wrote/edited the paper. EMB reviewed research data and wrote/edited the paper. DF-G performed research. AR performed research. KH performed research, reviewed research data and wrote/edited the paper. KRM reviewed data and wrote/edited the paper. SC reviewed research data and wrote/edited the paper and RAB designed research, analysed data, and wrote the paper.

Funding

Patient consent for publication

Not applicable

Ethics approval

All samples were obtained under approval by the Institutional Review Board at the Johns Hopkins University, School of Medicine.

Provenance and peer review

Not commissioned; externally peer reviewed.

Supplementary materials

Supplementary material associated with this article can be found in the online version at doi:10.1016/j.ard.2025.07.016.

Orcid

Nikhil Ranjan: http://orcid.org/0000-0003-0650-2928
Robert A. Brodsky: http://orcid.org/0000-0001-5741-1255

REFERENCES

[1] Aguiar CL, Erkan D. Catastrophic antiphospholipid syndrome: how to diagnose a rare but highly fatal disease. Ther Adv Musculoskelet Dis 2013;5 (6):305–14.

[2] Miyakis S, Lockshin MD, Atsumi T, Branch DW, Brey RL, Cervera R, et al. International consensus statement on an update of the classification criteria for definite antiphospholipid syndrome (APS). J Thromb Haemost 2006;4 (2):295–306.

[3] Cohen H, Isenberg DA. How I treat anticoagulant-refractory thrombotic antiphospholipid syndrome. Blood 2021;137(3):299–309.

[4] Farmer-Boatwright MK, Roubey RA. Venous thrombosis in the antiphospholipid syndrome. Arterioscler Thromb Vasc Biol 2009;29(3):321–5.

[5] Crowther MA, Ginsberg JS, Julian J, Denburg J, Hirsh J, Douketis J, et al. A comparison of two intensities of warfarin for the prevention of recurrent thrombosis in patients with the antiphospholipid antibody syndrome. N Engl J Med 2003;349:1133–8.

[6] Nayer A, Ortega LM. Catastrophic antiphospholipid syndrome: a clinical review. J Nephropathol 2014;3(1):9–17.

[7] Agostinis C, Durigutto P, Sblattero D, Borghi MO, Grossi C, Guida F, et al. A non-complement-fixing antibody to beta2 glycoprotein I as a novel therapy for antiphospholipid syndrome. Blood 2014;123(22):3478–87.

[8] Carrera-Marín A, Romay-Penabad Z, Papalardo E, Reyes-Maldonado E, García-Latorre E, Vargas G, et al. C6 knock-out mice are protected from thrombophilia mediated by antiphospholipid antibodies. Lupus 2012;21(14):1497–505.

[9] Fischetti F, Durigutto P, Pellis V, Debeus A, Macor P, Bulla R, et al. Thrombus formation induced by antibodies to beta2-glycoprotein I is complement dependent and requires a priming factor. Blood 2005;106(7):2340–6.

[10] Pierangeli SS, Girardi G, Vega-Ostertag M, Liu X, Espinola RG, Salmon J. Requirement of activation of complement C3 and C5 for antiphospholipid antibody-mediated thrombophilia. Arthritis Rheum 2005;52(7):2120–4.

[11] Chaturvedi S, Braunstein EM, Brodsky RA. Antiphospholipid syndrome: complement activation, complement gene mutations, and therapeutic implications. J Thromb Haemost 2021;19(3):607–16.

[12] Gavriilaki E, Yuan X, Ye Z, Ambinder AJ, Shanbhag SP, Streiff MB, et al. Modified Ham test for atypical hemolytic uremic syndrome. Blood 2015;125 (23):3637–46.

[13] Maga TK, Nishimura CJ, Weaver AE, Frees KL, Smith RJ. Mutations in alternative pathway complement proteins in American patients with atypical hemolytic uremic syndrome. Hum Mutat 2010;31(6):E1445–60.

[14] Osborne AJ, Breno M, Borsa NG, Bu F, Frémeaux-Bacchi V, Gale DP, et al. Statistical validation of rare complement variants provides insights into the molecular basis of atypical hemolytic uremic syndrome and C3 glomerulopathy. J Immunol 2018;200(7):2464–78.

[15] Fearon DT. Identification of the membrane glycoprotein that is the C3b receptor of the human erythrocyte, polymorphonuclear leukocyte, B lymphocyte, and monocyte. J Exp Med 1980;152(1):20–30.

[16] Anderson KL, Smith KA, Pio F, Torbett BE, Maki RA. Neutrophils deficient in PU.1 do not terminally differentiate or become functionally competent. Blood 1998;92(5):1576–85.

[17] Wilson JG, Ratnoff WD, Schur PH, Fearon DT. Decreased expression of the C3b/C4b receptor (CR1) and the C3d receptor (CR2) on B lymphocytes and of CR1 on neutrophils of patients with systemic lupus erythematosus. Arthritis Rheum 1986;29(6):739–47.

[18] Eriksson O, Mohlin C, Nilsson B, Ekdahl KN. The human platelet as an innate immune cell: interactions between activated platelets and the complement system. Front Immunol 2019;10:1590.

[19] Khera R, Das N. Complement receptor 1: disease associations and therapeutic implications. Mol Immunol 2009;46(5):761–72.

[20] Erdei A, Kovács KG, Nagy-Baló Z, Lukácsi S, Mácsik-Valent B, Kurucz I, et al. New aspects in the regulation of human B cell functions by complement receptors CR1, CR2, CR3 and CR4. Immunol Lett 2021;237:42–57.

[21] Java A, Liszewski MK, Hourcade DE, Zhang F, Atkinson JP. Role of complement receptor 1 (CR1; CD35) on epithelial cells: a model for understanding complement-mediated damage in the kidney. Mol Immunol 2015;67(2 Pt B):584–95.

[22] Vandendriessche S, Cambier S, Proost P, Marques PE. Complement receptors and their role in leukocyte recruitment and phagocytosis. Front Cell Dev Biol 2021;9:624025.

[23] Hourcade DE, Mitchell LM, Medof ME. Decay acceleration of the complement alternative pathway C3 convertase. Immunopharmacology 1999;42:167–73.

[24] Kremlitzka M, Polgár A, Fülöp L, Kiss E, Poór G, Erdei A. Complement receptor type 1 (CR1, CD35) is a potent inhibitor of B-cell functions in rheumatoid arthritis patients. Int Immunol 2013;25(1):25–33.

[25] Oliveira LC, Kretzschmar GC, Dos Santos ACM, Camargo CM, Nisihara RM, Farias TDJ, et al. Complement receptor 1 (CR1, CD35) polymorphisms and soluble CR1: a proposed anti-inflammatory role to quench the fire of "Fogo Selvagem" pemphigus foliaceus. Front Immunol 2019;10:2585.

[26] Wilson JG, Murphy EE, Wong WW, Klickstein LB, Weis JH, Fearon DT. Identification of a restriction fragment length polymorphism by a CR1 cDNA that correlates with the number of CR1 on erythrocytes. J Exp Med 1986;164:50–9.

[27] International Society of Blood Transfusion Working Group on Red Cell Immunogenetics and Blood Group Terminology: Blood Group Allele Tables Amsterdam. ISBT; 2024. https://www.isbtweb.org.

[28] Moulds JM, Moulds JJ, Brown M, Atkinson JP. Antiglobulin testing for CR1-related (Knops/McCoy/Swain-Langley/York) blood group antigens: negative and weak reactions are caused by variable expression of CR1. Vox Sang 1992;62(4):230–5.

[29] Herrera AH, Xiang L, Martin SG, Lewis J, Wilson JG. Analysis of complement receptor type 1 (CR1) expression on erythrocytes and of CR1 allelic markers in Caucasian and African American populations. Clin Immunol Immunopathol 1998;87(2):176–83.

[30] Zorzetto M, Bombieri C, Ferrarotti I, Medaglia S, Agostini C, Tinelli C, et al. Complement receptor 1 gene polymorphisms in sarcoidosis. Am J Respir Cell Mol Biol 2002;27(1):17–23.

[31] Cooling L. Blood groups in infection and host susceptibility. Clin Microbiol Rev 2015;28(3):801–70.

[32] Wu PC, Lee YQ, Möller M, Storry JR, Olsson ML. Elucidation of the low-expressing erythroid CR1 phenotype by bioinformatic mining of the GATA1-driven blood-group regulome. Nat Commun 2023;14(1):5001.

[33] Gutiérrez L, Caballero N, Fernández-Calleja L, Karkoulia E, Strouboulis J. Regulation of GATA1 levels in erythropoiesis. IUBMB Life 2020;72(1):89–105.

[34] Pevny L, Simon MC, Robertson E, Klein WH, Tsai SF, D'Agati V, et al. Erythroid differentiation in chimaeric mice blocked by a targeted mutation in the gene for transcription factor GATA-1. Nature 1991;349(6306):257–60.

[35] Barbhaiya M, Zuily S, Naden R, Hendry A, Manneville F, Amigo MC, et al. 2023 ACR/EULAR antiphospholipid syndrome classification criteria. Ann Rheum Dis 2023;82(10):1258–70.

[36] Chaturvedi S, Braunstein EM, Yuan X, Yu J, Alexander A, Chen H, et al. Complement activity and complement regulatory gene mutations are associated with thrombosis in APS and CAPS. Blood 2020;135(4):239–51.

[37] Pineton de Chambrun M, Larcher R, Pène F, Argaud L, Demoule A, Jamme M, et al. CAPS criteria fail to identify most severely-ill thrombotic antiphospholipid syndrome patients requiring intensive care unit admission. J Autoimmun 2019;103:102292.

[38] Ross GD, Yount WJ, Walport MJ, Winfield JB, Parker CJ, Fuller CR, et al. Disease-associated loss of erythrocyte complement receptors (CR1, C3b receptors) in patients with systemic lupus erythematosus and other diseases involving autoantibodies and/or complement activation. J Immunol 1985;135(3):2005–14.

[39] Stoute JA, Odindo AO, Owuor BO, Mibei EK, Opollo MO, Waitumbi JN. Loss of red blood cell-complement regulatory proteins and increased levels of circulating immune complexes are associated with severe malarial anemia. J Infect Dis 2003;187(3):522–5.

[40] Cole MA, Ranjan N, Gerber GF, Pan XZ, Flores-Guerrero D, McNamara G, Chaturvedi S, Sperati CJ, McCrae KR, Brodsky RA. Complement biosensors identify a classical pathway stimulus in complement-mediated thrombotic microangiopathy. Blood 2024;144(24):2528–45. PMID: 39357054; PMCID: PMC11862816. doi: 10.1182/blood.2024025850.

[41] Wong WW, Farrell SA. Proposed structure of the F' allotype of human CR1. Loss of a C3b binding site may be associated with altered function. J Immunol 1991;146(2):656–62.

[42] Venturelli V, Maranini B, Tohidi-Esfahani I, Isenberg DA, Cohen H, Efthymiou M. Can complement activation be the missing link in antiphospholipid syndrome? Rheumatology (Oxford) 2024;63:3243–54.

[43] Martínez-Flores JA, Serrano M, Pérez D, Lora D, Paz-Artal E, Morales JM, et al. Detection of circulating immune complexes of human IgA and β 2 glycoprotein I in patients with antiphospholipid syndrome symptomatology. J Immunol Methods 2015;422:51–8.

[44] Martínez-Flores JA, Serrano M, Pérez D, Cámara A G, Lora D, Morillas L, et al. Circulating immune complexes of IgA bound to beta 2 glycoprotein are strongly associated with the occurrence of acute thrombotic events. J Atheroscler Thromb 2016;23(10):1242–53.

[45] Smith BO, Mallin RL, Krych-Goldberg M, Wang X, Hauhart RE, Bromek K, et al. Structure of the C3b binding site of CR1 (CD35), the immune adherence receptor. Cell 2002;108:769–80.

[46] Noris M, Remuzzi G. Overview of complement activation and regulation. Semin Nephrol 2013;33(6):479–92.

[47] Kisserli A, Schneider N, Audonnet S, Tabary T, Goury A, Cousson J, et al. Acquired decrease of the C3b/C4b receptor (CR1, CD35) and increased C4d deposits on erythrocytes from ICU COVID-19 patients. Immunobiology 2021;226(3):152093.

[48] López-Benjume B, Rodríguez-Pintó I, Amigo MC, Erkan D, Shoenfeld Y, Cervera R, et al. Eculizumab use in catastrophic antiphospholipid syndrome (CAPS): descriptive analysis from the "CAPS registry". Autoimmun Rev 2022;21:103055.

[49] Faguer S, Ribes D. Early use of eculizumab for catastrophic antiphospholipid syndrome. Br J Haematol 2022;196(2):e12–4.

[50] Bodó I, Amine I, Boban A, Bumbea H, Kulagin A, Lukina E, et al. Complement inhibition in paroxysmal nocturnal hemoglobinuria (PNH): a systematic review and expert opinion from central Europe on special patient populations. Adv Ther 2023;40(6):2752–72.

[51] Gerber GF, DeZern AE, Chaturvedi S, Brodsky RA. A 15-year, single institution experience of anticoagulation management in paroxysmal nocturnal hemoglobinuria patients on terminal complement inhibition with history of thromboembolism. Am J Hematol 2022;97(2): E59–62.

Myositis

Enhanced proteasome activity in perifascicular myofibres is a hallmark of dermatomyositis and its inhibition is efficient in preclinical models

Léa Debrut [1,2,#], Margherita Giannini [1,3,#,*], Giulia Quiring [1],
Simone Perniola [4], Daniela Rovito [2], Céline Keime [2], Béatrice Lannes [5],
Aleksandra Nadaj-Pakleza [6], Jean-Baptiste Chanson [6], Anne-Laure Charles [1],
Bernard Geny [1,7], Daniel Metzger [2], Gilles Laverny [2,#], Alain Meyer [1,3,#]

[1] UR3072 Centre de Recherche en Biomédecine, Université de Strasbourg, Strasbourg, France

[2] Université de Strasbourg, CNRS, Inserm, IGBMC UMR 7104-UMR-S 1258, Illkirch, France

[3] Explorations Fonctionnelles Musculaires, Service de Physiologie, Centre de Référence des Maladies Autoimmunes Rares, Hôpitaux Universitaires de Strasbourg, Strasbourg, France

[4] Clinical Immunology Unit, Fondazione Policlinico Universitario A. Gemelli-IRCCS, Rome, Italy

[5] Département d'Anatomopathologie, Hôpitaux Universitaires de Strasbourg, Strasbourg, France

[6] Service de Neurologie, Centre de Référence des Maladies Neuromusculaires NEIdF, ERN EURO-NMD, Hôpitaux Universitaire de Strasbourg, Strasbourg, France

[7] Service de Physiologie et Explorations fonctionnelles, Hôpitaux Universitaires de Strasbourg, Strasbourg, France

ABSTRACT

Objectives: This study aims to characterise the molecular pathways underpinning perifascicular muscle fibre alterations to identify repositionable molecules for dermatomyositis (DM) treatment, and validate potential candidates in preclinical models.

Methods: RNA-sequencing was performed to determine the transcriptome of microdissected peri- and endofascicular myofibres from 7 patients with untreated and early DM (symptoms <6 months), 6 with other inflammatory myopathies and 5 without neuromuscular disease. The molecular pathways characterising DM perifascicular fibres were determined and used to explore databases of repositionable drugs. The top candidate molecule was validated in cellular and animal preclinical models.

Results: Microdissected myofibre transcriptomic analysis revealed that upregulation of the proteasome pathway, prevailing in perifascicular myofibres, is a hallmark of DM. Immunostaining experiments conducted in a validation cohort showed that in patients with DM, β5i (encoded by PSMB8) was predominantly expressed in the cytoplasm of muscle fibres within the perifascicular region, which also predominantly expressed MxA and HLA-I. Experiments in human myotubes showed that interferon (IFN)-β enhances the expression of proteasome catalytic subunit β5i and chymotrypsin-like activity in myofibres. Computational drug repurposing analysis based on the DM perifascicular myofibre transcriptomic signature identified ixazomib (a proteasome inhibitor) as the drug with the highest therapeutic potential. In human myotubes, ixazomib prevented IFN-β-induced DM-like lesions (atrophy, major histocompatibility complex class I [MHC-I] expression and mitochondrial dysfunctions) without impacting the expression of interferon-

*Correspondence to Dr Margherita Giannini, Pr Alain Meyer.
E-mail addresses: gianninim@unistra.fr (M. Giannini), alain.meyer7@gmail.com (A. Meyer).
Handling editor Josef S. Smolen.
[#] These authors are equal contributed.

stimulated genes (ISGs). Moreover, experimental myositis (EM) mice treated with ixazomib recovered muscle strength and normalised serum creatine kinase levels. While ISG expression was unchanged in muscles of ixazomib-treated EM mice, sarcolemmal MHC-I expression was abolished, myofibre size variability was normalised, and inflammatory infiltrate was decreased. *Conclusions:* Enhanced proteasome activity in perifascicular myofibres is a hallmark of DM; its inhibition, deemed effective in preclinical models, may represent a new therapeutic strategy for this disease.

WHAT IS ALREADY KNOWN ON THIS TOPIC

- Dermatomyositis (DM) is defined by a specific alteration pattern of the perifascicular myofibres. However, the underlying mechanisms are unknown, and current treatments are empirical and only partially effective.

WHAT THIS STUDY ADDS

- Perifascicular muscle fibres in early DM are characterised by interferon-β-induced upregulation of the proteasome pathway that contributes to the other key characteristics of the disease (ie, major histocompatibility complex class I expression, mitochondrial dysfunctions, and atrophy of perifascicular fibres).
- Proteasome inhibitors, predicted *in silico* as candidate repurposed drugs based on this new insight, are effective in preclinical models of DM.

HOW THIS STUDY MIGHT AFFECT RESEARCH, PRACTICE OR POLICY

- These findings encourage future trials testing proteasome inhibition in patients with DM.

INTRODUCTION

Inflammatory myopathies (IMs) are a group of rare autoimmune diseases leading to muscle weakness, although the underlying mechanisms are not fully known. Dermatomyositis (DM) is the most frequent IM subset and induces the highest mortality rate [1]. At the myopathological level, DM is defined by specific alterations of perifascicular fibres, that include atrophy, expression of type I interferon (IFN-I)-stimulated genes (ISGs) and of the major histocompatibility complex class I (MHC-I), as well as mitochondrial dysfunctions [2]. Inflammatory infiltrates and capillary injuries are also present in the muscles of patients with DM. The prevalence and severity of these histological features vary according to the autoantibody status, indicating several DM subsets [3].

Current treatments, based on the empirical use of corticosteroids and immunomodulators, allow only a partial recovery and expose to numerous side effects and frequent relapses [4]. Hence, to identify new DM treatment strategies, the underlying mechanisms need to be unravelled.

There is evidence that muscle fibres play a direct role in DM pathophysiology. Indeed, DM muscle cells deliver an IFN-I autocrine effect [5] while mitochondrial dysfunctions in DM muscle fibres sustain inflammation [6]. Myofibre sarcolemmal MHC-I expression may contribute to the activation, expansion, and survival of CD8+ T cells [7]. Moreover, we have recently shown that the selective inactivation of the glucocorticoid receptor in muscle fibres suppresses the therapeutic response of glucocorticoids in experimental myositis (EM) [8]. Thus, targeting muscle fibres may represent a relevant therapeutic strategy for DM.

Bulk transcriptomic analysis has revealed that IFN-I signalling, pattern recognition receptors, dendritic cell maturation, and T-cell exhaustion signalling are higher in DM muscle

compared to other IM subsets [9,10]. However, these analyses did not identify molecular pathways specifically deregulated in myofibres (as opposed to the other components of the muscle cells), nor the mechanisms underpinning the distinctive changes in perifascicular muscle fibres in DM.

Only 2 studies have analysed microdissected DM muscle fibres with 1 highlighting a reduction in titin protein in DM perifascicular muscle fibres [11], while the second revealed increased expression of several interferonogenic pattern recognition receptors in MHC-I expressing DM muscle fibres [12]. Neither study used RNA-sequencing for their analysis.

To further unveil the deregulated pathways in DM perifascicular fibres, using RNA-sequencing, we established the transcriptome of laser capture microdissected peri- and endofascicular myofibres from early untreated patients with DM, patients with other IMs as well as individuals without neuromuscular disease (NMD). The resulting findings revealed molecular pathways that characterise DM perifascicular fibres and allowed the identification of repositionable molecules for DM treatment. The efficacy of the candidate drug with the highest therapeutic potential was validated in both cellular and animal preclinical models.

METHODS

Methods are detailed in the Supplementary material.

RESULTS

Proteasome pathway upregulation prevailing in perifascicular muscle fibres is a hallmark of DM

To unravel the molecular pathways underpinning perifascicular muscle fibre alterations in DM, we compared the transcriptome of microdissected deltoid perifascicular (n > 300) and endofascicular (n > 300) myofibres (Supplementary Fig S1) from 13 early (symptoms for less than 6 months) untreated patients with IM (DM: n = 7; IM other than DM: n = 6) and 5 patients without NMD, the characteristics of which are shown in Table 1.

Next-generation sequencing analysis revealed that 865 genes were differentially expressed among the perifascicular fibres of the 3 groups of patients (Fig 1A, left panel). Among the latter, 479 genes were selectively deregulated in patients with DM (Fig 1B, left panel). The levels of the top 15 deregulated genes in DM perifascicular fibres compared to no NMD perifascicular fibres are presented in Figure 1C (left panel) and D. The most differentially expressed transcript in the perifascicular fibres of patients with DM was PSMB8 (encoding the proteasome subunit beta type-8, which is responsible for the chymotrypsin-like activity of the immunoproteasome), whose expression was 47-fold higher than in the patients without NMD (P = 1.31E-21) and 3-fold higher than in the patients without DM IM (P = .008) (Fig 1C left panel, D). Genes coding for previously reported hallmark biomarkers of DM perifascicular fibres (ie, IFI6, ISG15, MHC-I subunits) were also found in this top list (Fig 1C left panel, D). The most deregulated pathway in DM

Patient	Age/sex	Muscle symptoms (wk)	CK (IU/L)	Autoantibodies	Extramuscular involvement
DM 1	57/M	8	696	None	DM skin rash
DM 2	51/F	24	1700	Anti-Mi2β	Dysphagia
DM 3	42/F	18	4700	Anti-Mi2β	DM skin rash + polyarthritis
DM 4	54/F	3	16,616	Anti-Mi2β	None
DM 5	65/F	12	1420	None	DM skin rash
DM 6	76/F	17	154	Anti-TIF1γ	DM skin rash + ILD
DM 7	26/F	12	NA	Anti-TIF1γ	DM skin rash
Other IM 1 (IMNM)	61/F	13	1490	Anti-SRP	None
Other IM 2 (IBM)	80/M	24	292	None	None
Other IM 3 (IMNM)	75/F	24	1135	None	Dysphagia
Other IM 4 (IMNM)	27/F	4	11,139	None	Dysphagia
Other IM 5 (IMNM/ scleromyositis)	60/F	24	391	None	Dysphagia, myocarditis, Raynaud's phenomenon, scleroderma pattern on capillaroscopy
Other IM 6 (IMNM)	52/M	13	4843	Anti-SRP	None
No NMD 1	56/F	None	112	None	None
No NMD 2	47/M	None	77	None	None
No NMD 3	51/F	None	66	None	None
No NMD 4	42/F	None	125	None	None
No NMD 5	43/F	None	63	None	None

CK, creatine kinase blood level at the time of muscle biopsy; DM, dermatomyositis; F, female; IBM, inclusion body myositis; ILD, interstitial lung disease; IM, inflammatory myopathy; IMNM, immune-mediated necrotising myopathy; IU, international unit; M, male; NA, not applicable; NMD, neuromuscular disorder.
No patient was treated with glucocorticoids or immunosuppressants. Anti-SSA, -SSB, -U1-RNP, -Scl70, -centromere, -Mi2β, -TIF1γ, -SAE1, -SAE2, -MDA5, -NXP2, -Jo-1, PL-7, -PL-12, -EJ, -OJ, -Zo, -SRP, and -HMGCR antibodies were investigated using D-Tek line immunoassay; anti-cN1A were investigated using Euroimmun line immunoassay.

perifascicular muscle fibres (compared to individuals without NMD and other patients with IM) was proteasome ($P = 9.23E−6$), followed by antiviral response (human papillomavirus infection pathway) ($P = 1.87E−4$) (Fig 1E left panel).

A fewer number of genes (n = 566) were differentially expressed between the endofascicular fibres of the 3 groups of patients (Fig 1A right panel). Of the latter, 218 genes were selectively deregulated in patients with DM (Fig 1B right panel), 113 (51%) of which were also selectively deregulated in the perifascicular fibres of this group (Supplementary Fig S2A). The levels of the top 15 deregulated genes in DM endofascicular fibres are shown in Figure 1C right panel. Among these 15 genes, 6 (40%) were shared with the top 15 deregulated genes in the perifascicular fibres of this group (Supplementary Fig S2B). However, the extent of the deregulation of these genes was lower in the endofascicular fibres compared to the perifascicular fibres (Fig 1D). The most differentially expressed transcript in the endofascicular fibres of patients with DM compared to patients without NMD was PSMB8, although the overexpression of this transcript was approximately 3-fold lower than in the perifascicular fibres (Fig 1C right panel, D). Similarly to the perifascicular fibres, the most deregulated pathway in DM endofascicular muscle fibres (compared to individuals without NMD and other patients with IM) was proteasome, followed by antiviral response (hepatitis C pathway), although the weight of these 2 pathways (P value) was lower in the endofascicular vs the perifascicular fibres (6.31E−4 and 0.0058, respectively, Fig 1E right panel).

To validate transcriptomic findings from microdissected fibres in the discovery cohort, we performed immunostaining experiments in an independent validation cohort (Table 2). In patients with DM, β5i (encoded by PSMB8) was predominantly expressed in the cytoplasm of perifascicular muscle fibres, colocalising with MxA and MHC-I. In contrast, β5i expression was: i) confined to a few MxA-positive fibres in antisynthetase syndrome (ASyS) and scleromyositis (SM), ii) limited to inflammatory cells and rare fibres in inclusion body myositis (IBM), iii)

absent in immune-mediated necrotising myopathy (IMNM), and non-NMD subjects (Fig 1F).

Taken together, these data highlight that the enhanced proteasome pathway, prevailing in perifascicular muscle fibres, is a hallmark of DM.

In early untreated patients with DM, the physiological transcriptomic signature of perifascicular muscle fibres is replaced by a pathological signature characterised by proteasome dysregulation

There are very few data regarding the physiological differences between muscle fibres according to their spatial location within the muscle fascicules. In addition to previously reported biomarkers of DM, PSMB8 expression prevailed in DM perifascicular fibres, but was also observed in DM endofascicular fibres. Thus, to further determine the molecular differences between endo- and perifascicular fibres in physiological conditions and in IM, the transcriptome of paired perifascicular and endofascicular fibres was compared in each of the 3 groups (Fig 2A). In patients without NMD, 83 genes were upregulated and 54 downregulated in perifascicular fibres compared to the endofascicular fibres (Supplementary Fig S3A). Pathway analyses revealed that these genes were mainly related to muscle tissue development and the generation of precursor metabolites as well as energy signalling pathways (Supplementary Fig S3B). The levels of the top 15 differentially expressed genes are presented in Supplementary Figure S3C. Of note, physiological PSMB8 expression was 2.1-fold lower in perifascicular fibres compared to the endofascicular fibres ($P = .0001$) (Supplementary Fig S4). In patients with IM, this transcriptomic signature of the perifascicular fibres was lost, and replaced by a specific perifascicular signature consisting of 18 overexpressed and 10 underexpressed genes (Fig 2A,B), mainly involved proteasome, mitophagy, mitochondrial functioning, and antiviral response pathways (Fig 2B).
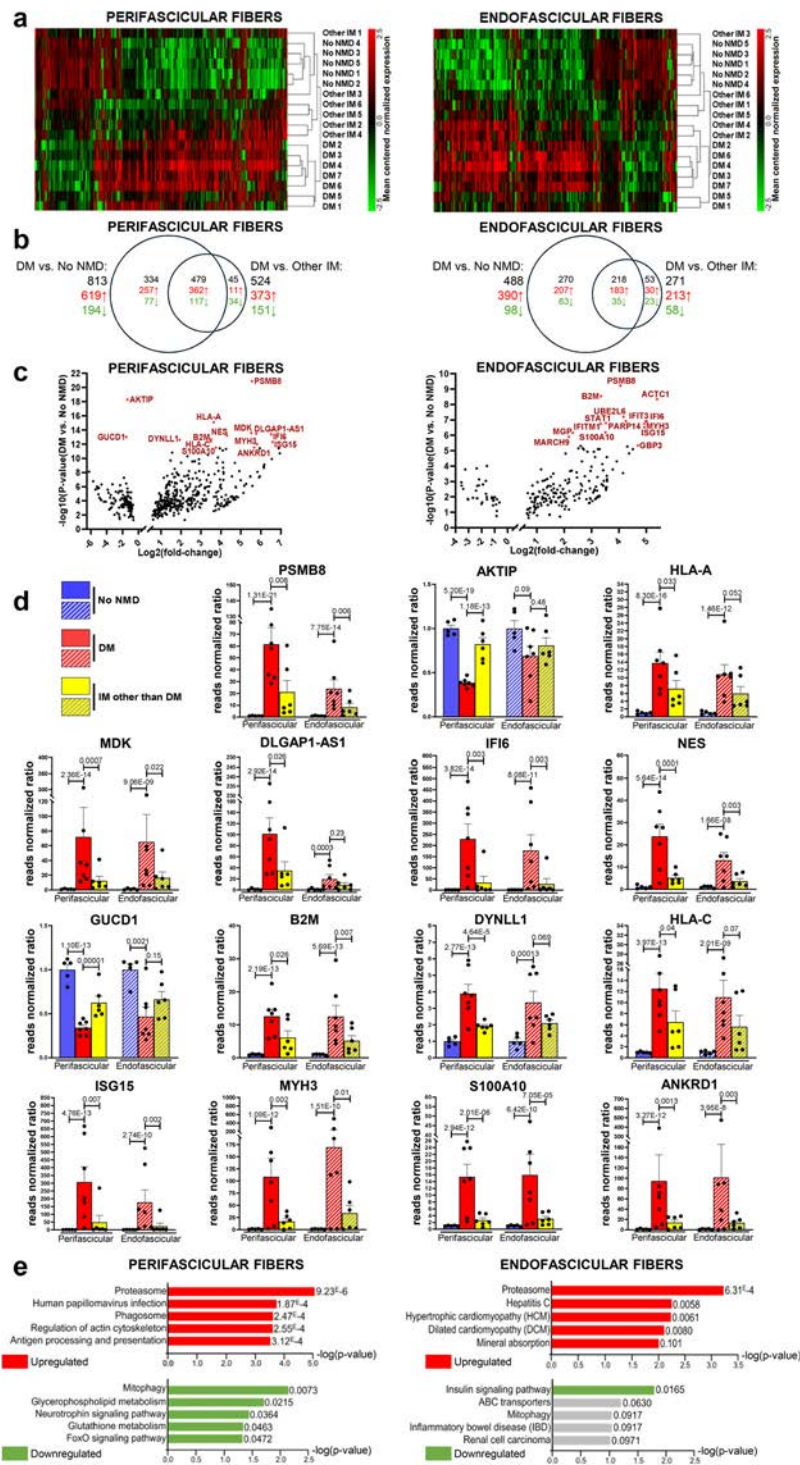
Figure 1. Deregulation of the proteasome pathway in muscle fibres is a hallmark of early untreated dermatomyositis (DM). (A) Heatmaps depicting the mean-centred normalised expression of differentially expressed genes (adj. $P < .05$) in perifascicular (n = 865) and endofascicular (n = 566) fibres of the deltoid muscles from patients with DM (n = 7), inflammatory myopathies (IMs) other than DM (n = 6), and without neuromuscular disease (NMD) (n = 5). (B) Venn diagram representation of the number of genes deregulated (P value <0.05 and $|\log_2 (\text{fold-change})| > \log_2(1.5)$) in perifascicular and endofascicular fibres of patients with DM (compared to other patients with IM and patients without NMD). (C) Volcano plot of the genes deregulated in DM perifascicular and endofascicular fibres compared to patients without NMD. The 15 most deregulated genes (according to P value; P value <.05 and $|\log_2 (\text{fold-change})| > \log_2(1.5)$) in DM perifascicular and endofascicular fibres are indicated in red. (D) Expression of the 15 most deregulated genes in DM perifascicular fibres (according to P value; P value <.05 and $|\log_2 (\text{fold-change})| > \log_2(1.5)$). The expression of each gene (normalised reads) is represented as the ratio between patients with IM and patients without NMD. Data are expressed as the mean + SEM. (E) Specifically deregulated pathways (upregulated [red] and downregulated [green]) in perifascicular and endofascicular fibres of patients with DM (compared to other patients with IM and patients without NMD). (F) Representative figures of immunostaining for β5i, MxA, MHC-I, and MHC-II in muscle from DM, antisynthetase syndrome (ASyS), scleromyositis (SM), immune-mediated necrotising myopathy (IMNM), inclusion body myositis (IBM), and patients without NMD. Black arrows indicate PSMB8 and MxA-positive fibres. Black arrowheads indicate PSMB8 and MxA-positive inflammatory cells. Scale bar: 100 μm. MHC-I, major histocompatibility complex class I.

IFN-β enhances myofibre expression of the proteasome catalytic subunit β5i and chymotrypsin-like activity

The IFN-I signature is an established hallmark of DM muscle fibres [9]. The present analysis revealed that proteasome upregulation represents an additional characteristic of DM perifascicular muscle fibres and a potential therapeutic target. The proteasome harbours 6 catalytic subunits in its catalytic core (20S), 3 of which are constitutive (β5, β1, and β2, respectively encoded by PSMB5, PSMB6, and PSMB7 and carrying the chymotrypsin-like, caspase-like, and trypsin-like activity, respectively) and 3 are inducible (β5i, β1i, and β2i, respectively encoded by PSMB8, PSMB9, and PSMB10 and carrying the same activities as the constitutive catalytic subunits) in inflammatory conditions (immunoproteasome) [13,14] (Fig 3A). The

proteasome also involves regulatory subunits PSMF1 (encoded by PI31) and the proteasome maturation protein (encoded by POMP) [13,14]. The expression and activity of each catalytic subunit of the 20S proteasome and their respective association with type I IFN signalling were hence studied in DM muscle fibres. PSMB8 was the most highly differentially expressed proteasome subunit in DM fibres (Fig 3A). Expression of the 2 other inducible subunits (β1i and β2i) and 1 of the constitutive subunits (β2) was increased, albeit to a much lesser extent (Fig 3A, Table 3). Transcript levels of genes encoding these subunits positively correlated with the expression of ISG15 in DM muscle fibres (R^2 from 0.36 to 0.51, $P < .05$) (Fig 3B). In contrast, the transcript levels of PSMF1, encoding the endogenous proteasome inhibitor PI31, were decreased in DM muscle fibres (1.2-fold vs no NMD in perifascicular fibres, $P = .042$ and 1.03-fold
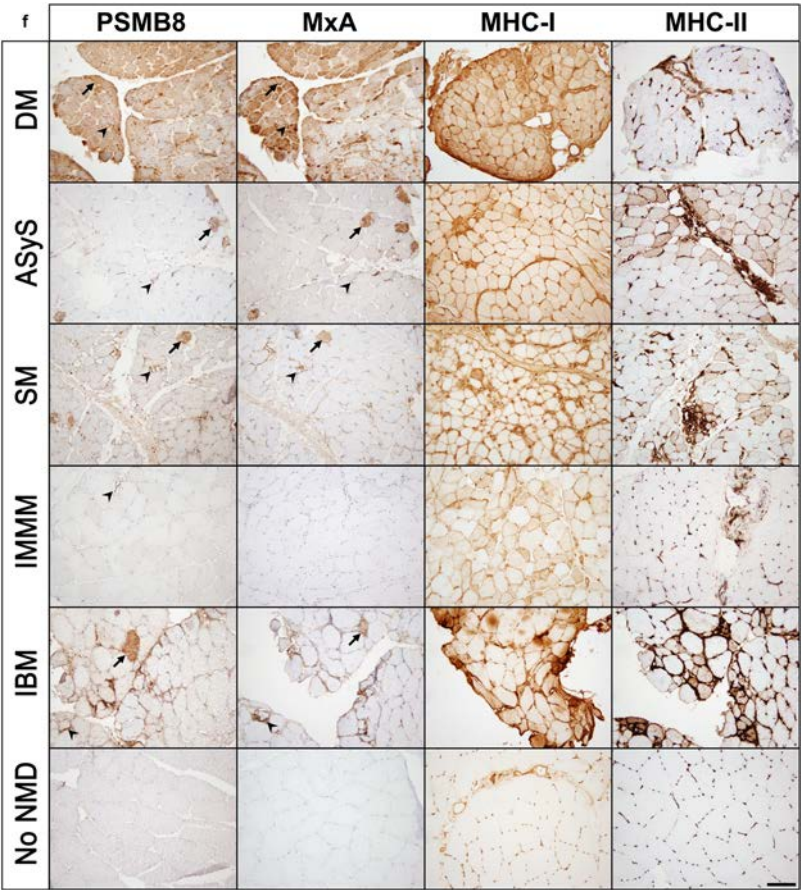
Figure 1. Continued.

in endofascicular fibres, $P = .792$) and negatively correlated with type I ISGs (R^2 from 0.36 to 0.51, $P < .05$) (Table 3).

IFN-β levels are known to be increased in the blood of patients with DM compared to patients without NMD and to patients with IM other than DM [15,16], and IFN-β-treated myotubes recapitulate *in vitro* the canonical characteristics of DM perifascicular muscle fibres (ie, IFN-I signature, MHC-I expression, mitochondrial dysfunctions, and atrophy) [6,10,17,18].

In a series of experiments designed to determine whether IFN-β stimulates the expression of proteasome subunits that is increased in DM muscle fibres, 5-day treatment of human myotubes with IFN-β (500 U/mL) was found to increase β5i subunit (PSMB8) protein levels by 5.6-fold (Fig 3C,D). In addition, IFN-β also induced proteasome chymotrypsin-like activity in human myotubes in a dose-dependent manner (Fig 3E).

Altogether, these results indicate that IFN-β, whose level is selectively increased in DM, contributes to the increased expression of catalytic proteasome subunits (mainly β5i) and chymotrypsin-like activity in DM muscle fibres.

In DM perifascicular muscle fibres, PSMB8 expression is mediated by type I IFN

Type I and type II IFNs exhibit partially overlapping transcriptional signatures [19]. While PSMB8 has been reported to be induced by both IFN types [20−25], MxA is primarily induced by type I IFNs, whereas major histocompatibility complex class II (MHC-II) is upregulated by type II IFNs [9,26]. Both IFN-I and IFN-II are elevated in the blood of patients with DM [16], but only type I ISGs and proteins (MxA)—and not type II

(MHC-II)—are detected in perifascicular fibres (Fig 1F, Supplementary Fig S5). To further investigate the relative contribution of each IFN type to PSMB8 expression in DM perifascicular fibres (Fig 4A), we assessed the ability of IFN-β (type I) and IFN-γ (type II) to induce PSMB8, in parallel with canonical IFNs response markers, MxA and MHC-II.

We queried the Interferome database, which compiles transcriptomic data from various cell types exposed to IFNs [27]. In agreement with previous reports [28,29], IFN-β preferentially upregulated MxA, whereas IFN-γ induced MHC-II levels. In addition, both IFN-β and IFN-γ had a similar potency to induce PSMB8 expression (Fig 4B). These results support that while PSMB8 is inducible by both IFN types, MxA and MHC-II are biomarkers of IFN-β and IFN-γ, respectively. Given that Interferome does not include transcriptomic datasets from skeletal muscle, we next assessed the expression of PSMB8, MxA, and MHC-II in human myotubes treated with IFN-β (500 U/mL) or IFN-γ (500 U/mL). In line with the *in silico* results, IFN-β and IFN-γ both induced PSMB8 transcript levels (Fig 4C) and chymotrypsin-like activity of the proteasome (Supplementary Fig S6A,B). In contrast, MxA, a hallmark of DM perifascicular fibres, was preferentially induced by IFN-β, while MHC-II expression, a hallmark of non-DM IM, was preferentially induced by IFN-γ (Fig 4C). These results indicate that PSMB8 expression in perifascicular fibres of DM is mediated by IFN-β rather than IFN-γ.

Proteasome inhibitors are repurposed candidate drugs for DM

To identify currently available candidate drugs targeting the molecular pathways underpinning perifascicular muscle fibres

Table 2

Individual characteristics of PSMB8 and MxA immunostainings in myofibres and immune cells of patients with inflammatory myopathies and without neuromuscular diseases

				PSMB8 positivity	
N	Sex/age (y)	IM-specific autoantibody	Diagnosis	Fibres	Immune cells
1	M, 39	Anti-NXP2	DM	Perif > endof	+
2[a]	F, 20	None	DM	Perif > endof	+
3	M, 71	Anti-TIF1γ	DM	Perif	−
4	F, 60	Anti-MDA5	DM	Perif > endof	+
5	F, 39	Anti-SAE1/2	DM	Perif > endof	+
6	F, 54	Anti-MI2ß	DM	Perif > endof	+
7[a]	F, 44	Anti-Jo-1	ASyS	Patchy	+
8	F, 73	Anti-PL-7	ASyS	Patchy	+
9	F, 46	Anti-Jo-1	ASyS	Patchy	+
10	F, 64	Anti-U1-RNP	SM	Patchy	+
11	F, 49	Anti-U1-RNP	SM	Patchy	+
12[a]	F, 27	Anti-U1-RNP	SM	Patchy	+
13[a]	M, 60	None	IMNM	−	+
14	F, 47	Anti-SRP	IMNM	−	+
15	M, 48	None	IMNM	−	+
16	M, 73	None	IBM	−	+
17	F, 49	Anti-cN1A	IBM	−	+
18[a]	M, 64	Anti-cN1A	IBM	Rare	+
19	M, 57	None	no NMD	−	−
20	M, 59	None	no NMD	−	−
21	F, 45	None	no NMD	−	−

ASyS, antisynthetase syndrome; DM, dermatomyositis; Endof, endofascicular fibres; IBM, inclusion body myositis; IM, inflammatory myopathy; IMNM, immune-mediated necrotising myopathy; NMD, neuromuscular disorder; Perif, perifascicular fibres; SM, scleromyositis.
No patient was treated with glucocorticoids or immunosuppressants. Anti-SSA, -SSB, -U1-RNP, -Scl70, -centromere, -Mi2β, -TIF1γ, -SAE1, -SAE2, -MDA5, -NXP2, -Jo-1, PL-7, -PL-12, -EJ, -OJ, -Zo, -SRP, and -HMGCR antibodies were investigated using D-Tek line immunoassay; anti-cN1A were investigated using Euroimmun line immunoassay.
[a] Patients whom representative pictures have been provided in Figure 1.

alterations in DM, the transcriptomic signature of DM perifascicular fibres (28 genes involved in proteasome, mitophagy, mitochondrial functioning, and antiviral response pathways, Fig 2B) was used for computational drug repurposing analysis, as described by Karatzas et al [30]. Nine chemical compounds were identified by at least 2 tools, with a predictive score <-50, thus possibly reversing the transcriptomic signature observed in DM perifascicular muscle fibres (Fig 5A,B). Among these, prednisolone (the current standard of care in DM treatment [4]), and a Janus kinase (JAK) inhibitor (a drug class for which case reports and series indicate efficacy in patients with DM) were highlighted, supporting the validity of this analysis. However, the drug with the highest predicted therapeutic potential was ixazomib, an inhibitor of the chymotrypsin-like activity of the constitutive catalytic subunits and the immunoproteasomes. An additional proteasome inhibitor, MG-132, was also identified with a high therapeutic score, which further reinforced the probability that targeting the chymotrypsin-like activity of the proteasome may constitute an effective therapeutic strategy for patients with DM.

These results indicate that targeting proteasome hyperactivity in DM perifascicular fibres is a potential innovative therapeutic strategy.

Proteasome inhibition is effective in an in vitro model of DM

To validate the *in silico* drug repurposing prediction gained from patients' muscle biopsies, and to investigate the link between high blood IFN-β, canonical DM perifascicular fibre lesions (atrophy, mitochondrial dysfunction, IFN-I signature, and MHC-I expression) and proteasome pathway upregulation,

IFN-β (500 U/mL)-treated human myotubes were cultured in the presence of ixazomib (40 nM added from day 2 to day 5 of IFN-β treatment) (Fig 6A).

As expected, ixazomib normalised chymotrypsin-like activity in IFN-β-treated myotubes (Fig 6B). Ixazomib prevented the IFN-β-mediated 40% reduction in myotube diameter (Fig 6C) as well as the 54% reduction in maximal mitochondrial respiration (Vmax) (Fig 6D).

Ixazomib treatment also reduced the IFN-β-induced expression of the MHC-I-protein (Fig 6E). By contrast, the 12.5-fold increase in IFN-β-induced ISG15 transcript levels was only partially mitigated by ixazomib (9-fold increase vs control) (Fig 6F). A similar partial effect of ixazomib was observed on other ISG (ie, IFIT3, IFI44, RSAD2, and IFIT 27) (Fig 6F).

Hence, proteasome inhibition prevents IFN-β-induced atrophy, mitochondrial dysfunction, and MHC-I without significantly impacting ISG expression in human myotubes indicating that proteasome mediates IFN-β-induced myotoxicity, downstream of the ISG activation.

We observed that, in DM perifascicular fibres, enhanced PSMB8 expression is mediated by IFN-β, rather than by IFN-γ. Accordingly, IFN-γ-treated myotubes have previously been used as an *in vitro* model of non-DM [29]. In human myotubes treated with IFN-γ (500 U/mL), other key features of DM perifascicular muscle fibres, such as atrophy, mitochondrial dysfunction, MHC-I expression, and the expression of ISGs other than MxA, were less prominent than in IFN-β-treated myotubes (Supplementary Fig S6A-F). To test the specificity of the therapeutic effect of proteasome inhibition on the myopathic actions of IFN-β, we repeated the *in vitro* experiment described above
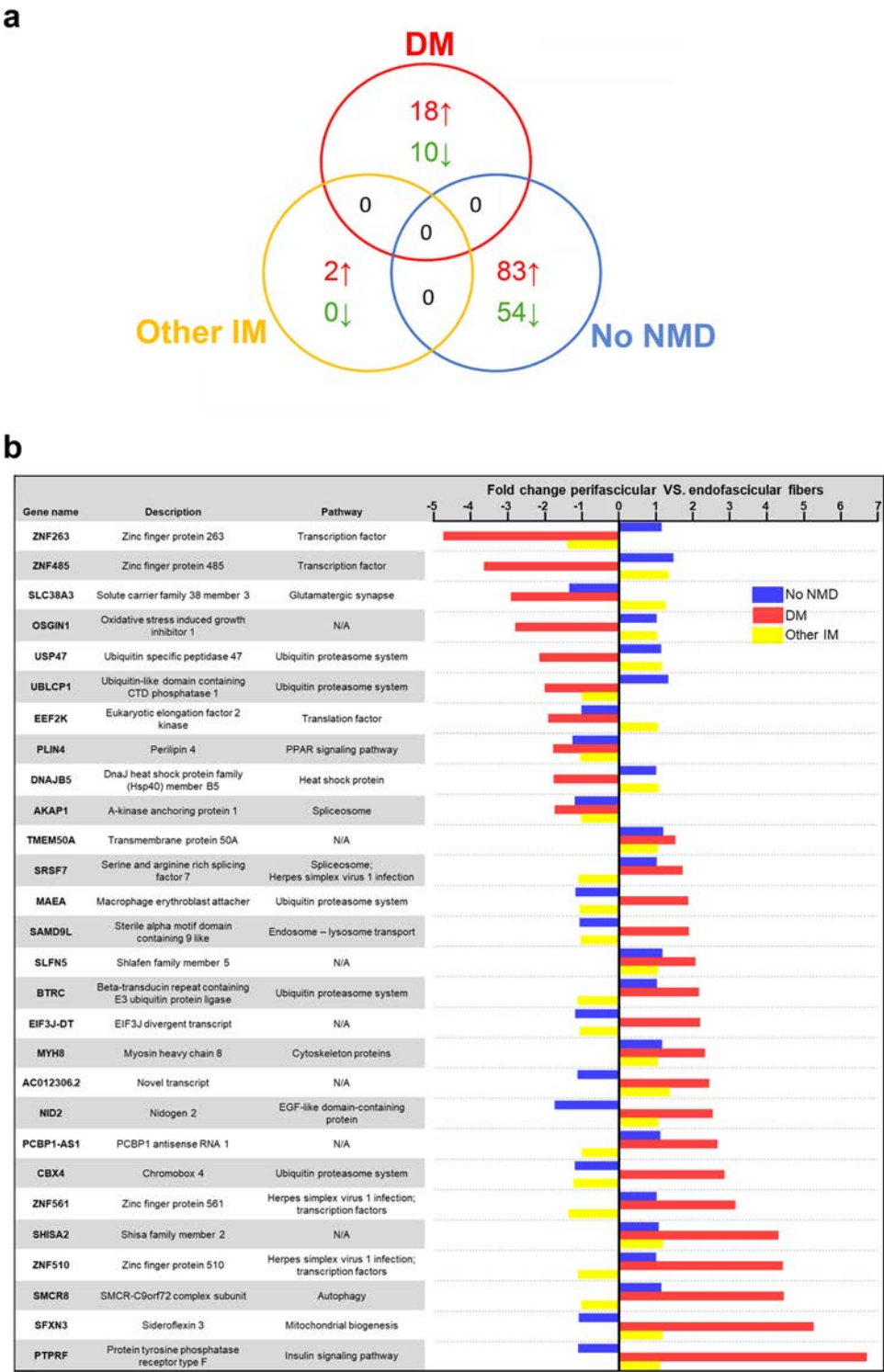
Figure 2. The transcriptomic signature of perifascicular muscle fibres is lost in early untreated patients with inflammatory myopathies (IMs) and replaced by a pathological signature in patients with dermatomyositis (DM). (A) Venn diagram of differently expressed genes (adj. $P < .05$ and $|\log_2$ (fold-change)$| > \log_2(1.5)$) between peri- and endofascicular fibres of the deltoid muscles from DM (n = 7), IM other than DM (n = 6), and patients without neuromuscular disease (NMD) (n = 5). (B) List of the 28 differentially expressed genes (adj. $P < .05$ and $|\log_2$ (fold-change)$| > \log_2(1.5)$) between peri- and endofascicular fibres of the deltoid muscles from patients with DM. Bar charts indicate fold change for DM (red), other IM (yellow), and no NMD (blue).

using human myotubes treated with IFN-γ (500 U/mL). Ixazomib normalised chymotrypsin-like activity in IFN-γ-treated myotubes, but did not reverse atrophy and mitochondrial dysfunction (Supplementary Fig S6B-D). Thus, unlike IFN-β, the myopathic effects of IFN-γ are independent of proteasome activation.

Proteasome inhibition is effective in an in vivo model of myositis

There is currently no animal model fully mimicking DM. However, we previously generated an EM model [31], representing an optimised version of C-protein-induced myositis [32] and shown to recapitulate key characteristics of DM (Fig 7A),
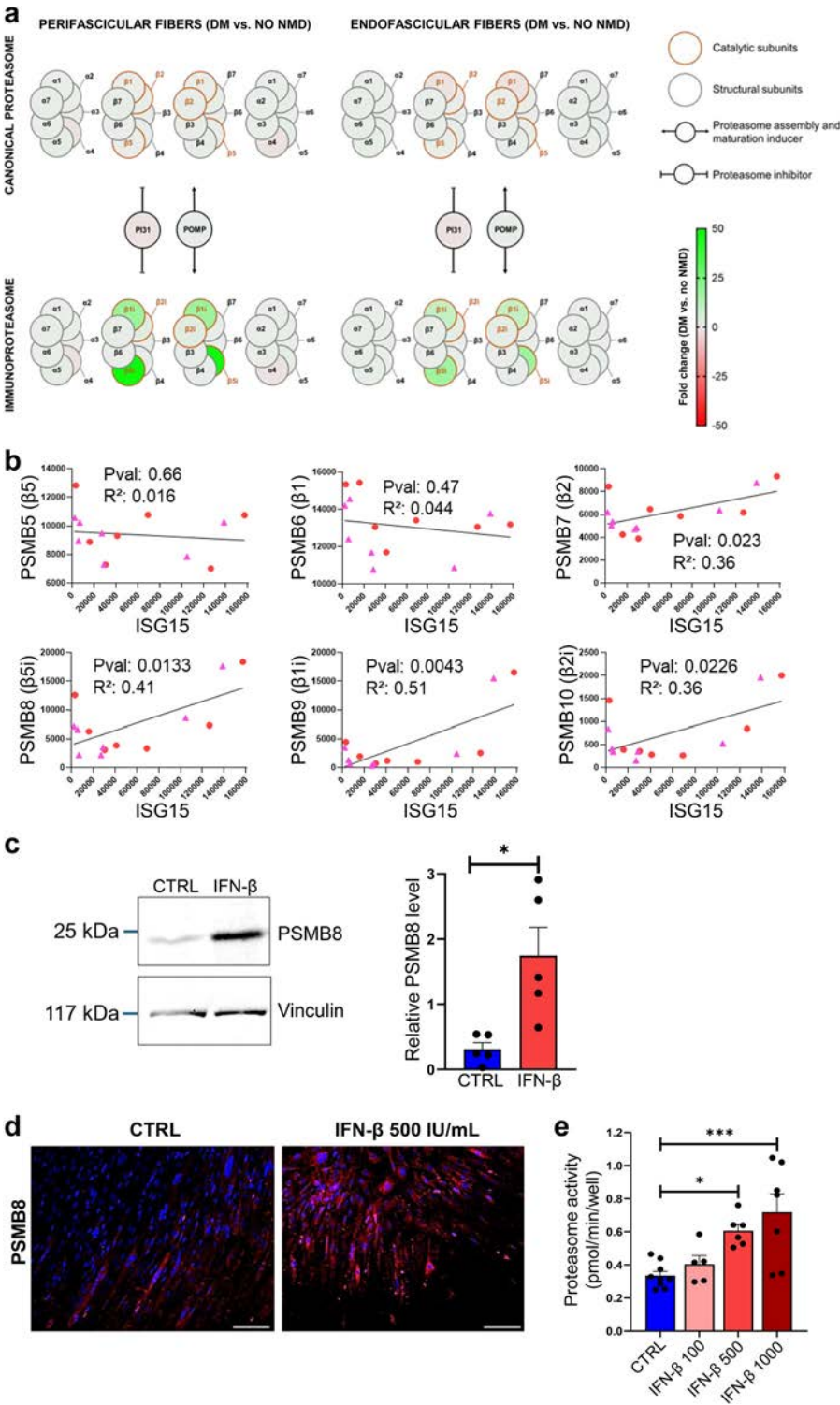
Figure 3. Interferon (IFN)-β enhances expression of proteasome catalytic subunit β5i and chymotrypsin-like activity in myofibres. (A) Heatmap depicting the expression of genes encoding the 20S proteasome and immunoproteasome subunit in perifascicular and endofascicular fibres of dermatomyositis (DM) compared to patients without neuromuscular disease (NMD). (B) Correlation between the expression of ISG15 and genes coding for proteasome catalytic subunits of the constitutive (PSMB5, PSMB6, PSMB7) and the immunoproteasome (PSMB8, PSMB9, PSMB10) in perifascicular (red circle) and endofascicular (pink triangle) DM fibres. (C) Representative immunoblot and quantification of proteasome β5i subunits (encoded by PSMB8) protein expression in human myotubes treated with IFN-β (500 U/mL) or vehicle (control, CTRL) for 5 days. n $\geq$ 4 for each condition. *: $P < .05$. (D) Representative immunostaining of PSMB8 expression in human myotubes treated with IFN-β (500 U/ml) or vehicle (control, CTRL) for 5 days. Scale bar: 100 µm. (E) Chymotrypsin-like activity in human myotubes treated with IFN-β (100 U/mL, 500 U/mL or 1000 U/mL) or vehicle (control, CTRL) for 5 days. Data are expressed as mean + SEM. *$P < .05$, ***$P < .001$. ISG, interferon-stimulated gene; POMP, proteasome maturation protein; PSMF1, proteasome inhibitor PI31 subunit.

including muscle weakness, elevated serum creatine kinase (CK) levels, muscle fibres atrophy, sarcolemmal MHC-I expression, elevated expression of several ISG and inflammatory infiltrate in the muscle [31] (Fig 7B-H, Supplementary Fig S7). Importantly, PSMB8 transcript levels (Fig 7I) and chymotrypsin-like activity (Fig 7J) were also increased in muscles of EM mice. Thus, the EM model enables further exploration *in vivo* of the potential effect of proteasome inhibition in DM at a preclinical stage.

Given that EM muscle defects are maximal from day 14 (D14) to day 21 (D21) after immunisation, we subsequently explored the therapeutic potential of proteasome inhibition using a single dose of ixazomib (5 mg/kg) [33,34] vs vehicle

only administered by gavage at D14 (Fig 7A). Ixazomib reduced chymotrypsin-like activity at D21 in gastrocnemius muscles of EM mice (Fig 7J). Moreover, ixazomib-treated EM mice normalised muscle strength and CK serum levels at D21 (Fig 7B,C). In agreement with the *in vitro* data, myofibre sarcolemmal MHC-I expression in ixazomib-treated EM mice was abolished (Fig 7F), fibre size variability was normalised (Fig 7D), and inflammatory infiltrates decreased (Fig 7H), while muscle IFIT3 expression remained high (Fig 7G). Taken together, these results show that proteasome inhibition is an effective therapeutic strategy in an *in vivo* preclinical model of DM.

Table 3

Genes encoding the proteasome subunits in dermatomyositis perifascicular and endofascicular fibres compared to patients without neuromuscular disease and their correlation with ISG15 expression in DM

Gene name	Protein	DM perif. vs no NMD perif.			DM endo. vs no NMD endo.			Correlation with ISG15 expression
		Fold change	*P* value	Adj. *P* value	Fold change	*P* value	Adj. *P* value	
PSMD3	26S proteasome regulatory subunit RPN3	−1.14	.461	.744	−1.01	.909	.974	R²: 0.00028 P val: .9549
PSMD9	26S proteasome regulatory subunit p27	1.18	.324	.631	−1.10	.612	.849	R²: 0.4501 P val: .0086
PSMD12	26S proteasome regulatory subunit RPN5	1.23	.227	.532	1.16	.229	.581	R²: 0.04923 P val: .4459
PSMD11	26S proteasome regulatory subunit RPN6	1.17	.382	.683	1.10	.528	.803	R²: 0.5294 P val: .0032
PSMD6	26S proteasome regulatory subunit RPN7	1.18	.191	.488	1.22	.046	.273	R²: 0.0002 P val: .9605
PSMD7	26S proteasome regulatory subunit RPN8	1.31	.081	.318	1.23	.255	.606	R²: 0.5513 P val: .0024
PSMD13	26S proteasome regulatory subunit RPN9	−1.11	.561	.807	1.07	.559	.823	R²: 0.01682 P val: .6586
PSMD14	26S proteasome regulatory subunit RPN11	−1.13	.660	.861	1.27	.118	.433	R²: 0.0053 P val: .804
PSMD8	26S proteasome regulatory subunit RPN12	1.62	.014	.112	1.37	.069	.332	R²: 0.0016 P val: .893
SHFM1	26S proteasome complex subunit SEM1	1.86	.014	.113	1.35	.111	.422	R²: 0.0437 P val: .476
PSMD4	26S proteasome regulatory subunit RPN10	1.09	.536	.791	1.00	.947	.986	R²: 0.1984 P val: .1105
PSMD2	26S proteasome regulatory subunit RPN1	−1.30	.073	.301	−1.29	.122	.441	R²: 0.2218 P val: .0891
PSMD1	26S proteasome regulatory subunit RPN2	−1.01	.937	.981	−1.05	.774	.925	R²: 0.1248 P val: .2153
ADRM1	Proteasome regulatory particle non-ATPase 13 (RPN13)	−1.02	.868	.955	−1.01	.930	.979	R²: 0.0014 P val: .8959
PSMC2	26S proteasome AAA-ATPase subunit RPT1	1.04	.812	.930	1.23	.075	.344	R²: 0.1389 P val: .1895
PSMC1	26S proteasome AAA-ATPase subunit RPT2	1.06	.755	.906	−1.01	.940	.984	R²: 0.2092 P val: .1001
PSMC5	26S proteasome AAA-ATPase subunit RPT6	−1.00	.982	.996	1.00	.943	.984	R²: 0.1279 P val: .2093
PSMC6	26S proteasome AAA-ATPase subunit RPT4	1.04	.826	.935	1.34	.012	.126	R²: 0.0014 P val: .8994
PSMC3	26S proteasome AAA-ATPase subunit RPT5	−1.05	.576	.816	−1.08	.364	.698	R²: 0.0265 P val: .5784
PSMC4	26S proteasome AAA-ATPase subunit RPT3	1.38	.054	.254	1.38	.035	.235	R²: 0.6509 P val: .0005
PSME1	PA28α (Proteasome activator complex subunit 1)	5.02	4.60E−11	3.01E−08	4.13	4.17E−08	1.55E−05	R²: 0.2128 P val: .0969
PSME2	PA28β (Proteasome activator complex subunit 2)	10.16	2.92E−11	1.99E−08	8.49	2.76E−08	1.17E−05	R²: 0.3579 P val: .0238
PSME3	PA28γ (Proteasome activator complex subunit 3)	−1.09	.688	.874	1.44	.007	.093	R²: 0.128 P val: .2091
PSME4	PA200 (Proteasome activator complex subunit 4)	1.18	.566	.809	1.14	.584	.835	R²: 0.0028 P val: .8558
PSMA6	Proteasome subunit α1	1.38	.147	.428	1.24	.193	.542	R²: 0.6617 P val: .0004
PSMA2	Proteasome subunit α2	1.01	.938	.981	1.09	.561	.824	R²: 0.1182 P val: .2288
PSMA4	Proteasome subunit α3	1.22	.174	.463	1.48	.010	.115	R²: 0.4151 P val: .0129
PSMA5	Proteasome subunit α5	2.27	8.06E−05	.003	1.92	.001	.034	R²: 0.4742 P val: .065
PSMA1	Proteasome subunit α6	1.20	.329	.635	1.53	.006	.085	R²: 0.097 P val: .2784
PSMA3	Proteasome subunit α7	1.52	1.61E−04	.005	1.62	4.40E−07	1.11E−04	R²: 0.1721 P val: .1402
PSMB6	Proteasome subunit β1	1.09	.538	.792	−1.06	.598	.842	R²: 0.0437 P val: .473
PSMB7	Proteasome subunit β2	1.48	5.85E−04	.013	1.37	.006	.080	R²: 0.3619 P val: .0229

(continued)

Table 3 (*Continued*)

Gene name	Protein	DM perif. vs no NMD perif.			DM endo. vs no NMD endo.			Correlation with ISG15 expression
		Fold change	*P* value	Adj. *P* value	Fold change	*P* value	Adj. *P* value	
PSMB3	Proteasome subunit β3	1.47	.006	.068	1.19	.130	.456	R²: 0.0848 *P* val: .3123
PSMB2	Proteasome subunit β4	1.49	.013	.107	1.56	.007	.092	R²: 0.4825 *P* val: .0058
PSMB5	Proteasome subunit β5	1.07	.520	.781	1.07	.520	.799	R²: 0.0162 *P* val: .6644
PSMB1	Proteasome subunit β6	1.23	.278	.588	1.04	.695	.889	R²: 0.1423 *P* val: .1836
PSMB4	Proteasome subunit β7	1.74	.005	.056	1.22	.130	.456	R²: 0.4243 *P* val: .0116
PSMB9	Proteasome subunit β1i	17.16	3.82E−10	1.66E−07	9.29	3.62E−06	5.12E−04	R²: 0.5061 *P* val: .0043
PSMB10	Proteasome subunit β2i	3.00	2.46E−04	.007	2.15	.015	.146	R²: 0.3629 *P* val: .0226
PSMB8	Proteasome subunit β5i	47.14	1.31E−21	2.22E−17	16.64	7.75E−14	5.92E−10	R²: 0.4121 *P* val: .0133
PSMF1	Proteasome inhibitor PI31 subunit	−1.20	.003	.042	−1.03	.792	.932	R²: 0.0588 *P* val: .4037
POMP	Proteasome maturation protein	1.49	.006	.065	1.12	.485	.779	R²: 0.1984 *P* val: .1105

DM, dermatomyositis; endo., endofascicular; NMD, neuromuscular disorder; perif., perifascicular.

R^2 value: coefficient of determination.

DISCUSSION

The lack of knowledge regarding the molecular mechanisms underpinning perifascicular fibre abnormalities in DM limits the development of treatments targeting the pathomechanisms of this disease.

We show herein that IFN-β-induced upregulation of the proteasome pathway in perifascicular muscle fibres is an early hallmark of DM that contributes to certain other key characteristics of the disease, including MHC-I expression, mitochondrial dysfunctions and perifascicular fibre atrophy. In keeping with both the role of IFN-I in DM [11,15] and the regulation of the proteasome expression [24], we found that PSMB8 is the most upregulated proteasome subunit in the perifascicular fibres of patients with DM. In addition, proteasome inhibitors, predicted *in silico* as candidate repurposed drugs based on this new insight, were observed to be effective in preclinical models of DM.

Bulk analysis has previously shown an increased expression of PSMB8 and chymotrypsin-like activity in the muscle of patients with DM as well as in other IM subtypes, mainly in IBM and ASyS, and to a lesser extent in IMNM [35,36]. Muscle β5i immunostaining has suggested that, in contrast to non-DM IM, enhanced proteasome expression and chymotrypsin-like activity in DM are prevalent in perifascicular fibres, although such activity has not been systematically assessed [35]. Our findings, based on an unbiased RNA-sequencing analysis of microdissected fibres, validated at the protein level in an independent cohort spanning all IM subtypes, confirm and expand these previous reports. The analyses were performed in untreated, early patients with DM (symptom duration <6 months). In muscle fibres, proteasome subunits overexpression colocalised with, and positively correlated to, the type I IFN signature. Moreover, IFN-β enhanced proteasome activity in human myotubes. Altogether, these findings indicate that increased proteasome activation in perifascicular fibres of patients with DM is associated with disease activity. These results pave the way for future studies aimed at assessing the sensitivity and specificity of PSMB8 immunostaining as a potential diagnostic and prognostic biomarker for DM in larger cohorts.

IFN-β is increased in the blood of patients with DM [15,16] and recapitulates the canonical characteristics of DM perifascicular muscle fibres in myotubes (ie, IFN-I signature, MHC-I expression, mitochondrial dysfunctions, and atrophy) [6,10,17,18]. However, the mechanism underlying the IFN-β effect on myofibres has remained largely unknown. In particular, while ISG15 was previously found to be highly upregulated in DM perifascicular fibres and in IFN-β-treated cells, targeting ISG15 did not prevent the effects of IFN-β on muscle cells [17]. The data presented herein shed new light on DM pathophysiology by revealing that IFN-β enhances proteasome activity in muscle fibres that subsequently underpin myofibre i) atrophy, ii) MHC-I expression, and iii) mitochondrial dysfunction, downstream of ISG upregulation. This finding is in line with previous independent observations, including i) the seminal pharmaceutics development of proteasome inhibitors for muscle wasting [37], ii) the reversion of IFN-induced MHC-I expression in myotubes [35], iii) the improvement of muscle function with bortezomib in a mouse model of myositis [38], and iv) the rescue of mitochondrial complex IV deficiency by proteasome inhibitors in fibroblasts derived from patients with mitochondrial monogenic diseases [39,40].

In contrast to DM, IFN-γ has been reported to play a prominent role in the pathogenesis of non-DM myopathies such as ASyS, SM, and IBM [36,29]. Consistent with these data, we observed β5i expression in muscle tissue from these patients, with a distribution distinct from the perifascicular pattern seen in DM. Additionally, *in vitro*, IFN-γ exerted a distinct myopathic effect compared to IFN-β, more closely resembling the features of non-DM muscle fibres [29]. Finally, in further contrast with IFN-β, the myopathic effects of IFN-γ occurred independently of proteasome activation. Comparative data on IFN-β- and IFN-γ-mediated proteasome regulation have so far been scarce [20,24], and, to our knowledge, absent in muscle cells. Here, we show that, in human myotubes, both IFN-β and IFN-γ similarly enhanced β5i proteasome activity, while IFN-β induced higher PSMB8 expression, suggesting differential regulation of proteasome components by the 2 cytokines. However, given that the *in vivo* biological activity of IFN-β and IFN-γ in the muscle tissue of
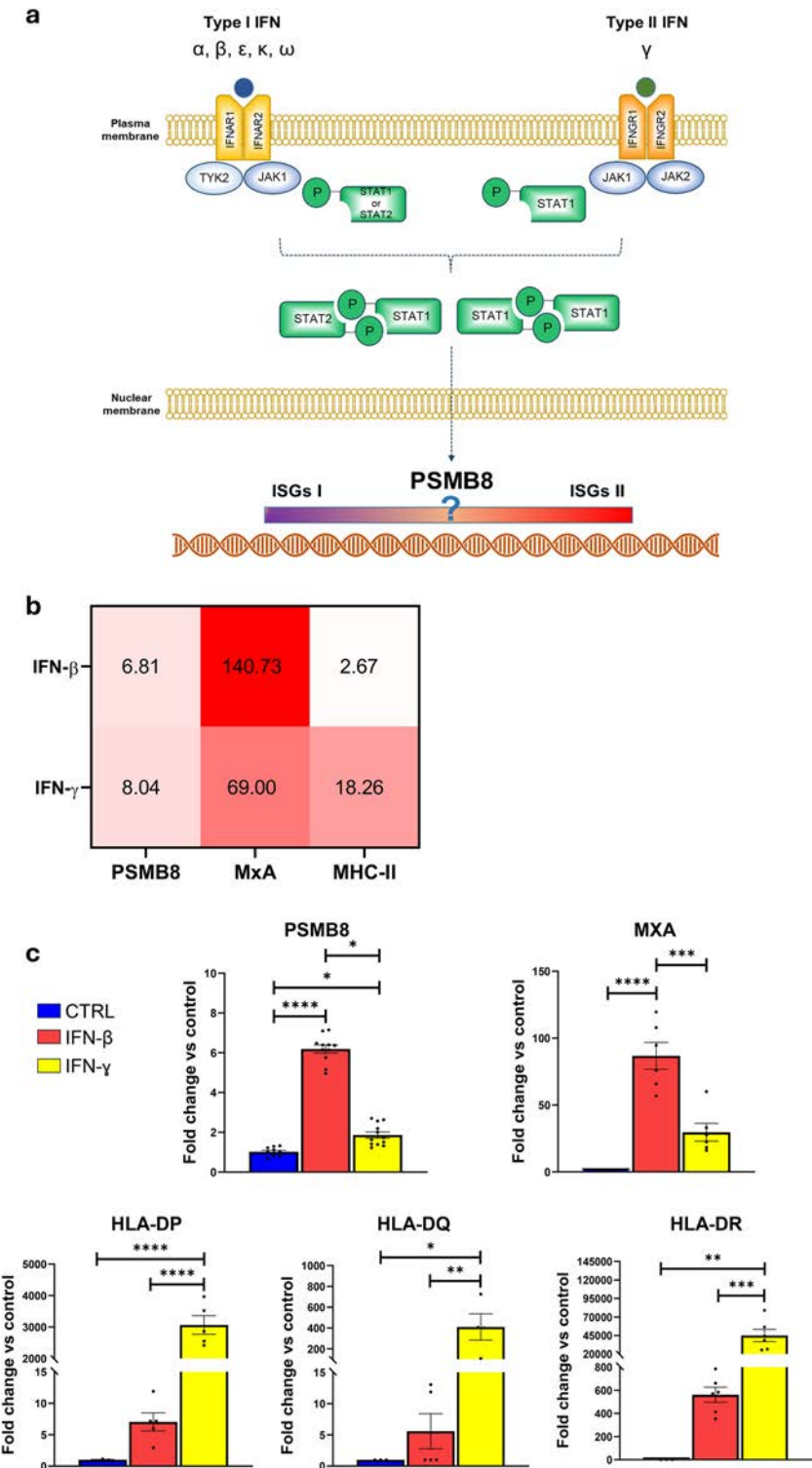
Figure 4. Interferons (IFNs) regulation of PSMB8 gene expression in an *in vitro* model of dermatomyositis (DM). (A) IFNs activation of JAK-STAT pathway. (B) Heatmap depicting the expression of PSMB8, MxA, and major histocompatibility complex (MHC)-II in fibroblasts treated with IFN-β (500 U/mL) or IFN-γ (500 U/mL), according to the datasets available on Interferome database. (C) PSMB8, MxA, and MHC-II gene expression in human myotubes treated with IFN-β (500 U/mL) or IFN-γ (500 U/mL). Data are expressed as the mean + SEM. *$P <$ .05, **$P < .01$, ***$P < .001$, ****$P < .0001$ vs the comparator indicated by the line. ISG, interferon-stimulated gene; JAK, Janus kinase.

patients with IM remains undefined, the clinical significance of this difference is uncertain. Myofibre mitochondrial dysfunctions [6] and MHC-I expression [41] participate in the development and maintenance of muscle inflammation in DM. In keeping with these observations, we found that inflammatory infiltrate was decreased in the muscle of EM mice treated with ixazomib further supporting a crosstalk between muscle fibres and immune cells, and therefore positioning muscle fibres as a therapeutic target in DM. However, in this model, a direct effect of ixazomib on immune cells.

Several strategies aiming at blocking the IFN-β pathway in DM are currently under investigation, which include direct targeting IFN-β itself (NCT05895786), its receptors (NCT06455449), and downstream JAK (NCT04972760) and/or Tyk2 (NCT05437263, NCT05335447) activation. Our data reveal that proteasome blockade is an additional putative strategy to block IFN-β pathway in DM. An 'on-target' therapeutic effect of proteasome inhibitors—consistent with their known pharmacodynamics—occurring downstream of IFN-β-driven transcriptomic stimulation, was supported by their ability to inhibit IFN-β−induced proteasome activation and IFN-β-induced myopathic effects without altering ISG expression. Comparative studies assessing the efficacy and tolerability of these candidate therapies warrant further investigation. Proteasome inhibition with bortezomib (included solely in the L1000CDS² database and identified as a candidate drug
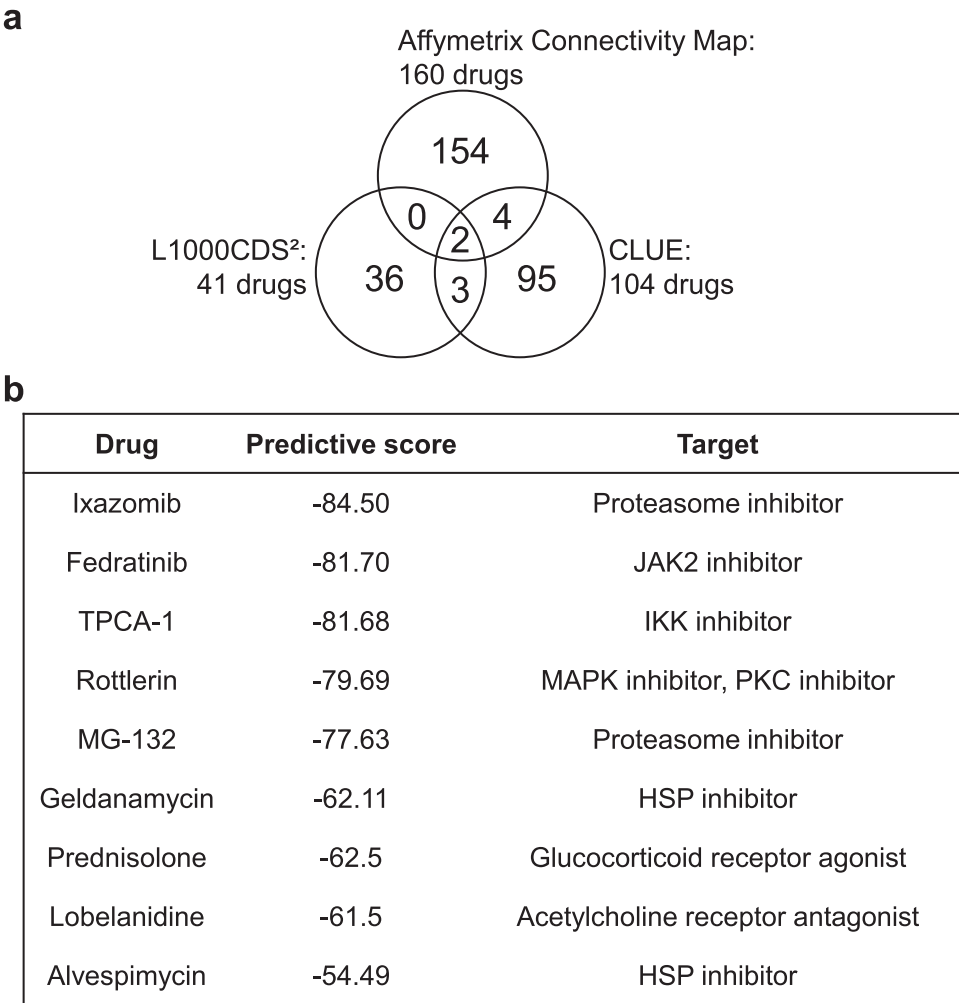
a

Affymetrix Connectivity Map:
160 drugs

L1000CDS²:
41 drugs

CLUE:
104 drugs

b

Drug	Predictive score	Target
Ixazomib	-84.50	Proteasome inhibitor
Fedratinib	-81.70	JAK2 inhibitor
TPCA-1	-81.68	IKK inhibitor
Rottlerin	-79.69	MAPK inhibitor, PKC inhibitor
MG-132	-77.63	Proteasome inhibitor
Geldanamycin	-62.11	HSP inhibitor
Prednisolone	-62.5	Glucocorticoid receptor agonist
Lobelanidine	-61.5	Acetylcholine receptor antagonist
Alvespimycin	-54.49	HSP inhibitor

Figure 5. Drug repurposing analysis. (A) Venn diagram of molecules identified by 3 drug repurposing tools. (B) Candidate repurposed drugs identified by at least 2 tools with a predictive score (see Methods section) <-50. HSP, heat shock protein; IKK, IκB kinase; JAK, Janus kinase; MAPK, mitogen-activated protein kinase; PKC, protein kinase C.

repurposed for DM by this tool) has been reported as an effective strategy in real-life treatment of systemic lupus erythematosus (SLE) [42,43], an autoimmune disease sharing clinical, pathophysiological, and genetic features with DM [6,44]. In this setting, the efficacy of proteasome inhibition has been hypothesised to be driven by the induction of apoptosis in plasma cells [42,43]. Although this mechanism might also participate in the therapeutic response observed herein in our EM mice model, our results derived from microdissected fibres and myotube experiments additionally support immunomodulation through the targeting of β5i hyperactivation in resident cells (ie, myofibres). Notably, selective inhibition of β5i has been shown to block the presentation of MHC-I-restricted antigens during the antiviral response [45], 2 pathways found to be specifically increased in DM perifascicular fibres in the present study. In both IFN-β-treated myotubes and EM myofibres, proteasome inhibition abolished MHC-I expression without affecting ISG expression. As a result, inflammatory infiltrate (mainly T cells in EM) [31] was decreased in ixazomib-treated mice muscle tissue.

Zetomipzomib (KZR-616), an inhibitor of the β5i and β1i immunoproteasome subunits not included in the databases of repositionable drugs, is currently in development for several autoimmune diseases. While it has shown positive effects in SLE in an open-label phase 1b/2 study [46], a 16-week intake of the treatment in 25 patients with active IM (including 13 DM and 12 non-DM IM), did not lead to a higher improvement vs placebo (the improvement was clinically meaningful in both groups).

Notwithstanding, improvement was nonetheless numerically greater with zetomipzomib with baseline correction to W16 (cross over) continuing throughout the open-label extension period up to 96 weeks [47]. Whether the improvement was greater in patients with DM vs patients without DM IM has not been provided to date. Our data further support the pursuit of the development of this drug in DM rather than in other IM subtypes.

Adverse events in patients with SLE treated with bortezomib have been frequently reported (ranging from 50% to 90%), although they were generally mild [42,43]. To improve the safety profile of this class of drugs, next-generation proteasome inhibitors have been developed. Ixazomib (used in our study) has demonstrated a lower incidence of serious adverse events in patients with multiple myeloma compared to bortezomib [48]. Although no serious adverse events related to zetomipzomib were reported in patients with IM [47] or in a Phase IIa trial in autoimmune hepatitis (NCT05569759), four patients died (including one in the placebo arm) in a Phase IIb trial evaluating this drug in active lupus nephritis (NCT05781750). Evidence suggestive of co-morbidities immediately prior to zetomipzomib exposure (e.g., possible systemic infection) and/or underlying disease characteristics (e.g., cardiovascular conditions) was present in these fatal cases [49]. Nevertheless, this study was stopped following a Food and Drug Administration hold. A partial hold imposed on the Phase IIa trial in autoimmune hepatitis (NCT05569759) was lifted in July 2025, and this study is currently ongoing.
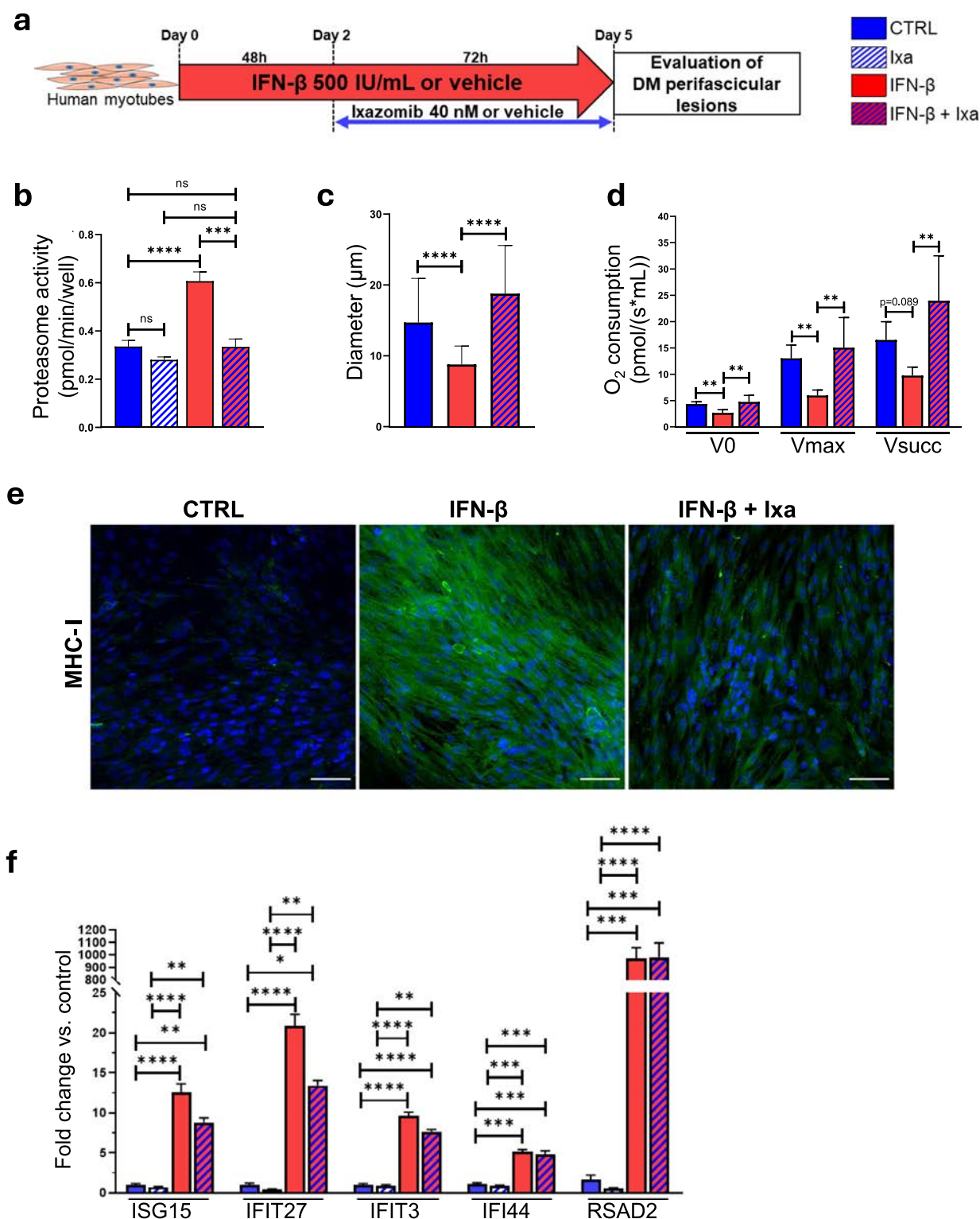
Figure 6. Proteasome inhibition is effective in an *in vitro* model of dermatomyositis (DM). (A) Experimental design: human myotubes treated with IFN-*β* (500 U/mL for 5 days) and ixazomib (Ixa, 40 nM) or vehicle added at day 2. (B) Chymotrypsin-like activity in human myotubes expressed as pmol/min/well (n ≥ 4). (C) Assessment of human myotube diameter (n ≥ 49 per group). (D) Mitochondrial respiration (n ≥ 5 per group). (E) Representative figure of major histocompatibility complex-I (MHC-I) immunostaining (green). Nuclei were stained with DAPI (blue). Scale bar: 100 μm. (F) Expression of interferon-stimulated genes MHC-I immunostaining (green). Nuclei were stained with DAPI (blue). Scale bar: 100 μm. (F) Expression of interferon-stimulated genes (n ≥ 9 per group). Data are expressed as the mean + SEM. *P < .05, **P < .01, ***P < .001, ****P < .0001. CTRL, control; IFN, interferon; V0: basal oxygen consumption with glutamate and malate; Vmax: ADP-stimulated respiration; Vsucc: succinate-stimulated respiration. ADP: adenosine diphosphate; DAPI: 4′,6-diamidino-2-phenylindole.
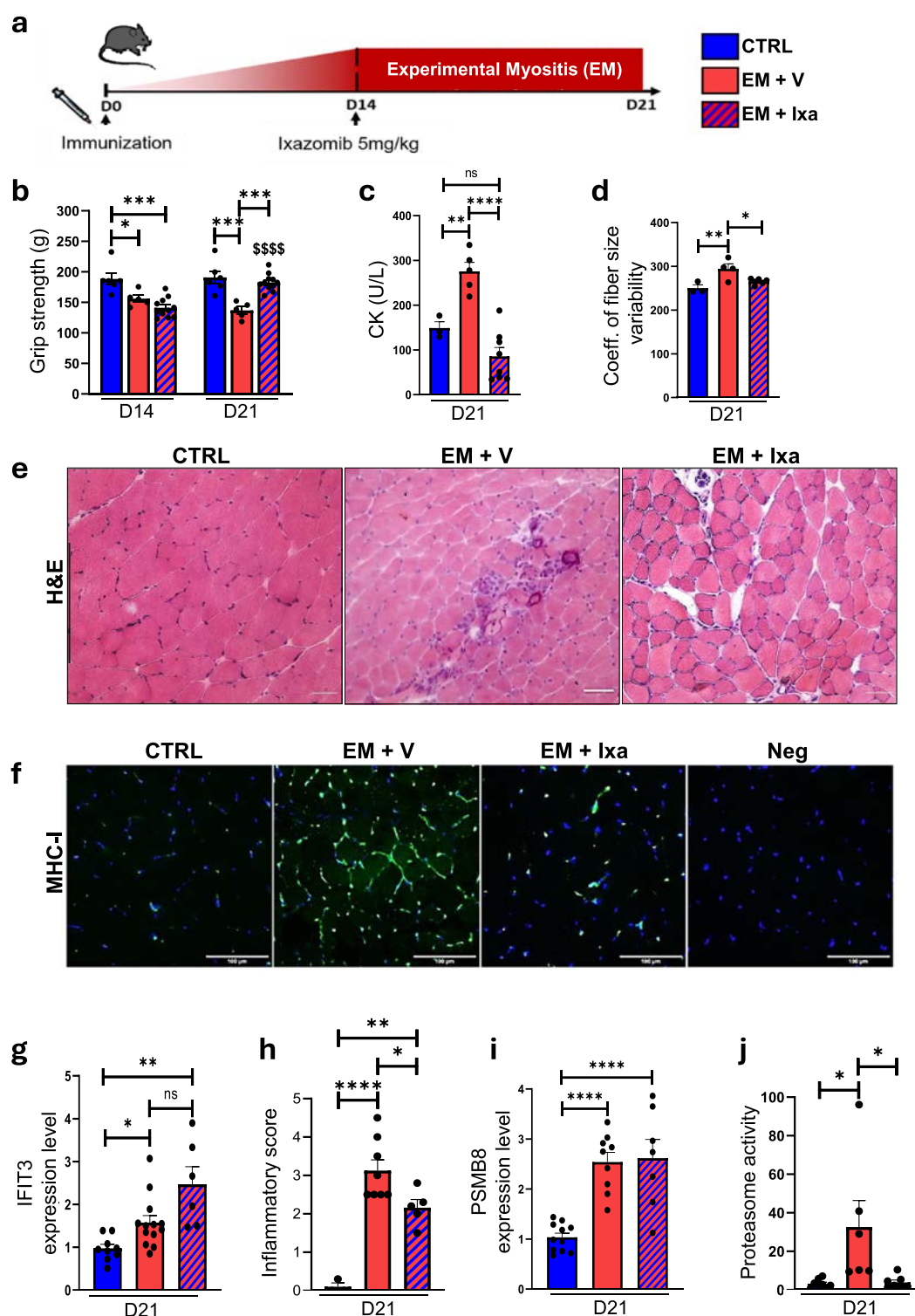
Figure 7. Proteasome inhibition is effective in experimental myositis (EM). (A) Experimental design: EM was induced at day 0 (D0), ixazomib (Ixa) or vehicle (V) was administered at D14, and mice were sacrificed at day 21 (D21). (B) Grip strength measurements (n ≥ 5) in mice at D14 and D21. (C) Serum creatine kinase (CK) levels at D21 in EM mice treated with Ixa or V, and in unimmunised mice (control, CTRL). (D) Coefficient of fibre size variability in gastrocnemius muscle of EM mice treated with Ixa or V, n ≥3. (E) Representative hematoxylin & eosin (H&E) staining of gastrocnemius cryosections at × 200 magnification. Scale bar: 100 μm. (F) Representative major histocompatibility complex-I (MHC-I) immunostaining (green) in the gastrocnemius muscle of EM mice treated with Ixa or V. Nuclei were stained with DAPI (blue). IgG was used as negative (Neg) control. Scale bar: 100 μm. (G) IFIT3 transcript levels normalised for housekeeping gene expression (18S), n ≥ 9 for each condition. (H) Histological inflammatory infiltrate score in H&E-stained slides from gastrocnemius muscle of EM mice treated with Ixa or V and in CTRL mice, at D21. Each dot represents the average score of 3 sections for each mouse (n ≥ 3 mice for each condition; 3 sections from each mouse were analysed). (I) PSMB8 transcript level normalised for housekeeping gene expression (18S), n ≥ 7 for each condition. (J) Chymotrypsin-like activity in gastrocnemius muscle of EM mice treated with Ixa or V and in CTRL mice, at D21 (n ≥ 3 for each condition). Data are expressed as the mean + SEM. ns: not significant ($P ≥ 0.05$), *$P < .05$, **$P < .01$, ***$P < .001$, ****$P < .0001$, $^{\$\$\$\$}P < .0001$ vs D14. DAPI: 4′,6-diamidino-2-phenylindole.

In conclusion, enhanced proteasome activity in perifascicular myofibres is a hallmark of DM and a likely therapeutic target.

Competing interests

None declared.

Acknowledgements

Contributors

LD, MG, GL, AM: substantial contributions to the conception or design of the work; or the acquisition, analysis, or interpretation of data for the work; drafting the work or revising it critically for important intellectual content; final approval of the version to be published; agreement to be accountable for all aspects of the work in ensuring that questions related to the accuracy or integrity of any part of the work are appropriately investigated and resolved. LD, MG: are joint junior authors. GL, AM: are joint senior authors. GQ, SP, DR, CK, BL, A-LC, BG, DM: substantial contributions to the acquisition of data for the work; drafting the work or revising it critically for important intellectual content; final approval of the version to be published. LD, MG, GL, AM: accept full responsibility for the work and/or the conduct of the study, had access to the data, and controlled the decision to publish. LD and MG are guarantors.

Funding

Patient consent for publication

Written informed consent was obtained from all participants. Patients were not involved in the design and conduct of this research, but patient associations will participate in disseminating the results of this research.

Ethics approval

This study was approved by the local Ethics Committee (No 6431). Written informed consent was obtained from all participants. The animal study was approved by the IGBMC Ethical Committee and the French Ministry (#35432-2022021417533158).

Provenance and peer review

Not commissioned; externally peer reviewed.

Data availability statement

Data will be shared on request from any qualified investigator.

Supplementary materials

Supplementary material associated with this article can be found in the online version at doi:10.1016/j.ard.2025.08.031.

Orcid

Léa Debrut: http://orcid.org/0000-0003-1534-8088
Margherita Giannini: http://orcid.org/0000-0002-4834-5804

REFERENCES

[1] Debrut L, Giannini M, Klein D, Spielmann L, Mertz P, Martin T, et al. Refining incidence and characteristics of inflammatory myopathies: a quadruple-source capture-recapture survey using the 2017 European League Against Rheumatism/American College of Rheumatology Classification Criteria. Arthritis Rheumatol. 2023 Oct;75(10):1850–5.

[2] Mammen AL, Allenbach Y, Stenzel W, Benveniste O. ENMC 239th Workshop Study Group. 239th ENMC International Workshop: classification of dermatomyositis, Amsterdam, the Netherlands, 14-16 December 2018. Neuromuscul Disord 2020 Jan;30(1):70–92.

[3] Pinal-Fernandez I, Casciola-Rosen LA, Christopher-Stine L, Corse AM, Mammen AL. The prevalence of individual histopathologic features varies according to autoantibody status in muscle biopsies from patients with dermatomyositis. J Rheumatol 2015 Aug;42(8):1448–54.

[4] Meyer A, Scirè CA, Talarico R, Alexander T, Amoura Z, Avcin T, et al. Idiopathic inflammatory myopathies: state of the art on clinical practice guidelines [corrected]. RMD Open 2018;4(suppl 1):e000784.

[5] Gallay L, Fermon C, Lessard L, Weiss-Gayet M, Viel S, Streichenberger N, et al. Involvement of type I interferon signaling in muscle stem cell proliferation during dermatomyositis. Neurology 2022 May 24;98(21):e2108–19.

[6] Meyer A, Laverny G, Allenbach Y, Grelet E, Ueberschlag V, Echaniz-Laguna A, et al. IFN-β-induced reactive oxygen species and mitochondrial damage contribute to muscle impairment and inflammation maintenance in dermatomyositis. Acta Neuropathol 2017 Oct;134(4):655–66.

[7] Fasth AER, Dastmalchi M, Rahbar A, Salomonsson S, Pandya JM, Lindroos E, et al. T cell infiltrates in the muscles of patients with dermatomyositis and polymyositis are dominated by CD28null T cells. J Immunol 2009 Oct 1;183(7):4792–9.

[8] Giannini M, Rovito D, Debrut L, Keime C, Lannes B, Charles A, et al. Muscle fibres play a critical role in therapeutic response of myositis to glucocorticoids through polarisation of the inflammatory infiltrate by a paracrine mechanism [abstract]. Arthritis Rheumatol 2022;74(suppl 9).

[9] Greenberg SA, Pinkus JL, Pinkus GS, Burleson T, Sanoudou D, Tawil R, et al. Interferon-alpha/beta-mediated innate immune mechanisms in dermatomyositis. Ann Neurol 2005 May;57(5):664–78.

[10] Pinal-Fernandez I, Casal-Dominguez M, Derfoul A, Pak K, Miller FW, Milisenda JC, et al. Machine learning algorithms reveal unique gene expression profiles in muscle biopsies from patients with different types of myositis. Ann Rheum Dis 2020 Sep;79(9):1234–42.

[11] Salajegheh M, Kong SW, Pinkus JL, Walsh RJ, Liao A, Nazareno R, et al. Interferon-stimulated gene 15 (ISG15) conjugates proteins in dermatomyositis muscle with perifascicular atrophy. Ann Neurol 2010 Jan;67(1):53–63.

[12] Suárez-Calvet X, Gallardo E, Pinal-Fernandez I, De Luna N, Lleixà C, Díaz-Manera J, et al. RIG-I expression in perifascicular myofibers is a reliable biomarker of dermatomyositis. Arthritis Res Ther 2017 Dec;19(1):174.

[13] Kloetzel PM. Antigen processing by the proteasome. Nat Rev Mol Cell Biol 2001 Mar;2(3):179–87.

[14] Collins GA, Goldberg AL. The logic of the 26S proteasome. Cell 2017 May 18;169(5):792–806.

[15] Liao AP, Salajegheh M, Nazareno R, Kagan JC, Jubin RG, Greenberg SA. Interferon β is associated with type 1 interferon-inducible gene expression in dermatomyositis. Ann Rheum Dis 2011 May;70(5):831–6.

[16] Bolko L, Anquetil C, Llibre A, Maillard S, Amelin D, Dorgham K, et al. Ultra-sensitive interferons quantification reveals different cytokine profile secretion in inflammatory myopathies and can serve as biomarkers of activity in dermatomyositis. Front Immunol 2025 Feb 12;16:1529582.

[17] Franzi S, Salajegheh M, Nazareno R, Greenberg SA. Type 1 interferons inhibit myotube formation independently of upregulation of interferon-stimulated gene 15. PLoS One 2013 Jun 4;8(6):e65362.

[18] Ladislau L, Suárez-Calvet X, Toquet S, Landon-Cardinal O, Amelin D, Depp M, et al. JAK inhibitor improves type I interferon induced damage: proof of concept in dermatomyositis. Brain 2018 Jun 1;141(6):1609–21.

[19] Platanias LC. Mechanisms of type-I- and type-II-interferon-mediated signalling. Nat Rev Immunol 2005 May;5(5):375–86.

[20] Hisamatsu H, Shimbara N, Saito Y, Kristensen P, Hendil KB, Fujiwara T, et al. Newly identified pair of proteasomal subunits regulated reciprocally by interferon gamma. J Exp Med 1996 Apr 1;183(4):1807–16.

[21] Niewerth D, Kaspers GJ, Assaraf YG, van Meerloo J, Kirk CJ, Anderl J, et al. Interferon-γ-induced upregulation of immunoproteasome subunit assembly overcomes bortezomib resistance in human hematological cell lines. J Hematol Oncol 2014 Jan 13;7:7.

[22] Jamaluddin M, Wang S, Garofalo RP, Elliott T, Casola A, Baron S, et al. IFN-beta mediates coordinate expression of antigen-processing genes in RSV-infected pulmonary epithelial cells. Am J Physiol Lung Cell Mol Physiol 2001 Feb;280(2):L248–57.

[23] Shin EC, Seifert U, Kato T, Rice CM, Feinstone SM, Kloetzel PM, et al. Virus-induced type I IFN stimulates generation of immunoproteasomes at the site of infection. J Clin Invest 2006 Nov;116(11):3006–14.

[24] Seifert U, Bialy LP, Ebstein F, Bech-Otschir D, Voigt A, Schröter F, et al. Immunoproteasomes preserve protein homeostasis upon interferon-induced oxidative stress. Cell 2010 Aug 20;142(4):613–24.

[25] Duncan CJ, Mohamad SM, Young DF, Skelton AJ, Leahy TR, Munday DC, et al. Human IFNAR2 deficiency: lessons for antiviral immunity. Sci Transl Med 2015 Sep 30;7(307) 307ra154.

[26] Lessard LER, Robert M, Fenouil T, Mounier R, Landel V, Carlesimo M, et al. Contribution of major histocompatibility complex class II immunostaining in distinguishing idiopathic inflammatory myopathy subgroups: a histopathological cohort study. J Neuropathol Exp Neurol 2024 Dec 1;83(12):1060–75.

[27] Rusinova I, Forster S, Yu S, Kannan A, Masse M, Cumming H, et al. Interferome v2.0: an updated database of annotated interferon-regulated genes. Nucleic Acids Res 2013 Jan;41(Database issue):D1040–6.

[28] Der SD, Zhou A, Williams BR, Silverman RH. Identification of genes differentially regulated by interferon alpha, beta, or gamma using oligonucleotide arrays. Proc Natl Acad Sci USA 1998 Dec 22;95(26):15623–8.

[29] Hou C, Periou B, Gervais M, Martin L, Berthier J, Baba-Amer Y, et al. Interferon-γ causes myogenic cell dysfunction and senescence in immune myopathies. Brain 2025 Apr 29;148(8):2883–98.

[30] Karatzas E, Kolios G, Spyrou GM. An application of computational drug repurposing based on transcriptomic signatures. Methods Mol Biol 2019;1903:149–77.

[31] Giannini M, Rovito D, Oulad-Abdelghani M, Messaddeq N, Debrut L, Quiring G, et al. Experimental myositis: an optimised version of C-protein-induced myositis. RMD Open 2025 Mar 5;11(1):e004558.

[32] Sugihara T, Sekine C, Nakae T, Kohyama K, Harigai M, Iwakura Y, et al. A new murine model to define the critical pathologic and therapeutic mediators of polymyositis. Arthritis Rheum 2007 Apr;56(4):1304–14.

[33] Micheletto MLJ, Hermes T de A, Bertassoli BM, Petri G, Perez MM, Fonseca FLA, et al. Ixazomib, an oral proteasome inhibitor, exhibits potential effect in dystrophin-deficient mdx mice. Int J Exp Pathol 2021 Feb;102(1):11–21.

[34] Millennium Pharmaceuticals Inc.. NINLARO (ixazomib) capsules, for oral use. Prescribing information. U.S. Food and Drug Administration; 2015 Available from: https://www.accessdata.fda.gov/drugsatfda_docs/label/2015/208462lbl.pdf.

[35] Bhattarai S, Ghannam K, Krause S, Benveniste O, Marg A, de Bruin G, et al. The immunoproteasomes are key to regulate myokines and MHC class I expression in idiopathic inflammatory myopathies. J Autoimmun 2016 Dec;75:118–29.

[36] Pinal-Fernandez I, Casal-Dominguez M, Derfoul A, Pak K, Plotz P, Miller FW, et al. Identification of distinctive interferon gene signatures in different types of myositis. Neurology 2019 Sep 17;93(12):e1193–204.

[37] Sánchez-Serrano I. Success in translational research: lessons from the development of bortezomib. Nat Rev Drug Discov 2006 Feb;5(2):107–14.

[38] Rayavarapu S, Coley W, Van der Meulen JH, Cakir E, Tappeta K, Kinder TB, et al. Activation of the ubiquitin proteasome pathway in a mouse model of inflammatory myopathy: a potential therapeutic target. Arthritis Rheum 2013 Dec;65(12):3248–58.

[39] Mohanraj K, Wasilewski M, Benincá C, Cysewski D, Poznanski J, Sakowska P, et al. Inhibition of proteasome rescues a pathogenic variant of respiratory chain assembly factor COA7. EMBO Mol Med 2019 May;11(5):e9561.

[40] Habich M, Riemer J. Stop wasting protein-proteasome inhibition to target diseases linked to mitochondrial import. EMBO Mol Med 2019 May;11(5):e10441.

[41] Okiyama N, Ichimura Y, Shobo M, Tanaka R, Kubota N, Saito A, et al. Immune response to dermatomyositis-specific autoantigen, transcriptional intermediary factor 1γ can result in experimental myositis. Ann Rheum Dis 2021 Sep;80(9):1201–8.

[42] Walhelm T, Gunnarsson I, Heijke R, Leonard D, Trysberg E, Eriksson P, et al. Clinical experience of proteasome inhibitor bortezomib regarding efficacy and safety in severe systemic lupus erythematosus: a nationwide study. Front Immunol 2021;12:756941.

[43] Alexander T, Sarfert R, Klotsche J, Kühl AA, Rubbert-Roth A, Lorenz HM, et al. The proteasome inhibitior bortezomib depletes plasma cells and ameliorates clinical manifestations of refractory systemic lupus erythematosus. Ann Rheum Dis 2015 Jul;74(7):1474–8.

[44] Bianchi M, Kozyrev SV, Notarnicola A, Sandling JK, Pettersson M, Leonard D, et al. Unraveling the genetics of shared clinical and serological manifestations in patients with systemic inflammatory autoimmune diseases. Arthritis Rheumatol 2025 Feb;77(2):212–25.

[45] Muchamuel T, Basler M, Aujay MA, Suzuki E, Kalim KW, Lauer C, et al. A selective inhibitor of the immunoproteasome subunit LMP7 blocks cytokine production and attenuates progression of experimental arthritis. Nat Med 2009 Jul;15(7):781–7.

[46] Rovin B, Saxena A, Leff R, Li E, Park E, Henig N. Zetomipzomib (KZR-616) demonstrates anti-inflammatory and immunomodulatory potential in patients with active lupus with or without lupus nephritis: results from the openlabel phase 1B/2 mission study. Lupus Sci Med 2023;10(suppl 1):A1–171.

[47] Aggarwal R, Goyal N, Lam D, Ng A, Leff R, Ray K, et al. Zetomipzomib demonstrates favorable long-term safety and tolerability profile without signs of immunosuppression: results from the PRESIDIO study and its open-label extension study in patients with dermatomyositis and polymyositis [abstract]. Arthritis Rheumatol 2023;75(suppl 9).

[48] Huang J, Zhang M, Lin J, Yang X, Huang P, Zheng X. Safety assessment of proteasome inhibitors real world adverse event analysis from the FAERS database. Sci Rep 2025 Apr 4;15(1):11628.

[49] Furie R, Anand N, Desai S, Lowe E, Muchamuel T, Palaniswamy K, et al. Efficacy and Safety Results of Zetomipzomib from the PALIZADE Phase 2b Clinical Trial in Patients with Lupus Nephritis [abstract]. Arthritis Rheumatol 2025;77(suppl 9).

Autoimmunity

Effects of different B-cell-depleting strategies on the lymphatic tissue

Carlo Tur[1,2,3,†], Markus Eckstein[4,†], Laura Bucci[1,2], Janina Auth[1,2],
Christina Bergmann[1,2], Simon Rauber[1,2], Melanie Hagen[1,2],
Danae-Mona Nöthling[1,2], Sebastian Böltz[1,2], Andreas Wirsching[1,2],
Koray Tascilar[1,2], Filippo Fagni[1,2], Giulia Corte[1,2], Aleix Rius Rigau[1,2], Yi Qin[1,2],
Panagiotis Garantziotis[1,2], Jule Taubmann[1,2], Jochen Wacker[1,2],
Andreas Ramming[1,2], Maria Antonietta D'Agostino[3], Sebastian Rauch[4],
Arndt Hartmann[4], Fabian Müller[5], Andreas Mackensen[5],
Ricardo Grieshaber-Bouyer[1,2], Georg Schett[1,2,3,6], Aline Bozec[1,2],
Maria Gabriella Raimondo [1,2,*]

[1] Department of Medicine 3 - Rheumatology and Immunology, Friedrich-Alexander-Universität Erlangen-Nürnberg and Uniklinikum Erlangen, Erlangen, Germany
[2] Deutsches Zentrum für Immuntherapie (DZI), Friedrich-Alexander-Universität Erlangen-Nürnberg und Uniklinikum Erlangen, Erlangen, Germany
[3] Division of Rheumatology-Fondazione Policlinico Universitario A. Gemelli IRCCS - Università Cattolica del Sacro Cuore, Rome, Italy
[4] Institute of Pathology and Comprehensive Cancer Center EMN, Friedrich-Alexander-Universität (FAU) Erlangen-Nürnberg and Universitätsklinikum Erlangen, Erlangen, Germany
[5] Department of Internal Medicine 5 - Hematology and Oncology, Friedrich-Alexander-Universität Erlangen-Nürnberg (FAU) and Universitätsklinikum Erlangen, Erlangen, Germany
[6] Karolinska Institutet, Stockholm, Sweden

ARTICLE INFO

ABSTRACT

Objectives: To assess the efficacy of new protein-based B cell depletion with glyco-engineered anti-CD20 antibody obinutuzumab (OBI) and the CD19/CD3 T cell engager blinatumomab (BLI) in patients with autoimmune diseases (AIDs) in comparison to rituximab (RTX) and CD19 chimeric antigen receptor (CAR) T cell therapy.
Methods: Sequential inguinal lymph node biopsies were taken before and after treatment with OBI-, BLI-, RTX- and CD19-CAR T cells in patients with AID. CD19+ and CD20+ B cells, plasma cells, T cells and macrophages were analysed by immunohistochemistry. Changes in follicular architecture (follicular dendritic cells, T follicular helper cells, proliferation) were also assessed.
Results: Baseline and follow-up lymph node biopsies from 24 patients with AID (OBI, 4; BLI, 4; RTX, 4; CD19-CAR T cells, 12) were analysed. B cell depletion was confirmed in all CD19-CAR T cell-treated patients but only in 1 (OBI) out of 12 protein-based B cell-treated patients. Likewise, follicular architecture was disrupted in all CD19-CAR T cell-treated patients but only in 1 (OBI)

https://doi.org/10.1016/j.ard.2025.06.2120

0003-4967/© 2025 The Authors. Published by Elsevier B.V. on behalf of European Alliance of Associations for Rheumatology (EULAR). This is an open access article under the CC BY license (http://creativecommons.org/licenses/by/4.0/).

out of 12 protein-based B cell-treated patients. B cell depletion efficacy in the lymph nodes was 100% for CD19-CAR T cells, 92% for OBI, 86% for RTX and 69% for BLI. Plasma cells were reduced but not depleted in all treatment approaches. CD3+ T cells and CD68+ macrophages remained unaffected. Peripheral blood B cell depletion occurred in all but 1 BLI-treated patient. B cell depletion was associated with stable drug-free remission, whereas a reduction in B cell numbers without depletion required retreatment with immunomodulatory drugs.

Conclusions: Protein-based B cell depletion reduces but usually does not deplete B cells in lymph nodes leaving the follicular architecture intact and being associated with disease recurrence.

WHAT IS ALREADY KNOWN ON THIS TOPIC

- Advanced protein-based B cell depleters, such as glycoengineered CD20 monoclonal antibody obinutuzumab (OBI) and CD19/CD3 T cell engager blinatumomab (BLI), are promising new therapeutic instruments for treatment of autoimmune disease (AIDs). It has been speculated that such B cell-depleting modalities achieve better clearance of tissue B cells in patients.

WHAT THIS STUDY ADDS

- By performing sequential lymph node biopsies, this study shows that advanced protein-based B cell depleters, like OBI and BLI, reduce but do not consistently deplete B cells in the lymph nodes. These results stand in contrast to the consistent full depletion of B cells associated with the disruption of follicular lymph node architecture after CD19 chimeric antigen receptor T cell therapy.

HOW THIS STUDY MIGHT AFFECT RESEARCH, PRACTICE OR POLICY

- Analysis of the lymph nodes may help to gain a better insight into the efficacy of advanced drugs to deplete B cells in lymphoid organs of patients with AID and to induce an 'immune reset'.

INTRODUCTION

Autoimmune diseases (AIDs), such as systemic lupus erythematosus (SLE), systemic sclerosis (SSc), rheumatoid arthritis (RA) and idiopathic inflammatory myopathies (IIM) are severe conditions that require timely, robust and sustained treatment with drugs that dampen the exaggerated immune response in order to prevent organ damage. B cells are considered to be an important therapeutic target as they contribute significantly to the pathogenesis of AIDs through autoantibody generation, antigen presentation and cytokine production. Therefore, B cell depletion is a key therapeutic approach in many AIDs [1]. The chimeric anti-CD20 antibody rituximab (RTX) is by far the most-studied B cell-depleting agent in AIDs, receiving therapeutic approval in 3 AIDs (RA, granulomatosis with polyangiitis and pemphigus vulgaris) and being widely used in many other AIDs [2]. Several studies have shown that therapeutic efficacy of RTX depends on the level of B cell depletion [2]. Hence, deeper depletion of peripheral B cells, a longer time before B cell reappearance and higher doses of RTX have all been associated with better clinical responses in the treatment of AIDs [2]. Importantly, RTX treatment has to be repeated to achieve sustained control of AIDs. These observations and data from tissue biopsies showing reduction but not depletion of B cells in the synovial membrane, bone marrow, tonsils and lymph nodes have been a motivation for engineering more advanced B cell-depleting strategies [3,4]. For instance, high-affinity CD20 targeting antibodies, such as ocrelizumab and ofatumumab, have been approved for the treatment of multiple sclerosis [1].

Deep B cell tissue depletion may induce a reset of autoimmunity and promote sustained drug-free remission. In line with this concept, autologous CD19-chimeric antigen receptor (CAR) T cell therapy—the most effective treatment for achieving B cell depletion in humans to date—has been shown to fully eradicate B cells from lymph nodes and induce long-lasting drug-free remission [5−12]. So far, it is unknown whether advanced protein-based B cell depletion can eradicate the B cell pool in the tissues. Advanced protein-based B cell depleters, such as glycoengineered CD20 monoclonal antibody obinutuzumab (OBI) and the CD19/CD3 T cell engager blinatumomab (BLI), have shown efficacy in AIDs, even in refractory cases [13−17]. OBI represents a next-generation anti-CD20 antibody with enhanced antibody-dependent cellular cytotoxicity and direct B cell killing compared with RTX [18,19]. The bispecific T cell engager BLI is a small molecule designed to co-engage T cells and CD19+ B cells, forming an immunological synapse that drives direct cytotoxicity [20]. OBI and BLI demonstrated B cell depletion in the circulation, but it is unclear to what extent these compounds deplete B cells in the lymphoid tissues [21,22]. Deep tissue depletion, however, may be a requirement for sustained responses in AIDs. Therefore, this study investigated the effects of OBI and BLI on B cell depletion and follicular architecture in the secondary lymphoid organs of patients with AID, comparing the effects of RTX and CD19-CAR T cell therapy.

METHODS

Patients

All patients had active AID when receiving B cell depletion. RTX and OBI were administered by standard protocol treatment [13,23], with 2 infusions (days 0 and 14) of 1000 mg of the respective antibody (Fig 1A). BLI was administered by an initial continuous infusion delivering a cumulative dose of 38.5 µg over 96 hours (days 0 to 4), followed by a second continuous infusion 1 week later with a cumulative dose of 112 µg over 96 hours (days 11 to 15). CD19-CAR T cells were manufactured by transfecting autologous T cells with a second-generation lentiviral vector encoding for a CD19-binding, 4-1BB costimulation-based CAR (MB-CART19.1; Miltenyi). CD19-CAR T cells were administered by a single infusion of 1×10^6 cells/kg body weight following standard lymphodepletion with cyclophosphamide and fludarabine [6]. Clinical response was defined as reduction of ≥4 in the Systemic Lupus Erythematosus Disease Activity Index 2000 score (SLEDAI-2K) in patients with SLE; achievement of American College of Rheumatology−European League Against Rheumatism (ACR−EULAR) moderate clinical response in patients with idiopathic inflammatory myopathies (IIM); moderate to good response in Disease Activity Score-28 (DAS-28) for RA; changes ≥2.5 in European Scleroderma Trials and Research Group activity index (EUSTAR-AI) for patients with SSc. Remission was defined by the Definition of Remission in SLE criteria for SLE (DORIS), ACR−EULAR major clinical response for IIM and values DAS-28 ≤2.6 for RA.
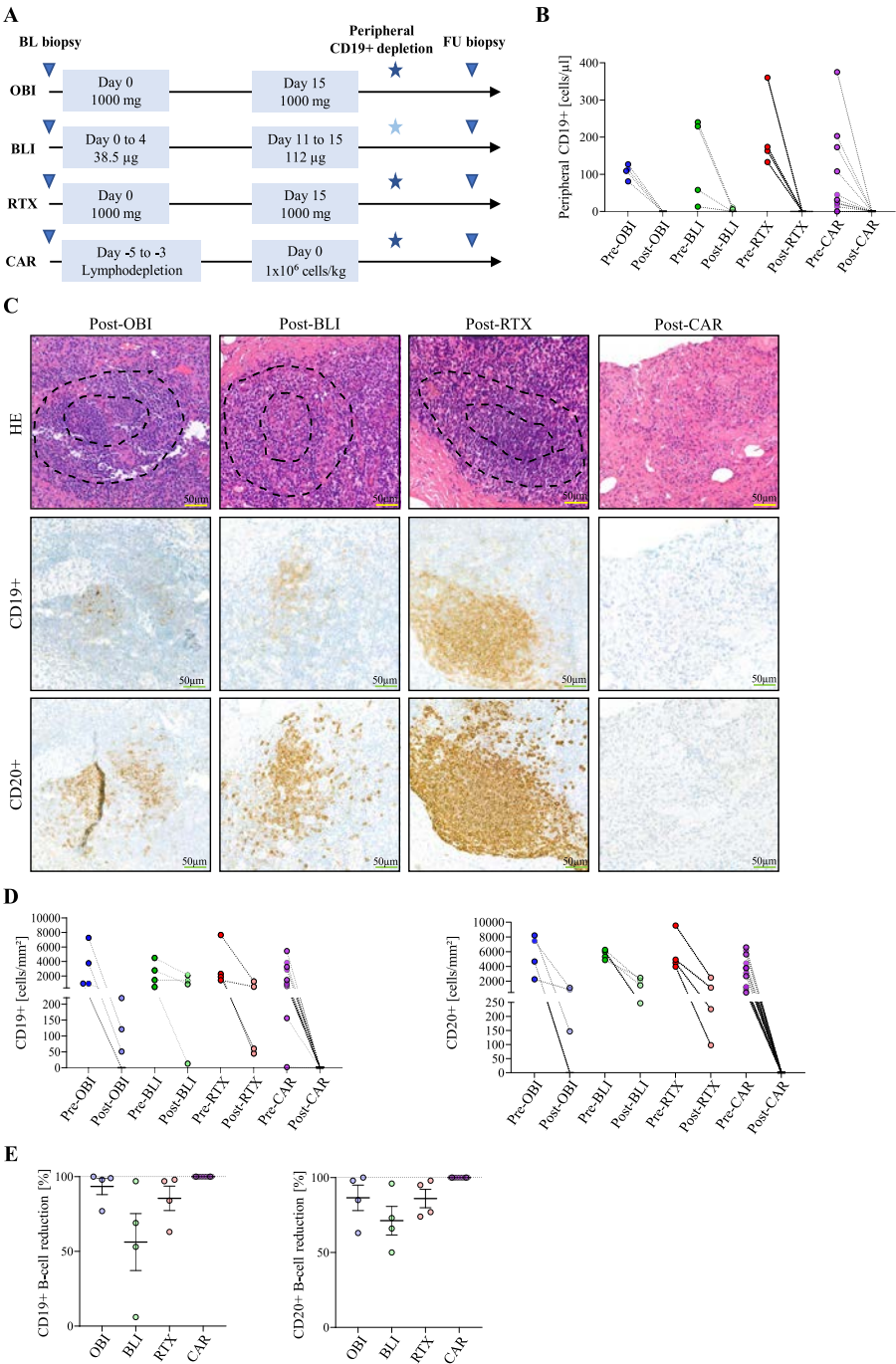
Figure 1. B cell depletion in peripheral blood and lymph nodes upon B cell targeting treatments. (A) Schematic representation of the different B cell-depleting regimens. OBI, obinutuzumab, N = 4; BLI, blinatumomab, N = 4; RTX, rituximab, N = 4; CAR, CD19-CAR T cells, N = 12. Blue triangles indicate the time of biopsy, both at baseline (BL) before treatment initiation and at follow-up (FU) after treatment. Follow-up biopsies were performed with full peripheral CD19+ B cell depletion (dark blue star). In the blinatumomab group, peripheral CD19+ B cells were not fully depleted in all patients (light blue star). (B) Quantification of CD19+ B cells in the peripheral blood of patients before (pre) and after (post) treatment. Bold dash indicates nondetectable cells. (C) Representative haematoxylin and eosin-stained images of lymph node biopsies obtained from each one representative OBI-, BLI-, RTX- and CAR-treated patient, together with representative immunohistochemistry pictures of CD19+ + and CD20+ + B cells corresponding to the same follicle structure. External dashed circles indicate follicular B cell areas in the lymph node tissue, whereas the internal dashed circles the germinal centre. Dashed circles are absent in the post-CAR image because the follicle structure is lost. (D) Quantitative pre- and posttreatment measures of CD19+ and CD20+ B cells in the lymph nodes, stratified by treatment conditions. Bold dash indicates not detectable. (E) Percent reduction of CD19+ and CD20+ B cells with different treatments. The dashed horizontal lines indicate 100%.

Lymph node biopsy

Biopsies from the inguinal lymph nodes were performed before and after therapy in each patient. The follow-up biopsy was performed before reappearance of circulating B cells, within 5 months after treatment, according to the visit schedule. Follow-up biopsies were done from the homolateral region, following topographic and ultrasound landmarks identified during the previous biopsy. In the cohort of patients treated with CD19-CAR T cells, the baseline biopsy was performed before the conditioning therapy. The biopsies were performed by 2 rheumatologists (CT/MGR), as previously described [12]. Briefly, ultrasound evaluation of the inguinal region was performed on patients lying in the supine position. The most accessible lymph nodes, located within 1 cm below the skin and away from major vessels and nerves, were selected. Biopsies were performed under ultrasound guidance (20 MHz linear probe, Esaote MyLabX90/X80) using sterile conditions. Local anaesthesia (10 mL of 2% mepivacaine) was administered, followed by a 0.5-cm skin incision to reduce skin resistance. A 16 G semiautomated biopsy needle (Precisa 1610-HS) was used for tissue retrieval. The wound was closed with adhesive plaster, and manual pressure was applied for 2 minutes, followed by a sandbag for 30 minutes to prevent hematoma. The conduct of this study was approved by the Institutional Review Board of the Friedrich-Alexander University of Erlangen-Nürnberg (#24-13-B). Written informed consent was obtained from all patients in accordance with the Declaration of Helsinki.

Conventional histology and immunohistochemistry

Morphological examination of the tissue specimen was performed by a board-certified pathologist (ME) on haematoxylin-eosin-stained tissue sections as described previously [12].

Immunohistochemical staining was performed using 2-μm-thick tissue sections transferred to positively charged adhesive slides (TOMO). All stainings were performed on a VENTANA Bench-Mark ULTRA autostainer platform (Ventana) according to accredited staining protocols in the routine immunohistochemistry facility of the Department of Pathology accredited and certified according to DIN EN ISO/IEC 17020. Briefly, slides were cut, deparaffinised and further processed on a BenchMark ULTRA autostainer. Antigen retrieval was carried out with CC1 reagent (Ventana) with different incubation times and temperatures (Supplementary Table S1). All lymph node-biopsy samples were stained for CD19 (pan B cell marker), CD20 (pan B cell marker), CD138 (plasma cells), CD23 (follicular dendritic cells [FDCs]), PD-1 (T follicular helper [TFH] cells), Ki67 (MIB1 antigen, proliferation fraction of germinal centre B cells), CD3 (T cells) and CD68 (macrophages) as described previously [12].

Evaluation of histopathology

Stained slides were digitised using a Hamamatsu S210 slide scanner (Hamamatsu) at × 400 magnification and imported into the open-source QuPath (v0.4.3) digital slide analysis environment. The area of interest for cell quantification per square millimetre of tissue area was defined as lymph node parenchyma excluding sclerotic areas and lymph node capsule annotated by a board-certified pathologist (ME). CD3, CD19, CD20, CD68 and CD138 cell populations were automatically quantified with the positive cell detection platform, results visually validated and target cell counts reported as the number of positive cells per square millimetre of the region of interest. To assess the architecture of the B cell maturation compartment (follicular area) of the lymph node, a semiquantitative score integrating general distribution and presence of B cells, architecture of the FDC network, proliferation rate of germinal centre B cells and presence of TFH cells was used, that has been described previously [12]. The detailed composition of the score is shown in the Supplementary Table S2. The analysis was performed by a pathologist (ME), who also performed intraobserver reliability and together with another board-certified pathologist (SR), the interobserver reliability. Scoring values were compared by calculating the single value agreement for summary scores of both observers.

Statistical analysis

Data are presented as medians with IQR or mean ± SD. Differences were analysed with the two-tailed Wilcoxon signed-rank test for paired data. To analyse changes in cell counts from pretreatment to posttreatment, we used linear mixed effects models. These included the natural logarithm of cell counts (+1 for each count to avoid log of 0 counts) as the independent variable, visit and treatment as categorical fixed effects including visit−treatment interaction terms and random intercepts for patient identifier and diagnosis to account for correlation within patients and diagnoses. CD19-CAR T cell therapy was the reference treatment level in the models; therefore, exponentiated coefficients of the treatment−visit interaction terms represent average ratios of cell counts for individual protein-based treatments to that of CD19-CAR T cell treatment at the follow-up visit. Two-tailed P values <.05 were considered statistically significant. Statistical analyses were performed using the open-source R software (version 4.4.3, R Foundation for Statistical Computing) and Prism software (version 10, GraphPad Software).

RESULTS

Patient characteristics

We analysed sequential inguinal lymph node biopsies from 24 patients undergoing different B cell targeting treatments: a group of 4 patients received OBI, BLI or RTX, respectively, whereas 12 patients (7 new cases and 5 previously described [12]) received CD19-CAR T cell therapy. Details on patient characteristics are summarised in Table 1 [12]. All patients received baseline and follow-up inguinal lymph node biopsies (Fig 1A). Follow-up biopsies were performed 69.2 days ± 36.3 (mean ± SD) after the first OBI infusion, 85.7 ± 43.5 days after the first RTX infusion and 60.8 ± 5.9 days after CD19-CAR T cell infusion. Due to the short half-life of BLI and associated earlier B cell recovery in the peripheral blood, follow-up biopsy was done earlier, 29.7 ± 3.2 days after the first BLI infusion.

Effects of treatments on circulating B cells and immunoglobulin levels

Depletion of circulating B cells was observed in all OBI-, RTX- and CD19-CAR T cell-treated patients as well as in most BLI-treated patients. One BLI-treated patient did not achieve peripheral B cell depletion (Supplementary Fig S1A). At the time of the follow-up biopsy, peripheral B cell depletion was present in all patients, except for 2 BLI-treated patients, including the one who never achieved B cell depletion and one who repopulated shortly before the biopsy (Fig 1B, Supplementary Fig S1A, and Supplementary Table S3).

Circulating immunoglobulin (Ig) levels were assessed at the time of lymph node biopsies across all treatment groups (Supplementary Fig S1B,C). Baseline IgG levels were very similar among the treatment groups. Virtually, no change of IgG levels was observed with RTX (−2%) and OBI (−7%), whereas decreases in IgG levels were more pronounced with BLI (−36%) and CD19-CAR T cells (−35%). No patient reached IgG levels below 400 mg/dL, defined as the threshold for intravenous Ig substitution (Supplementary Table S3). IgM levels decreased slightly by 17% with RTX treatment and more pronounced with OBI (−35%), BLI (−49%) and CD19-CAR T cells (−58%) (Supplementary Table S3).

Reduction but not elimination of B cells by protein-based B cell depletion in lymph nodes

Microscopic evaluation of inguinal lymph nodes was performed by immunohistochemistry with quantification of B cells by staining for CD19 and CD20 (Fig 1C). In all 12 CD19-CAR T cell-treated patients, B cells were depleted (P value for CD19+ and CD20+ cells before and after CD19-CAR T cells = .0005). In contrast, in all but 1 (OBI-treated) patient, B cells were not depleted. OBI showed robust (CD20+, −92%; CD19+, −96%) reduction of B cells in the lymph node. Reduction of B cells was less pronounced in BLI-treated patients (CD20+, −69%; CD19+, −47%) and RTX-treated patients (CD20+, −86%; CD19+, −86%) (Supplementary Table S4) (Fig 1D,E). Mixed model analysis, accounting for the variability due to the different diseases, confirmed that CD19-CAR T cells have a stronger and more consistent depleting capacity compared with protein-based approaches, whereas among the latter, OBI showed a numerically superior reduction (lower count ratio) of B cells (Table 2) [12].

Table 1
Patient characteristics

	OBI (n = 4)	BLI (n = 4)	RTX (n = 4)	CAR (n = 12)
Demographic characteristics				
Age (y), mean (SD)	38 (16.7)	60.2 (2.8)	54 (9.8)	38 (14.7)
Sex, female (N)	4	2	2	7
Type of autoimmune disease (N)				
SLE	3	0	0	4
SSc	0	0	0	7
IIM	1	0	2	1
RA	0	4	2	0
Disease duration, months mean (SD)	69 (51.1)	207 (72.1)	35.5 (15.1)	33 (24)
Autoantibodies to (N)				
ANA	4	0	3	12
dsDNA	3	0	0	4
Sm	1	0	0	1
Scl-70	0	0	0	6
Jo-1	1	0	1	1
ACPA/RF	0	4	2	0
Others[a]	4	0	2	3
Concomitant medication (N)				
Glucocorticoids	1	0	0	0
Methotrexate	0	0	1	0
Hydroxychloroquine	3	0	0	0
Mycophenolate mofetil	2	0	0	0
Previous treatments (N)				
Cyclophosphamide	2	0	0	3
Mycophenolate mofetil	1	0	1	9
Azathioprine	3	0	1	3
Rituximab	0	4	-	4
Methotrexate	1	4	2	9
Anticytokine mAbs	1	4	2	7
JAK inhibitors	0	4	1	1
Other drugs[b]	1	2	2	7

ACPA/RF, anticitrullinated peptides antibodies/rheumatoid factor; ANA, antinuclear antibodies; anti-PM/Scl, antipolymyositis/scleroderma; anti-SSA/Ro52, anti−Sjögren's-syndrome-related antigen A autoantibodies/Ro52; BLI, blinatumomab; CAR, CD19 chimeric antigen receptor T cells; dsDNA, double-stranded DNA; IIM, idiopathic inflammatory myopathies; JAK, Janus kinase; Jo1, anti-Jo1 antibodies; mAb, monoclonal antibody; OBI, obinutuzumab; RA, rheumatoid arthritis; RTX, rituximab; Scl-70, scleroderma 70; SLE, systemic lupus erythematosus; Sm, anti-Smith; SSA/Ro60, anti−Sjögren's-syndrome-related antigen A/Ro60; SSc, systemic sclerosis.

Categorical variables: numbers, continuous variables: mean, SD.

[a] Each one has reactivity in OBI: anti-SSA/Ro52, antinucleosome, antihistone, anticardiolipin antibodies, anti-β2-glycoprotein I antibodies and lupus anticoagulant. Each one reactivity in CAR: antiribonucleoprotein, anti-SSA/Ro52, anti-SSA/Ro60, antinucleosome, anti-PM/Scl, anti-Ku and antithreonyl-tRNA synthetase (Th)/anti-RNA processing complex to antibodies. Each one has reactivity in RTX: anti-SSA/Ro52 and anti-PM/Scl.

[b] Other drugs: intravenous immunoglobulins, leflunomide, abatacept and hydroxychloroquine. Among the 12 CAR patients, data from 5 were previously published [12].

Some cells expressing the common plasmablast/plasma cell marker CD138 were still found in the lymph nodes after treatment in all 4 groups (Supplementary Fig S1D,E and Supplementary Table S4). Analysis of CD138+ plasmablasts/plasma cells showed incomplete depletion with all treatments. CD19-CAR T cells reduced plasmablasts/plasma cells by 59%, OBI by 54%, RTX by 32% and BLI by 7%.

Maintenance of follicular structures in the lymph nodes after protein-based B cell depletion

We next assessed changes in the follicular structure in the lymph nodes in all treatment groups, including the number of FDCs, the number of TFH cells and the proliferation rate in the follicles before and after treatment (Fig 2A). These data were included in a combined B cell compartment architecture score (Fig 2B, Supplementary Fig S2A-D, and Supplementary Table S5). In all CD19-CAR T cell-treated patients, the follicular lymph node architecture was completely disrupted (median B cell

compartment score posttreatment [IQR]: 0.0 [0-0]). Among the patients treated with protein-based B cell-depleting agents, only 1 (OBI-treated) exhibited dissolution of the follicular architecture in the lymph nodes, whereas all others retained some degree of follicular structure. In OBI-treated patients, the median (IQR) of the B cell compartment score was 4.5 (0.75-6.75), in the BLI-treated patients 5.5 (1.75-7.75) and RTX-treated patients 4.5 (2.25-7.5), all showing maintained follicular structures. Baseline follicular architecture scores were lowest in BLI-treated patients, which may be explained by the fact that 3 out of 4 BLI-treated patients previously received RTX within 10 months before.

To test the robustness of the previously established combined B cell compartment architecture score, a second pathologist re-evaluated all included lymph node biopsies (n = 48) independently leading to a single agreement value of summarised scores of 87.5% (42/48 cases). The maximum deviation of summarised scores of discrepantly scored cases amounted +1 and −1 score points in 5 versus 1 cases, respectively. These results underline the observer-

Table 2

Differential effect of individual protein-based B cell treatments compared with CD19-CAR T cells on cell counts at follow-up

Treatment	Count ratio (95% CI)	*P* value	Percent higher compared with CAR (95% CI)
CD19			
BLI	190.8 (19.7-1850.4)	.0001	18,983% (1868%-184,939%)
OBI	11.7 (1.2-113.6)	.035	1072% (21%-11,261%)
RTX	60.0 (6.2-581.4)	.0012	5896% (518%-58,037%)
CD20			
BLI	525.6 (85.0-3248.0)	<.0001	52,457% (8404%-324,700%)
OBI	53.9 (8.7-333.2)	<.0001	5292% (773%-33,225%)
RTX	234.7 (38.0-1450.5)	<.0001	23,371% (3698%-144,951%)

BLI, blinatumomab; CAR, CD19 chimeric antigen receptor T cells; OBI, obinutuzumab; RTX, rituximab.
Ratios are exponentiated treatment−visit interactions.

independent robustness of utilising our score to describe global architectural changes of B cell maturation compartment changes. Intraobserver re-evaluation showed 100% concordance.

T cells and myeloid cell numbers in the lymph nodes of patients receiving cell and protein-based B cell depletion

To assess whether the effects of protein and cell-based B cells targeting are specific to the B cell compartment or affect other cells, we quantified the numbers of T cells and macrophages before and after treatments with OBI, BLI, RTX and CD19-CAR T cells (Fig 2C and D, Supplementary Table S4). Neither T cell nor macrophage numbers were affected by any of the B cell-targeted treatment approaches.

Clinical responses

Data on clinical responses after 3 months were available from 22 patients. All 12 CD19-CAR T cell-treated patients achieved clinical responses (assessed by SLEDAI-2K reduction in SLE, ACR−EULAR major clinical response in IIM or EUSTAR-AI in SSc) as well as a drug-free state (Fig 3A). In the OBI, RTX and BLI cohorts, clinical response was not followed by a sustained drug-free state (Fig 3A). Effects on SLEDAI scores in individual patients with SLE are shown in Supplementary Table S6.

DISCUSSION

This study shows that various protein-based B cell targeting therapies, including traditional chimeric anti-CD20 antibody RTX, glycoengineered anti-CD20 antibody OBI and anti-CD19 T cell engager BLI, effectively reduce B cells in the lymph nodes but usually do not achieve complete B cell depletion in the tissue. In contrast, CD19-CAR T cell-based B cell targeting induced consistent B cell depletion in the lymph nodes and abrogation of follicular structures. This deep, consistent tissue depletion in CD19-CAR T cell-treated patients highlights their ability to migrate actively into tissues and kill cells in lymphoid tissues, bone marrow and even the central nervous system [12,24−26].

All treatments effectively induced peripheral B cell depletion, though BLI showed less consistent results due to the molecule's short half-life [27]. Peripheral B cell depletion, however, does not indicate depletion in the tissues, requiring the drug to reach sufficient concentrations in tissues and the presence of a sufficient number of effectors. Proteins, ie, antibodies, generally rely on passive diffusion to penetrate tissues and require additional factors, such as the availability of effector cells and/or

complement components, to eliminate target cells [28]. Ultrasound-guided lymph node biopsy allows to analyse B cell depletion in the tissue of patients with AIDs in a safe and well-tolerated way [12,29,30].

OBI demonstrated good but incomplete reduction of B cells, although 1 patient achieved complete B cell depletion suggesting the principal possibility to clear the lymph node from B cells by protein-based approaches. This finding aligns with previous studies demonstrating OBI's superior effectiveness in eliminating B cells compared with RTX in both peripheral blood and tissues while still not achieving complete B cell depletion in the tissue [18,22,31−33]. Enhanced killing by OBI compared with RTX may be based on higher antibody-dependent cellular cytotoxicity. In contrast, RTX primarily relies on complement-dependent cytotoxicity, which is associated with an increased propensity for internalisation of CD20/CD20 antibody complexes by B cells [34], a key mechanism of resistance to type I anti-CD20 antibodies [35]. In accordance, our study did not show complete depletion of B cells from the lymph nodes of RTX-treated patients. These data support previous studies showing no B cell depletion in lymph nodes [4,12,36] or other organs such as the spleen, bone marrow and synovium 1 to 3 months after RTX infusion, despite B cell depletion in the peripheral blood [37−39].

BLI is a small molecule, comprising a single-chain variable fragment and lacking an Fc fragment, which would allow a more uniform distribution and deeper penetration into tissues [40]. Due to the missing Fc fragment, antibody recycling is not possible accounting for its short half-life of only about 2 hours [27]. We accounted for the shorter half-life by performing an earlier rebiopsy 1 month after the start of treatment, yet we still did not observe complete B cell depletion in the lymph nodes. This finding aligns with previous reports on nonlymphoid target organs, such as the liver and synovium, where tissue B cells were reduced but not completely depleted at comparable (28 days) [41] and later (90 days) [16] time points following BLI treatment. Notably, due to feasibility, exposure to BLI was lower in these patients as compared to patients with lymphoma, in whom BLI is administered in several 4-week-long infusion cycles. Therefore, exposure to the drug by two 1-week infusion cycles might have been incomplete, preventing full B cell depletion in the tissues despite the ability of BLI to penetrate into the lymph nodes based on the small size of the molecule.

We further show that deep B cell depletion—observed in CD19-CAR T cell-treated patients—led to the loss of follicular structure associated with the abrogation of FDCs and TFH cells as well as decreased cell proliferation in the lymph nodes. On the one hand, breakdown of follicular structure in the lymph nodes requires full B cell depletion, suggesting that residual B cells appear to be sufficient to provide signals to retain FDCs (eg, lymphotoxin-beta) and TFH cells (eg, CD40) in the lymph node [42,43]. On the other hand, less pronounced changes in follicular architecture were also seen with protein-based B cell depleters. This effect may also contribute to the reduced follicular architecture scores in BLI-treated patients at baseline, as they had been exposed to RTX approximately 8 to 10 months before starting BLI treatment. One patient received anti-TNF treatment 6 weeks before BLI, a treatment that has also been associated with B cell decrease in the germinal centre [44]. These observations suggest that a combination of protein-based therapies may exert either cumulative or synergistic effects on lymphoid tissue, which should be assessed with dedicated interventional studies. An excellent example supporting this concept is the combination of rituximab and belimumab, which showed additive effects on
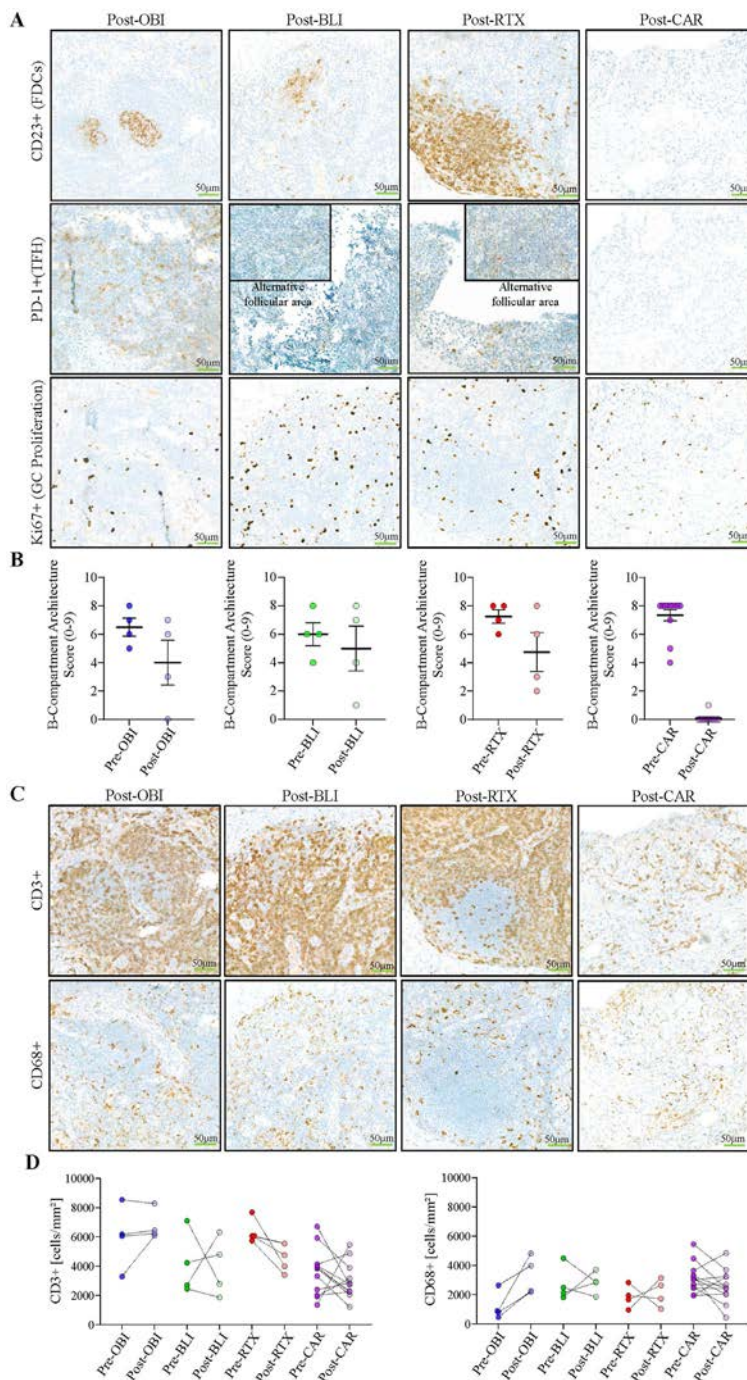
Figure 2. Changes of the follicular compartment of lymph nodes after B cell depletion (A) Representative immunohistochemistry images of posttreatment lymph node biopsies obtained from 1 representative patient per treatment condition. Although the follicular architecture (presence of CD23+ follicular dendritic cell network [FDC], presence of PD-1+ T follicular helper [TFH] cells) is preserved after treatment with obinutuzumab (OBI), blinatumomab (BLI) and rituximab (RTX), germinal centres are completely eradicated following CD19 chimeric antigen receptor T cell (CAR) treatment. Proliferation rate of germinal centre B cells (measured with Ki67) is also reduced. Pictures were taken at × 200 magnification on a Zeiss Axio Imager A2 microscope. (B) Pre- and posttreatment follicular architecture scores stratified by different treatment conditions. (C) Representative hematoxylin and eosin-stained images of posttreatment lymph node biopsies showing unaltered presence of regularly distributed CD3+ T cells and CD68+ macrophages in all 4 treatments. Pictures were taken at × 200 magnification on a Zeiss Axio Imager A2 microscope. (D) Quantitative pre- and posttreatment measures of CD3 + T cells and CD68+ macrophages.

B cell depletion in the salivary glands compared with rituximab alone, indicating that neutralisation of increased BAFF expression in conjunction with rituximab treatment could enhance the cell-depleting effect of rituximab [45]. Overall, the less pronounced changes in follicular architecture that we observed with protein-based B cell inhibitors, also after RTX pre-exposure, do not appear to be sufficient to induce drug-free remission. Thus, although CD19-CAR T cell-treated patients experienced drug-free remission, this was not the case in protein-based B cell-treated patients, who required either retreatment or rescue treatment. This observation supports previous studies showing that a greater and more sustained depletion of B cells in the peripheral blood is associated with better clinical responses in AID [31,46−48], transplantation [36] and cancer [22]. Although larger-scale studies are needed to confirm whether B cell depletion in secondary lymphoid organs directly correlates with clinical outcomes in patients with AID, our findings support

this hypothesis by extending the focus from the peripheral blood to lymphoid tissues and specifically to the entire follicle structure. Indeed, introducing lymph node biopsy as a clinical tool to assess B cell depletion could enhance treatment monitoring and play a pivotal role in tailoring therapeutic strategies. Another important aspect is the use of long-term follow-up biopsies as a strategy to assess B cell repletion and follicle reconstitution in the lymphoid organs of patients who have achieved drug-free remission, as we recently observed 1 year after CD19-CAR T cell therapy [49], paving the way for further analyses investigating the qualitative changes of the 'new' repopulating B cells and their correlation with persistent clinical response.

Our data also reveal the persistence of CD138+ plasmablasts/plasma cells in lymph nodes across all treatment groups. However, the decrease observed in CD19-CAR T cell-treated patients is likely due to the robust depletion of the CD19 +CD138+ plasmablast fraction, as previously described [12].

A

	OBI 1	OBI 2	OBI 3	OBI 4	BLI 1	BLI 2	BLI 3	BLI 4	RTX 1	RTX 2	RTX 3	RTX 4
	SLE	IIM	SLE	SLE	RA	RA	RA	RA	RA	RA	IIM	IIM
LN Clearance												
Clinical response												
Remission												
Drug-Free State												

	CAR 1	CAR 2	CAR 3	CAR 4	CAR 5	CAR 6	CAR 7	CAR 8	CAR 9	CAR 10	CAR 11	CAR 12
	SLE	SSc	SLE	SSc	SLE	SLE	SSc	SSc	SSc	SSc	IIM	SSc
LN Clearance												
Clinical response												
Remission		n.a.		n.a.				n.a.	n.a.	n.a.		n.a.
Drug-Free State												

Figure 3. Clinical response. (A) Summary of outcomes in all patients according to different treatments 3 months after therapy. Colour legend: green indicates achievement, red indicates nonachievement and light blue indicates not available. Lymph node (LN) clearance indicates B cell depletion and follicular architecture disruption in the lymph node. Clinical response label is based on SLE Responder Index (SRI), ACR−EULAR Moderate Clinical Response (IIM), Disease Activity Score-28 response (RA) and American College of Rheumatology Composite Response Index in Systemic Sclerosis (ACR-CRISS). Remission label is based on DORIS remission (SLE), ACR−EULAR Major Clinical Response (IIM), DAS-28 remission−(RA) and is not applicable (n.a.) in SSc and assessed at 3-month follow-up based on drug-free state, indicating absence of immunosuppressive treatments. Concomitant treatments at 3-month follow-up were obinutuzumab (OBI) 1: hydroxychloroquine (HCQ) and OBI; OBI 2, mycophenolate mofetil and OBI; OBI 3, CD19-CAR T cells; OBI 4, CD19-CAR T cells planned after bridging therapy with OBI (follow-up at 3 months not available); blinatumomab (BLI) 1, etanercept; BLI 2, teclistamab; BLI 3, filgotinib; BLI, follow-up at 3 months not available; rituximab (RTX) 1, only RTX; RTX 2, methotrexate and RTX; RTX 3, only RTX; and RTX 4, only RTX. All CD19-CAR T cell-treated patients were drug-free at 3-month follow-up. ACR−EULAR, American College of Rheumatology−European League Against Rheumatism; CAR, CD19 chimeric antigen receptor T cells; DAS-28, Disease Activity Score-28; DORIS, Definition of Remission in SLE; IIM, idiopathic inflammatory myopathies; RA, rheumatoid arthritis; SLE, systemic lupus erythematosus; SSc, systemic sclerosis.

This aligns with single-cell RNA sequencing data from bone marrow biopsies taken 58.5 days post-therapy—comparable to our biopsy time point (60.8 days)—which showed persistence of plasma cells [50]. Additionally, this finding supports the observed persistence of circulating IgG, which declines after treatment but remains above the threshold not requiring supplementation in all groups. A more pronounced reduction in IgM across all treatments corresponds to the observed decrease in the B cell pool in all patients.

This study has several limitations. First, tissue depletion effects of T cell engagers may be underestimated as they depend on the type of molecule and dosage. BLI is a small molecule with good tissue penetration but a short half-life. We acknowledged this by earlier biopsy in BLI-treated patients but did not find depletion despite earlier sampling. In addition, the dose of BLI used here is still lower than the one used in the cancer indication, which requires a continuous infusion over a 4-week period. Nonetheless, the second infusion cycle of BLI had a 3-times higher dose than the first infusion cycle in this work, providing an overall 2-times higher drug exposure than in the first study with BLI [18]. A further limitation is the small number of patients included in the protein-based anti-B cell treatment groups compared with the CD19-CAR T cell cohort, which supports the more exploratory nature of the results. However, despite the small sample size, when considering the data from the protein-based strategies collectively, we still observe a lack of sustained and robust depletion in secondary lymphoid organs, contrasting the findings from CD19-CAR T cell therapy. A further limitation is that the type of AIDs in the different treatment groups is not balanced. However, we do not believe that there are significant differences in depletion efficacy in lymph nodes among different diseases, as highlighted by the consistency of depletion observed with CD19-CAR T cell therapy across various diseases. Furthermore, patients with SLE may show impaired antibody-based depletion due to low complement levels and Fc-receptor polymorphisms related to SLE. However, this effect might have mitigated and not enhanced the response to OBI, as most of the OBI-treated patients had SLE. Another limitation in comparing CD19-CAR T cells with protein-based B cell depletion is that the former is preceded by additional lymphodepletion treatment, whereas the latter is not. The extent to which lymphodepletion contributes to tissue B cell depletion is unclear, as lymphodepletion allows the expansion of CD19-CAR T cells in the patient. Direct depletion of B cells in the lymph node seems, however, less likely, as 1 patient received the same dose of cyclophosphamide only 6 days before the pretreatment biopsy, and no signs of B cell depletion in the lymph node were found.

In summary, this study demonstrates that protein-based B cell-targeting agents reduce B cells in secondary lymphoid organs but do not achieve sustained deep depletion. In contrast, deep tissue B cell depletion was consistently observed in a larger cohort of CD19-CAR T cell-treated patients. These findings underscore the significant differences in the B cell-depleting capacity of cell-based therapies, which impact their potential to induce drug-free remission in patients with AID. Whether this sustained drug-free remission eventually signifies the cure of AID remains to be determined and depends on longer follow-ups. Nonetheless, these findings push the limits of current treatment goals in AID from on-drug suppression of disease to off-drug remission. Improvement of strategies of protein-based B cell depletion by new molecules or antibody combinations may open the boundaries of protein-based B cell depletion in the future coming closer to a 'cell-therapy-like effect.'

Competing interests

Contributors

CT, ME, GS and MGR conceived and designed the study. CT and MGR collected the samples. CT and ME collected and analysed the data. All authors interpreted the data. CT, ME and MGR wrote the first version of the manuscript, and all authors critically revised and approved the final version. All authors had full access to all the data in the study and had final responsibility for the decision to submit for publication. CT and ME contributed equally to this work. MGR is responsible for the overall content as guarantor.

Patient consent for publication

Consent was obtained directly from the patients.

Ethics approval

All procedures were performed in accordance with the Good Clinical Practice guidelines of the International Council for Harmonization and covered by license 24-13-B of the Institutional Review Board. Self-reported and biological sexes were identical in all patients. All participants gave written informed consent according to CARE guidelines and in compliance with the Declaration of Helsinki principles. No commercial sponsor was involved.

Provenance and peer review

Not commissioned; externally peer reviewed.

Data availability statement

Not applicable

Patient and public involvement

Not applicable.

Supplementary materials

Supplementary material associated with this article can be found in the online version at doi:10.1016/j.ard.2025.06.2120.

Orcid

Maria Gabriella Raimondo: http://orcid.org/0000-0003-2020-6711

REFERENCES

[1] Schett G, Nagy G, Krönke G, Mielenz D. B-cell depletion in autoimmune diseases. Ann Rheum Dis 2024;83:1409–20. doi: 10.1136/ard-2024-225727.

[2] Carter LM, Ehrenstein MR. Vital EM. Evolution and trajectory of B-cell targeted therapies in rheumatic diseases. Lancet Rheumatol 2025;7:e355–67. doi: 10.1016/S2665-9913(24)00338-2.

[3] Anolik JH, Barnard J, Owen T, Zheng B, Kemshetti S, Looney RJ, et al. Delayed memory B cell recovery in peripheral blood and lymphoid tissue in systemic lupus erythematosus after B cell depletion therapy. Arthritis Rheum 2007;56:3044–56. doi: 10.1002/art.22810.

[4] Ramwadhdoebe TH, van Baarsen LGM, Boumans MJH, Bruijnen STG, Safy M, Berger FH, et al. Effect of rituximab treatment on T and B cell subsets in lymph node biopsies of patients with rheumatoid arthritis. Rheumatology (Oxford) 2019;58:1075–85. doi: 10.1093/rheumatology/key428.

[5] Schett G, Mackensen A, Mougiakakos D. CAR T-cell therapy in autoimmune diseases. Lancet 2023;402:2034–44. doi: 10.1016/S0140-6736(23)01126-1.

[6] Mackensen A, Müller F, Mougiakakos D, Böltz S, Wilhelm A, Aigner M, et al. Anti-CD19 CAR T cell therapy for refractory systemic lupus erythematosus. Nat Med 2022;28:2124–32. doi: 10.1038/s41591-022-02017-5.

[7] Müller F, Taubmann J, Bucci L, Wilhelm A, Bergmann C, Völkl S, et al. CD19 CAR T-cell therapy in autoimmune disease—a case series with follow-up. N Engl J Med 2024;390:687–700. doi: 10.1056/NEJMoa2308917.

[8] Pecher AC, Hensen L, Klein R, Schairer R, Lutz K, Atar D, et al. CD19-targeting CAR T cells for myositis and interstitial lung disease associated with anti-synthetase syndrome. JAMA 2023;329:2154–62. doi: 10.1001/jama.2023.8753.

[9] Wang W, He S, Zhang W, Zhang H, DeStefano VM, Wada M, et al. BCMA-CD19 compound CAR T cells for systemic lupus erythematosus: a phase 1 open-label clinical trial. Ann Rheum Dis 2024;83:1304–14. doi: 10.1136/ard-2024-225785.

[10] Nicolai R, Merli P, Moran Alvarez P, Bracaglia C, Del Bufalo F, Marasco E, et al. Autologous CD19-targeting CAR T cells in a patient with refractory juvenile dermatomyositis. Arthritis Rheumatol 2024;76:1560–5. doi: 10.1002/art.42933.

[11] Lidar M, Rimar D, David P, Jacoby E, Shapira-Frommer R, Itzhaki O, et al. CD-19 CAR-T cells for polyrefractory rheumatoid arthritis. Ann Rheum Dis 2025;84:370–2. doi: 10.1136/ard-2024-226437.

[12] Tur C, Eckstein M, Velden J, Rauber S, Bergmann C, Auth J, et al. CD19-CAR T-cell therapy induces deep tissue depletion of B cells. Ann Rheum Dis 2025;84:106–14. doi: 10.1136/ard-2024-226142.

[13] Furie RA, Rovin BH, Garg JP, Santiago MB, Aroca-Martínez G, Zuta Santillán AE, et al. Efficacy and safety of obinutuzumab in active lupus nephritis. N Engl J Med 2025;392:1471–83. doi: 10.1056/NEJMoa2410965.

[14] Furie RA, Aroca G, Cascino MD, Garg JP, Rovin BH, Alvarez A, et al. B-cell depletion with obinutuzumab for the treatment of proliferative lupus nephritis: a randomised, double-blind, placebo-controlled trial. Ann Rheum Dis 2022;81:100–7. doi: 10.1136/annrheumdis-2021-220920.

[15] Rovin BH, Furie RA, Ross Terres JA, Giang S, Schindler T, Turchetta A, et al. Kidney outcomes and preservation of kidney function with obinutuzumab in patients with lupus nephritis: a post hoc analysis of the NOBILITY trial. Arthritis Rheumatol 2024;76:247–54. doi: 10.1002/art.42734.

[16] Bucci L, Hagen M, Rothe T, Raimondo MG, Fagni F, Tur C, et al. Bispecific T cell engager therapy for refractory rheumatoid arthritis. Nat Med 2024;30:1593–601. doi: 10.1038/s41591-024-02964-1.

[17] Subklewe M, Magno G, Gebhardt C, Bücklein V, Szelinski F, Arévalo HJR, et al. Application of blinatumomab, a bispecific anti-CD3/CD19 T-cell engager, in treating severe systemic sclerosis: a case study. Eur J Cancer 2024;204:114071. doi: 10.1016/j.ejca.2024.114071.

[18] Mössner E, Brünker P, Moser S, Püntener U, Schmidt C, Herter S, et al. Increasing the efficacy of CD20 antibody therapy through the engineering of a new type II anti-CD20 antibody with enhanced direct and immune effector cell-mediated B-cell cytotoxicity. Blood 2010;115:4393–402. doi: 10.1182/blood-2009-06-225979.

[19] Herter S, Herting F, Mundigl O, Waldhauer I, Weinzierl T, Fauti T, et al. Pre-clinical activity of the type II CD20 antibody GA101 (obinutuzumab) compared with rituximab and ofatumumab in vitro and in xenograft models. Mol Cancer Ther 2013;12:2031–42. doi: 10.1158/1535-7163.MCT-12-1182.

[20] Grakoui A, Bromley SK, Sumen C, Davis MM, Shaw AS, Allen PM, et al. The immunological synapse: a molecular machine controlling T cell activation. Science 1999;285:221–7. doi: 10.1126/science.285.5425.221.

[21] Rogala B, Freyer CW, Ontiveros EP, Griffiths EA, Wang ES, Wetzler M. Blina-tumomab: enlisting serial killer T-cells in the war against hematologic malignancies. Expert Opin Biol Ther 2015;15:895–908. doi: 10.1517/14712598.2015.1041912.

[22] Goede V, Fischer K, Busch R, Engelke A, Eichhorst B, Wendtner CM, et al. Obinutuzumab plus chlorambucil in patients with CLL and coexisting conditions. N Engl J Med 2014;370:1101–10. doi: 10.1056/NEJMoa1313984.

[23] Edwards JC, Szczepanski L, Szechinski J, Filipowicz-Sosnowska A, Emery P, Close DR, et al. Efficacy of B-cell-targeted therapy with rituximab in patients with rheumatoid arthritis. N Engl J Med 2004;350:2572–81. doi: 10.1056/NEJMoa032534.

[24] Grupp SA, Kalos M, Barrett D, Aplenc R, Porter DL, Rheingold SR, et al. Chimeric antigen receptor-modified T cells for acute lymphoid leukemia. N Engl J Med 2013;368:1509–18. doi: 10.1056/NEJMoa1215134.

[25] Minopoulou I, Wilhelm A, Albach F, Kleyer A, Wiebe E, Schallenberg S, et al. Anti-CD19 CAR T cell therapy induces antibody seroconversion and complete B cell depletion in the bone marrow of a therapy-refractory patient with ANCA-associated vasculitis. Ann Rheum Dis 2025;84:e4–7. doi: 10.1016/j.ard.2025.01.008.

[26] Kochenderfer JN, Wilson WH, Janik JE, Dudley ME, Stetler-Stevenson M, Feldman SA, et al. Eradication of B-lineage cells and regression of lymphoma in a patient treated with autologous T cells genetically engineered to recognize CD19. Blood 2010;116:4099–102. doi: 10.1182/blood-2010-04-281931.

[27] Mocquot P, Mossazadeh Y, Lapierre L, Pineau F, Despas F. The pharmacology of blinatumomab: state of the art on pharmacodynamics, pharmacokinetics, adverse drug reactions and evaluation in clinical trials. J Clin Pharm Ther 2022;47:1337–51. doi: 10.1111/jcpt.13741.

[28] Gong Q, Ou Q, Ye S, Lee WP, Cornelius J, Diehl L, et al. Importance of cellular microenvironment and circulatory dynamics in B cell immunotherapy. J Immunol 2005;174:817–26. doi: 10.4049/jimmunol.174.2.817.

[29] van Baarsen LG, de Hair MJ, Ramwadhdoebe TH, Zijlstra IJ, Maas M, Gerlag DM, et al. The cellular composition of lymph nodes in the earliest phase of inflammatory arthritis. Ann Rheum Dis 2013;72:1420–4. doi: 10.1136/annrheumdis-2012-202990.

[30] Fiechter RH, Bolt JW, van de Sande MGH, Aalbers CJ, Landewé RBM, Maas M, et al. Ultrasound-guided lymph node biopsy sampling to study the immunopathogenesis of rheumatoid arthritis: a well-tolerated valuable research tool. Arthritis Res Ther 2022;24:36. doi: 10.1186/s13075-022-02728-7.

[31] Looney CM, Strauli N, Cascino MD, Garma H, Schroeder AV, Takahashi C, et al. Development of a novel, highly sensitive assay for quantification of minimal residual B cells in autoimmune disease and comparison to traditional methods across B-cell-depleting agents. Clin Immunol 2023;248:109265. doi: 10.1016/j.clim.2023.109265.

[32] Looney CM, Schroeder A, Tavares E, Garg J, Schindler T, Vincenti F, et al. Obinutuzumab effectively depletes key B-cell subsets in blood and tissue in end-stage renal disease patients. Transplant Direct 2023;9:e1436. doi: 10.1097/TXD.0000000000001436.

[33] Reddy V, Klein C, Isenberg DA, Glennie MJ, Cambridge G, Cragg MS, et al. Obinutuzumab induces superior B-cell cytotoxicity to rituximab in rheumatoid arthritis and systemic lupus erythematosus patient samples. Rheumatology (Oxford) 2017;56:1227–37. doi: 10.1093/rheumatology/kex067.

[34] Lim SH, Vaughan AT, Ashton-Key M, Williams EL, Dixon SV, Chan HT, et al. Fc gamma receptor IIb on target B cells promotes rituximab internalization and reduces clinical efficacy. Blood 2011;118:2530–40. doi: 10.1182/blood-2011-01-330357.

[35] Reddy V, Cambridge G, Isenberg DA, MJ Glennie, Cragg MS, Leandro M. Internalization of rituximab and the efficiency of B cell depletion in rheumatoid arthritis and systemic lupus erythematosus. Arthritis Rheumatol 2015;67:2046–55. doi: 10.1002/art.39167.

[36] Kamburova EG, Koenen HJ, Borgman KJ, ten Berge IJ, Joosten I, Hilbrands LB. A single dose of rituximab does not deplete B cells in secondary lymphoid organs but alters phenotype and function. Am J Transplant 2013;13:1503–11. doi: 10.1111/ajt.12220.

[37] Audia S, Samson M, Guy J, Janikashvili N, Fraszczak J, Trad M, et al. Immunologic effects of rituximab on the human spleen in immune thrombocytopenia. Blood 2011;118:4394–400. doi: 10.1182/blood-2011-03-344051.

[38] Thurlings RM, Vos K, Wijbrandts CA, Zwinderman AH, Gerlag DM, Tak PP. Synovial tissue response to rituximab: mechanism of action and identification of biomarkers of response. Ann Rheum Dis 2008;67:917–25. doi: 10.1136/ard.2007.080960.

[39] Rehnberg M, Amu S, Tarkowski A, Bokarewa MI, Brisslert M. Short- and long-term effects of anti-CD20 treatment on B cell ontogeny in bone marrow of patients with rheumatoid arthritis. Arthritis Res Ther 2009;11:R123. doi: 10.1186/ar2789.

[40] Holliger P, Hudson PJ. Engineered antibody fragments and the rise of single domains. Nat Biotechnol 2005;23:1126–36. doi: 10.1038/nbt1142.

[41] Bargou R, Leo E, Zugmaier G, Klinger M, Goebeler M, Knop S, et al. Tumor regression in cancer patients by very low doses of a T cell-engaging antibody. Science 2008;321:974–7. doi: 10.1126/science.1158545.

[42] Cerny A, Zinkernagel RM, Groscurth P. Development of follicular dendritic cells in lymph nodes of B-cell-depleted mice. Cell Tissue Res 1988;254:449–54. doi: 10.1007/BF00225818.

[43] Yusuf I, Stern J, McCaughtry TM, Gallagher S, Sun H, Gao C, et al. Germinal center B cell depletion diminishes CD4+ follicular T helper cells in autoimmune mice. PLoS One 2014;9:e102791. doi: 10.1371/journal.pone.0102791.

[44] Anolik JH, Ravikumar R, Barnard J, Owen T, Almudevar A, Milner EC, et al. Cutting edge: anti-tumor necrosis factor therapy in rheumatoid arthritis inhibits memory B lymphocytes via effects on lymphoid germinal centers and follicular dendritic cell networks. J Immunol 2008;180:688–92. doi: 10.4049/jimmunol.180.2.688.

[45] Mariette X, Barone F, Baldini C, Bootsma H, Clark KL, De Vita S, et al. A randomized, phase II study of sequential belimumab and rituximab in primary Sjögren's syndrome. JCI Insight 2022 Dec 8;7(23):e163030.

[46] Vital EM, Dass S, Buch MH, Henshaw K, Pease CT, Martin MF, et al. B cell biomarkers of rituximab responses in systemic lupus erythematosus. Arthritis Rheum 2011;63:3038–47. doi: 10.1002/art.30466.

[47] Vital EM, Dass S, Buch MH, Rawstron AC, Emery P. An extra dose of rituximab improves clinical response in rheumatoid arthritis patients with initial incomplete B cell depletion: a randomised controlled trial. Ann Rheum Dis 2015;74:1195–201. doi: 10.1136/annrheumdis-2013-204544.

[48] Dias SS, Rodriguez-Garcia V, Nguyen H, Pericleous C, Isenberg D. Longer duration of B cell depletion is associated with better outcome. Rheumatology (Oxford) 2015;54:1876–81. doi: 10.1093/rheumatology/kev036.

[49] Tur C, Eckstein M, Schett G, Raimondo MG. Response to the correspondence on "CD19-CAR T-cell therapy induces deep tissue depletion of B cells". Ann Rheum Dis 2025. doi: 10.1016/j.ard.2025.03.006.

[50] Strati P, Li X, Deng Q, Marques-Piubelli ML, Henderson J, Watson G, et al. Prolonged cytopenia following CD19 CAR T cell therapy is linked with bone marrow infiltration of clonally expanded IFNgamma-expressing CD8 T cells. Cell Rep Med 2023;4:101158. doi: 10.1016/j.xcrm.2023.101158.

Autoimmunity

Autoantibody reactome analysis reveals diagnostic biomarkers and molecular classification for relapsing polychondritis

Yongmei Liu[1,a], Mengzhu Zhao[2,3,a], Lei Zhang[4,a], Jing Luo[5,a], Linlin Cheng[1,a], Haoting Zhan[1,a], Mansheng Li[6], Zijuan Zhang[7], Siyu Wang[1], Xinxin Feng[1], Min Feng[5], Haolong Li[1], Zhan Li[1], Jingdi Zhang[1], Yong Hou[3,***], Xiaobo Yu[6,**], Yongzhe Li[1,*]

[1] Department of Clinical Laboratory, State Key Laboratory of Complex, Severe and Rare Diseases, Peking Union Medical College Hospital, Peking Union Medical College and Chinese Academy of Medical Sciences, Beijing, China

[2] Department of Rheumatology, The First Affiliated Hospital, Zhejiang University School of Medicine, Hangzhou, China

[3] Key Laboratory of Rheumatology and Clinical Immunology, Department of Rheumatology, Peking Union Medical College Hospital, Peking Union Medical College and Chinese Academy of Medical Science, Ministry of Education, National Clinical Research Center for Dermatologic and Immunologic Diseases, Ministry of Science & Technology, Beijing, China

[4] Department of Rheumatology, The First Affiliated Hospital of Zhengzhou University, Zhengzhou, China

[5] Department of Rheumatology, The Second Hospital of Shanxi Medical University, Taiyuan, China

[6] State Key Laboratory of Medical Proteomics, Beijing Proteome Research Center, National Center for Protein Sciences-Beijing (PHOENIX Center), Beijing Institute of Lifeomics, Beijing, China

[7] Department of Pathology, State Key Laboratory of Complex Severe and Rare Diseases, Molecular Pathology Research Centre, Peking Union Medical College Hospital, Chinese Academy of Medical Sciences and Peking Union Medical College, Beijing, China

A R T I C L E   I N F O

A B S T R A C T

Objectives: The lack of effective biomarkers for relapsing polychondritis (RP) poses a significant challenge in its early diagnosis and treatment. This study aimed to identify novel autoantibodies and elucidate the pathogenesis and molecular heterogeneity of RP.

Methods: Plasma samples from 467 RP patients, 164 healthy controls (HCs), and 186 disease controls (DCs) were analysed using 2 sequential microarrays and enzyme-linked immunosorbent assay to sequentially discover, validate, and verify new autoantibodies. Machine learning and differential analysis were used to identify diagnosis-specific autoantibodies and their correlation with disease activity, recurrence, and remission.

Results: The RP group had 1344 elevated autoantibodies, discriminating RP patients from HCs. These antigenic targets were associated with pathways involving autoimmune responses, infections, and cardiovascular lesions. Two molecular subtypes characterised by distinct organ involvement and prognosis highlighted the heterogeneity of RP. Notably, 14 new autoantibodies were identified, which differentiated RP versus HCs and DCs with a sensitivity of 41% and 49.7% and a specificity of 91.7% and 90.5%, respectively. Among them, 6 autoantibodies showed better diagnostic performance and were consistently verified. Specifically, anti-C4B was positively

*Correspondence to Prof Yongzhe Li.

**Correspondence to Prof Xiaobo Yu.

***Correspondence to Prof Yong Hou.

E-mail addresses: houyongjia@hotmail.com (Y. Hou), yuxiaobo@ncpsb.org.cn (X. Yu), yongzhelipumch@126.com (Y. Li).

Handling editor Josef S. Smolen

[a] Yongmei Liu, Mengzhu Zhao, Lei Zhang, Jing Luo, Linlin Cheng, and Haoting Zhan contributed equally to this work.

correlated with disease activity, and increased anti-KRT16 predicted RP recurrence within 1 year. In addition, anti-C4B, anti-FNBP4, and anti-KRT10 decreased from acute attack to remission. Furthermore, the deposition of C4B protein in tracheal tissues, coupled with its reduction in plasma of RP patients, indicated that abnormal complement activation might be related to the pathological mechanism of RP.

Conclusions: The 14 autoantibodies promoted a noninvasive early detection of RP, predicted disease recurrence and provided new insights into the understanding of RP pathogenesis.

WHAT IS ALREADY KNOWN ON THIS TOPIC

- The diagnostic and therapeutic landscape of relapsing polychondritis (RP) is constrained by the absence of robust biomarkers and a limited understanding of the underlying pathological mechanisms.

WHAT THIS STUDY ADDS

- This investigation reveals the presence of 2 distinct molecular subtypes in RP, characterised by unique clinical phenotypes, thereby underscoring the heterogeneity of this condition.
- The identification of 14 novel autoantibodies represents a significant advancement, offering potential as diagnostic biomarkers for RP.
- The diagnostic performance of the 14 autoantibodies is significant, with a specificity of more than 90% and sensitivity of 41% and 49.7% in differentiating RP from healthy controls and disease controls, respectively.
- The anti-C4B and anti-KRT16 autoantibodies are potentially useful in the assessment of disease activity and the prediction of recurrence, extending their clinical relevance beyond diagnosis.

HOW THIS STUDY MIGHT AFFECT RESEARCH, PRACTICE OR POLICY

- The discovery of these plasma autoantibodies represents a potential improvement in the early diagnostic accuracy and precision medicine approaches in the management of RP. This work lays the foundation for the development of targeted and personalised therapeutic interventions, potentially ameliorating clinical outcomes for patients with RP.

INTRODUCTION

Relapsing polychondritis (RP) is a rare autoimmune disorder characterised by recurrent inflammation of cartilage-rich organs, including ears, nose, respiratory tract, eyes, and joints, with a reported incidence ranging from 0.71 to 4.5 per million individuals [1,2]. Its aetiology and pathogenesis remain elusive despite the extensive research. Potential triggers, including infection and chemical or mechanical trauma, cause protein degradation, cartilage antigen exposure, and a subsequent autoimmune response culminating in cartilage destruction [3−7]. Therefore, early diagnosis and treatment are needed to prevent disease progression and improve patient prognosis.

The mean diagnostic delay is 14.4 months due to the relatively insidious onset and heterogeneity of RP, with a misdiagnosis rate of 47% [8]. Autoantibodies against type II collagen (COL2) or matrilin-1 have limited sensitivity and specificity in RP diagnosis [9]. Cartilage oligomeric protein (COMP), identified as potential biomarker for monitoring disease activity, remains inadequately validated [9]. Thus, specific diagnostic biomarkers are urgently needed, along with the discovery of the potential pathological mechanisms underlying RP.

High-density protein microarray technology represents a promising approach for screening autoantibodies in autoimmune diseases, particularly those where autoantibodies play a pivotal role in disease pathogenesis [10]. Li et al. [11] successfully discovered anti-PTX-3 and anti-DUSP11 with positivity values of 27.56% and 31.80%, respectively, in patients with ACPA-negative rheumatoid arthritis using HuProt microarray. Moreover, 12 new autoantibodies were identified to diagnose Sjögren's syndrome, the autoantigens of which are involved in disease development through exposure to the immune system due to cell death or tissue damage [12]. Nevertheless, comprehensive studies on autoantibodies in RP are scarce.

This study identified more elevated autoantibodies in RP patients than in control groups, elucidated the signalling pathways and biological processes involving specific autoantigens in RP pathogenesis, and characterised the molecular subtypes based on the heterogeneity of autoantibody expression in RP patients. Furthermore, 2 phases of protein microarrays were used sequentially in a large cohort to discover new autoantibodies qualified as RP biomarkers. Enzyme-linked immunosorbent assay (ELISA) was performed to verify the feasibility of these new autoantibodies. Three novel autoantigens for RP patients were further detected in pathological tissues.

METHODS

Study population and samples

A total of 467 RP patients were recruited from Peking Union Medical College Hospital, the First Hospital of Zhengzhou University, and the Second Hospital of Shanxi Medical University from July 2017 to April 2024. RP diagnosis fulfilled the criteria of McAdam, Damiani-Levine, or Michet [13−15]. RP patients with other autoimmune diseases, tumours, haematological disorders, or immunodeficiency diseases were excluded. One hundred sixty-four healthy controls (HCs) and 186 patients with other autoimmune diseases (DCs) were enrolled as controls during the same period. The DCs group comprised 60 patients with rheumatoid arthritis, 51 with Behçet's disease, and 75 with antineutrophil cytoplasmic antibodies associated vasculitis, diagnosed according to the corresponding classification criteria [16−19]. All participants were divided into discovery, validation, and verification cohorts. Participants in the 3 cohorts were mutually exclusive. The flowchart of autoantibody identification is shown in Figure 1. Demographic and clinical characteristics of participants at the time of blood collection were recorded. Detailed information of cohorts and follow-up patients is described in Supplementary Methods and Supplementary Tables S1-S4.

High-density protein microarrays for candidate autoantibody screening

High-density protein microarray (AAbMap1.0) developed by ProteomicsEra Medical Co., Ltd was used to find novel
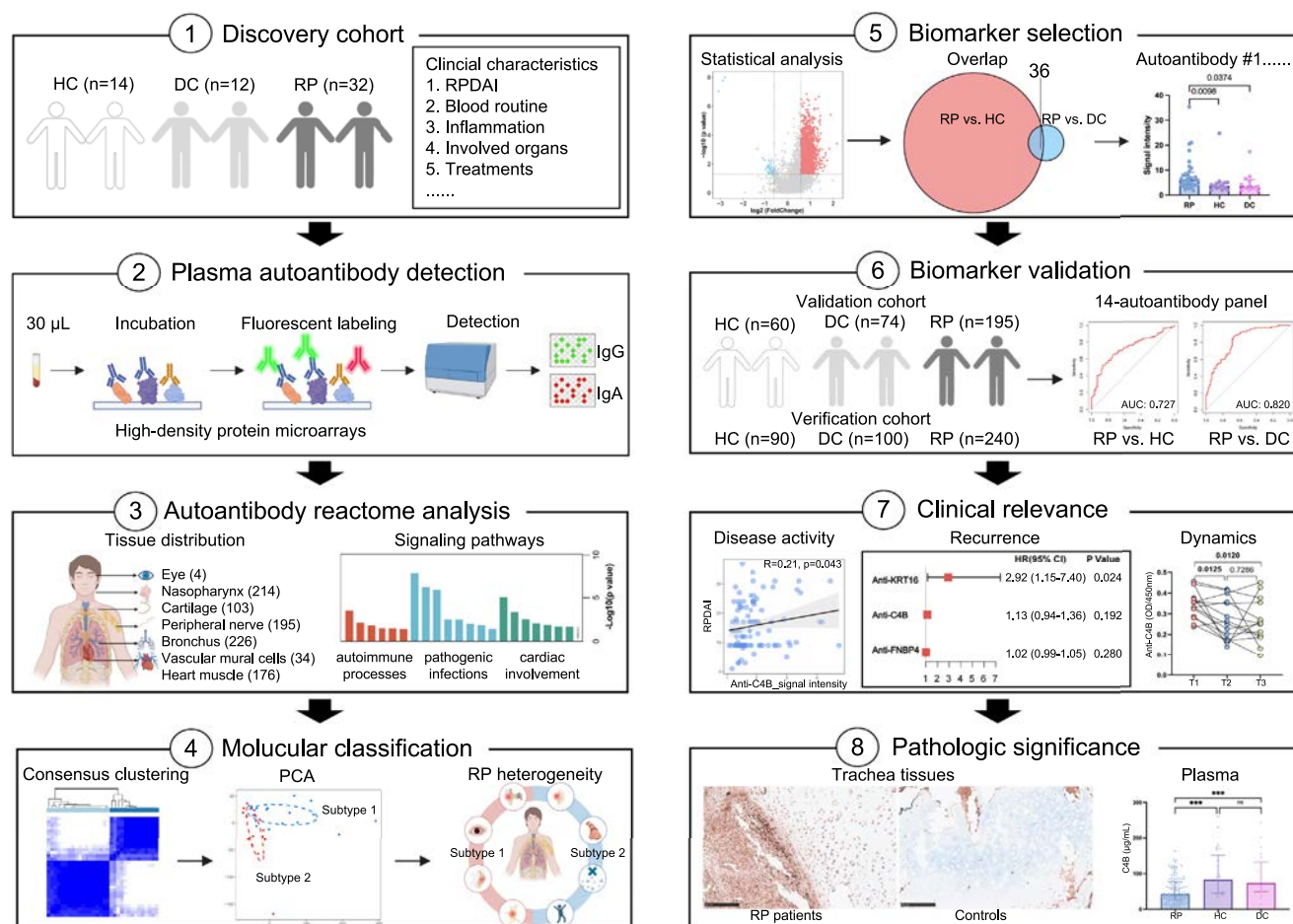
Figure 1. Workflow of plasma autoantibody reactome analysis of RP. DC, disease control; PCA, principal component analysis; RP, relapsing polychondritis.

autoantibodies in the discovery cohort [20]. The microarray is printed with 2382 proteins, 60 clinically applied autoantigens, and 1486 peptides in duplicate. Among these, 677 peptides had post-translational modifications (PTMs), while 809 peptides did not (Appendix). The detailed information of proteome array was provided in Supplementary Methods.

Plasma samples were centrifuged and diluted with blocking solution (5% skim milk/phosphate buffer saline (PBS)-0.05% Tween-20) at a ratio of 1:130. The microarray was blocked for 30 minutes and incubated with diluted plasma at room temperature for 2 hours. After washing, the microarray was incubated with 2 μg/mL Cy3-labelled anti-human IgG H + L and Alexa Fluor-labelled anti-human IgA (Jackson ImmunoResearch, 709-165-149 and 109-605-011) at room temperature in the dark for 1 hour, followed by a thorough wash. The anti-human IgG antibody showed no binding to human IgM and minimal cross-reactivity with IgA protein, demonstrating >5.8-fold lower intensity compared to IgG (Supplementary Fig S1C). The microarray was scanned using the GenePix 4300A microarray scanner (Molecular Devices). The signal intensity of autoantibodies was normalised using the signal-to-noise ratio, calculated as the average signal divided by average negative control spots.

Candidate autoantibodies should satisfy 3 criteria: (1) RP versus HCs, P values obtained from the Wilcoxon test < 0.05 and fold change (FC) >1.5; (2) RP versus DCs, $P < 0.05$ and FC > 1.5; (3) overlap of autoantibodies meeting both criteria (1) and (2).

Construction of focused protein array for novel autoantibody validation

In total, 32 IgG and 4 IgA candidate autoantigens selected through the high-density protein microarray were precoated in duplicate to construct a focused protein array, provided by ProteomicsEra Medical Co., Ltd. The reagents for focused array and data acquirement were same to those of high-density protein microarray, but protocol modifications including plasma dilution (1:100) and half incubation time.

ELISA assay for autoantibodies and C4B protein measurement

Antigenic peptides and proteins selected for verification were purchased from ChinaPeptides Co., Ltd. and Absea Biotechnology Ltd., respectively. The high-binding 96-well Maxisorp immunoplate (Thermo Scientific, 446469) was coated with 100 ng complement 4B (C4B; 1 μg/mL), 100 ng formin binding protein 4 (FNBP4; 1 μg/mL), 100 ng keratin 2 (KRT2; 1 μg/mL), 100 ng KRT10 (1 μg/mL), 150 ng KRT16 (1.5 μg/mL), or 100 ng dynein cytoplasmic 1 heavy chain 1 (DYNC1H1; 1 μg/mL) diluted in 100 μL of ELISA coating buffer (Solarbio, C1055) and incubated overnight at 4°C. Next, the coated plate was washed, blocked by 1% bovine serum albumin/PBS and incubated at room temperature for 1 hour. Then, diluted plasma (1:50) was added, and the plate was incubated for 2 hours at room temperature and further washed. Horseradish peroxidase-conjugated anti-human IgG antibody (1:130000, Abcam, ab6759) was

added to each well for 1 hour at room temperature, followed by colour development. The colorimetric signal was detected at an optical density of 450 nm (OD450), and the blank was subtracted from the OD450 readings of all samples. Also, anti-human IgG showed negligible reactivity with IgA and IgM, demonstrating >13.7-fold and >9.4-fold lower signals, respectively, compared to IgG targets (Supplementary Fig S1D).

Plasma C4B proteins were measured using a commercial ELISA Kit (Abcam, ab277717) according to the manufacturer's instructions. Raw data were processed using the linear regression method in the GraphPad software.

Immunohistochemistry analysis of autoantigens in biopsy tissues

Immunohistochemical staining of tracheal tissues of 2 RP patients and 2 controls was performed using anti-C4B (10 µg/mL, Abcam, ab66791), anti-KRT16 (1:200, Invitrogen, PA5-109897), and anti-FNBP4 (1:200, Invitrogen, PA5-59035) on the platform of BenchMark ULTRA Autostainer (v12.3, Ventana Medical Systems) according to the manufacturer's recommendations. The images were analysed using the NIS-Elements microscope.

XGBoost-based machine learning model

An XGBoost machine learning model using validation data was developed to discriminate RP patients from DCs and HCs. After log2-transformation and Z score normalisation of 36 autoantibodies, the dataset was randomly divided into training and testing sets (7:3). Cross-validation was performed in the training set by applying a stratified 10-fold split and a repetition of 10 times, resulting in 100 internal training/validation splits to ensure a robust estimation of the model performance. Parameters were tuned using a grid search algorithm with 10-fold cross-validation implemented in the 'caret' package, and then the optimal parameters were selected to retrain the XGBoost model. Finally, the performance of the model was further evaluated in the independent testing set.

Bioinformatics analysis

Unbiased hierarchical cluster analysis, principal component analysis (PCA), multiple correspondence analysis, enrichment analysis, and unsupervised consensus cluster analysis were carried out using 'pheatmap', 'limma', 'FactoMineR', 'clusterProfiler', and 'ConsensusClusterPlus' packages, respectively, using R (4.1.3). Detailed procedures were provided in Supplementary Methods.

Statistical analysis

Statistical analysis was conducted using Prism (8.0), R (4.1.3), and IBM SPSS Statistics (26.0). T-test and Wilcoxon test were applied to analyse normally and non-normally distributed data, respectively. The χ^2 test was performed for categorical variables. Pearson or Spearman correlation coefficients were calculated between the autoantibody levels and clinical parameters. $P < 0.05$ was considered statistically significant.

RESULTS

Plasma autoantibody reactome analysis of RP patients

The study design is illustrated in Figure 1. Among RP patients, 15 had active disease, and 17 were in an inactive stage,

involving respiratory tract (78.1%), ears (56.3%), nose (65.6%), joints (43.8%), etc. (Supplementary Table S2). Plasma autoantibody detection by high-density protein microarray was reproducible, with intra-array and interarray correlation coefficients of 0.99 and 0.98, respectively (Supplementary Fig S1A). Representative scanned microarray images are presented in Supplementary Figure S1B.

A total of 1344 IgG autoantibodies were upregulated in RP patients compared to HCs ($P < 0.05$ and FC > 1.5), which clustered 100% (32/32) of RP patients and 92.86% (13/14) of HCs (Fig 2A). PCA further confirmed a clear separation between RP patients and HCs (Supplementary Fig S2). Among these autoantigens, 20% were proteins, 36% were antigenic peptides with PTMs, and 43% were non-PTM peptides (Supplementary Figs S3, S4, Appendix). The average positive rate of autoantibodies against clinically applied autoantigens and novel autoantigens was 26.92% and 34.24% in RP patients, respectively, higher than 4.95% and 6.07% observed in HCs (Fig 2B).

The 1344 autoantigens were mapped to the UniProt database for 504 unique IDs (since multiple peptides can correspond to different regions of a protein). Finally, 354 autoantigens demonstrated specific tissue localisation after excluding uncertain data. Among these, 103 autoantigens were localised to cartilage tissue or chondrocytes. Specifically, autoantibodies targeting COL2 alpha 1 (COL2A1) and COL6A3 were significantly increased in RP patients (Fig 2C,D; Supplementary Table S5). Our study agreed with previous research [21−23] that identified anti-COL2 as a potential diagnostic marker for RP. Notably, the number of newly identified autoantibodies is 100-fold more than prior reports. In addition, many autoantigens were enriched in tissues or organs frequently affected in RP patients (Fig 2C), suggesting the reliability of autoantibody screening.

Kyoto Encyclopedia of Genes and Genomes pathway enrichment analysis revealed that the 504 autoantigenic proteins were primarily involved in 3 functional categories: autoimmune processes, pathogenic infections, and cardiac involvement (Fig 2E). Autoimmune-related pathways included complement and coagulation cascades, extracellular matrix receptor interaction, and proteoglycan, which included some glycoproteins or collagenous proteins, such as FN1, COL6A2, COL6A3, HSPG2, SV2A, COL2A1, and COL6A1, the main targets of anticartilage antibodies in RP [9]. Furthermore, autoantigens were significantly localised in collagen-containing extracellular matrix (Fig 2F), indicating that immune responses targeting cartilage and proteoglycans represented pivotal etiological factors in RP pathogenesis.

Eight pathways associated with infections and 7 pathways related to cardiac lesions were also identified (Fig 2E). Cardiac involvement was observed in approximately 20% of RP patients, mostly manifesting as subclinical changes. Routine transthoracic echocardiography and electrocardiogram monitoring in these patients mitigate acute complication risks [24,25]. RP-specific autoantigens are involved in the pathogenesis of hypertrophic cardiomyopathy, atherosclerosis, and other cardiovascular conditions, highlighting the pathogenic significance of these antigenic proteins identified in damaged heart valves, myocardium, or pericardium in RP patients.

Molecular subtypes of RP based on autoantibodies expression profiles

Consensus clustering analysis was used to explore the molecular heterogeneity underlying RP diversity, revealing that 1344 autoantibodies stratified RP patients into 2 molecular subtypes
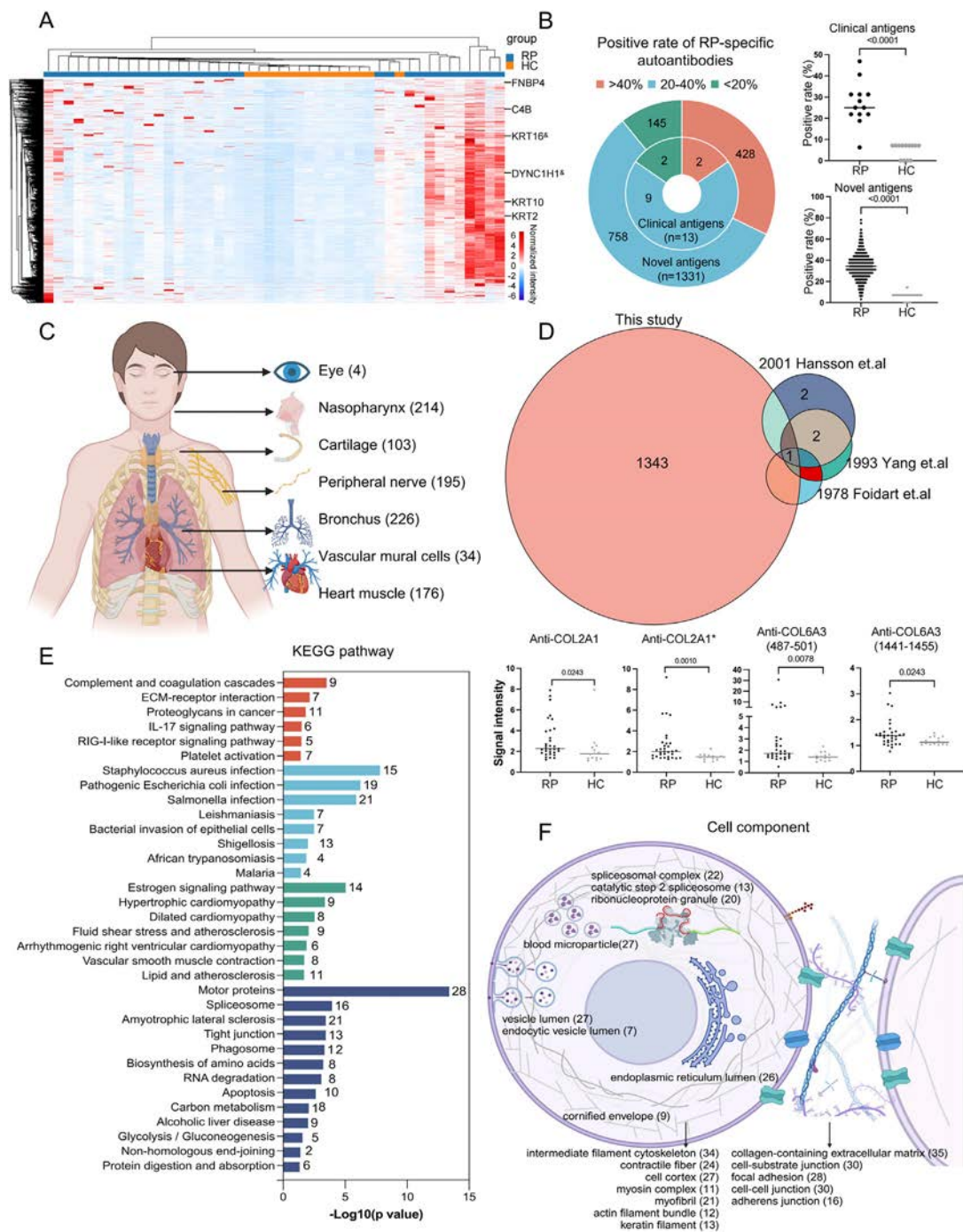
Figure 2. Upregulated autoantibodies in RP patients identified by high-density protein microarray. A, Hierarchical clustering analysis of autoantibodies increased in RP compared to HCs ($P < 0.05$, FC > 1.5), where 100% of RP patients and 92.86% of HCs were clustered. Some representative autoantibodies are labelled on the right. B, Comparison of positive rate of autoantibodies against novel autoantigens between RP patients and HCs. The positivity threshold was defined as the mean + 2SD of each autoantibody of the HCs group. C, Tissue enrichment of RP-related autoantigens. D, Venn diagram comparing the number of upregulated autoantibodies in RP patients newly identified in this study (N = 1343) with those identified in previous studies (N = 1). Scatter plots show the comparison of anti-COL2A1 and anti-COL6A3 autoantibodies between RP patients and HCs, whose autoantigens were enriched in cartilage tissue or chondrocytes. *Indicates a citrulline modification on the COL2A1 peptide. E, Significantly enriched signalling pathways associated with RP-specific autoantigens (N = 504) identified using the KEGG database ($P < 0.05$). Red, blue, and green boxes indicate signalling pathways associated with autoimmune processes, infections, and cardiac involvement, respectively. Bar length represents −Log10 (P value); adjacent number indicates autoantigen counts per category. F, Significantly enriched cellular components related to RP-specific autoantigens identified by GO analysis ($P < 0.05$). C and F, Images created with BioRender.com. GO, Gene Ontology; HC, healthy control; KEGG, Kyoto Encyclopedia of Genes and Genomes; RP, relapsing polychondritis.

with distinct separation (Fig 3A,B). RP patients classified as subtype 1 showed 457 specific autoantibodies involved in humoral immune response, intermediate filament cytoskeleton organisation, and positive regulation of tau-protein kinase activity, whereas subtype 2 only showed 12 specific autoantibodies associated with negative regulation of activation-induced cell death

of T cell (Supplementary Fig S5A, Fig 3C). Additionally, a higher rate of active disease, mechanical ventilation and recurrence within 3 months were found in subtype 1 patients, alongside more extensive organ involvement, including nervous system only in the subtype 1, as well as high RP-specific autoantibodies (Fig 3E,F, Supplementary Fig S5B,C).
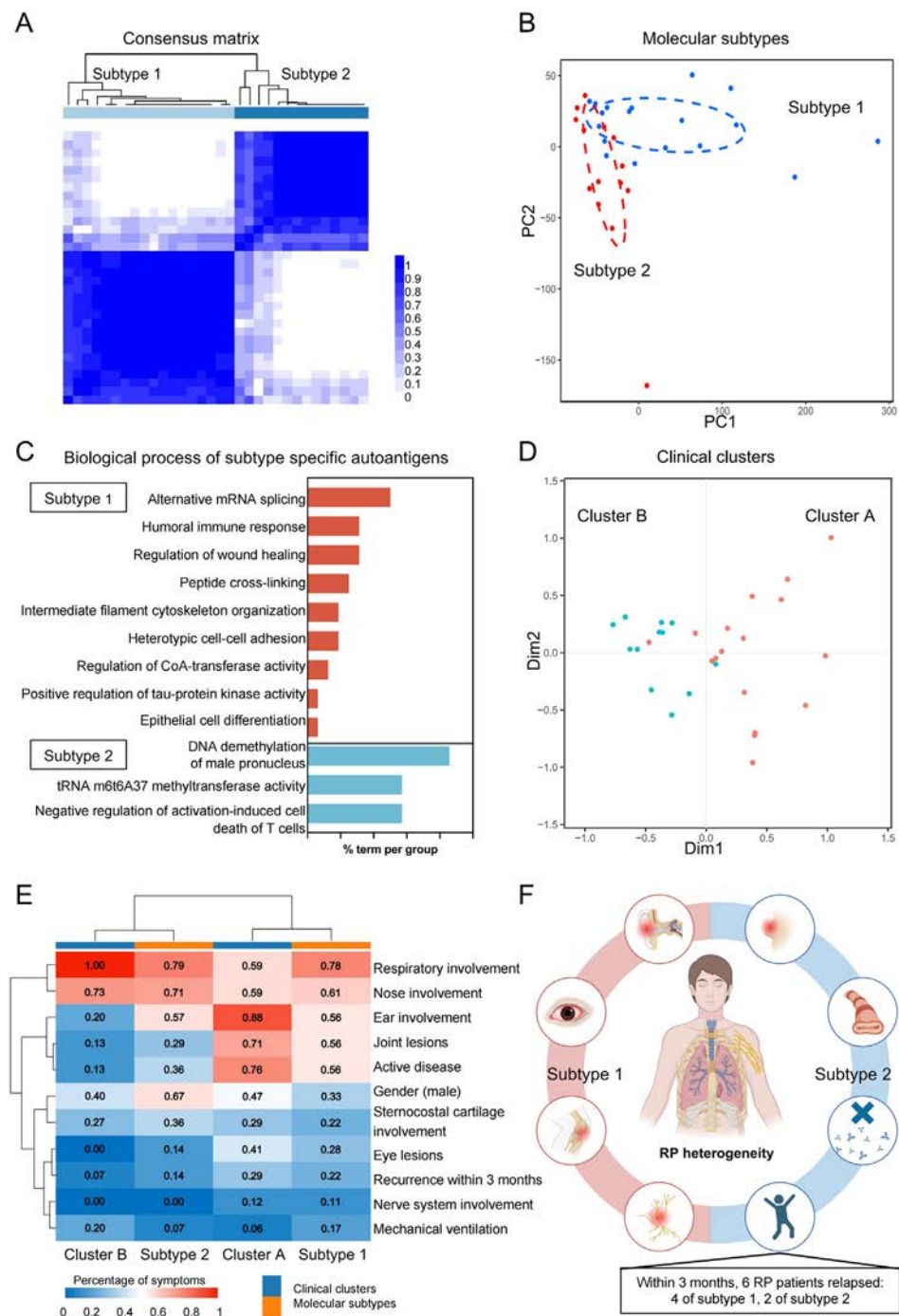
Figure 3. Molecular classification of RP patients based on plasma autoantibody profiles. A, The consensus matrix heatmap reveals 2 molecular subtypes of RP patients. The vertical and horizontal axes of consensus matrix heatmap represent the RP samples, heatmap showing darker blue represents greater similarity as measured by Pearson distances between RP patients. B, PCA of molecular subtypes 1 and 2 in RP patients, showing remarkable differences between 2 subtypes. C, Biological processes of specific autoantigens associated with 2 molecular subtypes. Red and blue boxes denote subtypes 1 and 2, respectively. D, Multiple correspondence analysis of clinical clusters A and B in RP patients, displaying clear separation from each other. E, Distribution of each clinical characteristic according to molecular subtypes and clinical classification clusters in the RP cohort, based on unbiased hierarchical clustering analysis. F, Illustration of differences in clinical manifestations, autoantibody expressions, and disease prognosis between molecular subtypes 1 and 2. F, Image created with BioRender.com. PCA, principal component analysis; RP, relapsing polychondritis.

Two clinical clusters (A and B) were identified within the same RP cohort using clinical data (Supplementary Fig S5C, Fig 3D). Patients in molecular subtype 1 and clinical cluster A mostly overlapped and shared similar clinical characteristics, including a higher rate of active disease, recurrence rate, and incidence of the non-airway phenotype involving ear, joint, eye, and nervous system lesions. Conversely, patients in subtype 2 and cluster B shared similar symptoms, predominantly respiratory and nasal symptoms (Fig 3E, Supplementary Fig S5D),

suggesting the potential of molecular classification in indicating RP heterogeneity, disease activity and prognosis.

Novel autoantibodies identified by high-density protein microarray

A total of 32 IgG and 4 IgA autoantibodies were identified as candidate biomarkers according to the screening criteria previously described (Fig 4, Supplementary Figs S6, S7).
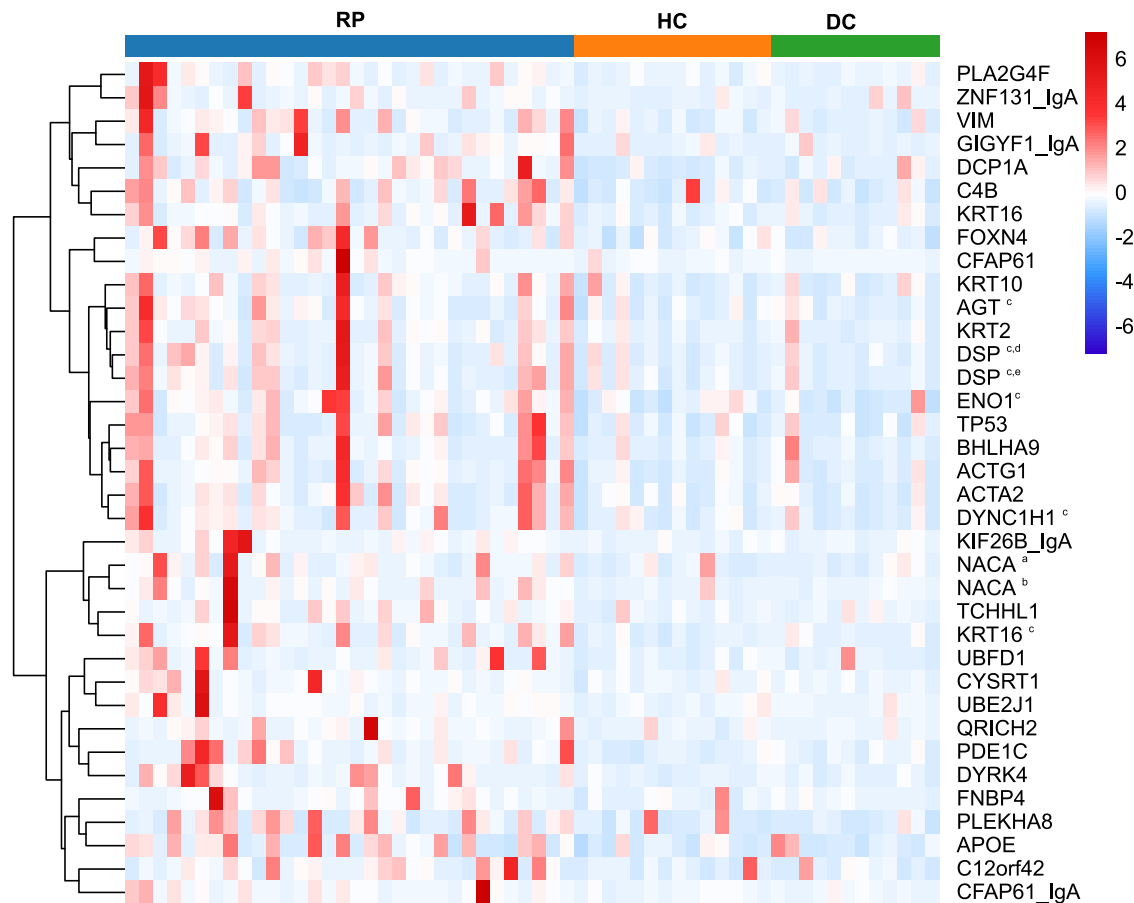
Figure 4. Identification of candidate autoantibodies for RP in the discovery cohort using high-density protein microarray. Heatmap of the signal intensities obtained from the 36 candidate autoantibodies in RP patients (N = 32), HCs (N = 14), and DCs (N = 12). Notes of candidate autoantibodies are shown in Table. DC, disease control; HC, healthy control; RP, relapsing polychondritis.

These 36 newly found autoantibodies differentiated RP patients from HCs and DCs with a sensitivity ranging from 18.8% to 53.1% and specificity exceeding 92%. Using the mean + 2SD of the HCs group as the positive threshold, the average seropositivity rate of 36 autoantibodies in RP patients (26.25%) was significantly higher than in HCs (6.03%) and DCs (7.78%). Details of candidate autoantibodies are shown in Table.

Validation of the 36 candidate autoantibodies by focused protein microarray

The validation study was performed using custom arrays displaying 36 proteins, with plasma from an expanded cohort comprising 195 RP, 60 HCs, and 74 DCs. An XGBoost-based machine-learning algorithm was used as a disease classifier to distinguish RP patients from HCs and DCs. The top 15 autoantibodies were obtained based on the importance scores quantifying each biomarker's contribution to the classification (Fig 5A). Among them, 8 and 12 autoantibodies allowed the distinction of RP from HCs or DCs, respectively, whereas 6 autoantibodies (anti-C4B, anti-FNBP4, anti-KRT2, anti-KRT10, anti-KRT16, and anti-DYNC1H1) exhibited discriminative capacity for RP against both HCs and DCs (Fig 5B, Supplementary Fig S8, Supplementary Table S6). The combined results of machine learning and differential analysis resulted in a diagnostic panel of 14 autoantibodies that achieved areas under the curve of 0.727 and 0.820 for distinguishing RP from HCs and DCs, respectively. The diagnostic specificity was 91.7% and 90.5%, and the sensitivity was 41% and 49.7%, respectively (Fig 5C, Supplementary Table S7).

Clinical correlation analysis revealed that anti-C4B levels were positively associated with C-reactive protein (CRP, P = .024, r = 0.17) and erythrocyte sedimentation rate (ESR, P = .030, r = 0.16) in total RP patients including active and inactive stage (Supplementary Fig S9). Further analysis of active patients showed that anti-C4B increased with the relapsing polychondritis disease activity index (RPDAI) scores, and the levels of CRP and ESR (Fig 5D), whereas no significant correlation was observed in inactive patients (data not shown). These findings suggested that high levels of anti-C4B indicated an exacerbation of disease inflammation.

Among 70 followed up RP patients, 19 experienced disease relapses within one year (Supplementary Table S3), characterised by high anti-C4B, anti-KRT16, and anti-FNBP4 levels (Fig 5E). Multivariate Cox proportional hazards regression revealed that elevated baseline anti-KRT16 was a risk factor for RP recurrence (Supplementary Fig S10), serving as a potential new autoantibody in predicting disease prognosis.

Verification of the diagnostic performance of autoantibodies by ELISA

Six autoantibodies that were significantly higher in RP patients compared to HCs and DCs were selected to confirm their levels by ELISA in a verification cohort consisting of 240 RP patients, 90 HCs, and 100 DCs.

All 6 autoantibodies were upregulated in the plasma of RP patients relative to both HCs and DCs groups (Fig 6A-6F), corroborating the protein microarray findings and reinforcing the potential of these novel autoantibodies as reliable diagnostic

Table

Novel autoantibodies identified for relapsing polychondritis by high-density protein microarray

Autoantigens	UniProt ID	Autoantigen types	Positive rate, % (N)			RP versus HCs		RP versus DCs		RP versus HCs + DCs		
			RP	HCs	DCs	P value	FC	P value	FC	Sensitivity	Specificity	AUC
IgG autoantibodies												
C12orf42	Q96LP6	Protein	13% (4)	7% (1)	8% (1)	.010	1.59	.037	1.62	0.344	0.923	0.724
FOXN4	Q96NZ1	Protein	31% (10)	0% (0)	0% (0)	.030	1.60	.020	1.64	0.406	0.962	0.715
PDE1C	Q14123	Protein	38% (12)	7% (1)	17% (2)	.000	1.75	.049	1.55	0.375	0.923	0.775
PLEKHA8	Q96JA3	Protein	13% (4)	14% (2)	0% (0)	.024	1.53	.004	2.40	0.375	0.923	0.742
DYRK4	Q9NR20	Protein	44% (14)	7% (1)	8% (1)	.001	2.42	.008	2.37	0.438	0.962	0.779
ACTA2	P62736-1	Peptide	41% (13)	0% (0)	8% (1)	.021	1.81	.017	1.81	0.438	0.962	0.724
QRICH2	Q9H0J4	Protein	13% (4)	7% (1)	0% (0)	.001	2.10	.013	2.03	0.188	0.923	0.77
FNBP4	Q8N3×1	Protein	6% (2)	7% (1)	0% (0)	.011	1.55	.049	1.75	0.219	0.923	0.716
UBFD1	O14562	Protein	31% (10)	0% (0)	8% (1)	.010	2.68	.009	1.89	0.313	0.962	0.746
TCHHL1	Q5QJ38	Protein	19% (6)	7% (1)	8% (1)	.010	1.92	.035	1.77	0.25	0.923	0.725
BHLHA9	Q7RTU4	Peptide	28% (9)	7% (1)	8% (1)	.024	2.02	.049	1.67	0.313	0.923	0.703
PLA2G4F	Q68DD2	Protein	34% (11)	0% (0)	8% (1)	.015	1.78	.023	1.77	0.406	0.923	0.725
CYSRT1	A8MQ03	Protein	16% (5)	7% (1)	0% (0)	.043	1.69	.017	1.73	0.281	0.923	0.71
ACTG1	P63261-1	Peptide	28% (9)	7% (1)	17% (2)	.005	2.05	.021	1.63	0.281	0.962	0.743
TP53	P04637	Peptide	28% (9)	7% (1)	8% (1)	.020	1.82	.049	1.67	0.281	0.962	0.707
NACA[a]	Q13765	Protein	13% (4)	7% (1)	0% (0)	.009	1.88	.014	2.10	0.188	0.962	0.74
NACA[b]	E9PAV3	Protein	16% (5)	7% (1)	0% (0)	.001	2.64	.016	2.74	0.531	0.923	0.767
C4B	P0C0L5	Peptide	9% (3)	7% (1)	0% (0)	.026	1.51	.033	1.67	0.375	0.962	0.709
ENO1[c]	P06733	Peptide	25% (8)	0% (0)	8% (1)	.024	1.52	.001	1.65	0.375	0.923	0.757
DYNC1H1[c]	Q14204	Peptide	28% (9)	7% (1)	8% (1)	.033	1.85	.014	1.85	0.375	0.923	0.718
KRT16	P08779	Peptide	38% (12)	7% (1)	17% (2)	.004	2.41	.033	1.96	0.344	0.923	0.74
KRT16[c]	P08779	Peptide	41% (13)	7% (1)	17% (2)	.001	2.21	.040	1.83	0.344	0.962	0.762
KRT10	P13645	Peptide	22% (7)	7% (1)	0% (0)	.007	1.75	.046	1.58	0.25	0.923	0.726
AGT[c]	P01019	Peptide	28% (9)	0% (0)	0% (0)	.012	1.56	.026	1.52	0.375	0.923	0.726
UBE2J1	Q9Y385	Protein	13% (4)	7% (1)	8% (1)	.007	1.97	.008	1.83	0.281	0.923	0.752
DCP1A	Q9NPI6	Protein	44% (14)	7% (1)	25% (3)	.000	2.63	.017	1.61	0.375	0.923	0.814
VIM	P08670-1	Peptide	41% (13)	7% (1)	17% (2)	.007	1.87	.043	1.65	0.375	0.923	0.727
APOE	P02649	Peptide	38% (12)	7% (1)	17% (2)	.006	1.94	.049	1.54	0.375	0.923	0.726
CFAP61	Q8NHU2	Protein	13% (4)	7% (1)	0% (0)	.048	1.90	.012	2.35	0.344	0.962	0.713
DSP[c,d]	P15924	Peptide	28% (9)	14% (2)	8% (1)	.016	1.78	.037	1.72	0.281	1.000	0.715
DSP[c,e]	P15924	Peptide	34% (11)	7% (1)	8% (1)	.028	1.77	.040	1.77	0.344	0.923	0.704
KRT2	P35908	Peptide	31% (10)	7% (1)	8% (1)	.028	2.08	.049	1.79	0.406	0.923	0.701
IgA autoantibodies												
KIF26B	Q2KJY2	Protein	28% (9)	7% (1)	8% (1)	.010	2.24	.028	2.14	0.406	0.923	0.728
GIGYF1	O75420	Protein	22% (7)	7% (1)	8% (1)	.023	2.06	.035	2.06	0.219	0.923	0.71
CFAP61	Q8NHU2	Protein	31% (10)	0% (0)	8% (1)	.028	1.88	.021	1.89	0.313	0.962	0.715
ZNF131	P52739	Protein	19% (6)	7% (1)	17% (2)	.004	2.29	.033	1.68	0.188	0.923	0.739

AUC, area under the curve; DCs, disease control, FC, fold change; HCs, healthy control; RP, relapsing polychondritis.

[a] The N→C terminal antigen sequence of NACA, corresponding to a region of amino acids 1-215.

[b] The N→C terminal antigen sequence of NACA corresponds to a region of amino acids 1881-2030.

[c] Indicates a post-translational modification of an antigenic peptide (citrulline modification).

[d] The N→C terminal antigen sequence of the DSP corresponds to a region within amino acids 2281-2297 where L-glutamine 2295 is absent.

[e] The N→C terminal antigen sequence of the DSP corresponds to a region within amino acids 2281-2297.

biomarkers for RP. Consistent with the observations in the validation cohort, the levels of new autoantibodies were positively correlated with the active disease markers ESR, CRP, and RPDAI, further underscoring their clinical relevance (Supplementary Fig S11).

Longitudinal monitoring demonstrated that anti-C4B, anti-FNBP4, and anti-KRT10 were significantly reduced (Fig 6G-6L) in response to effective treatment and subsequent disease remission, suggesting a potential role for these novel autoantibodies in the pathogenesis of RP and in the assessment of disease control. To further elucidate the prognostic significance of these autoantibodies, future studies involving expanded cohorts are warranted to validate the correlation between autoantibody levels and disease outcomes.

Level of C4B autoantigen in the pathological tissues and plasma of RP patients

Given that C4B is a plasma protein, we hypothesise that its tissue deposition may precipitate pathological alterations. Immunohistochemical analysis revealed that C4B protein was higher in chondrocytes of tracheal tissues in RP patients with respiratory involvement than in normal tracheal cartilage tissues. C4B was predominantly located within the cytoplasm of chondrocytes and largely absent from the cartilage matrix (Fig 7A,C-D), which was also attached to the mucosal layer of the trachea, such as columnar epithelial cells, glandular cavities, and diffuse inflammatory infiltrating cells (Fig 7B). The same was observed for KRT16 and FNBP4 proteins (Supplementary Fig S12).

Interestingly, plasma C4B was lower in RP patients, especially in patients with positive anti-C4B (Fig 7E-7F). However, no significant correlation between anti-C4B titres and plasma C4B concentrations was observed in either HCs ($P = .089$, $r = −0.35$) or RP ($P = .99$, $r = 8e-04$) groups (Fig 7G-H).

DISCUSSION

RP diagnosis is hampered or delayed in subjects lacking blood biomarkers based on current criteria, particularly in those presenting with atypical symptoms. This study identified a large set of upregulated autoantibodies (n = 1344) in RP patients
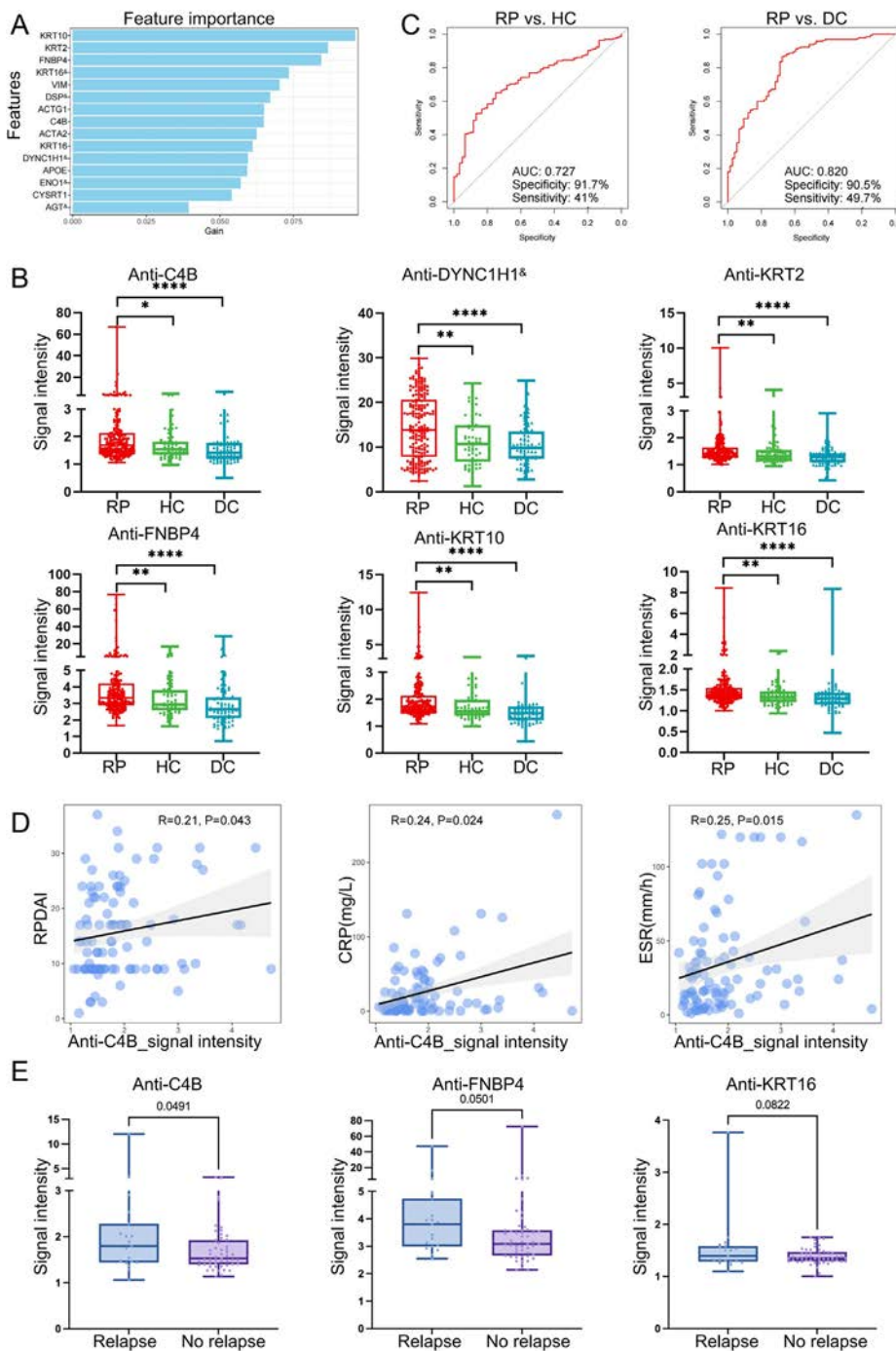
Figure 5. Establishment of 14-autoantibody panel in the validation dataset using focused protein microarray. A, Top 15 contributing autoantibodies identified by ranking importance analysis based on the XGBoost algorithm. B, Signal intensities of anti-C4B, anti-FNBP4, anti-KRT16, anti-DYNC1H1, anti-KRT10 and anti-KRT2 autoantibodies in RP patients (N = 195), HCs (N = 60), and DCs (N = 74). C, Receiver operating characteristic curves of the 14-autoantibody panel for RP discriminating HCs (right) and DCs (left) groups. The area under the curve, sensitivity, and specificity in receiver operating characteristic analysis are annotated in the bottom-right corner. D, Correlation between the anti-C4B levels and RPDAI scores, CRP, and ESR in RP patients with active disease. E, Plasma levels of anti-C4B, anti-FNBP4, and anti-KRT16 in RP patients with or without disease recurrence in one year. DC, disease control; HC, healthy control; RP, relapsing polychondritis.
[&] Indicates a post-translational modification of DYNC1H1 peptide.

associated with different signalling pathways, including autoimmune responses, microbial infections, and cardiac involvement. In addition, 2 molecular subtypes of RP with divergent clinical features were delineated. Two-phase microarray strategy and traditional method were used in different cohorts with a large number of subjects to profile 14 novel autoantibodies for the diagnosis, activity assessment, and recurrence prediction of RP.

Considering the diverse clinical presentations observed in RP patients, subgroup analysis is instrumental in refining treatment strategies and management approaches to mitigate disease-related damage. Studies conducted in France, Japan, and the United States classified RP patients based on clinical features, revealing that distinct subgroups were associated with divergent pathological mechanisms. For instance, blood phenotypes were associated with paraneoplastic syndrome whereas respiratory phenotypes were related to the immune response against tracheal cartilage [26−28]. However, molecular subgroups derived from genomics, proteomics, or autoantibody profiles are lacking. Our study elucidated an internal heterogeneity in RP patients based on autoantibody data, and 2 molecular subtypes were identified. Subtype 1 RP patients exhibited a marked increase in autoantibody levels, accompanied by a higher prevalence of involvement in the joints, eyes, and nervous system, as well as a greater recurrence rate and active disease. Furthermore, subtype 1-specific autoantigens were involved in the biological process of the humoral immune response. In contrast, subtype 2 RP patients demonstrated negligible antibody expression. RP is acknowledged as an autoimmune disease modulated by both humoral and cellular immune mechanisms, in which antibody response to cartilage tissue occurs in parallel with pro-inflammatory cytokine synthesis, chondrocyte apoptosis, and cartilage matrix destruction [29]. A Swedish study of 97 RP patients found that anti-COL2/9/11, anti-matrilin1, and anti-COMP antibodies were elevated in RP patients, albeit with a
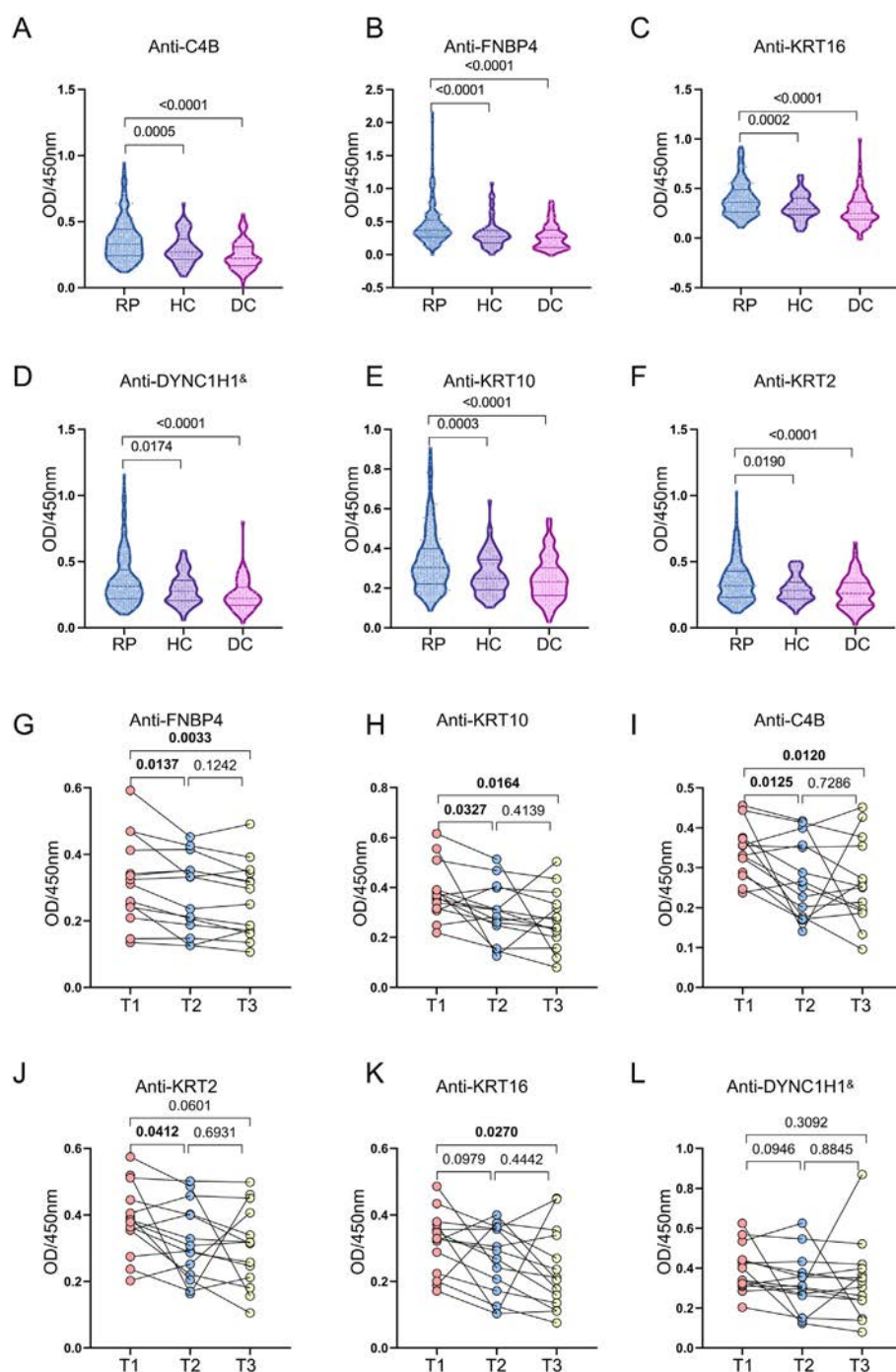
Figure 6. ELISA verification of autoantibodies associated with RP diagnosis in a large cohort. A-F, OD values of anti-C4B (A), anti-FNBP4 (B), anti-KRT16 (C), anti-DYNC1H1 (D), anti-KRT10 (E), and anti-KRT2 (F) in RP patients (n = 240), HCs (n = 90) and DCs (n = 100) groups.G-L, Dynamic trend of 6 autoantibodies during hospitalisation. The X-axis represents the sampling time points post-admission. Time 1 (T1): first day of hospitalisation; T2: mid-disease course; T3: final day before discharge. ELISA, enzyme-linked immunosorbent assay; OD, optical density; RP, relapsing polychondritis.
[&] Indicates a post-translational modification of DYNC1H1 peptide.

positive response rate ranging from only 13% to 21% [22]. RP is also considered to be a Th1-related autoimmune disease [9]. Based on these observations, our hypothesis is that RP patients with different molecular subtypes have different immune response patterns, with subtype 1 patients primarily driven by humoral immunity and subtype 2 driven by cellular immune responses. Further research is warranted to explore changes in lymphocyte subsets and cytokine profiles among RP patients, with the aim of delineating the pathogenesis heterogeneity to achieve personalised precision treatment and prognosis improvement.

The signalling pathway involving specific autoantigens was intimately related to cartilage injury and autoimmune process. Autoantigen distribution in the collagen-rich extracellular matrix and proteoglycans suggested that RP patients had active immune responses targeting cartilage tissues [30]. C4B was predominantly localised in the cytoplasm of chondrocytes. Given

immune complexes, C1q, C3, and C4d [31−33] as well as apoptotic chondrocytes [34] were detected in affected tissues of RP, we speculated that C4B originated from C4 cleavage induced by immune complex-mediated C1 activation [35] and/or apoptotic chondrocytes-induced MBL activation [36]. Furthermore, chondrocytes phagocytose cellular debris and exogenous antigens [37,38] and serve as antigen-presenting cells [39]. Thus, chondrocytes might internalise excessive C4B and present it to effector T cells to initiate anti-C4B antibody response. The implication of anti-C4B antibody in RP remains unknown. C4B-specific nanobodies have been shown to hinder endogenous regulators from facilitating Factor I-mediated C4B conversion [40]. This mechanism bears resemblance to the heightened complement activation observed in lupus nephritis, where anti-C3 antibodies impede Factor H and complement receptor 1 [41].

High-density protein microarray and focused microarrays were applied successively in different cohorts to profile RP-
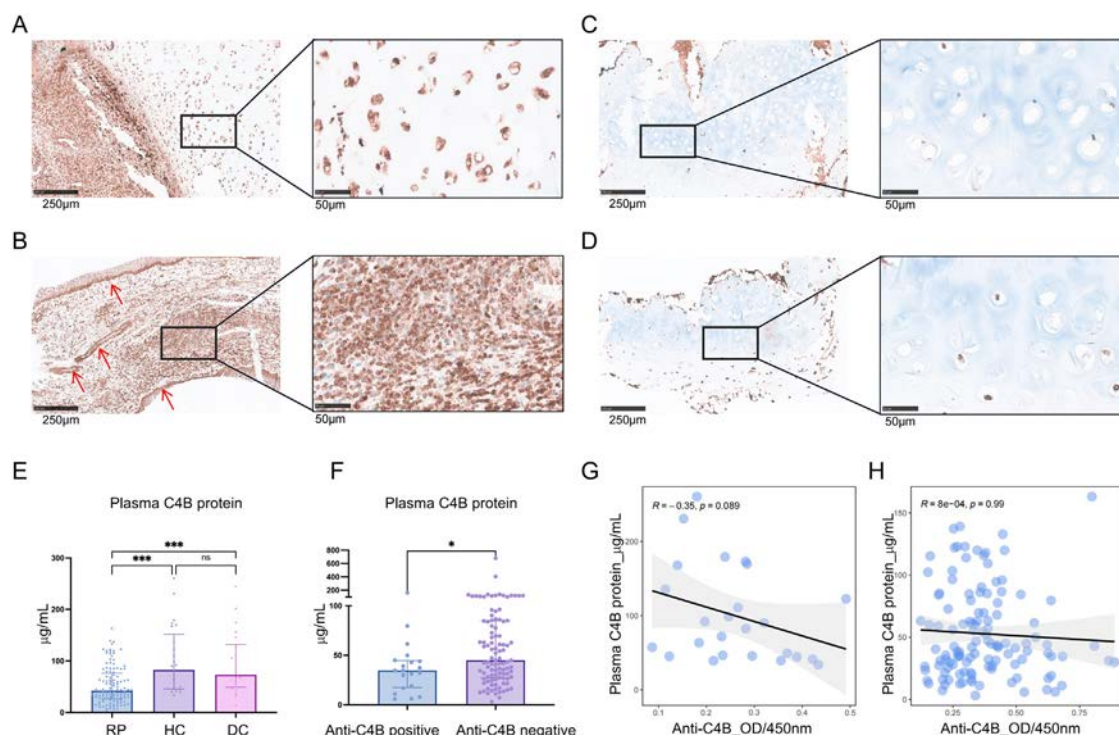
Figure 7. Analysis of C4B autoantigen in pathological tissues and plasma of RP patients. A-D, Immunohistochemical detection of C4B protein deposition in tracheal tissues from 2 RP patients with respiratory involvement (A-B) and 2 controls (C-D). A, C, and D, Images show the localisation of C4B protein in the chondrocytes and cartilage matrix. B, Image displays the mucosal tissue of the trachea, with red arrows indicating columnar epithelial cells and glandular lumina, and a black box showing infiltrating inflammatory cells. E. Scatter plots demonstrating the plasma C4B concentration (μg/mL) in RP patients (N = 125), HCs (N = 25), and DCs (N = 22). F, Comparison of plasma C4B protein between RP patients with and without anti-C4B seropositivity. The positive cut-off value of anti-C4B was considered as mean OD + 2SD of HCs from the verification cohort. G, H, Correlation between the anti-C4B levels and plasma C4B concentrations in HCs (G) and RP patients (H). DC, disease control; HC, healthy control; RP, relapsing polychondritis.

specific autoantibodies due to the urgent demand for reliable markers to diagnose RP patients. A 14-autoantibody panel was constructed that distinguished RP patients from HCs and DCs with a sensitivity of 59.4% and 78.1% and a specificity of 92.9% and 91.7%, respectively, in a discovery cohort, and a sensitivity of 41% and 49.7% and a specificity of 91.7% and 90.5%, respectively, in a validation cohort. Moreover, ELISA confirmed the diagnostic efficacy of novel autoantibodies in the verification cohort. Overall, the 14 autoantibodies, first reported here, represented the promising specific diagnostic markers for RP.

Notably, positive associations were observed between novel autoantibodies and ESR, CRP, and RPDAI in both the validation and verification cohorts of RP patients. Furthermore, elevated anti-KRT16 antibody was first found as a risk factor for disease recurrence in RP patients within one year. In addition, several studies demonstrated that autoantibody titres were related to treatment in RP, with reductions in anticartilage and anti-COL2 antibodies observed following steroid treatment or clinical remission [21,42]. Two case reports also documented that COMP and urinary COL2 peptide were downregulated after treatment [43,44]. In this study, anti-FNBP4, anti-KRT10, and anti-C4B antibodies exhibited a gradual decline from acute attack to remission, and anti-FNBP4 and anti-KRT10 antibodies were positively correlated with RPDAI. These findings suggest that the newly identified autoantibodies have the potential to assess disease activity, predict disease relapse, and reflect treatment effects.

The RP-specific autoantigens identified in our study were significantly enriched in the tracheal tissue of RP patients, indicating pathogenic potential. The KRT16 and FNBP4 proteins were localised to intermediate filaments and nucleoplasm, respectively. The release of intracellular autoantigens from dying cells, ineffective clearance of apoptotic debris, and protein

modification during inflammatory responses may render these antigens targets of B-cell responses [45−47]. Notably, the antigens recognised by anti-DSP, anti-DYNC1H1, and anti-AGT antibodies were modified by citrullination, a PTM that can generate new epitopes and enhance protein immunogenicity, driving pathological autoantibodies production [48−50]. Further investigation of novel autoantigens might provide new insights into the pathogenesis of RP.

Despite extensive research on various autoimmune disorders, the aetiology, pathogenesis, treatment response, and prognosis of RP remain relatively unexplored. The 14-autoantibody panel developed in this study filled the research gap and promoted the early diagnosis and timely treatment of RP. A limitation of the current study is that patients with polyspecific antibodies like systemic lupus erythematosus were not included. To further validate the clinical utility of this panel, future studies should undertake external cohort validation, incorporating multiple disease controls and RP patients from diverse ethnic backgrounds and geographic regions. This will enable the assessment of the optimal methodology for each autoantibody assay and the establishment of reference intervals for RP diagnosis. The titres of anti-COL2 in discovery RP cohort were consistent with previous reports, which were not prioritised for subsequent analysis due to not meeting our criteria for candidate biomarker. Anti-COL9/11, matrilin-1, and COMP antibodies were not validated due to their absence on the discovery arrays. Minimal anti-human IgG cross-reactivity with IgA/IgM, though potentially affecting absolute IgG quantification, is unlikely to compromise novel antigen identification or relative differences between RP and controls. Additionally, continued effort is still needed to elucidate the role of autoantigens and their corresponding autoantibodies in the pathophysiology of RP.

In conclusion, a panel of novel autoantibodies was identified and validated in RP patients using large-scale, unbiased screens. This study provides a fundamental insight into the heterogeneity and pathogenesis of RP and underscores the potential of plasma autoantibodies as biomarkers for future clinical assessment of RP.

Competing interests

The authors declare that the research was conducted in the absence of any commercial or financial relationships that could be construed as a potential conflict of interest.

CRediT authorship contribution statement

Yongmei Liu: Writing − review & editing, Writing − original draft, Visualization, Validation, Project administration, Methodology, Investigation, Data curation. **Mengzhu Zhao:** Writing − review & editing, Writing − original draft, Supervision, Project administration, Methodology, Investigation, Data curation. **Lei Zhang:** Writing − review & editing, Validation, Resources, Project administration, Investigation, Data curation. **Jing Luo:** Writing − review & editing, Validation, Supervision, Resources, Project administration, Investigation, Data curation. **Linlin Cheng:** Writing − review & editing, Writing − original draft, Visualization, Validation, Methodology, Funding acquisition. **Haoting Zhan:** Writing − review & editing, Visualization, Validation, Project administration, Methodology, Investigation, Data curation. **Mansheng Li:** Writing − review & editing, Visualization, Software, Methodology. **Zijuan Zhang:** Writing − review & editing, Validation, Resources, Methodology, Investigation, Data curation. **Siyu Wang:** Writing − review & editing, Resources, Investigation, Data curation. **Xinxin Feng:** Writing − review & editing, Resources, Investigation, Data curation. **Min Feng:** Writing − review & editing, Project administration, Investigation, Data curation. **Haolong Li:** Writing − review & editing, Validation, Methodology, Investigation. **Zhan Li:** Writing − review & editing, Visualization, Investigation, Data curation. **Jingdi Zhang:** Writing − review & editing, Investigation, Data curation. **Yong Hou:** Writing − review & editing, Writing − original draft, Supervision, Resources, Project administration, Methodology, Conceptualization. **Xiaobo Yu:** Writing − review & editing, Supervision, Resources, Project administration, Methodology, Conceptualization. **Yongzhe Li:** Writing − review & editing, Writing − original draft, Supervision, Resources, Project administration, Methodology, Funding acquisition, Conceptualization.

Contributors

YZL, XBY, YH, LLC, MZZ, and YML conceived the project and designed experiments. YML and HTZ carried out experiments with help from LLC and XBY. YML, MSL, and LLC analysed the experimental results. YZL, LZ, JL, and MF provided the clinical samples. ZJZ assisted in performing immunohistochemical experiments. MZZ, LZ, MF, SYW, XXF, and HLL collected clinical data. ZL and JDZ collected laboratory data and searched literature. YML wrote the manuscript. YZL supervised work and acquired fundings. All authors contributed to the article and approved the submitted version.

Patient consent for publication

Not applicable.

Ethics approval

This study was approved by the Medical Ethics Committee of the Peking Union Medical College Hospital (I-23PJ540), the First Hospital of Zhengzhou University (2023-KY-0467), and the Second Hospital of Shanxi Medical University ([2024] YX-No.384). All the participants provided written informed consent.

Provenance and peer review

Not commissioned; externally peer reviewed.

Data availability statement

Data are available upon reasonable request. All data relevant to the study are included in the article or uploaded as supplementary information. Data are available from the corresponding author (E-mail: yongzhelipumch@126.com) upon reasonable request.

Supplementary materials

Supplementary material associated with this article can be found in the online version at doi:10.1016/j.ard.2025.06.001.

Orcid

Mengzhu Zhao: http://orcid.org/0000-0001-5476-7037
Jing Luo: http://orcid.org/0000-0003-2702-120X
Mansheng Li: http://orcid.org/0000-0002-0778-0965

REFERENCES

[1] Butterton JR, Collier DS, Romero JM, Zembowicz A. Case records of the Massachusetts General Hospital. Case 14-2007. A 59-year-old man with fever and pain and swelling of both eyes and the right ear. N Engl J Med 2007;356 (19):1980–8.

[2] Sharma A, Gnanapandithan K, Sharma K, Sharma S. Relapsing polychondritis: a review. Clin Rheumatol 2013;32(11):1575–83.

[3] Alissa H, Kadanoff R, Adams E. Does mechanical insult to cartilage trigger relapsing polychondritis? Scand J Rheumatol 2001;30(5):311.

[4] Berger R. Polychondritis resulting from intravenous substance abuse. Am J Med 1988;85(3):415–7.

[5] Dahlqvist A, Lundberg E, Ostberg Y. Hydralazine-induced relapsing polychondritis-like syndrome. Report of a case with severe chronic laryngeal complications. Acta Otolaryngol 1983;96(3-4):355–9.

[6] Furer V, Wieczorek RL, Pillinger MH. Bilateral pinna chondritis preceded by glucosamine chondroitin supplement initiation. Scand J Rheumatol 2011;40 (3):241–3.

[7] Menge T, Rzepka R, Melchers I. Monoclonal autoantibodies from patients with autoimmune diseases: specificity, affinity and crossreactivity of MAbs

binding to cytoskeletal and nucleolar epitopes, cartilage antigens and myco-bacterial heat-shock protein 60. Immunobiology 2002;205(1):1–16.

[8] Lin DF, Yang WQ, Zhang PP, Lv Q, Jin O, Gu JR. Clinical and prognostic characteristics of 158 cases of relapsing polychondritis in China and review of the literature. Rheumatol Int 2016;36(7):1003–9.

[9] Liu Y, Li X, Cheng L, Zhan H, Huang Y, Li H, et al. Progress and challenges in the use of blood biomarkers in relapsing polychondritis. Clin Exp Immunol 2023;212(3):199–211.

[10] Li S, Song G, Bai Y, Song N, Zhao J, Liu J, et al. Applications of protein microarrays in biomarker discovery for autoimmune diseases. Front Immunol 2021;12:645632.

[11] Li K, Mo W, Wu L, Wu X, Luo C, Xiao X, et al. Novel autoantibodies identified in ACPA-negative rheumatoid arthritis. Ann Rheum Dis 2021;80(6):739–47.

[12] Longobardi S, Lopez-Davis C, Khatri B, Georgescu C, Pritchett-Frazee C, Lawrence C, et al. Autoantibodies identify primary Sjogren's syndrome in patients lacking serum IgG specific for Ro/SS-A and La/SS-B. Ann Rheum Dis 2023;82(9):1181–90.

[13] Damiani JM, Levine HL. Relapsing polychondritis−report of ten cases. Laryngoscope 1979;89(6 Pt 1):929–46.

[14] McAdam LP, O'Hanlan MA, Bluestone R, Pearson CM. Relapsing polychondritis: prospective study of 23 patients and a review of the literature. Medicine (Baltimore) 1976;55(3):193–215.

[15] Michet Jr. CJ, McKenna CH, Luthra HS, O'Fallon WM. Relapsing polychondritis. Survival and predictive role of early disease manifestations. Ann Intern Med 1986;104(1):74–8.

[16] International Team for the Revision of the International Criteria for Behcet's D. The International Criteria for Behcet's Disease (ICBD): a collaborative study of 27 countries on the sensitivity and specificity of the new criteria. J Eur Acad Dermatol Venereol. 2014;28(3):338–47.

[17] Aletaha D, Neogi T, Silman AJ, Funovits J, Felson DT, Bingham 3rd CO, et al. 2010 Rheumatoid arthritis classification criteria: an American College of Rheumatology/European League Against Rheumatism collaborative initiative. Arthritis Rheum 2010;62(9):2569–81.

[18] Arend WP, Michel BA, Bloch DA, Hunder GG, Calabrese LH, Edworthy SM, et al. The American College of Rheumatology 1990 criteria for the classification of Takayasu arteritis. Arthritis Rheum 1990;33(8):1129–34.

[19] Chung SA, Langford CA, Maz M, Abril A, Gorelik M, Guyatt G, et al. 2021 American College of Rheumatology/Vasculitis Foundation Guideline for the Management of Antineutrophil Cytoplasmic Antibody-Associated Vasculitis. Arthritis Rheumatol 2021;73(8):1366–83.

[20] Ren J, Wang H, Wei C, Yang X, Yu X. Development of a protein microarray for profiling circulating autoantibodies in human diseases. Proteomics Clin Appl 2022;16(6):e2100132.

[21] Foidart JM, Abe S, Martin GR, Zizic TM, Barnett EV, Lawley TJ, et al. Antibodies to type II collagen in relapsing polychondritis. N Engl J Med 1978;299 (22):1203–7.

[22] Hansson AS, Heinegård D, Piette JC, Burkhardt H, Holmdahl R. The occurrence of autoantibodies to matrilin 1 reflects a tissue-specific response to cartilage of the respiratory tract in patients with relapsing polychondritis. Arthritis Rheum 2001;44(10):2402–12.

[23] Yang CL, Brinckmann J, Rui HF, Vehring KH, Lehmann H, Kekow J, et al. Autoantibodies to cartilage collagens in relapsing polychondritis. Arch Dermatol Res 1993;285(5):245–9.

[24] Gergely Jr. P, Poór G. Relapsing polychondritis. Best Pract Res Clin Rheumatol 2004;18(5):723–38.

[25] Yin R, Zhao M, Xu D, Wang Q, Li M, Zhang W, et al. Relapsing polychondritis: focus on cardiac involvement. Front Immunol 2023;14:1218475.

[26] Dion J, Costedoat-Chalumeau N, Sène D, Cohen-Bittan J, Leroux G, Dion C, et al. Relapsing polychondritis can be characterized by three different clinical phenotypes: analysis of a recent series of 142 patients. Arthritis Rheumatol 2016;68(12):2992–3001.

[27] Ferrada M, Rimland CA, Quinn K, Sikora K, Kim J, Allen C, et al. Defining clinical subgroups in relapsing polychondritis: a prospective observational cohort study. Arthritis Rheumatol 2020;72(8):1396–402.

[28] Shimizu J, Yamano Y, Kawahata K, Suzuki N. Relapsing polychondritis patients were divided into three subgroups: patients with respiratory involvement (R subgroup), patients with auricular involvement (A subgroup), and overlapping patients with both involvements (O subgroup), and each group had distinctive clinical characteristics. Medicine (Baltimore) 2018;97(42):e12837.

[29] Arnaud L, Mathian A, Haroche J, Gorochov G, Amoura Z. Pathogenesis of relapsing polychondritis: a 2013 update. Autoimmun Rev 2014;13(2):90–5.

[30] Krishnan Y, Grodzinsky AJ. Cartilage diseases. Matrix Biol 2018;71-72:51–69.

[31] Head E, Starr A, Kim RC, Parachikova A, Lopez GE, Dick M, et al. Relapsing polychondritis with features of dementia with Lewy bodies. Acta Neuropathol 2006;112(2):217–25.

[32] Valenzuela R, Cooperrider PA, Gogate P, Deodhar SD, Bergfeld WF. Relapsing polychondritis. Immunomicroscopic findings in cartilage of ear biopsy specimens. Hum Pathol 1980;11(1):19–22.

[33] Homma S, Matsumoto T, Abe H, Fukuda Y, Nagano M, Suzuki M. Relapsing polychondritis. Pathological and immunological findings in an autopsy case. Acta Pathol Jpn 1984;34(5):1137–46.

[34] Ouchi N, Uzuki M, Kamataki A, Miura Y, Sawai T. Cartilage destruction is partly induced by the internal proteolytic enzymes and apoptotic phenomenon of chondrocytes in relapsing polychondritis. J Rheumatol 2011;38 (4):730–7.

[35] Mortensen SA, Sander B, Jensen RK, Pedersen JS, Golas MM, Jensenius JC, et al. Structure and activation of C1, the complex initiating the classical pathway of the complement cascade. Proc Natl Acad Sci U S A. 2017;114(5):986–91.

[36] Martin M, Blom AM. Complement in removal of the dead - balancing inflammation. Immunol Rev 2016;274(1):218–32.

[37] Mitchell NS, Shepard N. Changes in proteoglycan and collagen in cartilage in rheumatoid arthritis. J Bone Joint Surg Am 1978;60(3):342–8.

[38] Castillo EC, Kourí JB. A new role for chondrocytes as non-professional phagocytes. An in vitro study. Microsc Res Tech 2004;64(3):269–78.

[39] Sengprasert P, Kamenkit O, Tanavalee A, Reantragoon R. The immunological facets of chondrocytes in osteoarthritis: a narrative review. J Rheumatol 2024;51(1):13–24.

[40] Zarantonello A, Presumey J, Simoni L, Yalcin E, Fox R, Hansen A, et al. An ultra-high-affinity complement c4b-specific nanobody inhibits in vivo assembly of the classical pathway proconvertase. J Immunol 2020;205(6):1678–94.

[41] Vasilev VV, Noe R, Dragon-Durey MA, Chauvet S, Lazarov VJ, Deliyska BP, et al. Functional characterization of autoantibodies against complement component c3 in patients with lupus nephritis. J Biol Chem 2015;290 (42):25343–55.

[42] Ebringer R, Rook G, Swana GT, Bottazzo GF, Doniach D. Autoantibodies to cartilage and type II collagen in relapsing polychondritis and other rheumatic diseases. Ann Rheum Dis 1981;40(5):473–9.

[43] Kraus VB, Stabler T, Le ET, Saltarelli M, Allen NB. Urinary type II collagen neoepitope as an outcome measure for relapsing polychondritis. Arthritis Rheum 2003;48(10):2942–8.

[44] Saxne T, Heinegard D. Serum concentrations of two cartilage matrix proteins reflecting different aspects of cartilage turnover in relapsing polychondritis. Arthritis Rheum 1995;38(2):294–6.

[45] Fletcher AJ, James LC. Coordinated neutralization and immune activation by the cytosolic antibody receptor TRIM21. J Virol 2016;90(10):4856–9.

[46] Matsuda KM, Kotani H, Yamaguchi K, Okumura T, Fukuda E, Kono M, et al. Significance of anti-transcobalamin receptor antibodies in cutaneous arteritis revealed by proteome-wide autoantibody screening. J Autoimmun 2023;135:102995.

[47] Burbelo PD, Iadarola MJ, Keller JM, Warner BM. Autoantibodies targeting intracellular and extracellular proteins in autoimmunity. Front Immunol 2021;12:548469.

[48] Valesini G, Gerardi MC, Iannuccelli C, Pacucci VA, Pendolino M, Shoenfeld Y. Citrullination and autoimmunity. Autoimmun Rev 2015;14(6):490–7.

[49] Sokolova MV, Schett G, Steffen U. Autoantibodies in rheumatoid arthritis: historical background and novel findings. Clin Rev Allergy Immunol 2022;63 (2):138–51.

[50] Kwon EJ, Ju JH. Impact of posttranslational modification in pathogenesis of rheumatoid arthritis: focusing on citrullination, carbamylation, and acetylation. Int J Mol Sci 2021;22(19):10576.

Crystal arthropathies

Deconstruction of tophi and synovium defines SPP1+ macrophages involved in extracellular matrix remodelling in gout

Hanlin Xu [1],[****], Zhechen Liu [1],[2], Xiaofeng Zhou [1],[2], Xiaoxi Ji [1],
Xingwang Liu [1], Xiaoxia Zhu [3], Liwei Lu [4], Nicola Dalbeth [5],[***],
Rui He [6],[7],[**], Yinghui Hua [1],[*]

[1] Department of Sports Medicine, Huashan Hospital, Fudan University, Shanghai, China
[2] Clinical Medical College, Fudan University, Shanghai, China
[3] Department of Rheumatology, Huashan Hospital, Fudan University, Shanghai, China
[4] Department of Pathology and Shenzhen Institute of Research and Innovation, The University of Hong Kong, Hong Kong, China
[5] Department of Medicine, The University of Auckland, Auckland, New Zealand
[6] Department of Immunology, School of Basic Medical Sciences, Fudan University, Shanghai, China
[7] National Clinical Research Center for Aging and Medicine, Huashan Hospital, Fudan University, Shanghai, China

ARTICLE INFO

ABSTRACT

Objectives: Gout is a prevalent condition characterised by high serum urate levels, leading to crystal deposition in the joints. Although many studies have explored the mechanisms underlying gout flares, the dynamics of tophus formation remain unknown. This study provides the first transcriptomic profile of the tophaceous gout joint and investigates immune-stromal cell interactions in the pathogenesis of tophus formation.

Methods: Single-cell transcriptomic profiling was conducted on 44,221 synovial tissue cells from patients with intercritical gout (without tophi) and tophaceous gout. Spatial transcriptomics showed gene expression patterns in the corona and fibrovascular zones of tophi. Gene expression pattern comparisons, pseudotime, and differential gene enrichment analyses were conducted on stage-specific macrophage subsets. Immunofluorescence and flow cytometry on the tophi samples validated the transcription results and visualised the spatial localisation of the macrophage-fibroblast subpopulation. Differential causal inference combined with Mendelian randomisation elucidated gene regulatory networks and their causal relationships with gout pathology.

Results: We identified *SPP1+/MMP9+/CHI3L1+* macrophages within the corona zone exclusive to tophaceous gout, exhibiting extracellular matrix regulation genes, enhanced integrin-mediated interactions with stromal cells and transitional potential towards osteoclast differentiation. Notably, coexpression of the fibroblast marker *S100A4* and *COL6A2* in these macrophages suggested a fibroblast-like phenotype. Distinct *CD4+* T-cell transcriptional profiles between disease states indicated a phenotypic shift from inflammatory to immune-regulatory subsets during tophus development.

*Correspondence to Prof. Yinghui Hua, Department of Sports Medicine, Huashan Hospital, Fudan University, Shanghai, China.
**Correspondence to Prof. Rui He.
***Correspondence to Prof. Nicola Dalbeth.
****Correspondence to Dr. Hanlin Xu.
E-mail addresses: hanlinxu@fudan.edu.cn (H. Xu), n.dalbeth@auckland.ac.nz (N. Dalbeth), ruihe@fudan.edu.cn (R. He), hua_cosm@aliyun.com (Y. Hua).
Handling editor Josef S. Smolen.
HX, ZL and XZ contributed equally.

Conclusions: This study reveals a novel macrophage population ($SPP1^+/MMP9^{+/}CHI3L1^+$) with dual immunomodulatory and matrix-remodelling capabilities, exclusively present in tophus tissues but absent in intercritical gout synovium or flare-associated synovial fluid. It may play a role in the pathogenesis of fibrosis and bone erosion in gout.

WHAT IS ALREADY KNOWN ON THIS TOPIC

- Although the cellular and molecular mechanisms of gout flares are well understood, the mechanism of tophaceous gout, particularly the formation of tophi, remains unclear. Tophi have a complex structure with both innate and adaptive immune system activation, together with extracellular matrix remodelling.

WHAT THIS STUDY ADDS

- This study identifies $SPP1^+/MMP9^+/CHI3L1^+$ macrophages as a unique subset specific to the tophi with osteoclast differentiation potential and active involvement in extracellular matrix remodelling.
- It emphasises the activation of the integrin-mediated interactions between macrophages, fibroblasts, and osteoblasts, linking chronic inflammation, fibrosis, and matrix remodelling.
- The study demonstrates coexpression of the fibroblast marker $S100A4$ and $COL6A2$ in these macrophages and indicates a close phenotypic association with fibroblasts.

HOW THIS STUDY MIGHT AFFECT RESEARCH, PRACTICE OR POLICY

- SPP1 levels could guide future prediction of tophus formation.
- The $SPP1^+/MMP9^{+/}CHI3L1^+$ macrophages represent a therapeutic target for tophus formation and matrix remodeling of joint tissue in gout.
- Further research into specific molecular mechanism regulating tophi-related macrophage and fibroblast phenotype changes could help us better develop targeted therapies of chronic gouty arthritis.

INTRODUCTION

Gout is a common condition caused by elevated serum urate levels. Monosodium urate (MSU) crystal formation in joints leads to recurrent gout flares [1]. These flares are characterised by intense, self-limiting inflammation, primarily driven by NLR Family Pyrin Domain Containing Protein (NLRP) 3 inflammasome activation and the release of mature interleukin (IL)-1β [2−4]. Persistent hyperuricaemia and intra-articular deposition of MSU crystals can lead to tophaceous gout, which is often associated with bone and cartilage damage, chronic gouty arthritis, and musculoskeletal disability [5−7].

Although the cellular and molecular mechanisms of gout flares are well understood, evidence regarding the processes driving tophaceous gout remains limited. Previous studies have detailed the cellular structure of tophi, highlighting the activation of innate and adaptive immune responses within these lesions, and extracellular matrix (ECM) remodelling in adjacent tissues [8]. Quantitative immunohistochemistry has shown that tophi are complex, highly organised granuloma-like structures comprising 3 layers—a central core of MSU crystals, a macrophage-rich corona zone, and an outer fibrovascular zone [9,10]. Recent studies have identified increased $HLA\text{-}DQA1^{high}$ classical monocytes and $PTGS2^{high}$ monocytes, alongside the

overactivation of $CD8^+$ T cells, in peripheral blood mononuclear cells (PBMCs) from patients with gout. Differentially expressed genes (DEGs) in PBMCs, T cells, and B cells from patients with advanced gout are significantly enriched in the osteoclast differentiation pathway [11]. However, the *in situ* gene expression patterns of cells within different layers of tophi remain poorly understood. The potential interactions between immune and stromal cells in various regions of the tophi and their roles in tophus formation are yet to be fully explored.

Advances in single-cell transcriptomics enable precise gene sequencing and transcriptome analysis of specific cell types [12,13]. This technology offers new insights into the interactions and adaptations of immune and stromal cells in healthy and arthritic joints [11,14]. Although single-cell RNA sequencing (scRNA-seq) offers high cellular resolution, the enzymatic tissue digestion required for this technique can disrupt native tissue architecture [15]. This limitation poses challenges in preserving the spatial organisation necessary for studying pathological cell-cell interactions and examining the distinct regional environments of tophi [16]. Spatial transcriptomics (ST) offers a complementary approach using spatially barcoded arrays on tissue sections to study tissue architecture and cell-cell interactions in detail at 55-μm resolution [17,18]. Thus, integrating scRNA-seq with ST provides a comprehensive approach to study cellular organisation and interaction networks within tophi.

In this study, we used scRNA-seq to analyse the single-cell gene expression profiles of joint-resident cells from patients with intercritical gout (without tophi) and those with tophaceous gout. Additionally, we applied ST technology to explore spatial gene expression patterns in the corona and fibrovascular zones of the tophi. The present study aimed to identify unique gene regulatory patterns involved in immune regulation, ECM remodelling, and joint destruction during gout progression.

RESULTS

Single-cell RNA sequencing reveals distinct immune and stromal cell clusters in patients with gout with or without tophi

We collected synovial samples from 5 patients with intercritical gout without tophi, which is characterised by joint pain, redness, swelling, and MSU crystal deposition in the synovium, as observed by arthroscopy. Additionally, we collected samples from 5 patients with tophaceous gout identified by intra-articular tophi (Supplementary Fig S1). Because of the cytotoxic effects of MSU crystals on cell viability, we selected 3 samples from each group with the highest cell viability for single-cell sequencing (Fig 1A).

After quality control, we analysed 44,221 cells from synovial tissue or tophus samples collected from 3 patients with intercritical gout and 3 with tophaceous gout (Supplementary Figs S2 and S3). The clinical characteristics of patients at the time of arthroscopic surgery are summarised in Supplementary Table S1. Following data integration with harmony to minimise sample-to-sample variation, the cells were classified into 18 broad cell type-annotated clusters.
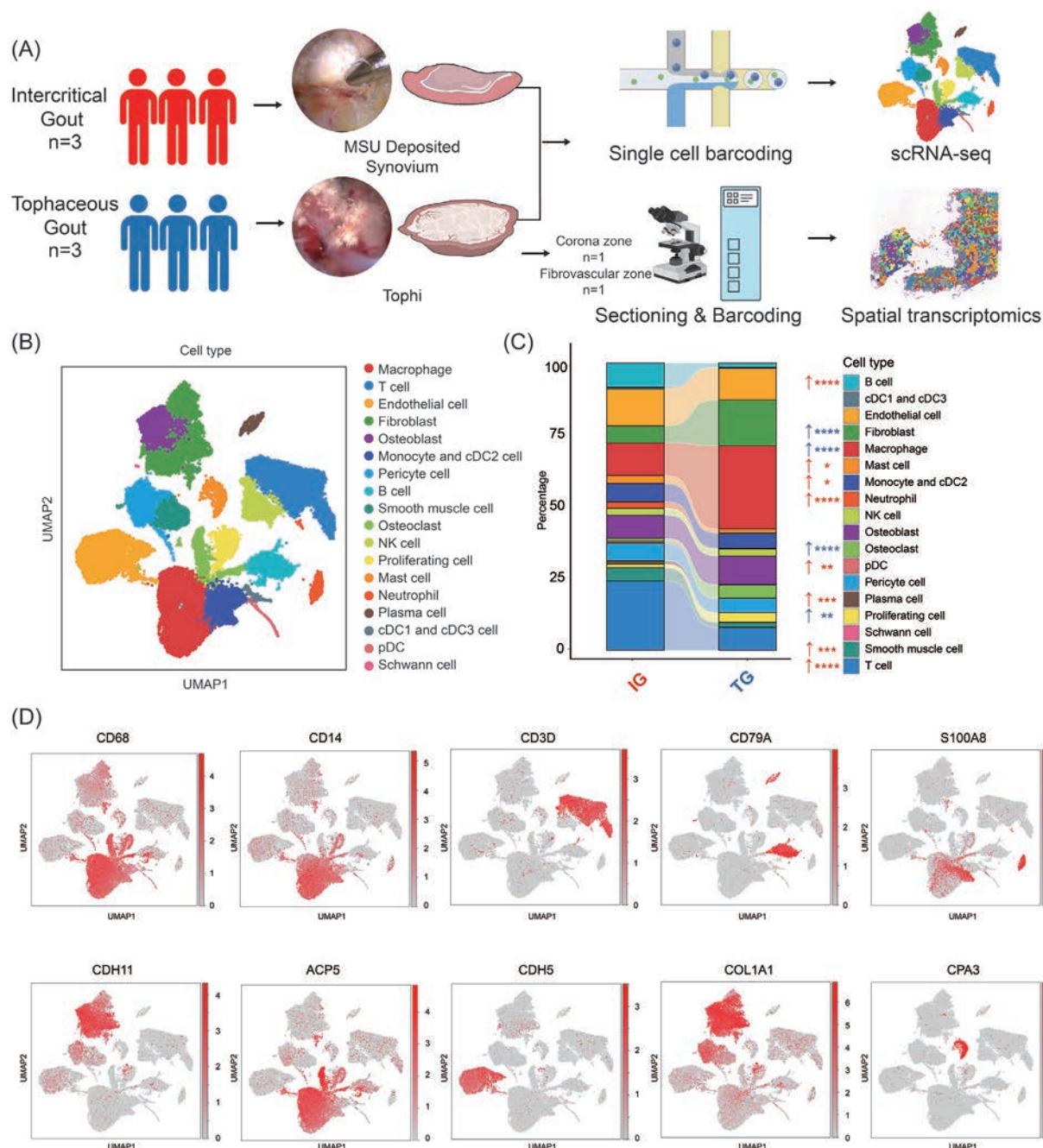
Figure 1. Single-cell RNA sequencing identifies distinct immune and stromal cell clusters in patients with gout with or without tophi. (A) Study design: single-cell RNA-seq (scRNA-seq) was performed on digested synovial or tophus tissue from 3 patients with intercritical gout without tophi and 3 patients with tophaceous gout, confirmed by arthroscopy. Spatial transcriptomics (ST) was performed on the corona and fibrovascular layers of the dissected tophi corresponding to the scRNA-seq sample. (B) Single-cell landscape of 44,221 identified cells, with dimensional reduction performed using uniform manifold approximation and projection (UMAP). (C) Distinct proportions of broad cell type-annotated clusters at different stages of gout. (D) UMAP plots showing the expression of canonical marker genes for broad cell-type-annotated clusters. ****$P < .0001$, ***$P < .001$, **$P < .01$, *$P < .05$. MSU, monosodium urate. NK cell, natural killer cell.

The main broad cell type-annotated clusters identified were as follows: macrophages (8908 cells), T cells (7092 cells), endothelial cells (5324 cells), fibroblasts (4834 cells), osteoblasts (3993 cells), monocytes and cDC2 (2587 cells), pericytes (2459 cells), B cells (2210 cells), smooth muscle cells (1404 cells), osteoclasts (1244 cells), natural killer cells (1088 cells), proliferating cells (1009 cells), mast cells (940 cells), and neutrophils (531 cells). We annotated distinct cell-type clusters based on manual identification using cell type-specific markers (Supplementary Table S2) defined by prior knowledge. The distribution of gene expression at the single-cell level was visualised using nonlinear, stochastic uniform manifold approximation and projection (UMAP) for dimension reduction (Fig 1B).

Differential abundances of various cell types across different stages of gout were acquired, which were expressed as frequencies within the total population per sample. In intercritical gout, neutrophils ($P < .0001$), B cells ($P < .0001$), T cells ($P < .0001$), monocytes ($P < .05$), and mast cells ($P < .05$) were significantly more abundant. Conversely, tophaceous gout was characterised by a significantly higher abundance of macrophages ($P < .0001$), fibroblasts ($P < .0001$), osteoclasts ($P < .0001$), and proliferating cells ($P < .01$)

(Fig 1C). The expression levels of key markers for each cell type-specific broad cell type-annotated cluster are shown in Figure 1D.

Mapping spatial gene expression in tophi using ST

Spatial gene expression patterns within different layers of tophus structures are an important but underexplored area [9]. Therefore, we conducted ST on 2 tophi samples—one from the corona zone and the other from the fibrovascular zone (Figs 1A and 2A).

After identifying the top variable genes and performing principal component analysis, we performed graph-based clustering of the tophus spot transcriptome (4313 spots), revealing 11 distinct clusters across the corona and fibrovascular zones (Fig 2A, B). Using robust cell-type decomposition (RCTD), we inferred the cellular composition of each spot in the ST data by leveraging the expression profiles of distinct cell types identified in single-cell transcriptomic data. In the multisample integration
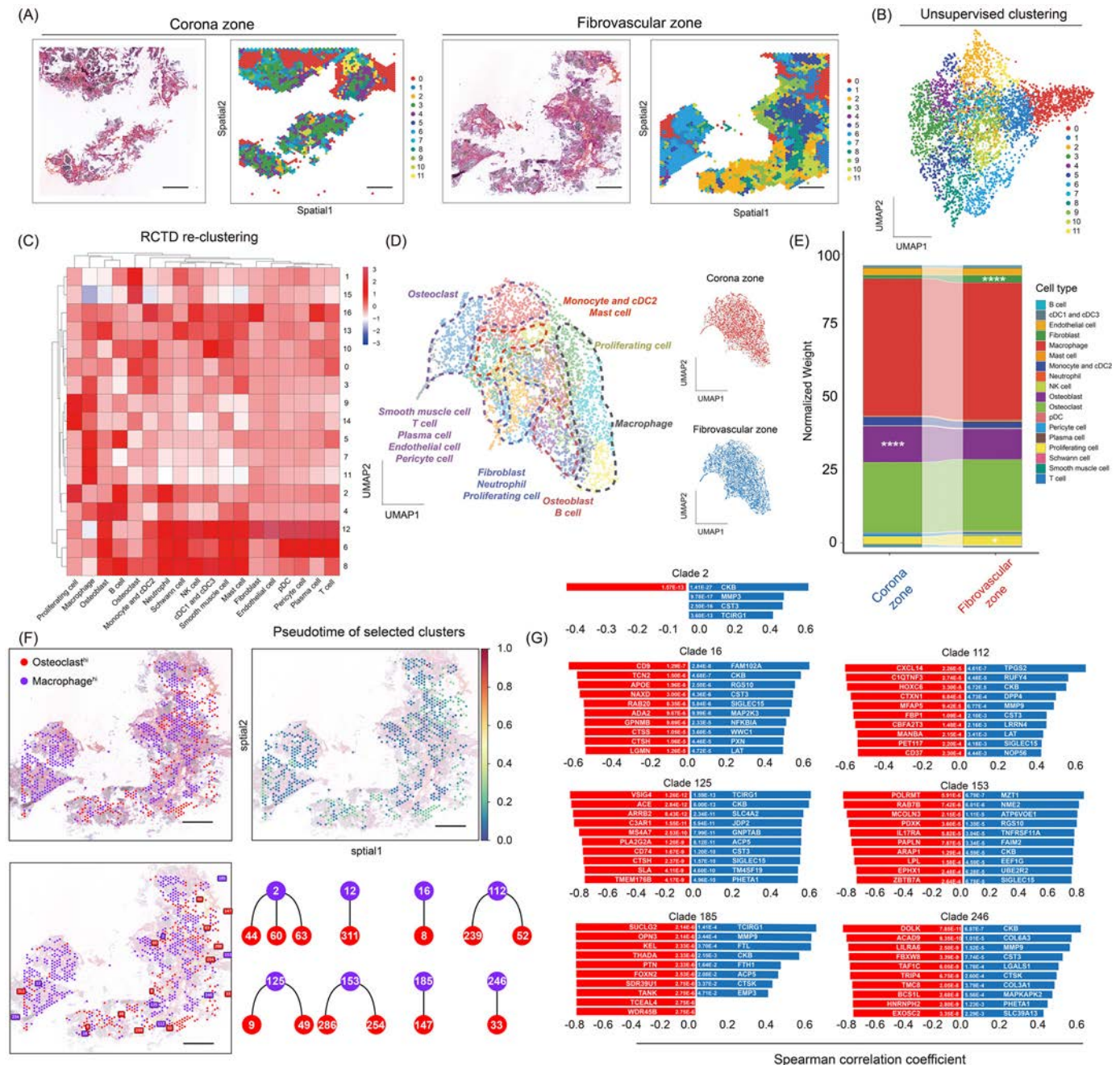

Figure 2. Spatial cell distribution and differentiation clades across zones. (A) Representative haematoxylin and eosin (H&E) image and corresponding spatial transcriptomics (ST) plot of the corona and fibrovascular zones (left to right). Scale bar = 550 μm. (B) Unsupervised clustering and uniform manifold approximation and projection (UMAP) visualisation of 4313 spots coloured by cluster. (C and D) Proportions of different cell types in each spot predicted by robust cell-type decomposition and dependent on cell-type abundance. The proportions of cell types in different spot clusters are shown. (E) Composition plots showing the relative abundance of each cell type according to sample. (F) Top left: The osteoclast^{high} and macrophage-^{high} clusters were selected for stLearn quasi-temporal analysis. Top right: pseudotime analysis of the selected clusters. Bottom left: segmentation of clusters into subclusters and inferred spatial trajectory of subcluster progression. Bottom right: dendrogram of spatial trajectory progression. Scale bar = 550 μm. (G) Transition markers identified genes involved in the inferred progression processes, revealing genes whose expression increases or decreases in pseudotime along spatial trajectories. ****$P < .0001$, ***$P < .001$ **$P < .01$, *$P < .05$. RCTD, robust cell-type decomposition.

workflow for ST, we reclustered the spots based on the cell-type composition predicted by RCTD, which estimates the proportion of each cell type within each spot (Fig 2C,D).

Reclustering revealed 16 distinct clusters, with varying cell-type abundances across each cluster, as visualised in a heatmap (Fig 2C). The major cell types in each cluster were predicted based on the distribution of mark gene expression (Fig 2D). Using the cell-type proportions predicted by the RCTD for each spot, we calculated the normalised cell-type composition weights for the corona and fibrovascular zone samples. Among all cell types, fibroblasts ($P < .0001$), mast cells ($P < .05$), and proliferating cells ($P < .05$) had higher weights in the corona zone samples, whereas osteoblasts ($P < .0001$) and proliferating cells ($P < .05$) were more abundant in the fibrovascular zone (Fig 2E).

Further ST analysis was performed to determine the cellular evolutionary and developmental trajectories in the tophi. We performed stLearn analysis on macrophage-rich and osteoclast-enriched clusters in the fibrovascular zone (Fig 2F) and corona zone (Supplementary Fig S4A), revealing the developmental transition of macrophages into osteoclasts. The cell populations of interest were segmented into subclusters in tissue sections. The pseudotime analysis of these subpopulations was displayed, with the inferred evolutionary and developmental trajectories represented by arrows and tree diagrams (Fig 2F, Supplementary Fig S4B). Furthermore, transition markers were identified to reveal the genes and signalling pathways involved in the inferred developmental processes. These genes exhibited increasing or decreasing expression along the pseudotime of the spatial trajectory. Genes associated with the spatial trajectory between subclusters (designated as 'clade') were identified (Fig 2G, Supplementary Figs S4C,D). The results showed that while genes supporting this differentiation trajectory overlapped across different regions, the variety and function of these genes were more diverse in the fibrovascular zone. Further enrichment analysis revealed that these transition markers were associated with lysosomal activity, consistent with the functional signature of osteoclast differentiation (Supplementary Fig S5).

Identification of SPP1-expressing tophaceous gout-associated macrophages in corona zone involved

Macrophages play a crucial role in gout flares and tophaceous gout [19]. Previous studies have identified M1 and M2 macrophages as primary subclusters; however, the boundaries between M1 and M2 are indistinct in UMAP plots following dimensional reduction and clustering, with only minor differences in expression levels [20]. Therefore, a graph-based unsupervised clustering method was used to assign classification labels termed cell subcluster identifiers to each cell, identifying 23 distinct macrophage subclusters (Fig 3A). Comparative analysis of cell composition revealed that subclusters M0 ($P < .0001$), M6 ($P < .0001$), and M9 ($P < .001$) were specifically present in the tophaceous gout group, whereas subclusters M1 ($P < .05$), M3 ($P < .001$), and M5 ($P < .01$) were specific to the intercritical gout group (Fig 3B,C).

We next predicted their sequential order along one or more virtual timelines, constructing cellular developmental or differentiation trajectories (Fig 3D, left). Consistent with the unsupervised clustering results, cells classified as M1, M3, and M5, along with those from intercritical gout, occupied the starting point of the pseudotime trajectory, whereas cells from tophaceous gout, particularly M0, M6, and M9, were found at the endpoint (Fig 3D, right). Thus, M0, M6, and M9 were identified as

tophaceous gout-associated macrophages (TGAMs), whereas M1, M3, and M5 were identified as intercritical gout-associated macrophages (IGAMs) (Fig 3E). To verify the differentiation relationship between macrophages and osteoclasts, we conducted pseudotime analysis across all macrophage and osteoclast populations and identified genes with significant expression changes along the pseudotime trajectory (Supplementary Fig S6, top left). These genes may drive changes in cell differentiation or function. Further analysis revealed that these genes were enriched in processes related to oxidative phosphorylation, arthritis, and reactive oxygen species (Supplementary Fig S6, top right). In addition, the pseudotime distribution of these cells revealed that IGAMs occupied the starting point and TGAMs were positioned at the endpoint (Supplementary Fig S6, bottom).

We screened the most DEGs in TGAMs and IGAMs. Notably, among the top 10 DEGs, we identified 2 marker genes, secreted phosphoprotein 1 (*SPP1*) and folate receptor beta (*FOLR2*), which have been recently recognised as representing mutually exclusive macrophage classifications (Fig 3F) [21−23]. We then conducted a pathway enrichment analysis using DEGs from the TGAM subclusters (Fig 3G). This analysis identified several pathways previously implicated in gout pathogenesis in TGAMs, including the nuclear factor kappa-B(NF-κB), NLRP, and tumor necrosis factor(TNF) signalling pathways (Fig 3G). Furthermore, we identified pathways associated with chronic inflammation, such as osteoclast differentiation and IL-17 signalling (Fig 3G).

The roles of SPP1 and FOLR2 in different gout phenotypes and their biological significance in tophus development warrant further investigation. To explore this, we examined the expression of *SPP1* and *FOLR2* in macrophage subclusters. The results revealed that the expression patterns of *SPP1* and *FOLR2* were closely aligned with the distribution of TGAMs and IGAMs (Fig 3H). The subclusters M0, M6, and M9 had the highest proportions of *SPP1*$^+$ cells and elevated levels of ECM-regulating genes, such as matrix metalloproteinases 9 (*MMP9*) and chitinase-3-like protein 1(*CHI3L1*). Conversely, subclusters M1, M3, and M5 contained almost no *SPP1*$^+$ cells and were predominantly composed of *FOLR2*$^+$ cells (Fig 3I). Furthermore, we reassessed the expression levels of *SPP1*, *FOLR2*, and *MMP9* in tophaceous gout and intercritical gout samples, confirming the significant presence of *SPP1*$^+$*MMP9*$^+$ macrophages in tophaceous gout samples and *FOLR2*$^+$ macrophages in intercritical gout samples (Fig 3J).

We then conducted flow cytometry on CD68$^+$ cells isolated from both intercritical and tophaceous gout digested joint tissues to validate the coexpression of SPP1, MMP9, and CHI3L1 (Supplementary Fig S7). Result showed a marked proportion of SPP1$^+$CHI3L1$^+$, SPP1$^+$MMP9$^+$, and CHI3L1$^+$MMP9$^+$ macrophage subsets in the tophaceous gout group compared to the intercritical gout group (Fig 3K). A strong correlation was also observed among the expressions of SPP1, MMP9, and CHI3L1 in macrophages. Specifically, the proportions of these double-positive populations in tophaceous gout samples reached approximately 2.74%, 0.75%, and 0.53%, respectively—significantly higher than in intercritical gout samples, where each subset accounted for less than 0.50%.

SPP1$^+$ TGAMs exhibit distinct characteristics related to ECM remodelling compared with gout flare-associated synovial fluid macrophages

The cellular phenotypic alterations induced by tophi are complex and profound. While we previously identified the critical
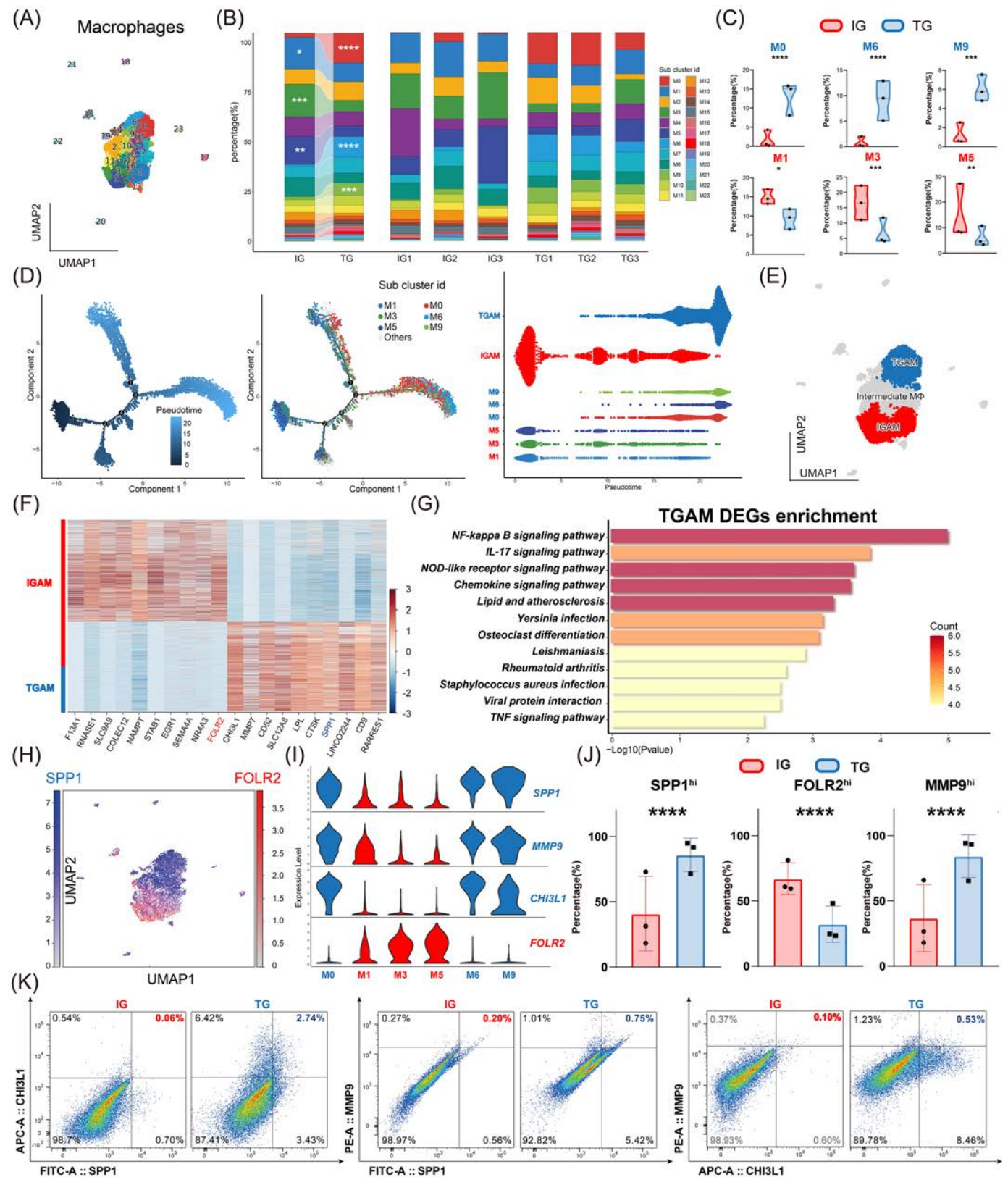
Figure 3. Identification of *SPP1*-expressing tophaceous gout-associated macrophages involved in extracellular matrix remodelling. (A) Uniform manifold approximation and projection (UMAP) plot of macrophages. (B) Proportions of macrophage subclusters across each sample. (C) Violin plots showing the distribution of the M1, M3, M5, M0, M6, and M9 subtypes in patients with intercritical gout and tophaceous gout. (D) Left: pseudotime differentiation pathway of tophaceous gout-associated macrophages (TGAMs). Right: distribution of cell counts across different subclusters of TGAMs in pseudotime analysis. (E) UMAP plot of macrophage reclustering based on sample-specific characteristics. (F) Heatmap depicting gene expression levels of the top 10 genes with the highest average Log2-fold change (avgLog2FC) in intercritical gout-associated macrophages (IGAMs) and TGAMs. (G) Enrichment analysis of differentially expressed genes (DEGs) in TGAMs. (H) UMAP plot showing the expression of *SPP1* and *FOLR2* in macrophages. (I) Violin plots showing gene expression in several sample-specific macrophage subtypes. (J) Gene expression levels of *SPP1*, *FOLR2*, and *MMP9* in intercritical gout and tophaceous gout samples. ****$P < .0001$, ***$P < .001$ **$P < .01$, and *$P < .05$. (K) Flow cytometry was performed on CD68$^+$ cells isolated from synovial tissues of intercritical gout (IG) and tophaceous gout (TG). Left: coexpression of SPP1 and CHI3L1. Middle: coexpression of SPP1 and MMP9. Right: coexpression of CHI3L1 and MMP9.

role of $SPP1^+$ TGAMs in tophi, we further explored the specificity of their gene expression profiles. Therefore, we performed an integrated analysis of single-cell data from tophi and synovial fluid from 3 patients with gout flares to identify genes specifically upregulated in chronic gouty arthritis [24]. Applying *CD68*, colony-stimulating factor-1 receptpr (*CSF1R*), cathepsin S (*CTSS*), and complement C1q A chain (*C1QA*) as markers for macrophages, we identified a distinct of macrophages population in the combined dataset following standard preprocessing and clustering procedures for downstream differential gene expression analysis (Fig 4A and Supplementary Figs S8 and S9). When compared to IGAMs, TGAMs specifically upregulated genes related to gout inflammation. In contrast, TGAMs exhibited elevated expression of specific genes, including *MMP12*, *MMP7*, collagen type VI alpha-3 chain (*COL6A3*), and *COL6A2* compared to flare-associated synovial fluid macrophages (FASFMs) (Fig 4B). Subsequent pathway enrichment analysis of these TGAMs-specific genes revealed a marked upregulation of ECM remodelling pathways, including protein digestion and absorption and ECM-receptor interaction (Fig 4C).

Genes such as *SPP1*, *CHI3L1*, and *COL6A2* exhibited low expression levels in FASFMs but were markedly upregulated across the TGAMs (Fig 4D). This pattern suggests the presence of a distinct cellular microenvironment within tophi that drives a transcriptional program not observed in acute inflammation. Furthermore, gene coexpression analysis revealed that *COL6A2* was positively correlated with both *SPP1* and *CHI3L1* (Fig 4E).

To validate the potential association between *SPP1* expression and gout development, we performed a Mendelian randomisation (MR) analysis. The scatter plot shows that 1 SD increase in *SPP1* expression is associated with a 0.6% increase in the risk of gout flare-ups ($P = 1.274 \times 10^{-5}$ for inverse variance weighted, 1.750×10^{-4} for weighted median, 4.263×10^{-2} for simple mode, and 7.636×10^{-3} for weighted mode) (Fig 4F). Additionally, the leave-one-single-nucleotide polymorphisms-out plot was used to estimate the MR effect size of *SPP1* expression on gout, treating it as an instrumental variable in the analysis (Fig 4G).

Stromal cells exhibited a proinflammatory phenotype in intercritical gout and an ECM-regulatory phenotype in tophaceous gout

A key feature of tophaceous gout is tissue matrix remodelling, which includes fibrosis and osteochondral matrix remodelling [8]. Cells involved in ECM regulation may play a critical role in the remodelling of the synovium and osteochondral ECM in tophaceous gout; however, the role has not been thoroughly described in previous studies [19,25]. We used an unsupervised approach to analyse the abundance of 17 identified fibroblast subclusters in intercritical gout and tophaceous gout, revealing 3 intercritical gout-specific subclusters and 4 tophaceous gout-specific subclusters (Fig 5A,B). By analysing the intersubtype correlation, we classified these subclusters into distinct functional subgroups (Fig 5C). We identified a subgroup of intercritical gout-associated fibroblasts, characterised by a strong inflammatory signature, comprising F3 ($P < .0001$), F9 ($P < .0001$), and F13 ($P < .05$). Conversely, tophaceous gout-associated fibroblasts (TGAFs) were classified into 2 groups—TGAF-1, which included F0 ($P < .0001$) and F1 ($P < .0001$), and TGAF-2, which included F5 ($P < .05$) and F8 ($P < .05$) (Fig 5B,C).

Notably, TGAF-2 exhibited a phenotype similar to $SPP1^+$ macrophages in tophi, characterised by increased expression of *SPP1*, *MMP9*, and *CD68*, along with DEGs associated with chronic inflammation and antigen processing (Fig 5D). Pathway analysis revealed that F3, F9, and F13 are primarily linked to ECM degradation and inflammatory responses, particularly complement regulation and IL-17/TNF/NF-κB signalling. Conversely, TGAF-1 was primarily associated with ECM interactions and protein digestion, contributing to tissue stability (Fig 5E). Cellular trajectory reconstruction analysis using gene counts and expression (CytoTRACE) analysis revealed that TGAMs possessed higher stemness and differentiation potential compared to TGAF-2 fibroblasts (Fig 5G). Further analysis on combination population of TGAM and TGAF-2 revealed that fibroblast8 closely aligns with TGAM in UMAP and pseudotime differentiation trajectories, indicating possible macrophage-fibroblast transition in gout (Fig 5H). Kyoto Encyclopedia of Genes and Genomes enrichment analysis of branch-dependent genes revealed that TGAF-2 plays a dual role in ECM remodelling and inflammatory responses at the endpoint (Fig 5F and Supplementary Fig S10).

We next performed immunofluorescence staining for S100A4, which is a classical fibroblast marker, CD68, as a macrophage marker, and SPP1 in serial sections of tophi. Notably, the corona zone adjacent to the tophus core exhibited an elevated triple-positive proportion ($S100A4^+SPP1^+CD68^+$) cells, indicative of potential macrophage-fibroblast intermediate states. In contrast, coexpression of these markers was weak and minimally colocalised in the fibrovascular zone (Fig 5I, top). Line profile analysis revealed clear intracellular colocalisation of these markers, and Mander's coefficients for S100A4/CD68 ($P < .0001$), S100A4/SPP1 ($P < .05$), and SPP1/CD68 ($P < .001$) were significantly elevated in the corona zone relative to the fibrovascular zone (Fig 5I, bottom). These findings offer spatial and protein-level evidence supporting the potential of a transitional cell population bridging TGAMs and TGAF-2 fibroblasts in the tophus microenvironment.

To further explore the role of SPP1 in the function of TGAMs and TGAF-2, we performed differential causal inference (DCI) analysis using SPP1 and CHI3L1 as seed nodes within these 2 pathways. Within the TGF-β signalling module, *SPP1* and *CHI3L1* displayed rewired causal relationships with core regulators, including *SMAD3*, *TGFB1*, *TGFBR1*, and *ALKBH5*. Notably, *SPP1* emerged as a central hub, receiving upstream input from *SMAD7* and exerting influence on downstream *SMAD3* family members, suggesting a potential role in modulating canonical TGF-β transcriptional output (Fig 5J, top). In the ECM-receptor interaction network, SPP1 was highly integrated into the regulatory architecture, forming directed edges with matrix-associated receptors (*CD44*, *SDC1*) and structural components (*FN1*, *COL1A1*, *COMP*). The directionality of these edges suggests that SPP1 may function as an upstream modulator of ECM assembly and remodelling (Fig 5J, bottom).

Osteoblasts also showed clear specificity at different stages of the disease. We identified 24 subclusters of synovial osteoblasts (Supplementary Fig S11A). Specifically, subclusters OB 2 ($P < .0001$), OB 3 ($P < .0001$), OB 5 ($P < .05$), and OB 6 ($P < .001$) were more prevalent in tophaceous gout, whereas subclusters OB 0 ($P < .0001$), OB 8 ($P < .0001$), OB 9 ($P < .01$), and OB 10 ($P < .01$) were significantly enriched in intercritical gout (Supplementary Figs S11B,C). Based on gene expression patterns, especially IL6, these subclusters were classified as tophaceous gout-associated osteoblasts (TGAOs) and intercritical gout-associated osteoblasts (IGAOs) (Supplementary Fig S11D). Enrichment analysis revealed that genes specific to IGAOs were primarily associated with proinflammatory responses, including
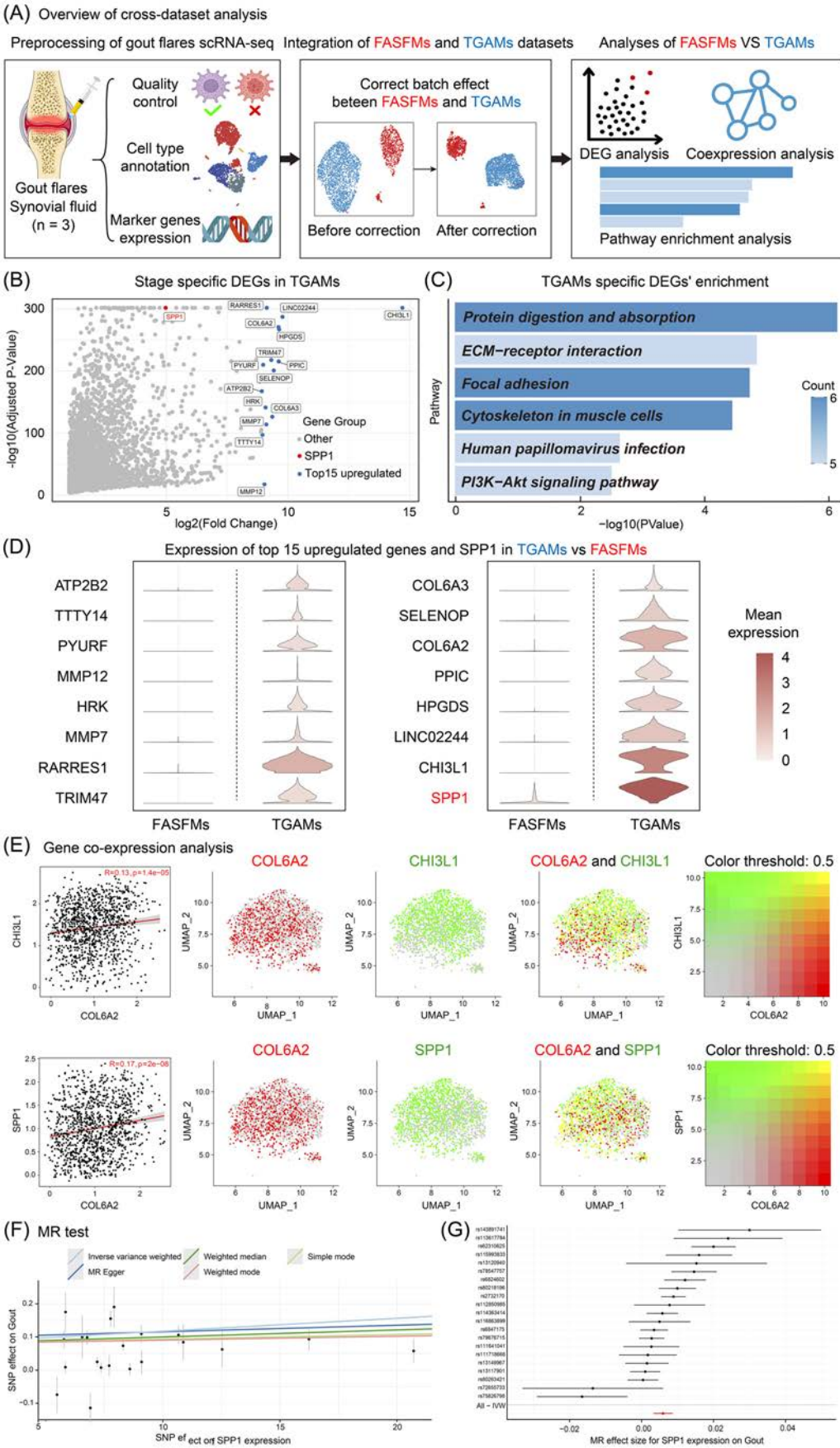
Figure 4. Identifying stage-specific genes in tophaceous gout-associated macrophages (TGAMs) and validating the relationship between *SPP1* and gout through Mendelian randomisation (MR). (A) Overview of the analytical workflow comparing TGAMs and flare-associated synovial fluid macro-phages (FASFMs). (B) Differential gene expression (DEG) analysis revealed a distinct transcriptional signature in TGAMs compared with FASFMs, highlighting *SPP1* and top 15 genes with the largest fold changes. (C) KEGG pathway enrichment analysis of TGAM-specific genes. (D) Violin plots showing the expression levels of the top 15 upregulated genes in TGAMs compared with FASFMs. (E) Top: correlation scatter plot and coexpression visualisation of *SPP1* and *COL6A2* genes in TGAMs. Bottom: correlation scatter plot and coexpression visualisation of *CHI3L1* and *COL6A2* genes in

complement regulation and classical gout-related pathways, such as TNF/NF-κB signalling, consistent with the patterns observed in IGAF subclusters. Conversely, TGAOs exhibited a markedly different functional profile, with a notable decrease in proinflammatory subclusters and an increase in genes associated with protein digestion and absorption, focal adhesion, and ECM-receptor interactions (Supplementary Fig S11E). To quantify functional divergence, gene set scoring revealed that IGAOs displayed higher inflammation scores, while TGAOs showed significantly increased protein-remodelling activity (Supplementary Fig S11F). Further DCI analysis revealed condition-specific regulatory rewiring centred on fibroblast activation protein (*FAP*), cathepsin B (*CTSB*), and cathepsin K (*CTSK*), spanning 4 representative pathways: ECM-receptor interaction, protein digestion and absorption, TNF signalling, and IL-17 signalling (Supplementary Fig S11G).

Activation of SPP1-CD44 signalling pathway in macrophages and fibroblasts within the tophus corona zone

Since we have identified tophi-specific subclusters of macrophages, fibroblasts, and osteoblasts with significant research potential, we next used single-cell and ST to assess the potential strength and spatial distribution of interactions within and between these cell populations.

Overall, single-cell sequencing revealed that the tophaceous gout group exhibited more frequent and robust intercellular interactions with fibroblasts and osteoblasts (Fig 6A,B). To further explore these interactions, we examined specific receptor-ligand pairs enriched in distinct cell populations. Bubble plots illustrate the receptor-ligand interactions between TGAMs and fibroblasts or osteoblasts, highlighting significant pairs, such as SPP1-CD44 interaction in TGAMs and collagen family-integrin interactions in fibroblasts (Fig 6C,D).

We also assessed cell communication probabilities based on the spatial expression profiles of ligands and receptors, considering the spatial distances and competitive interactions between the receptor-ligand pairs. The communication directions among cells within the corona and fibrovascular zones are illustrated in stained tissue sections (Fig 6E,F). Pathways were ranked based on normalised communication intensities, with a bar graph showing the top 10 signalling pathways and heatmaps illustrating the relative interaction strengths among cell types within these pathways (Fig 6E,F). In the corona zone, the SPP1-related pathway was most prominent, whereas in the fibrovascular zone, complement and collagen pathways were predominant (Fig 6E,F).

In the SPP1-related pathway within the corona zone, the most prominent receptor-ligand pair identified was SPP1-CD44, with macrophages, fibroblasts, and osteoblasts as senders or receivers (Fig 6G). We then used the tradeSeq package to identify DEGs significantly regulated by this signalling pathway, revealing genes modulated by SPP1 signalling (Fig 6H,I). The pathways enriched in these genes included focal adhesion, ECM-receptor interactions, and protein digestion (Fig 6J). This finding indicates that *SPP1*$^+$ macrophages and fibroblasts may regulate downstream TGAF and TGAO through SPP1-CD44

signalling, as previously defined. In the collagen pathways of the fibrovascular zone, fibroblasts act as primary sender cells that modulate other fibroblasts, osteoblasts, and osteoclasts. The most prominent ligands identified were members of the collagen type I family, while the receptors included CD44 and endogenous integrins (Fig 6K). The DEGs regulated by these collagen pathways were closely associated with ECM regulation (Fig 6L, M), with enriched pathways involving ECM-receptor interactions and protein digestion (Fig 6N).

Differential abundance and distinct transcriptional profiles of specific T-cell clusters in intercritical and tophaceous gout

The role of T cells in gout, particularly in tophi, has not been reported in detail [9]. Validated T-cell classification marker genes provide a reliable basis for identifying cell types in gout [11]. Therefore, we used specifically expressed genes as markers for each cell subcluster (Fig 7A). A list of the cell clusters and their annotated cell types is provided in Supplementary Table S3. In this study, T cells were present in both intercritical gout and tophaceous gout, with primary heterogeneity between the 2 groups observed in the *CD4*$^+$ T-cell subpopulations. Among *CD4*$^+$ T cells, *CD4*$^+$ naive T cells (*CCR7*$^+$) were more abundant in intercritical gout than in tophaceous gout ($P < .0001$), whereas CD4$^+$ regulatory T cells (*CTLA4*$^+$ *FOXP3*$^+$) were significantly elevated in tophaceous gout ($P < .01$) (Fig 7B,C). Further pseudotime trajectory analysis revealed that undifferentiated *CD4*$^+$ T cells (*CCR7*$^+$) gradually differentiated into *CTLA4*$^+$ *FOXP3*$^+$ cells along the trajectory (Fig 7D). Consistent with this finding, cells from tophaceous gout were found at the endpoint of the pseudotime trajectory, with a similar distribution observed only in *CTLA4*$^+$ *FOXP3*$^+$cells (Fig 7E).

To further explore the relationship between phenotypic changes in *CD4*$^+$T cells and *SPP1*$^+$ macrophages, we conducted an additional cell-chat analysis. The comparison of intercellular communication signal intensities between groups showed that, whether acting as ligand or receptor cells, *CTLA4*$^+$ *FOXP3*$^+$ and TGAMs exhibited stronger communication intensities than IGAMs (Fig 7F). The bubble plot of the receptor-ligand interaction analysis between TGAMs and *CTLA4*$^+$ *FOXP3*$^+$ identified unique receptor-ligand pairs, such as Peptidylprolyl Isomerase A-Basigin (PPIA-BSG) and SPP1-CD44 (Fig 7G,H).

DISCUSSION

Tophi plays a central role in gout-associated joint damage. In this study, we used scRNA-seq and ST to analyse cellular heterogeneity and spatial distribution of immune-stromal populations in tophi and synovial tissues from patients at different stages of gout. Our most significant finding is the identification of a specialised phenotypic subgroup, *SPP1*$^+$ TGAMs, which we demonstrate for the first time to be highly related to the progression from chronic inflammatory processes to tophus development and ECM reorganisation (Fig 8). *SPP1*$^+$ macrophages coexpressed immunoregulatory and matrix-remodelling markers, exhibiting a fibroblast-like phenotype. They also displayed enhanced osteoclast differentiation capacity and engaged in

---

TGAMs. (F) Mendelian randomisation scatter plot shows that for each SD increase in *SPP1* expression, the risk of gout flare-ups increases by 0.6% (P values: 1.274×10^{-5} for inverse variance weighted, 1.750×10^{-4} for weighted median, 4.263×10^{-2} for simple mode, and 7.636×10^{-3} for weighted mode). (G) The leave-one-single-nucleotide polymorphisms (SNPs)-out plot assesses the effect of SNP used as instrumental variables in the MR analysis. ****$P < .0001$, ***$P < .001$, **$P < .01$, and *$P < .05$. ECM, extracellular matrix; KEGG, Kyoto Encyclopedia of Genes and Genomes.
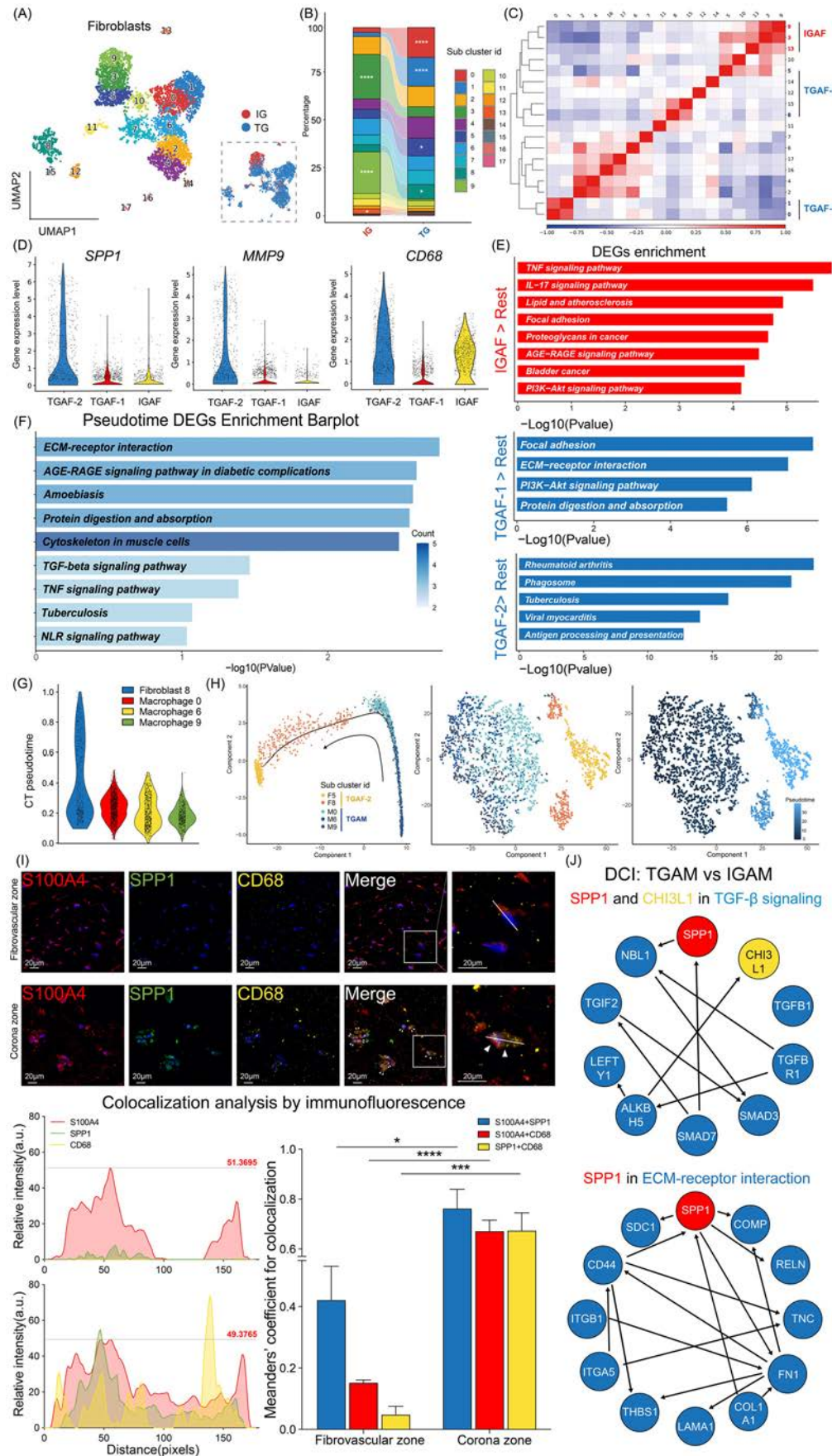
Figure 5. Fibroblasts and osteoblasts exhibited a proinflammatory phenotype in intercritical gout but an extracellular matrix (ECM)-regulatory phenotype in tophaceous gout. (A) Uniform manifold approximation and projection (UMAP) and dot plots of fibroblasts from intercritical gout and tophaceous gout samples. (B) Proportions of fibroblast subclusters in each sample. (C) Heatmap of intersubtype correlation analysis. (D) Violin plots showing gene expression in several sample-specific fibroblast subtypes. (E) Enrichment analysis of differential gene expressions (DEGs) in the intercritical gout-associated fibroblasts (IGAFs), tophaceous gout-associated fibroblast (TGAF)-1, and TGAF-2. (F) Kyoto Encyclopedia of Genes and Genomes (KEGG) enrichment bar plot of branch-dependent genes in pseudotime analysis. (G) Assessment of cellular differentiation potential in tophaceous

integrin-mediated crosstalk with fibrovascular niche components, including fibroblasts, osteoblasts, and regulatory T cells (Tregs).

SPP1, a multifunctional member of the small integrin binding ligand N-linked glycoprotein family, participates in diverse pathophysiological processes including skeletal homeostasis, inflammatory modulation and tissue fibrosis [26,27]. Our study reveals that this multifaceted protein exhibits stage-specific cellular expression patterns in gout pathogenesis. $SPP1^+$ TGAMs were exclusively detected in the tophi microenvironment (absent in other disease stages and peripheral blood) [11]. They displayed an increased expression of fibrosis-related genes, such as $CHI3L1$ and $MMP9$. CHI3L1 promotes profibrotic macrophage differentiation in pulmonary fibrosis, directly interacts with collagen I, and is involved in ECM remodelling [28]. MMP9, which is also well known for its role in ECM remodelling, is regulated by SPP1 and CHI3L1 [29,30].

Notably, the functional specialisation of $SPP1^+$ TGAMs arises from their anatomical confinement within tophus niches. Unlike other fibrotic conditions, gout manifests organised, crystal-centred multilayered structure. Within the fibrovascular zone, $SPP1^+$ TGAMs engage in a macrophage-to-osteoclast differentiation trajectory. This observation is further supported by our single-cell transcriptomic data. Pseudotemporal trajectory analysis revealed significant enrichment of genes involved in lysosomal activity and calcium-dependent protein binding—hallmark pathways essential for osteoclastic bone resorption [31,32]. Consequently, the osteoclastic differentiation of $SPP1^+$ TGAMs within the fibrovascular zone provides a mechanistic explanation for the characteristic bone erosion observed in tophaceous gout. Spatially distinct in function, corona zone-localised $SPP1^+$ TGAMs (vs fibrovascular zone populations) demonstrated unique integrin-mediated cell cross-talks with fibroblasts. This spatial functional heterogeneity suggests that $SPP1^+$ TGAMs may differentially regulate ECM degradation and synthesis according to their microenvironmental localisation, thereby helping maintain the intricate structural organisation of the tophus.

Interestingly, unlike their well-characterised immunosuppressive phenotype in tumour tissues, $SPP1^+$ macrophages exhibit a distinct transcriptional activation profile central to the gout pathogenesis, particularly IL-17 pathways, which may initiate and sustain the chronic inflammatory loop within the tophi [33−37]. IL-17A was previously proved to promote the differentiation of monocytes into $SPP1^+$ macrophages. These macrophages remodel fibrillar collagen via TGF-β1-mediated signalling pathways [38]. This IL-17-SPP1 self-reinforcing loop of matrix degradation and fibrogenesis likely drives the progressive encapsulation characteristic of mature tophi. Moreover, COL6A2, a widely expressed ECM component that is critical for maintaining tissue structural integrity and regulating diverse cellular processes, was identified as one of the most significantly upregulated genes at chronic gouty arthritis stage [39]. Elevated

$COL6A2$ expression has been shown to promote vascular remodelling and immune microenvironment reorganisation via activation of the PI3K−Akt and TGF-β signalling pathways in renal carcinoma [40]. Consistently, we found that $SPP1^+$ TGAMs in tophi similarly exhibit hyperactivation of these analogous pathways, underscoring their role in driving ECM pathological remodelling.

This unique transcriptional profile suggests that $SPP1^+$ TGAMs retain moderate inflammatory activity relative to intercritical macrophages while predominantly acquiring enhanced collagen VI-dependent ECM-regulatory functions compared with clusters of FASFM. Notably, a distinct cellular subset, tentatively termed TGAF2, was observed to share a similar transcriptional pattern, characterised by coupregulation of $SPP1$, $MMP9$, and $CD68$—features consistent with macrophage-to-myofibroblast transition under persistent inflammatory stimulation [41]. We also identified $S100A4$ within TGAM-specific gene modules, implying a potential phenotypic shift towards a collagen-producing and fibroblast-like state. The functional interplay between these 2 cellular subsets and their potential for transition warrants further investigation.

Cell communication and phenotypic interactions between $SPP1^+$ TGAMs and rest cells reveal immunoregulatory networks. Enhanced SPP1-CD44 interaction between $SPP1^+$ TGAMs and fibroblasts may be part of a broader regulatory network. For instance, SPP1-CD44 signalling could activate PI3K/AKT, suppress apoptosis, and maintain ECM homeostasis, supporting its role in matrix regulation [42]. SPP1-CD44 signalling functions not as a standalone ligand-receptor event, but as a context-dependent axis that integrates upstream transcriptional cues and downstream signalling to regulate ECM remodelling. Likewise, previous studies have linked SPP1-CD44 interactions to Th17 differentiation and T-cell exhaustion [29,43]. Our findings supported this in tophaceous gout, showing a shift towards SPP1-CD44 between $SPP1^+$ TGAMs and naive T cells as well as Tregs. This interaction suggests that the local microenvironment may favour Treg induction over Th17 polarisation. The Th17/Treg axis plays a pivotal role in maintaining immune homeostasis during gout. During gout remission, the Treg/Th17 ratio increases in peripheral blood, and Tregs exhibit elevated $CTLA4$ expression, which is critical for their immunosuppressive function [14]. Our analysis confirmed an increased proportion of Tregs in tophaceous gout, along with elevated $CTLA4$ expression, suggesting that $SPP1^+$ TGAMs may promote immune suppression by facilitating Treg differentiation [14].

While this study provides novel insights into the cellular dynamics of gout, certain limitations should be considered in interpreting the findings: (1) the spatial resolution of current transcriptomic approaches and the restricted diversity of available sample types impose constraints on data interpretation. Although the integration of ST with scRNA-seq improves spatial resolution and cell-type mapping, the inherent ∼55 μm resolution limit of the 10× Visium platform, combined with the

---

gout-associated macrophages (TGAMs) and TGAFs by Cellular trajectory reconstruction anlysis using gene counts and expression (CytoTRACE). (H) Left: pseudotime analysis of TGAMs and TGAF-2. Middle: UMAP downscaling of TGAMs and TGAF-2. Right: UMAP downscaling of TGAMs and TGAF-2 with pseudotime. (I) Top: representative multiplex immunofluorescence images showing S100A4 (red), SPP1 (green), CD68 (yellow), and 4',6-diamidino-2-phenylindole (DAPI) (blue) staining in the fibrovascular zone (top) and corona zone (bottom). Merged and magnified views are presented to highlight areas of triple-marker colocalisation. Bottom: line intensity profiles show fluorescence signal distribution across representative regions of interest (ROI). Bar graphs quantify pairwise colocalisation using Manders' coefficients for S100A4/SPP1, S100A4/CD68, and SPP1/CD68. ****$P <$ .0001, ***$P <$ .001, **$P <$ .01, *$P <$ .05. (J) Differential causal interactions centred on $SPP1$ and $CHI3L1$ within the transforming growth factor (TGF)-β signalling pathway (left) and ECM-receptor interaction pathway (right), inferred from differential causal inference (DCI) analysis comparing TGAMs and intercritical gout-associated macrophages (IGAMs). Arrows represent the direction of inferred regulatory influence. CT, cellular trajectory.
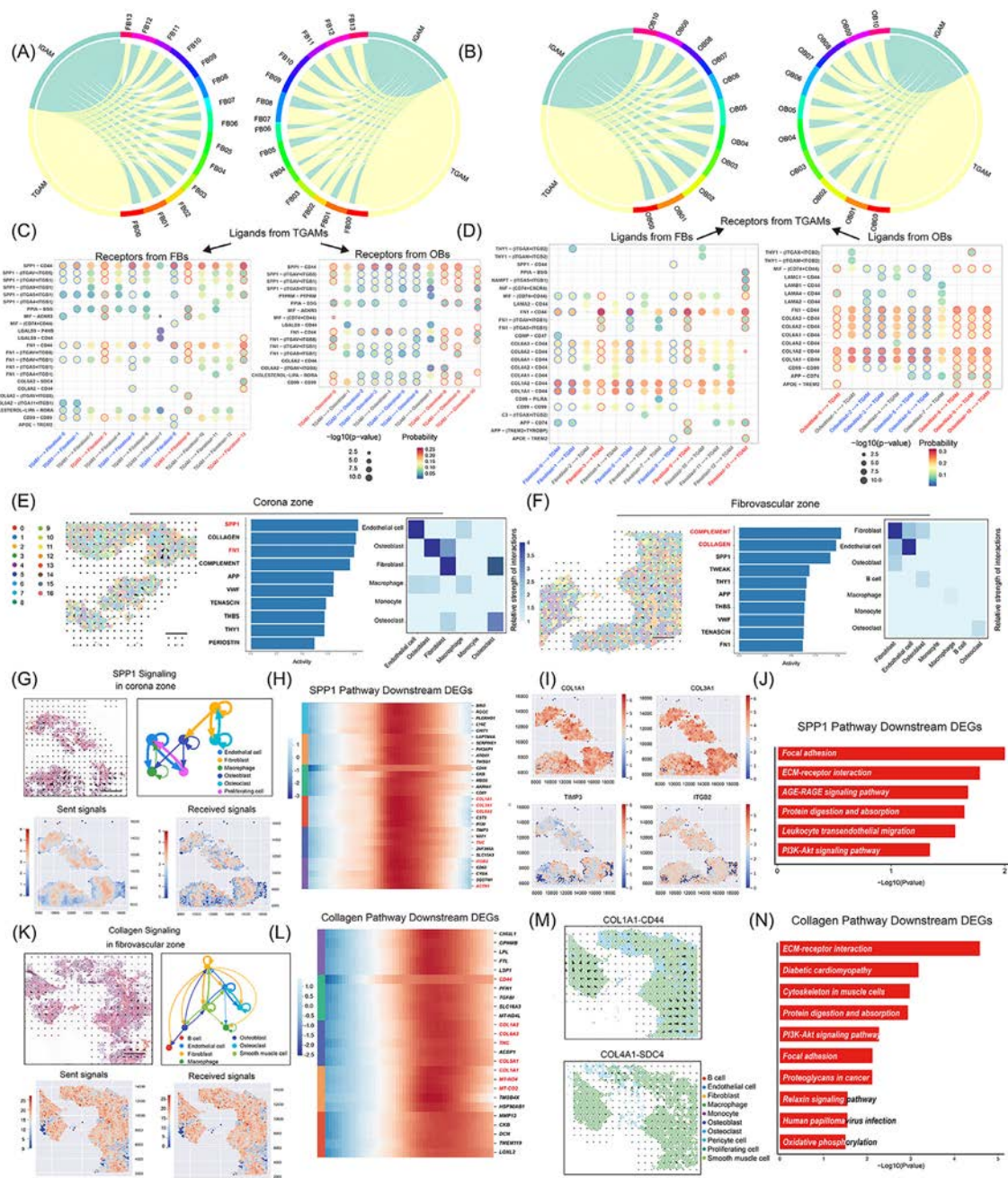
Figure 6. Cell communication analysis suggests a high activation of SPP1-CD44 in the tophus corona zone. (A, B) Cell-cell communication between intercritical gout-associated macrophages (IGAMs) and fibroblasts or osteoblasts. The left side of the circle shows the sending cells, and the right side shows the receiving cells. (C, D) Bubble plot of receptor-ligand interaction analysis between tophaceous gout-associated macrophages (TGAMs) and fibroblasts or osteoblasts. (E, F) Left: image-level directionality of cell communication pathways in the corona zone or fibrovascular zone. Middle: the top 10 signalling pathways, with values normalised to reflect the strength of intercellular communication. Right: heatmap showing the relative interaction strengths among cell types involved in the top 10 signalling pathways. (G) Top left: directionality of cell communication in the SPP1 signalling pathway. Top right: network diagram of interactions within the SPP1 signalling pathway. Bottom: heatmap of sent and received signal intensities. (H) Heatmap of differential gene expressions (DEGs) regulated by the SPP1 signalling pathway. (I) Relationship between DEGs and the SPP1-related pathways. (J) Enrichment analysis of DEGs regulated by the SPP1 signalling pathway. (K) Top left: directionality of cell communication in the collagen signalling pathway. Top right: network diagram of interactions within the collagen signalling pathway. Bottom: heatmap of sent and received signal intensities. (L) Heatmap of DEGs regulated by the collagen signalling pathway. (M) Representative receptor-ligand pair in the collagen pathway. (N) Heatmap of DEGs regulated by the collagen signalling pathway. ****$P < .0001$, ***$P < .001$ **$P < .01$, *$P < .05$.

limited number and diversity of tissue samples, restricts precise gene localisation and comprehensive identification of rare or transitional cell states. (2) Although CytoTRACE effectively highlights stemness differences between TGAMs and TGAF2 populations, definitive experimental evidence supporting cell state transitions and direct intercellular interactions is still required. Future studies incorporating lineage tracing and coimmunoprecipitation approaches will be necessary to validate potential transition events and confirm functional cell-cell communication networks.

In conclusion, this study revealed key cell-type and subtype transitions at various stages of gout, identifying *SPP1*^{+} TGAMs as a crucial population linking ECM remodelling to inflammatory processes associated with gout. This study offers new insights into the pathophysiology of gout, indicating that targeting the critical *SPP1*^{+} macrophage may provide an effective
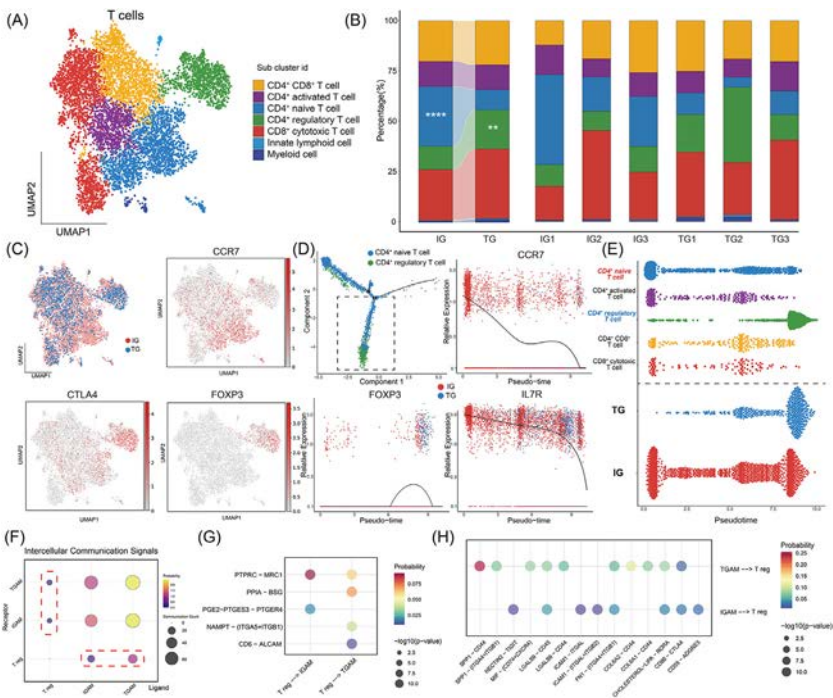
Figure 7. Differential abundance and distinct transcriptional profiles of specific T-cell clusters between intercritical gout and tophaceous gout. (A) Annotated uniform manifold approximation and projection (UMAP) plot of T cells. (B) Proportions of the annotated T-cell subclusters in each sample. (C) UMAP plots of the expression of canonical marker genes of *CD4*⁺ naive T cells and regulatory T cells. (D) Top left: pseudotime distribution of T cells, with a dashed box indicating Lineage 2. The rest of the plot shows differential gene expressions (DEGs) of pseudotime Lineage 2 expressed throughout pseudotime. (E) Distribution of cell counts across different subtypes and samples along Lineage 2 in pseudotime analysis. (F) Comparison of intercellular communication signal intensities between *CD4*⁺ regulatory T cells and tophaceous gout-associated macrophages (TGAMs) or intercritical gout-associated macrophages (IGAMs). (G, H) Bubble plot of receptor-ligand interaction analysis between TGAMs and *CD4*⁺ regulatory T cells. ****P < .0001, ***P < .001, **P < .01, *P < .05.
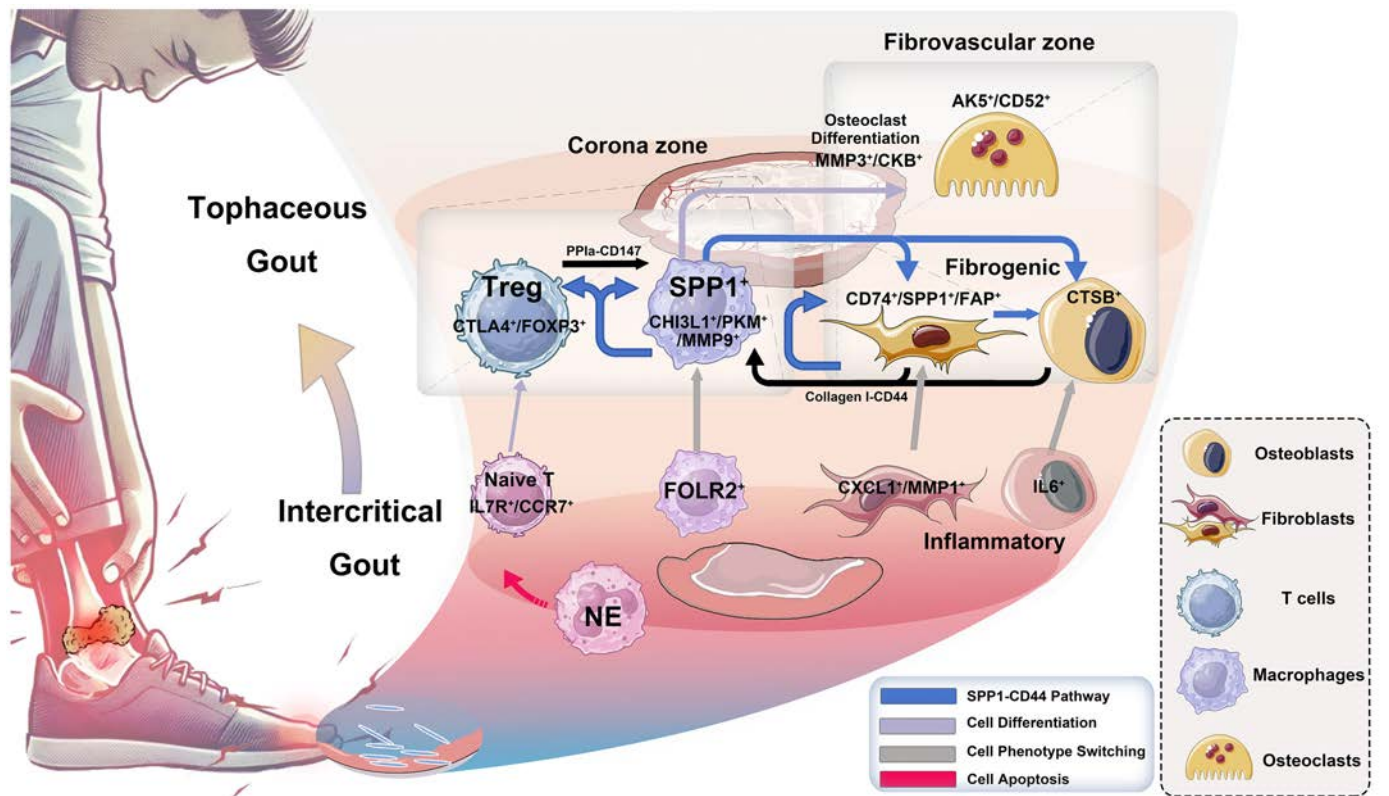
Figure 8. Schematic of tophaceous gout patterns based on transcriptomics. Schematic illustrating the phenotypic changes and differentiation pathways of cells between intercritical gout and tophaceous gout, highlighting the role of SPP1-CD44 receptor-ligand interactions among tophaceous gout-associated macrophages (TGAMs), fibroblasts, and osteoblasts in linking inflammation to extracellular matrix (ECM) remodelling in tophi. Treg, regulatory T-cell. NE, Neutrophilic Granulocyte; CTSB, Cathepsin B.

strategy for inhibiting tophus formation and preventing tissue fibrosis, and osteoclast differentiation, ultimately blocking the formation of tophi and preventing joint damage.

METHODS

Detailed experimental methods and technical details are provided in the Supplementary Materials.

Competing interests

Acknowledgements

Contributors

YH is responsible for the overall content as the guarantor. ND, RH, and LL supervised and designed the study and also edited the manuscript. YH, XZ (Zhu), XL, and XJ included patients and collected surgical samples. HX performed all sample processing, data analysis, and manuscript drafting. ZL and XZ (Zhou) contributed to data analysis and manuscript drafting.

Funding

Patient consent for publication

All participants provided written informed consent.

Ethics approval

The experimental protocols involving human specimens were approved by the Ethics Committee of Huashan Hospital (KY2020-060).

Provenance and peer review

Not commissioned; externally peer reviewed.

Data availability statement

Data are available on reasonable request.

Supplementary materials

Supplementary material associated with this article can be found in the online version at doi:10.1016/j.ard.2025.09.003.

Orcid

Hanlin Xu: http://orcid.org/0000-0001-6828-620X
Zhechen Liu: http://orcid.org/0009-0007-1984-3912
Xiaofeng Zhou: http://orcid.org/0009-0000-9776-1188
Xiaoxi Ji: http://orcid.org/0009-0006-4390-4108
Xingwang Liu: http://orcid.org/0009-0003-0402-7593
Liwei Lu: http://orcid.org/0000-0002-8634-0967
Nicola Dalbeth: http://orcid.org/0000-0003-4632-4476
Rui He: http://orcid.org/0000-0001-5288-9786
Yinghui Hua: http://orcid.org/0000-0002-0767-1267

REFERENCES

[1] Dalbeth N, Gosling AL, Gaffo A, Abhishek A. Gout. Lancet 2021;397:1843–55. doi: 10.1016/S0140-6736(21)00569-9.

[2] Shi M, Luo J, Ding L, Duan L. Spontaneous resolution of acute gout: mechanisms and therapeutic targets. RMD Open 2023;9:e003586. doi: 10.1136/rmdopen-2023-003586.

[3] Martinon F, Pétrilli V, Mayor A, Tardivel A, Tschopp J. Gout-associated uric acid crystals activate the NALP3 inflammasome. Nature 2006;440:237–41. doi: 10.1038/nature04516.

[4] Chen C-J, Shi Y, Hearn A, Fitzgerald K, Golenbock D, Reed G, et al. MyD88-dependent IL-1 receptor signaling is essential for gouty inflammation stimulated by monosodium urate crystals. J Clin Invest 2006;116:2262–71. doi: 10.1172/JCI28075.

[5] Dalbeth N, Collis J, Gregory K, Clark B, Robinson E, McQueen FM. Tophaceous joint disease strongly predicts hand function in patients with gout. Rheumatology (Oxford) 2007;46:1804–7. doi: 10.1093/rheumatology/kem246.

[6] Schlesinger N, Thiele RG. The pathogenesis of bone erosions in gouty arthritis. Ann Rheum Dis 2010;69:1907–12. doi: 10.1136/ard.2010.128454.

[7] Xu H, Qin H, Hua Y, Dalbeth N. Contributions of joint damage-related events to gout pathogenesis: new insights from laboratory research. Ann Rheum Dis 2023;82:1511–5. doi: 10.1136/ard-2023-224679.

[8] Chhana A, Dalbeth N. The gouty tophus: a review. Curr Rheumatol Rep 2015;17:19. doi: 10.1007/s11926-014-0492-x.

[9] Dalbeth N, Pool B, Gamble GD, Smith T, Callon KE, McQueen FM, et al. Cellular characterization of the gouty tophus: a quantitative analysis. Arthritis Rheum 2010;62:1549–56. doi: 10.1002/art.27356.

[10] Palmer DG, Hogg N, Denholm I, Allen CA, Highton J, Hessian PA. Comparison of phenotype expression by mononuclear phagocytes within subcutaneous gouty tophi and rheumatoid nodules. Rheumatol Int 1987;7:187–93. doi: 10.1007/BF00541376.

[11] Gu H, Yu H, Qin L, Yu H, Song Y, Chen G, et al. MSU crystal deposition contributes to inflammation and immune responses in gout remission. Cell Rep 2023;42:113139. doi: 10.1016/j.celrep.2023.113139.

[12] Pandey A, Bhutani N. Profiling joint tissues at single-cell resolution: advances and insights. Nat Rev Rheumatol 2024;20:7–20. doi: 10.1038/s41584-023-01052-x.

[13] Saliba A-E, Westermann AJ, Gorski SA, Vogel J. Single-cell RNA-seq: advances and future challenges. Nucleic Acids Res 2014;42:8845–60. doi: 10.1093/nar/gku555.

[14] Yu H, Xue W, Yu H, Song Y, Liu X, Qin L, et al. Single-cell transcriptomics reveals variations in monocytes and Tregs between gout flare and remission. JCI Insight 2024;9:e179067. doi: 10.1172/jci.insight.179067.

[15] Luecken MD, Theis FJ. Current best practices in single-cell RNA-seq analysis: a tutorial. Mol Syst Biol 2019;15:e8746. doi: 10.15252/msb.20188746.

[16] Castillo RL, Sidhu I, Dolgalev I, Chu T, Prystupa A, Subudhi I, et al. Spatial transcriptomics stratifies psoriatic disease severity by emergent cellular ecosystems. Sci Immunol 2023;8:eabq7991. doi: 10.1126/sciimmunol.abq7991.

[17] Rao A, Barkley D, França GS, Yanai I. Exploring tissue architecture using spatial transcriptomics. Nature 2021;596:211–20. doi: 10.1038/s41586-021-03634-9.

[18] Ståhl PL, Salmén F, Vickovic S, Lundmark A, Navarro JF, Magnusson J, et al. Visualization and analysis of gene expression in tissue sections by spatial transcriptomics. Science 2016;353:78–82. doi: 10.1126/science.aaf2403.

[19] Tao H, Mo Y, Liu W, Wang H. A review on gout: looking back and looking ahead. Int Immunopharmacol 2023;117:109977. doi: 10.1016/j.intimp.2023.109977.

[20] Zhao L, Ye W, Zhu Y, Chen F, Wang Q, Lv X, et al. Distinct macrophage polarization in acute and chronic gout. Lab Invest 2022;102:1054–63. doi: 10.1038/s41374-022-00798-4.

[21] Matusiak M, Hickey JW, van IJzendoorn DGP, Lu G, Kidziński L, Zhu S, et al. Spatially segregated macrophage populations predict distinct outcomes in colon cancer. Cancer Discov 2024;14:1418–39. doi: 10.1158/2159-8290.CD-23-1300.

[22] Nalio Ramos R, Missolo-Koussou Y, Gerber-Ferder Y, Bromley CP, Bugatti M, Núñez NG, et al. Tissue-resident FOLR2+ macrophages associate with CD8 + T cell infiltration in human breast cancer. Cell 2022;185 1189-207.e25. doi: 10.1016/j.cell.2022.02.021.

[23] Henlon Y, Panir K, McIntyre I, Hogg C, Dhami P, Cuff AO, et al. Single-cell analysis identifies distinct macrophage phenotypes associated with prodisease and proresolving functions in the endometriotic niche. Proc Natl Acad Sci USA 2024;121:e2405474121. doi: 10.1073/pnas.2405474121.

[24] Chang J-G, Tu S-J, Huang C-M, Chen Y-C, Chiang H-S, Lee Y-T, et al. Single-cell RNA sequencing of immune cells in patients with acute gout. Sci Rep 2022;12:22130. doi: 10.1038/s41598-022-25871-2.

[25] Sutherland TE, Dyer DP, Allen JE. The extracellular matrix and the immune system: a mutually dependent relationship. Science 2023;379:eabp8964.

[26] Bellahcène A, Castronovo V, Ogbureke KUE, Fisher LW, Fedarko NS. Small integrin-binding ligand N-linked glycoproteins (SIBLINGs): multifunctional proteins in cancer. Nat Rev Cancer 2008;8:212–26. doi: 10.1038/nrc2345.

[27] Song Z, Chen W, Athavale D, Ge X, Desert R, Das S, et al. Osteopontin takes center stage in chronic liver disease. Hepatology 2021;73:1594–608. doi: 10.1002/hep.31582.

[28] Cao Y, Rudrakshala J, Williams R, Rodriguez S, Sorkhdini P, Yang AX, et al. CRTH2 mediates profibrotic macrophage differentiation and promotes lung fibrosis. Am J Respir Cell Mol Biol 2022;67:201–14. doi: 10.1165/rcmb.2021-0504OC.

[29] Dong L, Hu S, Li X, Pei S, Jin L, Zhang L, et al. SPP1+ TAM regulates the metastatic colonization of CXCR4+ metastasis-associated tumor cells by remodeling the lymph node microenvironment. Adv Sci (Weinh) 2024;11:e2400524. doi: 10.1002/advs.202400524.

[30] Mazzali M, Kipari T, Ophascharoensuk V, Wesson JA, Johnson R, Hughes J. Osteopontin—a molecule for all seasons. QJM 2002;95:3–13. doi: 10.1093/qjmed/95.1.3.

[31] Zaidi M, Moonga BS, Huang CLH. Calcium sensing and cell signaling processes in the local regulation of osteoclastic bone resorption. Biol Rev Camb Philos Soc 2004;79:79–100. doi: 10.1017/s1464793103006262.

[32] Zaidi M, Alam AS, Shankar VS, Bax BE, Bax CM, Moonga BS, et al. Cellular biology of bone resorption. Biol Rev Camb Philos Soc 1993;68:197–264. doi: 10.1111/j.1469-185x.1993.tb00996.x.

[33] Desai J, Steiger S, Anders H-J. Molecular pathophysiology of gout. Trends Mol Med 2017;23:756–68. doi: 10.1016/j.molmed.2017.06.005.

[34] Li Y, Zheng Y, Huang J, Nie R-C, Wu Q-N, Zuo Z, et al. CAF-macrophage crosstalk in tumour microenvironments governs the response to immune checkpoint blockade in gastric cancer peritoneal metastases. Gut 2025;74:350–63. doi: 10.1136/gutjnl-2024-333617.

[35] Qi J, Sun H, Zhang Y, Wang Z, Xun Z, Li Z, et al. Single-cell and spatial analysis reveal interaction of FAP+ fibroblasts and SPP1+ macrophages in colorectal cancer. Nat Commun 2022;13:1742. doi: 10.1038/s41467-022-29366-6.

[36] Sathe A, Mason K, Grimes SM, Zhou Z, Lau BT, Bai X, et al. Colorectal cancer metastases in the liver establish immunosuppressive spatial networking between tumor-associated SPP1+ macrophages and fibroblasts. Clin Cancer Res 2023;29:244–60. doi: 10.1158/1078-0432.CCR-22-2041.

[37] Raucci F, Iqbal AJ, Saviano A, Minosi P, Piccolo M, Irace C, et al. IL-17A neutralizing antibody regulates monosodium urate crystal-induced gouty inflammation. Pharmacol Res 2019;147:104351. doi: 10.1016/j.phrs.2019.104351.

[38] Fabre T, Barron AMS, Christensen SM, Asano S, Bound K, Lech MP, et al. Identification of a broadly fibrogenic macrophage subset induced by type 3 inflammation. Sci Immunol 2023;8:eadd8945. doi: 10.1126/sciimmunol.add8945.

[39] Lamandé SR, Bateman JF. Collagen VI disorders: insights on form and function in the extracellular matrix and beyond. Matrix Biol 2018;71-72:348–67. doi: 10.1016/j.matbio.2017.12.008.

[40] Yang Y, Fan R, Zhang B, Liu K. COL6A2 in clear cell renal cell carcinoma: a multifaceted driver of tumor progression, immune evasion, and drug sensitivity. J Transl Med 2025;23:875. doi: 10.1186/s12967-025-06793-9.

[41] Zhuang T, Chen M-H, Wu R-X, Wang J, Hu X-D, Meng T, et al. ALKBH5-mediated m6A modification of IL-11 drives macrophage-to-myofibroblast transition and pathological cardiac fibrosis in mice. Nat Commun 2024;15:1995. doi: 10.1038/s41467-024-46357-x.

[42] Liu Q, Zeng H, Yuan Y, Wang Z, Wu Z, Luo W. Osteopontin inhibits osteoarthritis progression via the OPN/CD44/PI3K signal axis. Genes Dis 2022;9:128–39. doi: 10.1016/j.gendis.2020.06.006.

[43] Zheng Y, Zhao L, Xiong Z, Huang C, Yong Q, Fang D, et al. Ursolic acid targets secreted phosphoprotein 1 to regulate Th17 cells against metabolic dysfunction-associated steatotic liver disease. Clin Mol Hepatol 2024;30:449–67. doi: 10.3350/cmh.2024.0047.

Osteoarthritis

Effect of intra-articular adipose-derived mesenchymal stromal cell versus placebo injection on pain and function in patients with knee osteoarthritis: the ADIPOA2 phase 2b randomised clinical trial

Yves-Marie Pers [1],*, Hubert Schrezenmeier [2], Sandrine Fleury-Cappellesso [3], Ulrich Nöth [4], Lars Rackwitz [4], Rosanna Ferreira [1], Francis Berenbaum [5], Adeline Ruyssen-Witrand [6], Rogier Martijn Thurlings [7], Olga Addimanda [8], Gina Lisignoli [9], Roberta Ramonda [11], Fintan Shannon [10], Leonardo Punzi [11], Athan Baillet [12], Andrew W. McCaskie [13,14], Stephen McDonnell [13,14], Jenny O'Callaghan [13], Tom Turmezei [15,16], Dimitri A. Kessler [17,18], Ramin Lotfi [2], Markus Rojewski [2], Aoife Duffy [10], Andrew Finnerty [10], Anaïck Moisan [3], Helene Brochot-Dechet [3], Mathilde Aubery-Rousselet [3], Amélie Michon [19], Jimena Bouzas-Rodriguez [19], Oliver Pullig [20], Sylvie Broussous [21], Erika Nogue [22], Maïlis Amico [22], Marie-Christine Picot [22,23], Frank Barry [10], Christian Jorgensen [1], on behalf of ADIPOA2 consortium

[1] Institute for Regenerative Medicine and Biotherapy, Univ Montpellier, INSERM UMR 1183, Clinical Immunology and Osteoarticular Diseases Therapeutic Unit, CHU Montpellier, Montpellier, France

[2] Institute of Transfusion Medicine, University of Ulm and Institute of Clinical Transfusion Medicine and Immunogenetics Ulm, Red Cross Blood Transfusion Service Baden-Württemberg-Hessen and University Hospital Ulm, Ulm, Germany

[3] EFS (Etablissement Français du Sang), Grenoble, St Ismier, and Toulouse Cedex 3, France

[4] Department for Orthopedic and Trauma Surgery, Berlin, Germany

[5] Rheumatology Department, Sorbonne University, INSERM CRSA, Hôpital Saint-Antoine, Paris, France

[6] Rheumatology Centre, Toulouse University Hospital, Centre d'Investigation Clinique de Toulouse CIC1436, Inserm, Team PEPSS « Pharmacologie En Population cohorteS et biobanqueS », University of Toulouse 3, Toulouse, France

[7] Rheumatology Department, Radboud University Medical Center, Nijmegen, The Netherlands

[8] IRCCS Istituto Ortopedico Rizzoli, Medicina e Rheumatologia, Bologna, Italy

[9] IRCCS Istituto Ortopedico Rizzoli, Laboratorio di Immunoreumatologia e Rigenerazione Tissutale, Bologna, Italy

[10] Regenerative Medicine Institute, University of Galway, Galway, Ireland

[11] Department of Medicine, Università Degli Studi Di Padova, Padova, Italy

[12] Rheumatology Department, CHU Grenoble Alpes, Hôpital Sud, Echirolles, France

[13] Division of Trauma and Orthopaedic Surgery, Department of Surgery, University of Cambridge, Addenbrooke's Hospital, Cambridge, UK

[14] Cambridge University Hospitals NHS Foundation Trust, Cambridge, UK

[15] Norfolk and Norwich University Hospital, Norwich, UK

*Correspondence to Dr Yves-Marie Pers, MD, PhD, IRMB, University of Montpellier, INSERM, CHU Montpellier, Montpellier, France; Clinical Immunology and Osteoarticular Diseases Therapeutic Unit, Lapeyronie University Hospital, 371 Avenue du Doyen Gaston Giraud, Montpellier Cedex 05 34295, France.

E-mail address: ym-pers@chu-montpellier.fr (Y.-M. Pers).

Hubert Schrezenmeier and Sandrine Fleury-Cappellesso contributed equally to this work.

Current affiliation of Olga Addimanda: Rheumatology Unit, AUSL of Bologna—Policlinico Sant'Orsola—AOU—IRCCS of Bologna, Bologna, Italy.

Handling editor Josef S. Smolen.

[16] *University of East Anglia, Norwich, UK*

[17] *Department of Radiology, University of Cambridge, Cambridge, UK*

[18] *Artificial Intelligence in Medicine Lab (BCN-AIM), Facultat de Matemátiques i Informática, Universitat de Barcelona, Barcelona, Spain*

[19] *ECRIN, Paris, France*

[20] *Department Tissue Engineering and Regenerative Medicine, University Hospital Würzburg, Würzburg, Germany*

[21] *Research and innovation Department, CHU Montpellier, Univ Montpellier, Montpellier Cedex 5, France*

[22] *Clinical Research and Epidemiology Unit (Public Health Department), CHU Montpellier, Univ Montpellier, Montpellier Cedex 5, France*

[23] *Centre de Recherche en Épidémiologie et Santé des Populations (CESP), INSERM, University Paris-Saclay, Villejuif, France*

ARTICLE INFO

ABSTRACT

Objectives: This study aims to evaluate the efficacy of intra-articular autologous adipose-derived *ex vivo* expanded mesenchymal stromal cells (ADSC) on patient-reported outcome (pain and function) in symptomatic mild-to-moderate tibiofemoral knee osteoarthritis (OA).

Methods: Participants were randomised in a prospective, double-blind, controlled phase 2b study to receive 1 single intra-articular injection in 3 separate groups: ADSC low dose 2×10^6 cells; ADSC high dose 10×10^6 cells; or saline placebo. The primary outcome was the rate of OsteoArthritis Research Society International (OARSI)/Outcome MEasures in Rheumatology (OMERACT) 'strict responders' defined by improvements from baseline reported to 0 to 100 mm scale in Western Ontario and McMaster University Osteoarthritis index (WOMAC) pain or physical function subscores ≥50% with minimal absolute changes ≥20 mm at 6 months. Secondary outcomes included an evaluation of WOMAC pain, WOMAC function, quality of life (36-Item Short Form Health Survey), WOMAC and Knee injury and OA Outcome Score global change, magnetic resonance imaging cartilage thickness changes and safety from baseline to 12-month follow-up.

Results: One hundred thirty-five patients were randomised from September 2016 to March 2022 (mean age, 58.3 [SD, 6.5] years; 58 [43%] women), 99 (73%) received allocated intervention, and 97 were analysed. After 6 months, treatment with ADSC versus placebo injection, 26 patients (47.3%) versus 23 patients (54.8%) were strict OARSI/OMERACT responders (relative risk 0.86 [95% CI: 0.58-1.28]; *P* = .46). Individuals showed different patterns in cartilage thickness change between timepoints across tibiofemoral articular surfaces, but overall secondary outcomes showed no significant-group differences.

Conclusions: Among patients with symptomatic mild-to-moderate knee OA, a single intra-articular injection of 2×10^6 or 10×10^6 autologous ADSC compared with injection of saline placebo did not significantly improve pain and function.

Trial registration number: ClinicalTrials.gov Identifier: NCT02838069, https://clinicaltrials.gov/study/NCT02838069/EudraCT number: 2015-002125-19, https://www.clinicaltrialsregister.eu/ctr-search/search?query=2015-002125-19.

INTRODUCTION

Osteoarthritis (OA) is a multifactorial, slowly progressive disorder of joints leading to irreversible damage to cartilage and subchondral bone and synovial inflammation [1]. It is the most common musculoskeletal disease in adults affecting more than 23% of the worldwide population over 50 to 79 years and a major cause of disability [2]. As a consequence of ageing and the prevalence of obesity, the cost of OA to healthcare systems is growing rapidly [3]. While end-stage disease can be treated with joint replacement, at earlier stages, there is no effective disease-modifying treatment for this condition.

Biological therapies, including platelet-rich plasma, bone marrow concentrate or lipoaspirate, as well as cell therapy are either not recommended or are recommended against by international guidelines for the treatment of knee OA [4,5]. These recommendations reflect the current lack of sufficient high-quality evidence supporting the routine use of these intra-articular injections. However, the use of mesenchymal stromal cells (MSCs) is an attractive therapy since, under the correct *in vitro* conditions, they display trilineage differentiation including a capacity to form cartilage and bone,

protection against tissue hypoxia, reduction of fibrosis, and local inflammation [6]. MSCs can be isolated from a large number of tissues, including bone marrow and adipose tissue [7,8]. Adipose-derived MSCs (ADSC) are similar to bone marrow-derived MSCs but easier to collect for clinical application with higher isolation yields. These cells, when injected in the knee joint in preclinical models, prevented OA onset, reduced synovitis, and osteophyte formation [9−11]. MSCs from different tissue sources have been used in nearly 3000 patients with a convincing safety profile [12]. In addition, several MSC-based therapies (such as Stempeucel, Temcell HS, Cartistem, Prochymal, Cellgram-AMI, Stemirac, Alofisel, Obnitix, and others) are approved in certain countries [13]. The Global Mesenchymal Stem Cells Market Size accounted for $1.7 billion (BN) in 2021 and is targeted to achieve a market size of $3.4 BN by 2030, despite high production costs [14]. In OA, MSC-based therapies, from both autologous and allogeneic tissues, have been assessed in randomised clinical trials and meta-analyses, and, independent of the cell origin (bone marrow, adipose or umbilical cord [UC]), have showed similar improvement in pain, function, quality-of-life scores and cartilage volume

WHAT IS ALREADY KNOWN ON THIS TOPIC

- Mesenchymal stromal cells (MSC)-based therapies, from both autologous and allogeneic tissues, showed encouraging results in pain, function, quality of life scores, and cartilage volume in osteoarthritis (OA).
- Previous data are based on small sample sizes and have been limited by a high risk of bias to allow for robust and definitive conclusions.

WHAT THIS STUDY ADDS

- We conducted a multicentric randomised double-blind placebo-controlled study in knee OA with a single intra-articular injection of autologous adipose-derived mesenchymal stromal cells (ADSC), manufactured by *ex vivo* Good Manufacturing Procedures (GMP) expansion, and compared with placebo saline injection.
- Among adults with symptomatic mild-to-moderate radiologically defined knee OA, treatment with autologous ADSC versus saline injection is safe but did not significantly improve knee pain or function.

HOW THIS STUDY MIGHT AFFECT RESEARCH, PRACTICE OR POLICY

- The phase II ADIPose-derived mesenchymal stromal cells in OsteoArthritis (ADIPOA2) study successfully tackled the challenge of harmonising and standardising GMP-compliant production of MSC therapy across several different manufacturing sites in Europe.
- Further research should consider the short lifespan of MSC and lack of cell engraftment once injected and might explore bioengineering and stratified approaches, targeting patient subgroups, to address the multifactorial nature of OA degradation.

[15,16]. However, these data are based on small sample sizes and have been limited by a high risk of bias in open or uncontrolled clinical trials, and particularly by the lack of blinding to allow for robust and definitive conclusions [17,18].

Here, we conducted a randomised, double-blinded trial in 6 European countries with robust methodology. This study evaluated the efficacy of a single intra-articular ADSC injection on reported symptoms and structure in patients with symptomatic mild-to-moderate knee OA. It was hypothesised that ADSC would lead to greater improvements in knee pain intensity and function at 6 months when compared with placebo saline injection.

MATERIALS AND METHODS

Study design

The ADIPose-derived mesenchymal stromal cell in OsteoArthritis (ADIPOA2) was a 3-arm phase 2b, multicentric, randomised, double-blind controlled trial (RCT). This trial was approved in France, Ireland, Italy, Netherlands, and Germany according to European and local regulation and the Voluntary Harmonization Procedure initial submission on 2 April 2016. The clinical trial is registered under EudraCT (number 2015-002125-19) and on clinicaltrials.gov (NCT02838069). All participants provided written informed consent. The trial protocol is available in Supplementary File 1.

A summary of ADSC procedure and manufacturing steps is available in Supplementary File 2. The autologous ADSC were produced and prepared at 4 sites in Europe (Toulouse and St Ismier, France; Galway, Ireland; Ulm, Germany). Details of the

ADSC characteristics, standardised production and delivery according to Good Manufacturing Procedures standards, are available in Supplementary File 2. The time between adipose tissue aspiration and injection of the ADSC into the knee was 15 to 16 days, where 1 day (≤24 hours) was required for transport of the lipoaspirate to the manufacturing centre, 13 to 14 days for cell culture and 1 day (≤24 hours at ±4°C) for delivery of the isolated and expanded ASC to the clinical centre for transport. For both ADSC groups together, the mean for viability was 93.7% and the median 93.0% ± 4.8%.

Patient selection and enrolment

Participants were recruited by orthopaedic and rheumatology clinicians in 5 European countries (France, Ireland, Italy, Netherlands, and Germany). All inclusion and noninclusion criteria are detailed in Table 1.

Interventions

Patients meeting the eligibility criteria were allocated to treatment groups in 3 arms: low-dose group (LD) 2×10^6 ADSC, high-dose group (HD) 10×10^6 ADSC and control group receiving saline. Eligible participants attended the clinic to complete questionnaires at 1, 3, 6, 9, and 12 months post treatment. Unscheduled visits were allowed at any time for safety reasons or for the assessment of any adverse events (AEs) as required.

In both ADSC arms, all the patients underwent an outpatient liposuction under local anaesthesia. In the control group, a sham lipoaspiration (without removing adipose tissue) was performed to mimic the procedure and to ensure that all interventions were fully blinded.

Participants in each group received 1 single intra-articular knee injection (volume 5 mL) under ultrasound guidance using a lateral patellofemoral approach by an experienced musculoskeletal radiologist/rheumatologist without local anaesthetic injection. The cell preparation consisted of either LD or HD cells suspended in a solution containing 4.5% of human albumin (Octapharma) supplemented with 10% of poly-ionic solution containing 5% glucose (Baxter or B/BRAUN). Pharmacists received the ADSC preparation, confirmed quality control data and conditioned also normal saline prepared by manufacturing centres in a syringe with 18 to 20 gauge needle in a separate room. Then, the radiologist/rheumatologist performed the knee injection using a physical barrier (such as a drape or a cloth screen) to ensure that the participant remained fully blinded to the treatment.

Randomisation and masking

Patients were randomly assigned to LD ADSC, HD ADSC, or placebo in a 1:1:1 allocation, and randomisation was stratified by centre with permuted blocks. The randomisation was performed online on a 24 h/d basis by the central randomisation web-service customised by the KKS Düsseldorf. Plastic surgeons who performed the liposuction and radiologists/rheumatologists who carried out the injections did not have any discussion about treatment allocation with patients and clinical observers. The investigator did not have access to the list of treatment codes used for blinding. Thereby, KKS transmitted the treatment code of the patient to each local pharmacy. Participants, assessors, and the biostatistician were blinded to group allocation.

Table 1

Eligibility criteria in ADIPOA2 study

Inclusion criteria	Exclusion criteria

1) Male or female between the ages of 45 and 70, inclusive, during screening.
2) BMI between 20 and 35 kg/m^2
3) Symptomatic mild-to-moderate osteoarthritis (OA) of the index knee as defined at baseline by the American College of Rheumatology (ACR):
  i. History of pain in the index knee ≥ 6 mo, AND
  ii. Kellgren and Lawrence (K-L) grade 2 or 3 only, on plain radiographs of the index knee (including fixed flexion), AND
  iii. Swelling of the index knee evaluated by the investigator (joint effusion or soft-tissue swelling)
4) Must meet the following pain criteria at the time of baseline visit since at least half of the days in the previous month:
  i. Western Ontario and McMaster Universities Osteoarthritis Index (WOMAC) pain subscores ≥ 40 mm on the 0 to 100 normalised scale
  ii. Visual analogue scale (VAS) pain rating of at least 40 on a 100-mm scale
  iii. Subject's global assessment of the contralateral knee <20 mm by 100 mm using VAS
5) NSAID washout of at least 2 d before screening and baseline
6) Written informed consent dated and signed before the beginning of any procedures related to the clinical trial
7) Subject beneficiary of a social security scheme
	1) Previous treatments acting on cartilage or bone metabolism (eg, oral or intravenous bisphosphonates <1 y previously, denosumab < 6 mo, strontium ranelate or teriparatide or raloxifene <7 d before selection, and oral glucosamine ≥1500 mg/d or chondroitin sulphate ≥1000 mg/d <3 mo previously)
	2) Has had any trauma to the index knee in the previous 12 mo before the screening visit
	3) Has OA of the index knee that meets K-L classification criteria of grade 1 or 4
	4) OA causing significant pain in any joint other than the identified knee, i.e., pain in hip, or contralateral knee (≥20 mm pain) as confirmed by a separate VAS at baseline for any other painful joint concerned
	5) Before the screening visit has received:
	  i. Oral corticosteroid therapy within the previous 3 mo, OR
	  ii. Intramuscular, intravenous or epidural corticosteroid therapy within the previous 6 mo, OR
	  iii. Intra-articular injection of corticosteroids in the index within the previous 6 mo, OR
	  iv. Intra-articular injection of hyaluronic acid in the index knee within the 6 mo. OR
	  v. Intra-articular injection of platelet-rich plasma in the index knee within the 6 mo.
	6) Inflammatory or other rheumatic diseases defined by clinical examination and previous serum markers (such as rheumatoid arthritis, autoimmune disorder, seronegative spondyloarthritis, gout or pseudogout [defined as acute episodic attacks of swollen, painful joint in a patient with X-ray chondrocalcinosis or CPPD crystals]), History or evidence of infectious arthritis, Paget's disease, ochronosis, Wilson's disease, primary osteochondromatosis
	7) History of articular fracture of the target knee joint
	8) History of heritable disorders (eg, hypermobility) and collagen gene mutations
	9) Immunodeficiency diseases
	
	10) Alcoholics not in treatment and still drinking (14 + drinks/wk)
	
	11) Subjects with poorly controlled diabetes mellitus (HbA1C >8%) or known concomitant vascular problems
	
	12) Planned longer stay outside the region that prevents compliance with the scheduled visit
	
	13) Severe misalignment of the knee (excessive varus or valgus ≥8°) at physical examination, as confirmed by standard radiograph
	
	14) Severe osteoporosis with previous symptomatic vertebral or hip fractures
	
	15) History of joint replacement of the knee or hip within the previous 12 mo
	
	16) Serious systemic diseases or infectious/inflammatory skin diseases around the affected knee
	
	17) Positive serology for HIV, hepatitis B, C and syphilis
	
	18) History of cancer or blood dyscrasias, or previous chemotherapy, radiotherapy, or immunotherapy
	
	19) Contraindication to MRI, including MRI-incompatible internal devices (pacemaker, neurostimulator, cochlear implant, ocular foreign bodies, foreign bodies close to neurovascular structures)
	
	20) Intolerance or allergy to local anaesthesia
	
	21) Anticoagulant treatment
	
	22) Overweight with body mass index (mass in kg/size in m^2) greater than 35 (obesity grade II).
	
	23) Participation in another clinical trial or treatment with another investigational product within 30 days before inclusion in the study.
	
	24) Abnormal blood tests:
	  i. Hepatic (alanine aminotransferase and/or aspartate aminotransferase > 2 × upper limit of normal [ULN])
	  ii. Renal (clearance < 30 ml/min/1.73 m^2)
	  iii. Pancreatic or biliary disease, except asymptomatic bile stones
	  iv. Blood coagulation disorders, anaemia (≤ 10 g/dL) or platelet count of ≤ 100 × 109/L
	
	25) Significant medical problems, such as uncontrolled hypertension, symptomatic heart failure, or any other clinically relevant condition or current medication that in the opinion of the investigator contraindicates the use of any of the study or rescue medications
	
	26) Pregnant or lactating women, or premenopausal women not using an acceptable form of birth control, are ineligible for inclusion
	
	27) Known allergies to protein products (horse or bovine serum, or porcine trypsin) used in the *ex vivo* cell production process
	
	28) Known hypersensitivity to study drug or additives: albumin, sodium caprylate, sodium chlorid, potassium chlorid, ciprofloxacin, cefazoline, heparin
	
	29) Cancer or immunodeficiency disease
	
	30) Prisoners or subjects who are involuntary incarcerated
	
	31) Patients subject to legal protection measures
	
	32) Lack in understanding the nature and aims of the study and/or difficulties in communication with the investigator.
	
	33) Subject in exclusion period for another protocol
	
	34) Subject who are in a dependency or employment with the sponsor or the investigator

BMI, body mass index; CPPD, Calcium PyroPhospate Deposition; MRI, magnetic resonance imaging; NSAIDs, non-steroidal anti-inflammatory drugs.

Outcome measures

Primary endpoint

The primary endpoint was the rate of 'strict responders' between the 2 experimental groups and the placebo group at 6 months postinjection as defined by the OsteoArthritis Research Society International (OARSI)/Outcome MEasures in Rheumatology (OMERACT) [19] as improvements from baseline ≥ 50% and minimal absolute changes ≥ 20 mm in Western Ontario and McMaster University Osteoarthritis index (WOMAC) pain or physical function subscores. As recommended [20−22], when 1 item was missing in the pain score and 3 or fewer were missing in the physical function score, they were replaced by the mean of the respective items in the subscale for each patient. In the presence of more missing data, the scores were not validated and the 6-month value was replaced by the score at 3-month score for 1 patient.

Secondary endpoints

Secondary self-reported symptom-related outcomes were collected at 1, 3, 6, and 12 months after treatment as follows: (1) absolute changes from baseline in knee pain intensity during the past 24 hours as measured on 0 to 100 mm visual analogue scale (VAS) scale; (2) absolute changes from baseline in scores on the pain subscale of the WOMAC; (3) absolute changes from baseline in scores on the physical function subscale of the WOMAC; (4) absolute changes from baseline in scores of the total WOMAC; (5) absolute changes from baseline in scores of the Knee injury and OA Outcome Score (KOOS) index [23]; (6) absolute changes from baseline in quality of life as measured by the 36-Item Short Form Health Survey (SF-36) questionnaire [24]; (7) OARSI/OMERACT response defined by improvements from baseline of at least 20% together with an absolute change of 10 mm on a 0 to 100 mm scale in at least 2 of the 3 next values: WOMAC pain, WOMAC function, and VAS pain; (8) proportion of patients reaching the minimal clinically important improvement [25] (MCII) in change from baseline in VAS pain (delta −19.9 mm); (9) proportion of patients reaching the MCII in change from baseline in WOMAC physical function (delta −9.1 mm). The rate of 'strict-responders' regarding OARSI/OMERACT definition was studied as a secondary endpoint at 1, 3, and 12 months.

Regarding structural assessment, in order to demonstrate the feasibility of the technique, cartilage across the tibiofemoral articular surfaces was quantitatively assessed using Cartilage Surface Mapping (CaSM) [26,27] for change in thickness between baseline and 12-month timepoints in a subsample from a single centre (Montpellier): 8 from the placebo group, 8 from the LD ADSC group, and 9 from the HD ADSC group. Magnetic resonance imaging (MRI) acquisition and analysis are detailed in Supplementary File 3.

Data regarding the consumption of medications to relieve pain (type and dose of painkillers) were collected. Safety endpoints included the number of AEs and percentage of patients who experienced AE, serious AE (SAE) including events related to the procedure such as infection, bleeding, knee pain, knee swelling, or knee replacement surgery.

Sample size calculation

According to the 2 previous studies of Rutjes et al [28] and Strand et al [29], the expected response rate is around 30% in the placebo group. In the ADSC-treated groups (LD and HD pooled), we assumed a clinical responder rate of around 55% (between 50% and 60%), based on our previous ADIPOA1 study after 6 months [16]. The sample size calculation was based on an expected difference in subject response rate (strict responders) of 25%. The number of subjects required for 80% power and an alpha error of 5%, under a 2-sided hypothesis with a ratio 1:2, was 138 (46 per group). Assuming a drop-out rate of 10%, a minimum of 153 patients were planned to be included (51 per group).

Statistical analysis

Data analysis

The primary and secondary analyses of efficacy endpoints were performed in the full analysis set, involving all patients who were randomly assigned and for whom measures of the primary outcome at baseline and at 6 months were available. The primary outcome was also analysed after excluding patients with a major deviation that could affect the evaluation of the primary endpoint (per-protocol set). Medication and AEs were analysed on the safety set defined as all randomised patients who received the injection. All statistical tests were bilateral with a confidence level of 95%. Statistical analyses were performed using SAS 9.4 (SAS Institute) and R version 4.4.0.

Main statistical analyses

The rate of strict responders at 6 months was compared between ADSC-treated (LD and HD groups pooled) and placebo patients using a chi-square test. Effect size was estimated using risk difference and a relative risk together with their 95% CIs.

Analysis of the changes from baseline at 1, 3, 6, and 12 months in knee pain intensity during the past 24 hours, in WOMAC pain, physical function, and total scores, in KOOS index and in SF-36 scores was performed using mixed models for repeated measurements including treatment, time, and treatment-time interaction as a fixed effect. Repeated measurements were taken into account using a random intercept. Comparison between ADSC-treated and placebo patients was performed using the estimated difference of treatment effects at 1, 3, 6, and 12 months together with their 95% CIs. Rate of responders, rate of strict responders, proportion of patients reaching MCII in change from baseline in VAS pain, and in WOMAC physical function were compared between the 2 groups using chi-square tests at each time individually.

For exploratory purpose, analysis of strict responder rate, responder rate, disability, and quality of life questionnaires will be performed for each dose of ADSC compared to the placebo as above.

Medication and AEs were compared between LD, HD, and Placebo groups using chi-square or Fisher exact tests.

Subgroups analyses

Post-hoc analysis was conducted to compare the proportion of strict responders at 6 months between ADSC-treated and placebo groups. These comparisons were performed within specific subgroups: patients aged 60 years old or older, patients with baseline knee pain ≤ 60 mm and > 60 mm and patients with a baseline total WOMAC score ≤50 mm and > 50 mm.

Cartilage thickness analysis

For this analysis, we included all patients from 1-single centre (Montpellier, $n = 25$). The subsample group combined ADSC-treated groups ($n = 17$) for comparison against those in the placebo group ($n = 8$) using Statistical Parametric Mapping [30]. Group was the only term included in the general linear model for
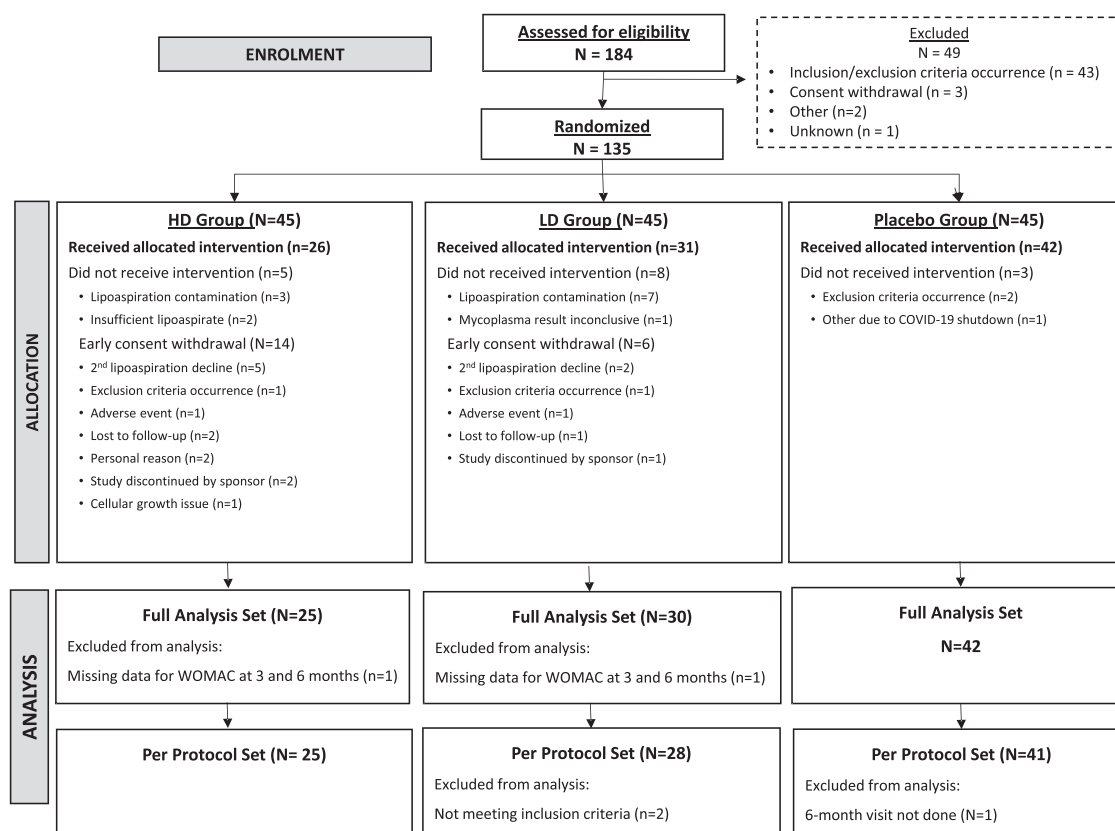
Figure 1. Flow chart of the ADIpose-derived mesenchymal stromal cells in OsteoArthritis phase 2 (ADIPOA2) study. ADIPOA2; HD, high dose; LD, low dose; WOMAC, Western Ontario and McMaster University Osteoarthritis index.

this feasibility analysis, looking for any significant vertex-wise difference between groups in cartilage thickness change between timepoints, $P < .05$ as the statistically significant level.

RESULTS

Characteristics of patients

Figure 1 provides a flow chart of patient enrolment, allocation to groups, follow-up, and analysis. A total of 135 patients from 184 individuals assessed for eligibility were enrolled between September 2016 and March 2022, in 9 clinical centres. Twelve-month follow-up was completed in March 2023. Baseline patient characteristics were comparable between groups (Table 2). Thirty-six patients did not receive intervention for different reasons (14 in the LD group, 19 in the HD group and 3 in the placebo group), mainly due to withdrawal of consent or bacterial contamination of the adipose tissue sample. These patient characteristics were similar to those who received the allocated intervention (in Supplementary File 4). Ninety-seven patients were included in the analysis (30 in the LD group, 25 in the HD group, and 42 in the placebo group). Two patients (1 in the LD group and 1 in the HD group) were excluded because of missing the main outcome. Three patients were also excluded from the per-protocol set because of major deviations (2 in the LD group and 1 in the placebo group). The ADSC-treated and placebo groups showed similar baseline characteristics.

Primary outcome

At 6 months, ADSC injection was not more effective than saline placebo injection on the primary outcome (Table 3 and Fig 2). We observed an improvement from baseline at day 35 in

both the ADSC-treated and saline injection groups in each parameter comprising the primary outcome, but the between-group difference was not significant. After 6 months, 26 patients in the ADSC-treated group (47.3%) and 23 patients in the placebo group (54.8%) were strict responders according to OARSI/OMERACT, respectively (relative risk, 0.86 [95% CI: 0.58-1.28]; $P = .46$). The 6-month rate of OARSI/OMERACT strict responders was not statistically significant either when comparing LD versus placebo (14 patients [46.7%] vs 23 patients [54.8%], respectively [relative risk, 0.85 (95% CI: 0.53-1.36); $P = .50$]) and HD versus placebo (12 patients [48%] vs 23 patients [54.8%], respectively [relative risk, 0.88 (95% CI: 0.54-1.43); $P = .59$]) (Supplementary Tables S9 and S10 and Supplementary Fig S6 in Supplementary File 4).

These results were confirmed on the per-protocol set with 47.2% of responders in the ADSC-treated group (25/53) and 56.1% in the placebo group (23/41) (relative risk, 0.84 [95% CI: 0.57-1.25]; $P = .39$).

Secondary outcomes

There was no statistically significant beneficial effect of ADSC on knee pain intensity at the different time points (1, 3, 6, and 12 months post treatment). All the secondary outcomes (WOMAC, KOOS, SF-36) showed no significant group differences (Fig 2 and Supplementary File 4). Secondary outcomes were also compared between groups (HD vs placebo and LD vs placebo) and did not differ significantly (Supplementary Tables S11-S14 and Supplementary Fig S6 in Supplementary File 4).

The 6-month proportion of patients reaching the MCII from baseline in VAS pain was elevated but similar in the ADSC group versus placebo, 33 patients (61.1%) versus 23 patients (56.1%), respectively (relative risk, 1.09 [95% CI: 0.77-1.53]; $P = .62$);

Table 2

Baseline characteristics of patients enrolled into the study and who received allocated intervention

Characteristics	HD group ($n = 25$)	LD group ($n = 30$)	Total ADSC group ($n = 55$)	Placebo group ($n = 42$)
Age, mean (SD), years	57.3 (7.7)	58.3 (6.0)	57.8 (6.8)	58.0 (6.9)
Women, no. (%)	10 (40.0)	16 (53.3)	26 (47.3)	23 (54.8)
Weight, mean (SD), kg	83.0 (14.4)	79.3 (15.6)	81.0 (13.2)	79.5 (16.0)
Height, mean SD), cm	172.1 (8.3)	170.4 (9.2)	171.2 (8.8)	169.7 (11.1)
BMI, mean (SD), kg/m^2	28.1 (3.8)	27.1 (3.7)	27.6 (3.8)	27.4 (3.3)
Medical history: diagnosis				
Diabetes, no. (%)	1 (0.9)	2 (1.8)	3 (1.3)	0 (0.0)
Hypertension, no. (%)	4 (3.4)	8 (7.2)	12 (5.3)	7 (3.9)
Dyslipidaemia, no. (%)	2 (1.7)	6 (5.4)	8 (3.5)	5 (2.8)
Osteoporosis, no. (%)	0 (0.0)	2 (1.8)	2 (0.9)	1 (0.6)
Medial meniscectomy of the index knee, no. (%)	5 (4.3)	5 (4.5)	10 (4.4)	4 (2.2)
Lateral meniscectomy of the index knee, no. (%)	3 (2.5)	0 (0.0)	3 (1.3)	3 (1.7)
Ligamentoplasty of the index knee, no. (%)	1 (0.9)	2 (1.8)	3 (1.3)	1 (0.6)
Knee pain VAS				
Score in the affected knee, mean (SD)/100 mm	70.2 (13.8)	66.5 (12.8)	68.2 (13.3)	64.7 (13.8)
Score in the contralateral knee, mean (SD)/100 mm	4.6 (6.0)	7.5 (6.5)	6.2 (6.4)	7.5 (6.4)
KOOS				
KOOS score pain, mean (SD)/100 mm	42.4 (13.5)	41.1 (10.9)	41.7 (12.0)	44.4 (15.8)
KOOS score symptoms, mean (SD)/100 mm	47.6 (15.7)	45.0 (16.8)	46.2 (16.2)	47.5 (19.8)
WOMAC questionnaire				
WOMAC pain subscore, mean (SD)/100 mm	54.4 (12.2)	57.7 (12.2)	56.2 (12.2)	56.9 ($\pm$ 14.4)
WOMAC stiffness subscore, mean (SD)/100 mm	63.0 (22.1)	63.8 (16.2)	63.4 (18.9)	62.5 (19.5)
WOMAC function subscore, mean (SD)/100 mm	58.8 (13.5)	58.3 (13.2)	58.5 (13.2)	52.7 (13.3)
WOMAC total score, mean (SD)/100 mm	58.2 (13.0)	58.5 (12.2)	58.4 (12.4)	54.9 (12.6)
SF-36				
Physical aggregate score, mean (SD)	31.7 (8.4)	30.0 (6.5)	30.8 (7.4)	35.1 (7.4)
Mental aggregate score, mean (SD)	51.5 (10.7)	52.4 (11.7)	52.0 (11.2)	51.8 (9.1)
Concomitant medication				
Paracetamol/acetaminophen, no. (%)	3 (12.0)	3 (10.0)	6 (10.9)	5 (11.9)
NSAIDs, no. (%)	1 (4.0)	2 (6.7)	3 (5.3)	3 (7.2)
Tramadol, no. (%)	0 (0.0)	0 (0.0)	0 (0.0)	1 (2.4)
Codeine, no. (%)	0 (0.0)	0 (0.0)	0 (0.0)	0 (0.0)
Morphine, no. (%)	0 (0.0)	0 (0.0)	0 (0.0)	0 (0.0)
Kellgren-Lawrence grade index knee				
II, no. (%)	7 (28.0)	9 (30.0)	16 (29.1)	19 (45.2)
III, no. (%)	18 (72.0)	21 (70.0)	39 (70.9)	23 (54.8)

ADSC, adipose-derived mesenchymal stromal cells; BMI, body mass index; HD, high dose; KOOS, Knee injury and Osteoarthritis Outcome Score; LD, low dose; NSAIDs, Non-steroidal anti-inflammatory drugs; SF-36, 36-Item Short Form Health Survey; VAS, visual analogue scale; WOMAC, Western Ontario and McMaster University Osteoarthritis index.

as well as patients reaching the MCII from baseline in WOMAC physical function (delta −9.1 mm), 40 patients (72.7%) versus 31 patients (73.8%), respectively (relative risk, 0.99 [95% CI: 0.77-1.25]; $P = .94$).

Subgroup analysis did not reveal a more pronounced effect within these different subgroups: age at baseline (≥60 years), Kellgren-Lawrence grade (2 vs 3), level of pain (VAS pain: ≤60 mm and >60 mm), and level of disability (WOMAC total score ≤ 50 mm and > 50 mm) (Supplementary Table S14 in Supplementary File 4).

Imaging analysis

Mean and SD cartilage thickness at baseline from all 25 individuals that underwent CaSM are shown in Supplementary File 3.

Although individuals showed different patterns of cartilage thickness change over time, no statistically significant differences were detected between groups in cartilage thickness change between any of the timepoints. Results for the baseline to 12-month analysis are shown in Supplementary File 3.

Adverse events

AEs occurred in a similar proportion between the 3 groups with 92.3% in the HD group, 90.3% in the LD group, and 85.7%

in the control group of patients with at least 1 AE ($P = .78$). AEs were minor and transient (Table 4). A few participants in both groups reported knee joint pain and swelling after injections. No complications associated with liposuction and injection were observed in the study. The number of SAEs was comparable between the 3 groups with 3.9% in the HD group, 2.3% in the LD group, and 1.4% in the control group ($P = .32$), and was unrelated to the procedure.

DISCUSSION

Regenerative medicine represents a promising opportunity for the biological treatment of OA, but only high-quality randomised controlled trials can determine its benefit. The ADIPOA2 phase 2b trial was designed to assess the efficacy and to determine the optimal dose of intra-articular injection of autologous ADSC for the treatment of symptomatic mild-to-moderate knee OA. Here, we report that a single autologous ADSC injection at a dose of either 2×10^6 or 10×10^6 cells was not more effective than saline placebo injection in improving knee pain and function. Similarly, all secondary outcomes showed no significant benefit. Pain scores improved extensively with 56% to 61% of participants in both groups achieving the MCII after 6 months. Additional exploratory analyses, limited by low statistical power, did not suggest a dose-response relationship or a treatment effect emerging before 6 months.

Table 3

Outcomes results between baseline and 6 mo by treatment group

	Total ADSC group ($n = 55$)	Placebo group ($n = 42$)	Group difference (95% CI)	Relative risk (95% CI)	*P* value
Primary outcome					
OARSI/OMERACT strict responders, no./*N* (%)	26/55 (47.3)	23/42 (54.8)	−7.5 (−27.5 to 12.5)	0.86 (0.58-1.28)	.46
Secondary outcomes					
Change from baseline in VAS pain in the affected knee, LSmean (SE), mm	−31.4 (4.0)	−24.9 (4.6)	−6.5 (−18.7 to 5.7)	-	.29
Change from baseline in WOMAC pain sub-score, LSmean (SE), mm	−24.1 (3.1)	−26.1 (3.5)	2.0 (−7.2 to 11.2)		.67
Change from baseline in WOMAC physical function subscore, LSmean (SE), mm	−25.7 (3.0)	−21.7 (3.5)	−4.0 (−13.1 to 5.1)		.39
Change from baseline in WOMAC total score, LSmean (SE), mm	−25.6 (3.0)	−24.1 (3.5)	−1.5 (−10.5 to 7.5)	-	.74
Change from baseline in KOOS pain sub-score, LSmean (SE), mm	21.6 (2.9)	19.2 (3.4)	2.4 (−6.4 to 11.2)	-	.59
Change from baseline in SF-36 physical aggregate score, LSmean (SE)	8.5 (1.3)	7.9 (1.6)	0.5 (−3.6 to 4.6)	-	.80
Change from baseline in SF-36 mental aggregate score, LSmean (SE)	0.6 (1.3)	0.7 (1.6)	0.03 (−4.1 to 4.0)	-	.99
Rate of OARSI/OMERACT response, no./*N* (%)	38/54 (70.4)	29/41 (70.7)	−0.4 (−18.9 to 18.1)	0.99 (0.77-1.29)	.97
Rate of patients reaching MCII change from baseline in VAS pain, no./*N* (%)	33/54 (61.1)	23/41 (56.1)	5.0 (−15.0 to 25.0)	1.09 (0.77-1.53)	.62
Rate of patients reaching MCII change from baseline in WOMAC physical function, no./*N* (%)	41/55 (74.6)	31/42 (73.8)	0.7 (−16.8 to 18.3)	1.01 (0.80-1.28)	.93
Rate of patients reaching MCII change from baseline in WOMAC physical function, no./*N* (%)	40/55 (72.7)	31/42 (73.8)	−1.1 (−18.8 to 16.7)	0.99 (0.77-1.25)	.91

KOOS, Knee injury and Osteoarthritis Outcome Score; LSmean, least square mean; MCII, minimal clinically important improvement; OARSI/OMERACT, OsteoArthritis Research Society International/Outcome MEasures in Rheumatology; SF-36, 36-Item Short Form Health Survey; VAS, visual analogue scale; WOMAC, Western Ontario and McMaster University Osteoarthritis index.
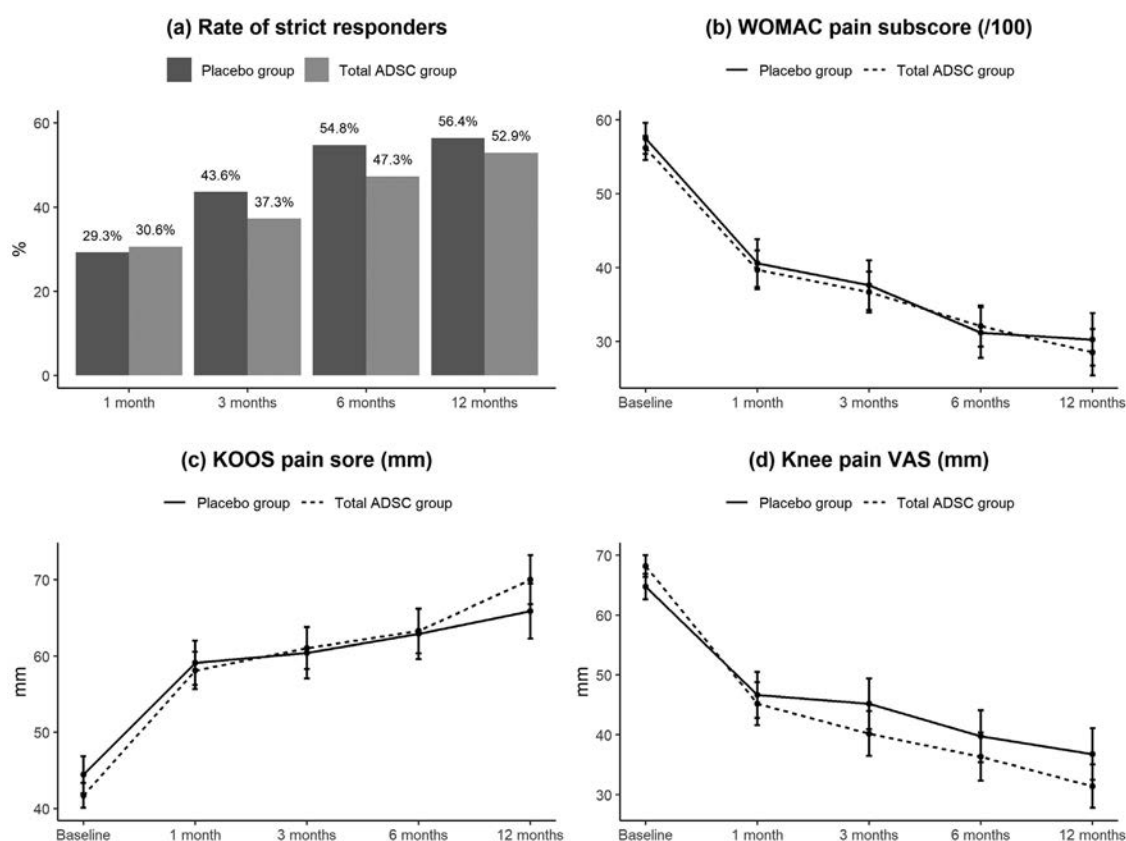

Figure 2. Evolution of knee pain VAS, WOMAC pain, KOOS pain and rate of OARSI/OMERACT strict responders throughout the study (0-12 mo). Dots: mean. Error bars: SD. KOOS, Knee injury and Osteoarthritis Outcome Score; OARSI, OsteoArthritis Research Society International; OMERACT, Outcome MEasures in Rheumatology; VAS, visual analogue scale; WOMAC, Western Ontario and McMaster University Osteoarthritis index.

Table 4
Medications and adverse events for each group (safety set)

Variables	HD group (n = 26)	LD group (n = 31)	Placebo group (n = 42)	P value
Acetaminophen use because of knee OA, baseline, no. (%)	2 (7.7)	3 (9.7)	4 (9.5)	1.00
Acetaminophen use because of knee OA, 1 mo, no. (%)	2 (7.7)	5 (16.1)	6 (14.3)	.70
Acetaminophen use because of knee OA, 3 mo, no. (%)	1 (3.8)	6 (19.4)	8 (19.0)	.17
Acetaminophen use because of knee OA, 6 mo, no. (%)	3 (11.5)	7 (21.9)	7 (16.7)	.59
Patients with at least 1 adverse event, no. (%)	24 (92.3)	28 (90.3)	36 (85.7)	.78
Adverse events	n = 128	n = 173	n = 211	
Adverse events related to albumin, no. (%)	1 (0.8)	0 (0.0)	0 (0.0)	.25
Adverse events related to study drug, no. (%)	3 (2.3)	4 (2.3)	3 (1.4)	.78
Adverse events intensity, no. (%)				
Mild	106 (82.8)	149 (86.6)	176 (83.8)	.14
Moderate	19 (14.8)	20 (11.6)	34 (16.2)	
Severe	3 (2.3)	3 (1.7)	0 (0.0)	
Knee joint pain, no.	3	2	2	
Knee swelling, no.	0	2	1	
Serious related adverse events, no. (%)	5 (3.9)	4 (2.3)	3 (1.4)	.32
Adverse events intensity, no. (%)				
Mild	0 (0.0)	1 (25.0)	0 (0.0)	.38
Moderate	3 (60.0)	1 (25.0)	3 (100.0)	
Severe	2 (40.0)	2 (50.0)	0 (0.0)	
Pneumonia, no.	1		1	
Knee replacement surgery, no.			1	
Breast cancer, no.		1		
Pulmonary embolism, no.		1		
Cellulitis, no.	1			
Limb fracture, no.	2			
Achilles rupture, no.		1		
Prostate surgery, no.		1		
Hypoxia, no.	1			
Hand oedema, no.			1	

HD, high dose; LD, low dose; OA, osteoarthritis.

Our results in this double-blind controlled study are not in agreement with the statistically significant benefits of ADSC compared with placebo for knee OA symptoms reported previously in a systematic review and meta-analysis [15,17,18]. A recent large open study followed 329 patients with knee OA for 24 months after ADSC injection with a second injection after 6 months. Half of the patients had severe OA (Kellgren-Lawrence grade 4), and the age of enrolment varied from 23 to 85 years. The authors described that 87.9% of patients improved at 24 months in terms of pain and function [31]. However, these results were obtained from open studies, with possible bias related to patient recruitment. It is entirely possible that the lack of blinding in prior trials influenced the reported improvement in symptoms [15,17,18]. A recent meta-analysis confirmed these limits and concluded that MSC injections may provide little to no pain relief or improvement in patients with knee OA [32]. Overall, 3 double-blind RCTs have been carried out using allogeneic BM-MSC [33] or autologous ADSC [34,35]. All these placebo-controlled studies showed positive results following cell injections. Two of them involved a few patients (less than 15 per treatment group), as well as no placebo pain VAS response in the control arm in one of the studies [34], which restricts their significance. However, a recent large Korean phase III study included over 250 patients and showed an improvement in pain and function parameters at 6 months after 1-single injection of 100×10^6 autologous ADSC (volume 3 mL), with no difference in change of cartilage defects between the groups [35]. Finally, a very large recent study involving 480 patients comparing cell injections from autologous bone marrow aspirate concentrate, autologous adipose stromal vascular fraction, and allogeneic human UC tissue-derived MSCs showed no superiority of either cell therapy versus corticosteroid injection (depomedrol) after 1 year [36]. This discrepancy may be due to differences in methodology of our RCT but also to biological differences as ADSC bioproduction, alternating cell culturing protocols, number of cells or volume injected, conditioned medium, interval, number of cell injections, outcome measures, patient characteristics, as well as design issues affecting risk of bias.

Furthermore, cartilage restoration using culture-expanded autologous MSCs has previously been attempted. However, the studies were limited to case series with small numbers of patients, and results were mitigated [37]. In a double-blind RCT of intra-articular allogeneic, culture-expanded bone marrow MSCs versus hyaluronate after partial medial meniscectomy in patients with osteoarthritic changes, the authors reported no evidence of structural cartilage restoration at 1 year, which was the primary endpoint of the trial [38]. Another phase III, 48-week RCT study of culture-expanded allogeneic UC-MSC implantation, despite the structural restoration assessed macroscopically and histologically, clinical outcomes such as pain and function at 48 weeks were not significantly superior to those experienced by patients who underwent microfracture [39]. So far, repair and regenerative strategies have been described and proposed over several years including specifically those using cell therapy (stem and stromal cell populations) but with limited high-level clinical trial evidence to date. Our findings do not support the use of ADSCs in subjects with symptomatic mild-to-moderate tibiofemoral knee OA. While MSC therapies have shown potential in preclinical studies, translating these effects into clinical benefits has proven challenging [40]. The efficacy of MSCs could be impacted by a number of variables, including inconsistencies in manufacturing protocols leading to differences in MSC properties and their paracrine factors among patients [41]. In the case of knee OA, targeting cartilage defect regeneration by MSCs could be disturbed by the formation of MSC-mediated endochondral ossification, thus reducing the formation of

good-quality tissue and the clinical outcome [42]. The repair functions of MSC injected might be also altered by a deleterious articular inflammatory environment [43], as well as the potential that cells undergo senescence following delivery which may contribute to joint alteration in a counterproductive manner [44]. It is important to consider the relatively short lifespan of MSCs and lack of cell engraftment once they have been injected [45]. By injecting such cells locally in an isolated manner, it seems difficult to modulate the microenvironment over the long term and thus counter the inexorable progression of OA. In addition, this discrepancy could be due to variations in the pathophysiology of OA phenotypes among patients. Future studies might explore a stratified approach, targeting patient subgroups more likely to respond based on specific biological markers or disease phenotypes (such as inflammatory OA).

Our study has several strengths that distinguish them from previous studies: a robust double-blind design, a real placebo (saline) control arm and a sham for adipose tissue extraction, a significative number of patients included, and a strong harmonised and standardised cell production. We should point out that, for the first time in a study, cell manufacturing was multicentric, with high-quality criteria. Our study also demonstrated the good safety and tolerability of this procedure without evidence of SAEs using autologous ADSC. This is also the first study to use whole articular surface cartilage thickness mapping to look at a treatment effects over time with this structural outcome measure. It will be important for future clinical trials to consider carefully the study inclusion phenotype and cartilage morphotype when looking for any significant structural effects of a treatment [46], since baseline heterogeneity in an outcome measure such as cartilage thickness will introduce noise that may overwhelm significant positive (or negative) therapeutic effects.

There are some limitations to our study. Due to appropriate double blinding of the study, we observed a large rate of responders which may explain why we did not reach our primary endpoint defined as strict OARSI/OMERACT responder rate. This substantial placebo response in both groups (70% OARSI/OMERACT responses) is quite usual, particularly in OA [47,48]. However, it also allows us to consider that the study's blinding methodology was perfectly respected, although we performed a sham lipoaspiration in the control arm. The required sample size was not reached. Indeed, the unexpectedly high rate of withdrawal and protocol deviations (including contamination) led to the need for a greater number of participants to preserve statistical power, which exceeded the scope of the original budget. Therefore, we performed a post hoc simulation assuming the same observed response rates; under these conditions, statistical significance was not achieved. However, we acknowledge that different response rates could have emerged with a larger sample, and that the study may have been underpowered to detect a treatment effect. In parallel with other studies, we found no improvement in terms of cartilage morphology between the placebo and combined treatment groups after injection over the 12-month study period as part of a feasibility analysis of the CaSM technique in a clinical trial setting. Subsequent analysis will be extended to all study participants with MRI available. Indeed, we aim to monitor patients at 2 years and beyond, both clinically and by imaging, in order to assess any long-term clinical or structural benefit and/or to delay knee replacement surgery.

To conclude, among patients with symptomatic mild-to-moderate knee OA, a single intra-articular injection of autologous ADSC compared with saline placebo did not result in a significant difference in pain and function over 12 months. These findings do not support the use of a single autologous ADSC injection for the management of knee OA. Further research should aim not only to refine MSC therapies but also to combine OA phenotype, bioengineering and gene therapeutic approaches to address the multifactorial nature of OA degradation.

Competing interests

CRediT authorship contribution statement

Yves-Marie Pers: Writing − review & editing, Writing − original draft, Validation, Investigation, Funding acquisition, Formal analysis, Data curation, Conceptualization. **Hubert Schrezenmeier:** Writing − review & editing, Validation, Resources, Methodology, Funding acquisition, Formal analysis, Conceptualization. **Sandrine Fleury-Cappellesso:** Writing − review & editing, Validation, Resources, Methodology, Funding acquisition, Formal analysis, Conceptualization. **Ulrich Nöth:** Writing − review & editing, Validation, Investigation, Funding acquisition, Data curation, Conceptualization. **Lars Rackwitz:** Writing − review & editing, Investigation. **Rosanna Ferreira:** Writing − review & editing, Investigation. **Francis Berenbaum:** Writing − review & editing, Validation, Investigation, Conceptualization. **Adeline Ruyssen-Witrand:** Writing − review & editing, Investigation, Data curation. **Rogier Martijn Thurlings:** Writing − review & editing, Investigation, Funding acquisition, Conceptualization. **Olga Addimanda:** Writing − review & editing, Investigation. **Gina Lisignoli:** Writing − review & editing, Validation, Investigation, Funding acquisition, Conceptualization. **Roberta Ramonda:** Visualization, Investigation. **Fintan Shannon:** Validation, Investigation. **Leonardo Punzi:** Validation, Investigation. **Athan Baillet:** Validation, Investigation. **Andrew W. McCaskie:** Writing − review & editing, Validation, Formal analysis, Data curation. **Stephen McDonnell:** Writing − review & editing, Validation, Formal analysis, Data curation. **Jenny O'Callaghan:** Writing − review & editing, Validation, Resources, Methodology, Data curation. **Tom Turmezei:** Writing − review & editing, Validation, Resources, Methodology, Formal analysis, Data curation. **Dimitri A. Kessler:** Writing − review & editing, Validation, Formal analysis, Data curation. **Ramin Lotfi:** Writing − review & editing, Validation, Resources, Methodology, Data curation, Conceptualization. **Markus Rojewski:** Writing − review & editing, Validation, Resources, Methodology, Formal analysis, Data curation. **Aoife Duffy:** Validation, Resources, Methodology. **Andrew Finnerty:** Validation, Resources, Methodology, Formal analysis. **Anaïck Moisan:** Validation, Resources, Methodology, Formal analysis, Data curation. **Helene Brochot-Dechet:** Validation, Resources, Methodology, Formal analysis, Data curation. **Mathilde Aubery-Rousselet:** Validation, Resources, Methodology, Formal analysis, Data curation. **Amélie Michon:** Resources, Project administration, Methodology, Investigation. **Jimena Bouzas-Rodriguez:** Validation, Resources, Project administration, Investigation. **Oliver Pullig:** Resources, Project administration, Investigation. **Sylvie Broussous:** Resources, Project administration, Funding acquisition. **Erika Nogue:** Writing − review & editing, Validation, Methodology, Formal analysis, Data curation. **Maïlis Amico:** Writing −

review & editing, Validation, Methodology, Formal analysis, Data curation. **Marie-Christine Picot:** Writing − review & editing, Validation, Methodology, Formal analysis. **Frank Barry:** Writing − review & editing, Validation, Supervision, Funding acquisition, Formal analysis, Data curation, Conceptualization. **Christian Jorgensen:** Writing − review & editing, Validation, Project administration, Investigation, Funding acquisition, Conceptualization.

Acknowledgements

Contributors

EN, MA, MCP analysed the results. Y-MP, HS, SF-C, FBarry, and CJ made substantial contributions to the conception and design of the study. SB, EN, MC-P, AM, and JB-R performed the randomisation, the statistical analysis plan, and administrative part. Y-MP, RF, FBerenbaum, AC, RMT, LP, FS, AB, OP, and CJ participated in the recruitment. HS, SFC, RL, MR, AD, AF, AM, HB-D, MAR, and FBarry contributed to cell production. AWM, JOC, TT, and DAK performed MRI analysis. The analyses and the interpretation of the data were conducted by Y-MP, HS, UN, FB, FBarry, and CJ. Y-MP, HS, FBarry, and CJ were involved in drafting the work. Y-MP is the guarantor of the study. All authors revised it critically for important intellectual content. All authors approved the final version to be published and agreed to be accountable for all aspects of the work.

Funding

Patient consent for publication

Consent obtained directly from patients.

Ethics approval

This trial was approved in April 2016 through the Voluntary Harmonization Procedure (VHP2015174) for France, Italy and the Netherlands. In Germany, having withdrawn from the VHP, the national competent authority Paul Ehrlich Institute approved the clinical trial in November 2018. The Ethics committees approved the clinical trial on the 8th October 2015 for France, 28th November 2016 for Germany, 29th November for the Netherlands, 12th January 2017 for Italy. Ireland were not included in the VHP procedure due to delays in validating the manufacturing facilities in Ireland. The clinical trial has been approved through national procedures, 30th September 2016 for Ireland. During the clinical trial, amendments were made to competent authorities to ensure that similar documents were approved in each country.

Provenance and peer review

Not commissioned, externally peer reviewed.

Patient and public involvement

Patients and/or the public were not involved in the design, or conduct, or reporting, or dissemination plans of this research.

Data availability statement

Y-MP and CJ had full access to all the data in the study and took responsibility for the integrity of the data and the accuracy of the data analysis. Data are available on reasonable request. Data will be provided from a locked, cleaned, and deidentified study database. Requests will be reviewed by the principal investigator before approval.

Supplementary materials

Supplementary material associated with this article can be found in the online version at doi:10.1016/j.ard.2025.07.026.

Orcid

Yves-Marie Pers: http://orcid.org/0000-0001-5927-3773

REFERENCES

[1] Martel-Pelletier J, Barr AJ, Cicuttini FM, Conaghan PG, Cooper C, Goldring MB, et al. Osteoarthritis. Nat Rev Dis Prim 2016;2:16072.

[2] GBD 2021 Osteoarthritis Collaborators. Global, regional, and national burden of osteoarthritis, 1990-2020 and projections to 2050: a systematic analysis for the Global Burden of Disease Study 2021. Lancet Rheumatol 2023;5:e508–22.

[3] Liu M, Jin F, Yao X, Zhu Z. Disease burden of osteoarthritis of the knee and hip due to a high body mass index in China and the USA: 1990-2019 findings from the global burden of disease study 2019. BMC Musculoskelet Disord 2022;23:63.

[4] Kolasinski SL, Neogi T, Hochberg MC, Oatis C, Guyatt G, Block J, et al. 2019 American College of Rheumatology/Arthritis Foundation Guideline for the Management of Osteoarthritis of the Hand, Hip, and Knee. Arthritis Care Res (Hoboken) 2020;72:149–62.

[5] Bannuru RR, Osani MC, Vaysbrot EE, Arden NK, Bennell K, Bierma-Zeinstra SMA, et al. OARSI guidelines for the non-surgical management of knee, hip, and polyarticular osteoarthritis. Osteoarthr Cartil 2019;27:1578–89.

[6] Pers YM, Ruiz M, Noël D, Jorgensen C. Mesenchymal stem cells for the management of inflammation in osteoarthritis: state of the art and perspectives. Osteoarthritis Cartilage 2015;23:2027–35.

[7] Chen Y, Shao J-Z, Xiang L-X, Dong XJ, Zhang GR. Mesenchymal stem cells: a promising candidate in regenerative medicine. Int J Biochem Cell Biol 2008;40:815–20.

[8] Pers Y-M, Jorgensen C. Mesenchymal stromal cells: updates and therapeutic outlook in rheumatic diseases. J Clin Med 2013;2:201–13.

[9] Murphy JM, Fink DJ, Hunziker EB, Barry FP. Stem cell therapy in a caprine model of osteoarthritis. Arthritis Rheum 2003;48:3464–74.

[10] ter Huurne M, Schelbergen R, Blattes R, Blom A, de Munter W, Grevers LC, et al. Antiinflammatory and chondroprotective effects of intraarticular injection of adipose-derived stem cells in experimental osteoarthritis. Arthritis Rheum 2012;64:3604–13.

[11] Desando G, Cavallo C, Sartoni F, Martini L, Parrilli A, Veronesi F, et al. Intra-articular delivery of adipose derived stromal cells attenuates osteoarthritis progression in an experimental rabbit model. Arthritis Res Ther 2013;15:R22.

[12] Thompson M, Mei SHJ, Wolfe D, Champagne J, Fergusson D, Stewart DJ, et al. Cell therapy with intravascular administration of mesenchymal stromal cells continues to appear safe: an updated systematic review and meta-analysis. EClinicalMedicine 2020;19:100249.

[13] Levy O, Kuai R, Siren EMJ, Bhere D, Milton Y, Nissar N, et al. Shattering barriers toward clinically meaningful MSC therapies. Sci Adv 2020;6:eaba6884.

[14] Mesenchymal stem cells market size - global industry, share, analysis, trends and forecast 2022−2030 [Internet]. Healthc. Pharm. 2022. https://www.acumenresearchandconsulting.com/mesenchymal-stem-cells-market Last update Feb 2025.

[15] Ma W, Liu C, Wang S, Xu H, Sun H, Fan X. Efficacy and safety of intra-articular injection of mesenchymal stem cells in the treatment of knee osteoarthritis: a systematic review and meta-analysis. Medicine (Baltimore) 2020;99:e23343.

[16] Pers Y-M, Rackwitz L, Ferreira R, Pullig O, Delfour C, Barry F, et al. Adipose mesenchymal stromal cell-based therapy for severe osteoarthritis of the knee: a phase I dose-escalation trial. Stem Cells Transl Med 2016;5:847–56.

[17] Tan SHS, Kwan YT, Neo WJ, Chong JY, Kuek TYJ, See JZF, et al. Intra-articular injections of mesenchymal stem cells without adjuvant therapies for knee osteoarthritis: a systematic review and meta-analysis. Am J Sports Med 2021;49:3113–24.

[18] Maheshwer B, Polce EM, Paul K, Williams BT, Wolfson TS, Yanke A, et al. Regenerative potential of mesenchymal stem cells for the treatment of knee osteoarthritis and chondral defects: a systematic review and meta-analysis. Arthroscopy 2021;37:362–78.

[19] Bellamy N, Buchanan WW, Goldsmith CH, Campbell J, Stitt LW. Validation study of WOMAC: a health status instrument for measuring clinically important patient relevant outcomes to antirheumatic drug therapy in patients with osteoarthritis of the hip or knee. J Rheumatol 1988;15:1833–40.

[20] Pham T, van der Heijde D, Altman RD, Anderson JJ, Bellamy N, Hochberg M, et al. OMERACT-OARSI initiative: Osteoarthritis Research Society International set of responder criteria for osteoarthritis clinical trials revisited. Osteoarthr Cartil 2004;12:389–99.

[21] Clement ND, Bardgett M, Weir D, Holland J, Gerrand C, Deehan DJ. What is the minimum clinically important difference for the WOMAC Index After TKA? Clin Orthop Relat Res 2018;476:2005–14.

[22] Ghomrawi HMK, Mandl LA, Rutledge J, Alexiades MM, Mazumdar M. Is there a role for expectation maximization imputation in addressing missing data in research using WOMAC questionnaire? Comparison to the standard mean approach and a tutorial. BMC Musculoskelet Disord 2011;12:109.

[23] Roos EM, Roos HP, Lohmander LS, Ekdahl C, Beynnon BD. Knee Injury and Osteoarthritis Outcome Score (KOOS)—development of a self-administered outcome measure. J Orthop Sports Phys Ther 1998;28:88–96.

[24] Ware JEJ, Sherbourne CD. The MOS 36-item short-form health survey (SF-36). I. Conceptual framework and item selection. Med Care 1992;30:473–83.

[25] Tubach F, Ravaud P, Baron G, Falissard B, Logeart I, Bellamy N, et al. Evaluation of clinically relevant changes in patient reported outcomes in knee and hip osteoarthritis: the minimal clinically important improvement. Ann Rheum Dis 2005;64:29–33.

[26] MacKay JW, Kaggie JD, Treece GM, McDonnell SM, Khan W, Roberts AR, et al. Three-dimensional surface-based analysis of cartilage MRI data in knee osteoarthritis: validation and initial clinical application. J Magn Reson Imaging 2020;52:1139–51.

[27] Kessler DA, MacKay JW, McDonnell SM, Janiczek RL, Graves MJ, Kaggie JD, et al. Segmentation of knee MRI data with convolutional neural networks for semi-automated three-dimensional surface-based analysis of cartilage morphology and composition. Osteoarthr Imaging 2022;2:100010.

[28] Rutjes AWS, Jüni P, da Costa BR, Trelle S, Nüesch E, Reichenbach S. Viscosupplementation for osteoarthritis of the knee: a systematic review and meta-analysis. Ann Intern Med 2012;157:180–91.

[29] Strand V, Baraf HSB, Lavin PT, Lim S, Hosokawa H. A multicenter, randomized controlled trial comparing a single intra-articular injection of Gel-200, a new cross-linked formulation of hyaluronic acid, to phosphate buffered saline for treatment of osteoarthritis of the knee. Osteoarthr Cartil 2012;20:350–6.

[30] Friston KJ, Holmes AP, Worsley KJ, Poline J-P, Frith CD, Frackowiak RSJ. Statistical parametric maps in functional imaging: a general linear approach. Hum Brain Mapp 1994;2:189–210.

[31] Freitag J, Wickham J, Shah K, Tenen A. Real-world evidence of mesenchymal stem cell therapy in knee osteoarthritis: a large prospective two-year case series. Regen Med 2022;17:355–73.

[32] Sadeghirad B, Rehman Y, Khosravirad A, Sofi-Mahmudi A, Zandieh S, Jomy J, et al. Mesenchymal stem cells for chronic knee pain secondary to osteoarthritis: a systematic review and meta-analysis of randomized trials. Osteoarthritis Cartilage 2024;32:1207–19.

[33] Vega A, Martin-Ferrero MA, Del Canto F, Alberca M, García V, Munar A, et al. Treatment of knee osteoarthritis with allogeneic bone marrow mesenchymal stem cells: a randomized controlled trial. Transplantation 2015;99:1681–90.

[34] Lee W-S, Kim HJ, Kim K-I, Kim GB, Jin W. Intra-articular injection of autologous adipose tissue-derived mesenchymal stem cells for the treatment of knee osteoarthritis: a phase IIb, randomized, placebo-controlled clinical trial. Stem Cells Transl Med 2019;8:504–11.

[35] Kim K-I, Lee MC, Lee JH, Moon Y-W, Lee W-S, Lee H-J, et al. Clinical efficacy and safety of the intra-articular injection of autologous adipose-derived mesenchymal stem cells for knee osteoarthritis: A phase III, randomized, double-blind, placebo-controlled trial. Am J Sports Med 2023;51:2243–53.

[36] Mautner K, Gottschalk M, Boden SD, Akard A, Bae WC, Black L, et al. Cell-based versus corticosteroid injections for knee pain in osteoarthritis: a randomized phase 3 trial. Nat Med 2023;29:3120–6.

[37] Copp G, Robb KP, Viswanathan S. Culture-expanded mesenchymal stromal cell therapy: does it work in knee osteoarthritis? A pathway to clinical success. Cell Mol Immunol 2023;20:626–50.

[38] Vangsness CTJ, Farr 2nd J, Boyd J, Dellaero DT, Mills CR, LeRoux-Williams M. Adult human mesenchymal stem cells delivered via intra-articular injection to the knee following partial medial meniscectomy: a randomized, double-blind, controlled study. J Bone Joint Surg Am 2014;96:90–8.

[39] Lim H-C, Park Y-B, Ha C-W, Cole BJ, Lee BK, Jeong HJ, et al. Allogeneic umbilical cord blood-derived mesenchymal stem cell implantation versus microfracture for large, full-thickness cartilage defects in older patients: a multicenter randomized clinical trial and extended 5-year clinical follow-up. Orthop J Sport Med 2021;9:2325967120973052.

[40] Pers Y-M, Soler-Rich R, Vadalà G, Ferreira R, Duflos C, Picot MC, et al. Allogenic bone marrow-derived mesenchymal stromal cell-based therapy for patients with chronic low back pain: a prospective, multicentre, randomised placebo controlled trial (RESPINE study). Ann Rheum Dis 2024;83:1572–83.

[41] Robb KP, Galipeau J, Shi Y, Schuster M, Martin I, Viswanathan S. Failure to launch commercially-approved mesenchymal stromal cell therapies: what's the path forward? Proceedings of the International Society for Cell & Gene Therapy (ISCT) Annual Meeting Roundtable held in May 2023, Palais des Congrès de Paris, Organize. Cytotherapy 2024;26:413–7.

[42] Khodabukus A, Guyer T, Moore AC, Stevens MM, Guldberg RE, Bursac N. Translating musculoskeletal bioengineering into tissue regeneration therapies. Sci Transl Med 2022;14:eabn9074.

[43] Fan M, Tong P, Yan L, Li T, Ren J, Huang J, et al. Detrimental alteration of mesenchymal stem cells by an articular inflammatory microenvironment results in deterioration of osteoarthritis. BMC Med 2023;21:215.

[44] Malaise O, Tachikart Y, Constantinides M, Mumme M, Ferreira-Lopez R, Noack S, et al. Mesenchymal stem cell senescence alleviates their intrinsic and seno-suppressive paracrine properties contributing to osteoarthritis development. Aging (Albany NY) 2019;11:9128–46.

[45] Barry F, Murphy M. Mesenchymal stem cells in joint disease and repair. Nat Rev Rheumatol 2013;9:584–94.

[46] Mobasheri A, Kapoor M, Ali SA, Lang A, Madry H. The future of deep phenotyping in osteoarthritis: how can high throughput omics technologies advance our understanding of the cellular and molecular taxonomy of the disease? Osteoarthr Cartil Open 2021;3:100144.

[47] Doherty M, Dieppe P. The 'placebo' response in osteoarthritis and its implications for clinical practice. Osteoarthr Cartil 2009;17:1255–62.

[48] Saltzman BM, Leroux T, Meyer MA, Basques BA, Chahal J, Bach Jr BR, et al. The therapeutic effect of intra-articular normal saline injections for knee osteoarthritis: a meta-analysis of evidence level 1 studies. Am J Sports Med 2017;45:2647–53.

Miscellaneous

Systematic literature review informing the EULAR points to consider for patient education in physical activity and self-management of pain during transitional care

Javier Courel-Ibáñez [1], Rafael Prieto-Moreno [2,3,*],
Erica Briones-Vozmediano [4], Patrocinio Ariza-Vega [5,6], Saskya Angevare [7],
Jordi Anton [8], Ilaria Bini [9], Daniel Clemente [10], Matilde Correia [11],
Wendy Costello [7], Diederik De Cock [12], Andrea Domjan [13], Leticia Leon [14],
Andrea Marques [15], Kirsten Minden [16,17], Ana Filipa Mourão [18],
Aurelie Najm [19], Seza Özen [20], Georgina Pimentel [21], Zainab Saleem [9],
Tomas Vetrovsky [22], Nico Wulffraat [23], Andrea Zacarias [8,24], Yeliz Prior [25],
Loreto Carmona [26], Fernando Estévez-López [2,3,27]

[1] Department of Physical Education and Sport, University of Granada, Granada, Spain

[2] Department of Education, Faculty of Education Sciences, CIBIS (Centro de Investigación para el Bienestar y la Inclusión Social) Research Centre, University of Almería, Almería, Spain

[3] Biomedical Research Unit, Torrecárdenas University Hospital, Almería, Spain

[4] University of Lleida, Faculty of Nursing and Physiotherapy, and Research Group in Healthcare, Biomedical Research Institute of Lleida, Lleida, Spain

[5] Instituto de Investigación Biosanitaria ibs.Granada, Granada, Spain

[6] Department of Physiotherapy, Faculty of Health Sciences, University of Granada, Granada, Spain

[7] European Network for Children with Arthritis and Autoinflammatory Diseases, Geneva, Switzerland

[8] Hospital Sant Joan de Déu, Pediatric Rheumatology Department, Universitat de Barcelona, Barcelona, Spain

[9] EULAR Young PARE and Anmar Young, Zürich, Switzerland

[10] Hospital Niño Jesús, Pediatric Rheumatology Unit, Madrid, Spain

[11] Centro Hospitalar e Universitário de Coimbra, Coimbra, Portugal

[12] Department of Public Health, Vrije Universiteit Brussel (VUB), Biostatistics and Medical Informatics Research Group, Brussels, Belgium

[13] Department of Rheumatology, Faculty of Medicine, University of Debrecen, Debrecen, Hungary

[14] Universidad Camilo Jose Cela, Health Sciences, Madrid, Spain

[15] Higher School of Nursing of Coimbra, Health Sciences Research Unit Nursing, Coimbra, Portugal

[16] Department of Pediatric Respiratory Medicine, Immunology and Critical Care Medicine, Charité Universitätsmedizin Berlin, Corporate Member of Freie Universität Berlin and Humboldt - Universität zu Berlin, Berlin, Germany

[17] Deutsches Rheuma-Forschungszentrum Berlin, Berlin, Germany

[18] Lisbon and Rheumatology Department, Centro Hospitalar de Lisboa Ocidental, Nova Medical School, Lisbon, Portugal

[19] University of Glasgow, Institute of Infection, Immunity and Inflammation, College of Medical Veterinary and Life Sciences, Glasgow, UK

*Correspondence to Dr Rafael Prieto-Moreno, University of Almería and Torrecárdenas University Hospital, Almería, Spain.
E-mail address: rafapriemor@gmail.com (R. Prieto-Moreno).
Social media: ✖ @javiercourel (J. Courel-Ibáñez), ✖ @Rafaprieto4 (R. Prieto-Moreno), ✖ @AntonJordi68 (J. Anton), ✖ @dclementega (D. Clemente), ✖ @LeticiaLeonM (L. Leon), ✖ @drsezaozen (S. Özen), ✖ @tomasvet (T. Vetrovsky), ✖ @ProfYelizPrior (Y. Prior), ✖ @carmona_loreto (L. Carmona), ✖ @FerEstevezLopez (F. Estévez-López)
Handling editor Josef S. Smolen.

[20] *Department of Pediatric Rheumatology, Hacettepe University, Ankara, Turkey*

[21] *Rheumatology Department, Unidade Local de Saúde de Coimbra, Coimbra, Portugal*

[22] *Charles University, Faculty of Physical Education and Sport, Prague, Czech Republic*

[23] *Department Pediatric Rheumatology, University Medical Center Utrecht, Utrecht, Netherlands*

[24] *Rheumatology Department, Hospital Clinic Barcelona, Universitat de Barcelona, Barcelona, Spain*

[25] *Centre for Human Movement and Rehabilitation, School of Health and Society, University of Salford, Salford, UK*

[26] *Instituto de Salud Musculoesquelética, Madrid, Spain*

[27] *Department of Social and Behavioral Sciences, Harvard T. H. Chan School of Public Health, Boston, MA, USA*

ARTICLE INFO

ABSTRACT

Objectives: To synthesise existing evidence on transitional care programmes for young people with juvenile-onset rheumatic and musculoskeletal diseases (jRMDs), focusing on their structure and implementation, the qualitative experiences and perceptions of those involved, and the quantitative outcomes associated with these programmes. Together with additional information, these insights have informed the European Alliance of Associations for Rheumatology (EULAR) Points to Consider for patient education in physical activity and self-management of pain in jRMDs during transitional care.

Methods: A systematic literature review was conducted with a broadened scope beyond patient education in physical activity and self-management of pain to provide a comprehensive overview of transitional care in rheumatology, aiming to optimise current strategies, support evidence-based approaches, and identify areas for clinical improvement. The search was conducted in PubMed and the Cochrane Library from inception until November 1, 2023. Descriptive, qualitative, and quantitative studies were included. Two researchers independently conducted the search, screening, data extraction, and quality assessment.

Results: From 31 studies, we identified 18 transitional care programmes with key approaches, including individualised and developmentally appropriate plans that often integrate educational strategies. These programmes, which generally aim to increase readiness to transfer, health-related quality of life, and continuity of care, frequently involved multidisciplinary teams and early intervention strategies. Young people with jRMDs and their families reported satisfaction with these transitional care experiences, particularly valuing early self-management support. While these programmes showed potential in promoting positive health outcomes and clinical practices, quantitative evidence supporting their effectiveness is limited, with few experimental studies confirming consistent benefits.

Conclusions: This systematic review highlights the diverse yet fragmented approaches in transitional care for jRMDs, emphasising the need for stronger quantitative evidence. Thus, it is important to conduct further experimental research to optimise existing programmes or develop new ones, ultimately contributing to a smoother transition to adult care and improved long-term outcomes.

INTRODUCTION

The core aims of transitional care are to assist in continuing to adult treatment and to improve physical, psychological, social, vocational, and illness-related outcomes of young people with juvenile-onset rheumatic and musculoskeletal diseases (jRMDs) [1]. Transitional care relies on 3 principles: (1) preparing young people and families for independent disease management and readiness to transfer from paediatric to adult care; (2) providing information and resources to enhance health- and disease-related knowledge, health literacy (ie, person's ability to find, understand, and use health-related information when making health-related decisions) [2], and self-management skills; and (3) offering individualised support through attentive, developmentally appropriate care according to the individual needs, preferences, and resources of young people with jRMDs [1,3,4]. Importantly, transitional care constitutes an opportunity to build attitudes, skills, and behaviours in childhood, adolescence, and young adulthood that likely provide valuable long-term benefits later in life [5].

The establishment of the Got Transition programme [6] (endorsed by the American College of Rheumatology) and the launch of the 2017 European Alliance of Associations for Rheumatology /Paediatric Rheumatology European Society (EULAR/PReS) general standards and recommendations in transitional care for young people with jRMDs [1] have been key-works in this field. Based on this foundational framework, new programmes have been developed and implemented, leading to new evidence that requires revision [7−9]. For example, a number of transitional care programmes [7,8] have been designed regarding the Six Core Elements of Health Care Transition designed by the Got Transition Framework [10], incorporating educational interventions that address topics such as understanding the transition policy and creating a plan of care. These programmes guide young people with jRMDs through structured conversations with patients, families, and healthcare providers to foster autonomy and self-management skills and prepare them for the transition adult care [8]. Although some of the existing EULAR recommendations address important aspects of transitional care (eg, patient education [11], physical activity [12], and self-management of pain [13]), they were not specifically designed for young people with jRMDs. This limits their applicability in transitional care, which requires specialised considerations to accommodate the developmental needs of these

WHAT IS ALREADY KNOWN ON THIS TOPIC

- The launch of the 2017 European Alliance of Associations for Rheumatology /Paediatric Rheumatology European Society (EULAR/PReS) European Alliance of Associations for Rheumatology (EULAR)/Paediatric Rheumatology European Society (PReS) standards and recommendations was a major step towards providing general guidance in transitional care for young people with juvenile-onset rheumatic and musculoskeletal diseases (jRMDs).
- The effectiveness and experiences of available transitional care programmes require revision to increase evidence-based knowledge and improve practice, outcomes, and implementation.
- There is a lack of consensus on best practices for transitional care programmes in rheumatology.

WHAT THIS STUDY ADDS

- While young people with jRMDs and their families generally express satisfaction with transitional care practices, they highlight the need for more personalised approaches that integrate their unique needs, preferences, and resources.
- The evidence base for transitional care in rheumatology from experimental quantitative studies remains limited.

HOW THIS STUDY MIGHT AFFECT RESEARCH, PRACTICE OR POLICY

- This review informs the EULAR Points to Consider for the patient education on physical activity and self-management of pain in jRMDs during transitional care.
- This task force encourages appropriate randomised controlled trials to evaluate existing patient education programmes focused on physical activity and self-management of pain during transitional care. If necessary, these programmes should be optimised or new ones developed.
- This task force highlights the importance of improving accessibility to transitional care by addressing barriers, especially for underrepresented groups with limited healthcare access, to ensure inclusivity and equal support in managing jRMDs.

young individuals (eg, avoid parental overprotection) [14−16]. The present systematic literature review aims to synthesise existing evidence on transitional care programmes for young people with jRMDs, focusing on their structure and implementation, the qualitative experiences and perceptions of those involved, and the quantitative outcomes associated with these programmes. These insights have informed the EULAR Points to Consider (PtC) for patient education in physical activity and self-management of pain in jRMDs during transitional care [17].

METHODS

Eligibility criteria and literature search

The steering group of the taskforce designed, registered, and conducted a systematic review according to the Preferred Reporting Items for Systematic Reviews and Meta-analyses [18] and the Cochrane Collaboration guidelines [19] (PROSPERO No: CRD42023481386). Three questions were formulated to synthesise evidence on practices, experiences, and outcomes in transitional care programmes for young people with jRMDs as well as their relatives, rheumatologists, and Health Professionals in Rheumatology (HPRs). These questions focus on understanding transitional care programmes in rheumatology for young

people with jRMDs, their families, and healthcare providers. The first question, 'How are transitional care programmes structured and implemented in rheumatology?', explores how these programmes are implemented by rheumatologists and HPRs, as well as the content provided. The second question, 'What are the experiences and perceptions of young people with jRMDs, families, and healthcare providers involved in transitional care programmes?', aims to capture the experiences, perceptions, and barriers faced by these groups. The third question, 'What are the benefits of transitional care interventions for young people with jRMDs and their families?', examines different outcomes, such as continuity of care, self-efficacy, disease-specific knowledge, and readiness to transfer to adult care.

The eligibility criteria of studies were determined according to the PICOS (Population, Intervention, Comparators, Outcomes, Study design) approach (Table 1).

Preparatory material for the initial planning meeting of the task force was developed based on a systematic literature review of PubMed and the Cochrane Library performed on October 1, 2021. To include an update on the results, we conducted this systematic literature review again on November 1, 2023. The search strategy consisted of a combination of relevant keyword variations in free terms, presented in Supplemental Table S1. Using a snowball technique, we included additional studies by performing backward (by checking reference lists) and forward (by checking citations) searches of the works included in the present review.

Study selection, data extraction, and quality assessment

The search was conducted by 2 researchers independently (JCI and RPM). Screening, data extraction, risk of bias and quality of evidence assessment were conducted by 2 researchers independently (JCI and RPM). Discrepancies were discussed for consensus or solved with a third researcher (FEL) if necessary. Eligibility criteria were applied to titles and abstracts (first-stage screening) and full texts of the remaining studies (second-stage screening). Risk of bias was assessed by the Clinical Appraisal Skills Programme for qualitative research [20]. For quantitative research, we used Cochrane risk of bias tool for randomised controlled trials (RCTs) [21], the Quality In Prognosis Studies tool for observational studies [22], and the Appraisal tool for cross-sectional studies [23].

RESULTS

The results of the search for this systematic review are shown in Figure 1. From 1600 studies, 98 were selected for full-text review, and 31 were included in this systematic review. For question 1, we identified 18 transitional care programmes (17 structured plans for young people with jRMDs and 1 for their parents) (Table 2) [24−49]. For questions 2 and 3, we found 25 studies. Of them, 2 were mixed-methods designs (ie, cross-sectional plus qualitative study) [7,49], 6 were qualitative [28,37,41,43,44,48], and 17 were quantitative. Specifically, among the quantitative studies, there were 5 intervention studies (1 RCT [42], 1 clinical trial protocol [50], and 3 quasi-experimental studies [16,38,40]), 5 cohort studies [8,30,32,33,47], 1 retrospective study [31], and 6 cross-sectional studies [24,29,39,45,46,51] (Table 3). The methodological quality is presented in Supplemental Tables S2-S5.

Table 1

Eligibility criteria of studies were determined according to PICOS (Population, Intervention, Comparators, Outcomes, Study design)

Clinical question	P	I	C	O	S
How are transitional care programmes in rheumatology structured and implemented?	Young people with jRMDs, their family and healthcare providers involved	Structured transitional care programmes	N/A	N/A	- Qualitative studies - Quantitative studies - Clinical trials protocol
What are the experiences and perceptions of young people with jRMDs, families, and health professionals involved in transitional care programmes?	Young people with jRMDs, their family or healthcare providers involved	Structured transitional care programmes	N/A	- Experiences - Perceptions - Barriers/facilitators	- Qualitative studies - Quantitative studies - Clinical trials protocol
What are the benefits provided by transitional care interventions in rheumatology for young people with jRMDs and their families?	Young people with jRMDs, their family and/or healthcare providers involved	Structured transitional care programmes	- Follow-up changes - Control group, - Other strategy - No comparator	- Continuity of treatment - Fatigue - Functional status - Knowledge - HRQoL - Pain management - Physical activity - Psychosocial health - Readiness to transfer - Self-management skills - Sexual health, - Vocation	- Qualitative studies - Quantitative studies - Clinical trials protocol

HRQoL, health-related quality of life; jRMD, juvenile-onset rheumatic and musculoskeletal disease; N/A, not applicable.

Question 1. How are transitional care programmes in rheumatology structured and implemented?

Common elements across the majority of transitional care programmes included: (1) the formulation of a specific written individual transition plan; (2) adopting a patient-centred, shared decision-making approach; (3) providing developmentally appropriate care; (4) initiating the process early; (5) involving a multidisciplinary team; and (6) offering educational resources.

Multidisciplinary teams usually involved paediatric and adult rheumatologists and nurses [24,25,34,39,42−44,51,52] with most programmes including HPRs such as physiotherapists [24,25,34,35,39,44,51], social workers [24,25,35,38,52], or occupational therapists [24,25,34]. Seven programmes included a coordinator [25,30,35,36,38,44,52]. Two studies included psychologists [35,52], and another study involved sexual/vocational counsellors [25].

Some programmes were structured in developmentally appropriate phases, with specific shared goals and contents adapted to young people's readiness and age [7,44,53]. Tools and formats of delivery vary in transitional care, and their effectiveness remains unclear. In addition to face-to-face consultations, most of the programmes also included telehealth (websites [7,30,35,36,41,43,53], web-based educational programmes [40−42], videos [36,42,43], and e-consulting [43]) and paper-based information (flyers [30,35,36], handbook [30,38], toolkit [7], or filofax [30]) with telephone [7,30,35,36,38] and e-mail [7,35] follow-up. One programme organised informal activities with peers, including meetings, workshops, and lectures [36].

Common self-management learning contents provided were disease management [7,25,35,36,38,42,44,51,52], education [7,24,25,30,34,35,38,42,44,50], social relationships [25,30,34,35,36], sexual health [24,25,30,34,38,42,52], disease-specific knowledge [25,30,35,36,42,52], physical activity

(including sports and exercise) [30,36,38,42], risk-taking behaviours [24,25,34,38,52], independent living and self-advocacy [24,25,30,38,52], diet [30,38,42,52], and psychosocial health [30,38,42,52], fatigue [36,42], financial counselling [24,25], communication skills [25,42], home/parental issues [30,34], self-confidence/body image [30,36], dental health [30], cybersafety [30], suicide [34,52], spirituality [34], cooking [36], disabilities [36], and pain management [42]. Contents for rheumatologists and HPRs were included in only 1 programme [30], addressing adolescent development, communication, and adolescent-friendly resources. Last, despite the essential role played by family and peers in transitional care in facilitating the transfer of responsibilities to young people [1,3], not all the programmes included dedicated resources for relatives [25,30,34,44] and peer support [7,24,30,36,43].

Question 2. What are the experiences and perceptions of young people with jRMDs, families, and healthcare providers involved in transitional care programmes?

In general, young people with jRMDs and their families were satisfied with the transitional care programmes [33,38−40,45]. They appreciated receiving early psychosocial, nonpharmacological interventions with the transition coordination to express their intimate concerns (ie, sports, school, friends, medication, body image, alcohol use, and contraception) [16]. Importantly, young people appealed for better understanding and integration of their individual needs, preferences, and resources during transitional care [28,37,43]. Parental education was valued by young people with jRMDs to gradually take over responsibility for their care [48]. Likewise, parents stated they would not give responsibility to their children without the programme assistance and admitted their overprotectiveness was due to lack of knowledge [16]. Both youth and parents recognised the role of
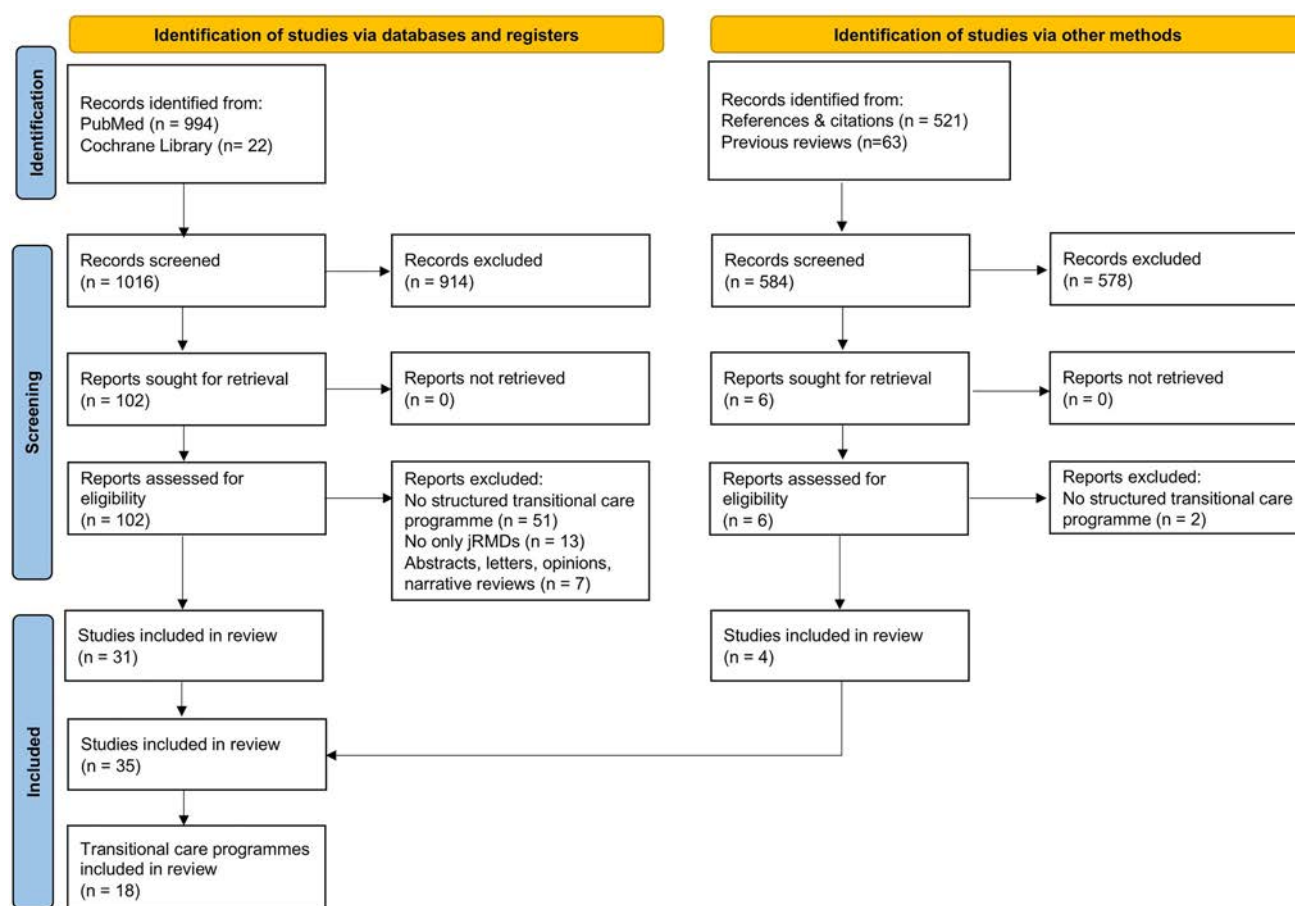
Figure 1. Flow chart of the study selection and inclusion process. jRMD, juvenile-onset rheumatic and musculoskeletal disease.

peer support to improve confrontation, identification, and fellowship [16].

Preliminary surveys and focused group discussions were used to guide the development of the transitional care programmes according to the experiences and expectations of young people with jRMDs [29,37,44,48]. This information served to identify missing topics during consultations [44] and the importance of gradual education, parental involvement, and adapted healthcare settings to match their expectations [37]. There is evidence reporting positive feedback on the access to the transition plan via website, the timeline learning steps, and the decision-making worksheet and emphasised the benefits of addressing mental health. In addition, young people valued self-management learning experiences outside the clinic (camps or conferences) and raised concerns on how to integrate the skills developed through the programmes in their daily routine [48].

The implementation of transitional care may improve the clinical practices and transfer administrative process through better documentation of transitional issues and higher multidisciplinary involvement [31]. However, reports on diet and home exercise remained poorly documented even after starting the programme [31]. Reported barriers to implementation included inadequate resources, coordination, and lack of specific training for rheumatologists and HPRs [29]. This is in line with the experience of rheumatologists and HPRs in having a lack of skills and self-confidence when dealing with young people with jRMDs [30]. The adoption of a structured transitional programme appeared to be manageable and was generally viewed positively, as it could contribute to

improved organisation, efficiency, follow-up care, structured communication, and availability of helpful resources [7]. Because each clinical setting may have unique needs and barriers to start implementing a transitional care practice, programmes should be flexible (eg, creating generic, but customisable, resources) and start the process with small changes [4,7].

Question 3. What are the benefits provided by transitional care interventions in rheumatology for young people with jRMDs and their families?

Transitional care programmes may have benefits in enhancing continuity of care [8,24,38,39,45] and may improve health-related aspects (ie, health-related quality of life, pain, and functional status) [32,33]. Some findings suggest that these programmes may enhance self-efficacy skills [45], vocational plans [32], disease-specific knowledge [32], and readiness to transfer to adult care [47]. In addition, 2 interventions found positive results on familiar relationships (ie, better parenting climate, autonomy support, reduction in parental control, and worry) [16] and possible improvements in parental knowledge and health-related quality of life [32]. Nevertheless, the knowledge and readiness acquired differed between programmes; some found difficulties with healthcare insurance, financial support, and decision-making autonomy about their care [47], while others reported issues with travel, booking appointments, or getting prescriptions [46]. These findings highlight the importance of effective communication

Table 2
Structure and contents of transitional care programmes in rheumatology

Programme	Studies	Age	Educational contents	Tools	Health care providers involved
Rheumatology transition programme	Rettig and Athreya, 1991 [24]	17-19	Vocational and financial counselling, alcohol education, birth control, parental independence. Parental education. Peer support.	Not reported	Paediatric rheumatologist, adult rheumatologist, social worker, nurse, internist rheumatologist, physical therapist, occupational therapist
Vancouver Young Adults with Rheumatic Diseases (YARD) clinic	Tucker and Cabral, 2005 [25]	14-18	Developmentally appropriate. Individualised plans. Education and self-management skills (disease, medications, skills in communication, educational/vocational career, finances/healthcare coverage, independent living, relationships outside the family, sexual health, risk-taking behaviours, family problems). Parental education.	Not reported	Coordinator, paediatric rheumatologist, adult rheumatology, nurse, social worker, physiotherapy, occupational therapy, vocational and sexual counselling services
Calgary Young Adults with Rheumatic Diseases (YARD) clinic	Miettunen, 2008 [26] Guelber, 2008 [27]	14-25	Developmentally appropriate. Individualised plans. Education and self-management skills (illness management, coverage, school, career counselling, personalised fitness programme).	Not reported	Coordinator (nurse), paediatric rheumatologist, adult rheumatology, nurse, physiotherapist, and social worker
Growing up and moving on	Shaw et al, 2004 [28,29] McDonagh, 2006 [30] Robertson et al, 2006 [31] McDonagh et al, 2007 [32] Shaw et al, 2007 [33]	11-17	Developmentally appropriate. Individualised plans. Education and self-management skills (disease, psychosocial health, social issues, parental issues, education and vocation, sexual health, self-confidence, body image, diet, dental health, exercise, cybersafety, independent living). Parental education. Peer support.	Websites Filofax Handbook Phone calls Flyers Templates	Coordinator, consultant rheumatologist
MAGICC (Moving on in Adolescence, Growing up In Collaboration and Coping)	Tattersall, 2012 [34]	10-25	Developmentally appropriate. Individualised plans. Education and self-management skills (HEADDS schema: home, education/employment, activities outside school and home, drugs, sexual health, suicide, spirituality). Parental education.	Not reported	Paediatric rheumatologist, adult rheumatologist, nurse, physiotherapist, occupational therapist
Berlin Transitions Program	Minden et al, 2014 [35]	16-20	Developmentally appropriate. Individualised plans. Joint consultations. Education and self-management skills (disease, health disease management, future plans and prospects, social environment, attitude and readiness for transition).	Websites Flyers Phone calls e-mails	Coordinator, paediatric rheumatologist, internal rheumatologist, physiotherapists, psychologists, social workers
Don't Retard	Hilderson et al, 2013 [36,37] Hilderson et al, 2016 [16]	14-16	Individualised plans. Education and self-management skills (disease, medication management and adherence, exercise, cooking, fatigue, school, friends, self-image, social issues, disabilities). Parental education. Peer support.	Websites Booklet DVD Phone calls Workshops Lectures	Coordinator, paediatric rheumatologist
Nationwide Children's Hospital	Jensen et al, 2015 [38]	15-26	Individualised plans. Education and self-management skills (medical management, occupation, hobbies, relationships).	Phone calls Workbook	Coordinator (social worker), paediatric rheumatologist, adult rheumatologist

(*continued*)

Table 2 (*Continued*)

Programme	Studies	Age	Educational contents	Tools	Health care providers involved
IWK Health Centre Pediatric Rheumatology Transition Clinic	Stringer et al, 2015 [39]	14-16	Individualised plans. Education and self-management skills (medical management and psychosocial health).	Not reported	Paediatric rheumatologist, adult rheumatologist, nurse, paediatric physiotherapist
Challenge your arthritis	Ammerlaan et al, 2014 [40] Ammerlaan et al, 2015 [41] Ammerlaan et al, 2017 [42]	16-25	Web-based educational programme. Education and self-management skills (disease, pain, fatigue, sport and exercise, nutrition, intimacy, communication skills at school or work).	e-Health News Videos Homework Games Chats	Paediatric rheumatologist, adult rheumatologist, nurse, peer trainers
University Medical Center Utrech	Ammerlaan et al, 2017 [43]	16-25	Individualised plans. Education and self-management (5 themes: treatment and medication; physical exercise, holidays, alcohol and drugs; relations, sexuality and pregnancy; dealing with pain, fatigue and emotions; study and work). Peer support.	Website Videos Stories Online consulting	Paediatric rheumatologist, adult rheumatologist, nurse
Clinical transition pathway for adolescents in Netherlands	Walter et al, 2017 [44] Walter et al, 2018 [45]	12-18	Individualised plans. Joint consultations. Education and self-management (medical care, psychosocial and vocational needs). Parental education.	Not reported	Coordinator (paediatric rheumatology nurse and adult rheumatologist), paediatric rheumatologist, adult rheumatology nurse, physiotherapists
McMaster Rheumatology Transition Clinic	McColl et al, 2021 [46]	14-17	Not reported	Not reported	Not reported
Got Transition	Overbury et al, 2021 [8] Teh et al, 2022 [47] Cox et al, 2023 [7] Carandang et al, 2022 [48] Chang et al, 2023 [49]	14-27	Education and self-management (Got Toolkit: self-care skills, education and resources, readiness). Parental education. Peer support.	Websites Phone calls e-mails	Paediatric rheumatologist, adult rheumatologist, nurse[a], child life specialist[a], physiotherapist[a]
ParTNerSTEPs (Parents in Transition—a Nurse-led Support and Transfer Educational Program)	Thomsen et al, 2022 [9]	Parents	Educational contents (adolescent's life with a chronic condition, independence, need for parents' support and expectations/emotions regarding the transfer, what to expect in adult care).	Websites Scripts	Paediatric rheumatologist, adult rheumatologist, nurse
TRACER (Transition to Adulthood Through Coaching and Empowerment)	Batthish, 2022 [50]	16-18	8-mo coaching intervention. Education and self-management (self-advocacy, medication management, general health, lifestyle issues, education/vocation, psychological and social well-being).	Not reported	Clinical psychologist
TTP (Tuebingen Transition Program)	Boeker et al, 2022 [51]	13-Not reported maximum age	Self-management, disease knowledge, reflection of the individual progress, and topics particularly relevant to adolescents (not specified). Parental involvement at the end of each visit.	Visits	Paediatric rheumatologist, adult rheumatologist, psychosocial team, physiotherapist. teachers
TCARD (Transition Clinic for Adolescents with Rheumatic Diseases)	García-Rodríguez et al, 2023 [52]	16-18	Self-management, knowledge and literacy, mental health (psychiatric disorders, drugs, suicide risk, education/vocation, sexual behaviour), nutrition, sports and physical activities, and rehabilitation.	Workshops Activities Counselling	Paediatric rheumatologist, adult rheumatologists, nutritionist, physical medicine and rehabilitation specialists, medical specialist in adolescent psychiatry, clinical psychologist, nurse, social worker

[a] Varied between studies/among countries.

and positive patient-provider relationships to identify individuals' needs, preferences, and resources to offer tailored contents during transitional care. Telehealth and e-consultation may play a role in better communication [41]. Ongoing clinical trials may provide new insights on the effectiveness of a face-to-face, coaching transition intervention (psychologist-driven) [50].

DISCUSSION

The present systematic review, informing the EULAR PtC for patient education in physical activity and self-management of pain in jRMDs during transitional care [17], aimed to synthesise existing evidence on transitional care programmes for young people with jRMDs, focusing on their structure and implementation,

Table 3

Studies characteristics examining transitional care programmes in rheumatology

Studies	Design	Population	Comparator	Main outcomes (instruments) and results	Risk of bias
Rettig and Athreya, 1991 [24]	Cross-sectional	36 (jRMDs) Aged 17-19 y UK	N/A	Continuity to adult care (%)[a]	High
Shaw et al, 2004 [29]	Cross-sectional	478 (HPRs) UK	N/A	Resources to be important: self-medication teaching packages and social skills training[b] Barriers for implementation: inadequate resources, coordination, and training[b]	Medium
Shaw et al, 2004 [28]	Qualitative	30 (JIA) Aged 13-30 y 23 (parents) UK	N/A	Young people with JIA and their parents call for developmentally appropriate care that address physical, social, psychological, and vocational issues	Medium
McDonagh et al, 2006 [30]	Cohort	194 (JIA) Aged 11, 14, 17 y 185 (parents) UK	Follow-up (6 months)	Acceptability[a] Educational resources usability[a]	Medium
Robertson et al, 2006 [31]	Retrospective	8 (centres) UK	Follow-up (12-24 months)	Documentation: Transitional issues (HEADS) ↑[c] Transitional readiness (ad hoc) ↑[c] Parental needs (ad hoc) ↑[c] MDT involvement (ad hoc) ↑	High
Shaw et al, 2007 [33] McDonagh et al, 2007 [32]	Cohort	308 (JIA) Aged 11, 14, 17 y 67% women 303 (parents) UK	Follow-up (12 months)	Young people with JIA: Satisfaction (Mind the Gap) ↑[c] Health-related quality of life (JAQQ) ↑[c] Arthritis-related knowledge (ad hoc) ↑[c] Vocational plans (ad hoc) ↑[c] Independent health behaviours (ad hoc) ↑ Parents: Satisfaction (Mind the Gap) ↑[c] Arthritis-related knowledge (ad hoc) ↑[c]	Low
Hilderson et al, 2013 [37]	Qualitative	11 (JIA) Aged 18-30 y 73% women	N/A	Experiences and expectations[b] 3 main themes emerged: preparation, parental involvement, and an adapted setting for the late-adolescent or early adult	Medium
Ammerlaan et al, 2014 [40]	Quasi-experimental	19 (JIA: 42%) Aged 16-25 y Netherlands	10 post intervention (1 month) Comparators: 9 face-to-face intervention	Technology acceptance (TAM)[a] High adherence and interaction[a] Perceived usefulness (0-10 Likert) ↔ Perceived user acceptance (0-10 Likert) ↑ Goals achievement ↔	High
Hilderson et al, 2015 [16]	Quasi-experimental	23 (JIA) Aged 14-16 y 74% women 23 (parents) UK	Follow-up (6-11 months)	Young people with JIA: Psychosocial health (PedsQL) ↑[d] Physical health (PedsQL) ↑ Pain and hurt (PedsQL) ↔ Communication (PedsQL) ↑ Daily activities (PedsQL) ↑ Health-related quality of life (VAS) ↑ Fatigue (MFI-20) ↓ Motivation (MFI-20) ↑ Parents: Worry (PedsQL) ↓[d] Behavioural control (PRS-YSR) ↓[d] Autonomy support (PVF) ↓ Promotion of independence ↓ Pain and hurt (PedsQL) ↔ Psychological control (PRS-YSR) ↓ Psychosocial health ↓ Physical health (PedsQL) ↓ Daily activities (PedsQL) ↑ Communication (PedsQL) ↓	Low

(*continued*)

Table 3 **(Continued)**

Studies	Design	Population	Comparator	Main outcomes (instruments) and results	Risk of bias
Jensen et al, 2015 [38]	Quasi-experimental	210 (JIA: 52%, SLE: 26%) Aged 15-26 y 79% women USA	Follow-up (6-8 months) Comparator: 26 controls	Continuity to adult care (%) ↑[c] Satisfaction (5-50 Likert)[a]	Medium
Stringer et al, 2015 [39]	Cross-sectional	51 (JIA: 82%) Aged 15-17 y 78% women Canada	27 Follow-up (adult care) Comparator: 13 no follow-up	Satisfaction (VAS) ↑ Disease control at transfer (ad hoc) ↔ Functional capacity (HAQ) ↔ Health-related quality of life (SF-36) ↓	Medium
Ammerlaan et al, 2015 [41]	Qualitative	13 (JIA: 42%) Aged 16-25 y Netherlands	N/A	High acceptability and feasibility for an online educational portal. Having access to their medical records increased their feelings of being in control; e-consult may lead to easier and better communication[b]	Medium
Ammerlaan et al, 2017 [42]	Randomised controlled trial	72 (JIA) Aged 16-25 y 88% women Netherlands	36 post intervention (1 month) Comparator: 36 controls	Learning experience (0-10 Likert)[a] Self-efficacy (Dutch- ASES) ↔ Health education impact (Dutch heiQ) ↔ Functional capacity (HAQ-DI) ↔ Perceived pain (0-10 Likert) ↔ Perceived well-being (0-10 Likert) ↔ Perceived fatigue (0-10 Likert) ↔ Perceived disease activity (0-10 Likert) ↔ Medication (DMARD and NSAID) ↔	Medium
Ammerlaan et al, 2017 [43]	Qualitative	HPRs	N/A	Young people demanded integrating young people priorities and respecting their decisions[b]	High
Walter et al, 2017 [44]	Qualitative	32 (JIA: 72%) Aged 14-20 y 69% women 33 (parents) Netherlands	N/A	Missed topics during consultations[b] Experiences of preparation for transfer[b] Self-management skills[b]	Medium
Walter et al, 2018 [45]	Cross-sectional	154 (JIA: 68%) Aged 12-14 y 64% women Netherlands	76 transferred to JIA clinic Comparator: 78 not transferred to JIA clinic	Continuity to adult care (%) ↑ Individual transitional plan (%)[e] ↑ [d] Satisfaction (OYOF-TES)[e] ↔ Self-efficacy (OYOF-SES)[e] ↔ Disease activity (ESR)[e] ↔ Vocational restrictions by the disease[e] ↔	Medium
McColl et al, 2021 [46]	Cross-sectional	70 (JIA: 87%, SLE: 13%) Aged 14-20 y 65 women Canada	N/A	Self-management skills (TRANSITION-Q)[a]	Medium
Overbury et al, 2021 [8]	Cohort	57 (JIA: 63%) Aged 14-27 y 75% women USA	N/A	Continuity to adult care (%)[a]	Medium
Teh et al, 2022 [47]	Cross-sectional	152 (JIA: 47%, SLE: 40%) Aged 15-22 y 65% women Singapore	111 aged <20 y Comparator: 41 aged ≥20 y	Medical healthcare knowledge (MKHU) ↓[d] Transitional readiness (TRAQ) ↓[d] Transition importance (0-10 Likert) ↔	Medium
Chang et al, 2023 [49]	Cross-sectional and qualitative	9 clinics USA	N/A	Organisational Readiness for Implementing Change (ORIC) Challenges, facilitators, and overall experience with the transition implementation process	Medium
Boeker et al, 2022 [51]	Cross-sectional	85 (JIA: 71%) Ages 18-44 y 71% women Germany	Average German population

Participants without continued care | Continuity to adult care (%)[a] Physical activity ↑ Health-related quality of life (EQ-5D-5L) ↓ Satisfaction (VAS) ↑ Disease activity (PGA) ↓ Physical activity ↑ Health-related quality of life (EQ-5D-5L) ↑ | Low |

Table 3 (*Continued*)

Studies	Design	Population	Comparator	Main outcomes (instruments) and results	Risk of bias
Carandang et al, 2022 [48]	Qualitative	39 (JIA: 85%) Aged 16-28 y 82% women USA	N/A	Recommendations on implementation: Frame healthcare transition as an opportunity for empowerment, implement a structured education plan and consider the role of parents[b]	Low
Cox et al, 2023 [7]	Cross-sectional and qualitative	6 clinics USA	N/A	Transition implementation (0-5 Likert) ↑[d] Results, suggestions and barriers[b] The programme improved organisation, efficiency, follow-up care, structured communication, and availability of helpful resources Main barriers included documenting the transition process, nonspecific documents and insufficient time	High

ASES, Arthritis Self-efficacy Scale; DMARD, disease-modifying antirheumatic drug; EQ-5D-5L, EuroQoL 5-Dimension 5-Level; ESR, erythrocyte sedimentation rate; HAQ, Health Assessment Questionnaire; HEADS, Home, Education, Activities, Drugs, Suicide; heiQ, Health Education Impact Questionnaire; HPR, Health Professional in Rheumatology; JAQQ, Juvenile Arthritis Quality of Life Questionnaire; JIA, juvenile idiopathic arthritis; jRMD, juvenile-onset rheumatic and musculoskeletal disease; MDT, multidisciplinary team; MFI, Modified Fatigue Index; MKHU, Medical Knowledge and Healthcare Usage; ; N/A, not applicable; NSAID, nonsteroidal anti-inflammatory drug; OYOF-SES, On-your-own-feet self-efficacy scale; OYOF-TES, On-your-own-feet transition experiences scales; PedsQL, Pediatric Quality of Life; PGA, Physician Global Assessment; PRS-YSR, Parental Regulation Scale−Youth Self-Report; PVF, Promotion of Volitional Functioning (Autonomy Support Scale); SF-36, 36-Item Short Form Survey; SLE, systemic lupus erythematosus; TAM, Technology Acceptance Model; TRAQ, Transition Readiness Assessment Questionnaire; VAS, visual analogue scale.

Change in scores: ↑ increments, ↓ decrements, ↔ no differences.

[a] No comparative analyses are available.

[b] Qualitative analyses.

[c] Results from partial sample.

[d] 75% with inactive disease.

[e] Clinical trial protocol, no results available

[f] Significant change, $P < .05$.

[g] Significant change, ES >0.30.

the qualitative experiences and perceptions of those involved, and the quantitative outcomes associated with these programmes. First, we observed a lack of consensus on practices for transitional care programmes in rheumatology, as existing programmes are markedly varied. Second, satisfaction with these programmes appears relatively good among young people with jRMDs and their families, although it remains unknown for healthcare professionals. Third, evidence supporting favourable outcomes remains limited, as few well-designed RCTs have evaluated the effectiveness of these programmes.

Structure and implementation of transitional care programmes in rheumatology: current practices and future directions

The considerable structural differences emerging from the identified programmes underscores the need for clearer and standardised guidance promoting evidence-based transitional care programmes in rheumatology. Indeed, a number of studies offered limited details on essential components (eg, programme duration, follow-up procedure, and delivery mode), suggesting that reporting quality in this field may benefit from improvement. Additionally, information on how well these programmes align with the unique needs, preferences and resources of young people and their families was also missing [54], offering limited insights into whether they are suitably tailored to serve young people with jRMDs. Despite these limitations, certain foundational principles from the 2017 EULAR/PReS (general) standards and recommendations [1] were reflected across the included studies. First, a dedicated coordinator to organise care, schedule follow-ups, serve as the primary contact for patients and families, and link paediatric and adult healthcare providers. Second, a multidisciplinary team including paediatric and adult rheumatologists and HPRs (eg, nurses, occupational therapists, physiotherapists, social workers, psychologists, and sports scientists) to ensure holistic care that addresses the unique medical, psychological, and social needs of each young person with jRMDs. Third, efficient communication between healthcare providers, young people with jRMDs and their families is essential to align treatment goals and foster informed engagement. Fourth, comprehensive care plans that combine, when indicated, pharmacologic and nonpharmacologic approaches, tailored to the evolving needs, preferences and resources of each young person. Fifth, to engage young people in informed shared decision-making to foster ownership and tailor care delivery to their needs, preferences, and resources, empowering them to self-manage their jRMDs.

Considering the high rates of physical inactivity [55,56] and challenges in self-management of pain commonly observed among young people with jRMDs [57−59], our task force identified the clinically relevant and timely need of developing specific guidelines for patient education in physical activity and self-management of pain during transitional care in rheumatology. This review, together with individual semistructured interviews and additional literature, informed the task force discussions that established the EULAR PtC on patient education in physical activity and self-management of pain for young people with jRMDs during transitional care [17]. By launching these EULAR PtC, we aim to optimise the design of transitional care programmes in rheumatology through clear, standardised guidance on patient education. This approach may support a smoother transition to adult care and fosters sustainable, long-term health outcomes.

Qualitative and quantitative evidence on transitional care programmes in rheumatology

Young people with jRMDs and their families generally express high satisfaction with existing transitional care programmes, appreciating initiatives that foster independence through early psychosocial support for young individuals and education for parents. The literature highlights the importance of peer support, education on self-management, and personalised transitional care tailored to individual needs, priorities, preferences, capabilities, resources, and contexts. In addition to these positive aspects, young people with jRMDs and their families also identified barriers to access transitional care such as insufficient resources and the need for coordinated, multidisciplinary, and specialised healthcare teams. While qualitative evidence is generally positive, the quantitative findings remain uncertain. The literature suggests that transitional care programmes may have the potential to enhance readiness to transfer, continuity of care, health literacy, and daily participation. However, most of these findings come from limited, individual studies with varying designs, highlighting the need for well-designed RCTs to establish robust quantitative evidence on key outcomes of transitional care.

Limitations

It is likely that not all existing transitional care programmes in rheumatology are included in this review, which may be considered the main limitation of this work. This may be explained by the exclusion of potentially relevant databases from our search (eg, CINAHL, PsycInfo, and PEDro) and the exclusion of transitional care programmes whose essential structural components were not described in detail in the screened manuscripts. Additionally, as most included studies focused on juvenile idiopathic arthritis and juvenile-onset systemic lupus erythematosus, the generalisability of our findings to other jRMDs is limited. Similarly, our results may not be relevant to people from minorities, populations at risk of social exclusion, and those underrepresented in research or with limited access to care. Moreover, as our literature review did not have temporal restrictions, the evolution of practices and resources must be considered when interpreting the findings (eg, some previously identified barriers may now be easier to overcome).

CONCLUSION

In conclusion, this systematic literature review synthesises the state-of-the-art in current transitional care practices in rheumatology. These insights, together with additional information, informed the discussions of the members of the task force establishing the EULAR PtC for patient education in physical activity and self-management of pain during transitional care. Further research is warranted to establish quantitative evidence on programme effectiveness and to explore additional areas critical for young people with jRMDs, such as healthy lifestyle, self-management of fatigue, sleep hygiene, mental health and social support, ensuring that transitional care evolves to meet their diverse needs. Importantly, to enhance the inclusivity and reach of transitional care, it is essential to address accessibility barriers, particularly for people from underrepresented groups with limited healthcare access.

Patient and public involvement

Patients and/or the public were involved in the design, conduction, reporting, and dissemination plans of this research. Refer to the Methods section for further details.

Patient consent for publication

Not applicable.

Ethics approval

Not applicable.

Provenance and peer review

Not commissioned; externally peer reviewed.

Data availability statement

Data sharing is not applicable as no datasets were generated and/or analysed for this study. All data relevant to the study are included in the article or uploaded as supplementary information.

Supplementary materials

Supplementary material associated with this article can be found in the online version at doi:10.1016/j.ard.2025.01.017.

Orcid

Javier Courel-Ibáñez: http://orcid.org/0000-0003-2446-1875

Rafael Prieto-Moreno: http://orcid.org/0000-0002-7301-5831

Erica Briones-Vozmediano: http://orcid.org/0000-0001-8437-2781

Patrocinio Ariza-Vega: http://orcid.org/0000-0003-2447-2179

Jordi Anton: http://orcid.org/0000-0002-8792-4219

Daniel Clemente: http://orcid.org/0000-0002-1605-7488

Leticia Leon: http://orcid.org/0000-0001-7142-0545

Kirsten Minden: http://orcid.org/0000-0003-2775-0111

Ana Filipa Mourão: http://orcid.org/0000-0002-0299-0963

Aurelie Najm: http://orcid.org/0000-0002-6008-503X

Seza Özen: http://orcid.org/0000-0003-2883-7868

Georgina Pimentel: http://orcid.org/0000-0001-5467-3399

Tomas Vetrovsky: http://orcid.org/0000-0003-2529-7069

Nico Wulffraat: http://orcid.org/0000-0001-9548-5562

Yeliz Prior: http://orcid.org/0000-0001-9831-6254

Loreto Carmona: http://orcid.org/0000-0002-4401-2551

Fernando Estévez-López: http://orcid.org/0000-0003-2960-4142

REFERENCES

[1] Foster HE, Minden K, Clemente D, Leon L, McDonagh JE, Kamphuis S, et al. EULAR/PReS standards and recommendations for the transitional care of young people with juvenile-onset rheumatic diseases. Ann Rheum Dis 2017;76(4):639–46. doi: 10.1136/annrheumdis-2016-210112.

[2] Šulinskaitė K, Zagurskienė D, Blaževičienė A. Patients' health literacy and health behaviour assessment in primary health care: evidence from a cross-sectional survey. BMC Prim Care 2022;23(1):223. doi: 10.1186/s12875-022-01809-5.

[3] Barnabe C, Chomistek K, Luca N, Hazlewood G, Barber CEH, Steiman A, et al. National priorities for high-quality rheumatology transition care for youth in Canada. J Rheumatol 2021;48(3):426–33. doi: 10.3899/JRHEUM.200790.

[4] McDonagh JE, Farre A. Transitional care in rheumatology: a review of the literature from the past 5 years. Curr Rheumatol Rep 2019;21(10):57. doi: 10.1007/s11926-019-0855-4.

[5] Cramm JM, Strating MMH, Nieboer AP. The role of team climate in improving the quality of chronic care delivery: a longitudinal study among professionals working with chronically ill adolescents in transitional care programmes. BMJ Open 2014;4(5):e005369. doi: 10.1136/bmjopen-2014-005369.

[6] National Alliance to Advance Adolescent Health. Got Transition program [Internet]. Available from: https://www.gottransition.org/. Accessed November 14, 2024.

[7] Cox J, Lyman B, Anderson M, Prothero MM. Improving transition care: a transition toolkit implementation project. J Nurse Pract 2023;19(3):104475. doi: 10.1016/j.nurpra.2022.10.004.

[8] Overbury RS, Huynh K, Bohnsack J, Frech T, Hersh A. A novel transition clinic structure for adolescent and young adult patients with childhood onset rheumatic disease improves transition outcomes. Pediatr Rheumatol Online J 2021;19(1):164. doi: 10.1186/s12969-021-00651-w.

[9] Thomsen EL, Esbensen BA, Hanghøj S, Hansson H, Boisen KA. Development of a complex intervention to support parents of adolescents with chronic illness transferring from pediatrics to adult care (ParTNerSTEPs). BMC Health Serv Res 2022;22(1):485. doi: 10.1186/s12913-022-07888-5.

[10] National Alliance to Advance Adolescent Health. Got transition: six core elements of health care transition [Internet]. Available from: https://www.got-transition.org/six-core-elements/. Accessed November 14, 2024.

[11] Zangi HA, Ndosi M, Adams J, Andersen L, Bode C, Boström C, et al. EULAR recommendations for patient education for people with inflammatory arthritis. Ann Rheum Dis 2015;74(6):954–62. doi: 10.1136/annrheumdis-2014-206807.

[12] Rausch Osthoff AK, Niedermann K, Braun J, Adams J, Brodin N, Dagfinrud H, et al. 2018 EULAR recommendations for physical activity in people with inflammatory arthritis and osteoarthritis. Ann Rheum Dis 2018;77(9):1251–60. doi: 10.1136/annrheumdis-2018-213585.

[13] Geenen R, Overman CL, Christensen R, Asenlöf P, Capela S, Huisinga KL, et al. EULAR recommendations for the health professional's approach to pain management in inflammatory arthritis and osteoarthritis. Ann Rheum Dis 2018;77(6):797–807. doi: 10.1136/annrheumdis-2017-212662.

[14] McDonagh JE, Farre A. Transitional care: time for a rethink? Nat Rev Rheumatol 2022;18(11):615–6. doi: 10.1038/s41584-022-00836-x.

[15] Pearce C, Newman S, Mulligan K. Illness uncertainty in parents of children with juvenile idiopathic arthritis. ACR Open Rheumatol 2021;3(4):250–9. doi: 10.1002/ACR2.11238.

[16] Hilderson D, Moons P, Van der Elst K, Luyckx K, Wouters C, Westhovens R. The clinical impact of a brief transition programme for young people with juvenile idiopathic arthritis: results of the DON'T RETARD project. Rheumatology (Oxford) 2016;55(1):133–42. doi: 10.1093/rheumatology/kev284.

[17] Courel-Ibañez J, Prieto-Moreno R, Briones-Vozmediano E, Ariza-Vega P, Angevare S, Anton J, et al. EULAR Points to Consider for patient education in physical activity and self-management of pain during transitional care. Ann Rheum Dis [Internet] 2024. doi: 10.1136/ard-2024-226448.

[18] Page MJ, McKenzie JE, Bossuyt PM, Boutron I, Hoffmann TC, Mulrow CD, et al. The PRISMA 2020 statement: an updated guideline for reporting systematic reviews. Syst Rev 2021;10(1):89. doi: 10.1186/s13643-021-01626-4.

[19] Cochrane Handbook for Systematic Reviews of Interventions. Wiley; 2019. doi: 10.1002/9781119536604.

[20] Noyes J, Booth A, Moore G, Flemming K, Tunçalp Ö, Shakibazadeh E. Synthesising quantitative and qualitative evidence to inform guidelines on complex interventions: clarifying the purposes, designs and outlining some methods. BMJ Glob Health 2019;4(Suppl 1):e000893. doi: 10.1136/bmjgh-2018-000893.

[21] Sterne JAC, Savović J, Page MJ, Elbers RG, Blencowe NS, Boutron I, et al. RoB 2: a revised tool for assessing risk of bias in randomised trials. BMJ 2019;366:l4898. doi: 10.1136/bmj.l4898.

[22] Hayden JA, van der Windt DA, Cartwright JL, Côté P, Bombardier C. Assessing bias in studies of prognostic factors. Ann Intern Med 2006;158(4):280–6.

[23] Downes MJ, Brennan ML, Williams HC, Dean RS. Development of a critical appraisal tool to assess the quality of cross-sectional studies (AXIS). BMJ Open 2016;6(12):e011458. doi: 10.1136/bmjopen-2016-011458.

[24] Rettig P, Athreya BH. Adolescents with chronic disease. Transition to adult health care. Arthritis Care Res 1991;4(4):174–80. doi: 10.1002/art.1790040407.

[25] Tucker LB, Cabral DA. Transition of the adolescent patient with rheumatic disease: issues to consider. Pediatr Clin North Am 2005;52(2):641–52. doi: 10.1016/j.pcl.2005.01.008.

[26] Miettunen P. The ins and outs of Canada's top transition clinics. CRAJ 2008;18(2):9–12.

[27] Guelber A. Life's transitions: Calgary's YARD clinic helps patients. Communications 2008;18(2):16–7.

[28] Shaw KL, Southwood TR, McDonagh JE, British Paediatric Rheumatology Group. User perspectives of transitional care for adolescents with juvenile idiopathic arthritis. Rheumatology (Oxford) 2004;43(6):770–8. doi: 10.1093/rheumatology/keh175.

[29] Shaw KL, Southwood TR, McDonagh JE, British Paediatric Rheumatology Group. Developing a programme of transitional care for adolescents with juvenile idiopathic arthritis: results of a postal survey. Rheumatology (Oxford) 2004;43(2):211–9. doi: 10.1093/rheumatology/keh018.

[30] McDonagh JE, Shaw KL, Southwood TR. Growing up and moving on in rheumatology: development and preliminary evaluation of a transitional care programme for a multicentre cohort of adolescents with juvenile idiopathic arthritis. J Child Health Care 2006;10(1):22–42.

[31] Robertson LP, McDonagh JE, Southwood TR, Shaw KL, British Society of Paediatric and Adolescent Rheumatology. Growing up and moving on. A multicentre UK audit of the transfer of adolescents with juvenile idiopathic arthritis from paediatric to adult centred care. Ann Rheum Dis 2006;65(1):74–80. doi: 10.1136/ard.2004.032292.

[32] McDonagh JE, Southwood TR, Shaw KL. British Society of Paediatric and Adolescent Rheumatology. The impact of a coordinated transitional care programme on adolescents with juvenile idiopathic arthritis. Rheumatology (Oxford) 2007;46(1):161–8. doi: 10.1093/rheumatology/kel198.

[33] Shaw KL, Southwood TR, McDonagh JE; British Society of Paediatric and Adolescent Rheumatology. Young people's satisfaction of transitional care in adolescent rheumatology in the UK. Child Care Health Dev. 2007;33(4):368-79. doi:10.1111/j.1365-2214.2006.00698.x

[34] Tattersall RS. The MAGICC and practical approach to rheumatology transition. Br J Hosp Med (Lond) 2012;73(10):552–7. doi: 10.12968/hmed.2012.73.10.552.

[35] Minden K, Niewerth M, Müther S. Berlin transition program: from adolescents to adults in rheumatology treatment. Z Rheumatol 2014;73(6):526–31. doi: 10.1007/s00393-014-1377-0.

[36] Hilderson D, Westhovens R, Wouters C, Van Der Elst K, Goossens E, Moons P. Rationale, design and baseline data of a mixed methods study examining the clinical impact of a brief transition programme for young people with juvenile idiopathic arthritis: the DON'T RETARD project. BMJ Open 2013;3(12):e003591. doi: 10.1136/bmjopen-2013-003591.

[37] Hilderson D, Eyckmans L, Van Der Elst K, Westhovens R, Wouters C, Moons P. Transfer from paediatric rheumatology to the adult rheumatology setting:

experiences and expectations of young adults with juvenile idiopathic arthritis. Clin Rheumatol 2013;32(5):575–83. doi: 10.1007/s10067-012-2135-9.

[38] Jensen PT, Karnes J, Jones K, Lehman A, Rennebohm R, Higgins GC, et al. Quantitative evaluation of a pediatric rheumatology transition program. Pediatr Rheumatol Online J 2015;13:17. doi: 10.1186/s12969-015-0013-0.

[39] Stringer E, Scott R, Mosher D, MacNeill I, Huber AM, Ramsey S, et al. Evaluation of a rheumatology transition clinic. Pediatr Rheumatol Online J 2015;13:22. doi: 10.1186/s12969-015-0016-x.

[40] Ammerlaan J, van Os-Medendorp H, Scholtus L, de Vos A, Zwier M, Bijlsma H, et al. Feasibility of an online and a face-to-face version of a self-management program for young adults with a rheumatic disease: experiences of young adults and peer leaders. Pediatr Rheumatol Online J 2014;12:10. doi: 10.1186/1546-0096-12-10.

[41] Ammerlaan JJ, Scholtus LW, Drossaert CH, van Os-Medendorp H, Prakken B, Kruize AA, et al. Feasibility of a website and a hospital-based online portal for young adults with juvenile idiopathic arthritis: views and experiences of patients. JMIR Res Protoc 2015;4(3):e102. doi: 10.2196/resprot.3952.

[42] Ammerlaan J, van Os-Medendorp H, de Boer-Nijhof N, Scholtus L, Kruize AA, van Pelt P, et al. Short term effectiveness and experiences of a peer guided web-based self-management intervention for young adults with juvenile idiopathic arthritis. Pediatr Rheumatol Online J 2017;15(1):75. doi: 10.1186/s12969-017-0201-1.

[43] Ammerlaan JW, van Os-Medendorp H, de Boer-Nijhof NC, Prakken B, Bijlsma JWJ, Kruize AA. The most important needs and preferences of patients for support from health care professionals: a reflective practice on (transitional) care for young adults with juvenile idiopathic arthritis. Patient Educ Couns 2017;100(10):1961–4. doi: 10.1016/j.pec.2017.03.018.

[44] Walter M, Hazes JM, Dolhain RJ, van Pelt P, van Dijk A, Kamphuis S. Development of a clinical transition pathway for adolescents in the Netherlands. Nurs Child Young People 2017;29(9):37–43. doi: 10.7748/ncyp.2017.e932.

[45] Walter M, Kamphuis S, van Pelt P, de Vroed A, Hazes JMW. Successful implementation of a clinical transition pathway for adolescents with juvenile-onset rheumatic and musculoskeletal diseases. Pediatr Rheumatol Online J 2018;16(1):50. doi: 10.1186/s12969-018-0268-3.

[46] McColl J, Semalulu T, Beattie KA, Alam A, Thomas S, Herrington J, et al. Transition readiness in adolescents with juvenile idiopathic arthritis and childhood-onset systemic lupus erythematosus. ACR Open Rheumatol 2021;3(4):260–5. doi: 10.1002/acr2.11237.

[47] Teh KL, Hoh SF, Chan SB, Gao X, Das L, Book YX, et al. Transition readiness assessment in adolescents and young adults with rheumatic diseases: the Singapore experience. Int J Rheum Dis 2022;25(3):344–52. doi: 10.1111/1756-185X.14277.

[48] Carandang K, Wells CK, Guglielmo D, Melcher K, Trimble M, Ardoin SP, et al. Adolescents' and young adults' recommendations for implementing healthcare transition in rheumatology: a mixed methods study. Arthritis Care Res (Hoboken) 2023;75(6):1228–37. doi: 10.1002/acr.24977.

[49] Chang JC, Sears C, Bitencourt N, Peterson R, Alperin R, Goh YI, et al. Implementation of rheumatology health care transition processes and adaptations to systems under stress: a mixed-methods study. Arthritis Care Res (Hoboken) 2023;75(3):689–96. doi: 10.1002/acr.24822.

[50] Batthish M. The TRACE Study: TRansition to Adulthood Through Coaching and Empowerment - A Pilot Randomized-Controlled Trial. Published 2022. https://clinicaltrial.be/fr/details/262090?per_page=100-&only_recruiting=0&only_eligible=0. Accessed June 12, 2024.

[51] Boeker LS, Kuemmerle-Deschner JB, Saur SJ, Klotsche J, Erbis G, Hansmann S. Health-related quality of life, continuity of care and patient satisfaction: long-term outcomes of former patients of the Tuebingen Transition Program (TTP) − a retrospective cohort study. Pediatr Rheumatol Online J 2022;20(1):121. doi: 10.1186/s12969-022-00776-6.

[52] García-Rodríguez F, Arana-Guajardo AC, Villarreal-Treviño AV, Negrete-López R, López-Rangel JA, Fortuna-Reyna BJ, et al. Design of a rheumatology transition clinic for a resource-constrained setting. Indian J Pediatr 2023;90(1):29–37. doi: 10.1007/s12098-022-04102-6.

[53] Nagra A, McGinnity PM, Davis N, Salmon AP. Implementing transition: ready steady go. Arch Dis Child Educ Pract Ed 2015;100(6):313–20. doi: 10.1136/archdischild-2014-307423.

[54] McDonagh JE, Minnaar G, Kelly K, O'Connor D, Shaw KL. Unmet education and training needs in adolescent health of health professionals in a UK children's hospital. Acta Paediatr 2006;95(6):715–9. doi: 10.1080/08035250500449858.

[55] Henderson CJ, Lovell DJ, Specker BL, Campaigne BN. Physical activity in children with juvenile rheumatoid arthritis: quantification and evaluation. Arthritis Care Res 1995;8(2):114–9. doi: 10.1002/art.1790080210.

[56] Bull FC, SS Al-Ansari, Biddle S, Borodulin K, Buman MP, Cardon G, et al. World Health Organization 2020 guidelines on physical activity and sedentary behaviour. Br J Sports Med 2020;54(24):1451–62. doi: 10.1136/bjsports-2020-102955.

[57] Nordal E, Rypdal V, Arnstad ED, Aalto K, Berntson L, Ekelund M, et al. Participation in school and physical education in juvenile idiopathic arthritis in a Nordic long-term cohort study. Pediatr Rheumatol Online J 2019;17(1):44. doi: 10.1186/s12969-019-0341-6.

[58] Schanberg LE, Anthony KK, Gil KM, Maurin EC. Daily pain and symptoms in children with polyarticular arthritis. Arthritis Rheum 2003;48(5):1390–7. doi: 10.1002/art.10986.

[59] Lim LSH, Ekuma O, Marrie RA, Brownell M, Peschken CA, Hitchon CA, et al. A population-based study of grade 12 academic performance in adolescents with childhood-onset chronic rheumatic diseases. J Rheumatol 2022;49(3):299–306. doi: 10.3899/jrheum.201514.

Epidemiology

The impact of population ageing on musculoskeletal disorders in 204 countries and territories, 1990-2021: global burden and healthcare costs

Shi-Yang Guan[1,2,3], Jin-Xin Zheng[4,5], Xin-Yu Feng[4,5], Shun-Xian Zhang[6], Shu-Zhen Xu[1,3], Peng Wang[7], Hong-Yan Cai[8], Hai-Feng Pan (ID)[1,3,*]

[1] Department of Epidemiology and Biostatistics, School of Public Health, Anhui Medical University, Hefei, Anhui, China

[2] Second Affiliated Hospital of Anhui Medical University, Hefei, Anhui, China

[3] Inflammation and Immune Mediated Diseases Laboratory of Anhui Province, Hefei, Anhui, China

[4] School of Global Health, Chinese Center for Tropical Diseases Research, Shanghai Jiao Tong University School of Medicine, Shanghai, China

[5] One Health Center, Shanghai Jiao Tong University-The University of Edinburgh, Shanghai, China

[6] Clinical Research Center, Longhua Hospital, Shanghai University of Traditional Chinese Medicine, Shanghai, China

[7] Teaching Center for Preventive Medicine, School of Public Health, Anhui Medical University, Hefei, Anhui, China

[8] Department of Nephrology, Anhui No.2 Provincial People's Hospital, Hefei, Anhui, China

ARTICLE INFO

ABSTRACT

Objectives: This study aims to quantify the impact of population ageing on the global burden and healthcare costs of musculoskeletal (MSK) disorders across 204 countries and territories from 1990 to 2021, stratified by geographic region, sociodemographic index (SDI), sex, and major MSK subcategories.

Methods: The global burden of MSK disorders attributed to population ageing was evaluated using decomposition analysis, while related healthcare costs were estimated through an extrapolation approach.

Results: Between 1990 and 2021, population ageing was the largest contributor to the increases in incident cases, prevalent cases, and disability-adjusted life-years (DALYs) in 33.3%, 37.7%, and 35.8% of countries and territories, respectively. Inverted U-shaped associations were observed between SDI and the proportions of incident cases, prevalent cases, and DALYs attributed to population ageing, with middle SDI countries exhibiting the highest proportions. Declines in incidence rates have partially offset the increase in incident cases due to population ageing globally. However, population ageing contributed more to the increases in prevalent cases and DALYs than increases in epidemiological rates. Males were more affected by population ageing globally, particularly in high and high-middle SDI countries, whereas females were more impacted in low-to-middle SDI countries. Osteoarthritis was the MSK disorder most influenced by population ageing globally, followed by gout and rheumatoid arthritis. In 2021, population ageing contributed US$96.0 billion to global healthcare costs for MSK disorders, equivalent to 0.10% of global gross domestic product.

*Correspondence to Prof Hai-Feng Pan.
E-mail address:* panhaifeng@ahmu.edu.cn (H.-F. Pan).
Handling editor Josef S. Smolen.

Conclusions: Over the past 3 decades, the global burden of MSK disorders attributed to population ageing has consistently increased. Public health strategies, tailored to SDI level, sex, and specific MSK subcategories, should not only enhance prevention efforts but also strengthen long-term management to mitigate the rising global burden and economic impact of MSK disorders driven by population ageing.

WHAT IS ALREADY KNOWN ON THIS TOPIC

- Population ageing has accelerated in recent decades, significantly contributing to the global burden of musculoskeletal (MSK) disorders.
- Despite extensive research on the global burden of MSK disorders, a critical gap remains in quantifying the net effect of population ageing, distinct from other concurrent drivers such as changes in epidemiological rates and population growth.

WHAT THIS STUDY ADDS

- In approximately one-third of countries and territories, population ageing has become the largest contributor to the increasing burden of MSK disorders.
- Inverted U-shaped associations were observed between the sociodemographic index (SDI) and the proportions of incident cases, prevalent cases, and disability-adjusted life-years (DALYs) attributed to population ageing, with middle SDI countries bearing the highest proportions.
- The decrease in incidence rates has partially offset the increase in incident cases driven by population ageing globally. However, population ageing contributed more to the increases in prevalent cases and DALYs than epidemiological rate increases.
- Males experience greater impact of population ageing globally, particularly in high and high-middle SDI countries. Females are more affected in low-to-middle SDI countries.
- Osteoarthritis is the most affected MSK disorder globally by population ageing, followed by gout and rheumatoid arthritis. In low SDI countries, neck pain is the most affected, while in high and high-middle SDI countries, gout is the most affected.
- In 2021, population ageing accounted for US$96.0 billion in global healthcare costs for MSK disorders, equivalent to 0.10% of the global gross domestic product, surpassing the costs attributed to common modifiable risk factors.

HOW THIS STUDY MIGHT AFFECT RESEARCH, PRACTICE OR POLICY

- This study provides timely evidence to inform targeted public health strategies and healthcare resource allocation to alleviate the global burden and economic impact of MSK disorders driven by population ageing and to promote healthier ageing worldwide.

INTRODUCTION

Over the past decades, rising life expectancy, driven by healthcare advancements and improved living standards, alongside declining fertility rates, has accelerated global population ageing [1]. According to the World Population Prospects 2024 by the United Nations, the global number of individuals aged 65 years and older is projected to double from 0.8 billion in 2024 to 1.6 billion by 2050, increasing their share of the total population from 10.2% to 16.4% [2]. This demographic transition presents unprecedented challenges to healthcare systems, as ageing populations face heightened risks of chronic diseases, functional decline, and disability [3]. Addressing these challenges requires both mitigating global burden and promoting healthy ageing, which focuses on maintaining functional ability and enhancing the quality of life in older adults [3].

Musculoskeletal (MSK) disorders, including low back pain, osteoarthritis (OA), neck pain (NP), gout, and rheumatoid arthritis (RA), are the leading causes of disability globally, contributing to 161.9 million disability-adjusted life-years (DALYs) in 2021 [4]. As populations age, the global burden of MSK disorders is expected to rise substantially due to their strong association with age-related degenerative processes, chronic inflammation, and long-term functional impairment [5,6]. Moreover, age-related factors such as sarcopenia, osteoporosis, and multimorbidity further exacerbate the severity of MSK disorders, which in turn increases healthcare demands and economic costs [5,6]. Despite extensive studies on the global burden and risk factors of MSK disorders [7−9], a critical knowledge gap remains in distinguishing the net effect of population ageing from other concurrent drivers, such as epidemiological shifts (eg, incidence and prevalence trends) and population growth. Without accurately quantifying these effects, it is difficult to develop targeted prevention and management strategies that effectively address the challenges posed by population ageing on MSK disorders.

To bridge this gap, we conducted a systematic analysis to comprehensively quantify the net impact of population ageing on the global burden and related healthcare costs of MSK disorders across 204 countries and territories from 1990 to 2021. This study disentangled the effects of population ageing from those of population growth and changes in age-specific epidemiological rates (eg, incidence, prevalence, and DALY rates), while accounting for geographic variation, sociodemographic factors, sex differences, and major MSK subcategories. These results offer essential evidence to guide targeted interventions aimed at alleviating the rising global burden and economic impact of MSK disorders in ageing populations and promoting healthier ageing worldwide.

METHODS

Data sources

The Global Burden of Diseases (GBD) 2021 study is a comprehensive global initiative led by the Institute for Health Metrics and Evaluation, in collaboration with researchers and institutions worldwide [4]. It aims to quantify the impact of 371 diseases and injuries on human health across 204 countries and territories from 1990 to 2021 [4]. The study utilises a wide array of data sources, including vital registration systems, surveys, censuses, and published population-based studies, to provide estimates of both fatal and nonfatal health outcomes, encompassing infectious and noncommunicable diseases, mental health conditions, and injuries [4]. As a key resource in global health research, GBD 2021 offers a robust framework for analysing global health dynamics, providing critical insights that inform policy decisions and strategies aimed at improving population health outcomes worldwide [4].

In this study, data on the global burden of MSK disorders were extracted from the GBD Results Tool, an interactive online platform that provides access to GBD 2021 estimates [4,10].

The incidence and prevalence of MSK disorders were estimated using the Bayesian metaregression tool DisMod-MR 2.1, which integrates data from various sources to yield consistent estimates [4,10]. Years lived with disability (YLDs) were calculated by multiplying the prevalence of each disorder by its associated disability weight, while years of life lost (YLLs) were determined by multiplying the number of deaths by standard life expectancy [4,10]. The sum of YLDs and YLLs provided the DALYs, which capture the overall burden of MSK disorders [4,10].

The 204 countries and territories are organised into 21 geographical regions, such as Western Europe, and further classified into 5 sociodemographic index (SDI) quintiles: low, low-middle, middle, high-middle, and high, based on an SDI score ranging from 0.0 (lowest development) to 1.0 (highest) [4]. More details on the case definitions and data sources for MSK disorders are available in Supplementary Table S1 and the related publications [4,8,10].

Decomposition method

To evaluate the impact of population ageing on the global burden of MSK disorders, we utilised a decomposition method that dissects changes in the number of incident cases, prevalent cases, and DALYs of MSK disorders into 3 distinct components: population ageing, population growth, and changes in age-specific rates [11,12]. This approach effectively mitigates potential inconsistencies that may arise from the selection of decomposition order and reference groups by systematically calculating the main effects and interactions of these components [11,12]. The decomposition method is grounded in the following equations [11,12]:

$$M_a = \sum_{i=1}^{20} N_1(s_{i2} - s_{i1})m_{i1}$$

$$M_p = \sum_{i=1}^{20} (N_2 - N_1)s_{i1}m_{i1}$$

$$M_m = \sum_{i=1}^{20} N_1 s_{i1}(m_{i2} - m_{i1})$$

$$I_{pa} = \sum_{i=1}^{20} (N_2 - N_1)(s_{i2} - s_{i1})m_{i1}$$

$$I_{pm} = \sum_{i=1}^{20} (N_2 - N_1)s_{i1}(m_{i2} - m_{i1})$$

$$I_{am} = \sum_{i=1}^{20} N_1(s_{i2} - s_{i1})(m_{i2} - m_{i1})$$

$$I_{pam} = \sum_{i=1}^{20} (N_2 - N_1)(s_{i2} - s_{i1})(m_{i2} - m_{i1})$$

The main effects of population ageing, population growth, and epidemiological rate changes are denoted as M_a, M_p, and M_m, respectively. Furthermore, the interactions among these components are captured in the terms I_{pa}, I_{pm}, I_{am}, and I_{pam} [11,12]. In this framework, m_{ij} represents the age-specific rate for the ith age group in year j, while s_{ij} reflects the proportion of the population within the same age group [11,12]. The population sizes for the 2 groups under comparison are labelled as $N1$ and $N2$ [11,12].

Through this structured methodology, we can effectively attribute the fluctuations in the incidence, prevalence, and DALYs directly to the impacts of population ageing, population growth, and changes in age-specific rates, as outlined below [11,12]:

$$A = M_a + 1/2 I_{am} + 1/2 I_{pa} + 1/3 I_{pam}$$

$$P = M_p + 1/2 I_{pm} + 1/2 I_{pa} + 1/3 I_{pam}$$

$$M = M_m + 1/2 I_{pm} + 1/2 I_{am} + 1/3 I_{pam}$$

Estimation of healthcare costs

To estimate the healthcare costs of MSK disorders attributed to population ageing, an extrapolation approach was adopted, which has been widely utilised in prior global economic evaluations of various noncommunicable diseases [13−15]. Specifically, the unit cost per MSK case in the United States was calculated as reference through dividing the total national expenditure on MSK-related healthcare by the number of prevalent MSK cases [16]. The U.S. MSK-related healthcare costs were then extrapolated to other countries and territories using a country-specific health spending ratio, defined as the ratio of per capita health expenditure in each country to that of the United States. Data on per capita health spending were obtained from the global health spending study [17]. Subsequently, the healthcare costs for each country were calculated through multiplying the number of prevalent MSK cases attributed to population ageing by the extrapolated per-case costs. All cost estimates were reported in 2021 U.S. dollars to ensure comparability across countries. Furthermore, the percentage of healthcare costs relative to gross domestic product (GDP) was calculated using GDP data from the World Health Organization Global Health Expenditure Database [18]. More details about the estimation of healthcare costs for MSK disorders attributed to population ageing are presented in Supplementary Methods and prior studies [13−15].

Statistical analysis

The decomposition analysis quantified both the absolute and relative contributions of population growth, population ageing, and epidemiological rate changes to the variations in incident cases, prevalent cases, and DALYs for MSK disorders from 1990 to each subsequent year through 2021 [11,12]. Absolute contributions were expressed as the numbers of incident cases, prevalent cases, and DALYs attributed to each component [11,12]. In contrast, relative contributions (attributed proportions) were calculated as the percentage of these attributed numbers relative to the total numbers in 1990 [11,12]. A positive contribution indicated an increase in incident cases, prevalent cases, and DALYs, while a negative contribution reflected a decrease [11,12].

For locations where population ageing made positive contributions, ratios (R) between the numbers of incident cases, prevalent cases, and DALYs attributed to epidemiological rate changes and those attributed to population ageing were calculated, to assess their comparative contributions [11,12]. An $R < −1$ indicated that the reductions in incidence, prevalence, and DALY rates completely offset the increases due to population ageing, while $R = −1$ suggested that reductions due to epidemiological rate changes equally counterbalanced the increases due to population ageing. If $−1 < R < 0$, it indicated that epidemiological

rate reductions mitigated, but did not fully counteract, the impact of population ageing [11,12]. Conversely, if $0 < R < 1$, it implied that the increases in incidence, prevalence, and DALY rates were lower than the effects of population ageing, whereas $R = 1$ denoted an equal contribution. An $R > 1$ suggested that the increases in incidence, prevalence, and DALY rates had greater effects than population ageing [11,12].

The associations between sociodemographic levels and attributed proportions, as well as the percentage of healthcare costs relative to GDP, were assessed using locally estimated scatterplot smoothing regression and Spearman's rank correlation, respectively [8]. All statistical analyses and visualisations were conducted using R version 4.2.3.

Patient and public involvement

This study relied solely on publicly available data, and no direct patient or public involvement was incorporated throughout the research process. Patients and the public were not involved in the development of the research question, selection of outcome measures, study design, or data collection and analysis. They also did not contribute to the interpretation of findings or the preparation of the manuscript.

RESULTS

Global population ageing from 1990 to 2021

From 1990 to 2021, the global population aged 65 and over increased from 325.6 million to 770.2 million, with the proportion of this age group in the total population rising from 6.1% to 9.8% (Supplementary Fig S1, Supplementary Table S2). Among the 5 SDI quintiles, high SDI countries had the highest proportion of the population aged 65 and over in 2021 (18.7%), while low SDI countries had the lowest proportion (3.3%). Except for low SDI countries, where the proportion remained stable (3.2% in 1990 and 3.3% in 2021), all other SDI quintiles experienced significant increases in the population aged 65 and over. The most pronounced rise occurred in high SDI countries, where the proportion increased from 11.8% to 18.7% (Supplementary Fig S1, Supplementary Table S2). More details about the changes in the proportions of the population aged 65 and over at the regional and national levels are presented in Supplementary Figures S1 and S2 and Supplementary Tables S2 and S3.

The impact of population ageing on the incidence, prevalence, and DALYs of MSK disorders

In 2021, MSK disorders accounted for 367.2 million incident cases, 1686.6 million prevalent cases, and 161.9 million DALYs globally, reflecting increases of 151.9 million, 821.5 million, and 75.6 million compared with 1990, respectively (Fig 1). Between 1990 and 2021, population ageing contributed to increases of 59.4 million incident cases, 299.4 million prevalent cases, and 27.2 million DALYs globally, with attributed proportions of 27.6%, 34.6%, and 31.6%, respectively (Figs 1 and 2).

Globally and across all SDI quintiles, the proportions of incident cases, prevalent cases, and DALYs attributed to population ageing steadily rose during this period (Supplementary Fig S3; Supplementary Tables S4-S6). Middle SDI countries exhibited the highest proportions of incident cases, prevalent cases, and DALYs attributed to population ageing (45.0%, 57.9%, and 51.8%, respectively) (Fig 2; Supplementary Tables S4-S6). Notably, compared with population growth and epidemiological rate changes, population ageing had the greatest impact on the increases in incident cases, prevalent cases, and DALYs in high-middle SDI countries, and on the increase in prevalent cases in middle SDI countries (Supplementary Fig S4; Supplementary Tables S4-S6).

Across geographic regions, East Asia reported the highest proportions of increases in incident cases, prevalent cases, and DALYs attributed to population ageing (52.7%, 68.5%, and 59.4%, respectively) (Fig 2; Supplementary Tables S4-S6). Furthermore, population ageing was the largest contributor to the increases in incident cases, prevalent cases, and DALYs in East Asia, Central and Eastern Europe, and High-income Asia Pacific, and to the increases in prevalent cases and DALYs in Western Europe (Supplementary Fig S4; Supplementary Tables S4-S6).

From 1990 to 2021, population ageing contributed to the increases in incident cases, prevalent cases, and DALYs in 95.6%, 94.6%, and 95.6% (195, 193, and 195/204) of countries and territories, respectively (Supplementary Figs S5-S7; Supplementary Tables S7-S9). Of these, the United Arab Emirates showed the highest attributed proportions for incident cases, prevalent cases, and DALYs (143.6%, 196.9%, and 173.4%, respectively). Furthermore, across 204 countries and territories, SDI showed inverted U-shaped associations with the attributed proportions of incident cases, prevalent cases, and DALYs, peaking in middle SDI countries (Fig 3). Notably, in 33.3%, 37.7%, and 35.8% (68, 77, and 73/204) of countries and territories, population ageing was the largest driver behind the increases in
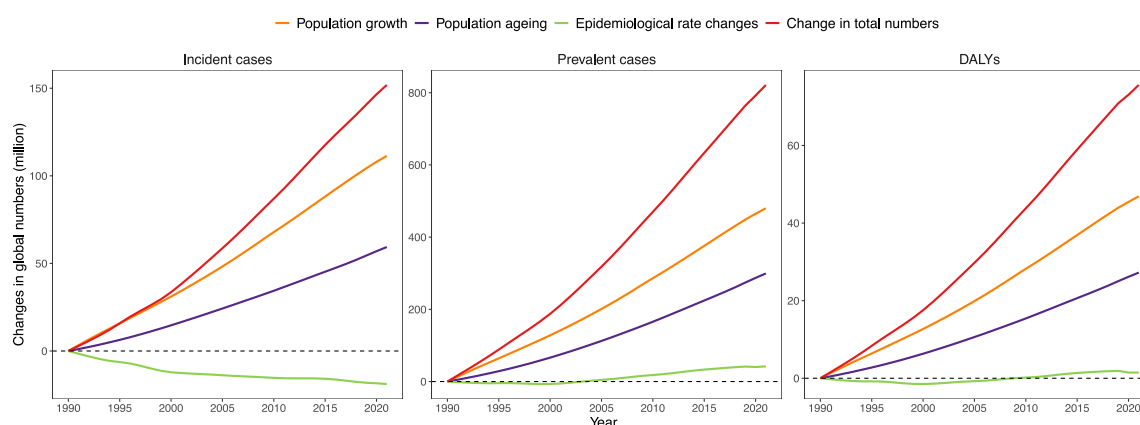

Figure 1. Changes in global numbers of incident cases, prevalent cases, and DALYs for MSK disorders attributed to population ageing, population growth, and epidemiological rate changes, 1990-2021. DALYs, disability-adjusted life-years; MSK, musculoskeletal.
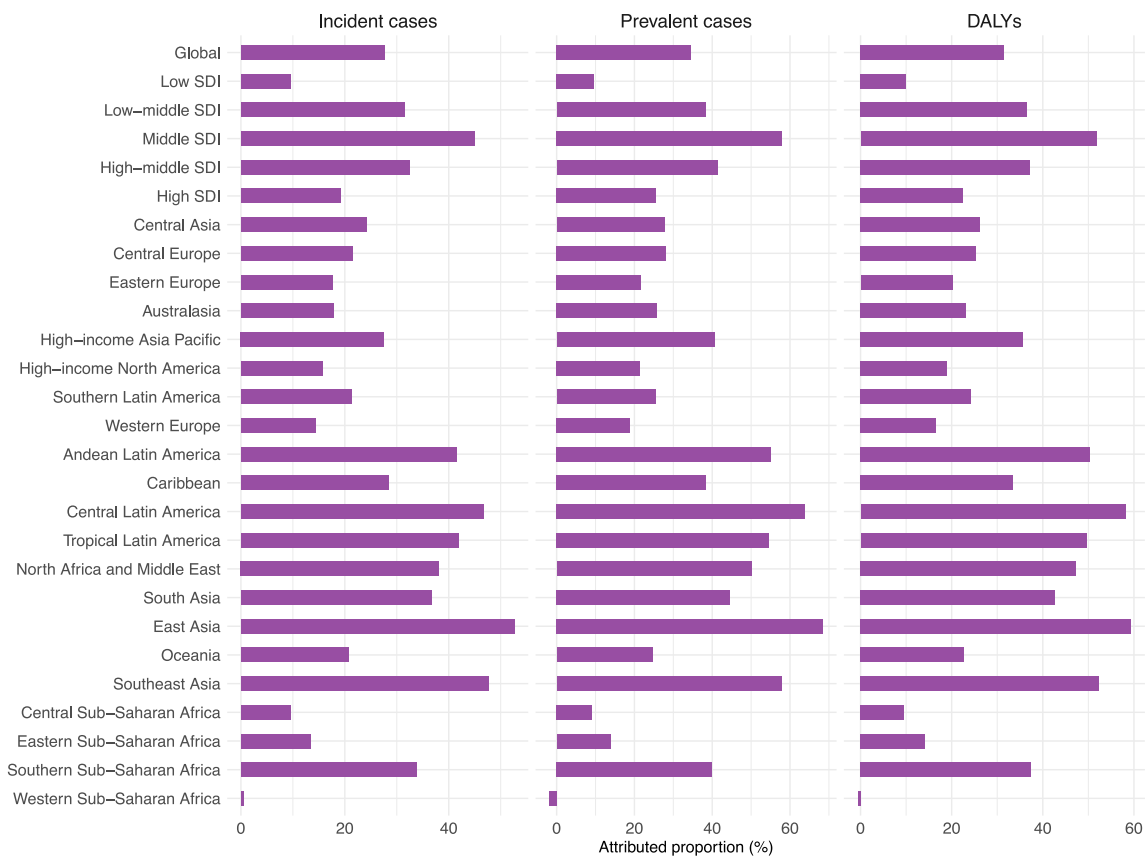
Figure 2. Proportions of incident cases, prevalent cases, and DALYs for MSK disorders attributed to population ageing globally and by SDI and geographic regions, 1990-2021. DALYs, disability-adjusted life-years; MSK, musculoskeletal; SDI, sociodemographic index.

incident cases, prevalent cases, and DALYs, respectively (Fig 4; Supplementary Figs S8 and S9; Supplementary Tables S7-S9).

Comparative contributions of changes in incidence, prevalence, and DALY rates vs population ageing

Between 1990 and 2021, the reduction in incidence rate led to a decrease of 18.9 million incident cases of MSK disorders globally, while increases in prevalence and DALY rates contributed to increases of 42.0 million prevalent cases and 1.5 million DALYs (Fig 1). Globally and across SDI quintiles, reductions in incidence rates partially offset the increases in incident cases driven by population ageing ($-1 < R < 0$), especially in low SDI countries ($R = -0.57$) (Supplementary Fig S10; Supplementary

Table S4). However, compared with the increases in prevalence and DALY rates, population ageing contributed more to the increases in prevalent cases and DALYs ($0 < R < 1$), particularly in high-middle SDI countries for prevalent cases ($R = 0.08$) and in middle SDI countries for DALYs ($R = 0.10$) (Supplementary Fig S10; Supplementary Tables S5 and S6).

Among the 12 geographic regions, reductions in incidence rates partially offset the increases in incident cases due to population ageing ($-1 < R < 0$), with Central Sub-Saharan Africa showing the strongest offsetting effect ($R = -0.37$) (Supplementary Fig S10; Supplementary Table S4). In contrast, population ageing contributed more to the increases in prevalent cases and DALYs than the increases in prevalence and DALY rates across most regions ($0 < R < 1$), with the most notable effects observed
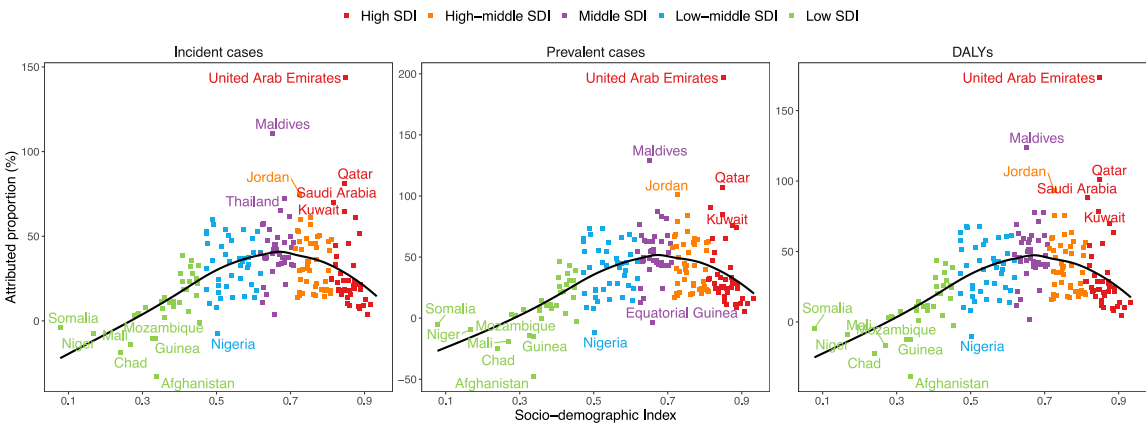

Figure 3. Association between SDI and proportions of incident cases, prevalent cases, and DALYs for MSK disorders attributed to population ageing in 204 countries and territories. DALYs, disability-adjusted life-years; MSK, musculoskeletal; SDI, sociodemographic index.
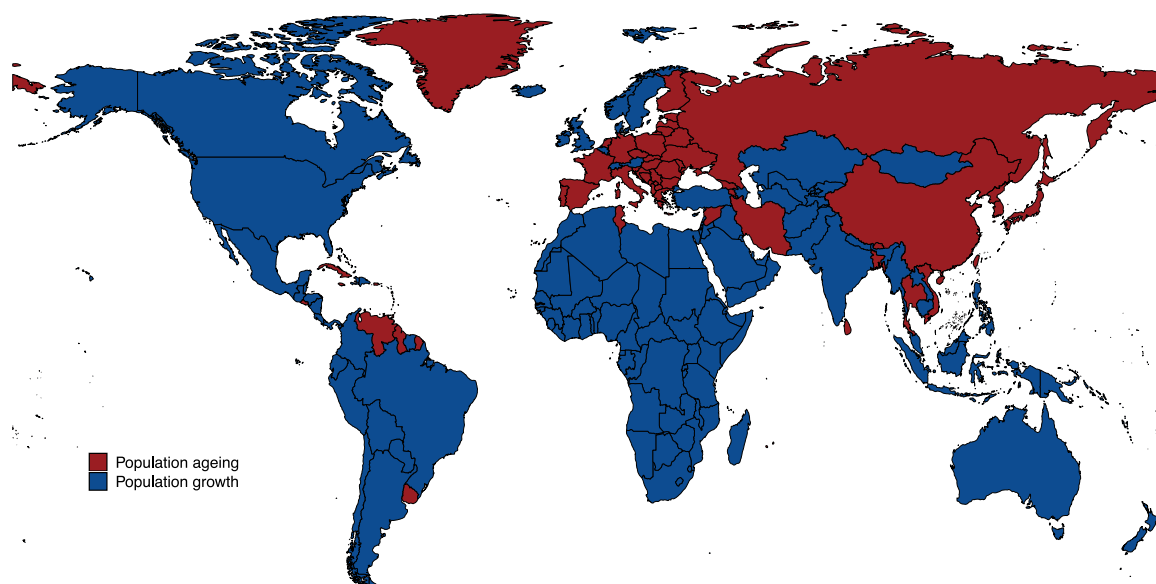
Figure 4. The largest contributor to the increase in DALYs for MSK disorders in 204 countries and territories, 1990-2021. DALYs, disability-adjusted life-years; MSK, musculoskeletal.

in Tropical Latin America (R = 0.03 and 0.02, respectively) (Supplementary Fig S10; Supplementary Tables S5 and S6).

At the national level, population ageing contributed more to the increases in incident cases, prevalent cases, and DALYs than increases in epidemiological rates in 47.5%, 88.7%, and 82.8% (97, 181, and 169/204) of countries and territories, respectively ($0 < R < 1$) (Fig 5; Supplementary Figs S11 and S12; Supplementary Tables S7-S9). Conversely, in 46.1%, 3.4%, and 8.8% (94, 7, and 18/204) of countries and territories, reductions in epidemiological rates partially offset the increases in incident cases, prevalent cases, and DALYs attributed to population ageing ($−1 < R < 0$), with Denmark exhibiting the strongest offsetting effect (R = −0.93, −0.29, and −0.43, respectively) (Fig 5; Supplementary Figs S11 and S12; Supplementary Tables S7-S9).

The impact of population ageing on incidence, prevalence, and DALYs by sex disparities

Over the past 30 years, males generally exhibited higher proportions of incident cases, prevalent cases, and DALYs attributed to population ageing than females globally, particularly in high and high-middle SDI countries (Fig 6; Supplementary Table S10). However, in low-to-middle SDI countries, females exhibited higher proportions attributed to population ageing (Fig 6; Supplementary Table S10).

At the regional level, males exhibited higher proportions of incident cases, prevalent cases, and DALYs attributed to population ageing across most regions, except in Andean Latin America, the Caribbean, South Asia, East Asia, and Eastern, Southern,
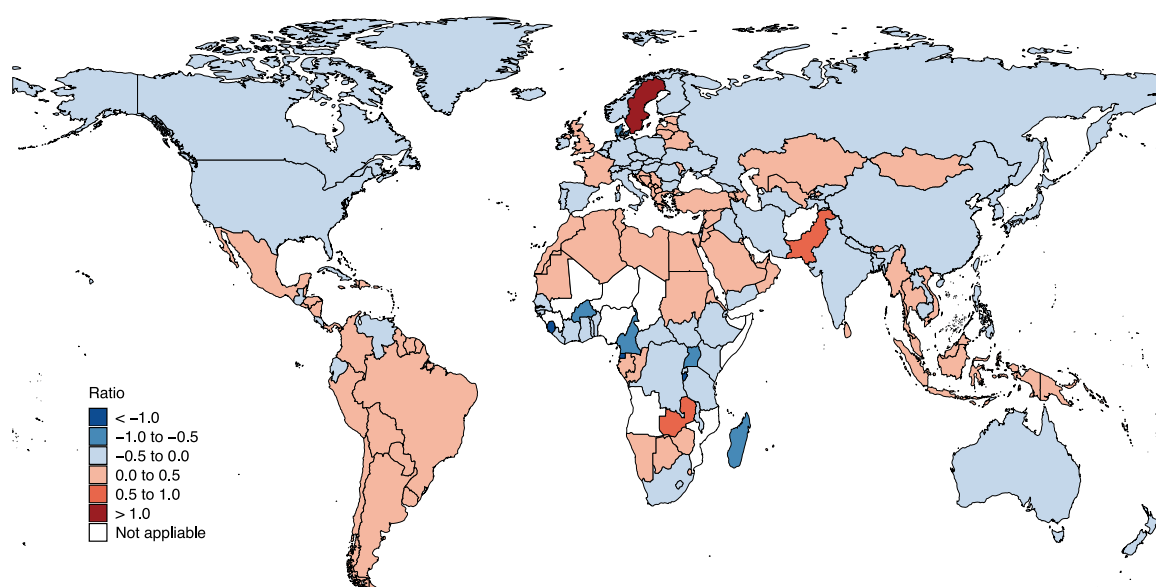

Figure 5. Ratios between the numbers of incident cases attributed to incidence rate changes and those attributed to population ageing in 204 countries and territories, 1990-2021. 'Not applicable' indicates population deageing associated decreases in incident cases.
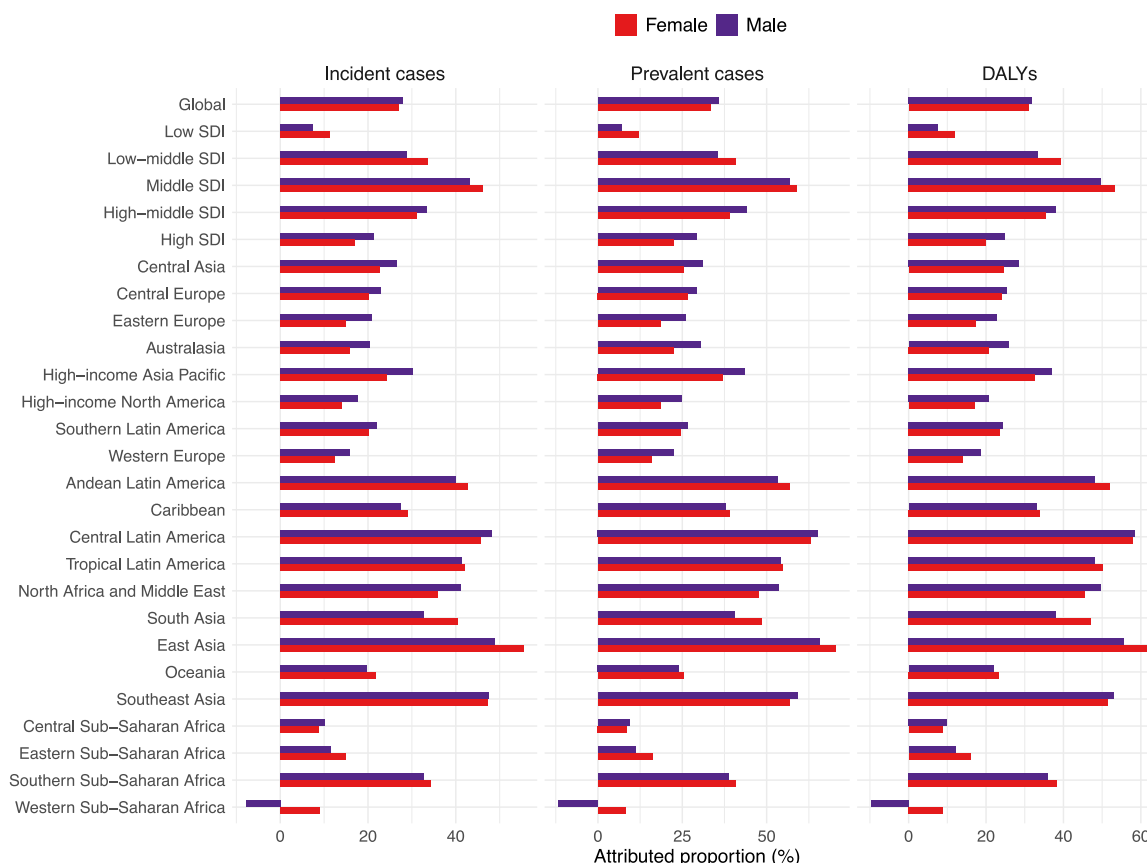
Figure 6. Sex differences in the proportions of incident cases, prevalent cases, and DALYs for MSK disorders attributed to population ageing globally and by SDI quintiles and geographic regions, 1990-2021. DALYs, disability-adjusted life-years; MSK, musculoskeletal; SDI, sociodemographic index.

and Western Sub-Saharan Africa, where females showed higher proportions (Fig 6; Supplementary Table S10). At the national level, males showed higher proportions of incident cases, prevalent cases, and DALYs attributed to population ageing in 58.8%, 59.8%, and 54.4% (120, 122, and 111/204) of countries and territories (Supplementary Figs S13-S15; Supplementary Table S11).

The impact of population ageing on incidence, prevalence, and DALYs by MSK subcategories

Between 1990 and 2021, among major MSK subcategories, OA was the most affected by population ageing globally, with attributed proportions of 49.4%, 60.9%, and 61.3% for incident cases, prevalent cases, and DALYs, respectively, followed by gout (49.2%, 56.7%, and 55.0%) and RA (29.7%, 44.2%, and 44.7%) (Supplementary Fig S16; Supplementary Table S12). For all other MSK subcategories, the attributed proportions were below 30% (Supplementary Fig S16; Supplementary Table S12).

Across most SDI quintiles, OA was the most affected MSK disorder by population ageing. However, NP was the most impacted in low SDI countries, with attributed proportions of 11.7%, 11.6%, and 11.7% for incident cases, prevalent cases, and DALYs, respectively (Supplementary Fig S16; Supplementary Table S12). Moreover, in high and high-middle SDI countries, gout was the most influenced for incident cases (38.8% and 58.4%, respectively) (Supplementary Fig S16; Supplementary Table S12).

Across most geographic regions, OA was the most impacted MSK disorder by population ageing. However, gout was the most impacted in Southern Latin America, South Asia, Europe, and Australasia for incident cases, as well as in High-income

North America and Australasia for prevalent cases (Supplementary Fig S16; Supplementary Table S12). Moreover, RA was the most affected in Central Sub-Saharan Africa for incident cases, as well as in Central Asia for prevalent cases and DALYs (Supplementary Fig S16; Supplementary Table S12).

At the national level, OA was the most affected by population ageing in 61.3%, 70.1%, and 72.1% (125, 143, and 147/204) of countries and territories for incident cases, prevalent cases, and DALYs, respectively (Fig 7; Supplementary Figs S17 and S18; Supplementary Table S13). Furthermore, gout was the most impacted in 25.0% (51/204) of countries and territories for incident cases. In contrast, all other MSK subcategories were the most affected in approximately 10% or fewer countries and territories (Fig 7; Supplementary Figs S17 and S18; Supplementary Table S13).

Healthcare costs for MSK disorders attributed to population ageing

Using 1990 as the baseline, population ageing contributed to US$96.0 billion in global healthcare costs for MSK disorders in 2021, accounting for 0.10% of global GDP. Across the 5 SDI quintiles, high SDI countries exhibited the highest healthcare costs (US$65.6 billion) and the greatest proportion of costs relative to GDP (0.12%). Among geographic regions, high-income North America reported the highest expenditure (US$37.6 billion), while the Caribbean had the highest percentage relative to GDP (0.19%). (Supplementary Figs S19 and S20; Supplementary Table S14).

At the national level, the United States had the highest healthcare costs (US$35.3 billion), while Cuba showed the highest cost proportion relative to GDP (0.31%) (Fig 8;
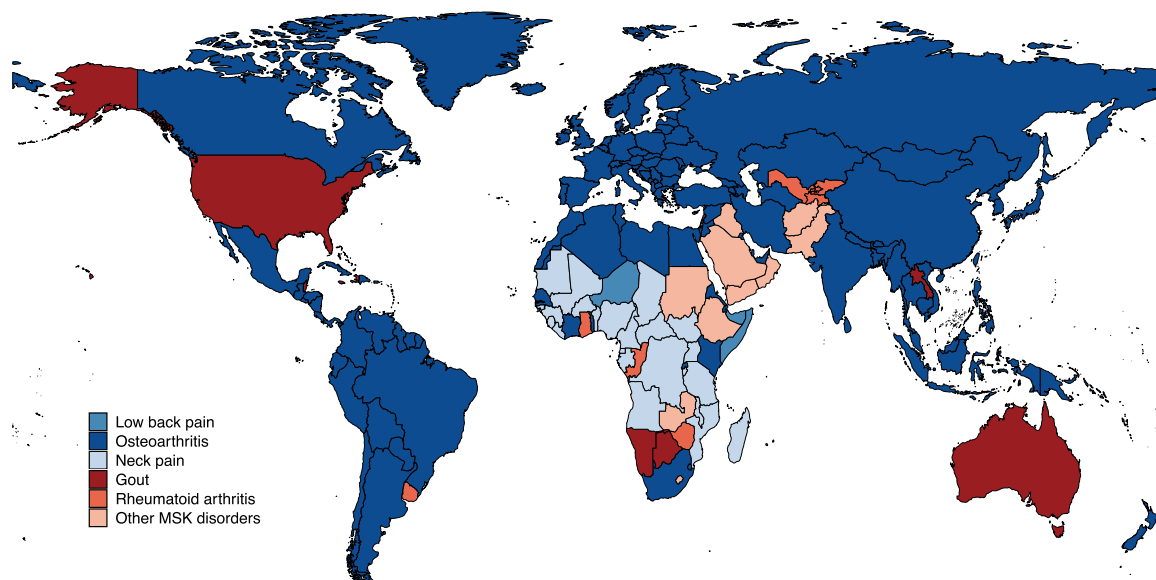
Figure 7. Predominant MSK category with the highest proportion of DALYs attributed to population ageing in 204 countries and territories, 1990-2021. DALYs, disability-adjusted life-years; MSK, musculoskeletal.
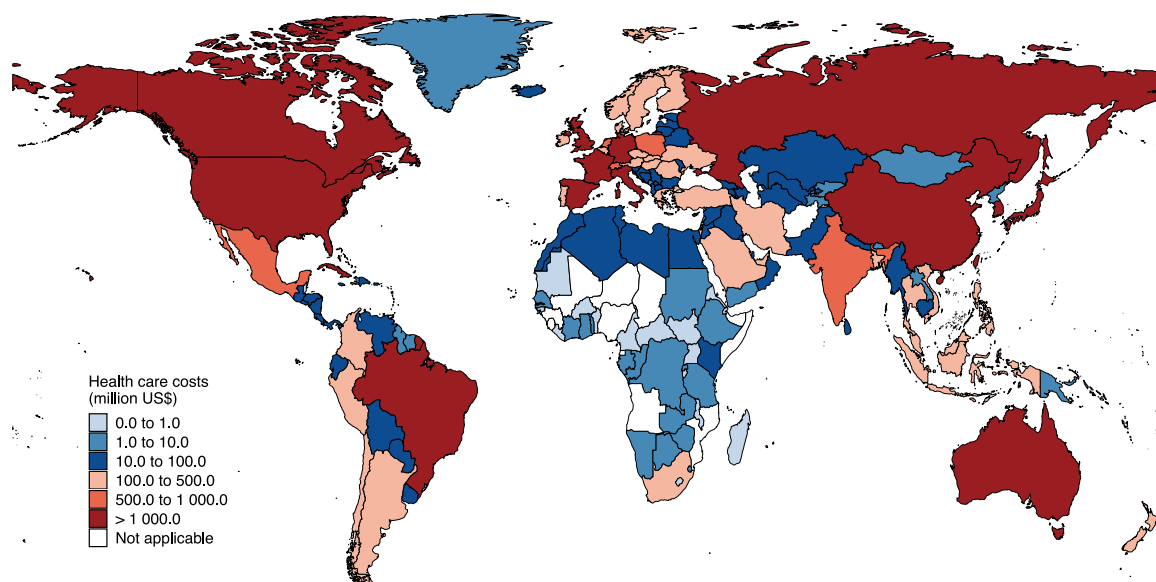

Figure 8. Healthcare costs for MSK disorders attributed to population ageing (million US$) in 204 countries and territories, 2021. 'Not applicable' indicates population deageing associated decreases in prevalent cases. MSK, musculoskeletal.

Supplementary Fig S21; Supplementary Table S15). Furthermore, there was a significantly positive correlation between SDI and the proportion of healthcare costs relative to GDP across 204 countries and territories (r_s = 0.688, $P < 0.001$) (Supplementary Fig S22).

To provide more policy-relevant insights, we further estimated the healthcare cost increases attributed to population ageing for MSK disorders over shorter time frames. Using 2011 and 2016 as alternative baselines, we assessed global healthcare costs across 204 countries and territories, stratified by geographic region and SDI quintile (Supplementary Figs S23-S30; Supplementary Tables S16-S19).

DISCUSSION

This study is the first comprehensive evaluation of the impact of population ageing on the global burden and healthcare costs

of MSK disorders across 204 countries and territories from 1990 to 2021. Our findings revealed that the global population aged 65 and over more than doubled during this period, with their share of the total population increasing from 6.1% to 9.8%. Furthermore, population ageing contributed to increasing proportions of incident cases, prevalent cases, and DALYs for MSK disorders globally and across all SDI quintiles. Notably, while high SDI countries had the largest proportion of elderly populations, middle SDI countries exhibited the highest relative burden of MSK disorders attributable to population ageing. This pattern likely reflects variations in the pace and context of demographic transitions. In middle SDI countries, the rate of population ageing has accelerated rapidly in recent decades, driven by gains in life expectancy and declining fertility rates [19]. However, many of these countries are still in the process of developing adequate healthcare infrastructure and chronic disease management systems, limiting their capacity to respond effectively to

the rising needs of ageing populations [19]. In contrast, high SDI countries, despite having larger proportions of elderly populations, often benefit from more advanced health systems and broader access to preventive care, which may help mitigate the impact of population ageing on MSK disorders [20]. These dynamics contribute to the observed inverted U-shaped association between SDI levels and the proportion of MSK burden attributable to population ageing, with the peak occurring in middle SDI countries. These findings highlight the need for SDI-specific public health strategies, particularly in middle SDI countries, where early interventions and targeted policies are urgently needed to alleviate the rising burden of MSK disorders driven by population ageing.

Encouragingly, our analysis showed that reductions in incidence rates have partially offset the rise in incident cases attributed to population ageing, especially in low SDI countries. This phenomenon is likely due to younger population structures in these countries, along with technological advancements that have alleviated traditionally high physical labour intensity and improved ergonomic conditions [8]. However, despite this progress, population ageing contributed more to the increases in prevalent cases and DALYs than epidemiological rate increases. This highlights the need not only for enhanced prevention efforts but also for improved long-term management strategies to alleviate the growing burden of MSK disorders attributed to population ageing.

At the national level, 46.1% of countries and territories experienced only partial offsets in incident cases due to declining incidence rates, while 88.7% and 82.8% of countries showed greater contributions of population ageing to the increases in prevalent cases and DALYs than those of epidemiological rate changes. In this context, valuable lessons could be drawn from countries like Denmark, which has significantly mitigated the adverse impact of population ageing through reductions in incidence, prevalence, and DALY rates. The approaches and policies implemented in Denmark, including a robust universal healthcare system, proactive early intervention strategies, and comprehensive rehabilitation services, could serve as models for other countries to address the escalating burden of MSK disorders in ageing populations [21].

Although the prevalence of MSK conditions is generally higher among females [7−9], our analysis showed that males experienced a greater relative impact of population ageing globally, particularly in high and high-middle SDI countries. In contrast, females were more affected in low-to-middle SDI countries. Beyond genetic and biological factors, these disparities likely reflect variations in demographic trends, behavioural risk exposures, and healthcare access. In high-income countries, where MSK disorders are most prevalent, the life expectancy gap between males and females has narrowed in recent decades, declining from 6.85 years in 1990 to 5.64 years in 2021 [2]. As more men in these countries reach older ages, their cumulative exposure to MSK-related risks increases, magnifying the ageing-related burden. By contrast, life expectancy for women in these countries has plateaued at consistently high levels [2], potentially leading to a 'ceiling effect', whereby further gains in longevity no longer translate into proportional increases in MSK burden. Moreover, men, particularly in high and high-middle SDI countries, are more likely to engage in physically demanding occupations and to smoke or consume alcohol, all of which are established risk factors for MSK disorders [8,22]. Conversely, in low-to-middle SDI countries, women often face greater health inequities, such as limited access to healthcare and higher prevalence of undernutrition, which could increase their vulnerability to age-related MSK disorders [23,24]. Taken together, the narrowing sex gap in life expectancy and cumulative exposure to MSK-related risk factors, particularly in high-income countries, likely explain the greater ageing-related burden among males, despite their lower baseline MSK prevalence.

Among major MSK subcategories, OA was the most affected by population ageing globally, followed by gout and RA. This is likely due to their strong association with ageing-related physiological changes, compounded by the rising prevalence of risk factors such as obesity and smoking over the past 3 decades [25,26]. However, in low SDI countries, NP was the MSK disorder most affected by population ageing. This finding is likely driven by the higher prevalence of labour-intensive industries, where prolonged physical strain, high work intensity, and poor occupational conditions contribute significantly to NP onset [27]. Additionally, in high and high-middle SDI countries, gout was the most affected MSK disorder for incident cases, likely linked to higher consumption of purine-rich foods, rising obesity rates, and declining physical activity levels [28]. These findings underscore the importance of developing public health strategies tailored to sex disparities and specific MSK subcategories in alleviating the growing burden of MSK disorders as population ageing accelerates.

Previous studies have shown that high body mass index, smoking, and occupational ergonomic factors accounted for US $60.5 billion, US$65.8 billion, and US$47.0 billion in global healthcare costs for MSK disorders in 2019, respectively [14,29,30]. Our study revealed that population ageing was responsible for US$96.0 billion in 2021, surpassing common modifiable risk factors as the leading driver of healthcare expenditures for MSK disorders. Therefore, in addition to mitigating modifiable risk factors, resource allocation strategies should place greater emphasis on addressing the health system challenges posed by population ageing. Notably, while middle SDI countries exhibited the greatest proportional burden of MSK disorders due to population ageing, high SDI countries incurred the highest absolute and relative healthcare costs. These results highlight the need to balance disease burden reduction with long-term economic sustainability. High SDI countries should prioritise cost-effective interventions to promote value-based healthcare, whereas middle SDI countries should seek diverse resources to expand affordable services amid demographic transitions.

This study has 3 significant strengths. First, it is the first comprehensive investigation assessing the impact of population ageing on the global burden and healthcare costs of MSK disorders across 204 countries and territories from 1990 to 2021, stratified by geographic regions, SDI, sex, and MSK subcategories. Second, the contribution of epidemiological rate changes was compared with population ageing, providing valuable insights into the potential benefits of strengthening both prevention and management efforts. By understanding how these factors interact, the findings could inform the development of targeted public health strategies that focus on early interventions, improved management, and policy reforms tailored to population ageing. Furthermore, traditional decomposition approaches often yield inconsistent or conflicting results depending on the choice of decomposition order and reference group, but the method applied in this study overcomes these limitations, providing robust and reliable evidence [11,12].

However, this study has several limitations that should be acknowledged. First, there is a potential underestimation of uncertainty in locations with limited data on MSK disorders, which may affect the accuracy of disease burden estimates,

particularly in low-income countries [4]. Second, due to the chronic and often insidious onset of many MSK disorders, it is difficult to determine their exact timing of onset and diagnosis. Consequently, the GBD study estimates incidence through the DisMod-MR 2.1 model, which integrates sparse and heterogeneous data sources. While this method provides internally consistent estimates, the modelled nature of incidence introduces uncertainty, and the resulting trends should be interpreted with appropriate caution. Third, while population ageing is primarily driven by increases in life expectancy and changes in fertility rates, the methodology used in this study does not differentiate between these 2 mechanisms [11,12]. This limitation may hinder a more nuanced understanding of how each factor contributes to the global burden of MSK disorders. Fourth, we were unable to compute 95% CIs for our estimates due to the lack of access to full posterior distributions of data from the GBD 2021 study. Future research should aim to refine methodologies and enhance data quality to provide deeper insights into the drivers of population ageing and their impact on MSK disorders worldwide. Additionally, our findings indicate that a considerable proportion of the increase in the global burden of MSK disorders cannot be explained by population ageing alone, but rather reflects changes in age-specific epidemiological rates. Although our decomposition model does not explicitly incorporate risk factor exposures, modifiable risk factors such as obesity, injury, and physical inactivity likely contributed to these observed rate changes, particularly for conditions like OA [8,9]. Therefore, beyond adapting health systems to ageing populations, early preventive strategies targeting modifiable risk factors are essential to mitigate future burden and promote healthy ageing.

CONCLUSIONS

Over the past 3 decades, the global burden of MSK disorders attributed to population ageing has steadily increased, with middle SDI countries experiencing the most pronounced impact. In approximately one-third of countries and territories, population ageing has emerged as the largest contributor to the growing burden of MSK disorders. In 2021, it accounted for US$96.0 billion in global healthcare costs for MSK disorders, equivalent to 0.10% of global GDP. Public health strategies, tailored to sociodemographic levels, sex disparities, and specific MSK subcategories, should not only enhance prevention efforts but also strengthen long-term management to address the growing burden of MSK disorders driven by population ageing.

Competing interests

All authors declare they have no competing interests.

Acknowledgements

The authors appreciate the team of the Institute for Health Metrics and Evaluation, University of Washington for their outstanding work in the GBD 2021 study.

Contributors

S-YG and H-FP conceived the idea, designed and supervised the study, and drafted the manuscript. S-YG, J-XZ, X-YF, S-XZ, S-ZX, PW, and H-YC contributed to the acquisition, analysis, or interpretation of data. S-YG and J-XZ performed the statistical analysis. S-YG, J-XZ, PW, and H-FP revised the manuscript. All authors revised the report and approved the final version before submission. S-YG and H-FP are the guarantors and attest that all listed authors meet authorship criteria and that no others meeting the criteria have been omitted.

Funding

This study was supported by grants from the National Natural Science Foundation of China (82273710).

Patient consent for publication

Patient consent for publication: Not applicable.Not commissioned; externally peer reviewed.

Ethics approval

Informed consent and institutional review board approval were waived by the Medical Ethics Committee of Anhui Medical University because the data utilised in this study were publicly available and did not contain identifiable personal information.

Provenance and peer review

Not commissioned; externally peer reviewed.

Data availability statement

Data used in the analyses can be obtained from the Global Health Data Exchange Global Burden of Disease Results Tool (https://vizhub.healthdata.org/gbd-results).

Patient and public involvement

Patients and/or the public were not involved in the design, or conduct, or reporting, or dissemination plans of this research.

Supplementary materials

Supplementary material associated with this article can be found in the online version at doi:10.1016/j.ard.2025.08.002.

Orcid

Hai-Feng Pan: http://orcid.org/0000-0001-8218-5747

REFERENCES

[1] GBD 2019 Demographics Collaborators. Global age-sex-specific fertility, mortality, healthy life expectancy (HALE), and population estimates in 204 countries and territories, 1950-2019: a comprehensive demographic analysis for the Global Burden of Disease Study 2019. Lancet 2020;396(10258):1160–203. doi: 10.1016/S0140-6736(20)30977-6.

[2] United Nations Population Division. World population prospects 2024 [Internet]. [updated n.d.; cited 2025 Aug 27]. Available from: https://population.un.org/wpp/

[3] World Health Organization. Ageing and health [Internet]. [updated n.d.; cited 2025 Aug 27]. Available from:. https://www.who.int/news-room/fact-sheets/detail/ageing-and-health

[4] GBD 2021 Diseases and Injuries Collaborators. Global incidence, prevalence, years lived with disability (YLDs), disability-adjusted life-years (DALYs), and healthy life expectancy (HALE) for 371 diseases and injuries in 204 countries and territories and 811 subnational locations, 1990-2021: a systematic analysis for the Global Burden of Disease Study 2021. Lancet 2024;403 (10440):2133–61. doi: 10.1016/S0140-6736(24)00757-8.

[5] Blyth FM, Briggs AM, Schneider CH, Hoy DG, March LM. The global burden of musculoskeletal pain-where to from here? Am J Public Health 2019;109 (1):35–40.

[6] Briggs AM, Woolf AD, Dreinhöfer K, Homb N, Hoy DG, Kopansky-Giles D, et al. Reducing the global burden of musculoskeletal conditions. Bull World Health Organ 2018;96(5):366–8. doi: 10.2471/BLT.17.204891.

[7] Safiri S, Kolahi AA, Cross M, Hill C, Smith E, Carson-Chahhoud K, et al. Prevalence, deaths, and disability-adjusted life years due to musculoskeletal disorders for 195 countries and territories 1990-2017. Arthritis Rheumatol 2021;73(4):702–14. doi: 10.1002/art.41571.

[8] Guan SY, Zheng JX, Sam NB, Xu S, Shuai Z, Pan F. Global burden and risk factors of musculoskeletal disorders among adolescents and young adults in 204 countries and territories, 1990-2019. Autoimmun Rev 2023;22(8):103361. doi: 10.1016/j.autrev.2023.103361.

[9] Guan SY, Zheng JX, Zhang SX, Xu S, Shuai Z, Cai HY, et al. Global burden of musculoskeletal disorders in adults aged 50 and over, 1990-2021: risk factors and sociodemographic inequalities. J Cachexia Sarcopenia Muscle 2025;16 (4):e70008. doi: 10.1002/jcsm.70008.

[10] Chen SH, Tang Y, Musonye HA, Pan HF. Global burden of diseases dataset, methodology and its use in rheumatic and musculoskeletal diseases. Int J Rheum Dis 2024;27(12):e15439. doi: 10.1111/1756-185X.15439.

[11] Cheng X, Tan L, Gao Y, Yang Y, Schwebel DC, Hu G. A new method to attribute differences in total deaths between groups to population size, age structure and age-specific mortality rate. PLoS One 2019;14(5):e0216613. doi: 10.1371/journal.pone.0216613.

[12] Cheng X, Yang Y, Schwebel DC, Liu Z, Li L, Cheng P, et al. Population ageing and mortality during 1990-2017: a global decomposition analysis. PLoS Med 2020;17(6):e1003138. doi: 10.1371/journal.pmed.1003138.

[13] Ding D, Lawson KD, Kolbe-Alexander TL, Finkelstein EA, Katzmarzyk PT, van Mechelen W, et al. The economic burden of physical inactivity: a global analysis of major non-communicable diseases. Lancet 2016;388(10051):1311– 24. doi: 10.1016/S0140-6736(16)30383-X.

[14] Chen N, Fong DYT, Wong JYH. Health and economic outcomes associated with musculoskeletal disorders attributable to high body mass index in 192 countries and territories in 2019. JAMA Netw Open 2023;6(1):e2250674. doi: 10.1001/jamanetworkopen.2022.50674.

[15] Weng Q, Chen Q, Jiang T, Zhang Y, Zhang W, Doherty M, et al. Global burden of early-onset osteoarthritis, 1990-2019: results from the Global Burden of Disease Study 2019. Ann Rheum Dis 2024;83(7):915–25. doi: 10.1136/ard-2023-225324.

[16] Dieleman JL, Beauchamp M, Crosby SW, DeJarnatt D, Johnson EK, Lescinsky H, et al. Tracking US health care spending by health condition and county. JAMA 2025;333(12):1051–61. doi: 10.1001/jama.2024.26790.

[17] Global Burden of Disease 2020 Health Financing Collaborator Network. Tracking development assistance for health and for COVID-19: a review of development assistance, government, out-of-pocket, and other private spending on health for 204 countries and territories, 1990-2050. Lancet 2021;398 (10308):1317–43. doi: 10.1016/S0140-6736(21)01258-7.

[18] World Health Organization. WHO global health expenditure database [Internet]. [updated n.d.; cited 2025 Aug 27]. Available from: https://apps.who.int/nha/database/Select/Indicators/en

[19] Kämpfen F, Wijemunige N, Evangelista Jr. B. Aging, non-communicable diseases, and old-age disability in low- and middle-income countries: a challenge for global health. Int J Public Health 2018;63(9):1011–2. doi: 10.1007/s00038-018-1137-z.

[20] GBD 2019 Universal Health Coverage Collaborators. Measuring universal health coverage based on an index of effective coverage of health services in 204 countries and territories, 1990-2019: a systematic analysis for the Global Burden of Disease Study 2019. Lancet 2020;396(10258):1250–84. doi: 10.1016/S0140-6736(20)30750-9.

[21] Birk HO, Vrangbæk K, Rudkjøbing A, Krasnik A, Eriksen A, Richardson E, et al. Denmark: health system review. Health Syst Transit 2024;26(1):1–186.

[22] GBD 2020 Alcohol Collaborators. Population-level risks of alcohol consumption by amount, geography, age, sex, and year: a systematic analysis for the Global Burden of Disease Study 2020. Lancet 2022;400(10347):185–235. doi: 10.1016/S0140-6736(22)00847-9.

[23] Shibli H, Aharonson-Daniel L, Feder-Bubis P. Perceptions about the accessibility of healthcare services among ethnic minority women: a qualitative study among Arab Bedouins in Israel. Int J Equity Health 2021;20(1):117. doi: 10.1186/s12939-021-01464-9.

[24] Alem AZ, Yeshaw Y, Liyew AM, Tessema ZT, Worku MG, Tesema GA, et al. Double burden of malnutrition and its associated factors among women in low and middle income countries: findings from 52 nationally representative data. BMC Public Health 2023;23(1):1479. doi: 10.1186/s12889-023-16045-4.

[25] Zhou XD, Chen QF, Yang W, Zuluaga M, Targher G, Byrne CD, et al. Burden of disease attributable to high body mass index: an analysis of data from the Global Burden of Disease Study 2021. EClinicalMedicine 2024;76:102848. doi: 10.1016/j.eclinm.2024.102848.

[26] GBD 2019 Tobacco Collaborators. Spatial, temporal, and demographic patterns in prevalence of smoking tobacco use and attributable disease burden in 204 countries and territories, 1990-2019: a systematic analysis from the Global Burden of Disease Study 2019. Lancet 2021;397(10292):2337–60. doi: 10.1016/S0140-6736(21)01169-7.

[27] GBD 2021 Neck Pain Collaborators. Global, regional, and national burden of neck pain, 1990-2020, and projections to 2050: a systematic analysis of the Global Burden of Disease Study 2021. Lancet Rheumatol 2024;6(3):e142–55. doi: 10.1016/S2665-9913(23)00321-1.

[28] GBD 2021 Gout Collaborators. Global, regional, and national burden of gout, 1990-2020, and projections to 2050: a systematic analysis of the Global Burden of Disease Study 2021. Lancet Rheumatol. 2024;6(8):e507–17. doi: 10.1016/S2665-9913(24)00117-6.

[29] Chen N, Fong DYT, Wong JYH. Health and economic burden of low back pain and rheumatoid arthritis attributable to smoking in 192 countries and territories in 2019. Addiction 2024;119(4):677–85. doi: 10.1111/add.16404.

[30] Chen N, Fong DYT, Wong JYH. The global health and economic impact of low-back pain attributable to occupational ergonomic factors in the working-age population by age, sex, geography in 2019. Scand J Work Environ Health 2023;49(7):487–95. doi: 10.5271/sjweh.4116.

Images in rheumatology

What lies beneath early-onset disc degeneration?

Haijun Tian[1,2], Baozhi Ding [1], Zeming Zeng[2], Shichang Zhao[2,**], Jie Zhao[1,*]

[1] Shanghai Key Laboratory of Orthopaedic Implants, Department of Orthopaedic Surgery, Shanghai Ninth People's Hospital, Shanghai Jiao Tong University School of Medicine, Shanghai, China
[2] Department of Orthopaedics, Shanghai Sixth People's Hospital Affiliated to Shanghai Jiao Tong University School of Medicine, Shanghai, China

A 42-year-old man presented with a 2-year history of low back pain and a recent onset of left-sided radiculopathy. His physical examination was notable for a positive left femoral nerve stretch test and 4/5 muscle strength in the left quadriceps. Computed tomography of the lumbar spine revealed a calcified disc herniation at the L3/4 level, accompanied by an intradiscal gas phenomenon (Fig, A,B). Further characterisation with sagittal T1-weighted magnetic resonance imaging confirmed the calcified herniation at the L3/4 level, and a special finding was that the intervertebral discs demonstrated markedly increased
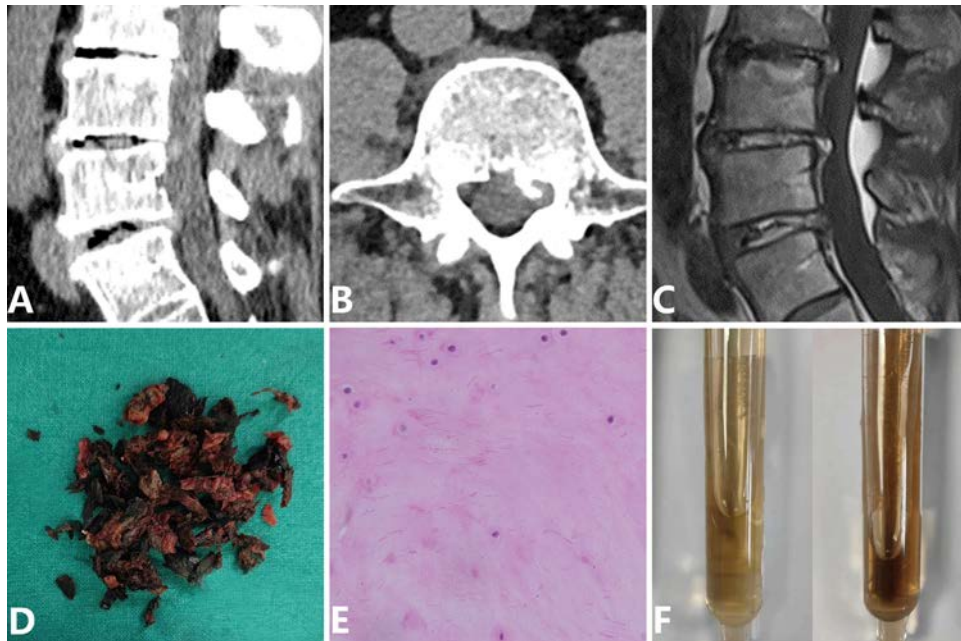

Figure. Alkaptonuria presenting with a calcified lumbar disc herniation and ochronotic pigment deposition. (A, B) Computed tomography showing a calcified herniated disc at L3/4 with an intradiscal gas phenomenon. (C) Sagittal T1-weighted magnetic resonance imaging confirming the calcified herniation at the L3/4 level. (D) Intraoperative photograph revealing a jet-black nucleus pulposus. (E) Histopathological examination of the disc material (haematoxylin and eosin stain). (F) Urine sample initially appears normal (left panel), then turns characteristically dark after 3 days of air exposure (right panel) due to homogentisic acid oxidation.

*Correspondence to Dr Jie Zhao, Department of Orthopaedic Surgery, Shanghai Ninth People's Hospital, Shanghai, China. **Correspondence to Dr Shichang Zhao, Department of Orthopaedics, Shanghai Sixth People's Hospital, 600 Yishan Road, Shanghai, China
E-mail addresses: zhaoshichang0404@163.com (S. Zhao), profzhaojie@126.com (J. Zhao).
Haijun Tian and Baozhi Ding contributed equally to this work.
Handling editor Josef S. Smolen.

T1-weighted signal intensity that surpassed the signal of adjacent vertebral marrow fat (Fig, C). During subsequent transforaminal lumbar interbody fusion, a striking finding was made: the nucleus pulposus was brittle and jet-black, resembling aged rubber (Fig, D). Histopathological examination of the excised disc material (haematoxylin and eosin stain) corroborated the diagnosis by revealing ochronotic pigment deposition within the degenerated disc tissue (Fig, E). The patient had no other remarkable systemic signs on initial presentation. What is the underlying diagnosis?

The answer is alkaptonuric ochronosis. The unusual intraoperative finding prompted a deeper investigation. A urine sample, though initially normal in colour, turned dark after being left to stand for 3 days (Fig, F). Genetic testing confirmed a homozygous mutation in the homogentisate 1,2-dioxygenase (*HGD*) gene. This case highlights that severe, early-onset disc degeneration with increased T1-weighted signal intensity that surpasses the signal of adjacent vertebral marrow fat, which may be attributed to the deposition of ochronotic pigment within the disc, is highly characteristic of ochronotic arthropathy and should raise suspicion for this diagnosis, even in the absence of classic scleral or cutaneous pigmentation [1−3].

Funding

None declared.

Competing interests

The authors declare no competing interests.

CRediT authorship contribution statement

Haijun Tian: Writing − review & editing, Writing − original draft, Data curation, Conceptualization. **Baozhi Ding:** Writing − review & editing, Writing − original draft, Data curation, Conceptualization. **Zeming Zeng:** Data curation. **Shichang Zhao:** Writing − review & editing, Conceptualization. **Jie Zhao:** Writing − review & editing, Conceptualization.

Patient consent for publication

Written informed consent was obtained from the patient for publication of this case and all accompanying images.

Ethics approval

Not applicable.

Provenance and peer review

Not commissioned; externally peer reviewed.

REFERENCES

[1] Bernardini G, Braconi D, Zatkova A, Sireau N, Kujawa MJ, Introne WJ, et al. Alkaptonuria. Nat Rev Dis Primers 2024;10(1):16. doi: 10.1038/s41572-024-00498-x.

[2] Chow WY, Norman BP, Roberts NB, Ranganath LR, Teutloff C, Bittl R, et al. Pigmentation chemistry and radical-based collagen degradation in alkaptonuria and osteoarthritic cartilage. Angew Chem Int Ed Engl 2020;59(29):11937–42. doi: 10.1002/anie.202000618.

[3] Di Matteo B, Marcacci M. Ochronosis. N Engl J Med 2021;384(5):461. doi: 10.1056/NEJMicm2025932.

Letter

A case of systemic lupus erythematosus with favourable pregnancy outcome following continued administration of anifrolumab during pregnancy

To the editor,

Systemic lupus erythematosus (SLE) is associated with an increased risk of adverse pregnancy outcomes (APOs), including preterm birth and preeclampsia, particularly in patients with active disease at conception [1]. Suppression of disease activity before and during pregnancy is crucial for improving pregnancy outcomes. Anifrolumab, a type I interferon (IFN) receptor antibody, has demonstrated efficacy in reducing SLE disease activity and glucocorticoid (GC) requirements in the treatment of uncontrolled lupus via the interferon pathway (TULIP)-1 and TULIP-2 trials as well as in real-world studies [2] and was approved in November 2021 in Japan. However, to the best of our knowledge, no reports exist on its use throughout pregnancy. This case

highlights the use of anifrolumab in an patient with SLE during pregnancy, with successful maternal and foetal outcomes.

Our patient was a 36-year-old Japanese woman diagnosed with SLE at the age of 7 based on the American College of Rheumatology 1997 classification criteria, including arthritis, lupus nephritis, lymphocytopenia, and positive antinuclear antibody and anti-DNA antibodies. After initial treatment with high-dose GC and tacrolimus (TAC), she was able to maintain low disease activity (systemic lupus erythematosus disease activity index 2000 = 2; low complement) on a GC dose of 9 mg/d of prednisolone (PSL), 2.5 mg/d of TAC, and 200 mg/d of hydroxychloroquine (HCQ). She was referred to our department at the age of 32 after a spontaneous abortion at 7 weeks' gestation. Following this, she conceived naturally and delivered a healthy female baby via caesarean section at 38 weeks due to breech presentation. In May X-1 year, minor disease flare was noted, with hypocomplementemia, lymphocytopenia, and anti-DNA antibody elevation (Fig). In November X-1 year, anifrolumab was initiated to reduce the GC dose after confirming no intention of pregnancy. PSL was gradually tapered to 5 mg/d by January X year. Unexpectedly, she conceived again in March X year. During pregnancy, she decided to continue using anifrolumab after careful discussions to ensure shared decision making. Ultrasounds confirmed normal foetal development and no evidence
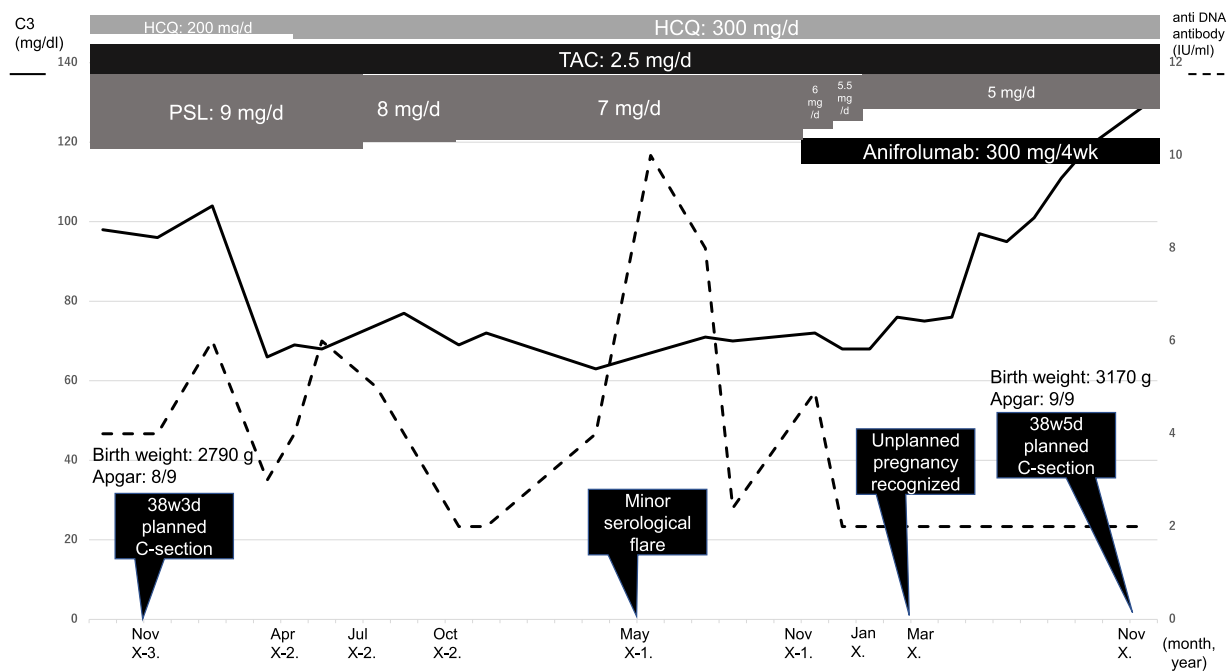

Figure. Clinical course of a systemic lupus erythematosus patient during pregnancy with exposure to anifrolumab. C-section, caesarean section; HCQ, hydroxychloroquine; PSL, prednisolone; SLE, systemic lupus erythematosus; TAC, tacrolimus.

of congenital heart block (CHB) although she was positive for anti-Sjögren's syndrome-related antigen A antibody. At 38 weeks and 5 days, the patient delivered a healthy 3170 g male baby via scheduled caesarean section. Apgar scores were 9 out of 10, and the newborn showed no birth defects, neonatal lupus, or CHB. Postpartum, both mother and child were stable. The clinical course from the first childbirth to the second under the use of anifrolumab is shown in the Figure.

Anifrolumab, a fully human IgG1 monoclonal antibody, is actively transported across the placenta via the foetal Fc receptor. Foetal exposure is expected to be minimal in early pregnancy and to increase progressively, reaching its peak near term. Animal studies in pregnant cynomolgus monkeys receiving anifrolumab showed no maternal, foetal, or postnatal toxicity. In clinical trials (TULIP-1, TULIP-2, and A phase II, randomized study to evaluate the efficacy and safety of MEDI-546 in subjects with systemic lupus erythematosus), limited pregnancy data revealed 20 exposures, with 1 spontaneous abortion, 1 preterm delivery, and 1 high-risk pregnancy (no details stated) [3]. However, real-world data on teratogenicity remain unavailable. Guidelines reflect this uncertainty. The 2022 to 2023 British Society for Rheumatology guideline offers no specific recommendation regarding anifrolumab use in pregnancy [4], whereas the 2024 European Alliance of Associations for Rheumatology recommendation advises its use only when no safer and effective alternatives are available [5].

In the present case, pregnancy was identified after the absolute critical period of organogenesis had passed (at 12 weeks' gestation). As disease activity was well controlled with anifrolumab and corticosteroids had been successfully tapered, continuation of anifrolumab was favoured. Through shared decision making, the patient opted against switching to pregnancy-compatible alternatives such as azathioprine or belimumab, and avoided the risks associated with re-escalating corticosteroid doses during pregnancy.

This case highlights the potential role of anifrolumab in maintaining disease control in pregnant patients with SLE while minimizing GC exposure. Elevated GC use during pregnancy has been associated with APOs, including preterm birth and premature rupture of membranes [6]. Moreover, previous studies have shown that pregnant women with SLE who develop complications often exhibit high IFN signatures throughout gestation [7]. Type I IFN signalling is also implicated in the pathogenesis of CHB, with increased IFN-response gene expression detected in affected foetal hearts [8]. Although purely theoretical and not evidence based at this stage, modulation of the IFN pathway by anifrolumab may offer additional benefits, including potential reduction in CHB risk.

In conclusion, we report, to our knowledge, for the first time, a pregnant woman with SLE successfully treated with anifrolumab throughout pregnancy, resulting in a healthy full-term newborn with no maternal or foetal complications.

Competing interests

None declared.

CRediT authorship contribution statement

Ayako Kitada: Writing − original draft, Data curation, Conceptualization. **Hiroto Tsuboi:** Writing − review & editing, Supervision. **Hiroshi Ebe:** Writing − review & editing, Data curation, Conceptualization. **Saori Abe:** Writing − review & editing. **Fumiyuki Shibasaki:** Writing − review & editing, Data curation. **Kotomi Murata:** Writing − review & editing, Data curation. **Moe Yamada:** Writing − review & editing. **Mami Yoshida:** Writing − review & editing. **Tomonori Hishinuma:** Writing − review & editing. **Fumina Kawashima:** Writing − review & editing. **Nana Uematsu:** Writing − review & editing. **Toshiki Sugita:** Writing − review & editing. **Masaru Shimizu:** Writing − review & editing. **Ayako Ohyama:** Writing − review & editing. **Hiromitsu Asashima:** Writing − review & editing. **Haruka Miki:** Writing − review & editing. **Yuya Kondo:** Writing − review & editing. **Isao Matsumoto:** Writing − review & editing, Supervision.

Patient consent for publication

Obtained.

Ethics approval

Not applicable.

Provenance and peer review

Not commissioned.

Orcid

Ayako Kitada: http://orcid.org/0000-0001-8031-7718
Hiroto Tsuboi: http://orcid.org/0000-0001-9067-0961
Hiroshi Ebe: http://orcid.org/0000-0003-0878-4017
Masaru Shimizu: http://orcid.org/0000-0001-6209-3239

REFERENCES

[1] Wind M, Fierro JJ, Bloemenkamp KWM, de Leeuw K, Lely AT, Limper M, et al. Pregnancy outcome predictors in systemic lupus erythematosus: a systematic review and meta-analysis. Lancet Rheumatol 2024;6(10):e667–83.

[2] Kubo S, Nakayamada S, Yoshikawa M, Miyazaki Y, Sakata K, Nakano K, et al. Peripheral immunophenotyping identifies three subgroups based on t cell heterogeneity in lupus patients. Arthritis Rheumatol 2017;69(10):2029–37.

[3] Tummala R, Abreu G, Pineda L, Michaels MA, Kalyani RN, Furie RA, et al. Safety profile of anifrolumab in patients with active SLE: An integrated analysis of phase II and III trials. Lupus Sci Med 2021 Feb 17;8(1):e000464.

[4] Russell MD, Dey M, Flint J, Davie P, Allen A, Crossley A, et al. British Society for Rheumatology guideline on prescribing drugs in pregnancy and breastfeeding: immunomodulatory anti-rheumatic drugs and corticosteroids. Rheumatology (Oxford) 2023;62(4):e48–88.

[5] Rüegg L, Pluma A, Hamroun S, Cecchi I, Perez-Garcia LF, Anderson PO, et al. EULAR recommendations for use of antirheumatic drugs in reproduction, pregnancy, and lactation: 2024 update. Ann Rheum Dis 2025;84(6):910–26.

[6] Okazaki Y, Taniguchi K, Miyamoto Y, Kinoshita S, Nakabayashi K, Kaneko K, et al. Glucocorticoids increase the risk of preterm premature rupture of membranes possibly by inducing ITGA8 gene expression in the amnion. Placenta 2022;128:73–82.

[7] Hong S, Banchereau R, Maslow BL, Guerra MM, Cardenas J, Baisch J, et al. Longitudinal profiling of human blood transcriptome in healthy and lupus pregnancy. J Exp Med 2019;216(5):1154–69.

[8] Clancy RM, Halushka M, Rasmussen SE, Lhakhang T, Chang M, Buyon JP. Siglec-1 macrophages and the contribution of IFN to the development of autoimmune congenital heart block. J Immunol 2019;202(1):48–55.

Ayako Kitada[1], Hiroto Tsuboi[1,*], Hiroshi Ebe[2], Saori Abe[1], Fumiyuki Shibasaki[1], Kotomi Murata[1], Moe Yamada[1], Mami Yoshida[1], Tomonori Hishinuma[1], Fumina Kawashima[1], Nana Uematsu[1], Toshiki Sugita[1], Masaru Shimizu[1], Ayako Ohyama[1], Hiromitsu Asashima[1], Haruka Miki[1], Yuya Kondo[1], Isao Matsumoto[1]

[1] Department of Rheumatology, Institute of Medicine, University of Tsukuba, Tsukuba-city, Ibaraki, Japan
[2] Department of Rheumatology, Ibaraki Seinan Medical Center Hospital, Sashima District, Ibaraki

*Correspondence to Dr Hiroto Tsuboi, Department of Rheumatology, Institute of Medicine, University of Tsukuba, 1-1-1 Tennodai, Tsukuba-city, Ibaraki 305-8575, Japan.
E-mail address: Hiroto-Tsuboi@md.tsukuba.ac.jp (H. Tsuboi).

Letter

Lidocaine-induced tear production in primary Sjögren's disease: neurologically induced lacrimation to broaden the horizon for treatment of ocular dryness?

Ocular dryness is a hallmark of patients with Sjögren's disease (SjD). Treatment remains largely symptomatic and is often inadequate, imposing a significant burden on patients [1]. Although inflammation is suggested to play a role in ocular dryness, the exact mechanisms remain obscure. Additionally, systemic anti-inflammatory therapies do not successfully alleviate ocular dryness.

In the recent RepurpSS-I trial, which tested the efficacy and safety of leflunomide−hydroxychloroquine combination therapy, we observed a significant decrease in systemic disease activity and robust anti-inflammatory responses, which were also without changes in ocular dryness (Fig, A) [2]. Surprisingly, as a serendipitous observation, we noted vigorous increased tear production in 12 patients who experienced partial transient facial nerve palsy (mean Schirmer score, affected side = 18.3 ± 4.05 mm vs non-palsy side = 6.42 ± 2.48 mm, $P = .002$) after a higher dose of local anaesthetic (lidocaine, 3.6 mL instead of 1.8 mL) during parotid biopsy procedures, irrespective of timepoint or treatment. Other ocular symptoms, apart from hyperlacrimation, were not observed. Multivariate analysis showed an increase in Schirmer score of ± 12.8 mm in the eyes with lidocaine-induced palsy compared with those in which no palsy occurred (see Fig, A-C and details in figure legend).

These results indicate the potential of drug-induced lacrimation via neurological pathways, which, to our knowledge, has not been observed previously. Such an effect was suggested upon systemic administration of pilocarpine, an agonist of muscarinic acetylcholine receptors that targets the parasympathetic nerves. However, meta-analysis did not confirm the efficacy on lacrimation, in some cases even showing contradictory results [3].

Lidocaine blocks facial signal conduction by inhibiting nerve fibre action potentials (inducing palsy). As a local anaesthetic, it mainly inhibits sensory neurons at low concentrations and motor neurons at higher doses, which typically reduces tear production rather than stimulates it, making it unlikely that lidocaine directly causes increased lacrimation. Tear secretion is primarily regulated through the parasympathetic, sympathetic, and sensory nervous systems. The lacrimal gland is mainly regulated through parasympathetic nerve fibres. The role of the sympathetic nervous system remains unclear and controversial [4,5]. However, it is generally believed that tear secretion is stimulated by parasympathetic nerve fibres and inhibited by sympathetic nerve fibres connected to the lacrimal gland. Therefore, the observed increase in lacrimation in our study could result from 1 of 2 pathways, leading to 2 hypotheses: increased stimulation of parasympathetic nerve fibres or reduced inhibition of sympathetic nerve fibres. Patients who experienced transient palsy received higher dosages of local anaesthetics (3.6 mL vs 1.8 ml) administered by 1 of the 2 maxillofacial surgeons performing the biopsies in our study (Fig, D). The first hypothesis suggests that lidocaine diffuses under the influence of gravity, reaches the superior cervical ganglion, blocks the sympathetic nerve pathway, and temporarily inhibits sympathetic inhibition of lacrimation. The second hypothesis involves pressure (ie, referred pain) from the higher dosage near the great auricular nerve. This pressure signals to the dorsal horn of the cervical spinal cord, but collaterals of these axons also end in the caudal subnucleus (sNc) of the spinal nucleus of the trigeminal nerve, resulting in a trigeminal parasympathetic reflex, similar to the pathophysiology of migraine [6]. Moreover, the sNc also corresponds with segmental innervation of the outermost so-called von Sölder dermatomes, which include the parotid and temporal areas, leading to referred pain from the neck to the head.

These hypotheses were tested by testing lidocaine diffusion on 2 head and neck specimens provided by our hospital's anatomy department. The maxillofacial surgeon, who also performed the biopsies during our study, mimicked the lidocaine injection using methylene blue dye (3.8 mL) instead of local anaesthetic, injected at the same location to observe fluid diffusion (Fig, D). The diffusion patterns indicated that both hypotheses were plausible (Fig, E).

These findings imply that ocular sicca may not be as irreversible as previously believed. Moreover, it suggests the future potential for drug-induced tearing through the modulation of neurological pathways. Further exploration of these pathways may reveal novel therapeutic options for SjD.
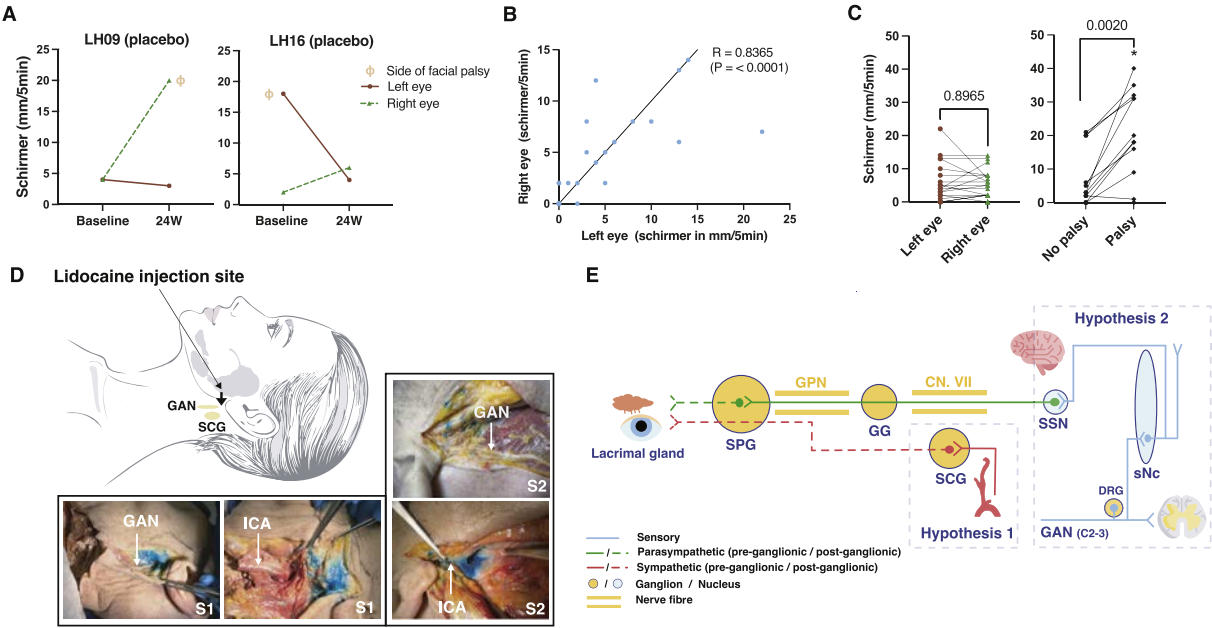
Figure. Lidocaine-induced tear production upon parotid biopsy: proposed neurological mechanisms of action. (A) Two representative donors in the placebo arm with lidocaine-induced palsy (φ) at baseline or at 24 weeks (W24). (B) A strong correlation (R) of left and right eye tear production was observed in non-palsy patients at baseline, indicating the normally observed coherence between tearing on both sides. (C) Left: Comparable lacrimation (Schirmer) of left and right eye in patients without palsy (n = 23). Right: Comparison between left/right eyes in palsy-affected patients. (D) Lidocaine injection site of a patient lying down when a parotid biopsy was performed by the craniofacial surgeon. Lidocaine diffuses dorsally due to gravity, potentially affecting the area surrounding the GAN or SPG. Left under and right: Four images of the experiment with 2 head specimens (labelled S1 and S2) to test the liquid (methylene blue, blue colour) diffusion. Different targeted areas were observed in the 2 head specimens; specimen 1 showed targeting of the GAN but no blue dye surrounding the ICA. In specimen 2, the blue dye did not surround the GAN but reached the deeper tissue layers and surrounded the superior cervical ganglion (SCG). (E) Two hypothesised mechanisms of action: 1. Reduced inhibition: Lidocaine injected in the parotid gland reaches the SCG via diffusion and leads to inhibition of the sympathetic nerves innervating the lacrimal gland. This leads to more activation of the parasympathetic nerves, inducing lacrimation; 2. Trigeminal parasympathetic reflex: Lidocaine affects the GAN by pressure or pain sensation, signalling the caudal part of the spinal nucleus and activating the parasympathetic pathway of lacrimation. CN. VII, facialis nerve; DRG, dorsal root ganglion; GAN, great auricular nerve; GC, geniculate ganglion; GPN, greater petrosal nerve; ICA, internal carotid artery; S1, specimen 1; S2, specimen 2; SCG, superior cervical ganglion; sNc, caudal part of spinal nucleus; SPG, sphenopalatine ganglion; SSN, superior salivatory nucleus.

Competing interests

All authors declare they have no competing interests.

Contributors

Data collection: EHMvdH. Data analysis: DR, EHMvdH. Data interpretation: DR, EHMvdH, RLAWB, HLL, JAGvR. Study design: HLL, JAGvR. Figures: DR, RLAWB, JAGvR. Supervision: RLAWB, HLL, JAGvR. Manuscript preparation: DR, Manuscript finalisation: DR, RLAWB, HLL, JAGvR.

Funding

This project was funded by ZonMw. The funder of this study had no role in the data collection, analysis, or writing of the report.

Patient consent for publication

Consent was obtained directly from the patients.

Ethics approval

The study (RepurpSS-I) was approved by the Local Ethics Committee of University Medical Center Utrecht (15-427/G-D), EudraCT, 2014−003140−12.

Provenance and peer review

Not commissioned; externally peer reviewed.

Orcid

Dewi Rijnenberg: http://orcid.org/0009-0008-0875-1200

REFERENCES

[1] Foulks GN, Forstot SL, Donshik PC, Forstot JZ, Goldstein MH, Lemp MA, et al. Clinical guidelines for management of dry eye associated with Sjögren disease. Ocul Surf 2015;13(2):118–32. doi: 10.1016/j.jtos.2014.12.001.

[2] van der Heijden E, Martine Hanna, Blokland SLM, Hillen MR, Lopes APP, van Vliet-Moret FM, Rosenberg AJWP, et al. Leflunomide−hydroxychloroquine combination therapy in patients with primary Sjögren's syndrome (RepurpSS-I): a placebo-controlled, double-blinded, randomised clinical trial. Lancet Rheumatol 2020;2(5):e260–9. doi: 10.1016/S2665-9913(20)30057-6.

[3] Wu J, Li D. Pilocarpine treatment of Sjögren's syndrome curative effect of meta-analysis of randomised controlled trials. Clin Exp Rheumatol 2024;42 (12):2490–8. doi: 10.55563/clinexprheumatol/lkk9qq.

[4] Jin K, Imada T, Hisamura R, Ito M, Toriumi H, Tanaka KF, et al. Identification of Lacrimal gland postganglionic innervation and its regulation of tear secretion. Am J Pathol 2020;190(5):1068–79. doi: 10.1016/j.ajpath.2020.01.007.

[5] Tangkrisanavinont V. Stimulation of lacrimal secretion by sympathetic nerve impulses in the rabbit. Life Sci 1984;34(24):2365–71. doi: 10.1016/0024-3205(84)90423-5.

[6] Edvinsson L. Aspects on the pathophysiology of migraine and cluster headache. Pharmacol Toxicol 2001;89(2):65–73. doi: 10.1034/j.1600-0773.2001.d01-137.x.

Dewi Rijnenberg [1], Eefje H.M. van der Heijden[1], Ronald L. A.W. Bleys[2], Helen L. Leavis[1,3], Joël A.G. van Roon[1,3,*]

[1] *Department of Rheumatology and Clinical Immunology, Utrecht University, University Medical Center Utrecht, Utrecht, The Netherlands*

[2] *Department of Anatomy, Division of Surgical Specialties, Utrecht University, University Medical Center Utrecht, The Netherlands*

[3] *Center of Translational Immunology (CTI) Research, Division of Laboratories, Pharmacy and Biomedical Genetics, Utrecht University, University Medical Center Utrecht, The Netherlands*

*Correspondence to Dr Joël A. G. van Roon.
E-mail address: j.vanroon@umcutrecht.nl (J.A.G. van Roon).

Correspondence

Correspondence on 'Pulmonary arterial hypertension in adults with Still's disease: another pulmonary manifestation associated with HLA-DRB1*15' by Boucly A, et al.

We read with great interest the article titled, 'Pulmonary arterial hypertension in adults with Still's disease: another pulmonary manifestation associated with HLA-DRB1*15' authored by Boucly A et al [1]. The authors identified a previously unappreciated association between HLA-DRB1*15 alleles and pulmonary arterial hypertension (PAH) in adult patients with Still's disease (SD). Whether this finding could be validated in the Chinese cohort of patients with SD was unknown.

We therefore collected clinical information for all patients with SD treated at the Department of Rheumatology, Renji Hospital, Shanghai Jiaotong School of Medicine, from April 2021 to July 2025 by chart review. All patients fulfilled the Yamaguchi diagnostic criteria [2]. Suspected PAH was defined by transthoracic echocardiography as pulmonary artery systolic pressure >40 mm Hg [3,4]. Patients with other known causes of pulmonary hypertension were excluded.

Between April 2021 and July 2025, 376 patients with SD were treated at our centre and only 5 cases (1.3%) were identified with suspected PAH, supporting that PAH might be a very rare complication in Chinese patients with SD. Human leukocyte antigen (HLA) typing was performed in 153 patients, including the above 5 patients with suspected PAH. HLA-DRB1*15 was detected in 59 of 153 (38.6%) patients, while none of the 5 patients with suspected PAH carried the HLA-DRB1*15 allele. Therefore, HLA-DRB1*15 allele seemed unlikely to be a genetic risk factor for PAH in Chinese adults with SD, at least based on our current data.

Previous studies have reported that the HLA-DRB1*15 allele is associated with hypersensitivity reactions to biologic agents in SD [5,6]. Taken together, these observations highlight the complexity of role HLA-DRB1*15 allele plays in the SD course. In our cohort, we found that HLA-DRB1*15 allele was significantly associated with drug-related adverse events of interleukin-6 receptor (IL-6R) inhibitors. It has been reported that IL-6R inhibitor treatment could trigger macrophage activation syndrome (MAS) in some patients with SD; therefore, it was not recommended in patients with SD with MAS. In our SD cohort, 11 patients experienced drug-related adverse events during or shortly after initiation of IL-6R inhibitors, including MAS (N = 5), liver dysfunction (N = 4), and acute infusion reactions (such as respiratory distress, cold sweats, nausea, or vomiting; N = 2). Among 10 of the 11 patients with genotyping data, we observed a significant elevated prevalence of HLA-DRB1*15 allele carriers (8/10, 80%) as compared to that of 17.1% in SD patients without adverse events on IL-6R inhibitors. Furthermore, HLA-DRB1*15-positive and -negative patients showed no differences in terms of the severity of SD, as measured by Pouchot score. Our findings indicate that potential genetic-therapeutic interactions should be carefully considered when initiating IL-6 blockade therapy in Chinese adults with SD.

Several potential limitations should be acknowledged. The retrospective and single-centre design is associated with possible selection and information biases. Moreover, the absence of confirmatory right heart catheterisation data limits the precision of PAH assessment. Additionally, genetic backgrounds may vary across ethnic groups, and thus our findings in Chinese patients with SD may not be generalizable to other populations, which warrants further investigation in multinational cohorts.

Funding

Competing interests

All authors declare they have no competing interests.

CRediT authorship contribution statement

Jingjing Li: Data curation, Formal analysis, Validation, Writing − original draft, Investigation, Methodology. **Ting Ma:** Data curation, Writing − original draft. **Wenwen Xu:** Conceptualization, Investigation, Validation, Writing − review & editing. **Ran Wang:** Methodology, Writing − review & editing. **Jie Chen:** Methodology, Writing − review & editing. **Qiong Fu:** Methodology, Supervision, Validation, Writing − review & editing.

Patient consent for publication

Not applicable.

Ethics approval

Not applicable.

Provenance and peer review

Not commissioned; externally peer reviewed.

Orcid

Jingjing Li: http://orcid.org/0009-0001-9166-3656
Qiong Fu: http://orcid.org/0000-0001-5873-6422

REFERENCES

[1] Boucly A, Mitrovic S, Carmagnat M, Savale L, Jaïs X, Taupin JL, et al. Pulmonary arterial hypertension in adults with Still's disease: another pulmonary manifestation associated with HLA-DRB1*15. Ann Rheum Dis 2025 Published online May 15. doi: 10.1016/j.ard.2025.04.016.

[2] Yamaguchi M, Ohta A, Tsunematsu T, Kasukawa R, Mizushima Y, Kashiwagi H, et al. Preliminary criteria for classification of adult Still's disease. J Rheumatol 1992;19(3):424–30.

[3] Avouac J, Airo P, Meune C, Beretta L, Dieude P, Caramaschi P, et al. Prevalence of pulmonary hypertension in systemic sclerosis in European Caucasians and metaanalysis of 5 studies. J Rheumatol 2010;37(11):2290–8. doi: 10.3899/jrheum.100245.

[4] Ma H, Wu H, Sun X, Wang Q, Zheng Y. The Evaluation of right ventricular synchrony by two-dimensional speckle tracking echocardiography in connective tissue disease-associated pulmonary arterial hypertension. Echocardiography 2025;42(1):e70060. doi: 10.1111/echo.70060.

[5] Saper VE, Ombrello MJ, Tremoulet AH, Montero-Martin G, Prahalad S, Canna S, et al. Severe delayed hypersensitivity reactions to IL-1 and IL-6 inhibitors link to common HLA-DRB1*15 alleles. Ann Rheum Dis 2022;81(3):406–15. doi: 10.1136/annrheumdis-2021-220578.

[6] Binstadt BA, Nigrovic PA. The conundrum of lung disease and drug hypersensitivity-like reactions in systemic juvenile idiopathic arthritis. Arthritis Rheumatol 2022;74(7):1122–31. doi: 10.1002/art.42137.

Jingjing Li [ID][1], Ting Ma[1], Wenwen Xu[1], Ran Wang[1], Jie Chen[1], Qiong Fu [ID][1,2,*]

[1] Department of Rheumatology, Renji Hospital, Shanghai Jiao Tong University School of Medicine, Shanghai, China

[2] Shanghai Immune Therapy Institute, Shanghai, China

*Correspondence to Dr Qiong Fu, Department of Rheumatology, Renji Hospital, Shanghai Jiao Tong University School of Medicine, Shanghai, China.

E-mail address: fuqiong5@163.com (Q. Fu).

Response

Response to correspondence on 'Pulmonary arterial hypertension in adults with Still's disease: another pulmonary manifestation associated with HLA-DRB1*15' by Boucly A, et al.

We thank Li et al [1] for their thoughtful correspondence on our article, 'Pulmonary arterial hypertension in adults with Still's disease: another pulmonary manifestation associated with HLA-DRB1*15' [2].

In their letter, the authors seek to clarify the existence of a possible association between HLA-DRB1*15 and pulmonary arterial hypertension (PAH) in Still's disease (SD) in a cohort of adult Chinese patients. This is an excellent initiative, given the severe lack of data in this population. In fact, in our series of 16 adult patients with SD-related PAH, there were no patients of Chinese ancestry and only 1 patient of Asian ancestry (Vietnamese), whose HLA status was unknown [2]. Furthermore, in the systematic review of adult cases of SD-related PAH we performed [2], there was only 1 patient of Chinese origin whose HLA status was unknown [3]. With regard to other pulmonary manifestations of SD (interstitial lung disease), data are also lacking for the Chinese population, as the main published papers come from North America, with cohorts predominantly composed of patients of European ancestry [4,5].

The fact that Li et al [1] found no association between HLA-DRB1*15 and pulmonary hypertension (PH) in a Chinese cohort is certainly an important message, but must be interpreted with caution. First, they did not perform right heart catheterisation, the gold standard for both confirming the diagnosis of PH and distinguishing between precapillary and/or postcapillary mechanisms [6]. In the absence of this systematic invasive haemodynamic evaluation, the diagnosis of PAH (ie, group 1 PH, characterised by progressive remodelling of small pulmonary arteries) cannot be confirmed with certainty. Moreover, the authors defined PH by transthoracic echocardiography as a pulmonary artery systolic pressure >40 mm Hg, although it is well-established that this is not a robust criterion and does not align with the European Society of Cardiology/European Respiratory Society recommendations for PAH screening, which are based

on tricuspid regurgitant velocity and indices of right ventricular function [6]. Additionally, the sample size was small (5 patients). The Chinese population is composed of different ethnic groups, and the authors did not specify the details of the ethnic groups in their cohort. However, data suggest a different distribution of HLA-DRB1 among the different populations living in China [7]. Finally, although 72.7% of our SD patients with PAH, for whom HLA typing was available, were positive for HLA-DRB1*15, 27.3% were negative [2], highlighting that although this HLA group appears to be a risk factor, genetics does not seem to be the only factor involved.

The other key message of the letter by Li et al [1] is that HLA-DRB1*15 was significantly associated with 'drug reactions' to interleukin (IL)-6 inhibitors in their patients. In our cohort, SD patients who had developed PAH also had a more frequent history of drug reactions to IL-1 or IL-6 inhibitors (37.5%) than those who did not have PAH (7.2%). Among the 6/16 PAH patients who had a history of drug reactions, HLA typing was available for 5 patients, and 4/5 (80%) were positive for HLA-DRB1*15 [2]. The crucial question is whether these 'drug reactions', found in a significant proportion of patients developing pulmonary involvement (whether interstitial or vascular) and often accompanied by recurrent macrophage activation syndrome (MAS) and eosinophilia, are a true drug hypersensitivity or not [8]. In our cohort, drug reactions to IL-1 and/or IL-6 inhibitors were all confirmed by a dermatologist and/or an allergologist, and included rashes atypical of SD (eg, nonevanescent, pruritic, urticarial, a fortiori in the presence of blood eosinophilia) or acute reactions (respiratory distress and swelling or Quincke oedema during or near the time of medication administration) [2]. Furthermore, 2 patients in the PAH+ group met the criteria for Drug Reaction with Eosinophilia and Systemic Symptoms (DRESS) syndrome (RegiSCAR [European Registry of Severe Cutaneous Adverse Reactions]for DRESS ≥4) [9]. Of the 11 patients described by Li et al [1] as having experienced 'drug-related adverse events' during or shortly after the initiation of IL-6R inhibitors, 2 had acute infusion reactions (such as respiratory distress, cold sweats, nausea or vomiting), 5 had MAS, and 4 had liver dysfunctions. While acute infusion reactions are likely to be drug-related adverse events, MAS and liver dysfunction are more debatable, as they may also be the result of a complication of hyperinflammatory forms of SD.

Drug-induced hypersensitivity is indeed not the only hypothesis to explain the development of these manifestations. Binstadt and Nigrovic [10] have put forward the 'Cytokine Plasticity Hypothesis', which suggests that targeted therapies, such as IL-1 and IL-6 blockers, modulate the milieu in which T cells

differentiate. This altered environment may foster a pathologic immune response triggered by exposure to common microbes or other exogenous or endogenous antigens rather than to the drugs themselves. According to this hypothesis, elevated IL-1 and IL-6 levels in SD lead to type 17 T helper (Th) cells (Th17) skewing in CD4 + Th cells and regulatory T cells (Tregs). Blocking IL-1 or IL-6 converts these cells into interferon-γ−producing Th1 cells and/or IL-4−producing Th2 cells, in particular CD4 + T cells recognising HLA-DRB1*15:XX-presented antigens (exogenous or endogenous) [10]. This may promote the occurrence of hyperinflammatory manifestations of SD, such as MAS, pulmonary complications, and explosive drug-like reactions to IL-1 or IL-6 inhibitors, in predisposed patients, such as those carrying HLA DRB1*15.

While Li et al [1] are right to call for caution in cases of HLA-DRB1*15 positivity, which is a biomarker for a more severe form of SD that should be, in our opinion, tested in all patients diagnosed with SD, it is worth remembering that the European Alliance of Associations for Rheumatology/Paediatric Rheumatology European Society recommendations for SD highlighted that there is insufficient evidence to withhold first-line IL-1 or IL-6 inhibitors in patients with new onset SD and HLA-DRB1*15 positivity [11]. Indeed, this could lead to missed treatment opportunities, since IL-1 or IL-6R inhibitors are and should be first-line treatment in SD [11]. However, the Task Force has included in its research agenda the need to better understand the pathophysiology of hyperinflammatory forms of SD, particularly the role of HLA DRB1*15 and the potential interaction with biological treatments [11].

FUNDING

Competing interests

None related to this work.

CRediT authorship contribution statement

Stéphane Mitrovic: Conceptualization, Data curation, Formal analysis, Investigation, Project administration, Validation, Visualization, Writing − original draft, Writing − review & editing. **Athénaïs Boucly:** Writing − review & editing. **Olivier Sitbon:** Writing − review & editing. **Bruno Fautrel:** Writing − review & editing. **David Montani:** Writing − review & editing.

Patient consent for publication

Not applicable.

Ethics approval

Not applicable.

Provenance and peer review

Not commissioned; externally peer reviewed.

Orcid

Stéphane Mitrovic: http://orcid.org/0000-0001-5244-7881
Athénaïs Boucly: http://orcid.org/0000-0001-6246-5557
Olivier Sitbon: http://orcid.org/0000-0002-1942-1951
Bruno Fautrel: http://orcid.org/0000-0001-8845-4274
David Montani: http://orcid.org/0000-0002-9358-6922

REFERENCES

[1] Li J, Ma T, Xu W, Wang R, Chen J, Fu Q. Correspondence on 'Pulmonary arterial hypertension in adults with Still's disease: another pulmonary manifestation associated with HLA-DRB1*15' by Boucly A, et al. Ann Rheum Dis 2025.

[2] Boucly A, Mitrovic S, Carmagnat M, Savale L, Jaïs X, Taupin JL, et al. Pulmonary arterial hypertension in adults with Still's disease: another pulmonary manifestation associated with HLA-DRB1*15. Ann Rheum Dis 2025 Sep;84(9):1538–48.

[3] Zeng F, Deng G, Luo H, Zuo X, Xie Y. Macrophage activation syndrome and pulmonary arterial hypertension in a patient with adult-onset Still disease: a case report. Medicine (Baltimore) 2019;98(44):e17427.

[4] Saper VE, Chen G, Deutsch GH, Guillerman RP, Birgmeier J, Jagadeesh K, et al. Emergent high fatality lung disease in systemic juvenile arthritis. Ann Rheum Dis 2019 Dec;78(12):1722–31.

[5] Saper VE, Ombrello MJ, Tremoulet AH, Montero-Martin G, Prahalad S, Canna S, et al. Severe delayed hypersensitivity reactions to IL-1 and IL-6 inhibitors link to common HLA-DRB1*15 alleles. Ann Rheum Dis 2022 Mar;81(3):406–15.

[6] Humbert M, Kovacs G, Hoeper MM, Badagliacca R, Berger RMF, Brida M, et al. 2022 ESC/ERS Guidelines for the diagnosis and treatment of pulmonary hypertension. Eur Respir J 2023 Jan;61(1):2200879.

[7] Fan B, Huang X, Zhang X, Huang L, Yang Z, Ma S, et al. Comprehensive research on the distribution of HLA-DRB1 in Chinese populations. HLA 2023 Mar;101(3):239–48.

[8] Mitrovic S, Boucly A, Sitbon O, Fautrel B, Montani D. Correspondence on: pulmonary arterial hypertension in adults with Still's disease: another pulmonary manifestation associated with HLA-DRB1*15—reply. Ann Rheum Dis 2025. doi: 10.1016/j.ard.2025.07.003.

[9] Kardaun SH, Sekula P, Valeyrie-Allanore L, Liss Y, Chu CY, Creamer D, et al. Drug reaction with eosinophilia and systemic symptoms (DRESS): an original multisystem adverse drug reaction. Results from the prospective RegiSCAR study. Br J Dermatol 2013 Nov;169(5):1071–80.

[10] Binstadt BA, Nigrovic PA. The conundrum of lung disease and drug hypersensitivity-like reactions in systemic juvenile idiopathic arthritis. Arthritis Rheumatol 2022;74(7):1122–31.

[11] Fautrel B, Mitrovic S, De Matteis A, Bindoli S, Antón J, Belot A, et al. EULAR/PReS recommendations for the diagnosis and management of Still's disease, comprising systemic juvenile idiopathic arthritis and adult-onset Still's disease. Ann Rheum Dis 2024 Nov;83:1614–27.

Stéphane Mitrovic [1,2,3,*], Athénaïs Boucly [4,5,6], Olivier Sitbon [4,5,6], Bruno Fautrel [1,2,7], David Montani [4,5,6]

[1] *Department of Rheumatology, Sorbonne University−APHP (Assistance Publique - Hôpitaux de Paris), Pitié-Salpêtrière Hospital, Paris, France*

[2] *CEREMAIA (Centre d'Etude et de Référence sur les Maladies AutoInflammatoires et les Amyloses), FAI^{2}R (Filière de Santé des Maladies Auto-Immunes et Auto-Inflammatoires Rares) Network, Paris, France*

[3] *INSERM UMRS 959, Immunology-Immunopathology-Immunotherapy (i3), Sorbonne University, Paris, France*

[4] *APHP, Hôpital Bicêtre, DMU Thorinno, Service de Pneumologie, Le Kremlin-Bicêtre, France*

[5] *Université Paris-Saclay, Faculté de Médecine, Le Kremlin-Bicêtre, France*

[6] *INSERM, UMR S_999, Le Kremlin-Bicêtre, France*

[7] *INSERM UMR 1136, Pierre Louis Institute of Epidemiology and Public Health, Equipe PEPITES, Sorbonne University-APHP, Paris, France*

*Correspondence to Dr Stéphane Mitrovic, Department of Rheumatology, Sorbonne University−APHP, Pitié-Salpêtrière Hospital, Paris, France.
E-mail address: stephane.mitrovic@aphp.fr (S. Mitrovic).

Correspondence

Correspondence on 'Janus kinase inhibitors and tumour necrosis factor inhibitors show a favourable safety profile and similar persistence in rheumatoid arthritis, psoriatic arthritis and spondyloarthritis: real-world data from the BIOBADASER registry' by Hernández-Cruz et al.

To the Editor,

We read with great interest the recent article by Hernández-Cruz et al [1], which presents valuable real-world evidence comparing the safety and persistence of Janus kinase inhibitors (JAKi) and tumour necrosis factor inhibitors (TNFi) across rheumatoid arthritis (RA), psoriatic arthritis (PsA), and axial spondyloarthritis (axSpA). Their analysis of 6826 patients from the BIOBADASER (Spanish Registry of Adverse Events for Targeted Therapies in Rheumatic Diseases) registry represents one of the largest real-life cohorts exploring this topic to date. The findings of comparable persistence between JAKi and TNFi, stratified by disease subtype, are both clinically relevant and timely [1].

However, one relevant methodological concern is that the analysis of drug persistence in the BIOBADASER study did not include prior assessment of medication adherence. Persistence was estimated solely based on time to discontinuation, without considering whether patients consistently took the treatment as prescribed. This limitation could impact the interpretation of the persistence outcomes, especially in real-world settings where adherence is a key determinant of long-term treatment continuation. Although the authors acknowledge various sources of bias and unmeasured confounding in the limitations section, the absence of adherence data is not explicitly addressed and should be taken into account when interpreting the findings. Persistence and adherence are distinct concepts [2,3]. A patient may remain on treatment but deviate from the prescribed regimen (nonadherence), leading to overestimated treatment benefits or masked safety issues. Administrative data may

thus provide an inflated picture of persistence in the absence of adherence metrics, such as the medication possession ratio or proportion of days covered. Ignoring adherence in persistence studies may, therefore, result in biased or overly optimistic estimates of treatment effectiveness and safety [4,5].

The clinical implications of this distinction are profound. The therapeutic efficacy and long-term benefits of treatments depend not only on maintaining therapy over time but also on correct and consistent administration. Suboptimal adherence has been associated with increased disease activity, flares, diminished quality of life, and higher healthcare costs [4]. In real-world database studies relying on administrative data or electronic medical records, the absence of adherence measures can result in biased or overly optimistic persistence estimates. As such, the conclusions regarding comparative effectiveness between JAKi and TNFi must be interpreted cautiously, recognising that unmeasured differences in adherence may contribute to observed differences in persistence and remission rates.

This distinction becomes even more relevant in the context of the evolving *6P Medicine* framework (Personalized, Predictive, Preventive, Participatory, Precision, and Persistent), where both adherence and persistence are considered integral to long-term treatment success [6]. Recognising the multidimensional nature of patient behaviour, this model advocates for a comprehensive assessment that integrates persistence, adherence, and other behavioural factors into clinical and policy decision-making. Of note, patients with RA, PsA, and axSpA classified as persistent in administrative databases may, in reality, show poor adherence, thereby inflating persistence figures and skewing interpretations of treatment durability. Additionally, overlooking adherence may mask the identification of individuals at risk of suboptimal outcomes who could benefit from supportive interventions to improve medication-taking behaviour.

Incorporating adherence assessment would enable a more accurate stratification of therapeutic outcomes and enhance the applicability of real-world persistence results in both clinical and policy contexts. Ultimately, this contributes to a more nuanced and clinically meaningful understanding of RA, PsA, and axSpA therapy performance, directly informing treatment guidelines, shared decision-making, and individualised care planning [7−10].

We commend the authors for their rigorous approach to evaluating persistence, but we strongly advocate for the inclusion of adherence data in future registry-based studies. Doing so would allow for a more granular and clinically meaningful interpretation of treatment continuation and its relation to both efficacy and safety. This is particularly important as healthcare systems increasingly adopt data-driven models to evaluate real-world effectiveness and value-based care in chronic inflammatory diseases.

Competing interests

All authors declare they have no competing interests.

Contributors

JB-B, AV-R and SC performed the investigation, analysed the data, provided resources, supervised the project, and wrote the original draft of the manuscript. JB-B also reviewed and edited the manuscript. The authors have read and agreed to the published version of the manuscript.

Funding

No funding or sponsorship was received for this study or the publication of this article.

Patient consent for publication

Not applicable.

Ethics approval

This article is based on previously conducted studies and does not contain any new studies with human participants or animals performed by any of the authors.

Provenance and peer review

Not commissioned; externally peer reviewed.

Medical writing/editorial assistance

No external or internal medical writing or editorial assistance was used in the preparation of this manuscript.

Orcid

Joaquín Borrás-Blasco: http://orcid.org/0000-0003-0248-4208

REFERENCES

[1] Hernández-Cruz B, Otero-Varela L, Freire-González M, Busquets-Pérez N, García González AJ, Moreno-Ramos M, et al. Janus kinase inhibitors and tumour necrosis factor inhibitors show a favourable safety profile and similar persistence in rheumatoid arthritis, psoriatic arthritis and spondyloarthritis: real-world data from the BIOBADASER registry. Ann Rheum Dis 2024;83:1189−99.

[2] Rodriguez Goicoechea M, Tejedor Tejada E, Borrás Blasco J. [Translated article] Persistence, current state of the art. Farm Hosp 2024;48:T141.

[3] de la Cueva Dobao P, Notario J, Ferrándiz C, López Estebaranz JL, Alarcón I, Sulleiro S, et al. Expert consensus on the persistence of biological treatments in moderate-to-severe psoriasis. J Eur Acad Dermatol Venereol 2019;33:1214−23.

[4] Borrás-Blasco J, Ramírez-Herráiz E, Navarro Ruiz A. El valor de la persistencia en el modelo de la Medicina 5P en enfermedades crónicas [The value of persistence in the 5P Medicine model for chronic diseases]. J Healthc Qual Res 2024;39:196−8.

[5] Borrás-Blasco J, Ramírez-Herráiz E, Navarro-Ruiz A. Influencia de la adherencia en el valor de persistencia dentro de la Medicina 6P [Influence of adherence on persistence value inside Medicina 6P]. J Healthc Qual Res 2025;40:101123.

[6] Borrás-Blasco J, Ramírez-Herráiz E, Navarro-Ruiz A. Integration of persistence in the 5P-medicine approach for age-related chronic diseases. Int J Qual Health Care 2024;36:mzae026.

[7] Valcuende-Rosique A, Borrás-Blasco J, Martínez-Badal S, Cortes X, Aparicio-Rubio C, Casterá-Melchor E. Evaluation of persistence, retention "rate" and prescription pattern of original infliximab and infliximab CT-P13 in biologic-naïve patients with ulcerative colitis. Farm Hosp 2022;46:296−300.

[8] Borrás-Blasco J, Valcuende-Rosique A, Cornejo S, Aparicio-Rubio C, Aguilar-Zamora M, Garijo-Bufort M, et al. Persistence after switching from adalimumab biosimilar MSB11022 to adalimumab biosimilar GP2017 in patients with chronic inflammatory rheumatic diseases. J Pharm Technol 2024:87551225241306675.

[9] Borrás-Blasco J, Cornejo S, Valcuende-Rosique A, Alcala R, Bono AN. Long-term persistence with secukinumab in patients with moderate-to-severe psoriasis. Farm Hosp 2024. In press.

[10] Borrás-Blasco J, Alcala R, Valcuende-Rosique A, Cornejo S. Long-term real-world persistence of guselkumab in patients with moderate-to-severe psoriasis. Actas Dermosifiliogr 2025. In press.

Joaquín Borrás-Blasco [ID] [1,*], Alejandro Valcuende-Rosique[2], Silvia Cornejo-Uixeda[1]

[1] *Pharmacy Department, Hospital de Sagunto, Sagunto, Spain*
[2] *Pharmacy Department, Alzira Hospital, Alzira, Spain*

***Correspondence to** Dr Joaquín Borrás-Blasco, Pharmacy Department, Hospital de Sagunto, Valencia, Spain.
E-mail address: jborrasb@gmail.com (J. Borrás-Blasco).

Response

Response to correspondence on 'Janus kinase inhibitors and tumour necrosis factor inhibitors show a favourable safety profile and similar persistence in rheumatoid arthritis, psoriatic arthritis and spondyloarthritis: real-world data from the BIOBADASER registry' by Hernández-Cruz et al.

Dear editor,

Thank you for your letter. Your comments on the difference between persistence and adherence are valid and scientifically solid [1]. We are aware of this. This matter is important in observational studies, especially those involving administrative claim databases from patients with chronic immune-mediated diseases attended by rheumatologists. It can also be extended to other electronic medical records, such as BIOBADASER (Spanish register of adverse events and effectiveness of advanced therapies -biologic, biosimilars and targeted synthetic drugs- in Rheumatic Diseases of the Spanish Society of Rheumatologist). The importance of adherence has been recognised in several recent articles. They inform about a great variability in persistence and adherence and highlight the difficulty in their evaluation, especially adherence [2−4].

BIOBADASER has a peculiar context that will be explained below. The Spanish healthcare system provides a 100% financial coverage for advanced therapies, including tumor necrosis factor inhibitors and Janus Kinase inhibitors. Patient payment is not necessary. The system covers all Spanish citizens [5]. All the advanced therapies prescribed by rheumatologists are approved by a committee (with the participation of rheumatologists, hospital pharmacists, nurses, and managers). After the approval of these therapies, the treatment is dispensed by professionals in hospital pharmacies. The pharmacist keeps an electronic record that helps us with adherence, verified in a first step. If the pharmacist detects adherence problems, they notify the treating rheumatologist. In this way, they can improve adherence in a dynamic way. This method has been standardised since 2014 and has been functioning in most rheumatology services [6].

In addition, BIOBADASER is not an administrative claims database. It is an initiative of rheumatologists coordinated by the research department of the Spanish Society of Rheumatology and has been functioning since the 2000s [7]. The objective of BIOBADASER is to evaluate both the safety and efficacy of advanced therapies. The inclusion of data is performed by experienced rheumatologists, and the reliability of the data is checked by on-site monitoring twice a year. Adherence is verified by checking clinical charts and pharmacy records. When advanced therapy is stopped because of inefficacy, the cause is recorded. If the cause is adherence, it is documented in the database [7−10].

Rheumatologists are aware of the differences in adherence and persistence, as your letter mentions. We also notice their impact on health outcomes, effectiveness, and related costs [2]. Rates of adherence in several rheumatic diseases of 9.3% to 94%, and of persistence of 23% to 80%, have been recently reviewed. However, there is a great variability due to the scarcity of observational studies, and above all, the difficulty in the adherence measurements [2].

We know the rate of adherence of different disease-modifying antirheumatic drugs (DMARDs) in Spanish patients with rheumatic diseases is about 79%. The study of Pombo-Suarez et al [11] revealed the adherence rates in 859 patients attended in 41 Rheumatology Services. In this case, the Compliance Questionnaire in Rheumatology assessed that the adherence rate was 79%. This rate was similar between biologics and conventional DMARDs—oral, subcutaneous, and intravenous (IV) [12]. Due to the COVID-19 pandemic, there was a remarkable reduction in the use of intravenous drugs in our patients. In fact, infliximab IV is rarely used currently in rheumatoid or psoriatic arthritis patients. Fewer drugs, simple doses, family support, as well as psychosocial conditions were the main determinants of adherence [11].

The study of Calvo-Alén et al [12] included patients with rheumatoid arthritis treated with different biologic drugs. The authors found there was 85% adherence using the medication possession ratio. The studies by Pombo-Suarez et al [11] and Calvo-Alén et al [12] included patients participating in BIOBADASER.

Another study of a smaller number of patients with rheumatoid arthritis, psoriatic arthritis, and ankylosing spondylitis revealed rates of adherence of 59.3%, 60.5%, and 76.2%, respectively (measured by medication possession ratio, Compliance Questionnaire in Rheumatology, and Morisky Medication Adherence Scale Questionnaire) [13].

We consider that the rates of adherence in patients with rheumatic diseases are high, as it is reported in the literature [11−13]. These facts reinforce our data of persistence. Since the appearance of the first biologic >25 years ago, Spanish

rheumatologists and pharmacists have been working together. Their aim is to improve the adherence in patients with inflammatory arthritis. It is noteworthy that adherence in patients with inflammatory arthritis is usually higher than that in patients with psoriasis without arthritis or inflammatory bowel disease [14]. Even though this was mentioned by the correspondence authors [1], our study deals only with inflammatory arthritis.

As a matter of fact, a structured adherence evaluation will improve the research. It is challenging in observational studies and is not the objective of our research. Our data about persistency are not disregarded because of this reason, considering the high adherence rates in our patients, which was similar between tumor necrosis factor and Janus Kinase inhibitors.

At long last, the 'treat to target' strategy in rheumatology was implemented around 2010 [15]. Since then and until now, one of the overarching principles is that 'The treatment of rheumatoid arthritis must be based on a shared decision between the patient and the rheumatologist' [16]. This has been extended to other immune-mediated and musculoskeletal conditions. We know that shared decision making improves the adherence and outcomes in our patients. In addition, the 'treat to target' strategy has presently added the treatment of comorbidities. To reach this, a multidisciplinary team is needed. This team includes rheumatologists, pharmacists, primary care specialists, pneumologists, etc. The 6P medicine model that you mention is true for oncology and haematology but is far from its implementation in rheumatology [17,18].

We appreciate your comments, and as you suggest, we could introduce adherence evaluation in future BIOBADASER investigations. If one of our objectives is adherence, the value and quality of them can be increased for the sake of our patients.

Thank you very much for your correspondence.

With our best regards.

Competing interests

All authors declare they have no competing interests.

CRediT authorship contribution statement

Blanca Hernández-Cruz: Writing − review & editing, Writing − original draft, Methodology, Investigation, Formal analysis, Conceptualization.

Acknowledgements

None.

Contributors

BHC prepared the response to this letter, as corresponding author. The rest approved the submission.

Funding

Patient consent for publication

Not applicable.

Ethics approval

None required.

Provenance and peer review

Not commissioned; externally peer reviewed.

Orcid

Blanca Hernández-Cruz: http://orcid.org/0000-0001-6423-3610

REFERENCES

[1] Correspondence on "Janus Kinase inhibitors and tumour necrosis factor inhibitors show a favourable safety profile and similar persistence in rheumatoid arthritis, psoriatic arthritis and spondyloarthritis: real world data from the BIOBADASER registry. Pending of cite. https://doi.org/10.1136/ard-2023-225271.

[2] Anghel LA, Farcaş AM, Oprean RN. Medication adherence and persistence in patients with autoimmune rheumatic diseases: a narrative review. Patient Prefer Adherence 2018;12:1151–66.

[3] Peter ME, Zuckerman AD, DeClercq J, Choi L, James C, Cooper K, et al. Adherence and persistence in patients with rheumatoid arthritis at an integrated health system specialty pharmacy. J Manag Care Spec Pharm 2021;27:882–90.

[4] Smolen JS, Gladman D, McNeil HP, Mease PJ, Sieper J, Hojnik M, et al. Predicting adherence to therapy in rheumatoid arthritis, psoriatic arthritis or ankylosing spondylitis: a large cross-sectional study. RMD Open 2019;5(1): e000585.

[5] Ministerio De Sanidad. Sistema Nacional de Salud [Internet]. [updated 2025 Jan 14; cited 2025 Jul 19]. Available from: https://www.sanidad.gob.es/organizacion/sns/home.htm.

[6] VV.AA. Monografías de Farmacia Hospitalaria y de Atención Primaria. Cambio de paradigma: de la participación a la validación (nº 14). Barcelona Bayer Hispania SL, 2020. pp 20-39 [updated 2020 Nov 1; cited 2025 jul 19].

[7] Carmona L. Registro de acontecimientos adversos de terapias biológicas en enfermedades Reumáticas: BIOBADASER. Rev Esp Reumatol 2004;31:210–3.

[8] Carmona L, Gómez-Reino J, González-González R. en representación del Grupo de Estudio BIOBADASER. Registro español de acontecimientos adversos de terapias biológicas en enfermedades reumáticas (BIOBADASER): informe de la situación a 14 de enero de 2005 [Spanish registry of adverse events of biological therapies in rheumatic diseases (BIOBADASER): report as of January 14, 2005]. Reumatol Clin 2005;1:95–111 Spanish.

[9] Biobadaser 3.0. Registro Español De Acontecimientos Adversos De Terapias Biológicas Y Biosimilares En Enfermedades Reumáticas [Internet]. [updated 2015 Oct 15; cited 2025 Jul 19]. Available from: https://biobadaser.ser.es/docs/ProtocoloBIOBADASER_V8_VersionFinal.pdf.

[10] Sanchez-Piedra C, Hernández Miguel MV, Manero J, Roselló R, Sánchez-Costa JT, Rodríguez-Lozano C, et al. Objectives and methodology of BIOBADASER phase III. Reumatol Clin (Engl Ed) 2019;15:229–36.

[11] Pombo-Suarez M, Maneiro Fernandez JR, Gomez-Reino JJ. Adherence to treatment in patients with rheumatoid arthritis from Spain. Patient Prefer Adherence 2021;15:111–7.

[12] Calvo-Alén J, Monteagudo I, Salvador G, Vázquez-Rodríguez TR, Tovar-Beltrán JV, Vela P, et al. Non-adherence to subcutaneous biological medication in patients with rheumatoid arthritis: a multicentre, non-interventional study. Clin Exp Rheumatol 2017;35:423–30.

[13] Núñez-Rodríguez J, González-Pérez Y, Nebot-Villacampa MJ, Zafra-Morales R, Obaldia-Alaña MC, Caso-González A. Adherencia terapéutica a fármacos biológicos en pacientes con artritis reumatoide, artritis psoriásica y espondilitis anquilosante. (Estudio ADhER-1) [Adherence to biological therapies in patients with rheumatoid arthritis, psoriatic arthritis and ankylosing spondylitis. (Study ADhER-1)]. Semergen 2021;47:81–90 Spanish.

[14] Kolios AGA, Hueber AJ, Michetti P, Mrowietz U, Mustak-Blagusz M, Sator PG, et al. ALIGNed on adherence: subanalysis of adherence in immune-mediated inflammatory diseases in the DACH region of the global ALIGN study. J Eur Acad Dermatol Venereol 2019;33:234–41.

[15] Smolen JS, Aletaha D, Bijlsma JWJ, Breedveld FC, Boumpas D, Burmester G, et al. Treating rheumatoid arthritis to target: recommendations of an international task force. Ann Rheum Dis 2010;69:631–7.

[16] Smolen JS, Landewé RBM, Bergstra SA, Kerschbaumer A, Sepriano A, Aletaha D, et al. EULAR recommendations for the management of rheumatoid

arthritis with synthetic and biological disease-modifying antirheumatic drugs: 2022 update. Ann Rheum Dis 2023;82:3–18.

[17] Bhamidipati K, Wei K. Precision medicine in rheumatoid arthritis. Best Pract Res Clin Rheumatol 2022;36:101742.

[18] Miyagawa I, Tanaka Y. Is precision medicine possible in rheumatic diseases? Lessons from selective use of targeted therapies in patients with psoriatic arthritis. Expert Rev Clin Immunol 2020;16:199–206.

Blanca Hernández-Cruz [ID] [a,*]

[a] *Rheumatology Service, Virgen Macarena University Hospital, Andalusian Health Service, Seville, Spain*

Correspondence to Dr Blanca Hernández-Cruz.
E-mail address: blancahcruz@gmail.com